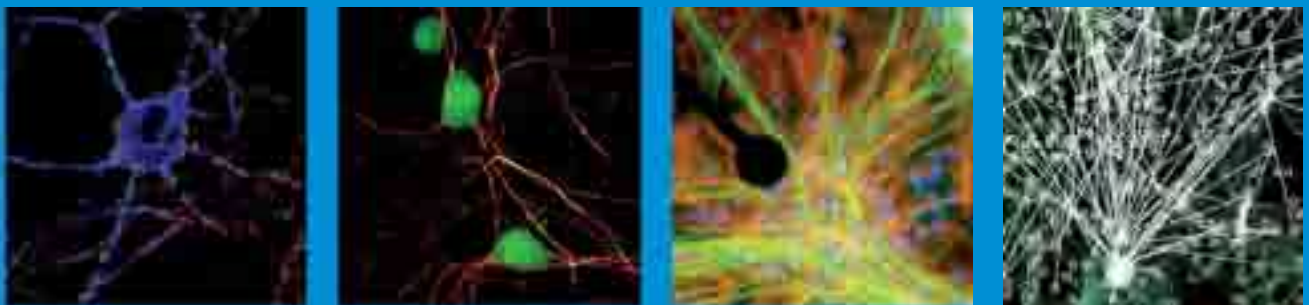


Proceedings

MEA Meeting 2010

June 29 - July 2, 2010, Reutlingen, Germany

7th International Meeting on Substrate-Integrated Microelectrode Arrays




BIO PRO
Baden-Württemberg GmbH


 **Bernstein
Center
Freiburg**

NMI 
achieving results

Baden-Württemberg

Where technology gets applied

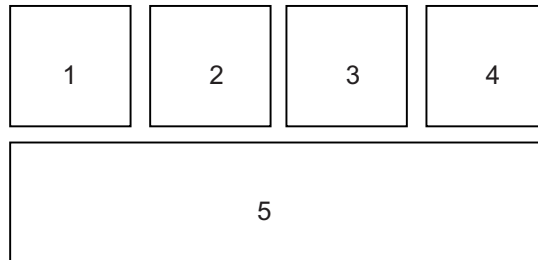
 Situated in the South-West of Germany, the state of Baden-Württemberg is home to one of the most exciting R&D infrastructures in the Life Sciences sector in Europe.

To get innovative technologies applied faster, BIOPRO works to develop novel concepts for translational research. 



Best pictures for cover image

Electrophysiological Tools for Neuroscience, Biotechnology and Biomedical Engineering



Cover images by courtesy of:

1. Daisuke Ito et al.: Long-term measurement of excitatory and inhibitory synapse densities with electrical activity during development of cultured rat cortical networks. *p. 20*
2. Tom Reimer et al.: Burst- induced inhibition in cortical neuronal networks *in vitro*. *p. 66*
3. Helena Hogberg et al.: Application of Micro Electrode Arrays (MEAs) as an emerging technology for developmental neurotoxicity. *p. 142*
4. Alessandro Maccione et al.: Functional connectivity maps in hippocampal cultures coupled to high resolutions MEAs underlie structural connectivity. *p. 193*
5. Michele Fiscella et al.: Recording of neural Activity of mouse retinal ganglion cells by means of an integrated high-density microelectrode array. *p. 106*

Conference Proceedings of the
7th International Meeting on Substrate-Integrated Microelectrode Arrays
June 29 - July 2, 2010, Reutlingen, Germany

Meeting Organisation and Imprint

- Organiser** NMI Natural and Medical Sciences Institute at the University of Tübingen
Markwiesenstrasse 55, 72770 Reutlingen, Germany
Phone: +49 7121 - 51 530 -0; Fax: +49 7121 - 51 530 16; E-Mail: info@nmi.de
Internet: www.nmi.de
- Co-organiser and Publisher** BIOPRO Baden-Württemberg GmbH
Breitscheidstraße 10, 70174 Stuttgart, Germany
Phone: +49 711 218 185 00; Fax: +49 711 218 185 02; E-Mail: info@bio-pro.de
Internet: www.bio-pro.de
Authorised Managing Director: Dr. Ralf Kindervater
- Co-organiser** Bernstein Center Freiburg
Hansastraße 9, 79104 Freiburg, Germany
Tel.: +49 (0)761 203 9549 ; Fax: +49 (0)761 203 9559 ; E-Mail: contact@bcf.uni-freiburg.de
Internet: www.bcf.uni-freiburg.de
- Organisation Team** Karla Burgert, Ira Digel, Nadja Gugeler, Priscilla Herrmann
E-Mail: meameeting@nmi.de
Internet: www.nmi.de/meameeting2010
- Scientific Programme Committee** Prof. Ulrich Egert, Institute of Microsystem Technology (IMTEK), University of Freiburg, Germany
Prof. Peter Fromherz, Max Planck Institute for Biochemistry, Martinsried, Germany
Dr. Michele Giugliano, University of Antwerp, Belgium
Dr. Daniel Granados-Fuentes, Washington University, St. Louis, USA
Dr. Yael Hanein, Tel-Aviv University, Israel
Prof. Andreas Hierlemann, Swiss Federal Institute of Technology, Zurich, Switzerland
Prof. Dr. Sven Ingebrandt, University of Applied Sciences, Kaiserslautern, Germany
Prof. Sung June Kim, Seoul National University, South Korea
Dr. Udo Kraushaar, NMI Natural and Medical Sciences Institute, Reutlingen, Germany
Prof. Shimon Marom, Faculty of Medicine, Technion, Haifa, Israel
Prof. Sergio Martinoia, University of Genova, Italy
Dr. Thomas Meyer, Multi Channel Systems MCS GmbH, Germany
Prof. Wim L.C. Rutten, University of Twente, The Netherlands
Prof. Bruce Wheeler, University of Illinois, Urbana, USA
Dr. Guenther Zeck, Max Planck Institute for Neurobiology, Martinsried, Germany
- Conference Chair** Dr. Alfred Stett, NMI Natural and Medical Sciences Institute, Reutlingen, Germany
- Sponsor** Multi Channel Systems MCS GmbH, Reutlingen, Germany (www.multichannelsystems.com)
- Editor** Alfred Stett
- Cover** Masicom UG, Kirchentellinsfurt, Germany
- Production** Fischbach Druck GmbH, Reutlingen
- ISBN** 3-938345-08-5

NMI Natural and Medical Sciences
Institute at the University of Tübingen

NMI
achieving results



BIOPRO Baden-
Württemberg GmbH

BIO  **PRO**
Baden-Württemberg GmbH

Bernstein Center Freiburg



Multi Channel Systems MCS GmbH

multichannel 
systems

Foreword

Substrate-Integrated Microelectrode Arrays: Electrophysiological Tools for Neuroscience, Biotechnology and Biomedical Engineering

7th International Meeting on Substrate-Integrated Microelectrode Arrays, June 29 - July 2, 2010, Reutlingen, Germany

The MEA community is continuously growing. There are currently more than 550 members subscribed to the MEA user group, the web-based scientific discussion group for MEA users¹. The technology and its applications are described in Wikipedia², in addition to the many papers in high-ranking journals reporting on the scientific outcome in laboratories worldwide. Multi Channel Systems recently counted more than 500 references featuring the use of their equipment. The community also sees the advent of new systems and suppliers – a good sign as it indicates a dynamic and healthy market. This development we have accounted for by offering exhibition space at this year's MEA meeting along with the opportunity for advertising in the proceedings book.

Without doubt, the passive arrays with up to hundreds of tiny electrodes have come of age and are now routine tools in electrophysiology, often used in combination with imaging, patch clamping and microfluidics. Using genetically modified cell and tissue samples, allows for investigation of the correlation of subcellular and population properties in large networks. The increasing complexity on the biological side is accompanied by the development of high-density sensor arrays with thousands of tightly-spaced electrodes and imbedded active electronics, that bear the potential to perform recordings from large cell populations at single-cell resolution. These arrays are now entering into market.

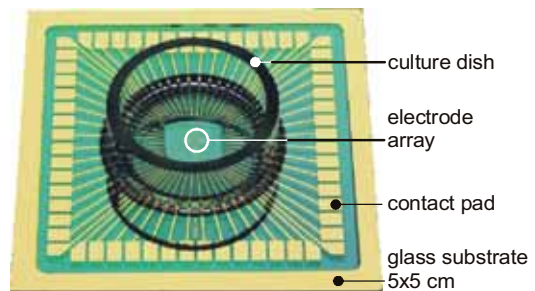
It is an honour and a great pleasure for the NMI and the co-organizers to welcome the approximately 200 participants from all over the world. Once again, the meeting has attracted students and senior researchers, MEA developers and new and experienced MEA users. More than 700 authors and co-authors from 24 countries have submitted papers for 28 oral and 125 poster presentations. Following the feedback from participants of the last meeting, an all-day poster session will be held to provide the opportunity for in-depth information exchange and networking.

We would like to thank the Scientific Programme Committee for reviewing and ranking the abstracts, and pre-selecting images for the best-picture award. The selected pictures merged to a collage for the cover page represent the diversity of themes that have been submitted – from subcellular studies to complex network analysis.

¹ <http://tech.groups.yahoo.com/group/mea-users/>

² http://en.wikipedia.org/wiki/Multi-electrode_array

microelectrode array



Standard Microelectrode Array (MEA). The substrate-integrated electrodes in the centre of the dish can be used both for stimulation and recording. Arrays with up to 1024 passive electrodes and 4096 active electrodes are available commercially from several suppliers. Many different layouts and types of electrodes, optimized for a wide range of applications, are manufactured by the NMI and delivered world-wide by Multi Channel Systems MCS to academic and industrial laboratories. MEAs are being used to address numerous questions in neuroscience, neurotechnology and cardiovascular research, as well as for drug testing in the pharmaceutical industry.

This year, the Bernstein Center Freiburg is co-organizer of the meeting. It aims to improve the understanding of brain dynamics and to explore the application of new insights and techniques in biomedicine and neurotechnology. It has provided important impulses for the programme of the meeting. Almost a tradition, BIOPRO Baden-Württemberg GmbH, as the state agency for the promotion of modern biotechnology and the life sciences, is again supporting the print version of the proceedings book. It will also be available online and offers a representative overview on current techniques and applications, which is helpful in particular for newcomers to the MEA user community.

We welcome you heartily to Reutlingen and wish you enthusiastic discussions and productive scientific exchange – with old and new friends and colleagues.

Enjoy the meeting!

Prof. Dr. Ulrich Egert
Bernstein Center Freiburg

Dr. Ralf Kindervater
CEO, BIOPRO Baden-Württemberg GmbH

Dr. Alfred Stett
Conference Chair;
Deputy Managing Director, NMI Reutlingen

Contents

Neuronal Dynamics and Plasticity 19

Long-term measurement of excitatory and inhibitory synapse densities
with electrical activity during development of cultured rat cortical networks 20

Daisuke Ito, Takumi Komatsu, Hiroki Tamate, Kazutoshi Gohara
Division of Applied Physics, Faculty of Engineering, Hokkaido University, Sapporo, Japan

Neuronal dynamics vs. connectivity: a computational model to explain how
in vitro neuronal networks exhibit well-defined patterns of activity 24

Paolo Massobrio¹, Matteo Garofalo^{1,2}, Valentina Pasquale², Sergio Martinoia^{1,2}
1 Neuroengineering and Bio-nano Technology Group (NBT), Department of Biophysical
and Electronic Engineering (DIBE), University of Genova, Genova (Italy).
2 Department of Neuroscience and Brain Technologies, Italian Institute of Technology (IIT), Genova (Italy)

Network Structure And The Origin Of Synchronized Bursts In Vitro 28

Samora Okujeni^{1,2,3}, Nila Mönig², Steffen Kandler^{1,2,3}, Oliver Wehberger^{1,2,3}, Ulrich Eger^{1,3}
1 Bernstein Center Freiburg, University Freiburg, Freiburg, Germany
2 Neurobiology & Biophysics, Institute of Biology III, Faculty of Biology, University Freiburg, Germany
3 Biomicrotechnology, Dept. Microsystems Engineering – IMTEK, University Freiburg, Germany

Effect of Ghrelin on the Network Development and Activity in Cultured Cortical Neurons of Newborn Rats30

Stoyanova Irina, le Feber Joost, Rutten Wim
Neurotechnology Group, Faculty of Electrical Engineering, Mathematics and Computer Sciences,
University of Twente, Enschede, the Netherlands

Effects of electrical stimulation to sympathetic neuron-cardiomyocyte coculture 34

*Akimasa Takeuchi¹, Hiromasa Tani¹, Masahide Mori¹, Hiroyuki Moriguchi¹, Keiko Miwa², Jong-Kook Lee²,
Makoto Noshiro³, Yasuhiko Jimbo¹*
1 Graduate school of Frontier Sciences, University of Tokyo, 5-1-5 Kashiwanoha, Kashiwa, Chiba, 277-8563 Japan
2 Research Institute of Environmental Medicine, Nagoya University, Furouchi, Chikusa, Nagoya, Aichi, 464-8601, Japan
3 Graduate School of Medical Sciences, Kitasato University, 1-15-1 Kitasato, Mimami, Sagamihara, Kanagawa, 252-0373 Japan

Temporal Coordination Of Bursting In Neuronal Cultures 38

Bikbaev Arthur, Frischknecht Renato, Heine Martin
AG Molecular Physiology, Leibniz Institute for Neurobiology, Magdeburg (Germany)

Spontaneous Cortical Column Recurrent Activity and Layer Sensitivity to Electrical Stimulation 40

Vincent Delattre¹, Michele Giugliano^{1,2} and Henry Markram¹
1 Laboratory of Neural Microcircuitry, Ecole Polytechnique Fédérale de Lausanne, Switzerland
2 Dept. Biomedical Sciences, Univ. Antwerp, Universiteitsplein 2, B-2610 Wilrijk (Belgium)

Software providing on-line high-resolution spatial mapping of single neurons 42

Patrick Dini^{1,2,3}, Maxime Ambarè³, Ulrich Eger^{1,3}
1 IMTEK – Department of Microsystems Engineering; University of Freiburg, Freiburg, Germany
2 Faculty of Biology; University of Freiburg, Freiburg, Germany
3 Bernstein Center for Computational Neuroscience Freiburg

Networks in dissociated culture follow native cortical development 44

Steffen Kandler^{1,2,3}, Samora Okujeni^{1,2,3}, Sebastian Reinartz³ & Ulrich Eger^{1,3}
1 Bernstein Center Freiburg
2 Neurobiology and Biophysics, Inst. Biology III
3 Biomicrotechnology, Dept. Microsystems Engineering; ALU Freiburg, Germany

Mapping of Paired-Pulse Activity in Hippocampal Slices with Multi-Transistor-Chip..... 46

Christoph Hermann, Peter Fromherz
Membran and Neurophysics, MPI of Biochemistry, Martinsried/Munich (Germany)

Functional and morphological comparison of patterned and random low density cultures of neurons grown on microelectrode arrays (MEAs)	47
<i>Marconi Emanuele¹, Messa Mirko¹, Baldelli Pietro^{1,3}, Casagrande Silvia³, Dante Silvia², Maccione Alessandro¹, Berdondini Luca¹, Benfenati Fabio¹</i>	
1 Italian Institute of Technology – NBT Department	
2 Italian Institute of Technology – Nanophysics Department	
3 Università di Genova - DIMES	
Network Activity Patterns in the Subthalamic Nucleus of the Rat	49
<i>Jan Stegenga, Richard van Wezel, Tjitske Heida</i>	
Mira institute of biomedical technology, Biomedical signals and systems group, University of Twente, Enschede, The Netherlands	
How to Reduce Stimulus/Response Variability in Cortical Neuronal Networks	51
<i>Oliver Wehberger^{1,2,3}, Samora Okujeni^{1,2,3}, Ulrich Egerl^{1,3}</i>	
1 Bernstein Center for Computational Neuroscience Freiburg	
2 Faculty of Biology	
3 IMTEK - Department of Microsystems Engineering, University of Freiburg, Freiburg, Germany	
Mapping of neuronal oscillations in acute hippocampal slices at high spatial resolution with Multi-Transistor Arrays	53
<i>Christian Stangl, Peter Fromherz</i>	
Max Planck Institute for Biochemistry, Dept. of Membrane and Neurophysics, Martinsried / Munich	
Spontaneous calcium transients in cultured cortical networks during development	54
<i>Yuzo Takayama, Hiroyuki Moriguchi, Kiyoshi Kotani, Yasuhiko Jimbo</i>	
Graduate School of Frontier Sciences, University of Tokyo, Japan	
Self-wiring Neural Network Model for the Simulation of Connective Topology and Burst Propagation in Neuronal Cultures	56
<i>T. Gritsun, J. le Feber and W.L.C.Rutten</i>	
Neurotechnology group, Faculty of Electrical Engineering, Mathematics and Computer Science (EEMCS), University of Twente, Enschede, the Netherlands	
Simultaneous Recording of Synaptic Plasticity in CA1 and CA3 of APP.V717I Transgenic Mice Using Microelectrode Arrays	58
<i>Seon-Ah Chong^{1,2}, Carmen Batic^{3,1}, Wolfgang Eberle¹, Fred Van Leuven⁴, Geert Callewaert²</i>	
1 Bio-Electronic Systems, IMEC vzw, Leuven, Belgium	
2 Research Group Neurodegeneration, KULeuven, Kortrijk, Belgium	
3 Laboratory of Solid State Physics and Magnetism, Department of Physics and Astronomy, KULeuven, Leuven, Belgium	
4 Experimental Genetics Group LEGTEGG, KULeuven, Leuven, Belgium	
Consequences of excessive 5-HT levels during development on signal propagation and short term plasticity in the rat barrel cortex in vitro	60
<i>Dirk Schubert, Martijn Selten, Thomas Slippens, Judith Homberg, Rembrandt Bakker, Rolf Kötter</i>	
Donders Institute for Brain, Cognition and Behaviour, Department of Cognitive Neuroscience, Radboud University Medical Centre, Nijmegen, The Netherlands	
Network hyperexcitability of cortical cultures from synapsin I knockout mice grown onto Micro-Electrode Arrays	62
<i>Michela Chiappalone¹, Valentina Pasquale¹, Mariateresa Tedesco², Sergio Martinoia^{1,2} and Fabio Benfenati^{1,3}</i>	
1 Department of Neuroscience and Brain Technologies, Italian Institute of Technology, Genova (Italy)	
2 Department of Biophysical and Electronic Engineering, University of Genova, Genova (Italy)	
3 Department of Experimental Medicine, Section of Physiology, University of Genova, Genova (Italy)	
Persistent effects of cholinergic activation in developing cerebral cortex cultures: a model for the role of sleep activity patterns in early development?	64
<i>Chiappalone Michela¹, Corner Michael², Le Feber Joost³</i>	
1 Department of Neuroscience and Brain Technologies, Italian Institute of Technology, Genova (Italy)	
2 Systems Biology Laboratory, Israel Institute for Technology - Technion, Haifa (Israel)	
3 MIRA Institute for Biomedical Engineering and Technical Medicine, University of Twente, Enschede (The Netherlands)	

Burst- induced Inhibition in Cortical Neuronal Networks <i>in vitro</i>	66
<i>Tom Reimer, Werner Baumann, Philipp Julian Koester, Jan Gimsa</i> University of Rostock, Chair for Biophysics, Gertrudenstrasse 11a, 18057 Rostock, Germany	
Long-term recordings from organotypic co-cultures of VTA-SN/PFC	68
<i>Elena Dossi¹, Francesca Gullo¹, Claudia Heine², Heike Franke², Mariapia Abbracchio³, Peter Illes², Enzo Wanke¹</i> 1 Department of Biotechnology and Biosciences, University of Milan-Bicocca, Milan, Italy 2 Rudolf-Boehm-Institute of Pharmacology and Toxicology, University of Leipzig, Leipzig, Germany 3 Department of Pharmacological Sciences, Laboratory of Molecular and Cellular Pharmacology of Purinergic Transmission, University of Milan, Milan, Italy	
Identification of Local Field Potentials and Spikes on MEA256 Platforms	70
<i>Gullo Francesca, Maffezzoli Andrea, Dossi Elena, Wanke Enzo</i> Department of Biotechnologies and Biosciences, University of Milano-Bicocca, Milan, Italy	
Up/down States Synchrony Studied in Cortical Networks: Roles of Ion Channels, Neurotransmitter Transporters and GABA Receptors	72
<i>Gullo Francesca, Maffezzoli Andrea, Dossi Elena, Wanke Enzo</i> Department of Biotechnologies and Biosciences, University of Milano-Bicocca, Milan, Italy	
From Neuron to Network: The Roles of Synaptic Proteins in Neuronal Network Activity	74
<i>Lavi Ayal, Sheinin Anton, Ashery Uri</i> Department of Neurobiology, Life Sciences Faculty, Tel Aviv University, Israel	
Chronic network stimulation enhances spontaneous spike rates	76
<i>Gregory J. Brewer¹, Michael D. Boehler¹, R A Pearson¹, A A DeMaris¹, A N Ide¹, Bruce C. Wheeler²</i> 1 Southern Illinois University School of Medicine, Springfield, IL USA 2 University of Florida, Gainesville, FL USA	
Toward panneuronal recording of multisensory information processing in the medicinal leech	78
<i>Daniel A. Wagenaar¹, John Nagarah¹, Pieter Laurens Baljon^{1,2}, and Cynthia Harley¹</i> 1 California Institute of Technology, Broad Fellows Program and Division of Biology, Pasadena CA, USA 2 Vrije Universiteit, Amsterdam, The Netherlands	
Calcium dynamics during bursting activity in neocortical cultures	80
<i>Matthew Goddard¹, Ulrich Eger^{1,2}</i> 1 Bernstein Center Freiburg, Univ. of Freiburg, Germany 2 IMTEK - Department of Microsystems Engineering, Univ. of Freiburg, Germany	
Stem Cell Derived Neuronal Networks	83
Interactions of P19 cell-derived neuronal networks and mouse cortical networks co-cultured on microelectrode array	84
<i>Yuzo Takayama, Hiroyuki Moriguchi, Atushi Saito, Kiyoshi Kotani, Yasuhiko Jimbo</i> Graduate School of Frontier Sciences, University of Tokyo, Japan	
Electrophysiological Properties Of Different Embryonic Stem Cell-Derived Neural Populations As Detected By The Microelectrode Array System	86
<i>Sebastian Illes¹, Stephan Theiss³, Alfons Schnitzler^{1,2}, Marcel Dihné^{1,2}</i> 1 Department of Neurology, Heinrich-Heine University, Moorenstr. 5, 40225 Düsseldorf, Germany 2 Institute of Clinical Neuroscience and Medical Psychology, Heinrich-Heine University, Universitätsstr.1, 40225 Düsseldorf, Germany 3 Result Medical, Friedenstraße 39, D-40219 Düsseldorf	
The Effects of AC Magnetic Fields on Neuronal Differentiation and Network Activities of P19EC Cells	88
<i>Atsushi Saito, Yuzo Takayama, Hiroyuki Moriguchi, Kiyoshi Kotani and Yasuhiko Jimbo</i> Graduate School of Frontier Sciences, University of Tokyo, Japan	

Neural Differentiation of Human Induced Pluripotent Stem Cells: Formation of Functional Neuronal Networks	90
<i>Riikka Äänismaa¹, Laura Ylä-Outinen¹, Juha Heikkilä¹, Riitta Suuronen^{1,2,3}, Heli Skottman¹, Susanna Narkilahti¹</i>	
1 Regea – Institute for Regenerative Medicine, University of Tampere, Tampere, Finland	
2 Department of Eye, Ear and Oral Diseases, Tampere University Hospital, Tampere, Finland	
3 Department of Biomedical Engineering, Tampere University of Technology, Tampere, Finland	
Plasticity of Human Embryonic Stem Cell –derived Neuronal Networks: Effect of Low-frequency Stimulation	92
<i>Laura Ylä-Outinen¹, Ismo Korhonen^{1,2}, Jarno E. Mikkonen¹, Jari Hyttinen², Susanna Narkilahti¹</i>	
1 Regea - Institute for Regenerative Medicine, University of Tampere and Tampere University Hospital, Tampere (Finland)	
2 Department of Biomedical Engineering, Tampere University of Technology, Tampere (Finland)	
Tracking the Network Development of hESC derived Neurons during Maturation	94
<i>Fikret Emre Kapucu¹, Jarno M. A. Tanskanen¹, Jarno E. Mikkonen², Laura Ylä-Outinen³, Susanna Narkilahti³, Jari A. K. Hyttinen¹</i>	
1 Department of Biomedical Engineering, Tampere University of Technology, Tampere, Finland	
2 Department of Signal Processing, Tampere University of Technology, Tampere, Finland	
3 Regea – Institute for Regenerative Medicine, University of Tampere and Tampere University Hospital, Tampere, Finland	
Human Pluripotent Stem Cells and Neuronal Networks Derived from Them: In Vitro Modeling, Toxicology Testing, and Patterning Approaches with Microelectrode Array Setup	96
<i>Laura Ylä-Outinen¹, Juha Heikkilä¹, Heli Skottman¹, Riitta Suuronen^{1,2,3}, Riikka Äänismaa¹, Susanna Narkilahti¹</i>	
1 Regea - Institute for Regenerative Medicine, University of Tampere and Tampere University Hospital, Tampere, Finland	
2 Department of Eye, Ear, and Oral Diseases, Tampere University Hospital, Tampere Finland	
3 Department of Biomedical Engineering, Tampere University of Technology, Tampere Finland	

Retinal Signalling 99

Changing dynamics of spontaneous waves during retinal development: a novel panretinal perspective achieved with the Active Pixel Sensor (APS) 4,096 electrodes array	100
<i>Evelyne Sernagor¹, Alessandro Maccione², Matthias H. Hennig³, Mauro Gandolfo⁴, Stephen J. Egle⁵, Luca Berdondini²</i>	
1 Institute of Neuroscience, Newcastle University Medical School, Newcastle upon Tyne, UK	
2 Department of Neuroscience and Brain Technologies, Italian Institute of Technology, Genova, Italy	
3 Institute for Adaptive and Neural Computation, School of Informatics, University of Edinburgh, Edinburgh, UK	
4 Department of Biophysical and Electronic Engineering, University of Genova, Genova, Italy	
5 Department of Applied Mathematics and Theoretical Physics, Cambridge University, Cambridge, UK	
Network oscillation in <i>rod degenerated (rd1)</i> retinas	104
<i>Günther Zeck^{1,2} and Jacob Menzler¹</i>	
1 Department of Computational and Systems Neuroscience, Max Planck Institute of Neurobiology, Martinsried, Germany	
2 NMI, Natural and Medical Sciences Institute at the University of Tübingen, Reutlingen, Germany	
Spatial and Temporal Patterns and Information Processing in Retinal Neurons	105
<i>Liang Pei-Ji, Jing Wei, Liu Wen-Zhong, Gong Hai-Qing, Zhang Pu-Ming</i>	
School of Life Sciences and Biotechnology, Shanghai Jiao Tong University, Shanghai, China	
Recording of Neural Activity of Mouse Retinal Ganglion Cells by Means of an Integrated High- Density Microelectrode Array	106
<i>Michele Fiscella¹, Urs Frey², David Jäckel¹, Jan Müller¹, Ralf Streichan¹, Ian L. Jones¹, Branka Roscic¹, Karl Farrow³, Botond Roska³, Andreas Hierlemann¹.</i>	
1 Bio Engineering Laboratory, ETH Zurich, Basel, Switzerland.	
2 Bio Engineering Laboratory, ETH Zurich, Basel, Switzerland; now at IBM Research, Zurich, Switzerland.	
3 Neural Circuits Laboratory, Friedrich Miescher Institute, Basel, Switzerland	
Electrical response of rabbit retinal ganglion cells and their intraretinal conduction after optic nerve crush	108
<i>Christian Leibig¹, Günther Zeck²</i>	
1 Membrane- and Neurophysics, Max Planck Institute for Biochemistry, Martinsried	
2 Computational- and Systems Neurobiology, Max Planck Institute of Neurobiology Martinsried, Germany	

Detailed Ex Vivo Electrophysiology Studies in Rabbit Sinoatrial (SA) Node	110
<i>Geoffrey Lewen², Hong Shi¹, Jia L. Zhu¹, Paul Levesque¹</i>	
1 Discovery Toxicology, Bristol-Myers Squibb Company, Princeton, NJ, USA	
2 Research Informatics, Bristol-Myers Squibb Company, Princeton, NJ, USA	
MEA-aided investigation of cardiac arrhythmia induced by electrical stimulation	113
<i>Binbin Xu¹, Sabir Jacquir¹, Stéphane Binczak¹, Gabriel Laurent¹, David Vandroux², Pierre Athias³, Jean-Marie Bilbault¹</i>	
1 Laboratoire Le2i UMR CNRS 5158, Université de Bourgogne, Dijon, France	
2 NVH Medecinal, Dijon, France	
3 Laboratoire LPPCE, CHU de Dijon, France	
Organotypic ventricular heart slices of guinea pig and pig to test for drug side effects	116
<i>Katharina Stürz¹, Elke Guenther¹, Michael Reppel², Jürgen Hescheler³ and Udo Kraushaar¹</i>	
1 Dept. of Electrophysiology, NMI Reutlingen, Germany	
2 University Medical Center Schleswig-Holstein, Lübeck, Germany	
3 Dept. of Physiology, Köln University, Germany	
To Study the Relevance of K _{ATP} Channels in Pharmacological Preconditioning Using MEA	118
<i>Thomas Pfeiffer¹, Jessica Ka-Yan Law^{2,3}, John Anthony Rudd², Chi-Kong Yeung², Sven Ingebrandt¹</i>	
1 Department of Informatics and Microsystems Technology, University of Applied Sciences Kaiserslautern, D-66482 Zweibrücken, Germany	
2 School of Biomedical Sciences, The Chinese University of Hong Kong (CUHK), Shatin, Hong Kong	
3 Bioengineering Graduate Program, The Hong Kong University of Science and Technology (HKUST), Clear Water Bay, Hong Kong	
Formation of Cardiac Cell Clusters on Commercial Multi-Electrode Arrays With Well Defined Biochemical Cues	120
<i>Li Wang^{1,3}, Li Liu¹, Qinghua Yuan¹, N. Magome¹, K. Aglatze¹ and Yong Chen^{1,2}</i>	
1 Institute for Integrated Cell-Material Science, Kyoto University, Kyoto 606-8507, Japan	
2 Ecole Normale Supérieure, UMR 8640, 24 rue Lhomond, 75005 Paris, France	
3 College of Chemistry and Molecular Science, Wuhan University, 430072, Wuhan, China	
Electrophysiological Studies of Human Embryonic Stem Cell –Derived Cardiomyocytes with Novel Microelectrode Arrays	122
<i>Kujala Ville¹, Ryyänen Tomi², Hyttinen Jari³, Lekkala Jukka², Kerkelä Erja¹, Aalto-Setälä Katriina^{1,4}</i>	
1 Regea – Institute for Regenerative Medicine, University of Tampere and Tampere University Hospital, Tampere, Finland	
2 Department of Automation Science and Engineering, Tampere University of Technology, Tampere, Finland	
3 Department of Biomedical Engineering, Tampere University of Technology, Tampere, Finland	
4 Heart Center, Tampere University Hospital, Tampere, Finland	
Detection Of Cardiac Activity From Ventricular Heart Slices Using Micro-Electrode Arrays	124
<i>Chung Yingying¹, Atan Shirhan¹, Zhang Guangqing¹, Wong Philip², Shim Winston¹</i>	
1 Research and Development Unit, National Heart Centre Singapore, Singapore	
2 Department of Cardiology, National Heart Centre Singapore, Singapore	
QT-time Evaluation for Drug-Screening Using a Rhesus Monkey Embryonic Stem Cell-Derived Cardiomyocyte Based Multi Electrode Array Test System	126
<i>Martin Lehmann¹, Filomain Nguemo¹, Ulrich Martin², Michael Reppel³, Jürgen Hescheler¹</i>	
1 University of Cologne, Cologne, Germany	
2 Hannover Medical School, Hannover, Germany	
3 Department of Cardiology, Medical University of Lübeck, Lübeck, Germany	
Anti-arrhythmic effects of very low density lipoproteins	128
<i>Yangzhen Shao, Azra Mijatovic, Sigfus Gizurarson, Truls Råmunddal, Jan Boren, Elmir Omerovic</i>	
Department of Molecular and Clinical Medicine/Cardiology, Wallenberg laboratory, Institute of Medicine at Sahlgrenska Academy, University of Gothenburg	
An in vitro method for studies of arrhythmogenesis in the heart - Electrophysiological effects of lysophosphatidylcholine on HL-1 cardiomyocytes.....	130
<i>Sigfus Gizurarson, Yangzhen Shao, Azra Miljanovic and Elmir Omerovic</i>	
Department of Molecular and Clinical Medicine/Cardiology, Wallenberg laboratory, Institute of Medicine at Sahlgrenska Academy, University of Gothenburg	

Perforated Multielectrode Array in Drug Discovery 134

Jonathan M. Levenson, Helen E. Gibson, David Gerber, Margaret Levin
Target Validation, Galenea, Corp., Cambridge, MA, USA

Cerebrospinal fluid of brain-trauma patients suppresses functional neuronal network activity 138

Marcel Dihné^{1,2}, Sebastian Illes¹, Stephan Theiss³, Alfons Schnitzler^{1,2}
1 Department of Neurology, Heinrich-Heine University, Moorenstr. 5, 40225 Düsseldorf, Germany
2 Institute of Clinical Neuroscience and Medical Psychology, Heinrich-Heine University, Universitätsstr.1, 40225 Düsseldorf, Germany
3 Result Medical, Friedenstraße 39, D-40219 Düsseldorf

Application of Micro Electrode Arrays (MEAs) as an Emerging Technology for Developmental Neurotoxicity 142

Helena T. Hogberg¹, Antonio Novellino², Tomasz Sobanski², Anna K. Bal-Price²
1 Johns Hopkins Bloomberg School of Public Health, Baltimore, Maryland, USA
2 European Commission, Joint Research Centre, Ispra, Italy

Neuronal Networks Coupled To MEAs: A Tool For In Vitro Neurotoxicity Assessment?
Results From An Inter-Laboratory Project 145

*Antonio Novellino¹, Anna Price¹, Taina Palosaari¹, Bibiana Scelfo¹, Maurice Whelan¹, Sergio Martinoia^{2,3},
Maria T Tedesco², Paolo D'Angelo², Michela Chiappalone³, Fabio Benfenati^{3,4}, Guenter W Gross⁵,
Alexandra Gramowski^{6,7}, Olaf Schroeder⁷, Timothy J Shafer⁸, Andrew FM Johnstone⁸*
1 JRC, Institute for Health and Consumer Protection, Ispra, Italy
2 KBTLab – DIBE and ett s.r.l., University of Genoa, Genoa, Italy
3 NeuroTech Lab – NBT, Italian Institute of Technology, Genoa, Italy
4 DIMES, Section of Physiology, University of Genoa, Genoa, Italy
5 Dept. Biol. Sciences and CNNS, University of North Texas, Denton TX, USA
6 Institute of Biological Sciences, University of Rostock, Rostock, Germany
7 NeuroProof GbmH, Rostock, Germany
8 Neurotoxicology Div., U. S. Environmental Protection Agency, RTP, NC, USA

Bioimpedance spectroscopy of an epithelial cell culture on a MEA chip 147

*H.D. Wanzenboeck¹, C. Peter¹, L. Schneider¹, M. Hufnagel¹, M. Fischeneder¹, A. Hoefler¹, S. Damnjanovic¹,
C. Fillafer², M. Wirth², F. Gabor² and E. Bertagnolli¹*
1 Vienna University of Technology, Institute for Solid State Electronics, Floragasse 7/1, A-1040 Vienna, Austria
2 University Vienna, Department of Pharmaceutical Technology and Biopharmaceutics, Althanstrasse 14, A-1090 Vienna, Austria

Actions Of Pyrethroid Insecticides On Cortical Networks: Comparison Of Relative Potencies Determined
Using MEAs To Relative Potencies Determined Using Motor Activity 149

Andrew F.M. Johnstone¹, Marcello Wolansky², Kevin M. Crofton¹ and Timothy J. Shafer¹
1 Integrated Systems Toxicology Division, U.S. Environmental Protection Agency, Research Triangle Park, NC, USA
2 Departamento de Química Biológica, Universidad de Buenos Aires, Buenos Aires, Argentina

Profiling of acute neurotoxic effects of insect repellents with MEA-neurochip technology 151

O. H.-U. Schroeder¹, D.G. Weiss², K. Jügel¹, A. Gramowski^{1,2}
1 NeuroProof GmbH, Rostock, Germany
2 Institute of Biological Sciences, Cell Biology and Biosystems Technology, University of Rostock, Rostock, Germany

New multi-target opioid peptides in drug development: Electrophysiological profiling using
MEA neurochip technology 153

*Alexandra Gramowski^{1,2}, Olaf Schröder², Konstantin Jügel², Andrzej Lipkowski³, Aleksandra Misicka-Kesik⁴,
Dirk Tourwé⁵, Dieter G. Weiss¹*
1 Institute of Biological Sciences, Cell Biology and Biosystems Technology, University of Rostock, Rostock, Germany;
2 NeuroProof GmbH, Rostock, Germany
3 Polish Academy of Science, Medical Research Centre, Warsaw, Poland
4 Faculty of Chemistry Warsaw University, Warsaw, Poland
5 Vrije Universiteit Brussel, Organic Chemistry, Brussel, Belgium

In vitro toxicity and cytotoxicity of the immunosuppressant cyclosporine A 155

Konstantin Jügel¹, Luise Schultz^{1,3}, O. H.-U. Schröder¹, Christophe Landry⁴, Romeo Cecchelli⁴,
Dagmar-Christiane Fischer³, Dieter Haffner³, Dieter G. Weiss², Alexandra Gramowski^{1,2}

1 NeuroProof GmbH, Rostock, Germany

2 Institute of Biological Sciences, Cell Biology and Biosystems Technology, University of Rostock, Rostock, Germany

3 Department of Pediatrics, University Children's Hospital Rostock, Rostock, Germany

4 Université Lille Nord de France, Laboratoire de Physiopathologie de la Barrière Hémato-encéphalique, Lens, France

Characterization of a mice model of human epilepsy with Multi-Electrode Arrays 157

Davide Boido^{1,2}, Enrico Ferrea^{1,2}, Diego Ghezzi¹, Pasqualina Farisello^{1,2}, Pietro Baldelli^{2,1}, Fabio Benfenati^{1,2}

1 Department of Neuroscience and Brain Technology, Italian Institute of Technology, Genova, Italy

2 Department of Experimental Medicine, Section of Physiology, University of Genova, Genova, Italy

The A-beta 42/40 Ratio Is a Driver of Acute Synaptotoxicity and LTP Impairment 159

Iryna Benilova^{1,2,3}, Seon-Ah Chong^{3,7}, Inna Kuperstein^{1,2}, Kerensa Broersen^{4,5}, Joost Schymkowitz^{4,5},
Frederic Rousseau^{4,5}, Carmen Bartic^{3,6}, Geert Callewaert⁷, Bart De Strooper^{1,2}

1 Department for Molecular and Developmental Genetics, Flanders Institute for Biotechnology (VIB), Leuven, Belgium

2 Laboratory for the Research of Neurodegenerative diseases, Center for Human Genetics, KU Leuven, Belgium

3 IMEC, MCP/ART, Heverlee, Belgium

4 SWITCH Lab, VIB, Leuven, Belgium

5 Vrije Universiteit Brussels (VUB), Belgium

6 Department of Physics and Astronomy, KU Leuven, Belgium

7 Research Group Neurodegeneration, KU Leuven, Kortrijk, Belgium

A MEA-based Assay of Adrenal Chromaffin Cells Spontaneous Firing Using Ion Channel Blockers 161

Andrea Marcantoni¹, Jonathan Rojo-Ruiz¹, Sara Gosso¹, Alberto Pasquarelli², Valentina Carabelli¹, Emilio Carbone¹

1 Department of Neuroscience; NIS Center, CNISM Research Unit, University of Torino, I-10125 Torino (Italy)

2 Institute of Electron Devices and Circuits, Ulm University, 89069 Ulm, Germany

Alcohol effects on cortical cultures 163

Kosmas Deligkaris, Jan Stegenga, Joost le Feber

University of Twente, Enschede, The Netherlands

Assessment of Neuroprotective Strategies Using MEAs 165

Geoff Mealing¹, Joseph S Tauskela¹, JP Thivierge^{1,2}, Anthony Krantis³

1 National Research Council, Institute for Biological Sciences, Synaptic Therapies & Devices, Building M-54, Montreal Rd
Campus, Ottawa, ON, Canada

2 School of Psychology, University of Ottawa, Ottawa, ON, Canada

3 QBM Cell Sciences, Ottawa, ON, Canada

Importance of multielectrode array recordings in drug discovery 167

Nicolas Redon¹, Christophe Lanneau¹, Pauline Cervello¹, Bruno Biton¹, Daniel Bertrand², Florence Oury-Donat²
and Patrick Avenet¹

1 Sanofi-Aventis R&D, Exploratory Unit, Chilly Mazarin, France.

2 Sanofi-Aventis R&D, Exploratory Unit, Montpellier, France

3 HiQscreen Sarl, Geneva, Switzerland

Signal Analysis, Statistics, and Software 169

Modeling of extracellular potentials recorded with multicontact microelectrodes 170

Gaute T. Einevoll

Norwegian University of Life Sciences, 1432 Aas, Norway

Identifying Electrically Active Cells In Neuronal Culture And Tissue Using

CMOS Based Multi-Transistor Arrays (MTAs) 174

Lambacher Armin¹, Vitzthum Veronika¹, Zeck Günther², Fromherz Peter¹

1 Membrane and Neurophysics, MPI for Biochemistry, Martinsried/Munich, Germany

2 Systems and Computational Neurobiology, MPI of Neurobiology, Martinsried/Munich, Germany

Investigating neuronal networks dynamics in hippocampal cultures by means of high-density CMOS-MEAs	175
<i>Mauro Gandolfo¹, Alessandro Maccione², Mariateresa Tedesco¹, Thierry Nieus², Kilian Imfeld³, Sergio Martinoia^{1,2}, Luca Berdondini²</i>	
1 Department of Biophysical and Electronic Engineering, University of Genova, Genova, Italy	
2 Department of Neuroscience and Brain Technology, Italian Institute of Technology, Genova, Italy	
3 Nanomedicine, Centre Suisse d'Electronique et de Microtecqnique, Landquart (Switzerland)	
Frame work for Comparing Spike Detection Algorithms for Real-Time Applications	179
<i>Pini Tandaitnik , Hugo Guterman</i>	
Ben-Gurion University, Beer-Sheva, Israel	
Signal and Noise Analysis of Low S/N Data Recorded from MEA	181
<i>V. Gautam and K.S. Narayan</i>	
Molecular Electronics Laboratory, Jawaharlal Nehru Centre for Advanced Scientific Research, Jakkur P.O., Bangalore, India.	
Where are the barrels? A signal based approach	183
<i>Rembrandt Bakker, Martijn Selten, Rolf Kötter, Dirk Schubert</i>	
Donders Institute for Brain and Cognition, University Medical Centre St. Radboud, Nijmegen, Netherlands	
NeuVision: a New Simulation Environment to Model Large-Scale Neuronal Networks Coupled to Micro-Electrode Arrays	185
<i>Marcello Mulas^{1,2}, Paolo Massobrio¹, and Sergio Martinoia^{1,2}</i>	
1 Neuroengineering and Bio-nanoTechnology Group, Department of Biophysical and Electronic Engineering (DIBE), University of Genova, Genova (Italy)	
2 Neuroscience and Brain Technology Department, Italian Institute of Technology, Genova, (Italy)	
Assessment of functionality modulation of in-vitro networks using an intra network burst correlation algorithm	187
<i>E. Biffi¹, A. Menegon², G. Regalia¹, S. Maida², A. Pedrocchi¹, G. Ferrigno¹</i>	
1 Politecnico di Milano, Bioengineering Department, Neuroengineering and Medical Robotics Laboratory, p.zza Leonardo da Vinci 32, 20133 Milano, Italy	
2 R&D Laboratory, Alembic, San Raffaele Scientific Institute, via Olgettina 60, 20132 Milano, Italy	
On The Statistics Of Biological Noise And Instrumentation Noise in Active and Inactive Cultures	189
<i>J.B. Destro-Filho¹, Sergio Martinoia²</i>	
1 School of Electrical Engineering, Federal University of Uberlandia, Brazil.	
2 Department of Biophysical and Electrical Engineering (DIBE), University of Genoa (UniGe), Genoa, Italy	
Exploring Granger Causality As A Tool For Understanding Connectivity In Patterned Networks	191
<i>Sankaraleengam Alagapan, Liangbin Pan, Eric Franca, Bruce Wheeler, Thomas Demarse</i>	
J. Crayton Pruitt Family Department of Biomedical Engineering, University of Florida, Gainesville, FL, USA	
Functional Connectivity Maps In Hippocampal Cultures Coupled To High Resolutions MEAs Underlie Structural Connectivity	193
<i>Alessandro Maccione¹, Matteo Garofalo¹, Thierry Nieus¹, Maria Teresa Tedesco², Enrico Commisso², Sergio Martinoia^{1,2} and Luca Berdondini¹</i>	
1 Neuroscience and Brain Technology Department, Italian Institute of Technology, Genova – Italy	
2 Neuroengineering and Bio-nano Technology Group (NBT), Department of Biophysical and Electronic Engineering (DIBE), University of Genova, Genova – Italy	
Investigating neuronal activity by SPYCODE data analyzer	195
<i>Luca Leonardo Bologna¹, Valentina Pasquale¹, Matteo Garofalo¹, Mauro Gandolfo², Pieter Laurens Baljon², Alessandro Maccione¹, Sergio Martinoia^{2,1}, and Michela Chiappalone¹</i>	
1 Department of Neuroscience and Brain Technology, Italian Institute of Technologies, Genova (Italy)	
2 Department of Biophysical and Electronic Engineering, University of Genova, Genova (Italy)	
Adaptive algorithms for burst and network burst detection	197
<i>Valentina Pasquale¹, Sergio Martinoia^{2,1} and Michela Chiappalone¹</i>	
1 Department of Neuroscience and Brain Technologies, Italian Institute of Technology, Genova (Italy)	
2 Department of Biophysical and Electronic Engineering, University of Genova, Genova (Italy)	

Simple Model of a Neuronal Network Reproducing Synchronous Bursts	199
---	-----

Masaki Nomura^{1,2}, Daisuke Ito³, Kazutoshi Gohara³, Toshio Aoyagi^{2,4}

1 Department of Mathematics, Kyoto University, Kyoto (Japan)

2 JST, CREST, Tokyo (Japan)

3 Division of Applied Physics, Hokkaido University, Sapporo (Japan)

4 Department of Applied Analysis and Complex Dynamical Systems, Kyoto University, Kyoto (Japan)

Online Spike Extraction for Bidirectional High-Density Microelectrode Arrays using Optimal Filters	201
--	-----

David Jäckel¹, Urs Frey², Jan Müller¹, Ian Jones¹, Muhammad Usman Khalid¹, Jan Sedivy³, Andreas Hierlemann¹

1 ETH Zurich, Department Biosystems Science and Engineering, 4058 Basel, Switzerland.

2 Bio ETH Zurich, Department Biosystems Science and Engineering, 4058 Basel, Switzerland.now at IBM Research, Zurich, Switzerland.

3 Department of Measurement, Czech Technical University, Prague, Czech Republic.

A Comprehensive and Efficient Python-based Framework for the Processing of Spiking Activity Data in MEA recordings	203
--	-----

Maffezzoli Andrea, Wanke Enzo

Department of Biotechnologies and Biosciences, University of Milano-Bicocca, Milan (Italy)

Epileptiform Firing Characteristics in Hippocampal Slices	205
---	-----

Zhang Pu-Ming¹, Gong Xin-Wei¹, Yang Fan², Liu Jian-Sheng², Lu Qin-Chi², Gong Hai-Qing¹, Liang Pei-Ji¹

1 School of Life Sciences and Biotechnology, Shanghai Jiao Tong University, Shanghai, China

2 School of Medicine, Shanghai Jiao Tong University, Shanghai, China

Unfolding the Properties of Biological Neural Networks with Multidimensional Reduction Techniques and Graph Theory	207
--	-----

Carrillo-Reid Luis, Garcia-Munoz Marianela, Arbuthnott Gordon

Okinawa Institute of Science and Technology, Okinawa, Japan

Electrical Stimulation, Implants, and Robotics _____ **209**

Subretinal electrical stimulation of isolated RCS rat retina with pulse trains and paired pulses	210
--	-----

Thoralf Herrmann, Alfred Stett

NMI Natural and Medical Sciences Institute at the University of Tübingen, Reutlingen, (Germany)

Real-time Characterization of Neuronal Response for Selective Stimulation	212
---	-----

Michelle L. Kuykendal¹, Gareth S. Givanasen¹, Martha A. Grover², Steve M. Potter¹, Stephen P. DeWeerth¹

1 Laboratory for Neuroengineering, Coulter Department of Biomedical Engineering, Georgia Institute of Technology, Atlanta, Georgia, USA

2 School of Chemical & Biomolecular Engineering, Georgia Institute of Technology, Atlanta, Georgia, USA

Voltage-controlled Stimulation Pulses May Be Lethal	214
---	-----

Jonathan C. Erickson

Washington and Lee University, Department of Physics-Engineering, Lexington, VA, USA

Wireless Stimulation of MEAs Inside the Incubator	216
---	-----

Chinmay Joag, Bruce Wheeler, Thomas DeMarse

J. Crayton Pruitt Department of Biomedical Engineering, University of Florida, Gainesville, FL, USA

Ex ovo culture: An <i>in vivo</i> model for microsensor implants	218
--	-----

Massimo Kubon¹, Meike Moschallski¹, Gorden Link¹, Simon Werner¹, Claus Burkhardt¹, Wilfried Nisch¹,

Beate Scholz¹, Burkhard Schlosshauer¹, Gerald Urban² and Martin Stelzle¹

1 NMI Natural and Medical Science Institute at the University of Tuebingen, Reutlingen, Germany

2 University of Freiburg, IMTEK, Laboratory of Sensors, Freiburg, Germany

Electric Stimulation Of Explanted Retina Using A Subretinal Implant Chip In A Video Projector Setup	220
---	-----

Andreas Padberg^{1,2}, Steffen Kibbel³, Thoralf Herrmann¹, Ulrich Egert², Alfred Stett¹

1 NMI Natural and Medical Sciences Institute at the University of Tuebingen, Reutlingen, (Germany)

2 IMTEK, Biomicrotechnology, Albert-Ludwigs-Universität Freiburg, Freiburg, (Germany)

3 Retina Implant AG, Reutlingen, (Germany)

Epiretinal stimulation of retina with CMOS Multi-Capacitor-Array	222
<i>Max Eickenscheid¹, Günther Zeck², Peter Fromherz¹</i>	
1 Max Planck Institute for Biochemistry, Department of Membrane and Neurophysics, Martinsried, Germany	
2 NMI Natural and Medical Science Institute, Reutlingen, Germany	
Tetanzation Dynamics in Human Neuroblastoma Cultures	223
<i>Ferrández J. M.^{1,2}, Lorente V.², Bongard M.^{1,3}, Díaz G.^{1,3}, delaPaz F.⁴, Fernández E.^{1,3}</i>	
1 Instituto de Bioingeniería, Universidad Miguel Hernández, Alicante	
2 Dpto. Electrónica, Tecnología de Computadoras, Univ. Politécnica de Cartagena,	
3 CIBER-BBN, Spain	
4 Departamento de Inteligencia Artificial, UNED, Spain	
A Closed-Loop System for Robotic Control using Human Neuroblastoma Cultures	225
<i>Ferrández J. M.^{1,2}, Lorente V.², Bongard M.^{1,3}, Díaz G.^{1,3}, delaPaz F.⁴, Fernández E.^{1,3}</i>	
1 Instituto de Bioingeniería, Universidad Miguel Hernández, Alicante	
2 Dpto. Electrónica, Tecnología de Computadoras, Univ. Politécnica de Cartagena,	
3 CIBER-BBN, Spain	
4 Departamento de Inteligencia Artificial, UNED, Spain	
Chronic Network Stimulation Enhances Evoked Action Potentials	227
<i>A. N. Ide¹, A. Andruska¹, M. Boehler¹, B. C. Wheeler³, G. J. Brewer^{1,2}</i>	
1 Department of Medical Microbiology, Immunology and Cell Biology, Southern Illinois University, School of Medicine, Springfield, IL 62794-9626, USA.	
2 Department of Neurology, Pharmacology, Southern Illinois University, School of Medicine, Springfield, IL 62794-9626, USA.	
3 J. Crayton Pruitt Family Department of Biomedical Engineering, University of Florida, Gainesville, FL 32611-6131, USA.	
Highly Stretchable PDMS-Based Multi-Electrode Array For Epidural Electrical Stimulation To Regain Motor Function After Spinal Cord Injury	229
<i>Alexandre Larmagnac^{1,2}, Pavel Musienko², Janos Vörös¹, Grégoire Courtine²</i>	
1 Laboratory of Biosensors and Bioelectronics, ETH Zurich, Switzerland	
2 Experimental Neurorehabilitation Laboratory, Department of Neurology, University of Zurich, Switzerland	
Neuro-Robot Vitroid, with simple coupling approach	231
<i>Suguru N. Kudoh, Naohiko Fujiwara, Hidekatsu Ito, Minori Tokuda and Ai Kiyohara</i>	
Department of Human System Interaction, School of Science and Technology, Kwansai Gakuin University, Sanda, Hyougo, Japan	
Electrodes, Surfaces and Setups	233
Bidirectional interfacing of carbon nanotube substrates to neuronal networks	234
<i>Luca Gambazzi¹, Francesca Maria Toma², Alan Le Goff^{2,3}, Kai Fuchsberger³, Sara Cipollone², Martin Stelzle³, Maurizio Prato², Henry Markram¹ and Michele Giugliano^{1,4}</i>	
1 Lab. of Neural Microcircuitry, Brain Mind Institute, EPFL, CH-1005 Lausanne, Switzerland	
2 Dept. Pharmaceutical Sciences, Univ. Trieste, P.le Europa 1, I-34127 Trieste (Italy)	
3 Naturwissenschaftliches und Medizinisches Institut, Reutlingen (Germany)	
4 Dept. Biomedical Sciences, Univ. Antwerp, Universiteitsplein 2, B-2610 Wilrijk (Belgium)	
Self-aligned growth and modification of neuronal network through electrically dynamic surfaces	236
<i>Jinwon Kim¹, Sungeun Lee¹, Yoonkey Nam², Sung June Kim¹</i>	
1 School of Electrical Engineering, Seoul National University, Seoul, Republic of Korea	
2 Department of Bio and Brain Engineering, Korea Advanced Institute of Science and Technology, Daejeon, Republic of Korea	
Miniaturized multi-well type neural assay platform on MEAs using cell-repulsive agarose hydrogel	239
<i>Yoonkey Nam, Jisoon Lim, Gaurav Goyal, Gyumin Kang</i>	
Department of Bio and Brain Engineering, KAIST, Daejeon, Korea	
Micro Pillar Electrodes on MEAs for Tissue Stimulation	241
<i>Jochen Held, Jens Heynen, Angelika Stumpf, Wilfried Nisch, Claus Burkhardt, Alfred Stett</i>	
NMI Natural and Medical Sciences Institute at the University of Tübingen, Reutlingen (Germany)	

On Microelectrode Impedance Measurements	243
<i>Jarno M. A. Tanskanen¹, Pasi Kauppinen¹, Tomi Ryyänen², Jukka Leikkala², Jari A. K. Hyttinen¹</i>	
1 Department of Biomedical Engineering, Tampere University of Technology, Tampere, Finland	
2 Department of Automation Science and Engineering, Tampere University of Technology, Tampere, Finland	
Scalloped electrodes for brain tissue recordings	245
<i>Patricia Vazquez, Maria Dimaki, Winnie E. Svendsen</i>	
DTU Nanotech, Technical University of Denmark, 2800 Kongens Lyngby, Denmark	
Solid Silver Microneedle Electrode Arrays for Intracellular Recording Applications	247
<i>Jochen Held¹, Joao Gaspar¹, Patrick Ruther¹, Matthias Hagner², Andreas Cismak³, Andreas Heilmann³, and Oliver Paul¹</i>	
1 Department of Microsystems Engineering (IMTEK), University of Freiburg, Freiburg (Germany)	
2 Department of Physics, University of Konstanz, Konstanz (Germany)	
3 Department of Biological Materials and Interfaces, Fraunhofer Institute for Mechanics of Materials Halle, Halle (Germany)	
Biocompatible MWNTs-based MEA for the study emergent activity in the cortical network	249
<i>G. Gabriel^{1,2}, I. Martin¹, A. Guimerà^{1,2}, M. Sánchez-Vives^{3,4}, R. Reig³, X. Palomer³, P. Godignon¹, R. Villa^{1,2}</i>	
1 Instituto de Microelectrónica de Barcelona (IMB-CNM), CSIC, Campus UAB, Barcelona, Spain	
2 CIBER-BBN, Networking Center on Bioengineering, Biomaterials and Nanomedicine.	
3 IDIBAPS (Institute of Biomedical Research August Pi y Sunyer), Barcelona, Spain	
4 ICREA (Institut Català de Recerca i Estudis Avançats), Barcelona, Spain	
Microelectrode cavity arrays (MECA) for parallel and high resolution ion channel recording	251
<i>Gerhard Baaken^{1,2}, Srujan Dondapati¹, Jürgen Rühle^{2,3}, Jan C. Behrends^{1,3}</i>	
1 Laboratory for Electrophysiology and Biotechnology, Department of Physiology, University of Freiburg, Freiburg, Germany	
2 Laboratory for Chemistry and Physics of Interfaces, Department of Microsystems Engineering – IMTEK, University of Freiburg, Freiburg, Germany	
3 Freiburg Materials Research Center (FMF), University of Freiburg, Freiburg, Germany	
In-Vitro Closed Loop Optical Electrophysiology of Networks I: Whole field Illumination Experimental Paradigm	253
<i>Ahmed El Hady^{1,2,3}, Kai Bröking^{1,3}, Oliver Schlüter⁵, Walter Stühmer^{2,3,4}, Fred Wolf^{3,4}</i>	
1 Max Planck Institute for Dynamics and Self Organization, Göttingen, Germany	
2 Max Planck Institute of Experimental Medicine, Göttingen, Germany	
3 Bernstein Focus for Neurotechnology, Göttingen, Germany	
4 Bernstein Center for Computational Neuroscience, Göttingen, Germany	
5 European Neuroscience Institute, Göttingen, Germany	
Effect of electrode dimensions on nerve fiber signal recordings	255
<i>Kiran Kumar Sriperumbudur, Philipp Julian Koester, Werner Baumann, and Jan Gimsa</i>	
University of Rostock, Chair for Biophysics, Gertrudenstrasse 11a, 18057 Rostock, Germany	
Insect neurons coupled to iridium oxide electrodes	257
<i>Katrin Göbbels¹, André van Ooyen², Andreas Offenhäusser³, Uwe Schnakenberg², Peter Bräunig¹</i>	
1 Institute of Biology II, RWTH Aachen University, 52074 Aachen, Germany	
2 Institute of Materials in Electrical Engineering (IWE 1), RWTH Aachen University, 52074 Aachen, Germany	
3 Institute of Bio- and Nanosystems (IBN-2), Forschungszentrum Jülich, 52425 Jülich, Germany	
Spike recordings from ganglion cell populations using a new type of carbon nanotubes surface multielectrodes	259
<i>Markus Bongard^{1,4}, Gemma Gabriel^{1,2}, Rosa Villa^{1,2}, Rodrigo Gomez², Nuria Benito³, Eduardo Fernandez^{1,4}</i>	
1 El Centro de Investigación Biomédica en Red en Bioingeniería, Biomateriales y Nanomedicina (CIBER BBN), Spain	
2 Universitat Autònoma de Barcelona, Centre Nacional de Microelectrònica (CNM-CSIC), Spain	
3 Cajal Institute (CSIC), Spain	
4 Universidad Miguel Hernández, Instituto de Bioingeniería, Spain	
Transparent NCD microelectrode array for spatially resolved detection in micro-areas of single cells	261
<i>E. Colombo^{1,2}, C. Pietzka¹, V. Carabelli², Z. Gao¹, P. Herfurth¹, Y. Men¹, M. Schneider³, E. Carbone², E. Kohn¹, A. Pasquarelli¹</i>	
1 Institute of Electron Devices and Circuits, Ulm University, 89069 Ulm, Germany	
2 Department of Neuroscience, NIS Center, 10125 Torino, Italy	
3 Experimental Anesthesiology Department, Ulm University Hospital, 89075 Ulm, Germany	

Accurate validation of extra-cellular neuronal recordings in culture	263
<i>Nitzan Herzog¹, Mark Shein², Yael Hanein²</i>	
1 Department of Bio-Medical Engineering,	
2 School of Electrical Engineering, Faculty of Engineering, Tel Aviv University, Tel Aviv, Israel.	
Polystyrene coated MEA	265
<i>Tomi Ryyänen¹, Ville Kujala², Laura Ylä-Outinen², Erja Kerkelä², Susanna Narkilahti², Jukka Leikkala¹</i>	
1 Department of Automation Science and Engineering, Tampere University of Technology, Tampere, Finland	
2 Regea – Institute for Regenerative Medicine, University of Tampere and Tampere University Hospital, Tampere, Finland	
Integration of Carbon Nanotubes in Microelectrode Arrays by Microcontact Printing and Electropolymerization for Neurostimulation and Biosensing Applications	267
<i>Kai Fuchsberger¹, Alan Le Goff², Ramona Gerwig¹, Claus Burkhardt¹, Janine Elit¹, Yingjia Li¹, Andreas Scheipers, Alfred Stett¹, Martin Stelzle¹</i>	
1 NMI Natural and Medical Sciences Institute at the University of Tuebingen, Reutlingen, Germany	
2 Department of Pharmaceutical Sciences, University of Trieste, Trieste, Italy	
CNT electrodes for MEAs and neuronal applications	269
<i>B. Stamm¹, K. Schneider², L. Pastewka³, C. Burkhardt¹, W. Nisch¹, M. Häffner², M. Fleischer², M. Moseler³, S. Di Giovanni⁴, D. P. Kern², A. Stett¹</i>	
1 NMI Natural and Medical Sciences Institute at the University of Tübingen, Reutlingen	
2 Institute of Applied Physics, University of Tübingen	
3 Fraunhofer Institute for Mechanics of Materials IWM, Freiburg	
4 Hertie Institute for Clinical Neuroscience, Tübingen	
Microscope Setup For Laser Manipulation And Long-Term Monitoring Of Neuronal Cell Cultures	271
<i>Torben Harbodt¹, Reinhard Galneder¹, Susann Schröder¹, Karl-Heinz Boven², Christian Hembd³, Alfred Stett¹</i>	
1 NMI Natural and Medical Sciences Institute at the University of Tübingen, Reutlingen, Germany	
2 Multi Channel System MCS GmbH, Reutlingen, Germany	
3 TILL Photonics GmbH, Gräfelfing, Germany	
Electrical and Optical Recording of Interactions between Small Neuronal Networks using Needle-Type Microelectrodes	273
<i>Aki Saito, Hiroyuki Moriguchi, Miho Goto, Atsushi Saito, Yuzo Takayama, Kiyoshi Kotani, Yasuhiko Jimbo</i>	
Graduate School of Frontier Sciences, University of Tokyo, 5-1-5 Kashiwanoha, Kashiwa-shi, Chiba 277-8563, Japan	
High-density micro-needles for in vitro neural studies	275
<i>D.E. Gunning¹, P. Hottowy², W. Dabrowski², J. P. Hobbs³, J.M. Beggs³, A. Sher⁴, A.M. Litke⁴, C.J. Kenney⁵, K. Mathieson¹</i>	
1 Department of Physics and Astronomy, University of Glasgow, Glasgow, UK	
2 Faculty of Physics and Applied Computer Science, AGH University of Science and Technology, Krakow, Poland	
3 Biocomplexity Institute, University of Indiana, Bloomington, IN, USA	
4 SCIPP, University of California Santa Cruz, Santa Cruz, CA, USA	
5 SLAC National Accelerator Laboratory, Menlo Park, CA, USA	
Polymeric Micro Technologies for Flexible Actuator Devices	277
<i>Rakefet Ofek Almog¹, Yelena Sverdllov¹, Tsvi Shmilovich¹, Slava Krylov¹, Aryeh Taub², Yosi Shacham-Diamand¹</i>	
1 Faculty of Engineering, Tel Aviv University, Tel Aviv, Israel	
2 Psychobiology Research Unit, Tel Aviv University, Tel Aviv, Israel	
Mussel-Inspired Polymer Coating for Surface Modification of MEA Applications	279
<i>Kyungtae Kang¹, Min Jee Jang², Insung S. Choi¹, Yoonkey Nam²</i>	
1 Molecular-Level Interface Research Center, Department of Chemistry, KAIST, Daejeon 305-701, Korea	
2 Department of Bio and Brain Engineering, KAIST, Daejeon 305-701, Korea	
All-polymer MEAs: Challenges, Features and Perspectives	281
<i>Axel Blau¹, Angelika Murr², Sandra Wolff³, Jens Wüsten², Francesco Difato¹, Christiane Ziegler³, Fabio Benfenati¹</i>	
1 The Italian Institute of Technology (IIT), Dept. of Neuroscience and Brain Technologies (NBT), Via Morego 30, 16163 Genoa, Italy, www.iit.it	
2 Institut für Mikrotechnik Mainz GmbH (IMM), Carl-Zeiss-Str. 18-20, 55129 Mainz, Germany, www.imm-mainz.de	
3 Nano+Bio Center (NBC) at the University of Kaiserslautern, Erwin-Schrödinger-Str. 13, 67663 Kaiserslautern, Germany, www.nbc.uni-kl.de	

Combining MEA and VSD to study cells in a pattern generator	283
<i>Pieter Laurens Baljon^{1,2}, John Nagarah¹, Daniel A. Wagenaar¹</i>	
1 Broad Fellows Program and Division of Biology, California Institute of Technology, Pasadena CA, United States	
2 Department of Biophysical and Electronic Engineering, University of Genova, Genova, Italy	
Transparent Multisuction Electrode Arrays For Tissue Immobilization And Simultaneous MEA And VSD Measurements	285
<i>John M. Nagarah¹, Pieter Laurens Baljon², Daniel A. Wagenaar¹</i>	
1 Broad Fellows Program, Division of Biology, California Institute of Technology, Pasadena, CA, USA	
2 Experimental Neurophysiology, Vrije Universiteit, Amsterdam, Netherlands	
Conducting Polymer Coated MEAs for Enhanced Signal Recording and Stimulation	287
<i>Vini Gautam and K.S. Narayan</i>	
Molecular Electronics Laboratory, Jawaharlal Nehru Centre for Advanced Scientific Research, Jakkur P.O., Bangalore, India	
Gold Shark Teeth Structures on MEAs - Electroplating of Nano-Structures on Metallic Microelectrodes	289
<i>Philipp Julian Koester¹, Carsten Tautorat¹, Tom Reimer¹, Michael Zwanzig², Werner Baumann¹, and Jan Gimsa¹</i>	
1 University of Rostock, Chair for Biophysics, Gertrudenstrasse 11a, 18057 Rostock, Germany.	
2 Fraunhofer Institute for Reliability and Microintegration (IZM), Gustav-Meyer-Allee 25, 13355 Berlin	
GO-Bio 3: PoreGenic [®] - 1. Whole-Cell Patch Clamp Recordings with a 3D-MEA chip	291
<i>Philipp Julian Koester¹, Carsten Tautorat¹, Jochen Held², Patrick Ruther², João Gaspar², Oliver Paul², Helmut Beikirch³, Jan Gimsa¹, and Werner Baumann¹</i>	
1 University of Rostock, Chair for Biophysics, Gertrudenstrasse 11a, 18057 Rostock, Germany.	
2 University of Freiburg, Department of Microsystems Engineering (IMTEK), Georges-Köhler-Allee 103, 79110 Freiburg, Germany	
3 University of Rostock, Faculty of Computer Science and Electrical Engineering, Institute of Electronic Appliances and Circuits, Albert-Einstein-Strasse 2, 18059 Rostock, Germany	
GO-Bio 3: PoreGenic [®] - 2. Cardiomyocyte Action Potential Recordings with a 3D-MEA chip	293
<i>Philipp Julian Koester¹, Carsten Tautorat¹, Jochen Held², Patrick Ruther², João Gaspar², Oliver Paul², Helmut Beikirch³, Jan Gimsa¹, and Werner Baumann¹</i>	
1 University of Rostock, Chair for Biophysics, Gertrudenstrasse 11a, 18057 Rostock, Germany.	
2 University of Freiburg, Department of Microsystems Engineering (IMTEK), Georges-Köhler-Allee 103, 79110 Freiburg, Germany	
3 University of Rostock, Faculty of Computer Science and Electrical Engineering, Institute of Electronic Appliances and Circuits, Albert-Einstein-Strasse 2, 18059 Rostock, Germany	
High-Resolution Amperometric Spikes From Chromaffin Cells Revealed By Boron-Doped Nanocrystalline Diamond Microelectrode Arrays	295
<i>Sara Gosso¹, Andrea Marcantoni¹, Yanlin Xu², Elisabetta Colombo^{1,2}, Zi-yao Gao², Erhard Kohn², Alberto Pasquarelli², Emilio Carbone¹, Valentina Carabelli¹</i>	
1 Department of Neuroscience, NIS Center, 10125 Torino, Italy	
2 Institute of Electron Devices and Circuits, Ulm University, 89069 Ulm, Germany	
Cell-a-V, a novel multi-well MEA for multi brainstructures research	297
<i>Taub Aryeh¹, Rabner Arthur², Shacham-Diamand Yosi²</i>	
1 Psychobiology Research Unity, Department of Psychology, Tel Aviv University, Tel Aviv, Israel	
2 Faculty of Engineering, Tel Aviv University, Tel Aviv, Israel	
Culture Techniques	299
NbActiv4 medium improvement to Neurobasal/B27 increases network activity which scales exponentially with synapse density	300
<i>Gregory J. Brewer¹, Torrie T. Jones¹, Michael D. Boehler¹, R A Pearson¹, A A DeMaris¹, A N Ide¹, Bruce C. Wheeler²</i>	
1 Southern Illinois University School of Medicine, Springfield, IL USA	
2 University of Florida, Gainesville, FL USA	
Towards in-vitro neuronal network models: In-vitro dual compartment neurofluidic system and functional connectivity in physically isolated neuronal cell culture	303
<i>Kanagasabapathi Thirukumaran T. , Ciliberti Davide and Decré Michel M.J.</i>	
Minimally Invasive Healthcare Department, Philips Research Laboratories Eindhoven, High Tech Campus 34(23), 5656 AE Eindhoven, The Netherlands	

Oscillatory activity in murine Langerhans islets	305
<i>Udo Kraushaar¹, Martina Düfer², Gisela Drews², Elke Guenther¹ and Peter Krippel-Drews²</i>	
1 Dept. of Electrophysiology, NMI Reutlingen, Germany	
2 Department of Pharmacology, University of Tübingen, Tübingen, Germany	
PDMS Microtunnels for MEA Recordings: Improvements in Mold Fabrication and Compatibility with Conventional MEAs	307
<i>Liangbin Pan¹, Gregory J. Brewer^{2,3}, Bruce C. Wheeler¹</i>	
1 J. Crayton Pruitt Family Department of Biomedical Engineering, University of Florida, Gainesville, USA	
2 Department of Medical Microbiology, Immunology and Cell Biology, Southern Illinois University, School of Medicine, Springfield, USA	
3 Department of Neurology, Southern Illinois University, School of Medicine, Springfield, USA	
Recordings of electrical activity in neuronal network patterned on MEA using Micropipette drawing method	309
<i>Miho Goto, Hiroyuki Moriguchi, Yuzo Takayama, Aki Saito, Kiyoshi Kotani, Yasuhiko Jimbo</i>	
Graduate School of Frontier Sciences, University of Tokyo	
Collective Activation in Clustered Neuronal Assemblies of Variable Size and Topology	310
<i>Mark Shein Idelson¹, Eshel Ben-Jacob² and Yael Hanein¹</i>	
1 School of Electrical Engineering, Tel-Aviv University, Tel-Aviv 69978, Israel	
2 School of physics and astronomy, Tel-Aviv University, Tel-Aviv 69978, Israel	
A Multielectrode Array Analysis of the Snail Brain	312
<i>Christopher A. Harris, Peter A. Passaro, Ildikó Kemenes, György Kemenes, Michael O'Shea</i>	
School of Life Sciences, University of Sussex, Brighton, United Kingdom	
Using Three-Dimensional Cell Culture Systems On Microelectrode Arrays For Biosensing Applications	314
<i>Andreas W. Daus¹, Michael Goldhammer² and Christiane Thielemann¹</i>	
1 University of Applied Sciences Aschaffenburg, BioMEMS and Bioelectronics Laboratory, Aschaffenburg, Germany	
2 University of Applied Sciences Aschaffenburg, Laboratory for EMC, Aschaffenburg, Germany	
Engineering the micro electrode environment with microfluidics: A new approach for cell culture patterning or controlled chemical stimulation	316
<i>Anja Kunze¹, Marc Heuschke², Michele Giugliano³ and Philippe Renaud¹</i>	
1 Laboratory Microsystems 4, Ecole Polytechnique Fédérale de Lausanne, Switzerland	
2 Ayanda Biosystems SA, Lausanne, Switzerland	
3 Dept. of Biomedical Sciences, University of Antwerp, Belgium	
Three Dimensional Recording from Neural Network Encapsulated in Hydrogel Constructs	318
<i>Lee Wonhee¹, Kim Euitae¹, Hynd R Mathew², Kim Sung June¹</i>	
1 School of Electrical Engineering and Computer Science, College of Engineering, Seoul National University, Seoul, Republic of Korea	
2 College of Nanoscale Science and Engineering, State University of New York, Albany, New York, USA	
Creating Unidirectional Neural Networks on a Chip	320
<i>Bradley J. Dworak¹, Kucku Varghese¹, Liangbin Pan¹, Gregory J. Brewer², and Bruce C. Wheeler¹</i>	
1 J. Crayton Pruitt Family Department of Biomedical Engineering, University of Florida, Gainesville, Florida, USA	
2 Departments of Neurology and Medical Microbiology Immunology and Cell Biology, Southern Illinois University, Springfield, Illinois, USA	

Active Arrays and Electronics **323**

Novel Neuronal Cellular and Network Measurements Enabled by a High-Density 11,011-Microelectrode CMOS Array	324
<i>Douglas J Bakkum^{1,2}, Urs Frey^{1,3}, Jan Mueller¹, Michele Fiscella¹, Hirokazu Takahashi², Andreas Hierlemann¹</i>	
1 ETH Zurich, Department of Biosystems Science and Engineering (D-BSSE), Basel, Switzerland	
2 Research Center for Advanced Science and Technology (RCAST), The University of Tokyo, Japan	
3 Now at IBM Research, Zurich, Switzerland	

512-electrode MEA System For Spatio-Temporal Distributed Stimulation and Recording of Neural Activity	327
<i>Pawel Hottowy^{1,2}, John M. Beggs³, E. J. Chichilnisky⁴, Wladyslaw Dąbrowski¹, Tomasz Fiutowski¹, Deborah E. Gunning⁵, Jon Hobbs³, Lauren Jepson⁴, Sergei Kachiguine², Keith Mathieson³, Przemysław Rydygier¹, Alexander Sher², Andrzej Skoczeń¹, Alan M. Litke²</i>	
1 Faculty of Physics and Applied Computer Science, AGH University of Science and Technology, Kraków, Poland	
2 Santa Cruz Institute for Particle Physics, University of California, Santa Cruz, USA	
3 Biocomplexity Institute, University of Indiana, Bloomington, USA	
4 Salk Institute for Biological Studies, La Jolla, USA	
5 Department of Physics and Astronomy, University of Glasgow, Glasgow, UK	
Bidirectional Interfacing of Neurons with a 32k Pixel CMOS Multi-Capacitor-Transistor-Array (MCTA)	331
<i>Thomas Gerling¹, Armin Lambacher¹, Björn Eversmann², Roland Thewes², Peter Fromherz¹</i>	
1 Department of Membrane and Neurophysics, Max Planck Institute for Biochemistry, Martinsried/Munich, Germany	
2 Corporate Research, Infineon Technologies AG, Munich, Germany	
Investigation of pharmacologically-induced epileptic spatial-temporal patterns on cortico-hippocampal slices by means of high-density microelectrode arrays	332
<i>Ferrea E.^{1,2}, Maccione A.¹, Baldelli P.^{1,2}, Benfenati F.^{1,2}, Berdondini L.¹</i>	
1 Department of Neuroscience and Brain Technologies, The Italian Institute of Technology, Genova, Italy;	
2 Department of Experimental Medicine, University of Genova, Genova, Italy	
MEA Based Multichannel System Employing ASIC for In Vivo and In Vitro Experiments	334
<i>Pawel Gryboś, Piotr Kmon, Robert Szczygiel, Mirosław Żołądz, Maciej Kachel</i>	
Department of Measurement and Instrumentation, AGH University of Science and Technology, Cracow, Poland	
Delta Compression of Neural Recordings for Highdensity CMOS-based Microelectrode Arrays	336
<i>Neil Joye, Michelangelo Carrozzo, Alexandre Schmid, Yusuf Leblebici</i>	
Microelectronic Systems Laboratory (LSM), Ecole Polytechnique Fédérale de Lausanne (EPFL), Lausanne, Switzerland	
AM Modulation-based CMOS Readout Circuit for High-density Microelectrode Arrays	338
<i>Neil Joye, Alexandre Schmid, Yusuf Leblebici</i>	
Microelectronic Systems Laboratory (LSM), Ecole Polytechnique Fédérale de Lausanne (EPFL), Lausanne, Switzerland	
Voltage and Current Stimulation Buffer for High-Density Microelectrode Arrays	340
<i>Paolo Livi¹, Flavio Heer¹, Urs Frey², Douglas J. Bakkum^{1,3}, Andreas Hierlemann¹</i>	
1 ETH Zurich, Bio Engineering Laboratory, Department of Biosystems Science and Engineering, Switzerland	
2 ETH Zurich, Bio Engineering Laboratory, Department of Biosystems Science and Engineering; now at IBM Research, Zurich, Switzerland	
3 Graduate School of Information Science and Technology, The University of Tokyo, Japan	
NeuroFETs: Field Effect Nano-Transistors Fabrication for Neural Recording	342
<i>Llibertat Abad^{1,2}, Matthieu Petit², Ghislain Bugnicourt^{2,3}, Thierry Crozes², Thierry Fournier² and Catherine Villard²</i>	
1 Fondation Nanosciences, 23 rue des Martyrs, F-38000 Grenoble.	
2 Institut Néel, CNRS / UJF - BP 166, F-38042 Grenoble cedex 9.	
3 INSERM U-836, Institut des Neurosciences Grenoble (GIN), Universit Joseph Fourier UMR-S 836, Grenoble, F-38042	
Plant Cells	345
Detecting Electrical Network Activity in Root Apex of <i>Zea mays</i> (L.) by Multielectrode Arrays (MEAs) [§]	346
<i>Masi Elisa, Mancuso Stefano</i>	
Laboratorio Internazionale di Neurobiologia Vegetale (LINV) – Department of Plant, Soil and Environmental Science, University of Florence, Italy	
List of Authors	351

Plant Cells

Detecting Electrical Network Activity in Root Apex of *Zea mays* (L.) by Multielectrode Arrays (MEAs)[§]

Masi Elisa^{1*}, Mancuso Stefano¹

¹ Laboratorio Internazionale di Neurobiologia Vegetale (LINV) – Department of Plant, Soil and Environmental Science, University of Florence, Italy

* Corresponding author. E-mail address: elisa.masi@unifi.it

The study of electrical network systems, integrated with chemical signalling networks, is a common trend in contemporary biology of electrically excitable cells of many multicellular organisms. At present, in plants, despite most cells are electrically excitable and active, full characteristics of the electrical network distribution and dynamics has not been established. Here, a 60-channels multielectrode array (MEA) is applied to study spatiotemporal characteristics of the electrical network activity of the root apex. Both intense spontaneous electrical activities and locally propagating electrical signals have been observed. Propagation of the spikes indicates the existence of excitable travelling waves in plants, similar to those observed in non-nerve electrogenic tissues of animals. Obtained data reveal synchronous electric activities of root cells emerging in a specific root apex region. The dynamic electrochemical activity of root apex cells is proposed to continuously integrate internal and external signalling for developmental adaptations in a changing environment.

1 Introduction

Electrically excitable cells are present in many multicellular organisms, especially in brains of animals, but also in lower animals such as sponges, which lack central nervous system and in animals having excitable epithelia, which can conduct signals via neuroid conduction. In plants, most cells are electrically excitable and active, releasing and propagating action potentials (APs), which may affect such central physiological processes as photosynthesis and respiration [1].

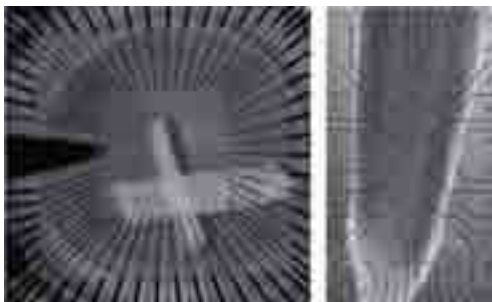


Fig. 1. Root apex longitudinal slice plated on a MEA array.

The first report describing electrical signals in plants was published over 200 years ago [2, 3, 4, 5] on carnivorous plants. Since then, many researchers have made detailed analyses of the electrical activity of single cells by using microelectrodes for intracellular recordings. However, such techniques cannot address integrated issues of how large assembly of cells can combine information both spatially and temporally.

This can be possible using the MEA approach, intensively used in neuroscience for any electrogenic animal tissues, and, here presented as its first application, also for plants tissues.

2 Materials and Methods

2.1 Plant material and MEA setup

Caryopses of *Zea mays* L. were soaked in distilled water and placed between damp paper towels in Petri dishes. Dishes were maintained in vertical position, incubated at 26 °C for 48 h, and used after roots reached a length of \approx 3 cm (usually after 2 days).

Longitudinal and transversal slices from the primary root tip were cut at 350 μ m thickness with a tissue slicer (Mod. 51425, Stoelting, Illinois, USA) and were stored submerged for 2 h in CaCl₂ 5 mM (pH 6.5) at room temperature (22 °C) before recording.

For recording, samples were plated on a multielectrode array (previously coated with nitrocellulose), consisting of 60 TiN/SiN microelectrodes (30 μ m \varnothing). We used MEAs arranged in a 8x8 matrix for transversal slices (200 μ m IED) and 6x10 matrix for longitudinal ones (500 μ m IED) (Multi Channel Systems[®] MCS, Reutlingen, Germany).

To achieve the best contact slices were fixed onto the MEA using an adhesive water permeable and water resistant tape (3M Micropore Surgical Tape)

[§] The results of the experiments here reported have been published on Masi et al. (2009). *PNAS* 106, 4048-4053.

that mediate close and flat adhesion of the slice to the MEA surface, allowing in the meantime superfusion of the tissue (Fig. 1).

Recordings were performed with tissues submerged in bath solution containing CaCl_2 5 mM (pH 6.5) at a flow rate of $1 \text{ mL}\cdot\text{min}^{-1}$ and temperature of $22 \pm 1 \text{ }^\circ\text{C}$.

2.2 Pharmacology

Spontaneous activity was monitored by bath perfusion with L-glutamate (Glu) and the glutamate receptor antagonist 6,7-Dinitroquinoxaline-2,4-dione (DNQX, 2.5 mM, pH 6.7, 2 h incubation) dissolved in 2.5% DMSO or the Ca^{2+} channel blocker gadolinium chloride (Gd^{3+} , 1 mM, 2 h incubation).

Glu was obtained from VWR, Gd^{3+} from Merck Pty Limited, CaCl_2 from JT Baker Chemical Co., all of the other chemicals were obtained from Sigma chemicals. Each solution was adjusted to pH 6.5 and used, without root sample, as negative control to check electrodes signal-to-noise ratio.

2.3 Data acquisition and analysis

Data were acquired with a MEA1060BC (Multi Channel Systems) at a sampling rate of 20 KHz. Dedicated software such as MC Rack (Multi Channel Systems) was used to control the hardware and record simultaneously field potentials from the 60 electrodes and to perform spike detection (achieved by setting the threshold at $-30 \mu\text{V}$, ≈ 5 times the basal noise). Further analysis such as spike coincidence analysis and rate were performed using custom built MatLab programs.

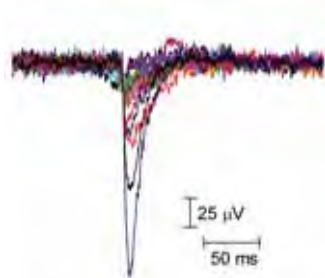


Fig. 2. Recordings of spontaneous spikes. Fifteen traces are superimposed to illustrate the typical shape and size. The signals are aligned at their maximum negative deflections. Data were digitized at 20 KHz.

3 Results

2.1 General characteristics of spontaneous activity

Spikes amplitude, whose shape remind to that recorded in animal cells, varies from 30 to 400 μV , with the duration of about 36-40 ms (Fig. 2).

Amplitude depends very much on the distance of the electrodes from the site of generation of the signal thus the data recorded must be regarded more for their

time characteristics (time of appearance) than for the absolute value of the amplitude.

It is also worth noting that, because of noise, the duration seems to be smaller for the spikes of small amplitude; in fact, in that case the tail can be confused with the noise of the signal. In particular, the duration of the spikes turned out to be proportional to their amplitude (Fig. 3). This linear dependence suggests that the electrical events have a fixed temporal duration determined by the physiological features of the cell membrane.

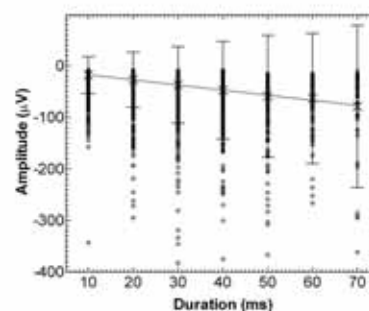


Fig. 3. Amplitude plotted against duration of action potentials. Black points, amplitude and duration for each spike; X, average values \pm SD; dotted line, linear fit for averaged values.

2.2 Effect of calcium and glutamate

As expected, the presence of calcium in the medium is critical for the quality of the signal. In fact, increasing external calcium concentration from 3 to 5 mM caused a significant ($P < 0.01$) increase in the rate of appearance of the spikes. The results are summarized in Table 1.

Table 1. Spike rate and amplitude in the root apex of maize in response to different pharmacological treatments (results reported as means \pm SD, $n = 15$)

	Rate (Spikes min^{-1})	Amplitude (μV)
CaCl_2 3 mM	3.0 ± 0.4	-51.50 ± 5.2
CaCl_2 5 mM	4.41 ± 0.7	-54.8 ± 6.3
Gd^{3+}	0.2 ± 0.07	-66.7 ± 7.2
Gd^{3+} recovery	3.6 ± 0.5	-97.7 ± 11.2
Glu 0.5 mM	9.32 ± 0.4	-53.1 ± 6.0
Glu 1 mM	26.96 ± 1.9	-102.7 ± 12.3
Glu 2 mM	31.32 ± 2.1	-61.3 ± 7.8
DNQX	0.13 ± 0.05	-41.7 ± 5.2
DNQX recovery	3.12 ± 0.3	-46.9 ± 5.0

Spikes were almost totally inhibited, at any external Ca^{2+} concentration, by incubating the root for 2 h in presence of 1 mM gadolinium (Fig. 4A and B). The detection of signals after overnight recovery of the root (the root was gently stirred in working solution) revealed a restoration of the electrical network activity (Fig. 4C).

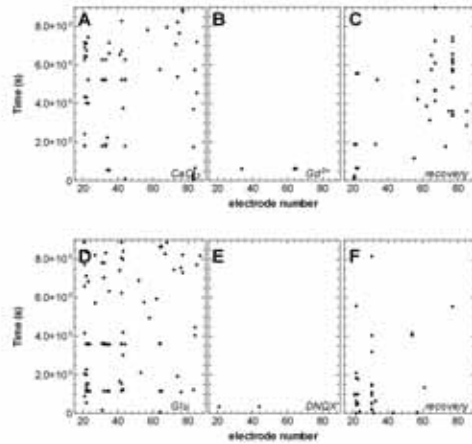


Fig. 4. Representative raster plots of spontaneous activity recorded from 60 electrodes (linear order) in maize root under the following conditions: (A) CaCl_2 5mM; (B) CaCl_2 plus Gd^{3+} 1 mM; (C) restored electrical activity after washing out of Gd^{3+} and overnight recovery; (D) Glu 1 mM plus CaCl_2 5 mM; (E) Glu 1 mM plus CaCl_2 5 mM plus DNQX 2.5 mM; (F) restored electrical activity after washing out of DNQX and overnight recovery.

Application of 0.5 mM L-glutamate to a solution containing 5 mM CaCl_2 enhanced significantly ($P < 0.001$) the rate of appearance of the spikes from 4.4 ± 0.7 to 9.3 ± 0.4 $\text{s} \cdot \text{min}^{-1}$; the effect at higher glutamate concentrations (1 and 2 mM) was even more marked as the rates increased to 26.7 ± 1.9 and 31.3 ± 2.1 $\text{s} \cdot \text{min}^{-1}$, respectively (Table 1). In all of the tested roots, the L-glutamate-evoked increase in activity was significantly ($P < 0.001$) attenuated to 0.13 ± 0.07 spikes per minute (Table 1 and Fig. 6 D and E) by the receptor antagonist DNQX (incubation 2 h; DNQX 2.5 mM). Here, again it was possible to restore the electrical activity of the root after overnight recovery (Fig. 6F).

2.3 Synchronization and propagation of the spikes

In maize root, the cells under study can be considered large with respect to the electrode (diameter of 80-100 μm on average), and homogeneous in morphology [6]. Therefore, by using an IED of 200 or 500 μm , it is reasonable to assume that the electrical signals generated by a single root cell will be detected by just one electrode [7].

The electrical activity in the maize root apex followed a specific pattern of activity with spikes that developed spontaneously on many electrodes at the same time forming periods of synchronized activity, separated by intervals of many seconds of no activity. This appears to be the first observation of synchronized electrical activity in plants.

The calculation of the coincidence probability between spikes trains measured at different groups of electrodes shows the highest peak at $\tau = 0$, evidence of the high amount of synchronized events and that

synchronization is a well-established phenomenon in root cells (Fig. 5).

Interestingly, treating the roots with L-glutamate (1 mM) led to a strong increase in the number of synchronized events compared with those recorded in the standard solution containing just CaCl_2 (Fig. 5)

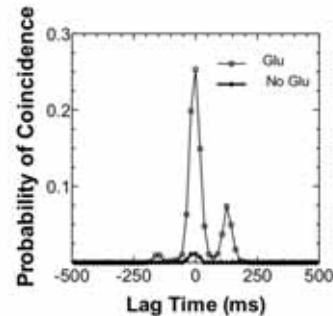


Fig. 5. Distribution of the coincidence probabilities measured between spikes trains obtained from couples of electrodes. The x axis represents the temporal shift $\tau \pm n\Delta t$ where the bin t is 18 ms, smaller than the average spike duration of ≈ 40 ms, larger than the propagation time (1.3 ± 1.2 ms).

Looking at the many synchronized events that have been recorded, they reveal to be composed of a quite complex spatiotemporal pattern where the electrical signals did not appear on all electrodes at exactly the same time (Fig. 6 Middle); the propagation of the spikes (Fig. 6 Bottom) indicates the existence of excitable traveling waves in plants, similar to those observed in non-nerve electrogenic tissues of animals.

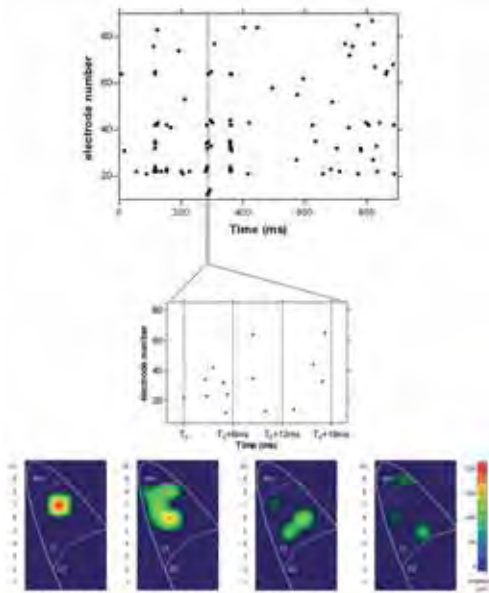


Fig. 6. Activity within synchronized periods. Raster plot of spontaneous activity (Top) shows correlated periods containing spatiotemporal patterns (Middle). A high-temporal-resolution map of the spatial propagation of a single impulse generated at the time 0 is shown (Bottom). A wide spread of the signal is evident.

2.4 Localization of activity in the root apex

The MEA approach for the study of electrical activity in the root apex have provided data from a quite large area of it, including meristem, transition

zone, and mature zone (Fig. 7). In each experiment performed, whatever the nature of the treatment, the most active root part was revealed to be the transition zone. This region, showed a higher electrical activity than the neighboring root apex zones (Fig. 8) and a higher collective activity of groups of cells, i.e., synchronization (data not shown).

3 Conclusion

Electrical events in plants are normally associated with an external stimulation [8, 9 10] but in the present study we demonstrate that a great number of spontaneously generated electrical signals exist in cells of the root apex.

Moreover, the generation of spikes showed a well definite model of action with the production of many events developing spontaneously in many electrodes at the same time, forming periods of synchronized activity, followed by periods of inactivity that can last several seconds (Fig. 6 Top). This behavior is well known in cortical structures of animals where is believed to be involved in information transmission and storage and here we hypothesized that it may have the same meaning in plants.

The fact that the electrical activity is mostly observed in the transition zone of the root apex, points to a possible physiological role of synchronized electrical activity in this region. A fine-tuning of the physiological and metabolic process in this very dynamic region could be controlled by such synchronized electrical activity.



Fig. 7. Image of a maize root apex. Meristem, transition zone (TZ) and mature zone (MZ) have been highlighted.

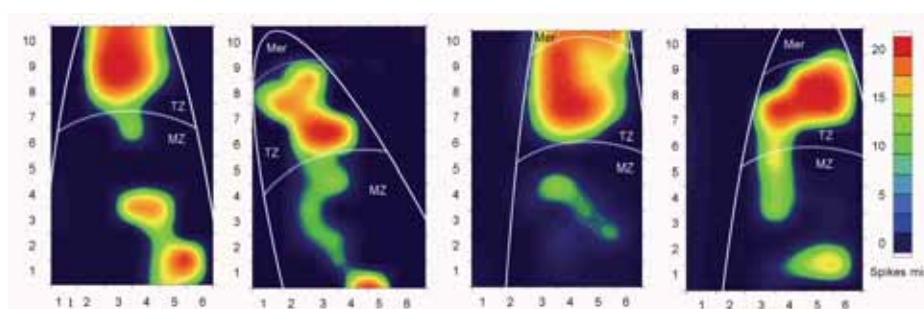


Fig. 8. Representative images of the spatial localization of the electrical activity in root apex of maize. Overall electrical activity measured as rate of appearance (spikes per minute) in 4 different roots/experiments (Mer, meristem; TZ, transition zone; MZ, mature zone).

References

- [1] Fromm J., Lautner S. (2007). Electrical signals and their physiological significance in plants. *Plant Cell Environm* 30, 249–257.
- [2] Bertholon M.L. (1783). De l'Electricité des Végétaux: Ouvrage dans lequel on traite de l'électricité de l'atmosphère sur les plantes, de ses effets sur l'économie des végétaux, de leurs vertus medicaux (P.F. Didotjeune, Paris).
- [3] Burdon-Sanderson J. (1873). Note on the electrical phenomena which accompany stimulation of a leaf of *Dionaea muscipula*. *Proc R Soc London* 21, 495–496.
- [4] Darwin C. (1875). *Insectivorous Plants* (Murray, London).
- [5] Darwin C., assisted by Darwin F. (1880). *Power of Movements in Plants* (Murray, London).
- [6] Baluska F., Kubica S., Hauskrecht M. (1990). Postmitotic "isodiametric" cell growth in the maize root apex. *Planta* 18, 269–274.
- [7] Lin Y., Chen C., Chen L., Zeng S., Luo Q. (2005). The analysis of electrode-recording horizon. *Conf Proc IEEE Eng Med Biol Soc* 7, 7345–7348.
- [8] Fromm J., Lautner S. (2007). Electrical signals and their physiological significance in plants. *Plant Cell Environm* 30, 249–257.
- [9] Felle H., Zimmermann M.R. (2007). Systemic signalling in barley through action potentials. *Planta* 226, 203–214.
- [10] Wildon D.C., et al. (1992). Electrical signalling and systemic proteinase inhibitor induction in the wounded plant. *Nature* 360, 62–65.

Active Arrays and Electronics

Novel Neuronal Cellular and Network Measurements Enabled by a High-Density 11,011-Microelectrode CMOS Array

Douglas J Bakkum^{1,2}, Urs Frey^{1,3}, Jan Mueller¹, Michele Fiscella¹, Hirokazu Takahashi², Andreas Hierlemann¹

¹ ETH Zurich, Department of Biosystems Science and Engineering (D-BSSE), Basel, Switzerland

² Research Center for Advanced Science and Technology (RCAST), The University of Tokyo, Japan

³ Now at IBM Research, Zurich, Switzerland

The brain's unique cognitive abilities are thought to emerge from the processing of information by networks of neurons. Multiunit recording techniques, typically multi-electrode arrays and functional imaging using Ca⁺⁺ or voltage sensitive dyes, have been developed to help understand such network dynamics. However, these techniques are not ideal. Accessible neurons are limited by number and location of electrodes in commercially available 60-electrode arrays, and the imaging techniques either have poor signal-to-noise or low temporal resolution, are subject to phototoxicity and photobleaching within an hour or two, and do not allow for neuronal stimulation. To address these limitations, we grew networks of cortical neurons and glia over a CMOS array with integrated circuitry containing 11,011 electrodes within a 3.4mm² area. The array's high resolution and flexible electrode configurations have allowed us to electronically 'image' network morphology, identify 'cell-assemblies', reconstruct sections of axonal arbors, and resolve the propagation of action potentials across axons. The unprecedented level of neuronal network access has already produced novel data, and further studies are expected to provide a wealth of additional data to advance our basic understanding of the brain's capabilities.

1 Introduction

The brain is arguably the most complex system studied in science. A human brain contains about one hundred billion neurons, each of which communicate electrically and chemically with tens of thousands of other neurons and make up about a quadrillion (10¹⁵) synaptic connections. The patterns and strengths of connections constantly change with experience, and no two brains are alike. The manipulation of action potentials filtering through the connections gives rise to perceptions, interpretation, memories, consciousness, imagination, language, and adaptive behavior. Such manipulations are thought to emerge from the collective activity of ensembles of neurons, but much remains unknown about the fundamental rules governing information processing in the brain. With this in mind, individual neurons have been studied extensively at the cellular and molecular levels. However, mainly due to technological limitations, little is yet known about how the activity of individual neurons can combine to produce behavior, learning, and memory.

Therefore, to investigate the population dynamics and plasticity of neural networks, a state-of-the-art 11,011-electrode complementary metal oxide semiconductor (CMOS) array was developed by the host laboratory (Fig.1) [1,2]. The densely packed electrodes allow 2-way access to *any* neuron grown over the array. Electrodes can both detect signals from

multiple neurons in parallel and electrically evoke new signals, providing a long-term (months) communication between a neural network and a computer. Within a few ms, 126 of the electrodes could be (re)configured into almost any arbitrary pattern to sample network activity (20kHz). Multiple neighboring electrodes could record the activity of an individual soma with signals up to 140 times rms noise. Likewise, any electrode(s) could be arbitrarily connected to a stimulation buffer in order to evoke neural activity, while stimulus artifacts that prevent signal recording were localized within 80µm and about 5ms.

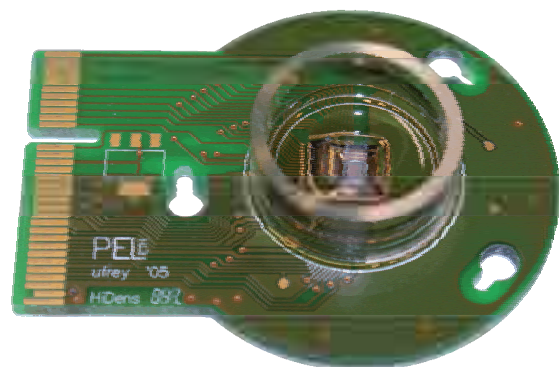


Fig. 1. The CMOS chip. Cells are grown over 11,011 electrodes located at the center of the ring.

2 Methods

2.1 Cell culture

Cells from E18 rat cortices dissociated in trypsin were grown in DMEM with 10% horse serum on top of the CMOS arrays. A thin layer of PEI and a 15 μ L drop of laminin were used for cell adhesion. Experiments were conducted inside an incubator to control environmental conditions.

2.1 CMOS array

The microsystem chip was fabricated in 0.6 μ m CMOS technology, is 7.5x6.1mm² in size, and features 11,011 metal electrodes, as well as 126 bidirectional circuitry channels capable of recording and stimulation. All 7 μ m diameter platinum (Pt) electrodes are placed within a 2.0x1.75mm² area (3,150 electrodes per mm²), and were realized during a 3-mask post-CMOS processing step. Flexibility in the electrode selection (126 can be selected at the same time) is attained through an analog switch matrix integrated underneath the electrode array, consisting of 13k SRAM cells and analog switches that define the routing from the electrodes to the amplifiers of the channel units. The SRAM cells store information about the traversed switches between connected electrodes and readout/stimulation channels. Dedicated algorithms optimize the routing for a defined configuration. See [1,2] for more details.

2.1 Electrical Stimulation and Recording

Electrically evoked activity was induced using biphasic voltage pulses between 100 to 400 μ s

duration and +/-0.7 to 1.3V magnitude per phase applied through built-in DACs and buffers. Data acquisition, visualization, and spike detection were controlled using a modified version of Meabench [3] interfaced with custom-designed software.

3 Results

The array's high resolution and flexible electrode configurations have allowed us to electronically 'image' network morphology (Fig.2) [2,4], identify 'cell-assemblies' (Fig.3), and reconstruct sections of axonal arbors (Fig.4). Furthermore, its signal-to-noise ratio was large enough to resolve the propagation of action potentials across continuous lengths of thin axons via spike-triggered averaging (Fig.5).



Fig. 2. Electrical 'images' of network topology. Average spike peaks from spontaneous recordings (1 min per configuration) are plotted for three cultures initially seeded with 10k, 5k, and 1k cells, aged 16, 16, and 26 days-in-vitro respectively. Due to an incubator malfunction, only 1 neuron remained alive in the 1k preparation. Neurons varied in footprint size, spike magnitude (*gray scale*), and firing profile (not shown). To sample all electrodes, 108 coherent 6x17-electrode recording configurations were scanned across the entire array. Note that some neurons may not have been active during the 1-min configuration duration.

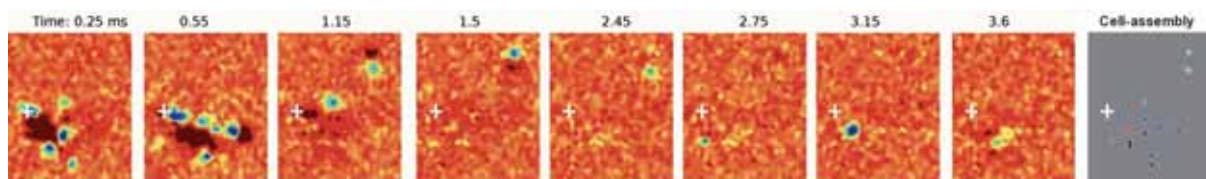


Fig. 3. Identification of 'cell-assemblies'. Spontaneous-spike-triggered averaging from one soma (*white plus*) showed that different neurons reliable fired together. The data suggest that some aspects of circuit connectivity can be inferred from a statistical analysis of spike-trains for different neurons ('cell-assemblies'). Somata are *green to blue* in color, representing recorded voltage. Latency from the triggered somatic action potential is given above each frame. The right graph plots the location of all detected somata, color-coded in latency. To sample all electrodes, coherent 6x17-electrode recording configurations were scanned across the entire array (108 total configurations).

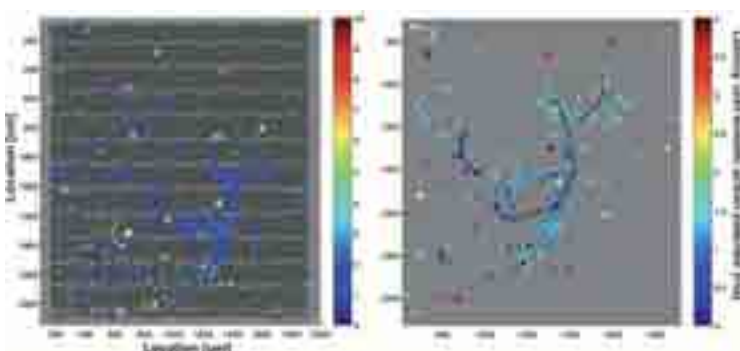


Fig. 4. Reconstructing axonal arbors via a stimulus "input map" for a single neuron. *Color* indicates the latency after a stimulus until an AP was recorded at the soma (*white plus*), with 50-75% (*smaller dots*) or >75% (*larger dots*) reliability within a 150 μ s window. Right: Continuous lengths of axons and some axonal branching appear possible to be mapped (*lines*). Ineffective sites (*gray dots*) surrounded many effective sites, suggesting stimulation range is local to an electrode. APV, CNQX, and BMI blocked synaptic activity.

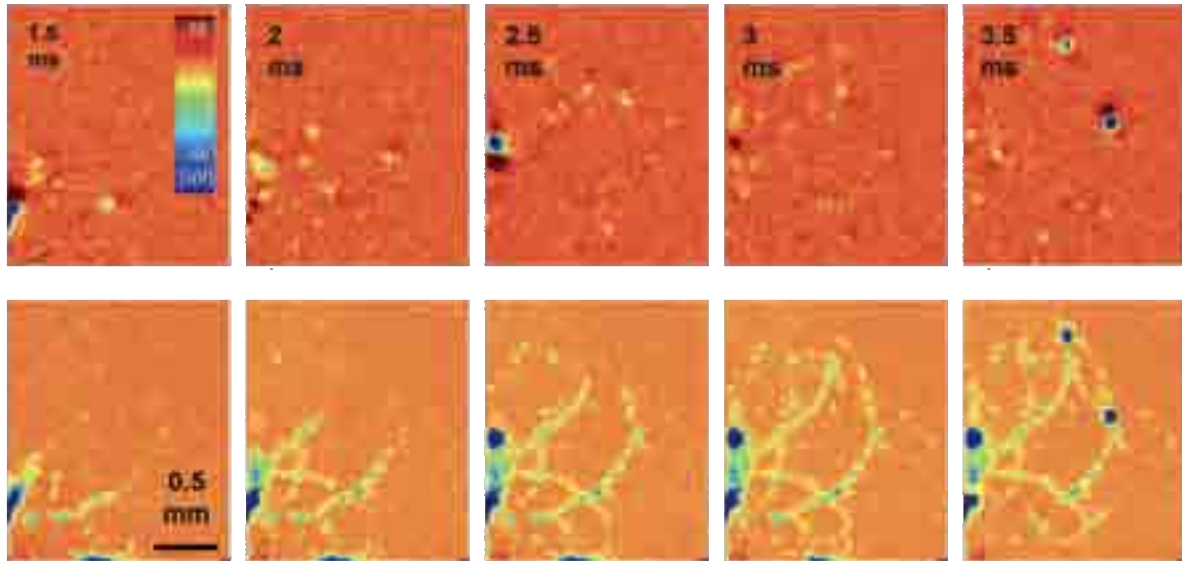
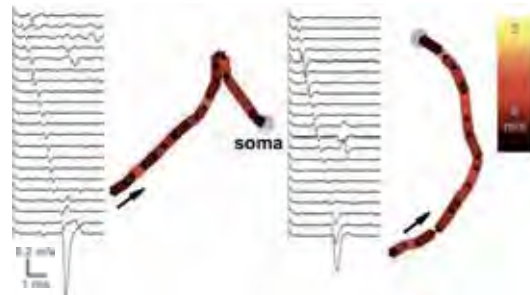


Fig. 5. Propagation of axonal APs. Top: Raw voltage traces (*top row*) and traces binned over 2 ms (*bottom row*) are color-coded. Stimuli applied to a single electrode (*arrow*) evoked a subset of neurons, and somatic APs (*blue*) were detected by multiple neighboring electrodes. The color scale was reduced in order to zoom-in on axonal APs (*yellow*). To sample all electrodes, coherent 6x17-electrode recording configurations were scanned across the array, and responses after 60 stimuli per configuration were averaged. Right: AP propagation in two selected neurons. Velocity (*color*) between electrodes (*black dots* and *voltage traces*) varied across axonal segments.



4 Conclusion

The system allows high spatial and temporal resolution two-way experimentation without a limit on experiment duration. This unprecedented level of neuronal network access has already produced novel data, and further studies are expected to provide a wealth of additional data that will advance our basic understanding of the brain's capabilities.

Acknowledgement

Financial support was kindly provided by ETH under the internal grant TH-00108, the TEPCO Research Foundation, the Japanese Society for the Promotion of Science, and an RCAST internal grant. We thank Hideo Sakai, Norio Tanada, and Takeshi Mita for assistance with culture maintenance.

References

- [1] Frey U, Sedivy J, Heer F, Pedron R, Ballini M, Mueller J, Bakkum D, Hafizovic S, Faraci FD, Greve F, Kirstein KU, Hierlemann A (2010). Switch-Matrix-Based High-Density Micro-electrode Array in CMOS Technology. *IEEE Journal of Solid-State Circuits*, 45(2)
- [2] U. Frey, U. Egert, F. Heer, S. Hafizovic, A. Hierlemann, (2009) Microelectronic system for high-resolution mapping of extracellular electric fields applied to brain slices. *Biosensors and Bioelectronics* 24 2191–2198
- [3] Wagenaar DA, DeMarse TB, Potter SM, (2005) MEABench: A toolset for multi-electrode data acquisition and on-line analysis. *IEEE EMBS Conf. on Neural Engineering*.
- [4] Bakkum DJ, Frey U, Mueller J, Fiscella M, Hierlemann A, Takahashi H. (2009) Accessing neuronal network activity with an 11,011 electrode CMOS array. *Proceedings of the 24th Symposium on Biological and Phys. Engr. (BPES)*, Sendai, Japan: 1A2-4.

512-electrode MEA System For Spatio-Temporal Distributed Stimulation and Recording of Neural Activity

Paweł Hottowy^{1,2*}, John M. Beggs³, E. J. Chichilnisky⁴, Władysław Dąbrowski¹, Tomasz Fiutowski¹, Deborah E. Gunning⁵, Jon Hobbs³, Lauren Jepson⁴, Sergei Kachiguine², Keith Mathieson⁵, Przemysław Rydygier¹, Alexander Sher², Andrzej Skoczeń¹, Alan M. Litke²

1 Faculty of Physics and Applied Computer Science, AGH University of Science and Technology, Kraków, Poland

2 Santa Cruz Institute for Particle Physics, University of California, Santa Cruz, USA

3 Biocomplexity Institute, University of Indiana, Bloomington, USA

4 Salk Institute for Biological Studies, La Jolla, USA

5 Department of Physics and Astronomy, University of Glasgow, Glasgow, UK

* Corresponding author. E-mail address: hottowy@agh.edu.pl

We present the design and preliminary test result of a large-scale MEA-based system for spatio-temporal distributed stimulation and recording of neural activity. The system is based on a 512-electrode array with 60 μm inter-electrode spacing and dedicated multichannel integrated circuits for independent stimulation and recording on all the electrodes. In the preliminary tests we stimulated individual neurons in rat retina and cultured cortical slices and recorded the evoked spikes as soon as 55 μs after the stimulation pulse on the stimulating electrode, and 5 μs after the pulse on other electrodes and were able to detect and classify even the low-latency spikes from directly activated neurons.

1 Introduction

Modern MEA-based systems can record neural activity with single cell resolution and with hundreds or even thousands of independent channels, but the electrical stimulation is usually limited to a few electrodes or several groups of electrodes repeating the same stimulation protocol. In contrast, two-way electrical communication with a large population of neurons, at the resolution of single cells and individual action potentials, requires a system capable of generating independently defined stimulation signals on large number of sites. This has to be combined with recording of the network response and minimal stimulus-related artifacts.

Here we present a 512-electrode system able to stimulate neuronal cells in general spatio-temporal patterns, with simultaneous low-artifact recording of the elicited activity. The system is based on a high-density MEA and can elicit complex, precisely defined patterns of action potentials in hundreds of individual neurons. We plan to use the system to investigate the mechanisms of information processing in brain tissue, and to develop stimulation techniques for high-resolution neural prostheses.

2 System design

The presented system is based on custom-designed MEA [1] and Application Specific Integrated Circuits (ASICs). Eight Stimchip ASICs [2] generate

the electrical stimulation signals independently on each electrode and eight Neuroplat chips [3] simultaneously record the neural activity. A photograph of the system is shown in fig. 1A.

The system is controlled by a PC running a Labview application, which generates the stimulation control signals based on user-defined input files and continuously records the neural activity on all the electrodes. The input files are generated with Matlab and allow for independent definition of stimulation amplitude and timing for each channel. The recorded data are analyzed off-line with custom software developed in Matlab and Java.

2.1 Multielectrode array

The MEA consists of 512 microelectrodes arranged in a hexagonal pattern, with 60 μm inter-electrode spacing (fig. 1B). The electrodes have a diameter of 5 μm and are routinely electroplated with platinum before the experiment for impedance reduction.

Arrays of this type have been used previously for large-scale recording of neural activity from retina [4,5] and cultured brain slices [6]. Smaller 61-electrode arrays with the same spatial resolution and electrical properties have been used for electrical stimulation of retinal ganglion cells in rodents and primates, using a previous version of the stimulation electronics [7] as well as the Stimchip ASIC [8].

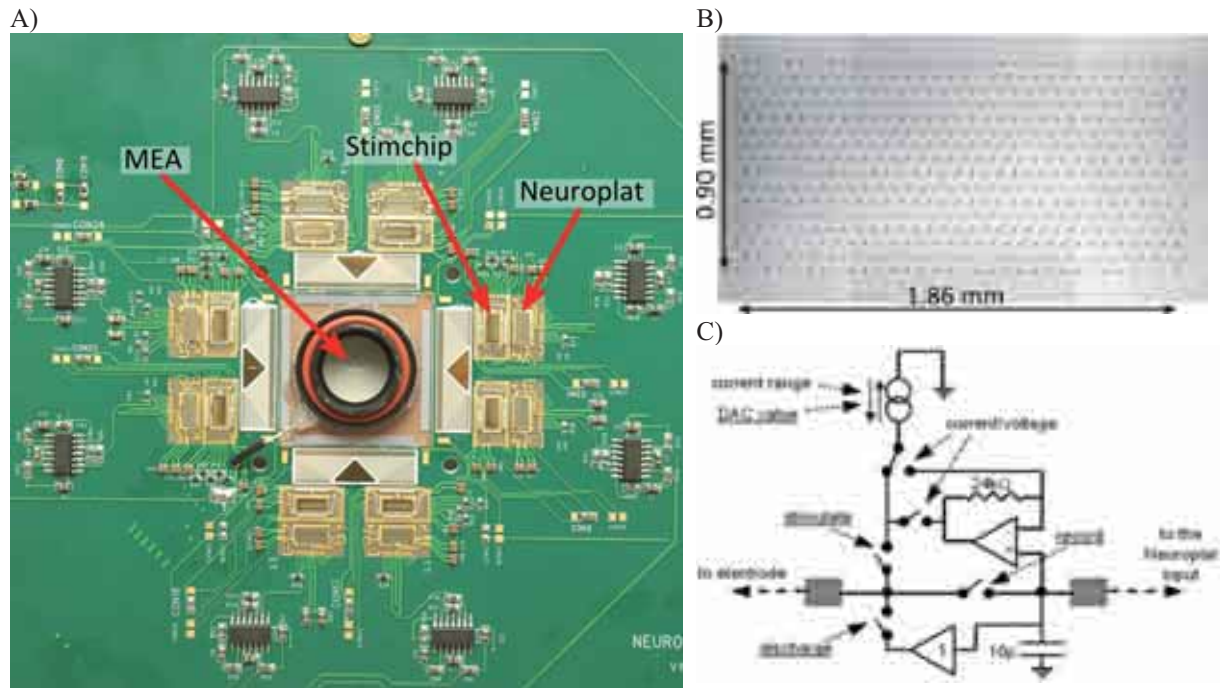


Fig. 1. A) Photograph of the Neuroboard. The array with chamber and eight sets of ASICs are located in the center. B) Microphotograph of the 512-electrode array. C) Functional diagram of single Stimchip channel with control signals. The real-time control signals are underlined.

2.2 Stimchip

The Stimchip ASIC includes 64 independent stimulation channels, circuitry for generating internal reference voltages, and a logic block that controls the operation of each channel based on digital commands sent from the control PC. Each channel comprises a programmable generator of arbitrary current waveform, a current-to-voltage converter, and artifact suppression circuitry (fig. 1C). The waveform generator is built of an 8-bit digital-to-analog converter and eight selectable output current buffers with maximum current ranging from 60 nA to 1 mA. The current waveform can be sent to the electrode either directly or via the current-to-voltage converter if voltage stimulation mode is selected [2].

During signal recording the electrode is connected to the input of the external amplifier through the closed *record* switch (fig. 1C). To avoid saturation of the amplifier by the large voltage signal generated by the stimulation pulse (either on the same channel, or one of the neighboring electrodes) the amplifier input can be disconnected from the electrode prior to the pulse and held at the constant potential, sampled before the stimulation pulse. In addition, the electrode-electrolyte interface can be actively discharged via a voltage follower before the electrode is reconnected to the amplifier input.

The shape of the stimulation signal and the states of all the switches in the circuitry are controlled with time resolution of 50 μ s, independently for each channel, by a stream of real-time data sent from the control computer (15 Mbit/s for each chip).

2.3 Neuroplat chip

The Neuroplat chip [3] comprises 64 independent recording channels, an analog multiplexer, bias circuitry and control logic. Each channel includes an AC-coupled amplifier, a band-pass filter, and a sample-and-hold circuit. The amplifier gain and the filter frequency range can be set by digital commands. The output signals on all the channels are sampled with a frequency of 20 kHz, multiplexed, and sent to the control computer for digitization and storage.

3 Preliminary tests

To evaluate the system performance, we stimulated and recorded activity from isolated rat retina and organotypic cultures of the rat cortex.

3.1 Stimulation protocol

We used charge-balanced triphasic stimulation pulses generated in current mode, with relative amplitudes of 2:-3:1 and durations of 50 μ s or 100 μ s per phase (fig. 2A). This pulse shape resulted in very low stimulus artifact that did not require post-pulse discharging. We recorded the elicited neural activity, on the stimulating electrode, as soon as 55 μ s after the stimulation pulse, and as early as 5 μ s after the pulse on the other, non-stimulating electrodes.

For each electrode, we used stimulation pulses with amplitudes (defined as the current value for the negative pulse phase) ranging from 0.1 to 4.0 μ A for the 50 μ s/phase pulses and 0.05 to 2.0 μ A for 100 μ s/phase pulses. The amplitude was increased in 5%

steps and stimulation pulse of given amplitude was repeated 100 times.

To reduce the experiment time, we grouped 512 electrodes in 64 eight-electrode patterns, with inter-electrode distance of 480 μm in each pattern. The electrodes within one pattern generated stimulation pulses simultaneously with a frequency of 2 Hz, and the pulses in next pattern were shifted by 7.5 ms. The whole stimulation procedure took ~ 1 hour and 50 minutes when both pulse durations were used.

3.2 Results

Stimulation of individual neurons

The four subplots in figure 2A show overlaid responses of a retinal ganglion cell (RGC) to stimulation pulses of different amplitudes recorded on the electrode generating the stimulation signal.

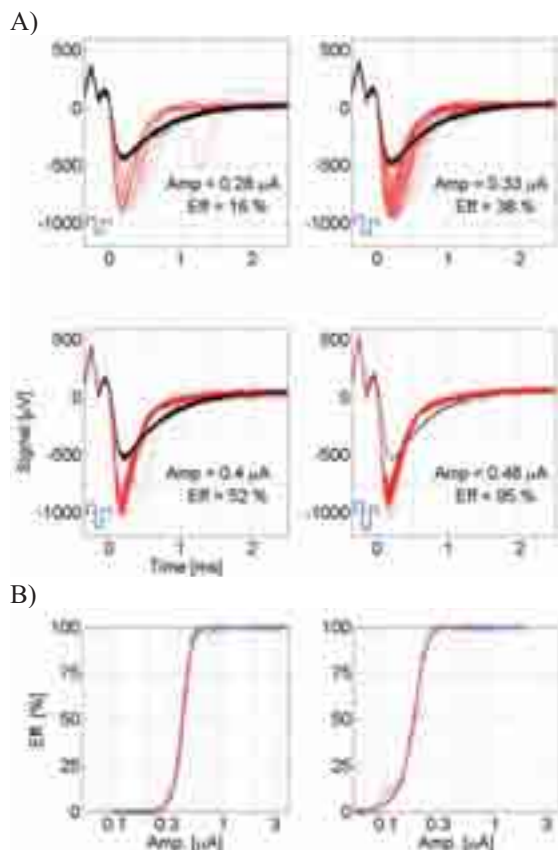


Fig. 2. Stimulation and recording of single RGC activity. A) Each subplot shows overlaid responses of retinal ganglion cell to 100 stimulation pulses recorded on the stimulating electrode. Four subplots correspond to various stimulation amplitudes. Black traces: artifacts only. Red traces: artifact combined with cell response. The blue trace illustrates the shape and timing of the stimulation current waveform. B) Stimulation efficiency as a function of current amplitude for 50 $\mu\text{s}/\text{phase}$ pulses (left) and 100 $\mu\text{s}/\text{phase}$ pulses (right).

Increasing the stimulation amplitude results in both, the smooth increase of the stimulation efficiency and stabilization of the elicited spike latency, while

the artifact level stays well within linear range of the Neuroplat chip ($\pm 3\text{mV}$ for a gain setting of 270).

Identification of activated cells

To reconstruct shape of the elicited neuronal signal, we averaged traces within each of the two classes shown in fig. 2A (subplot no. 4, current amplitude 0.48 μA) and subtracted the averaged waveforms [7]. The same procedure was applied to the six electrodes adjacent to the stimulating electrode. The elicited waveforms are virtually identical to the signals recorded from the same neuron spiking spontaneously, as shown in fig. 3A.

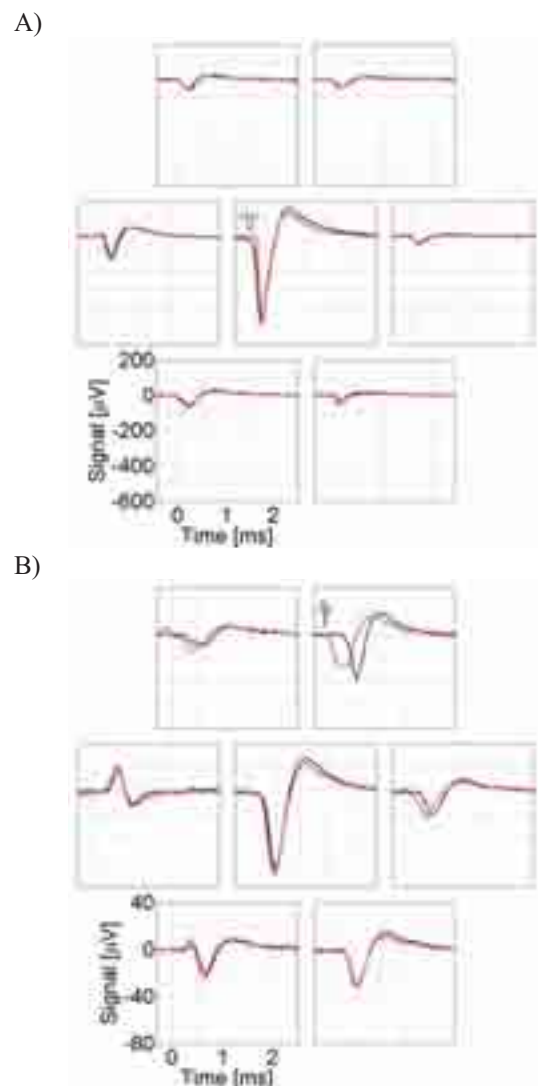


Fig. 3. A) Average shape of recorded elicited spike from retinal ganglion cell shown on seven electrodes (blue traces) compared with shape of signal recorded from the same neuron spiking spontaneously (red traces). The blue trace illustrates the timing of the stimulation pulse. B) Identical analysis for neuron in cultured rat cortical slice.

Activation of neurons in cultured rat cortical slices required in general higher stimulation currents than retinal ganglion cells. As shown in fig. 3B, the cell's response to a pulse of 4.0 μA recorded on the

stimulating electrode is significantly distorted. However, the signals on all of the neighboring electrodes are very well preserved and allow for unambiguous identification of the activated cell.

Spatial map of stimulation thresholds

Some of the identified neurons were effectively stimulated by several different electrodes, located near the cell bodies or axons. Fig. 4A shows averaged signals recorded from a retinal ganglion cell on 24 electrodes, including all the 6 electrodes that effectively stimulated the cell. Four of these electrodes (labelled with '1' to '4') recorded somatic signal from the stimulated neuron, with the two remaining electrodes ('5' and '6') recording axonal spikes.

The stimulation efficacies as a function of current amplitudes are shown in fig 4B for each of the six electrodes. The cell was stimulated with the lowest threshold current by the electrode that also recorded the largest signal from this neuron. However, the other electrodes near the soma show a similar stimulation threshold to the electrodes close to the axon.

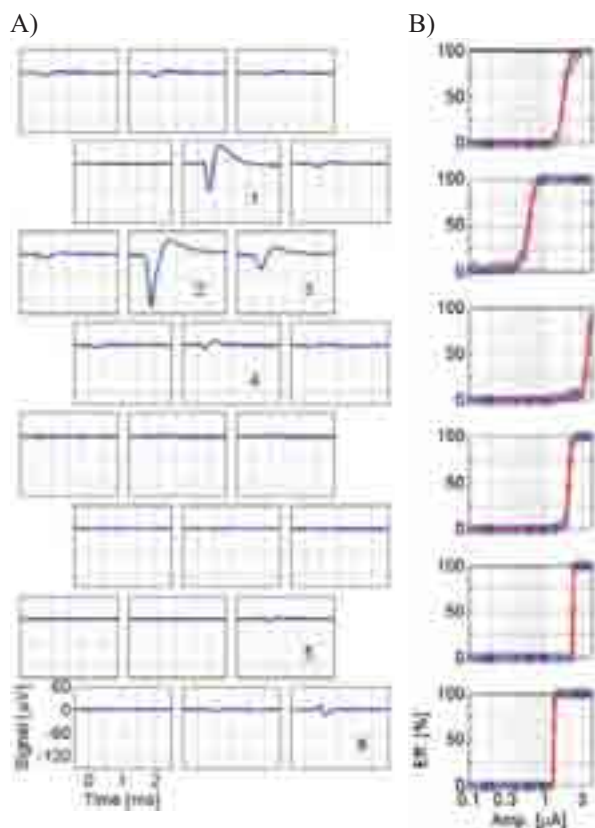


Fig. 4. A) Averaged signal recorded from an RGC. The electrodes that stimulated the cell are labelled (1-6). B) Stimulation efficiency as a function of current amplitude for each of the electrodes 1-6 (top to bottom). Pulse duration: 50 µs/phase.

4 Summary

We have developed a large-scale system that is capable of stimulating hundreds of neurons with arbitrarily defined patterns of stimulation currents, with simultaneous recording of the elicited activity. In the preliminary experiment, we were able to stimulate individual neurons in rat retina and cultured cortical slices, and record the evoked low-latency spikes from directly stimulated neurons with minimal distortions. Software for automated classification of elicited neural responses is currently under development.

Acknowledgement

This work was supported by the National Institutes of Health Grant EB004410 (J.B. and A.M.L.), National Science Foundation Grant PHY-0417175 and the McKnight Foundation (A.M.L.), Polish Ministry of Science and Higher Education (W.D.), RCUK (K.M.), EPSRC (D.E.G.), and the Burroughs Wellcome Fund Career Award at the Scientific Interface (A.S.).

References

- [1] Mathieson K., Kachiguine S., Adams C., Cunningham W., Gunning D., O'Shea V., Smith K. M., Chichilnisky E.J., Litke A. M., Rahman M. (2004). Large-area microelectrode arrays for recording of neural signals. *IEEE Transactions on Nuclear Science*, 51, 2027-2031.
- [2] Hottowy P., Dąbrowski W., Skoczeń A., Wiącek P. (2008). An integrated multichannel waveform generator for large-scale spatio-temporal stimulation of neural tissue. *Analog Integrated Circuits and Signal Processing*, 55, 239-248.
- [3] Gryboś P., Dąbrowski W., Hottowy P., Fiutowski T., Bielewicz B. (2006). Neuroplat64 – low noise CMOS integrated circuit for neural recording applications. *Proceedings of the 5th International Meeting on Substrate-Integrated Micro Electrode Arrays*, 208-209.
- [4] Litke A. M., Bezayiff N., Chichilnisky E. J., Cunningham W., Dąbrowski W., Grillo A. A., Grivich M., Gryboś P., Hottowy P., Kachiguine S., Kalmar R.S., Mathieson K., Petrusca D., Rahman M., Sher, A. (2004). What does the eye tell the brain? Development of a system for the large scale recording of retinal output activity. *IEEE Transactions on Nuclear Science*, 55, 239-248.
- [5] Pillow J.W., Shlens J., Paninski L., Sher A., Litke A.M., Chichilnisky E.J., Simoncelli E. P., (2008). Spatio-temporal correlations and visual signaling in a complete neuronal population. *Nature*, 454, 995-999.
- [6] Tang A., Jackson D., Hobbs J., Chen W., Smith J. L., Patel H., Prieto A., Petrusca D., Grivich M. I., Sher, A., Hottowy, P., Dąbrowski, W., Litke A. M., Beggs J. M., (2008). A Maximum Entropy Model Applied to Spatial and Temporal Correlations from Cortical Networks In Vitro. *Journal of Neuroscience*, 28, 505-518.
- [7] Sekirnjak C., Hottowy P., Sher A., Dąbrowski W., Litke A. M., Chichilnisky E. J. (2006). Electrical Stimulation of Mammalian Retinal Ganglion Cells With Multielectrode Arrays. *Journal of Neurophysiology*, 95, 3311-3327.
- [8] Hottowy P., Dąbrowski W., Kachiguine S., Skoczen A., Fiutowski T., Sher A., Rydygier P., Grillo A. A., Litke A. M., (2008). An MEA-based system for multichannel, low artifact stimulation and recording of neural activity. *Proceedings of the 6th International Meeting on Substrate-Integrated Micro Electrode Arrays*, 259-262.

Bidirectional Interfacing of Neurons with a 32k Pixel CMOS Multi-Capacitor-Transistor-Array (MCTA)

Thomas Gerling¹, Armin Lambacher¹, Björn Eversmann², Roland Thewes², Peter Fromherz¹

¹ Department of Membrane and Neurophysics, Max Planck Institute for Biochemistry, Martinsried/Munich, Germany

² Corporate Research, Infineon Technologies AG, Munich, Germany

We report on a closed-loop-experiment with an A-cluster neuron of a pedal ganglion from the pond snail *Lymnaea stagnalis*. For that kind of experiments neurons with a soma diameter between 50-80 μm were taken. A description of the preparation and the cell extraction can be found in [1]. The neurons were cultured for 24 hours on the laminin fragment *IKVAV* on the chip surface.

The CMOS-MCTA chip has a 2 mm² high-density sensor and stimulation array of 32768 bidirectional pixel which are arranged in 128 rows and 256 columns with a pitch of 8.775 μm in each dimension. Each row of the array has its own differential readout amplifier and an on-chip 9 bit analog-to-digital-converter (ADC). Due to the fabrication by an extended CMOS technology the sensor transistor with its intrinsic poly-silicon gate is buried in the chip and is connected to the interface capacitor via a metallic pathway. That interface capacitor consists of a platinum spot isolated by a biocompatible dielectric layer made of TiO₂/ZrO₂ to avoid any Faradaic currents across the surface. This layout allows recording and stimulation with the same pixel, i.e. the interface is bidirectional. For recording the array can be readout with a full frame rate of 2.4 kHz. For stimulation externally and/or internally generated stimulation pulses can be applied for each row of the array.

For the closed-loop-experiment an array of 9x9 pixel was chosen and repetitive biphasic voltage pulses of raising and falling ramps are applied [2]. To allow for immediate readout after stimulation, the selected columns can be reset to their operating points as described in [3] [4]. Thus recording of neuronal signals on a stimulating pixel can be achieved after 650 μs .

References

- [1] N. I. Syed, H. Zaidi, P. Lovell. In vitro reconstruction of neuronal circuits: A simple model approach. In *Modern Techniques in Neuroscience Research*. U. Windhorst and H. Johansson, editors. Springer, Berlin. 361-377, 1999
- [2] I. Schoen, P. Fromherz. Extracellular stimulation of mammalian neurons through repetitive activation of Na⁺ channels by weak capacitive currents on a silicon chip. *J Neurophysiol* 100: 346-357, 2008
- [3] B. Eversmann, M. Jenkner, F. Hofmann, C. Paulus, R. Brederlow, B. Holzapfl, P. Fromherz, M. Merz, M. Brenner, M. Schreiter, R. Gabl, K. Plehnert, M. Steinhauser, G. Eckstein, D. Schmitt-Landsiedel, R. Thewes. A 128x128 CMOS biosensor array for extracellular recording of neural activity. *IEEE J. Solid State Circ* 38: 2306-2317, 2003
- [4] A. Lambacher, M. Jenkner, M. Merz, B. Eversmann, R.A. Kaul, F. Hofmann, R. Thewes, P. Fromherz. Electrical imaging of neuronal activity by multi-transistor-array (MTA) recording at 7.8 μm resolution. *Appl Phys A* 79: 1607-1611, 2004

Investigation of pharmacologically-induced epileptic spatial-temporal patterns on cortico-hippocampal slices by means of high-density microelectrode arrays

Ferrea E.^{1,2*}, Maccione A.¹, Baldelli P.^{1,2}, Benfenati F.^{1,2}, Berdondini L.¹

¹ Department of Neuroscience and Brain Technologies, The Italian Institute of Technology, Genova, Italy;

² Department of Experimental Medicine, University of Genova, Genova, Italy

* Corresponding author. E-mail address: enrico.ferrea@iit.it

Microelectrode arrays (MEAs) are largely employed to study electrical activity in neuronal tissues [1]. Nevertheless, commercially available MEAs provide a limited number of recording sites and do not allow a precise identification of spatial-temporal oscillations. To overcome this limitation, high density MEAs based on CMOS technology were recently developed [2,3]. The platform used here enables extracellular electrophysiological recordings from 4096 electrodes arranged in a squared area of 2.7 mm x 2.7 mm with inter-electrode distance of 21 μm , at a sampling rate of 7,7 kHz/electrode. Here, we report preliminary validation results demonstrating the capabilities of this platform to acquire from the whole array electrophysiological activity from brain slices, with the aim to study the impact of convulsant agents on murine cortico-hippocampal slices.

1 Methods/Statistics

1.1 Experimental Protocol

Epileptic-like discharges were induced on horizontal hippocampal slices (400 μm in thickness) by applying 4-aminopyridine (200 μM) or picrotoxin (100 μM) [4]. Spontaneous activity was recorded up to one hour from the slice coupled with the CMOS-MEA (fig.1).

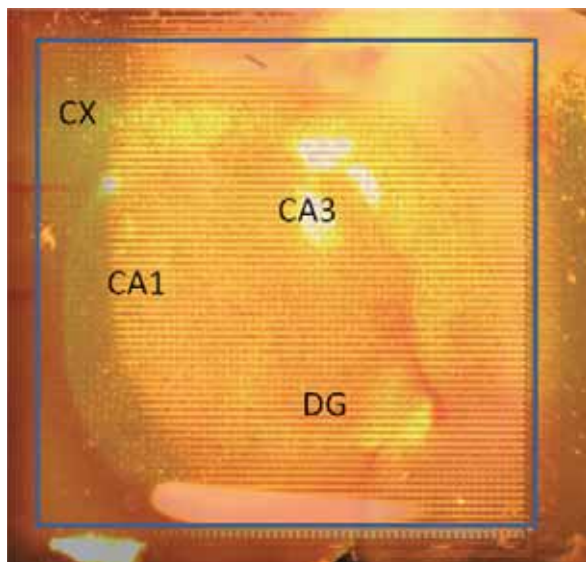


Fig. 1. 400 μm thick brain slice over the CMOS-MEA providing simultaneous recording from 4096 microelectrodes.

Our high density MEA platform was coupled with a perfusion system and temperature control to keep the

brain slice under healthy conditions and for drug treatments.

The inlet was provided by a pump fluxing 5 mL/min of heated solution, while the level of media in the dish was maintained by an outlet connected to a vacuum pump. Slices were kept in position by using custom-made anchors.

2 Results

The recording performances and the large recording area of the chip permit the observation of fast propagating activities involving multiple slice areas (Fig 2.a,d). Fig 2.c,d shows a propagation pattern from the hippocampus to para-hippocampal regions. Thanks to the unique features of the platform, we were able to precisely follow the spread of activity during long-lasting epileptic-like discharges induced in slices by the perfusion of convulsant drugs (fig 2.b). Interestingly, results show that not all the regions are always involved in these propagations. Moreover, this technology enables the clear identification of epileptic foci and the classification of the different propagation trajectories.

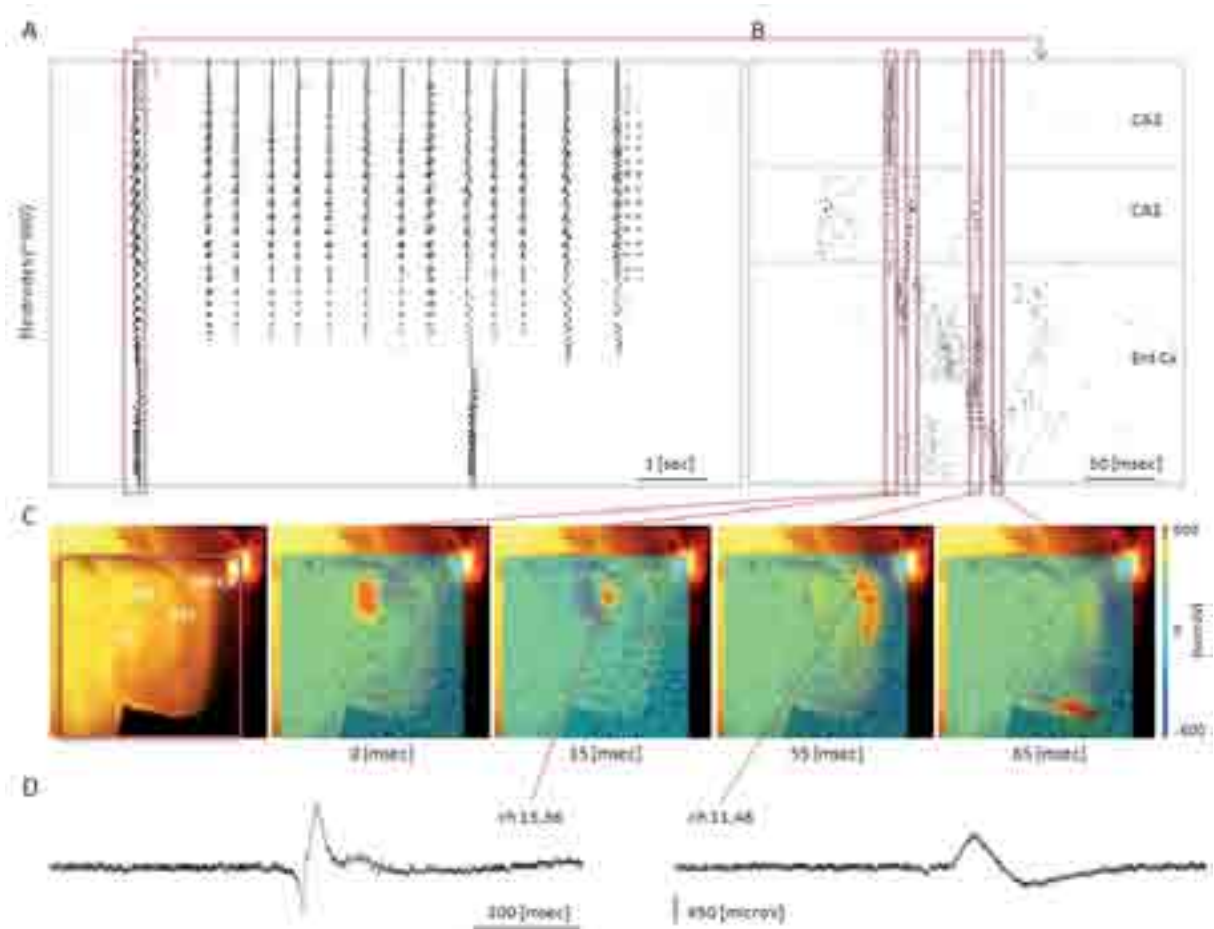


Fig 2 (a) raster plot representation of a train of fast inter-ictal events recorded by ~900 electrodes, (b) close-up on the first inter-ictal event involving the activation of different slice areas (see (c)). (c) Superimposition on the slice image of a red square representing the recording area of the device; the following images show a false colour-map of the voltage values recorded at different instances (b). Signal propagation from CA3 to CA1 and to Entorhinal Cortex can be appreciated in detail. (d) Raw data of two representative channels showing alternate phases of hyper- and de-polarisation.

3 Conclusion/Summary

High-resolution MEAs offer a unique opportunity to record from relatively large portions (2.7 mm x 2.7 mm active area) of brain tissue, at a high spatial resolution (4096 electrodes) and high sampling frequency. Here, we show that the APS-MEA platform is particularly suitable to study *in vitro* models of temporal lobe epilepsy.

References

- [1] Morin F., et al., *Journal of Bioscience and Bioengineering*, 2:131-143, 2005.
- [2] Frey U, et al., *Biosensors & Bioelectronics* 24 2191-8, 2009.
- [3] Berdondini, L., et al., *Lab Chip*, 9: 2644-51, 2009.
- [4] Avoli M., et al., *Journal of Physiology* 493.3: 707-717, 1996.

MEA Based Multichannel System Employing ASIC for In Vivo and In Vitro Experiments

Paweł Gryboś¹, Piotr Kmon¹, Robert Szczygieł¹, Mirosław Żołędź¹, Maciej Kachel¹

¹ Department of Measurement and Instrumentation, AGH University of Science and Technology, Cracow, Poland

* Corresponding author. E-mail address: pgrybos@agh.edu.pl, kmon@agh.edu.pl

This paper presents the design and measurements of low noise multichannel system for recording extra-cellular neuronal signals using micro electrode arrays. System is based on the integrated circuit containing 64 readout channels combined with the MEA electrodes. Electronic chip is fabricated in CMOS 180 nm technology and occupies $5 \times 2.3 \text{ mm}^2$ of silicon area. A single readout channel is built of an AC coupling circuit at the input, a low noise preamplifier, a band-pass filter, and a second amplifier. In order to reduce the number of output lines, the 64 analog signals from readout channels are multiplexed to a single output by an analog multiplexer. The chip is optimized for low noise and good matching performance and has the possibility of pass-band tuning. The low cut-off frequency can be tuned in the 1 Hz - 60 Hz range while the high cut-off frequency can be tuned in the 3.5 kHz - 15 kHz range. For the nominal gain setting at 44 dB and power dissipation per single channel of $220 \mu\text{W}$, the equivalent input noise is in the range from $6 \mu\text{V}$ - $11 \mu\text{V}$ rms depending on the band-pass filter settings. The chip has good uniformity concerning the spread of its electrical parameters from channel to channel. The spread of a gain calculated as standard deviation to mean value is about 4.4% and the spread of the low cut-off frequency set at 1.6 Hz is only 0.07 Hz. Chip parameters and the data acquisition are controlled thanks to the signals generated by the PXI equipped with the measurement card and managed by the LabVIEW based software.

1 Methods

The ASIC comprises three main blocks: 64 AC coupling circuits at the inputs, 64 analog channels with the amplifiers and filters, and an analog 64:1 multiplexer. Its photo is depicted in the Fig. 1. The proposed architecture of a single readout channel is shown in Fig. 2. It consists of three main sections: AC coupled input preamplifier, band-pass filter stage with AC coupled output and second amplifier.



Fig. 1. Photo of a 64-channel chip: input pads are at the top side, control and output pads are at the bottom side, power supply and test pads are on the left and right side.

The analog channel amplifies and filters small amplitude biopotential signals, which are typically in the range from tens to hundreds of μV with the frequency spectrum from a few Hz to a few kHz. The signals are recorded with respect to common reference electrode INREF immersed in physiological saline solution. The low and the high cut-off frequencies of the channel are controlled by external signals S1, S2, S3 and by the V_R_Gate input. The signals from the

64 channels are sampled at the same moment and subsequently are multiplexed through the analog multiplexer to the output of the ASIC. The bandwidth of single channel is limited to 15 kHz. The nominal frequency of the multiplexer's operation is 5 MHz what results in about 75 kHz sampling frequency per single channel. It allows to avoid an aliasing problem and to develop system comprising much more than 64 recording channels.

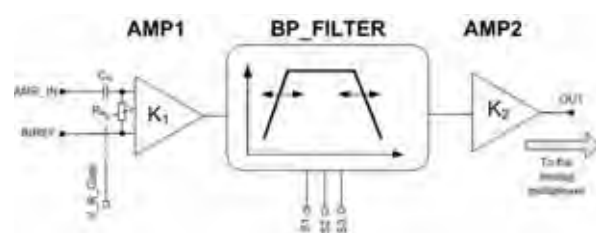


Fig. 2. Simplified block diagram of a single readout channel.

2 Results

The PCB prototype board equipped with the MEA electrodes, described ASIC and a LVDS controller was designed (Fig. 3). The measurements are run with an application written in the LabVIEW environment controlling the measurement card. For the multiplexer data acquisition and chip measurements PXI (PCI eXtensions for Instrumentation) module was used, equipped with high-speed analog/digital output card (NI-PXI 6733) and 100 MS/s, 14-Bit Digitizer (NI-PXI 5122). An

output card serves as a source of multiplexer control signals and source of input test signals for analog channels. The digitizer acquires the output signal for further processing i.e. decimation and demultiplexation. We made an experiment using our prototype board and MEA multichannel electrodes. Into the saline solution in which electrodes were immersed we dipped a metal round electrode with the signal conveyed from the generator. The 64 recorded signals are depicted in the Fig. 4.

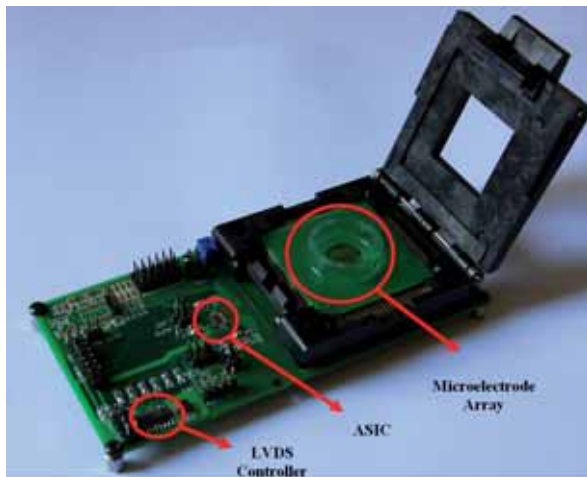


Fig. 3. Test setup for the ASIC measurements.

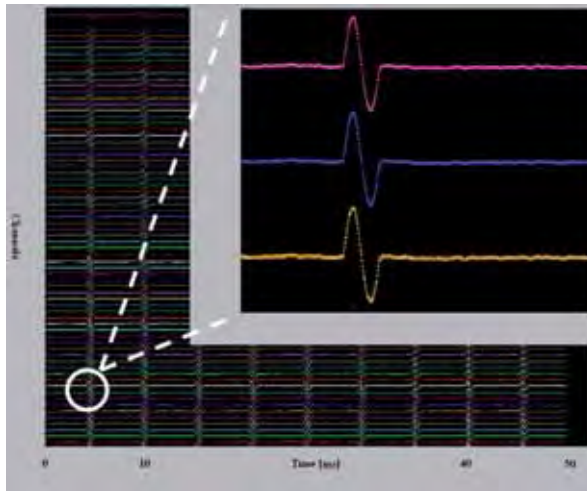


Fig. 4. Signals recorded with the MEA usage.

3 Conclusions

The multichannel neural recording system built with the MEA electrodes and with the ASIC was presented. Its main parameters are shown in the Table I. The low noise performance of the ASIC, implemented AC coupling at the inputs, good channel-to-channel uniformity and low power consumption make the designed electronic chip an universal multi-channel readout ASIC for experiments with alive neuronal cells. In the near future the results of the In Vitro measurements held on the described system will be presented. Based on the presented ASIC and the MEA electrodes the system comprising 256 recording channels is being built which results will be presented on the conference.

TABLE I
SUMMARY OF BASIC PARAMETERS OF THE MEASUREMENT SYSTEM

Parameter	Value
Gain	44 dB
Tuning range for low cut-off frequency	1 - 60 Hz
Tuning range for high cut-off frequency	3.5 - 15 kHz
Equivalent input noise (depending on the pass band setting)	6 - 11 μ V
Power per channel	220 μ W
Linearity for input signals	2 mV
Spread of gain and low cut-off frequency	4.4 %
Spread of high cut-off frequency	1.8 %
Power supply voltage	± 1.1

Acknowledgement

This research and development project was supported by Polish Ministry of Science and Higher Education in the years 2008-2010.

Delta Compression of Neural Recordings for High-density CMOS-based Microelectrode Arrays

Neil Joye^{*}, Michelangelo Carrozzo, Alexandre Schmid, Yusuf Leblebici

Microelectronic Systems Laboratory (LSM), Ecole Polytechnique Fédérale de Lausanne (EPFL), Lausanne, Switzerland

^{*} Corresponding author. E-mail address: neil.joye@epfl.ch

Recent high-density CMOS-based MEAs contain thousands of electrodes. Hence, an off-chip acquisition system performing data compression prior to visualization and analysis on a computer is required in order to handle the large amount of data generated by active MEAs. Since significant information is discarded with conventional spike detection algorithms, a delta compression algorithm is implemented on a Xilinx Virtex 5 FPGA. An experimental setup is developed in order to verify the functionality of the data acquisition system, implemented on the FPGA platform, independently from the CMOS front-end. It is shown that if the signal-to-noise ratio (SNR) of the input signal is higher or equal to 10 dB, delta compression is suitable for high-density MEAs.

1 Introduction

Modern MEAs are realized with increasingly high density of electrodes, causing stringent constraints on the CMOS circuits in charge of the analog front-end, analog to digital conversion and data transmission. Acquiring an array of 64 x 64 electrodes at a sampling rate of 10 kSamples/s generates an amount of data to be transmitted for processing equal to 490 MB/s [1]. Thus, data compression has to be accomplished before analyzing the recorded data on a dedicated computer.

Conventional spike detection algorithms perform thresholding of the amplitude of the signal in order to capture the majority of action potentials. However, important information such as the neural activity above or below the threshold level is discarded. Delta compression has been presented as a possible solution [2]. The temporal derivative of the neural signal is calculated in the digital domain and its value transmitted only if it exceeds a determined threshold.

2 Readout System

The readout circuitry is targeted for a 128 x 128 CMOS-based MEA, as depicted in Fig. 1. Each readout channel, which consists of a low-noise amplifier connected to an 8-bit ADC, acquires data by scanning all electrodes in one zone. A zone is defined as a sub-array of 64 x 4-6 electrodes. In this preliminary study, 25 electrodes in one zone are sensed.

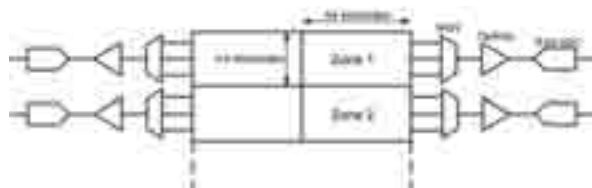


Fig. 1. Overview of the readout circuitry.

Considering zones of 64 x 4 electrodes, which correspond to 64 zones, the total data output rate is equal to 256 MB/s if a sampling frequency of 20 kHz and 8-bit ADCs are considered. A delta compression algorithm is thus implemented on a Xilinx Virtex 5 FPGA, as depicted in Fig. 2. A low-pass 30th order Finite Impulse Response (FIR) filter, which eliminates the signal high-frequency noise, and an Ethernet interface are also implemented. The delta compression algorithm is performed by computing the difference between two successive samples. For each pixel, when 256 samples have been acquired and temporarily saved on the FPGA, the transmitted data is either the recorded signal if the delta compression algorithm has detected activity, or the running average of the signal.

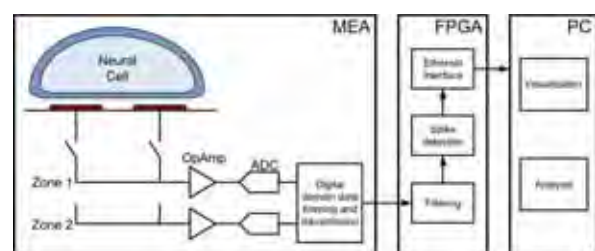


Fig. 2. System overview and data flow.

3 Results

An experimental setup has been developed in order to verify the functionality of the data acquisition system, implemented on the FPGA, independently from the CMOS front-end. Artificial spikes generated with the tool presented in [3] are generated using an arbitrary waveform generator in order to simulate the recorded extracellular signals. This software allows varying the SNR of generated signals. The compression ratio and the false events versus the SNR

of input signals are measured and presented in Fig. 3. The delta compression algorithm performance dramatically drops for SNRs smaller than 10 dB. Thus, for small SNRs, spike detection techniques based on the nonlinear energy operator, for example, should be used as a more appropriate solution [4], [5].

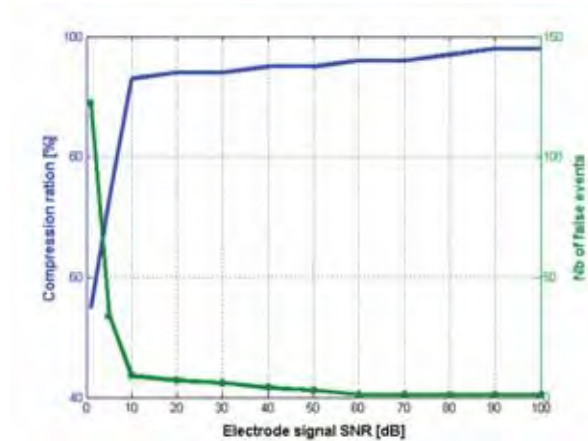


Fig. 3. Compression ratio and number of false events versus the SNR of the artificial neural spikes.

4 Conclusion

A delta compression algorithm is implemented on a FPGA platform in order to compress neural recorded signals. If the SNR of the input signal is higher or equal to 10 dB, our experiments show that the delta compression is suitable for high-density CMOS-based MEAs.

Acknowledgement

This work has been conducted with the support of the Swiss NSF grant number 205321-116780, and the EPFL STI Seed Grant.

References

- [1] K. Imfeld, S. Neukom, A. Maccione, Y. Bornat, S. Martinoia, P.-A. Farine, M. Koudelka-Hep, and L. Berdondini (2008): Large-scale, high-resolution data acquisition system for extracellular recording of electrophysiological activity. *IEEE Trans. on Biomed. Eng.*, 55, 2064-2073.
- [2] J. N. Y. Aziz, K. Abdelhalim, R. Shulyzki, R. Genov, B. L. Bardakjian, M. Derchansky, D. Serletis, and P. L. Carlen (2009): 256-channel neural recording and delta compression microsystem with 3D electrodes. *IEEE J. Solid-State Circuits*, 44, 995-1005.
- [3] L. S. Smith and N. Mtetwa (2007): A tool for synthesizing spike trains with realistic interference. *J. Neurosci. Methods*, 159, 170-180.
- [4] S. Mukhopadhyay and G. C. Ray (1998): A new interpretation of nonlinear energy operator and its efficacy in spike detection. *IEEE Trans. on Biomed. Eng.*, 45, 180-187.
- [5] J. Holleman, A. Mishra, C. Diorio, and B. Otis (2008): A micro-power neural spike detector and feature extractor in .13 μ m CMOS. In *Proc. IEEE Custom Integrated Circuits Conference (CICC)*, 333-336.

AM Modulation-based CMOS Readout Circuit for High-density Microelectrode Arrays

Neil Joye^{*}, Alexandre Schmid, Yusuf Leblebici

Microelectronic Systems Laboratory (LSM), Ecole Polytechnique Fédérale de Lausanne (EPFL), Lausanne, Switzerland

^{*} Corresponding author. E-mail address: neil.joye@epfl.ch

An innovative readout channel, based on analog amplitude modulation (AM) of the signals recorded by each electrode, is developed for high-density CMOS-based MEAs. This new readout method enables the design of a low-noise amplification stage while still reading the extracellular activity sensed by the whole array. Hence, the circuit architecture provides an efficient solution to the major limitation of high-density active MEAs related to the real-time transmission of every electrode input. CMOS implementation of the readout channel is presented. Each pixel contains a double-balanced CMOS mixer having a size of $26.5 \times 26.5 \mu\text{m}^2$. It is shown that in the case where signals from five different pixels are simultaneously recorded, the dominant noise source of the system is the noise generated in the two-stage operational amplifier. Furthermore, the maximum number of pixels which can be contained in a single readout channel is limited by the thermal noise of each pixel which sums up at the amplifier input node. A maximum limit of 20 pixels is estimated.

1 Introduction

CMOS-based MEAs have recently emerged as devices enabling a large number of closely spaced electrodes to be fabricated along their readout circuits [1], [2]. In order to read the full array, the front-end amplifiers must be integrated in each chip [1]. However, the pixel area is limited by the size of the amplifiers. A second approach where the amplification stage is located outside the array has been adopted in [2]. However, only a limited number of electrodes can simultaneously be recorded.

Thus, a new method where a single amplification stage simultaneously records the activity from several electrodes is investigated. As presented in Fig. 1, each recorded signal is modulated in the AM domain, using V_n of different frequencies for each electrode in a row. The sum of the modulated signals is performed in the current mode, and amplified before analog-to-digital conversion. Each signal is then recovered by digital demodulation on a FPGA.

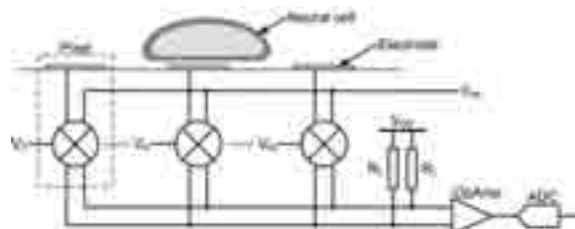


Fig. 1. Conceptual schematic of the readout architecture.

2 Readout Architecture

In each pixel, an active CMOS mixer is implemented in $0.18 \mu\text{m}$ CMOS technology, as

described in Fig. 2. This pixel circuitry is implemented for devices based on oxide-semiconductor field-effect transistors (OSFETs), as presented in [3]. Electrodes will be fabricated by post-fabrication steps based on oxide recession of the CMOS dices followed by the deposition of a dielectric layer. The mixer consists of a transconductance stage (M_1 and M_2) connected to two switching pairs (M_3 to M_6) driven by a local oscillator signal V_{LO} . The electrode is connected to the gate of the input transistor M_1 . The sensed signal is modulated by the sinusoidal signal V_{LO} . The pixel with its calibration transistors M_a and M_b has a size of $26.5 \times 26.5 \mu\text{m}^2$. Moreover, square electrodes with an optimum length of $7 \mu\text{m}$ are considered, which has been derived using cell-electrode models adapted from [4] and [5]. A two-stage operational amplifier occupying an area of $43.6 \times 33.8 \mu\text{m}^2$ and dissipating $20 \mu\text{W}$ is used.

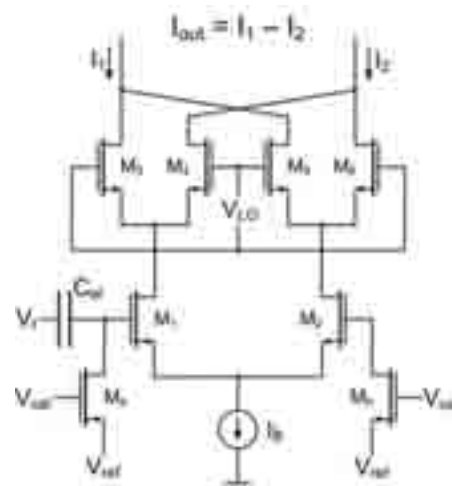


Fig. 2. CMOS mixer circuit implemented in each pixel.

3 Results

A post-layout simulation of the noise spectral density of the mixer referred to the input of the amplifier is depicted in Fig. 3, for the case where signals from five different pixels are simultaneously recorded. Modulation frequencies are set between 50 and 150 kHz. Using a model adapted from [5], the electrode-electrolyte noise spectral density at the input of the mixer is evaluated at 100 nV/sqrt(Hz) for the case where a typical configuration encountered in electrophysiological experiments is considered. Its value at the amplifier input node is thus approximately 80 nV/sqrt(Hz), which derives from the gain of a mixer. Thus, the noise contribution of the cell-electrode interface is the dominant noise source of the system, as observed in Fig. 3.

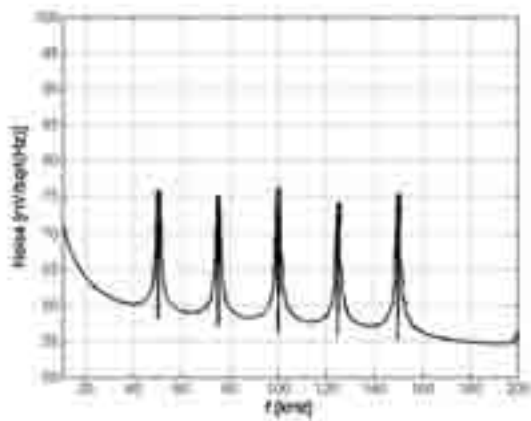


Fig. 3. Post-layout simulation of the noise spectral density at the input of the front-end amplifier. Five pixels are simultaneously readout.

4 Conclusion

A novel readout architecture for high-density MEAs is presented. The front-end amplification stage records several electrodes, simultaneously. Moreover, design constraints related to the flicker noise are relaxed, as a benefit of the operation at higher frequencies. However, the number of electrodes which can simultaneously be recorded is limited by the thermal noise of each pixel which sums up at the amplifier input node. A maximum limit of 20 pixels is estimated.

Acknowledgement

This work has been conducted with the support of the Swiss NSF grant number 205321-116780, and the EPFL STI Seed Grant.

References

- [1] K. Imfeld, S. Neukom, A. Maccione, Y. Bornat, S. Martinoia, P.-A. Farine, M. Koudelka-Hep, and L. Berdondini (2008): Large-scale, high-resolution data acquisition system for extracellular recording of electrophysiological activity. *IEEE Trans. on Biomed. Eng.*, 55, 2064-2073.
- [2] U. Frey, J. Sedivy, F. Heer, R. Pedron, M. Ballini, J. Mueller, D. Bakkum, S. Hafizovic, R. D. Faraci, F. Greve, K.-U. Kirstein, and A. Hierlemann (2010): Switch-matrix-based high-density microelectrode array in CMOS technology. *IEEE J. Solid-State Circuits*, 45, 467-482.
- [3] B. Eversmann, M. Jenkner, F. Hofmann, C. Paulus, R. Brederlow, B. Holzapfl, P. Fromherz, M. Merz, M. Brenner, M. Schreiter, R. Gabl, K. Plehnert, M. Steinhauser, G. Eckstein, D. Schmitt-Landsiedel, and R. Thewes (2003): A 128 x 128 CMOS biosensor array for extracellular recording of neural activity. *IEEE J. Solid-State Circuits*, 38, 2306-2317.
- [4] N. Joye, A. Schmid, and Y. Leblebici (2009): Electrical modeling of the cell-electrode interface for recording neural activity from high-density microelectrode arrays. *Neurocomputing*, 73, 250-259.
- [5] N. Joye, A. Schmid, and Y. Leblebici (2009): A cell-electrode interface noise model for high-density microelectrode arrays. In *Proc. Ann. Int. Conf. of the IEEE EMBS (EMBC)*, 3247-3250.

Voltage and Current Stimulation Buffer for High-Density Microelectrode Arrays

Paolo Livi^{1*}, Flavio Heer¹, Urs Frey², Douglas J. Bakkum^{1,3}, Andreas Hierlemann¹

¹ ETH Zurich, Bio Engineering Laboratory, Department of Biosystems Science and Engineering, Switzerland

² ETH Zurich, Bio Engineering Laboratory, Department of Biosystems Science and Engineering; now at IBM Research, Zurich, Switzerland

³ Graduate School of Information Science and Technology, The University of Tokyo, Japan

* Corresponding author. E-mail address: paolo.livi@bsse.ethz.ch

We report on a reconfigurable buffer for voltage and current stimulation of electrogenic cells, cultured on a CMOS high-density microelectrode array. In voltage mode, the circuit is a high-output-current class-AB voltage follower. In current mode, the circuit is a type-II current conveyor using the same amplifier with increased gain. The electrical characterization of the buffer is presented as well as stimulation results of on-chip cultured neurons.

1 Introduction

The possibility to stimulate neuronal cultures is a crucial feature for many interesting neuroscience experiments. Stimulation is needed to trigger and analyze specific network characteristics/dynamics, or to induce, e.g., plastic behavior. Neurons can be stimulated by either current or voltage signals with typical amplitudes of 100-1000mV or 5-10 μ A and durations of 50-900 μ s [1].

Here we report on a stimulation buffer circuit for a CMOS-based microelectrode array featuring 11,016 metal electrodes (7 μ m diameter) and 126 channels for bidirectional (recording and stimulation) communication with electrogenic cells [2]. The important features of this circuit include: (i) a single circuit for both, voltage and current stimulations; (ii) the use of a single operational amplifier, which reduces the required area (160x120 μ m²); and (iii) low power consumption (102 μ W in the quiescent state), which prevents heating the delicate cells.

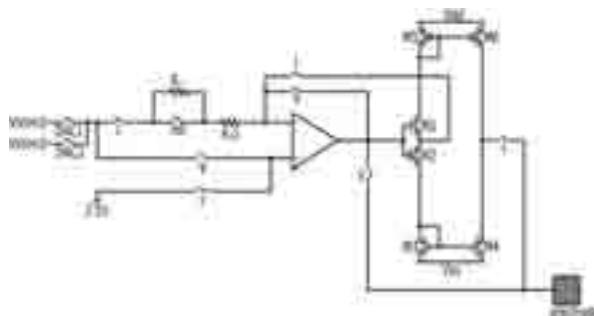


Fig. 1. Circuit schematic of the proposed voltage and current stimulation buffer. The label “V” means the switch is on in V-mode, while “I” means on in I-mode.

2 The Proposed Circuit

The circuit is shown in Fig. 1. A set of digitally controlled switches defines the current or voltage stimulation configuration. The input (V_{stim}) is always provided as a voltage using two integrated 10bit digital-to-analog converters.

In voltage mode, a voltage follower configuration is used, so that the input voltage, V_{stim} , is copied at the output (i.e., at the electrode). The circuit provides low output impedance approximating then an ideal voltage source. Large output current is needed in order to drive the large electrode-electrolyte capacitance (several nF), but power consumption has to be kept low. A class AB structure is a suitable approach, since it can provide large output currents when needed, still using a small bias current.

In current mode, the circuit implements a positive current conveyor of type II [3], with high output impedance, so that an ideal current source is approximated. The applied input voltage drops on resistor R_{C1} (10k Ω) creating a current that is conveyed at the electrode through the output stage built by transistors M1-M6. When the switch HR is open, the resistor R_C (90k Ω) is connected in series to R_{C1} reducing then the range of the current that can be generated. In particular, if only resistor R_{C1} is used, the circuit can provide an output current with good linearity up to 300 μ A, or up to 30 μ A, if resistor R_C is connected as well. The same operational amplifier is used as in voltage mode, but with increased gain (for stability reasons).

3 Results

3.1 Electrical Characterization

The chip was fabricated in an industrial 0.6 μ m 3M2P CMOS process. The power supply is 5V. The electrical characterization of the stimulation circuit for current and voltage configuration was carried out. The

circuit has good linearity (13 bit in voltage mode, 7 bit in current mode) for input voltages between 0.5V and 3.5V. Fig. 2 shows the response to a biphasic voltage stimulus ($\pm 1V$ in amplitude, period of $500\mu s$): the top graph is the input signal, the second one is the response in voltage mode, and the last two are the responses in current mode. These measurements were performed with a $15nF$ load connected to the circuit. The reason, why such a big capacitive load was used, is that we wanted to characterize the circuit in a worst case scenario (in normal operation the circuit has to drive only one electrode, corresponding to roughly $500pF$). Given such a load, the circuit in voltage mode shows a rising time of $70\mu s$ (corresponding to a bandwidth of $14kHz$). The slightly increasing response (should be flat) for negative currents in the current mode is due to the output impedance of the circuit that is not large enough. This problem will be solved in a next version using a cascaded output stage.

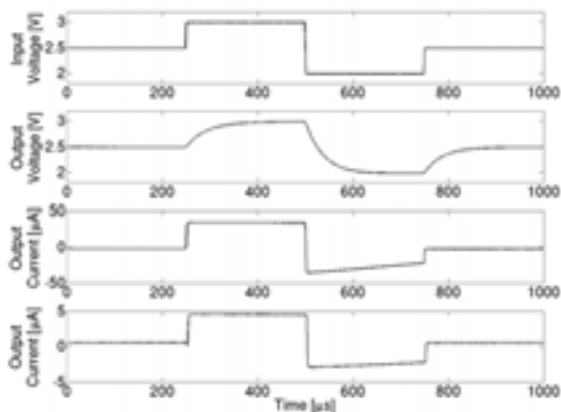


Fig. 2. Output characteristics for a biphasic voltage pulse.

3.2 Neuronal Stimulation Experiments

Physiological measurements were carried out as well. Fig. 3 shows 40 traces of triggered electrical activity upon stimulation (biphasic pulse, $\pm 1.2V$ amplitude, $500\mu s$ per phase, $300ms$ inter-stimulation interval) of neuronal cells, cultured directly on the chip. Responses have been collected in this case at $606\mu m$ distance from the stimulation site.

Fig. 4 shows responses of one soma to stimuli of various amplitudes and durations.

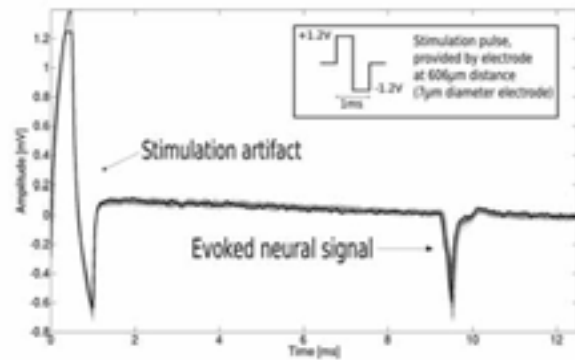


Fig.3. Stimulation and triggered response of cultured neurons on the chip.

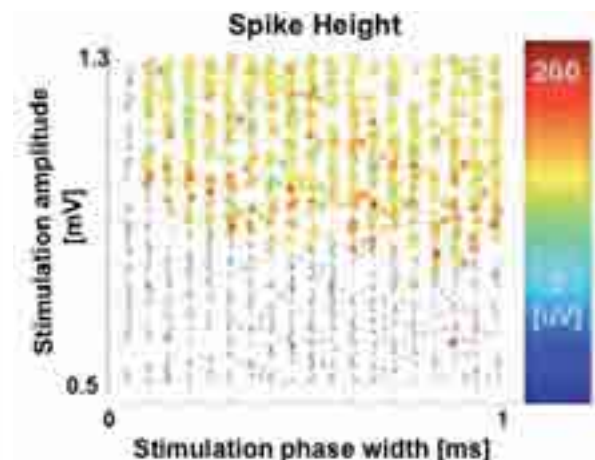


Fig.4. Responses of one soma to different stimuli; ineffective stimuli are in grey.

4 Conclusions

A compact circuit, capable of providing both voltage and current stimuli has been presented and characterized. The circuit is part of a CMOS-based high-density MEA system and can provide very localized stimulation (e.g., to selected single cells). The chip has been successfully used for thousands of stimulations and recordings from neuronal cells.

Acknowledgement

The authors thank M. Ballini, J. Rothe and J. Müller at ETH Zurich, for help in the electrical characterization of the circuit.

References

- [1] D. A. Wagenaar, J. Pine, J. Potter, "Effective parameters for stimulation of dissociated cultures using multi-electrode arrays", *J. of Neuroscience*, 2004
- [2] U. Frey et al., "Switch-Matrix-Based High-Density Microelectrode Array in CMOS Technology," *Solid-State Circuits, IEEE Journal of*, vol.45, no.2, pp.467-482, Feb. 2010
- [3] C. Toumazou et al., "Analog IC Design: The Current-Mode Approach", London: Peter Peregrinus, 1990

NeuroFETs: Field Effect Nano-Transistors Fabrication for Neural Recording

Llibertat Abad^{1,2}, Matthieu Petit², Ghislain Bugnicourt^{2,3}, Thierry Crozes², Thierry Fournier² and Catherine Villard^{2*}

1 Fondation Nanosciences, 23 rue des Martyrs, F-38000 Grenoble.

2 Institut Néel, CNRS / UJF - BP 166, F-38042 Grenoble cedex 9.

3 INSERM U-836, Institut des Neurosciences Grenoble (GIN), Université Joseph Fourier UMR-S 836, Grenoble, F-38042.

* Corresponding author. E-mail address: catherine.villard@grenoble.cnrs.fr

The present work tackles with the coupling of model neuron networks with functionalized silicon surfaces and the integration of nano field effect transistors to stimulate and record their activity (neuroFETs project).

1 Background/Aims

The principal aim of this work is the fabrication of field effect nano-transistors (nanoFETs) arrays for neural stimulation and/ or recording of constrained *in-vitro* neuron networks. These nano-transistors are fabricated on SOI wafers (Silicon-On-Insulator) using photolithography techniques. The principle of operation of these devices is the local variation of the voltage within the gap between the neuron and the nanoFET, modulating the conductance of the transistor channel.

The work of Patolsky et al. [1], after the seminal work of P. Fromhertz's group [2], has inspired this work. These authors recorded neuron action potentials with nanotransistors arrays built from silicon nanowires according to a bottom-up approach. Nevertheless, this method restricts the geometries of measurable networks to neuron chains. Our project is in contrast based on a top-down fabrication approach, suitable for looped neuron network topologies.

2 Results

2.1 Chip fabrication process

The device is started on a uniformly boron implanted (10^{17} to 10^{19} at/cm³) SOI wafer (SOITEC). NanoFETs arrays are fabricated using deep UV (DUV) photolithography, electron beam lithography and reacting ion etching (RIE).

We summarize briefly the chip fabrication process in the fig 1. In a first DUV photolithographic step, the contact pads and electrical tracks to connect the transistors (source and drain) are defined by a lift-off process of gold. In a more sophisticated second step electron-beam lithography is used to define the silicon bridges (around 100 nm wide). This should conform the nanoFET channels. Protected with the thin film Al mask, the top silicon layer is etched by Reactive Ion Etching (SF₆).

It is well known that a maturation of at least one week after neuron plating is necessary to obtain fully differentiated active cells. NanoFETs arrays have to survive at least this period of time with a high yield, while submerged into culture medium maintained at 37°C. Moreover, insulation between nanoFETs has to be ensured. We have thus chosen a high dielectric material, HfO₂, deposited by atomic layer deposition (ALD) as an encapsulation layer to protect the surface. ALD is expected to provide low defect deposited materials, enabling a reduction of the dielectric thickness compatible with the further step of neuron growth.

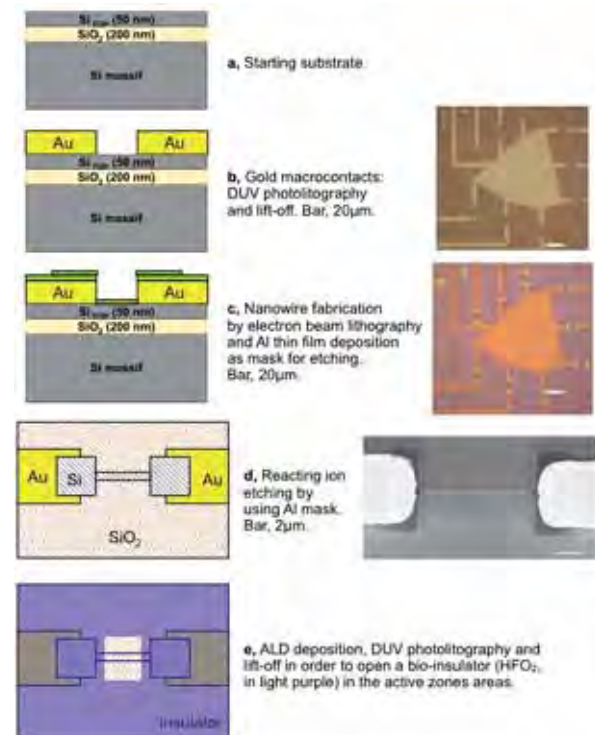


Fig. 1. Main technological steps leading to the fabrication of field effect nanotransistor (nanoFET) arrays.

2.2 Neuron alignment on nanoFETs

For the proper placement of cells in the active zone area, we used patterning adhesion techniques based on UV lithography and lift-off of poly-L-lysine that promotes neuron adhesion to the surface [3].

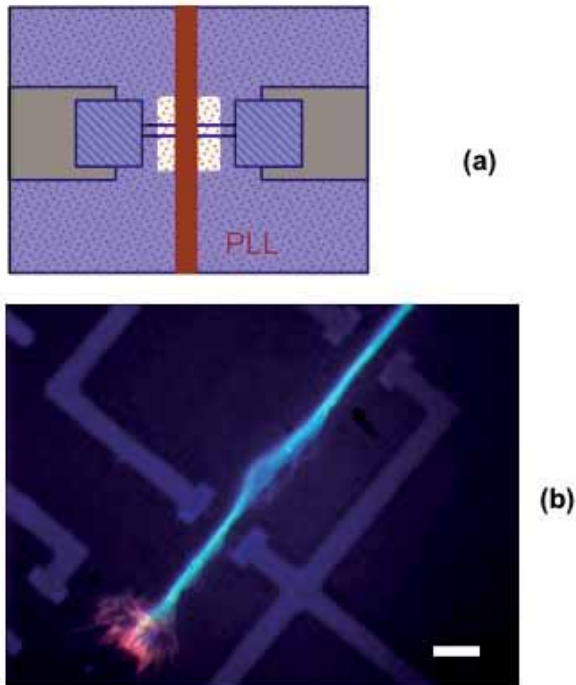


Fig. 2. (a) Adhesive Poly-L-lysine patterning made from UV lithography and lift-off. (b) Immunolabelled neurite crossing two nanoFETs. Actin in red (growth cone) and tubulin in green. Bar, 5 μm .

2.3 Control electronics of nanoFETs

We have developed, with the support of the electronic pole of the Néel Institute, an original instrumentation allowing to follow the propagation in real time of a neural signal within a triangular network instrumented by 12 nanoFETs (sampling frequency of 100 kHz). This detection is based by the generation, by micro controllers, of monophasic voltage pulses at a frequency of 100 Hz. These voltage signals are then converted into biphasic current pulses that feed the nanoFETs while avoiding thermal or electrochemical offsets.

3 Summary

Well-defined nanotransistors have been obtained by this approach and first tests are still in progress. We have performed preliminary experiments of contrast adhesion and subsequently correct soma positioning and neuritic guidance in the active nanofabricated areas.

Acknowledgement

We thank the “Programme Physique-Chimie pour le Vivant” of the french research national agency (ANR) and the Nanoscience Foundation (Grenoble) for their supports.

References

- [1] F. Patolsky, B. Timko, G. Yu, Y. Fang, AB Greytak, G. Zheng and CM Lieber (2006). Detection Stimulation and Inhibition of neuronal signals with high-density nanowire transistor arrays. *Science*, 313, 1100-04
- [2] R. A. Kaul, N. I. Syed and P. Fromherz (2004). Neuron-Semiconductor Chip with Chemical Synapse between Identified Neurons, *Phys. Rev. Lett.* 92, 038102-1-4.
- [3] S. Gory-Fauré, J. Brocard, P.O. Amblard, A. Depaulis, P. Salin, E. Dumas, S. Roth et C.Villard, Ordered Neural Networks Grown on Patterned MEA, *In: Stett A (ed). Proceedings MEA Meeting 2006. Stuttgart: BIOPRO Baden-Wuerttemberg GmbH 2006*; 194-195.

Culture Techniques

NbActiv4 medium improvement to Neurobasal/B27 increases network activity which scales exponentially with synapse density

Gregory J. Brewer¹, Torrie T. Jones¹, Michael D. Boehler¹, R A Pearson¹, A A DeMaris¹, A N Ide¹, Bruce C. Wheeler²

¹ Southern Illinois University School of Medicine, Springfield, IL USA

² University of Florida, Gainesville, FL USA

We find spike rates of 0.5/second (Hz) for rat embryonic hippocampal neurons cultured in Neurobasal/B27, lower than cultures in serum-based media and offering an opportunity for improvement. NbActiv4TM was formulated by addition of creatine, cholesterol and estrogen to Neurobasal/B27 that synergistically produced an 8-fold increase in spontaneous spike activity. The increased activity with NbActiv4 correlated with a 2-fold increase in immunoreactive synaptophysin bright puncta and GluR1 total puncta. Characteristic of synaptic scaling, immunoreactive GABA α puncta also increased 1.5-fold and NMDA-R1 puncta increased 1.8-fold. Resting respiratory demand was decreased and demand capacity was increased in NbActiv4, indicating less stress and higher efficiency. We also found that while synaptophysin synapse density increased linearly with development, spike rates increased exponentially in developing neuronal networks. Synaptic receptor components NR1, GluR1 and GABA-A also increase linearly but with more excitatory receptors than inhibitory. These results suggest that the brain's information processing capability gains more from increasing connectivity of the processing units than increasing processing units, much as internet information flow increases much faster than the linear number of nodes and connections. They also show that NbActiv4 is an improvement to Neurobasal/B27 for cultured networks with an increased density of synapses and transmitter receptors which produces higher spontaneous spike rates in neuron networks.

1 Background/Aims

The most interesting property of neurons is their long-distance propagation of signals as spiking action potentials. Since 1993, Neurobasal/B27TM has been used as a serum-free medium optimized for hippocampal neuron survival. Neurons on microelectrode arrays (MEA) were used as an assay system to increase spontaneous spike rates in media of different compositions. Neuronal network output in the cortex as a function of synapse density during development has not been explicitly determined. Synaptic scaling in cortical brain networks seems to alter excitatory and inhibitory synaptic inputs to produce a representative rate of synaptic output. Here, we cultured rat hippocampal neurons over a 3 week period to correlate synapse density with the increase in spontaneous spiking activity. We followed the network development as synapse formation and spike rate in two serum-free media optimized for either a) neuron survival (Neurobasal/B27) or b) spike rate (NbActiv4).

2 Methods/Statistics

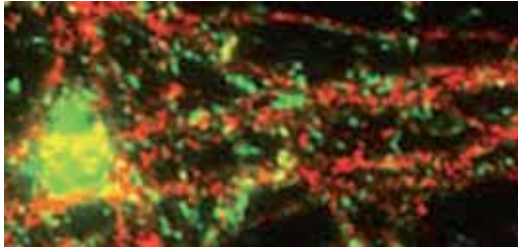
Spontaneous activity was recorded for rat embryonic hippocampal neurons plated at 500 cells/mm² in either Neurobasal/B27/Glutamax or

NbActiv4 on MEAs from Multichannel Systems (30 μ m diameter electrodes, 200 μ m spacing). Immunocytochemistry for synaptic markers GABA receptor- α , NMDA receptor NR1, synaptophysin or glutamate receptor GluR1 was performed on cultures plated at 160 cells/mm² on glass coverslips. Digital analysis of synapse density was conducted with Image-Pro software to avoid double counting and long strings of unresolved synapses. Student's t-test or 2-factor ANOVA was used to determine differences in conditions.

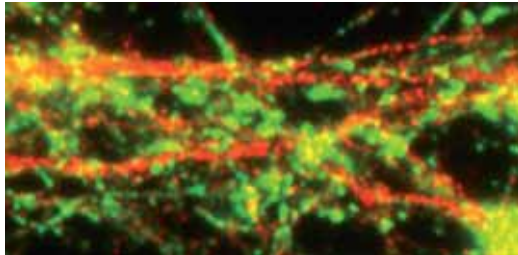
3 Results

We find spike rates of 0.5/second (Hz) for rat embryonic hippocampal neurons cultured in Neurobasal/B27, lower than cultures in serum-based media and offering an opportunity for improvement. NbActiv4TM was formulated by addition of creatine, cholesterol and estrogen to Neurobasal/B27 that synergistically produced an 8-fold increase in spontaneous spike activity (Brewer et al., 2008). The increased activity with NbActiv4 correlated with a 2-fold increase in immunoreactive synaptophysin bright puncta and GluR1 total puncta (Fig. 1).

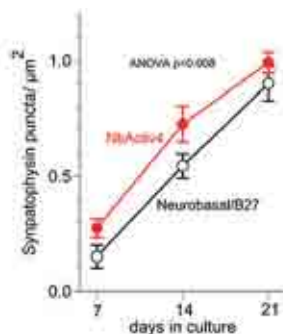
A) Synapses in Neurobasal/B27 at day 14



B) Synapses in NbActiv4 at day 14



C) Synaptophysin



D) GluR1 counts

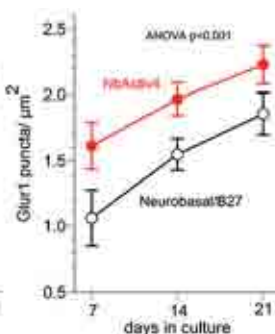


Fig. 1: Synapses stained for synaptophysin (green) and postsynaptic AMPA receptors GluR1 (red). Immunostain at 14 days for neurons cultured in A) Neurobasal/B27, B) NbActiv4, development of synapse density measured as C) synaptophysin, D) GluR1 counts. From Brewer et al. *J. Neural Eng.* 6 (2009) [PM:19104141](#)

Characteristic of synaptic scaling, immunoreactive GABA β puncta also increased 1.5-fold and NMDA-R1 puncta increased 1.8-fold. Resting respiratory demand measured as oxygen consumption was decreased and demand capacity was increased in NbActiv4, indicating less stress and higher efficiency. We also found that while synaptophysin synapse density increased linearly with development, spike rates increased exponentially in developing neuronal networks (Fig. 2). Synaptic receptor components NR1, GluR1 and GABA-A also increase linearly but with more excitatory receptors than inhibitory.

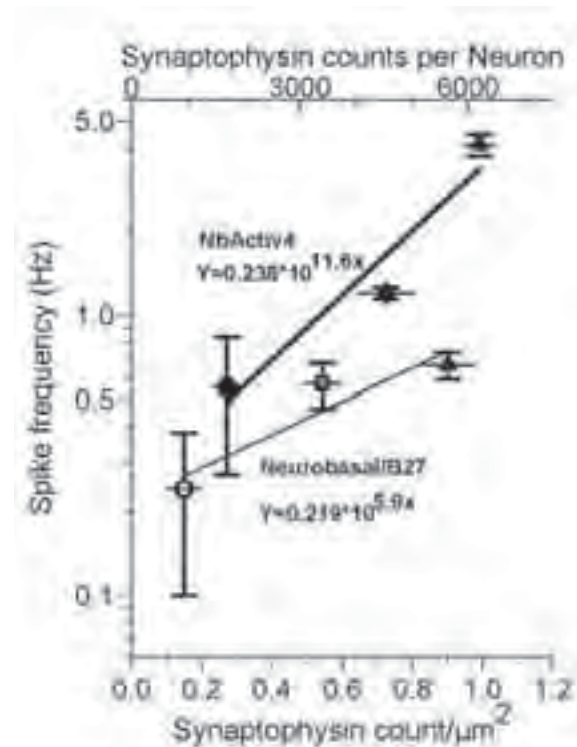


Fig. 2: The frequency of action potentials increases as an exponential function of synapse density. From Brewer et al. *J. Neural Eng.* 6 (2009) [PM:19104141](#)

4 Conclusion/Summary

These results show that development of synapses is nearly linear with time in culture on a planar substrate. However, information flow measured as spike rate increases exponentially. The 6000 synapses per neuron that we achieved approaches the 18,000 synapses per neuron in the rat hippocampus, but is much smaller than the 50,000 synapses per neuron in the human cortex (Braitenberg & Schuz, 2004). This suggests that the brain's information processing capability gains more from increasing connectivity of the processing units than increasing processing units, much as internet information flow increases much faster than the linear number of nodes and connections. They also show that NbActiv4 is an improvement to Neurobasal/B27 for cultured networks with an increased density of synapses and transmitter receptors which produces higher spontaneous spike rates in neuron networks.

Conflict of interest

Brewer receives royalties from invention of Neurobasal, B27 (trademarks of Invitrogen) and NbActiv4®. He also owns BrainBits LLC, the manufacturer and supplier of NbActiv4.

The full report of this work is published in J. Neural Eng. 6 (2009) 014001 doi:10.1088/1741-2560/6/1/014001

References

- [1] G. J. Brewer, M. D. Bohler, T. T. Jones, and B. C. Wheeler. 2008. NbActiv4 medium improvement to Neurobasal/B27 increases neuron synapse densities and network spike rates on multielectrode arrays. *J Neurosci. Methods* 170:181-187.
- [2] V. Braitenberg and A. Schuz. Density of Neurons. In: *Cortex: Statistics and geometry of neuronal connectivity*, 2nd edition, Springer, Berlin: 2004, p. 19-35.

Towards in-vitro neuronal network models: In-vitro dual compartment neurofluidic system and functional connectivity in physically isolated neuronal cell culture

Kanagasabapathi Thirukumaran T.¹, Ciliberti Davide¹ and Decré Michel M.J.¹

¹ Minimally Invasive Healthcare Department, Philips Research Laboratories Eindhoven, High Tech Campus 34(23), 5656 AE Eindhoven, The Netherlands.
E-mail: thiru.kanagasabapathi@philips.com

In-vitro neural network models are promising tools for gaining insight into many chronic brain diseases and their treatment options. As a first step towards building such in-vitro neural network models, we demonstrate a dual compartment neurofluidic system with inter-connected microchannels to connect neurons from their respective compartments on a planar microelectrode arrays (MEAs). Cell culture protocols of dissociated rat cortical neurons in such devices, axonal growth through microchannels, and analyses of functional connectivity between compartments through electrophysiological studies are presented in this work.

1 Introduction

We aim to provide insights into pathological neurodegenerative diseases and their treatment modalities that lack sufficient understanding by developing an in-vitro neuronal network system that supports specific neuronal pathways. In continuation of our work presented at the MEA Meeting 2008 [1], we present our progress in the development of a dual-compartment neurofluidic device with microchannels connecting the two compartments, integrated with Micro-Electrode Arrays (MEAs), and results of electrophysiological recordings. In the present work, we discuss protocols for successfully maintaining cultures of dissociated rat cortical neurons in such devices for long-term studies (up to DIV 35), inter-compartment neurite growth through histological staining and analyses of functional connectivity between compartments through electrophysiological studies.

2 Methods

As per the approved protocols for the care and use of lab animals in the Netherlands, primary cultures of Rat embryonic cortical neurons were prepared as reported in earlier work [2]. Polydimethylsiloxane (PDMS) devices [3] used for this study have two microfluidic compartments with the microchannels preventing the movement of cells between compartments [4]. The preparation of Microelectrode arrays (MEAs) and the integration of PDMS devices to MEAs are reported elsewhere [2]. The electrophysiological network activity from the device was acquired using a MEA1060 system

[MEA 1060-Inv-Standard amplifier, MultiChannel Systems, Germany]. With the total medium volume of the reservoirs being 0.24 ml, particular care was taken to prevent excessive evaporation during the recording sessions. A sterile recording box was custom built to maintain 90% relative humidity and 5% CO₂ supply. Electrophysiological recordings were analysed using the Spike manager toolset [5].

3 Results and discussion

The cells in the compartments were provided with nutrients by the medium contained in the two reservoirs connected to the compartments. Each reservoir, with a volume of ~60µl provides sufficient nutrients for the culture. However, later in their developmental stage (~DIV 7), the cells in the centre of the compartment were observed to be depleted with oxygen and other nutrients. This resulted in cell death in the centre of the compartment propagating towards the periphery. To circumvent the issue of low oxygen and supplement availability to the cells, the culture medium in the reservoir was changed at more frequent intervals. Cultures with a medium change frequency of three times per week are electrophysiologically active for up to DIV 35.

Visual observation of the culture over the developmental period indicates neurite growth across the compartment from DIV 3. Neurites were observed to cross-over to the adjacent compartment through the microchannels along the whole length of the compartment (8 mm). NeuN and Neurofilaments histological staining shows the presence of extensive dendritic and axonal

arborization within the compartment of origin, as well as propagation of neurites to the other compartment through the microchannels (Figure 1). Analysis of the network activity recorded from electrodes in both compartment reveals high correlation in the spontaneous activity of spike trains across the barrier.

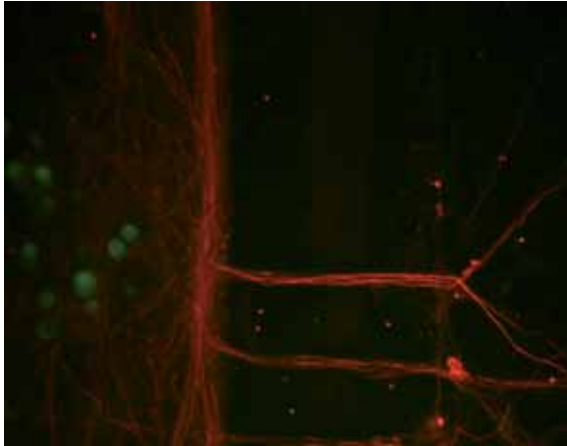


Figure 1: NeuN and Neurofilaments histological staining to show the neurite propagation through microchannels

4 Conclusion

Closed compartment neurofluidic systems similar to those presented in this work are often challenged by very low volume of medium available to the cell culture. We addressed this issue by implementing a medium change protocol that helps in supplying cells with fresh oxygen and supplements over the complete developmental period, while prolonging cell viability in the devices described. The microchannels offer the necessary physical isolation of somata between the compartments, neurites were observed to propagate through them into adjacent compartments.

Electrophysiological recordings of spontaneous activity in the dual compartment device show a strong network cross-correlation (CC) between compartments suggesting the presence of neuronal network pathways across microchannels. Cross-correlogram between one sample electrode in compartment A (Electrode 33) and all the electrodes in both the compartments is as shown in Figure 2. In this figure, correlation of network activity within the same compartment is observed to be higher than the correlation with electrodes in the adjacent compartment. Further, electrical stimulation of cells between compartments and their corresponding cross-correlation analysis confirmed functional connectivity across the compartments.

Based on the results presented in this work and on our recent progress in culturing heterogeneous

cell types in dual-compartment device, we believe the system is capable of being expanded into a

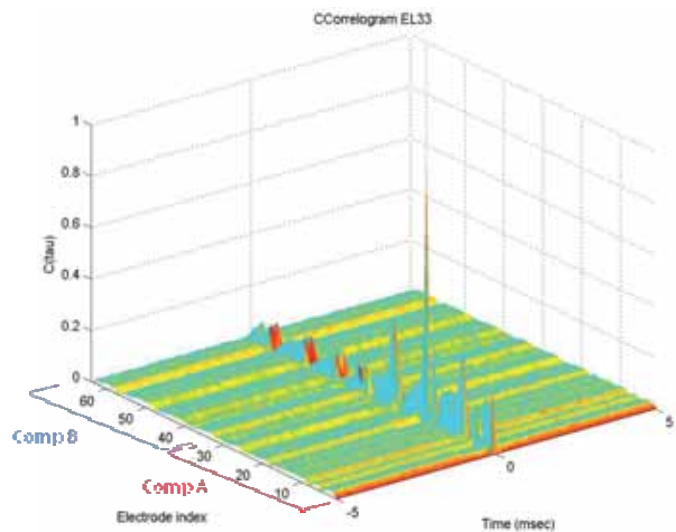


Figure 2: 3D plot of cross-correlation of spontaneous activity in two compartments

multi-compartment device with the flexibility to culture neuronal subpopulations including those of Cortical, Thalamus and Basal Ganglia, thereby providing a new tool to establish in-vitro network models for specific neuronal pathways.

Acknowledgement

TTK supported by a Point-One grant (Brainmimick project) from the Dutch government. The authors thank Prof. Sergio Martinoia for his valuable inputs in the analysis of electrophysiological data during the course of this work, for allowing us to use the Spike manager toolset and Brunella Tedesco for her assistance in histological staining presented in this work.

References

- [1] Thirukumar T. Kanagasabapathi, K.W., Ger J.A. Ramakers and Michel M.J. Décré. In-vitro compartmented neurofluidic system for studying neural networks Proceedings of MEA Meeting 2008, (Reutlingen, Germany), July 2008: p. 323-324.
- [2] Thirukumar T. Kanagasabapathi, G.J.A.R.a.M.M.J.D., In-vitro neuronal networks in PDMS-based closed-compartmented device. Proceedings of World Congress 2009, (Munich, Germany), September 2009.
- [3] McDonald, J.C., et al., Fabrication of microfluidic systems in poly(dimethylsiloxane). *Electrophoresis*, 2000. 21(1): p. 27-40.
- [4] Taylor, A.M., et al., Microfluidic multicompartiment device for neuroscience research. *Langmuir*, 2003. 19(5): p. 1551-1556.
- [5] A. Vato, L. Bonzano, M. Chiappalone, S. Cicero, F. Morabito, A. Novellino, G. Stillo, Spike manager: a new tool for spontaneous and evoked neuronal networks activity characterization. *Neurocomputing*, 2004. 58-60: p. 1153 - 1161

Oscillatory activity in murine Langerhans islets

Udo Kraushaar^{1*}, Martina Düfer², Gisela Drews², Elke Guenther¹ and Peter Krippeit-Drews²

¹ Dept. of Electrophysiology, NMI Reutlingen, Germany

² Department of Pharmacology, University of Tübingen, Tübingen, Germany

* Corresponding author. E-mail address: udo.kraushaar@nmi.de

The islets of Langerhans consist for more than 80% of beta-cells regulating blood glucose level by insulin secretion. Insulin release is directly linked to cell metabolism in stimulus-secretion coupling (SSC). Glucose-induced mitochondrial ATP production increases the ATP/ADP ratio next to ATP-dependent K⁺ channels (K_{ATP} channels), thus inhibiting these channels. The corresponding depolarization opens voltage-dependent Ca²⁺ channels resulting in Ca²⁺ influx and eventually exocytosis of insulin-containing vesicles. During constant glucose concentrations between ~6 and ~20 mM Ca²⁺ action potentials are grouped in bursts, leading to oscillatory activity. Oscillations in membrane potential, cytosolic Ca²⁺ concentration and insulin secretion are indicative of normal beta-cell function. Oscillations of individual islets in turn lead to overall pulsatile insulin secretion, necessary for an efficient effect of insulin on target tissues. The mechanism which induces oscillatory activity in islets at a constant glucose concentration is the rise of a Ca²⁺ induced K⁺ current (I_{K_{slow}}), consisting mainly of K_{ATP} current and SK4 current. SK4 has been identified recently [1] as a promising new target of insulinotropic substances. The methods for investigating membrane oscillations comprise imaging, sharp electrode and patch-clamp recordings, techniques which are cost intensive and require high technical skills. Here we introduce a new method using microelectrode arrays (MEA) to record electrical activity from Langerhans islets. The advantages of this approach are its simplicity and the possibility to perform high-throughput measurements, relevant factors for a test system suitable to explore new and effective anti-diabetic drugs.

1 Methods

Mouse islets were isolated by collagenase digestion of the pancreas, handpicked and cultured in RPMI 1640 medium supplemented with 10 % fetal calf serum.

After 1 day in culture single islets were transferred into a MEA bath chamber (Multichannel Systems, Germany) and positioned using a glass pipette attached to a micromanipulator. Recordings were online filtered (10 Hz - 3 kHz), sampled at 5-25 kHz and offline low pass filtered at 70 Hz. Substances were either applied by bath perfusion or added directly into the bath. All experiments were performed at 37° C.

2 Results and Conclusion

Typical oscillatory patterns recorded from an islet on a MEA are displayed in figure 1A. 15 mM glucose elicited burst activity at regular intervals of several seconds followed by periodic inactivity. This activity corresponds to the well known Ca²⁺ action potential burst activity obtained by microelectrode recording of a beta-cell (Figure 1B).

Changes in extracellular glucose level altered the burst duration which is in accordance with the physiological behaviour. The sulfonyl urea (SU) tolbutamide known to block K_{ATP} channels in beta-cells was also capable to evoke burst activity showing the mode of action of this class of insulinotropic anti-diabetic drugs in a MEA-based recording of islet electrical activity. As expected, opening of K_{ATP} channels with diazoxide silenced the signal confirming the role of K_{ATP} channels.

To summarize, MEA-based recordings of islet oscillatory activity seem to be a promising new approach to study beta-cell function and thus can serve as a novel test system to rapidly explore new and effective anti-diabetic drugs.

References

- [1] Düfer M, Gier B, Wolpers D, Krippeit-Drews P, Ruth P, Drews G (2009) Enhanced glucose tolerance by SK4 channel inhibition in pancreatic beta-cells. *Diabetes* 58:1835-1843
- [2] Drews G, Krippeit-Drews P, Düfer M (2010) Electrophysiology of Islet Cells In *The Islets of Langerhans Advances in Experimental Medicine and Biology*. Ed.: S. Islam, Springer, p. 554.

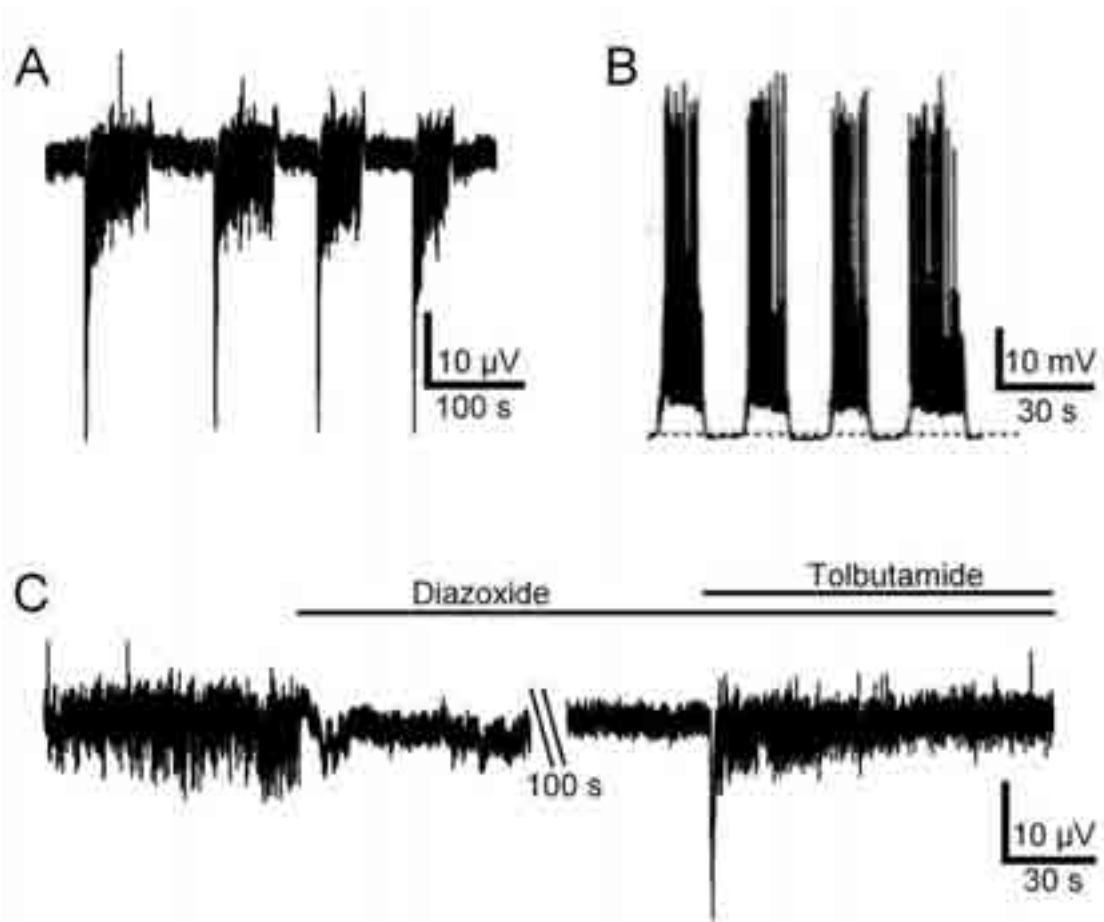


Fig. 1 Oscillatory field potentials in murine Langerhans islets. A: Periodic burst activity in 15 mM glucose. Strong negative voltage deflections indicate the beginning of the burst. B: exemplary data of intracellularly recorded membrane potential changes in the presence of 15 mM glucose in the patch-clamp configuration. Trains of Ca^{2+} action potentials alternate with periods of inactivity. Data from Drews et al. 2010. C: Pharmacological activation and inactivation of KATP channels alters the activity of the islet. In the presence of 30 mM glucose, which constantly activates the islet, stimulation of KATP channels by diazoxide suppresses the field potentials. Application of the competitive KATP channel inhibitor tolbutamide dramatically increases field potential activity. Data in A and C from same cell.

PDMS Microtunnels for MEA Recordings: Improvements in Mold Fabrication and Compatibility with Conventional MEAs

Liangbin Pan¹, Gregory J. Brewer^{2,3}, Bruce C. Wheeler^{1*}

1 J. Crayton Pruitt Family Department of Biomedical Engineering, University of Florida, Gainesville, USA

2 Department of Medical Microbiology, Immunology and Cell Biology, Southern Illinois University, School of Medicine, Springfield, USA

3 Department of Neurology, Southern Illinois University, School of Medicine, Springfield, USA

* Corresponding author. E-mail address: bwheeler@ufl.edu

We are developing a PDMS device with two wells and multiple micro-tunnels. This device is specifically designed for compatibility with MEAs from a popular vendor (MultiChannelSystems) so as to maximize use of the pre-existing electrode contacts. The mold fabrication process consists of a formation of two layers of SU-8 film. We reordered the fabrication steps to permit alignment of the tall mask to the small tunnel mold structures. This eliminates the complex but commonly used but steps involved in the creation of intermediate metal alignment patterns (sputtering, photolithography and etching). PDMS is then cast in the SU-8 mold and the PDMS structures are aligned on the MEA, followed by cell culturing. In this paper we describe in more detail the successful fabrication of molds and PDMS tunnel devices, and have constructed two separate cortical networks connected by unidirectional axons and include data from spontaneous activity recorded using the MEA. Very near future goals are analyzing the spontaneous signals and network stimulation.

1 Introduction

Micro-devices with micro-tunnels can be used to construct predefined and compartmentalized neuronal networks to investigate neuron-neuron or neuron-glia interaction [1]-[4]. These tunnels provide a means to constrain network connectivity and perhaps dictate unidirectional growth of axons to communicate between compartments. In combination with MEAs they can facilitate research into the relationships between multiple sub-networks with defined interconnections [5]. Although creation of the microtunnel device from a mold is straightforward, the creation of the mold itself is often quite complex. Here we report a modified mold fabrication procedure that reduces that complexity.

2 Materials and Methods

2.1 Fabrication of Micro-tunnel Devices

The fabrication process of a mold consists of the formation of two layers of SU-8 film, the first layer for the thin structure of micro-tunnels and a thicker second layer for the culture wells, as shown in Fig. 1. Briefly, a standard 4-inch, single-side polished clean silicon wafer was treated on an HMDS hotplate for 1 min. Photoresist SU-8 2002 was spun on at a thickness of 3 μm , exposed with the micro-tunnel mask, post-exposure baked and developed. Then the alignment marks of the first SU-8 film on the wafer were covered. Next, the photoresist SU-8 2050

(Microchem, Inc) was spun on at a thickness of 120 μm . Then the tapes covering the alignment marks were removed and the wafer was soft-baked. The culture well mask was aligned with the alignment marks of the first SU-8 film and the second SU-8 film was exposed, post-exposure baked and developed. This eliminates the commonly used but complex steps involved in the creation of intermediate metal alignment patterns (sputtering, photolithography and

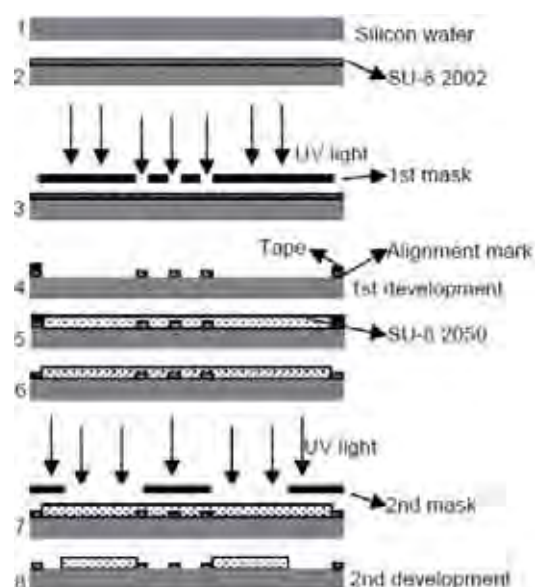


Fig. 1. Fabrication protocol for the SU-8 mold.

etching). Then mixed polydimethylsiloxane (PDMS) was poured on the wafer slowly. After the PDMS spread the whole wafer, the wafer was put on a hotplate for curing PDMS. The cured PDMS layer was peeled off the wafer and stocked for use. A customized punch was used to punch two rectangular wells for culture and another smaller circular well was punched out to expose the reference electrode of the MEA. Finally, a 3 mm thick circular PDMS ring was attached around the wells to form a chamber for holding cell culture media. Before cell culture, the surfaces of MEAs and coverslips were coated with poly-D-lysine (PDL) solution (100 $\mu\text{g}/\text{ml}$, diluted in borate buffer at a pH of 8.5) overnight. The next day the surfaces were rinsed three times by sterilized DI water and then dried. Each device was aligned with an MEA by using a customized aligner in such a way that two rows of electrodes lie underneath the micro-tunnels and each well contains three rows of electrodes.

2.2 Cell culture

Embryonic E18 rat cortical tissue was purchased from BrainBits, Inc. (Springfield, Illinois, USA) and dissociated according to the vendor's protocol. Twenty μl cell suspension was added in well A. Next the MEAs were placed in the incubator for 10 minutes. Then 300 μl of culture media was added into the media chamber of each device. After around ten days, neurons were plated in well B.

3 Results

The SU-8 mold consists of structures for micro-tunnels and culture wells, as shown in the right panel of Fig. 2.

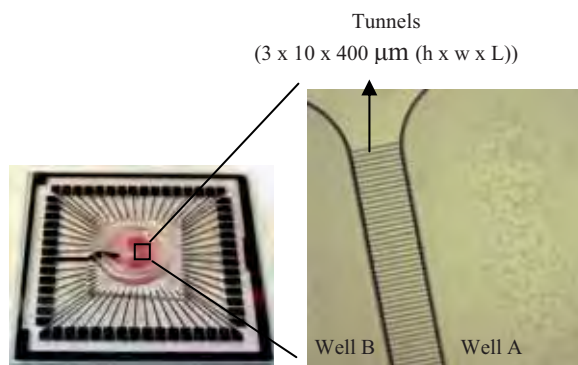


Fig. 2. Micro-tunnel device integrated with an MEA

A primary feature of the tunnel device is its ability to be easily integrated with an MEA, as shown in the left panel of Fig.2. There is no leak of cell culture media and the neurons in Well A can survive for at least one month. The axons of the neurons in Well A grow through the tunnels and reach Well B about 6 days after plating. Then the cells plated later in Well B form connections with the axons from well A. In this way, two separate networks connected with

unidirectional axons are formed from Well A to Well B. Spontaneous activity was recorded on DIV 10 of the cells in Well A, B, and within the tunnels. Fig.3 shows tonic spikes recorded by the two rows of electrodes underneath the tunnels. By comparing the timing of spikes from the same tunnel (i.e., a cross correlogram), the time delays of the spike propagation from one electrode to another can be measured and verified the presence of unidirectional propagation of spikes along the tunnels.

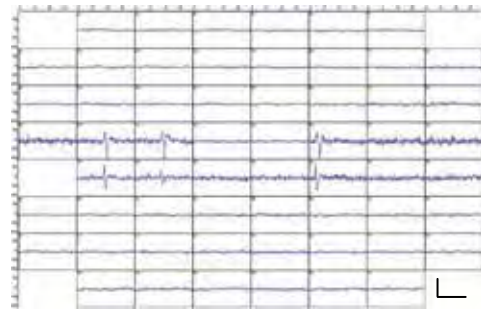


Fig. 3. Spontaneous activity recorded from the MEA with tunnels (Scale 100 μV , 10 ms).

4 Conclusions

A PDMS device with two culture wells and multiple microtunnels were fabricated and integrated with a commercial MEA. Then the unidirectional connections between two networks were formed and spontaneous and electrophysiological activity in the tunnels were recorded.

Acknowledgement

This work was supported in part by National Institute of Health research grant PHS 1 R01 NS052233.

References

- [1] Taylor A. M., Blurton-Jones M., Rhee S. W., Cribbs D. H., Cotman C. W., Jeon N. L., (2005). A microfluidic culture platform for CNS axonal injury, regeneration and transport. *Nature Methods*, 2, 599–605.
- [2] Park J., Koito H., Li J., Han A., (2009). Microfluidic compartmentalized co-culture platform for CNS axon myelination research. *Biomedical Microdevices*, 11(6), 1145–1153.
- [3] Berdichevsky Y., Staley K.J., Yarmush M.L., (2010). Building and manipulating neural pathways with microfluidics. *Lab on a Chip*, 10, 999–1004.
- [4] Shi P., Nedelec S., Wichterle H., Kam L. C., (2010). Combined microfluidics/protein patterning platform for pharmacological interrogation of axon pathfinding. *Lab on a Chip*, 10, 1005–1010.
- [5] Dworak B. J., Wheeler B. C., (2009). Novel MEA platform with PDMS microtunnels enables the detection of action potential propagation from isolated axons in culture. *Lab on a Chip*, 9, 404–410.

Recordings of electrical activity in neuronal network patterned on MEA using Micropipette drawing method

Miho Goto^{1*}, Hiroyuki Moriguchi¹, Yuzo Takayama¹, Aki Saito¹, Kiyoshi Kotani¹, Yasuhiko Jimbo¹

¹ Graduate School of Frontier Sciences, University of Tokyo

* Corresponding author. E-mail address: gotob@bmpe.k.u-tokyo.ac.jp

We developed new recording method for extracellular electrical activity of neuronal network combining MEA based recording system with our cell patterning methods "Micropipette drawing". It was confirmed that the electrical signals could be detected though there are agarose gel layer between MEA and cells. The shapes and power spectra of electrical signals are compared with those of normal culture.

1 Background

To study relationships between configurations of neuronal networks and their dynamics is one of the useful approaches to understand mechanisms of the information processing in a brain. Although there are a lot of cell patterning techniques, most of them required photo-mask fabrication process and large equipment. To overcome this, we developed a simple patterning method named "Micropipette drawing" and combined with Microelectrode Array (MEA) based recording system to detect neuronal electrical activity controlling the network configurations.

2 Methods

The surface of MEA was coated with 2 % (w/v) agarose gel to make a cell non-adhesive layer. Then the cell-adhesive solution, poly-D-lysine, were drawn onto the agarose layer by using glass pipette to make the spot patterns and line patterns. The size of patterns is 60 - 80 μm in diameter and 5 - 10 μm in width. Neuronal cells of the cortex obtained from 18 - 19 days-old rat embryos were plated and cultured on these patterns. After 7 - 13 days *in vitro*, the electrical activities were detected.

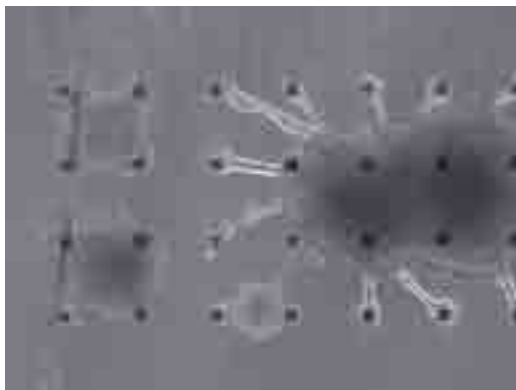


Fig. 1. Patterned neuronal networks on MEA

3 Results

The patterned networks were cultured on MEA keeping the configurations more than two weeks (Fig.1). Electrical activities detected after 17 days *in vitro* are shown in Fig. 2. The signal to noise ratio was sufficient to detect the electrical activity though the distance between cells and electrodes was larger than that of normal culture without agarose gel coating. This result suggests that this recording method combining with Micropipette drawing enables us to study the dynamics associating with its configurations.

4 Summary

We developed the simple method for recording neuronal activity in cultured network patterned on MEA combining our original technique, Micropipette drawing. This technique assists us to reveal the information processing in a brain from a fundamental level.

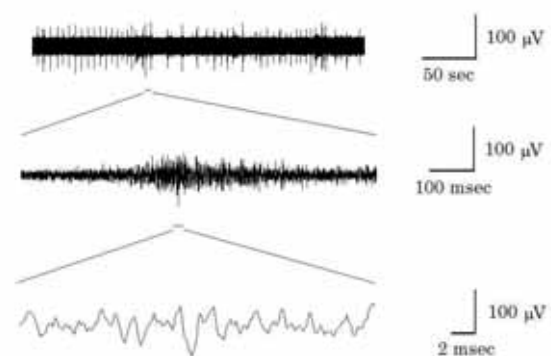


Fig. 2. Electrical activities detected from patterned cells

Collective Activation in Clustered Neuronal Assemblies of Variable Size and Topology

Mark Shein Idelson¹, Eshel Ben-Jacob² and Yael Hanein¹

¹ School of Electrical Engineering, Tel-Aviv University, Tel-Aviv 69978, Israel

² School of physics and astronomy, Tel-Aviv University, Tel-Aviv 69978, Israel

* Corresponding author. E-mail address: markshei@post.tau.ac.il

Developing neuronal networks exhibit spontaneous coordinated activity patterns in the form of synchronized bursts of action potentials. These patterns are modulated by a combination of intrinsic electrophysiological properties of single neurons and interactions between these neurons as manifested by the network morphology and synaptic connections. Consequently, mapping the network bursts (NBs) as a function of the network topology may shed light on the underlying principles governing their activity. To address this issue experimentally, we used poly-d-lysine (PDL) and carbon nanotube (CNT) based network engineering to induce self-organization of cultured neurons into clustered networks of different sizes and topologies. These clusters were coupled to micro electrode arrays (MEAs) for long term electrical activity recordings. By varying the size of the clusters from few to hundreds of neurons, we found that clusters of a few tens of neurons already exhibit NBs and that the duration and rate of NBs increases with the cluster size. Furthermore, the NBs are characterized by innate coherent network oscillations in the range of 25 to 100 Hz. We show that two clusters coupled by a bundle of extensions, exhibit both individual and mutual NBs in which mutual NBs are characterized by long activation delays (tens of ms) between the two clusters. In contrast to small clusters and uniform networks that exhibit fast and spatially distributed recruitment during NBs, networks of many connected clusters are characterized by slow sequential activation of the clusters in the network.

1 Introduction

Neuronal networks are made of basic interacting building blocks, neurons and glia cells. These networks possess well identified structural and functional characteristics which extend beyond the basic functionality of their building blocks. More specifically, developing neuronal networks exhibit spontaneous coordinated activity patterns in the form of synchronized bursts of action potentials [1]. These patterns are modulated by a combination of intrinsic electrophysiological properties of single neurons [2] and interactions between these neurons as manifested by the network morphology and synaptic connections [3]. Consequently, mapping the collective activity of the network, in addition to characterization of single neurons, is necessary for the understanding of the underlying principles governing this activity.

To experimentally address this issue, we utilized micro-patterning techniques to form small clustered networks of various sizes and topologies, coupled to micro electrode arrays (MEAs). We began by monitoring the activity of very small clusters (the smallest clusters that showed spontaneous electrical network activity) of several tens of neurons. Next, we examined how such activity varies as the networks size increases and compared it to that of large (10^6 neurons) uniform networks. Next, we investigated the interaction between pairs of coupled networks. Finally we examined the activity patterns of networks of several coupled clusters.

2 Methods

Two general approaches were used to engineer clustered neuronal networks. In the first, patterning was achieved by selective adhesion of cells to rough surfaces (using carbon nanotube (CNT) islands)[4]. In the second, patterning was achieved by selective adhesion of cells to adhesive surface chemistry (by soft lithography of Poly-D-Lysine (PDL))[5]. In the first approach, the CNT islands were used as both the patterning substrate and the electrodes. In the latter, PDL islands were patterned on top of commercial MEAs.

3 Results

Utilizing the natural propensity of neurons to cluster and by varying the pattern design and the cell plating density we were able to form four different basic network models. Uniform coating of PDL promoted the adherence and limited the mobility of cell bodies, thus resulting in uniform networks (fig. 1A). On the other hand, when plating cells on smooth surfaces with CNT/PDL islands, most of the cells attached or migrated to the rough/adhesive surfaces forming neuro-glia clusters. Patterning islands with high inter-island distances resulted in the formation of electrically isolated clusters (fig. 1B). Increasing the plating density and the island's size enabled the formation of clusters with increasing sizes. Decreasing the inter-island distances increased the

probability of adjacent clusters to connect through bundles of neuronal processes. Consequently, a large spectrum of linked clustered networks of various sizes was created, ranging from small networks of two coupled clusters (fig. 1C) to networks of several connected clusters (fig. 1D).

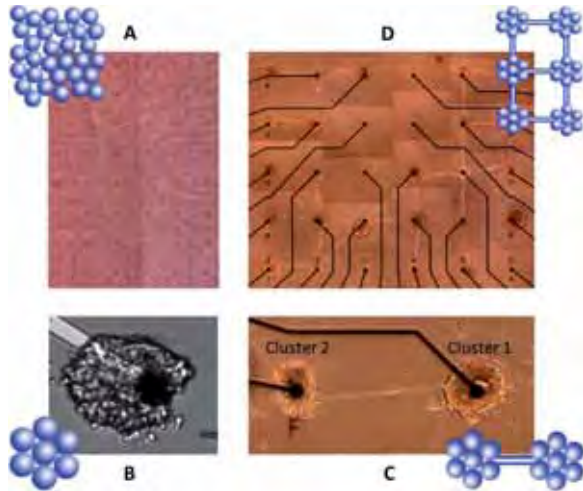


Fig. 1. Different patterning approaches result in networks with different topologies: (A) uniform network, (B) isolated cluster, (C) coupled clusters, (D) network of clusters.

The electrical activity in all of these networks was typified by spontaneous networks bursts (NBs) - short time intervals of intense collective activation followed by longer intervals of sporadic activity (fig. 2). NBs were observed even in very small clusters of several tens of neurons and their rate increased with cluster's size. In addition, isolated clusters showed persistent synchronous oscillations in the gamma frequency range (fig 2B).

The activation profile within a NB was markedly different for each of the four network models. Large uniform networks and isolated clusters exhibited similar NB profiles (fig. 2A,B). The NBs were characterized by a fast recruitment (tens of ms) of the whole population, followed by a slower decay (hundreds of ms) in the network firing rate and were activated in an all or none manner (with the exception of aborted NBs [6]). On the other hand, the NB activity propagation in coupled networks was characterized by long delays (hundreds of ms), and conditional activation (many NBs did not propagated to adjacent clusters) (fig 2C). Furthermore, in large clustered networks, NB propagation persisted over several seconds and often exhibited recurrent activation loops in which clusters were activated more than once during the same NB (fig. 2D). In addition, uniform networks exhibited a spatially distributed activation order while clustered network exhibited sequential activation through the pathways connecting the clusters.

4 Summary

Synchronized network bursting is a generic characteristic of neuronal cultures spanning networks of various sizes and topologies. Using engineered neural networks we show that NB activity profiles differ in accordance with the network topology; from all or none highly synchronized activity to conditional and sequential activation patterns.

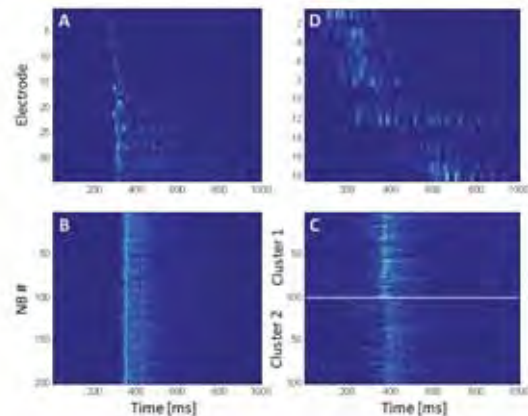


Fig. 2. The activity profiles of the 4 networks presented in figure 1. (A) and (D) show one NB recorded by multiple electrodes in a uniform network (fig. 1A) and a network of clusters (fig 1D), respectively. Electrode order was rearranged according to the activity center of mass during the NB window. (B) 200 consecutive NBs recorded from an isolated cluster (fig 1B) in which traces are temporally aligned to maximize the correlations between them. (C) 100 consecutive NBs in a network of two coupled clusters (top and bottom relate to the right and left clusters in figure 1C, respectively).

Acknowledgement

We thank Inna Brainis and Moshe David-Pur for their technical assistance.

References

- [1] Ben-Ari, Y., Developing networks play a similar melody. *Trends Neurosci*, 2001. 24(6): p. 353-60.
- [2] Shein, M., et al., Management of synchronized network activity by highly active neurons. *Phys Biol*, 2008. 5(3): p. 36008.
- [3] Baruchi, I., et al., The emergence and properties of mutual synchronization in in vitro coupled cortical networks. *Eur J Neurosci*, 2008. 28(9): p. 1825-35.
- [4] Shein, M., et al., Engineered neuronal circuits shaped and interfaced with carbon nanotube microelectrode arrays. *Biomed Microdevices*, 2009. 11(2): p. 495-501.
- [5] Sorkin, R., et al., Compact self-wiring in cultured neural networks. *Journal of Neural Engineering*, 2006. 3(2): p. 95-101.
- [6] Eytan, D. and S. Marom, Dynamics and effective topology underlying synchronization in networks of cortical neurons. *J Neurosci*, 2006. 26(33): p. 8465-76.

A Multielectrode Array Analysis of the Snail Brain

Christopher A. Harris*, Peter A. Passaro, Ildikó Kemenes, György Kemenes, Michael O'Shea

School of Life Sciences, University of Sussex, Brighton, United Kingdom

*Corresponding author. Email address: C.A.Harris@sussex.ac.uk

We have developed a technique for recording from up to 252 extracellular electrodes on the intact CNS of the mollusc *Lymnaea stagnalis*. The preparation consists of the whole CNS, pressed against the electrode array and connected by sensory nerves to the chemosensory epithelia of the esophagus and lip. A complex rhythmic pattern, characteristic of feeding, was recorded in several ganglia following stimulation with sucrose, dopamine or depolarization of a feeding-command neuron (the CV1a). The technique also allowed us to monitor the electrophysiological consequences of associative conditioning of feeding behaviour.

1 Background and methods

Planar multielectrode arrays (MEA) are often used to study organotypic brain slices or dissociated cultures of neurons. Natural synaptic connectivity and 3D structure is lost in such preparations however and stimulation of sensory tissues is not possible. Here we present a technique for using planar MEAs to record from the intact CNS of the mollusc *Lymnaea stagnalis*. Although networks in the molluscan CNS have been extensively investigated using intracellular microelectrodes, it has not previously been possible to record electrically from large numbers of neurons simultaneously. Little is therefore known about the population coding properties of, and interactions between, neural networks in the CNS.

The preparation consists of the intact brain connected by sensory nerves to the chemosensory epithelia of the esophagus and lip. A ring of blu-tack along the dish wall is used to stabilize the preparation. Thin slips of glass are used to press individual de-sheeted ganglia against the electrode array, which produces signal-to-noise ratios of up to 1:16 and allows photographs to be taken in which individual cells can be resolved (Fig. 1). Silicone perfusion tubes are inserted into the dish to transport fluid into and out of the dish. We use MEAs and software from Multi Channel Systems to record activity extracellularly at 5-10 kHz. The time from dissection to recording is approx. 20 min.

2 Results and conclusion

Complex patterns of spontaneous neuronal activity were recorded from all ganglia in the CNS. From the buccal ganglia, the region of the CNS containing the feeding central pattern generator, a rhythmic pattern of activity characteristic of feeding was readily induced either by depolarizing an identified feeding command neuron (the CV1a) or by perfusing chemosensory epithelia with 20 mM sucrose, a gustatory stimulus known to activate feeding (Fig. 1). This activity had a structure typical of feeding: duration of approx. 6 s and distinct spatio-temporal phases mirroring the protraction, rasp and swallow phases of feeding behaviour. Perfusing the CNS with 1-2 mM dopamine induced a similar rhythmic pattern of activity. Activity induced by sucrose was distributed widely throughout the CNS, notably in ganglia controlling locomotion, a behaviour that must be coordinated with feeding. The MEA also enabled us to monitor electrophysiological consequences of the associative conditioning of feeding behaviour. Many of these findings were presented in a recent publication [1].

The results suggest that MEA recording from an intact CNS enables distributed, multiple-source neural activity to be analysed in the context of biologically relevant behaviour, behavioural coordination and behavioural plasticity.

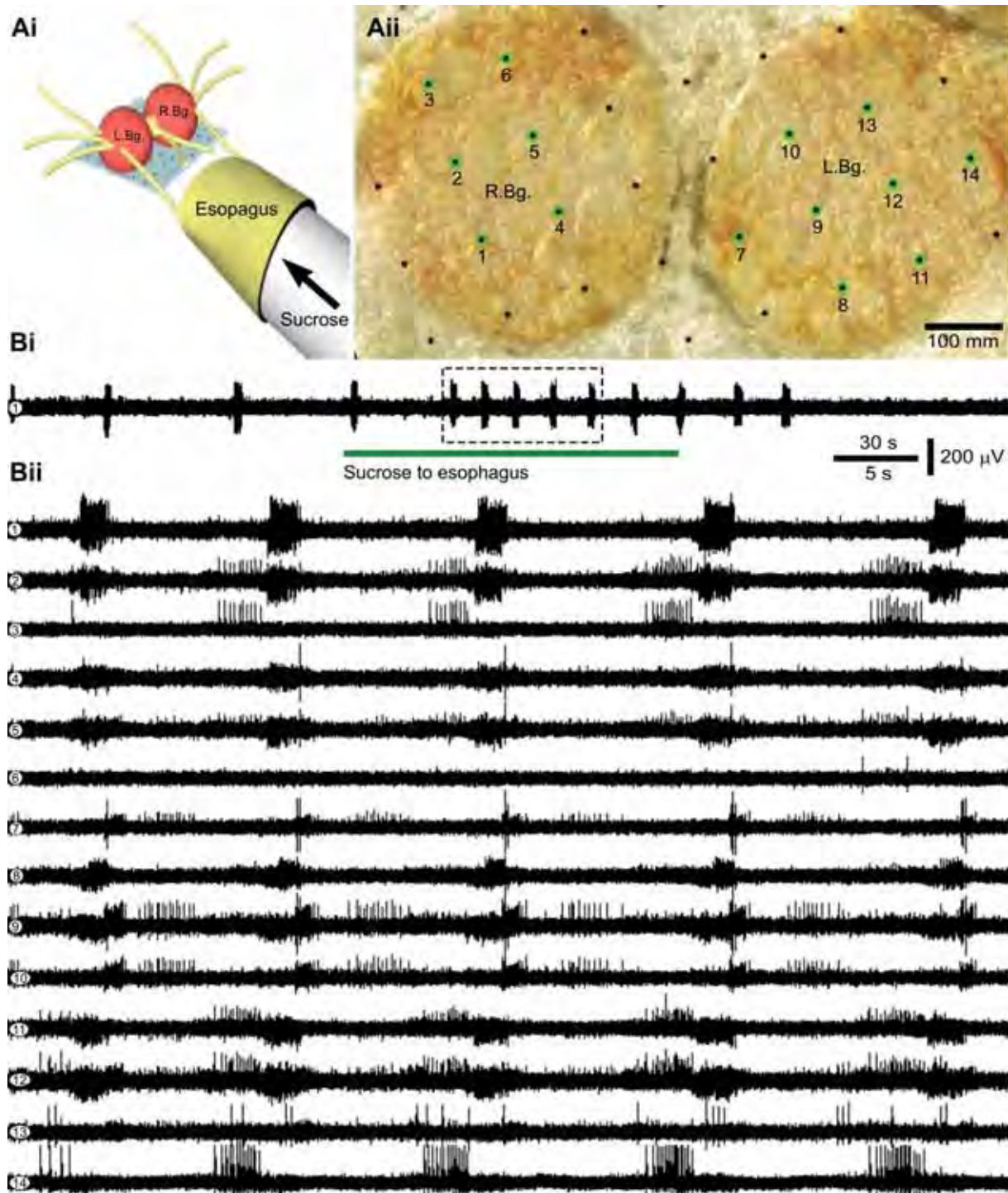


Fig 1. Multielectrode array (MEA) recording from the buccal ganglia during rhythmic feeding motor output triggered by perfusion of the esophagus with sucrose. (Ai) 3D schematic and (Aii) photomicrograph of the paired left and right buccal ganglia (L.Bg. and R.Bg.) on the MEA. Numbers indicate where the traces in (B) were recorded simultaneously. (Bi) A bout of several fictive feeding cycles was induced by perfusion of the esophagus with sucrose. The window defined by the dashed line shows the region of the recording expanded in (Bii). Each feeding cycle lasts approx. 6 s and consists of a sequential pattern of spikes and bursts that is synchronized across both buccal ganglia (see electrodes 3 and 14; 1 and 8; 4 and 7). (Figure from [1] with permission from Elsevier.)

Acknowledgement

This work was supported by the Biotechnology and Biological Sciences Research Council.

References

- [1] Harris CA, Passaro PA, Kemenes I, Kemenes G, O'Shea M. (2010) Sensory driven multi-neuronal activity and associative learning monitored in an intact CNS on a multielectrode array. *Journal of Neuroscience Methods* 186(2):171-8.

Using Three-Dimensional Cell Culture Systems On Microelectrode Arrays For Biosensing Applications

Andreas W. Daus^{1*}, Michael Goldhammer² and Christiane Thielemann¹

¹ University of Applied Sciences Aschaffenburg, BioMEMS and Bioelectronics Laboratory, Aschaffenburg, Germany

² University of Applied Sciences Aschaffenburg, Laboratory for EMC, Aschaffenburg, Germany

* Corresponding author. E-mail address: andreas.daus@h-ab.de

There is an ongoing discussion whether electromagnetic fields (EMF) at mobile phone frequencies causes health effects. Research on biological effects of EMF has primarily been done in monolayer *in vitro* studies. However, the *in situ* environment of a cell in a living organism differs from monolayer models. Cells within a tissue are organized in a three-dimensional (3D) architecture and interact with neighbouring cells and with the extracellular matrix by biochemical and mechanical cues. In monolayer studies, cultures are grown in a two-dimensional (2D) arrangement and cell-cell as well as cell-ECM interactions are obviously different from live tissue. As a novel approach, we use scaffold-free three dimensional cell culture systems, so called spheroids, on microelectrode arrays (MEA) to investigate possible impacts of electromagnetic exposure on the communication between electrogenic cells *in vitro*.

1 Introduction

Electrogenic cells and their origin tissues are since long target of research focusing on possible biological effects associated with radio frequency electromagnetic fields. Although there is only little evidence of major health risk arising from the exposure of the human body to EMF at mobile phone frequencies, some of the published results are inconsistent and obviously knowledge gaps remain.

In vitro studies are widely established to investigate possible interactions between biological tissue and EMF in a controlled environment. Therefore, cells grown in monolayer on Petri dishes are considered as an appropriate paradigm to mimic *in vivo*-like conditions. However, the *in situ* environment of a cell in a living organism differs from monolayer *in vitro* models. The aim of this study was to improve the physiological relevance of cell-based assays in electromagnetic exposure studies by using three-dimensional *in vitro* models.

2 Methods

Tissue from chicken heart and brain (stage 28-29, Hamburger and Hamilton, 1951) was mechanically dissected and enzymatically dissociated with Trypsin/EDTA. 2×10^6 cells were cultivated in 35-mm dishes containing 2ml cell culture medium (DMEM with 10%FCS and 2%CS). The dishes were placed on a gyratory shaker, allowing cells to reaggregate into scaffold-free three-dimensional spheroids. We used MEA-Chips (Multi Channel Systems, Germany) with 60 flat microelectrodes to record the electrical activity of cardiac myocyte spheroids. MEAs (Ayanda Biosystems, Switzerland) with pyramid-shaped

electrodes were employed to study neuronal spheroids. The spheroids were plated on poly-D-lysine treated MEAs and were allowed to settle down.

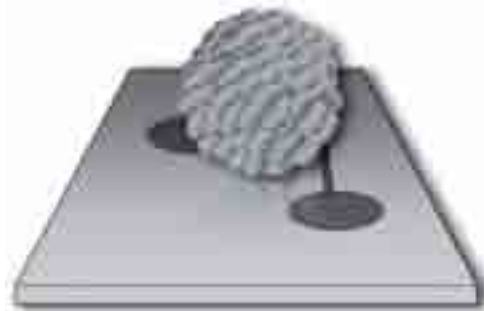


Fig. 1. Spheroid on MEA

Action potentials were recorded extracellularly with a sampling rate of 10kHz and analysed offline with a custom-made matlab-based software tool. To generate defined electromagnetic fields for exposure of spheroids, we developed a flexible TEM cell based setup. This so-called stripline consists of two metallic elements, a ground plane, and, in a defined distance above, the septum. The radio frequency energy was generated by a signal generator, amplified and fed into the septum through a coaxial connector. This resulted in a homogeneous well-defined electromagnetic field between the two metallic elements, where the biological sample was placed (Fig. 2). This setup is not based on standing waves and thus suitable for a large range of sample bins, frequencies and field strengths, respectively SAR levels. Conditions in the stripline were simulated at 900MHz by finite element (FE) calculation. Since experiments can be performed inside a CO₂ incubator, long-term exposures are possible.

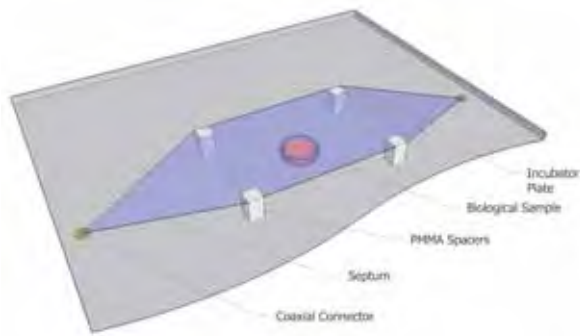


Fig. 2. Stripline

3 Results

Fully dissociated cardiac myocyte and neuronal cells from chicken embryo reaggregated to 3D spheroids within the first day *in vitro*. In case of cardiac myocytes, spheroids were self-contractile and action potentials occurred continuously with a maximum beating rate of 1.5Hz. Cardiac myocyte spheroids were contractile up to 45div, whereas in parallel experiments cardiac myocytes grown in monolayers irreversible discontinued contractions after 12div. Electrical activity of neuronal spheroids appeared in single spikes and bursts. FE-simulations were carried out to investigate the field distribution within stripline and spheroid respectively. To obtain reproducible exposure conditions, constant and homogenous fields are necessary. In the exposure setup used, we observed minor inhomogeneities at the bottom of the spheroid, but apart from that a homogeneous and well-defined electromagnetic field. The

inhomogeneities originate from the microelectrode and only affect a marginal part of the spheroid, which has a diameter of approximately 200 μ m. Hence, electrode artefacts carry less weight in spheroids compared to monolayer cultures grown on microelectrode arrays. In initial experiments, spheroids were exposed to 900MHz. Preliminary results indicate no impact of electromagnetic fields on the signal pattern of electrogenic cells.

4 Conclusion

We found, that spheroids in combination with microelectrode arrays are a novel promising tool for electromagnetic exposure studies. This approach combines a number of beneficial properties: (i) Cells within spheroids are grown in a three-dimensional architecture and resemble tissues better in terms of structural and functional properties than monolayer cultures. (ii) Cardiac spheroids are suitable to study long-term effects over several weeks, which was not feasible with monolayer cultures. (iii) Inhomogeneities in the electromagnetic field due to electrodes and conducting lines of the MEA chip have only minor influence on the field distribution within the spheroid if exposure parameters are chosen carefully. Common patch-clamp recordings could probably cause field intensifications respectively SAR inhomogeneities.

Acknowledgement

This work was supported by the BMBF (17N2208 PT-AIF).

References

- [1] Pampaloni F, Reynaud EG, Stelzer EH. 2007. The third dimension bridges the gap between cell culture and live tissue. *Nat Rev Mol Cell Biol* 8:839-845.
- [2] Bousse L. 1996. Whole cell biosensors. *Sens Actuators* 34:270-275.
- [3] Bartholoma P, Gorjup E, Monz D, Reiningger-Mack A, Thielecke H, Robitzki A. 2005. Three-dimensional *in vitro* reaggregates of embryonic cardiomyocytes: a potential model system for monitoring effects of bioactive agents. *J Biomol Screen* 10: 814-822.
- [4] Layer PG, Robitzki A, Rothermel A, Willbold E. 2002. Of layers and spheres: the reaggregate approach in tissue engineering. *Trends Neurosci* 25:131-134.

Engineering the micro electrode environment with microfluidics: A new approach for cell culture patterning or controlled chemical stimulation

Anja Kunze^{1*}, Marc Heuschkel², Michele Giugliano³ and Philippe Renaud¹

¹ Laboratory Microsystems 4, Ecole Polytechnique Fédérale de Lausanne, Switzerland

² Ayanda Biosystems SA, Lausanne, Switzerland

³ Dept. of Biomedical Sciences, University of Antwerp, Belgium

* Corresponding author. E-mail address: anja.kunze@epfl.ch

By enhancing the environment of micro electrode arrays with microfluidic channels we cultured primary neuronal cells in patterned two- and three dimensional structures. Alternatively, the same microfluidic channels can be used to generate a local chemical stimulation over a two-dimensional neuronal cell culture. We demonstrate that a significantly different of spontaneous activity pattern was recorded from the same neuronal cell culture under perfusion of 4.5 μ M bicuculline at 20 nl/s and 200 nl/s.

1 Introduction

Micro electrode arrays (MEAs) are becoming more and more commonly used for neuroscience studies. The range of applications reaches from drug tests [1], over impedance and electrophysiological studies of artificial network structures [2] to activity measurement of brain slices. Currently, neuronal cells are mostly seeded homogenously over the planar MEA, which is in contrast to their natural environment that supports three dimensions. Enhancing the MEA workspace with microfluidic channels can provide the cells with an artificial 3D structure close to their natural environment. We have designed and fabricated a microfluidic device that supports the patterning of neuronal cell cultures in 2D and 3D, or that can be used for controlled chemical stimulation of 2D cell cultures.

2 Methods

2.1 Cell culture patterning in microfluidics

Figure 1a and 1b present the concept of patterning neuronal cells in a 2D or 3D layered culture. The microfluidic channels are molded in poly(dimethyl-siloxane) (PDMS) over a silicon master. The silicon master was fabricated with standard photolithography and deep reactive ion etching. The design for the master consists of four inlets, which are leading into a main channel and one outlet. The main channel is used as a cell culture chamber. The PDMS device was bonded to a glass cover slide and treated with poly(ethylenimine) (PEI). Neuronal cells were extracted from the cortex of E19 embryonic rats. The 2D cell culture pattern is then achieved through selective injection of the cells in the

preferred inlet channels and generating a laminar flow pattern in the culture-chamber with a syringe pump. For the 3D pattern, cells were gently mixed in a liquid agarose-alginate hydrogel solution before injection, and the laminar cell layers are cooled down below the gelling temperature of the hydrogel to immobilize the pattern.

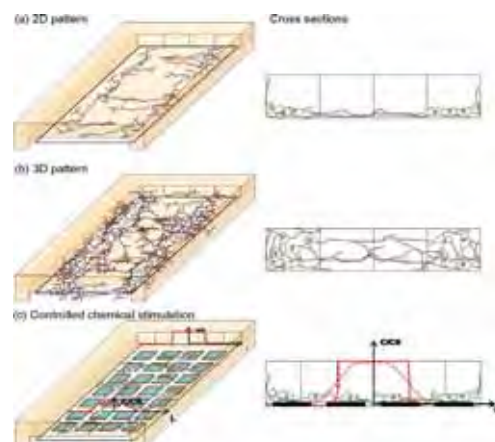


Fig. 1. Drawing of the general concept of using microfluidic channels to pattern (a) 2D neuronal cell culture, (b) 3D culture and (c) a chemical gradient over a 2D neuronal cell culture on MEAs.

2.2 Controlled chemical stimulation

For a controlled chemical stimulation, a six inlet PDMS microfluidic channel covers five rows of a standard 8 x 8 200 μ m spacing MEA, as sketched in Fig. 1c and 2. The microfluidic device was mounted over the MEA after the neuronal cell culture was fully established at 8 days *in vitro* (DIV). We used 4.5 μ M bicuculline to locally suppress inhibition of neurons in a homogenous culture of cortical neurons [3]. The GABA-A receptor antagonist, was added to serum

free culture medium and perfused over the cell culture at 20 nl/s and 200 nl/s. We assume that cells are exposed to equal velocities, because of the flat flow profile in shallow channels.

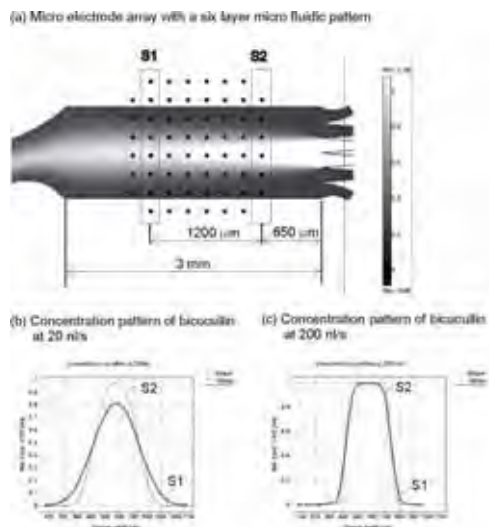


Fig. 2. The microfluidic design added to a 8 x 8 microelectrode array and the two different generated concentration profiles of bicuculline dependent on the flow rate.

3 Result

3.1 Cell culture pattern

Two-dimensional and three-dimensional structures of cortical neurons were cultured in a three layer pattern in the microfluidic device. We observed neurite extension between separated cell layer in both cultures. Viable cell cultures were measured with fluoresceine diacetate after 8 DIV. Figure 3 shows the obtained 2D and 3D neuronal cell culture patterns.

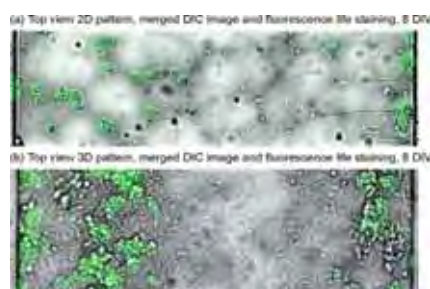


Fig. 3. (a) 2D and (b) 3D cell culture patterns and live staining after 8 DIV.

3.2 Chemical stimulation with bicuculline

A controlled chemical stimulation experiment using non-patterned 2D cell cultures is illustrated in Fig. 4. After covering the neuronal cell culture with the PDMS microfluidic device, spontaneous activity decreased. The controlled exposition of 4.5 μ M bicuculline at 20 nl/s to neuronal cells, located in the middle of the main microfluidic channel, reactivated spike and bursting activity. With a ten times higher

flow rate the burst activity increased, while no more single spikes were detected

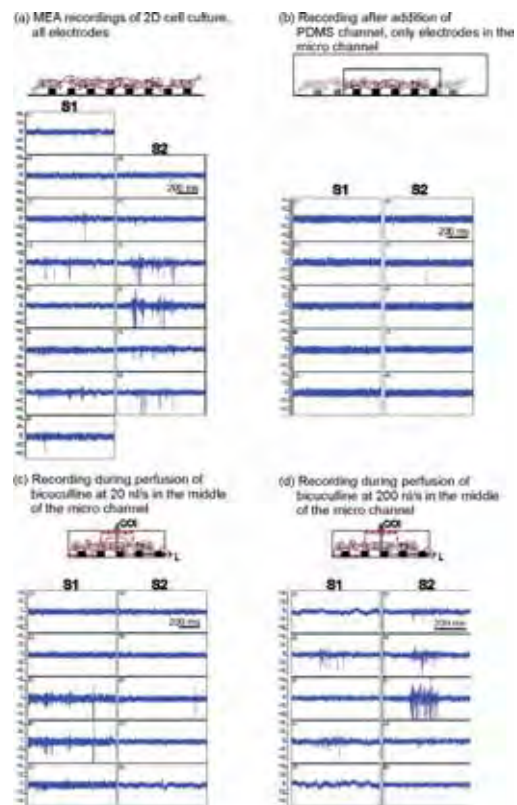


Fig. 4. MEA recordings of intrinsic (a and b) and locally stimulated activity measurement (c and d) of dissociated cortical neurons cultured for 8 DIV.

4 Conclusion

The capability of the microfluidic device to pattern two-dimensional and three-dimensional cell cultures for studies on neuronal network development has been demonstrated. The microfluidic device also allows stimulating cell cultures with a controlled chemical pattern on MEA, which can be of high interest for pharmacology and toxicology studies.

References

- [1] M. Parviz and G. W. Gross. (2007): Quantification of zinc toxicity using neuronal networks on microelectrode arrays. *NeuroToxicology*, 28, 520-531
- [2] B. J. Dworak and B. C. Wheeler (2009). Novel MEA platform with PDMS microtunnels enables the detection of action potential propagation from isolated axons in culture. *Lab on a Chip*, 9, 404-410.
- [3] X. Li et al (2007). Long-term recording on multi-electrode array reveals degraded inhibitory connection in neuronal network development. *Biosensors and Bioelectronics*, 22, 1538-1543.

Three Dimensional Recording from Neural Network Encapsulated in Hydrogel Constructs

Lee Wonhee^{1*}, Kim Euitae¹, Hynd R Mathew², Kim Sung June¹

¹ School of Electrical Engineering and Computer Science, College of Engineering, Seoul National University, Seoul, Republic of Korea

² College of Nanoscale Science and Engineering, State University of New York, Albany, New York, USA

* Corresponding author. E-mail address: wonhee88@gmail.com

Cells cultured using traditional 2D culture methods typically demonstrate a very different morphology and biochemical functions when compared to those found in vivo. Further, this cyto-architecture is difficult to compose by culturing different cells simultaneously in vitro. In this study we have developed a novel hydrogel culture system for the construction of 3D matrices for neural cell culture. The functionality of 3D-cultured neural networks has been investigated along with cell viability. In addition we have demonstrated that these cells form functional synapses and have successfully recorded neural activities from these 3D matrices using both 2D and/or 3D electrodes to show the feasibility of developed 3D culture method.

1 Introduction

Cell culture has been used as an important method in the area of neuroscience. It has been carried out with only one cell type in the specially designed structures such as planar MEA [1]. However, cellular tissues in natural brain are not composed of single cell type but several different types of cells and their structure is too complex to analyze. In addition, cultured network of neurons is too far from that in natural brain tissues because previous neuron culture has been executed on the two dimensional (2D) planar surface not on the three dimensional (3D) space. These features make the morphology of neurons and astrocytes different from those in natural brain tissue and limit the span of life of culture. As a result of these problems, the need for the development of new 3D co-culture method is increasing.

While many studies have been performed about 3D culture and co-culture, most of them have not been integrated but executed separately. Moreover, in the case of co-culture, cell types have been quite limited to stem cells and precursor cells. Nowadays, many tests have been tried to build 3D culture constructs using hydrogel materials such as collagen, polyethylene-glycol. Hydrogel materials are unique in the sense that they make oxygen and nutrients effectively transferred to encapsulated cells and that their pore size is small enough to hold cell bodies and large enough to pass the neurites of neurons by.

Until now, few studies have dealt with co-culture of neurons and glial cells – particularly astrocytes. As a consequence, the developmental patterns and life spans of these cells co-cultured in 3D hydrogel constructs have not been investigated completely.

This paper demonstrates that neural cells cultured in 3D hydrogel constructs show good viability and

form functional synapses by confocal imaging and electrical recording of neural activities using both 2D (planar) MEAs and multi-shank 3D electrodes.

2 Materials and Methods

Primary hippocampal neurons (E18) and astrocytes (P1) were encapsulated and cultured together within a thermo-gelated protein-based hydrogel, Matrigel at cell densities of ~5000 cells/uL and ~1000 cells/uL, respectively. To overcome the contraction of Matrigel constructs, and then cell death which occur when neurons are cultured at high cell density in thick hydrogel matrices, 3D hydrogel construct were polymerized and cultured on a semi-permeable membrane prior to adhesion on the microelectrode arrays (MEAs) where neural recordings were performed. Multi-shank electrodes possessing three dimensionally arranged sites were inserted in the Matrigel constructs containing functional neural networks and we recorded both spontaneous and evoked neural activities in each MEA and multi-shank electrode (Fig.1). The impedance changes of MEAs and multi-shank electrodes both before and after hydrogel polymerization were measured and validated by electrochemical impedance spectroscopy. Neural activity recording was executed using MEAs and multi-shank electrodes separately, and then results were compared. The viability of cells was confirmed through confocal microscopy after Immunocytochemical staining for III tubulin for neurons and GFAP for astrocytes.

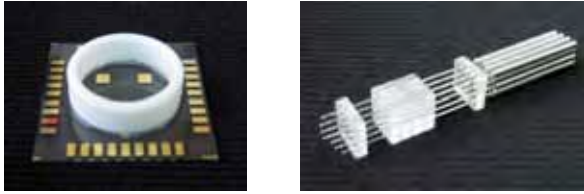


Fig. 1. MEA (Left) and Multi-shank electrode (Right)

3 Results

Neural cells were successfully cultured in 3D matrices over a period of up to 2 weeks. No significant decrease in cell viability at the concentration of 5 mg/mL of Matrigel at a cell density of 5000 cells/uL was observed (Fig.2a). Also the morphological similarity [2] of astrocytes to those in natural brain and viability of the cells in the 3D culture constructs were demonstrated through the confocal microscope imaging (Fig.2b). Impedance changes of both MEAs and multi-shank electrodes were found to not be significantly different following either coating with Matrigel (133% increased) or insertion into three dimensional constructs (275% increased). The neural activity recording by 2D MEAs and 3D multi-shank electrodes showed distinct hit-rate and different waveforms when compared to each other (Fig.3). The hit-rate of MEAs was too low to record neural activity from 3D cultured neural networks because of the distance between electrode sites and neurons. The impedance difference of electrode sites made different type signals recorded, such as action potential or local field potential.

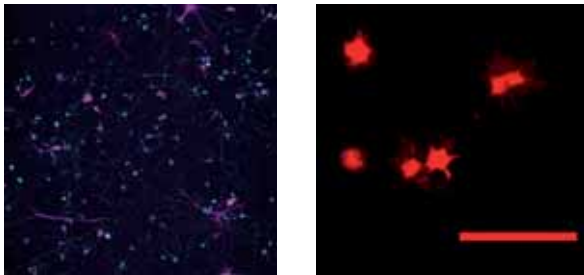


Fig. 2. a. Projected image of the 3D hydrogel culture construct (Left). b. Stellate shape of astrocytes in 3D hydrogel culture construct (Right).

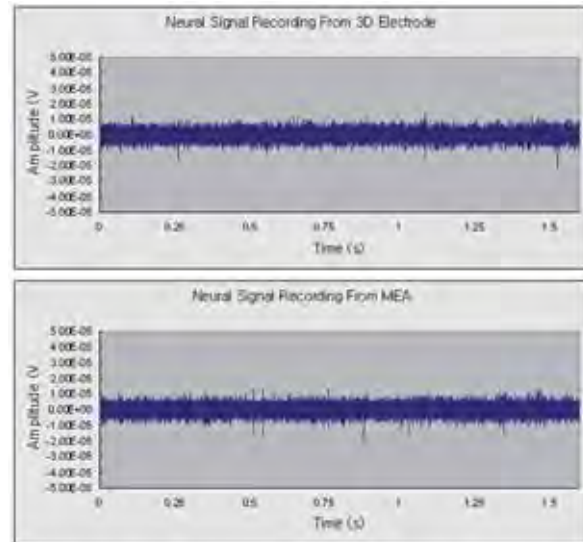


Fig. 3. Neural signal recording results both from multi-shank electrode (3D electrode, upper graph) and from MEA (lower graph).

4 Conclusion and Discussion

Neural networks can be cultured in 3D hydrogel constructs. The viability of constructs was determined using confocal imaging and immunostaining. The functionality of MEAs containing 3D constructs was confirmed by electrical recording of neural network activity. The hit-rate of neural activity recording from MEAs and multi-shank electrodes demonstrates the importance of the distance between electrode sites and neurons and the different waveforms indicates the necessity of impedance adjustment of electrode sites.

Acknowledgement

This work was supported in part by Pioneer Research Program through the National Research Foundation of Korea funded by the Ministry of Education, Science and Technology (2010-0002249) and in part by the National Institute of Biomedical Imaging and Bioengineering under Agreement Number EB007782 (M.R.H.).

References

- [1] Jun, S. B., Hynd, M. R., Dowell-Mesfin, N., Smith, K. L., Turner, J. N., Shain, W., and Kim, S. J. (2007) Low-density neuronal networks cultured using patterned poly-L-lysine on microelectrode arrays, *J Neurosci Methods* 160, 317-326.
- [2] Bushong, E. A., Martone, M. E., Jones, Y. Z., and Ellisman, M. H. (2002) Protoplasmic astrocytes in CA1 stratum radiatum occupy separate anatomical domains, *J Neurosci* 22, 183-192.

Creating Unidirectional Neural Networks on a Chip

Bradley J. Dworak¹, Kucku Varghese¹, Liangbin Pan¹, Gregory J. Brewer², and Bruce C. Wheeler^{1*}

¹ J. Crayton Pruitt Family Department of Biomedical Engineering, University of Florida, Gainesville, Florida, USA

² Departments of Neurology and Medical Microbiology Immunology and Cell Biology, Southern Illinois University, Springfield, Illinois, USA

*Corresponding author. Bruce.wheeler@bme.ufl.edu

Previously we have shown how to utilize microtunnel structures to create communicating subpopulations of neurons in separate compartments or wells. Here we report that, by timing the addition of different populations of neurons to the different compartments, unidirectional axonal growth can be established, thereby creating the potential for creating defined neural networks whose direction of connections is pre-designed. The fabrication methodology involves creating SU-8 molds and casting PDMS tunnel structures. The approach is straightforward: one well is plated with neurons and axons are allowed to grow until they are at the point of emerging into the next well. Then that well is plated, and so on. The hypothesis is that, once the first axons fill the tunnel, then axons from the second population are unlikely to grow in the reverse direction. That this is the case is supported by experiments in which the fluorescent dyes, DiO and DiI, are used to mark the different cell populations followed by fluorescence imaging at appropriate intervals. Practical guidelines for this procedure are also given. A full version of the work described in this abstract has been submitted to a fully peer reviewed journal

1 Introduction

Recently there has been an increasing interest in developing in vitro neural networks to study various aspects of brain function such as information processing and synaptic connectivity in both normal and diseased states¹⁻⁶. In order to achieve this, it is necessary to have well defined geometries of connected neurons. Currently such networks are obtained by techniques such as photolithography⁷, surface topography⁸, laser ablation⁹, microcontact printing¹⁰, and physical confinement¹¹.

In our work we have achieved a directional network by plating neurons in a PDMS chamber consisting of multiple wells linked by tunnels. Subpopulations of our network were plated at different times, thereby giving axons from earlier subpopulations the time required to extend out through the tunnels to the adjoining wells. This method isolates the axons enabling electrophysiological recordings only from axons if necessary and the sequential plating allows for very well controlled unidirectional neuronal circuits. The PDMS chambers can be easily attached to coverslips and MEAs.

2 Methods

2.1 Overall concept

The prototype consists of five square culture wells. The wells are arranged in a configuration of four periphery wells placed at 90 degree angles from the central well. A set of 11 microtunnels connects

each peripheral well to the central well. The well and tunnel structure was fabricated from casted PDMS.

2.2 Surface Preparation and Cell Culture

PDMS chambers and coverslips were plasma cleaned and attached together to form a device. These devices were then coated with PEI for 30 mins at 37°C. Devices were then rinsed multiple times with sterile water. The final rinse was left overnight in the incubator. Prior to starting the cell cultures, the devices were rinsed again multiple times with cell culture medium.

E18 cortical tissue from BrainBits LLC was treated with papain and triturated 10-15 times followed by centrifugation and re-suspension of the cell pellet. All the media from the wells was aspirated and cells (1uL vol. of cell suspension) were very carefully plated in 2 of the five outer wells and allowed to settle for 20 mins in the incubator. The chambers were then flooded with media. Once the axons were observed to have extended through the tunnels into the adjoining wells (4-7 DIV), the central well was plated in the same manner described above. Finally after another 4-7 DIV when the axons from the central well had extended into the two remaining outer wells, those wells were also plated.

Visualization of axonal growth was obtained by optical verification using DiI and DiO dyes.

3 Results

Axons were observed to grow through the tunnels into adjoining wells within 3-7 days. The times

required for this growth was dependant on the density of cells near the entrance to the tunnels. Alternating between DiI and DiO for subsequent platings made it possible to view the directionality of the neurons. Once tunnels were filled with axons in one direction, axons from the next plating did not extend back into the already filled tunnels.

Figure 1 shows a composite of images taken with red and green filters at 7 DIV. The cells in Well A were plated first (with DiI) and axons can be seen extending into the central well, Well C. Well C was plated (cells with DiO) on 5 DIV and no axons are seen extending towards Well A. Figure 2 shows a different view of the same chamber in Figure 1 with just the green filter. Axons plated on 7 DIV can be seen extending from Well C to Well E that has not yet been plated whereas as no axons are seen extending into the tunnels towards Well A which was plated before Well C.

In conclusion, our technique of wells in combination with tunnels and timed plating achieved the desired connectivity. That is, directional connections between neural populations in Well A to Well C and further on to Well E. Future applications of this technology may be useful for example, in creating defined network topologies, or among different cell populations representing different brain areas.



Fig. 1. Unidirectional growth as a result of sequential plating



Fig. 2. Neurons showing unidirectional growth

Acknowledgement

We thank the NIH for funding.

References

- [1] Feinerman, O., Rotem, A., and Moses, E.: 'Reliable neuronal logic devices from patterned hippocampal cultures', *Nature Physics*, 2008, 4, (12), pp. 967-973
- [2] Bettencourt, L.M.A., Stephens, G.J., Ham, M.I., and Gross, G.W.: 'Functional structure of cortical neuronal networks grown in vitro', *Physical Review E*, 2007, 75, (2)
- [3] Takaki, M., Nakayama, S., Misawa, H., Nakagawa, T., and Kuniyasu, H.: 'In vitro formation of enteric neural network structure in a gut-like organ differentiated from mouse embryonic stem cells', *Stem Cells*, 2006, 24, (6), pp. 1414-1422
- [4] Markram, H., Gupta, A., Uziel, A., Wang, Y., and Tsodyks, M.: 'Information processing with frequency-dependent synaptic connections', *Neurobiology of Learning and Memory*, 1998, 70, (1-2), pp. 101-112
- [5] Kudoh, S.N., Kiyohara, A., and Taguchi, T.: 'The Heterogeneous Distribution of Functional Synaptic Connections in Rat Hippocampal Dissociated Neuron Cultures', *Electronics and Communications in Japan*, 2009, 92, (6), pp. 41-49
- [6] Varghese K, Molnar P, Das M, Bhargava N, Lambert S, et al. (2010) A New Target for Amyloid Beta Toxicity Validated by Standard and High-Throughput Electrophysiology. *PLoS ONE* 5(1): e8643
- [7] Kleinfeld, D., Kahler, K.H., and Hockberger, P.E.: 'Controlled Outgrowth of Dissociated Neurons on Patterned Substrates', *Journal Of Neuroscience*, 1988, 8, (11), pp. 4098-4120
- [8] Clark, P., Connolly, P., Curtis, A.S.G., Dow, J.A.T., and Wilkinson, C.D.W.: 'Topographical Control of Cell Behavior .2. Multiple Grooved Substrata', *Development*, 1990, 108, (4), pp. 635-644
- [9] Corey, J.M., Wheeler, B.C., and Brewer, G.J.: 'Compliance of Hippocampal-Neurons to Patterned Substrate Networks', *Journal Of Neuroscience Research*, 1991, 30, (2), pp. 300-307
- [10] Branch, D.W., Corey, J.M., Weyhenmeyer, J.A., Brewer, G.J., and Wheeler, B.C.: 'Microstamp patterns of biomolecules for high-resolution neuronal networks', *Medical & Biological Engineering & Computing*, 1998, 36, (1), pp. 135-141
- [11] Suzuki, I., Sugio, Y., Jimbo, Y., and Yasuda, K.: 'Stepwise pattern modification of neuronal network in photo-thermally-etched agarose architecture on multi-electrode array chip for individual-cell-based electrophysiological measurement', *Lab On A Chip*, 2005, 5, (3), pp. 241-247

Electrodes, Surfaces and Setups

Bidirectional interfacing of carbon nanotube substrates to neuronal networks

Luca Gambazzi¹, Francesca Maria Toma², Alan Le Goff^{2,3}, Kai Fuchsberger³, Sara Cipollone², Martin Stelzle³, Maurizio Prato², Henry Markram¹ and Michele Giugliano^{1,4}

¹ Lab. of Neural Microcircuitry, Brain Mind Institute, EPFL, CH-1005 Lausanne, Switzerland

² Dept. Pharmaceutical Sciences, Univ. Trieste, P.le Europa 1, I-34127 Trieste (Italy)

³ Naturwissenschaftliches und Medizinisches Institut, Reutlingen (Germany)

⁴ Dept. Biomedical Sciences, Univ. Antwerp, Universiteitsplein 2, B-2610 Wilrijk (Belgium)

Among the materials proposed for bidirectional electrical interfacing with the central nervous system, multiwalled carbon nanotubes (CNTs) are the most interesting. Beyond excellent chemical and thermal stability, this nanomaterial has exceptional biocompatible properties (Harrison & Atala, 2007), ultra-light weight, high mechanical strength, very large surface area and excellent electrical properties (Keefer *et al.*, 2008; Gabay *et al.*, 2007). In addition, unexpected “endogenous” interactions between CNTs substrates and intrinsic neuronal and synaptic properties have been reported (Cellot *et al.*, 2008; Mazzatenta *et al.*, 2007; Lovat *et al.*, 2005). These interactions lead to speculate on the intriguing potential use of CNTs substrates to directly engineer cellular properties. For these reasons, CNTs represent an obvious choice for future neuroprosthetic devices, at the level of interfacing the neural tissue with “smart” electrodes. Along these motivations, we report a systematic study of hybrid CNTs-neuronal networks *in vitro*, explicitly taking advantage of microphotolithography and contact microprinting. We obtained thin-film depositions of CNTs over glass-substrate microelectrode arrays (MEAs), chronically coupled to cultured networks of postnatal hippocampal neurons. This allowed us for the first time to examine at the network-level, the way MWCTNs bidirectionally interacts with the spontaneous neuronal activity and its emergence *ex vivo*, as first observed at the single-cell level in Lovat *et al.* (2005) and Mazzatenta *et al.*, (2007).

1 Methods/Statistics

Hippocampal dissociated neuronal cultures were grown on glass-substrate arrays of titanium nitride (TiN) planar microelectrodes. Commercially available multi-walled carbon nanotubes (CNTs) were functionalized by the cycloaddition reaction (Georgakilas *et al.*, 2002) and solubilised in N,N-dimethylformamide (DMF) (0.01mg/mL) to be drop-casted or microprinted on MEAs as a thin-film. Commercial water-soluble oxidized CNTs were used to micro-contact printing, through PDMSbased micro-moulds, modified from (Zhou *et al.*, 2006).

Several patterns of CNTs spatial deposition and printing were considered (e.g. coating the entire MEA, only 50% of its inner area, and only few electrodes), in order to address preliminary the relationship between the spatial extent of the deposition and the impact on spontaneous and evoked electrical activity.

MEAs were sealed by fluorinated Teflon membranes, allowing multisite electrophysiological recording and electrical stimulation (Multichannel Systems GmbH, Reutlingen, Germany) inside a low-humidity (i.e. electronic-friendly) incubator at 37°C, 9% O₂, 5% CO₂, and 65% R.H., ensuring long-term stability of recording conditions. Recordings were processed off-line by custom C++ software,

identifying the time of occurrence of multi-unit activity and its typical extracellular waveforms. Subsequent data analysis was performed in Matlab (The MathWorks, Inc., Natick, MA, USA), involving the manipulation of individual spike times across the MEAs, as well as the computation of the spike times histogram (Van Pelt *et al.*, 2004).

2 Results

Electrically conductive CNT thin-films, dispersed over the entire MEA surface, neither short-cut together nor shunted functionally individual electrodes. On the contrary, they increased the electrodes sensitivity. As a result, electrodes located below CNT thin-films depositions detected extracellular activity of (~40%) higher peak amplitude. Due to the increased signal-to-noise ratios, MEAs coated by CNT thin-films further detected ~100% more spikes.

Neuronal networks growing and developing on CNT thin-films showed qualitatively the same stereotypical spontaneous emergent electrical activity of control networks: irregular alternating epochs of asynchronous firing and of short bursts of network-wide activity. However, (i) the number of bursts per minute became significantly higher after 10-12 days *in vitro*, in networks growing on CNTs. This is

consistent with our previous intracellular observations (Lovat *et al.*, 2005; Mazzatenta *et al.*, 2007). In addition, (ii) the duration of these synchronous epochs decreased compared to control. When quantified in terms of the temporal profile of the firing probability during a network burst (Van Pelt *et al.*, 2004), networks growing on CNTs displayed a (iii) significantly higher upstroke velocity (i.e. speed of ignition of a network burst).

(i)-(iii) suggest a higher degree of network connectivity, consistent with the predictions of a mathematical model of emerging irregular network bursting in cultured networks (Giugliano *et al.*, 2004).

Throughout the first three weeks *in vitro*, pairwise spike-timing cross-correlations between trains, detected at distinct MEA electrode, became progressively larger (~ 0.7 on the average, after 2 weeks) in networks growing on CNT thin-films compared to control (~ 0.3). This suggests a significantly higher functional connectivity, possibly resulting from anatomical connectivity.

Finally, when neighbouring MEA electrodes were employed to deliver biphasic extracellular stimuli in a bipolar configuration, the number of spikes elicited in the first few milliseconds following the stimulation (i.e. its so-called “direct” effect) was on the average only slightly larger than the control, in networks growing on CNT thin-films. However, the number of spikes elicited 40-50 milliseconds after the stimulation (i.e. the “recurrent” effect of the stimulus) displayed a massive increase (~ 9 folds) when comparing networks growing on CNT thin-films to control networks.

This suggests an increase in the charge-transfer efficiency of MEA electrodes, located below CNT thin-films depositions. More importantly, this result also strengthens the hypothesis of a denser synaptic connectivity and hints at a spatially extended effect of the electrical stimulation, recruiting farther units in CNT thin-films neuronal networks than in control conditions.

3 Conclusion/Summary

We focused on the recently described “endogenous” functional interactions arising when CNTs and neuronal networks are coupled. Beyond the expected improvements in terms of electrical impedance of MEA electrodes coated by CNTs, we explicitly addressed the impact on collective neuronal activity at the network-level, in the case of spatially extended CNT thin-film depositions.

Our results confirm and extend to the network-level our previous observations, carried out intracellularly at the level of postsynaptic evoked/spontaneous responses.

In addition, these results set the ground for a mechanistic interpretation of the (sub)cellular interaction between CNTs and neurons, potentially

relevant for the future neuroengineering of neuronal tissue in direct contact to CNT-based brain implants.

Acknowledgement

We are grateful to Dr. L. Ballerini, Dr. S. Grün and K.-H. Boven for discussions, and to J. Meystre, S. Garcia, and K. Antonello for excellent technical assistance.

References

- [1] Harrison BS, Atala A (2007) Carbon nanotube applications for tissue engineering. *Biomaterials* 28: 344-353.
- [2] Keefer EW, Botterman BR, Romero MI, Rossi AF, Gross GW (2008) Carbon nanotube coating improves neuronal recordings. *Nature Nanotech* 3: 434-439.
- [3] Gabay T, Ben-David M, Kalifa I, Sorkin R, Abrams ZR, *et al.* (2007) Electro-chemical and biological properties of carbon nanotube based multi-electrode arrays. *Nanotechnology* 18: 035201.
- [4] Cellot G, Cilia E, Cipollone S, Rancic V, Sucapane A, *et al.* (2008) Carbon nanotubes might improve neuronal performance by favouring electrical shortcuts. *Nature Nanotech*: 16.
- [5] Mazzatenta A, Giugliano M, Campidelli S, Gambazzi L, Businaro L, *et al.* (2007) Interfacing neurons with carbon nanotubes: electrical signal transfer and synaptic stimulation in cultured brain circuits. *J Neurosci* 27: 6931-6936.
- [6] Lovat V, Pantarotto D, Lagostena L, Cacciari B, Grandolfo M, *et al.* (2005) Carbon nanotube substrates boost neuronal electrical signaling. *Nano Lett* 5: 1107-1110.
- [7] Georgakilas V, Kordatos K, Prato M, Guldi D, Holzinger M, *et al.* (2002) Organic functionalization of carbon nanotubes. *J Am Chem Soc* 124: 760-761.
- [8] Zhou Y, Hu L, Grüner G (2006) A method of printing carbon nanotube thin films. *Applied Physics Letters* 88: 3109.
- [9] Van Pelt J, Wolters P, Corner M, Rutten W, Ramakers G (2004) Long-term characterization of firing dynamics of spontaneous bursts in cultured neural networks. *IEEE transactions on bio-medical engineering* 51: 2051-2062.
- [10] Giugliano M, Darbon P, Arsiero M, Lüscher H-R, Streit J (2004) Single-neuron discharge properties and network activity in dissociated cultures of neocortex. *J Neurophysiol* 92: 977-996.

Self-aligned growth and modification of neuronal network through electrically dynamic surfaces

Jinwon Kim¹, Sungeun Lee¹, Yoonkey Nam², Sung June Kim^{1*}

¹ School of Electrical Engineering, Seoul National University, Seoul, Republic of Korea

² Department of Bio and Brain Engineering, Korea Advanced Institute of Science and Technology, Daejeon, Republic of Korea

* Corresponding author. E-mail address: kimsj@snu.ac.kr

Planar microelectrode arrays (MEAs) as a cell-based biosensor have been widely used with dissociated neuronal cell cultures to study the signal processing of neural networks related with their geometries and to detect neurotoxins. In the application of MEAs, surface engineering techniques have provided simple, ordered neuronal networks, which have facilitated analysis of neural signal from the neural networks and neuronal recording through alignment between neuron and electrode. Here we introduce a new surface engineering technique that can provide self-aligned neuronal networks and modify network geometry during the cultivation. The method, using protein resistant property and electrically desorbable property of poly-ethylene glycol (PEG), forms the cell adhesive bio-molecular patterns by localized desorption of PEG evoked by electrical pulses and re-adsorption of the cell adhesive bio-molecules on the activated bare surface. A variety of neuronal patterns of width ranging from 5 μ m to 100 μ m were fabricated and neurons are self-aligned to a micro-electrode array by natural processes. Also, modification of neuronal network geometry during the cultivation was tried.

1 Introduction

Surface engineering techniques have provided new tools to further explore signal processing of neural networks related with their geometries. The surface patterning methods such as micro-contact printing and photo-lithography enable design of simple, ordered neuronal networks for synaptic plasticity study. However, since bio-molecular surface patterns by the current approaches are pre-determined and static before neuronal cell culture, study on functional change of neuronal network induced by their geometrical change has not been direct. Stimuli-responsive surfaces recently attracting extensive interest provide dynamic change in bio-molecular surface patterns by various external stimulations[1-2]. Application of stimuli-responsive surface to dissociated neuronal cell culture is expected to enable modification of neuronal network geometry during the cultivation and to facilitate studying functional change of neuronal network by their geometrical change.

2 Materials and Methods

2.1 Fabrication of MEAs

Cell culture plates with individually addressable electrodes were fabricated using a semiconductor process. The electrodes were fabricated with a variety of shapes including line shapes with widths ranging from 5 μ m to 100 μ m. Indium Tin Oxide (ITO, 200nm) was used as a conductive metal layer on a glass substrate. The metal patterns and contact sites were patterned by wet etching with ITO etchant (LCE-12K), following photolithography. A Teflon ring was then

attached to the culture plate with polydimethylsiloxane (PDMS, Sylgard 184; Dow Corning, Midland MI) to make a culture chamber. The commercial MEAs of Multichannel systems were used for self-alignment experiment, too.

2.2 Surface patterning of bio-molecules using electrically dynamic surfaces

We propose electrically dynamic surfaces to form patterned neuronal networks and to modify neuronal network geometry during the cultivation. The new method forms cell-adhesive bio-molecular pattern in the wet condition like cell culture condition and self-align hippocampal neurons onto electrodes by natural processes. The method uses a polymer, Poly(L-lysine)-grafted-poly(ethylene glycol) (PLL-g-PEG), with protein resistant property and electrically desorbable property. The cell adhesive bio-molecular patterns are formed by localized, electrically programmable desorption of the protein resistant polymer and re-adsorption of the cell adhesive bio-molecules. Poly(L-Lysine) label with FITC (FITC-PLL) or Laminin were used as the the cell adhesive bio-molecules. During cultivation, neuronal network modification is guided by bio-molecular pattern change using additional protein resistant polymer desorption and cell adhesive bio-molecule re-adsorption. Figure 1 shows the processes of stepwise forming the cell-adhesive bio-molecular surface patterns for modification of network geometry.

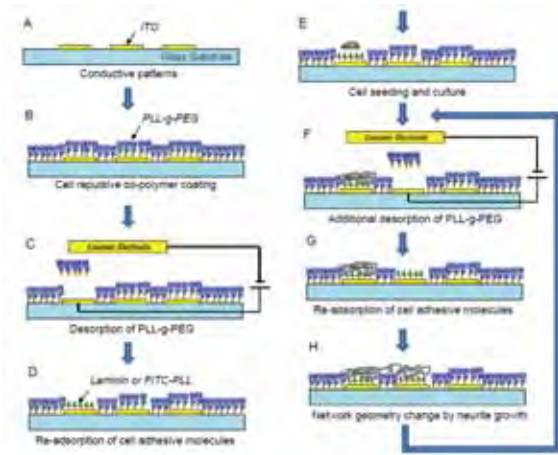


Fig. 1. The schematic of electrically dynamic surfaces

2.3 Culture and immunostaining of primary hippocampal neurons

Primary hippocampal neurons were obtained as previously described [3]. Briefly, hippocampi were obtained and dissociated from the brain of embryonic day 18 rat pups (Sprague–Dawley rats; KOATECH, Korea). They were seeded at densities of 100 cells/mm² on culture plates in serum-free neurobasal media (GIBCO) supplemented with B27 (GIBCO) and 0.5mM L-glutamine (Fluka, Biochemica, Milwaukee, WI). Cultures were maintained at 37 °C in a 5% CO₂, 95% air humidified atmosphere. Half of the media was replaced with fresh media twice a week. To identify the elongation of neuritis on the electrode surfaces, we performed immunocytochemistry at beta-III-tubulin. Hippocampal cells were fixed in cold (4 °C) 4% paraformaldehyde in HBSS for 30 minutes and immunostained with fluorochrome-conjugated antibodies (Texas Red anti-mouse, Molecular Probes, Inc., OR).

3 Results and Discussion

3.1 Formation of patterned neuronal network

Figure 2 shows the realization of a patterned neuronal network using electrically dynamic surfaces in sequence. Figure 2A shows the stable immobilization of PLL-g-PEG-TRIC (Red fluorochrome-conjugated PLL-g-PEG) on the glass substrate. The fluorescence intensity on the ITO electrode was slightly lower since ITO was less transparent than glass. The immobilized PLL-g-PEG-TRIC was completely desorbed from the ITO electrode activated by electrical pulse (Figure 2B). A 3V voltage pulse with 1 second duration was enough to initiate desorption of PLL-g-PEG. Cell-adhesive FITC-PLL pattern was formed by the selective re-adsorption onto the activated bare ITO electrode.

PLL-g-PEG, protein resistant polymer, in 10mM HEPES buffer adjusted to pH=7.4 successively blocks adsorption of FITC-PLL on unintended surfaces except the activated bare surfaces (Figure 2C). Figure 2D shows a patterned neuronal network. It was shown that cell attachment and neurite growth were confined on the ITO surface where FITC-PLL was re-adsorbed.

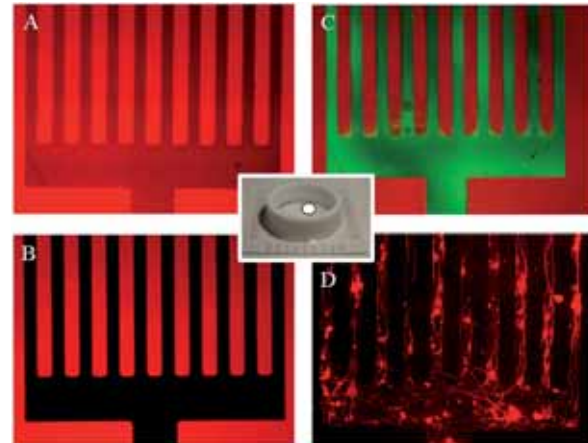


Fig. 2. The sequential realization of a patterned neuronal network

3.2 Minimum pattern size applicable to neuronal network design

To verify the minimum pattern size that can be realized by electrically dynamic surfaces, neuronal patterns with various dimensions from 5µm to 100µm are tried. Figure 3 shows the hippocampal neuronal networks of which beta-III-tubulin was immunostained with red fluorescence to identify the cell attachment and neurite elongation. The elongation of neurites along electrodes as well as cell clustering was more obvious on the narrow electrodes, as expected. It is known that the dimensions of the cell adhesive protein patterns influence the compliance of the hippocampal neurons [4]. Cell clustering decreased considerably on large electrodes. Cell attachment was rarely observed on the PLL-g-PEG modified glass regions surrounding the ITO electrodes.

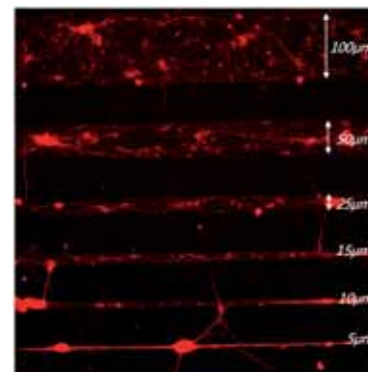


Fig. 3. The neuronal networks formed on electrodes with diverse dimensions

3.3 Self-alignment of neurons onto micro-electrode array

Figure 4 shows the hippocampal neurons self-aligned to the micro-electrodes for facilitated electrical recording. It is known that the efficiency of neuronal recording depends on the alignment between neuron and electrode [5-6]. When the cell body is partially covering the electrode surface, the amplitude of recorded neural signal is proportion to the ratio of the covered electrode area and the entire electrode area. That is to say, the correct alignment increases the amplitude of recorded neural signal by reducing the leakage current through tight sealing. Figure 4 also shows that the cell attachment and neurite growth cannot be confined to the electrode surface. A 3V voltage pulse with a long duration of 20 second was applied.

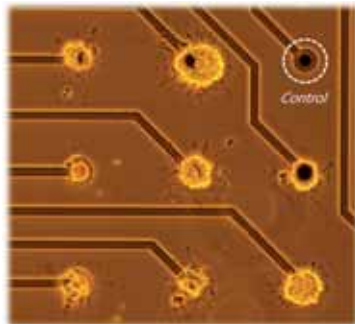


Fig. 4. Self-aligned neuronal network

3.4 Network geometry modification during the cultivation

Additional desorption of PLL-g-PEG and re-adsorption of cell-adhesive molecules during the cultivation result in the obvious change in neuronal network geometry by neurite growth on top of the added cell-adhesive molecular patterns. The cell death by the exposure of neurons to cell-adhesive molecules and electrical pulses for PLL-g-PEG was negligible. The immobilization of PLL-g-PEG in the culture media was stable enough to block adsorption of cell-adhesive molecules on unintended surfaces during the additional re-adsorption process.

4 Conclusion

The proposed method as neuronal cell patterning method provides a self aligned patterning of neurons to microelectrodes and a neuronal network geometry modification during the cultivation. The electrically dynamic surfaces of the PLL-g-PEG are flexible with regard to the choice of cell adhesive molecules. The proposed method can be easily combined with other conventional surface patterning methods. We expect this new method can be a useful tool to facilitate study on functional change of neuronal network by their geometrical change.

Acknowledgement

This work was financially supported by the Technology Innovation Program (10033657) funded by the Ministry of Knowledge Economy (MKE) of Korea and the Brain Korea 21 Project, the Department of Electrical Engineering, Seoul National University.

References

- [1] Mendes, P.M. (2008) : *Stimuli-responsive surfaces for bio-applications*. Chem Soc Rev, **37**(11), 2512-29
- [2] Tang, C.S., et al. (2006): *Dynamic, electronically switchable surfaces for membrane protein microarrays*. Anal Chem, **78**(3), 711-7
- [3] Dowell-Mesfin, N.M., et al. (2004): *Topographically modified surfaces affect orientation and growth of hippocampal neurons*. J Neural Eng, **1**(2), 78-90
- [4] Corey, J.M., B.C. Wheeler, and G.J. Brewer (1991): *Compliance of hippocampal neurons to patterned substrate networks*. J Neurosci Res, **30**(2), 300-7
- [5] Buitengeweg, J.R., W.L. Rutten, and E. Marani (2002): *Modeled channel distributions explain extracellular recordings from cultured neurons sealed to microelectrodes*. IEEE Trans Biomed Eng, **49**(12 Pt 2), 1580-90
- [6] Fromherz, P., et al. (1991): *A Neuron-Silicon Junction - a Retzius Cell of the Leech on an Insulated-Gate Field-Effect Transistor*. Science, **252**(5010), 1290-1293.

Miniaturized multi-well type neural assay platform on MEAs using cell-repulsive agarose hydrogel

Yoonkey Nam^{*}, Jisoon Lim, Gaurav Goyal, Gyumin Kang

¹ Department of Bio and Brain Engineering, KAIST, Daejeon, Korea

^{*} Corresponding author. E-mail address: ynam@kaist.ac.kr.

We present a novel MEA platform based on cell-repulsive agarose hydrogel patterning technique for various MEA applications including cell-based biosensors and neurophysiological studies. This is a simple but versatile ‘add-on’ technique that can be easily adopted in plain neurobiology laboratories. The proposed approach could be an alternative for large-scale multi-well type MEAs for realizing high-throughput functional neural assay systems.

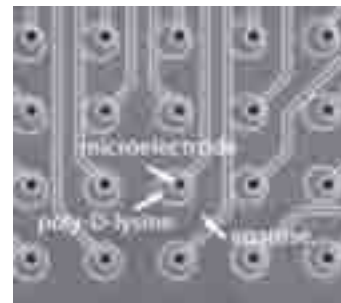
1 Introduction

High-throughput neurophysiological screening process is required to utilize dissociated neuronal networks in various MEA applications. It is desirable to have multitude of multichannel systems to probe multiple cultured neuronal networks simultaneously. To increase the throughput, multi-well type MEAs have been proposed and some are commercially available. Here, we propose a different strategy for simple experiments that do not require large number of electrodes. We used cell-repulsive agarose hydrogel to fabricate large-scale integrated microwell array on MEAs. Using this technique, various types of micro-scale neuronal networks can be formed and probed using an MEA. We show that sixty of micro-scale neuronal networks can be probed simultaneously using a single multichannel system. Some of the results were published previously [1].

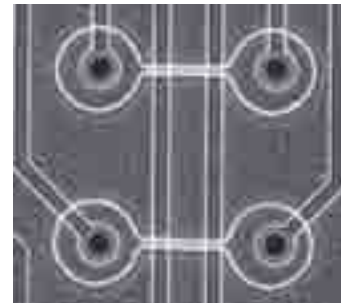
2 Methods

Agarose hydrogel structures were cast using micro-molding in capillary (MIMIC) technique. First, PDMS (polydimethylsiloxane) molds were fabricated by soft-lithography. The PDMS mold was placed on an MEA that was coated with poly-D-lysine. The patterns on the mold were aligned with microelectrodes using a custom-build contact aligner. Boiled 2%(w/v) agarose solution was filled and the whole assembly was cooled and dried for 24 hr. The PDMS mold was carefully removed and dried agarose structures (microwells and grooves) were left on the MEA surface.

Dissociated E18 rat hippocampal neurons were cultured for up to 3 weeks. Neurobasal medium supplemented with B27 was used without serum. Cell plating density was 600 – 800 cells/mm². The development of network activity was investigated by electrical recording and stimulation starting at 5 days in vitro (DIV).



(a)



(b)

Fig. 1. Fabricated agarose hydrogel structures on MEAs. (a) Multi-microwell array, (b) two microwells connected by microgrooves, ((a) from [1] - Reproduced by permission of The Royal Society of Chemistry (RSC))

3 Results

Designed agarose structures were microwells (diameter: 100 μm) and microgrooves (width: 10 μm). Microwells were aligned with microelectrodes such that each well had one electrode (diameter: 30 μm) that can record or stimulate a neuronal network inside the well. We constructed two different types of agarose structures : isolated microwell arrays and microwell networks connected by microgrooves (Fig 1).

Neurons did not adhere to background areas where agarose hydrogel was uniformly coated. It was highly repulsive to neuronal adhesion. The quality of

repulsiveness was maintained throughout the culture period. In each microwell, ten neurons were located on average and these neurons eventually formed a small neural cluster.

Concerning the spontaneous activity, isolated microwells generated spontaneous electrical activity as early as 5 DIV. Cluster networks generated synchronized bursting activity at 14 DIV. Pharmacological agents such as NMDA, bicuculline, CNQX, and AP5 modulated electrical activities from each microwells and this indicated that these networks were electrically functional through chemical synapses. In case of the clustered networks, the propagation of bursts could be measured. We also stimulated the cluster networks and recorded time-delayed responses.

4 Conclusion

In summary, we have presented a novel MEA platform based on cell-repulsive agarose hydrogel patterning technique for various MEA applications including cell-based biosensors and neurophysiological studies. This is a simple but versatile ‘add-on’ technique that can be easily adopted in plain neurobiology laboratories. The proposed approach could be an alternative for large-scale multi-well type MEAs for realizing high-throughput functional neural assay systems.

References

- [1] Kang G, Lee JH, Lee CS, Nam Y., Agarose microwell based neuronal micro-circuit arrays on microelectrode arrays for high throughput drug testing, *Lab Chip*. 2009 Nov 21;9(22):3236-42.

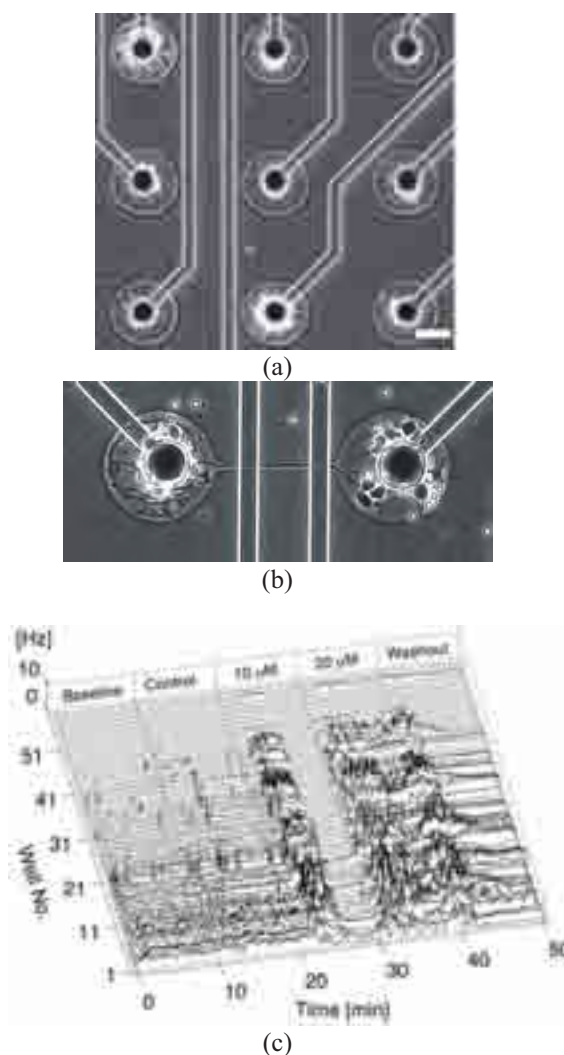


Fig. 2. Patterned neuronal networks on MEAs. (a) Micro-scale neuronal network arrays, (b) 2-node neuronal cluster network, (c) NMDA response from 60 microwells recorded from a single MEA. ((a), (c) from [1] - Reproduced by permission of The Royal Society of Chemistry (RSC))

Micro Pillar Electrodes on MEAs for Tissue Stimulation

Jochen Held*, Jens Heynen, Angelika Stumpf, Wilfried Nisch, Claus Burkhardt, Alfred Stett

NMI Natural and Medical Sciences Institute at the University of Tübingen, Reutlingen (Germany)

* Corresponding author. E-mail address: jochen.held@nmi.de

For stimulation of cells within tissue samples on MEAs, micro pillar electrodes have been developed. The micro pillars were fabricated using gold electroplating – a method applicable to every substrate. After electroplating of the pillar, a passivation layer is deposited. Insulated pillars with open tips were fabricated with a diameter of approximately 30 μm and heights between 10 and 50 μm .

1 Introduction

Depth stimulation of tissue *in vivo* or *in vitro* is a challenge for planar micro electrode arrays (MEAs). It is possible to penetrate the tissue gently with three-dimensional (3D) electrodes [1-3] to locate the electrode tip in the vicinity of the target cells. The stimulation amplitudes can thus be lower and the spatial resolution is higher than with MEAs with planar electrodes located at the surface of neuronal tissue [2,3]. In this paper we present the integration of gold (Au) pillars on glass MEAs with Ti lines and a silicon nitride (Si_xN_y) passivation layer [4]. Pillars with diameters of approximately 30 μm and a height of roughly 50 μm have been fabricated.

2 Fabrication

The fabrication process of the micro pillar electrodes is schematically shown in Fig. 1. The first fabrication steps are similar to planar MEAs [Fig. 1 (a)]. The process of micro pillar fabrication starts with the deposition of the seed layer for the later electroplating [Fig. 1 (b)]. The seed layer consists of a metal stack of titanium (Ti, 15 nm) acting as an adhesion layer and Au (145 nm). After metallisation, lithography with a thick photoresist was done [Fig. 1 (c)]. The positive photoresist AZ®40XT-11D (AZ Electronic Materials) was used. With this resist it is possible to realise resist thickness up to 60 μm in one single spin coating step. Holes with diameters of approximately 30 μm could thus be realised. These fabricated holes were used as a template for the next step the electroplating of Au [Fig. 1 (d)]. The Au was electroplated with a current density of approximately 8 mA/cm^2 . According to the overall applied charge, pillars with a height of 10 to 50 μm could be produced. The seed layer was then removed by dry etching [Fig. 1 (f)]. In the next step a passivation layer Si_xN_y was deposited [Fig. 1 (g)]. For stimulation purposes, the metal had to be exposed at the pillar tip.

This was done using a mask-less lithography and etch-back process of the photoresist [Fig. 1 (h)].

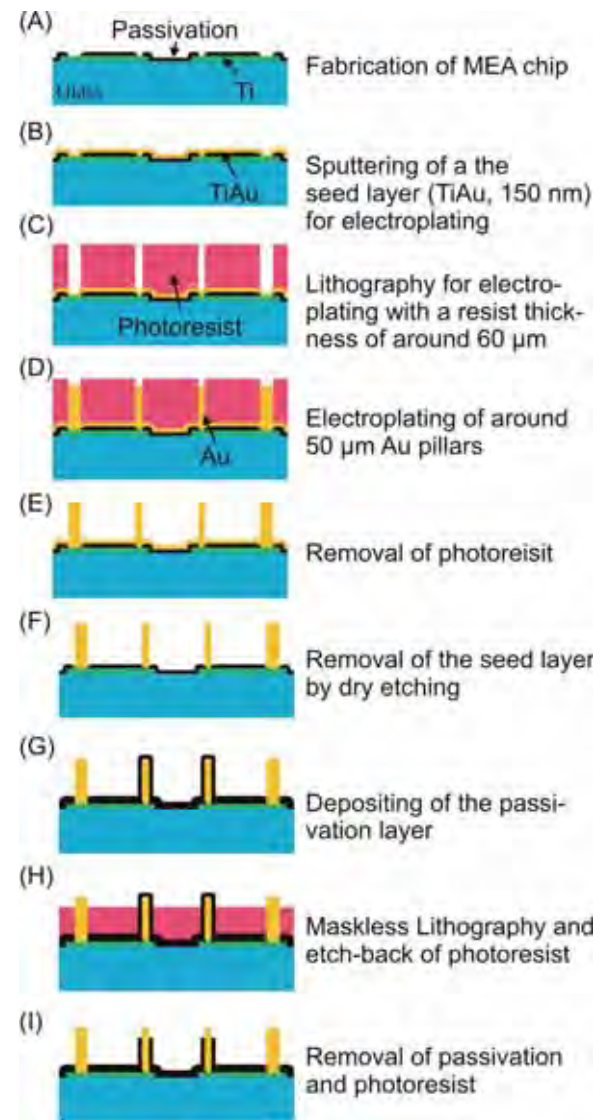


Fig. 1. Schematics of the fabrication process of Au micro pillars.

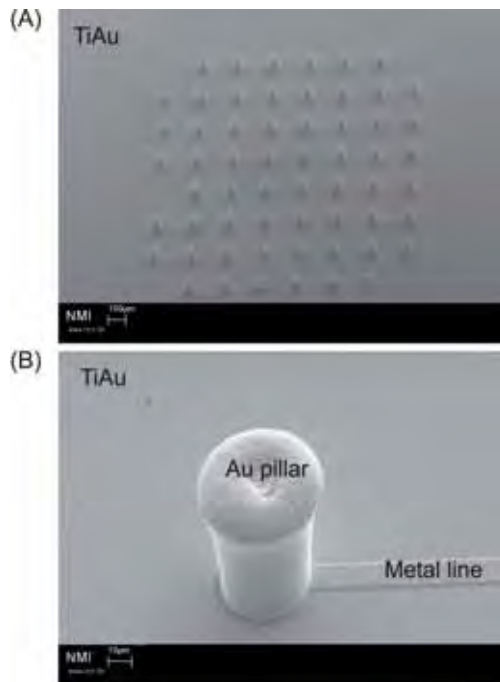


Fig. 2. SEM image of an electroplated Au pillar array after removal of the photoresist with the seed layer.

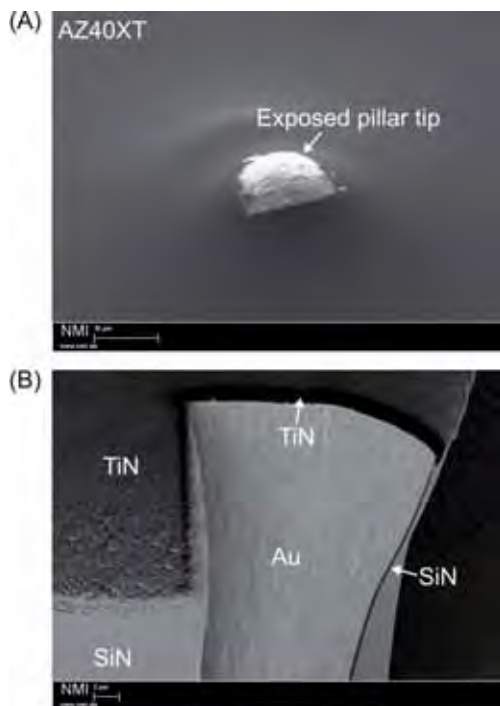


Fig. 3. SEM image (A) of an exposed micropillar tip surrounded by photoresist and (B) a cross-section of an pillar tip with TiN.

The opening process was based on references [5,6]. The pillar tip was then free of photoresist; the Si_xN_y at the tip of the pillar was removed by dry etching in a CF_4 plasma. In the last step TiN was deposited and the photoresist removed [Fig. 1 (i)].

Figure 2 shows SEM images of an Au micro pillar after electroplating and the removal of the photoresist. In Fig. 3 (A) shows an SEM image of a micro pillar embedded in photoresist after the tip opening process. Figure 3 (B) presents a cross-section of the micro pillar tip with selectively deposited TiN at the tip.

3 Conclusions

We established processes for the routine fabrication of micro pillar electrodes on planar MEAs using gold electroplating. Insulated pillars with diameters of approximately $30\ \mu\text{m}$ and heights of roughly $50\ \mu\text{m}$ and with open tips were generated. The advantage of the developed method is that it can be integrated on different MEA substrates. The developed 3D electrodes can be used for stimulation within a neuroprosthesis or for *in vitro* experiments with brain slices.

Acknowledgement

Supported by German Ministry for Education and Research (BMBF), grant 0312035A.

References

- [1] Thielecke H., Impidjati I., Zimmermann H., Fuhr G. R. (2005) Gentle cell handling with an ultra-slow instrument: creep-manipulation of cells. *Microsystems Technologies*, vol. 11, no. 11, pp. 1230-1241.
- [2] Butterwick A., Vankov A., Huie P., Vijayraghavan K., Loudin J., Palanker D. (2007) Progress Towards a High-Resolution Retinal Prosthesis. *Ophthalmic Technologies XVII*, vol. 6426A, pp. 1-9.
- [3] Loudin J. D., Simanovskii D. M., Vijayraghavan K., Sramek C. K., Butterwick A. F., Huie P., McLean G. Y., Palanker D. V. (2007). Optoelectronic retinal prosthesis: system design and performance. *J. Neural Eng.*, vol. 4, pp. S72-S84.
- [4] Stett A., Egert U., Guenther E., Hofmann F., Meyer T., Nisch W., Haemmerle H. (2003). Biological Application of Microelectrode Arrays in Drug Discovery and Basic Research. *Analytical and Bioanalytical Chemistry*, vol. 377, no. 3, pp. 486-495.
- [5] Held J., Gaspar J., Koester P. J., Tautorat C., Hagner M., Cismak A., Heilmann A., Baumann W., Ruther P., Paul O. (2009). Hollow Microneedle Electrode Arrays for Intracellular Recording Applications. *in Tech. Digest IEEE MEMS'09 Conf.*, pp. 220-223.
- [6] Held J. (2009). Microneedle Electrode Arrays for Cellular Recording Applications, *PhD Thesis University of Freiburg*.

On Microelectrode Impedance Measurements

Jarno M. A. Tanskanen^{1*}, Pasi Kauppinen¹, Tomi Ryynänen², Jukka Lekkala²,
Jari A. K. Hyttinen¹

¹ Department of Biomedical Engineering, Tampere University of Technology, Tampere, Finland

² Department of Automation Science and Engineering, Tampere University of Technology, Tampere, Finland

* Corresponding author. E-mail address: jarno.m.tanskanen@tut.fi

Microelectrode (ME) electric impedances influence the quality of the measured bioelectric signals. In this paper, we describe our impedance measurement setup utilized in characterization of our in-house produced microelectrode arrays (MEAs) and compare our MEAs with corresponding commercial MEAs. We also discuss the impedance measurements.

1 Introduction

Microelectrode (ME) electric impedances set limits to the measurable bioelectric phenomena and influence the quality of the measured signals. In this paper, we describe our impedance measurement (IM) setup utilized in characterization of our in-house produced microelectrode arrays (MEAs), and compare the impedance performance of our MEAs with the corresponding commercial MEAs (Multi Channel Systems GmbH (MCS), Reutlingen, Germany). The IM [1, 2] setup was devised to measure impedances as seen by the preamplifiers during actual cell measurements. We conclude that our in-house MEAs [3, 4] are usable from the impedance point of view. Some IM observations are also commented upon. IMs of MEA MEs have also in been addressed by Becq *et al.* [5].

2 Methods

2.1 Equipment

Impedances were measured using Solartron 1260A Impedance/Gain-phase Analyzer (Solartron Analytical, Hampshire, UK) connected to Solartron 1294A Impedance Interface, whose non-human interface was utilized. 1294A was connected to a MEA via MEA1060-Inv contacting adapter (model: MEA1060-INV-CA, MCS). Connections to the contacting adapter were made with banana-to-0.76 mm plug test adapters (model: 4691, Pomona Electronics, Everett, WA, USA).

2.2 MEAs and MEA handling procedure

We measured standard commercial 59-ME MEAs (model: 200/30iR-Ti-gr, MSC) with glass rings, electrode diameters of 30 μm and interelectrode distances of 200 μm , and a large embedded reference electrode. Our in-house MEAs [3] were topologically similar, except for an additional identical large electrode on the opposite side of the MEA for the application of greater stimulation currents creating

somewhat homogenous field over the ME area. Our electrode material was titanium with no coating, thus, the electrode surface was titanium oxide.

The MEAs were let stabilize at least over night in room temperature in isotonic saline (sodium chloride 9 mg/ml, Baxter), rinsed with distilled water, and let stabilize for at least one hour filled with the cell culture medium prior to measurement. Contact pins of the contacting adapter were cleaned with 70 % alcohol in the beginning of each measurement session and MEA contact pads were cleaned with the alcohol, wiped dry, and visually inspected for residue. Temperature of a MEA was allowed to stabilize for at least three minutes in the contacting adapter. The measurement temperature was approximately 37°C.

2.3 Impedance measurement protocol

The measurement current was set to 10 μA and the frequency range to 0.1 Hz to 8 kHz with three measurement frequency points per decade and a measurement point at 1 kHz. Frequencies were swept from higher to lower. Current settling time was set to 30 s prior to each sweep. Measurement integration time was 5 s. Data was recorded to a standard laptop PC using SMaRT software (Solartron Analytical).

The 1294A four-terminal connectors were connected as described in [2] for two-terminal configuration. In terms of Solartron 1294A connector naming conventions, “GEN HI” and “V input HI” were interconnected and connected to an ME, and “GEN LO/INPUT” and “V input LO” interconnected and connected to the embedded ground electrode. The measurement also was tested with “GEN HI” and “V input HI” connected to the embedded ground and “GEN LO/INPUT” and “V input LO” to the ME. With in-house MEAs, the ground electrode on the same side of the MEA as in the commercial MEAs was used.

3 Results

Two-terminal IM results at 1 kHz of three commercial and five in-house MEAs are shown in Fig. 1. From Fig. 1, it is seen that the commercial MEAs exhibited lower impedances and greater ME-to-ME consistency, whereas the in-house MEAs can still be taken to be well usable. Impedance spectroscopy results between two commercial and two in-house MEAs are presented in Fig. 2. Whereas the impedances of the in-house MEAs are generally higher than those of the commercial ones, the behavior of the impedance as a function of frequency is very similar. Also, as seen in Fig. 2, the impedance behavior between the MEs of a MEA is fairly consistent.

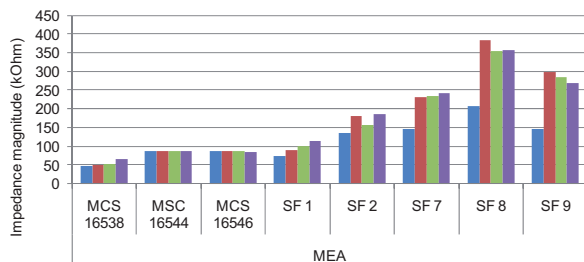


Fig. 1. Impedances measured at 1 kHz of three commercial (MSC) and five in-house (SF) MEAs. Four MEs (different color bars) were measured from each MEA.

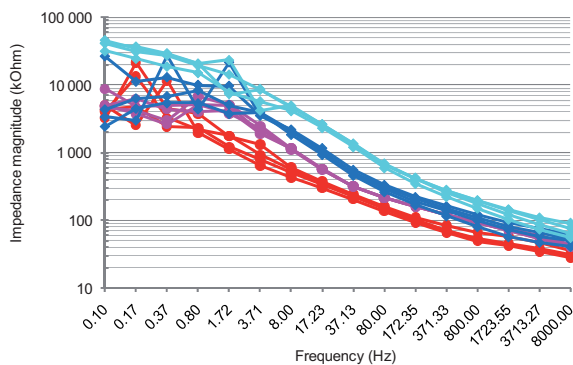


Fig. 2. Impedance spectroscopy results for two commercial MEAs (red and pink filled circles) and two in-house MEAs (blue and cyan filled diamonds) for four MEs per MEA.

4 Conclusions

In this paper, we have described the IM setup used to assess our in-house produced MEAs and compared their ME impedance performance with that of the corresponding commercial ones. Even though our current process did not produce MEs of equal performance, the results are encouraging, and further development of our in-house MEA production is justified. Also, we can conclude that not having MEs coated with titanium nitride did not increase the impedances as much as anticipated and that the resulting impedances can be taken to be sufficiently low for successful cellular measurements. The impedance spectroscopy results were found sufficiently consistent.

5 Discussion

Titanium nitride surface of the commercial MEs helps to achieve lower impedances as compared with plain titanium MEs. Nevertheless, we have successfully used our in-house MEAs in cellular measurements [5], confirming that the higher impedance is not detrimental to the measurement capability.

As illustrated in Fig. 1, esp. for in-house MEAs SF 8 and SF 9, our MEs were not of very consistent quality. This was found to be due to a poor quality commercial photolithography mask, resulting in ME size variation. We have now found a new mask supplier to achieve consistent ME size and performance.

It was found that even changing lead connection order, as described in Section 2.3, affected the results, and sometimes resulted in partial recovery of the impedance increase caused by earlier IMs of the same ME. Here, the results are shown for the setup resulting in the lowest impedances for the commercial MEAs, complying best with the manufacturer specifications.

The low frequency IMs of the impedance spectroscopy were found to affect the MEs to a varying extent, ranging from changes in the surface color of our in-house MEA MEs to the destruction of the MEs. The surfaces were inspected using light microscopy and the destruction of MEs was evident already in repeated IMs. Thus, the first measurements on any ME are shown in the results, and the results in the low frequency range in Fig. 2 have to be taken with caution, although no actual ME breakdown is evident.

We continue to develop our ME IM protocol to achieve more robust and ME-friendly IMs.

Acknowledgement

The work was funded by Academy of Finland (decision numbers: 122947 and 123359).

References

- [1] Grimnes, S., Martinsen, Ø. G. *Bioimpedance & Bioelectricity Basics*. (2000). New York, NY, USA: Academic Press.
- [2] Agilent Technologies. *Agilent Impedance Measurement Handbook: A Guide to Measurement Technology and Techniques*. Available (sited May 11, 2010): <http://cp.literature.agilent.com/litweb/pdf/5950-3000.pdf>
- [3] Ryyänen, T., Kujala, V., Ylä-Outinen, L., Kerkelä, E., Narkilahti, S., Lekkala, J. Polystyrene coated MEA. In *Conf. Proc. 7th Int Meeting on Substrate-Integrated Micro Electrode Arrays*, June 29-July2, 2008, Reutlingen, Germany, in press.
- [4] Kujala, V., Ryyänen, T., Hyttinen, J., Lekkala, J., Kerkelä, E., Aalto-Setälä, K. Electrophysiological studies of human embryonic stem cell -derived cardiomyocytes with novel microelectrode Arrays. In *Conf. Proc. 7th Int Meeting on Substrate-Integrated Micro Electrode Arrays*, June 29-July2, 2008, Reutlingen, Germany, in press.
- [5] Becq, G., Bienkowski, G., Diard, J. P., Villard, C. About MEA impedance measurement and analysis. In *Conf. Proc. 6th Int. Meeting on Substrate-Integrated Micro Electrode Arrays*, July 8-11, 2008, Reutlingen, Germany, pp. 277-278.

Scalloped electrodes for brain tissue recordings

Patricia Vazquez, Maria Dimaki, Winnie E. Svendsen¹

¹ DTU Nanotech, Technical University of Denmark, 2800 Kongens Lyngby, Denmark

A novel fabrication technique for three dimensional electrodes of around 60 μm is explained. The obtained electrodes aim at recording brain slices signals *in vitro*, with their height and shape playing a crucial role in obtaining good quality signals since they avoid dead cell layers of the tissue. This technique solves the common challenge of fabricating high aspect ratio structures in silicon and their metallization to obtain active electrodes. On top of this, a good control over the profile of the pillars is reached without the need of time-consuming calibration experiments.

1 Introduction

1.1 Out of plane electrodes for brain slice recordings

As reported previously, out of plane electrodes improve the signal to noise ratio of electrical activity recorded from neuron cells [1], and seem to be the trend for solutions in this area. Namely, carbon nanotubes, nanowires, and three dimensional electrodes fabricated by clean room processes mark the lead in the field [2-5].

Three dimensional electrodes above 50 μm of height have proved to be of great interest for brain tissue studies, since they can penetrate the dead cell layers at the surface of the brain slice, thus reducing the distance to the active cells.

In this work, a novel fabrication technique for three dimensional electrodes of around 60 μm is explained. It provides a good control over the profile of the pillars, which can be sharpened by the tuning of the height and slope of small steps that make the general outline of the electrode. Moreover, these steps ease the final metallization of the electrodes, which is a common problem in the fabrication of high aspect ratio MEMS devices.

2 Methods

2.1 Challenges: high aspect ratio shapes in dry etching

One important issue in the control of the profile of the structures is to compensate reentrant etching that appears with high aspect ratio structures, as it has the effect of producing faster etching at the bottom of the structures. A combination of the techniques shown by [3] and [6] allows tackling this problem. Sacrificial pillars around the main electrode stop the plasma molding that provokes this effect, and consecutive anisotropic and isotropic etch provides an easy method for tuning the sidewall angle of the high aspect ratio structures.

In addition, the use of a silicon-on-insulator wafer (SOI) facilitates the whole process, since the pillars will lie on an insulator layer, typically silicon oxide, and are thus independent from each other as individually addressable electrodes.

2.2 Fabrication sequence

The main steps in the fabrication process are as follow: during the first step, the areas of the electrodes are defined by photolithography; this is done by spinning a thick resist layer of 4.2 μm . The etching is then performed in an inductively coupled plasma etcher (ICP), and it stops automatically when it reaches the insulator layer, in this case a 0.4 μm layer of silicon oxide (an adding advantage of using an SOI wafer). The thus obtained pillars, with heights of about 50 μm , form the skeleton that will shape the final array of electrodes. In order to enhance the conductivity of the electrodes, at this stage the wafer is heavily doped in a furnace, and wires are patterned and metalized by standard lift-off. Finally, with the purpose of ensuring the insulation of the array, a layer of 200 μm of silicon nitride is deposited and etched away on the active sites of the pillars to expose the areas that are meant to become the actively measuring electrodes.

3 Results

Three dimensional electrodes of about 60 μm have been fabricated for brain slice activity recording. The technique used produced some singular forms of pillars with a scallop profile that facilitated the control of the sharpening of the electrodes and their consequent metallization.

The use of sacrificial pillars around the main electrode protect it from being etched faster at the bottom, as it is shown in figure 1.

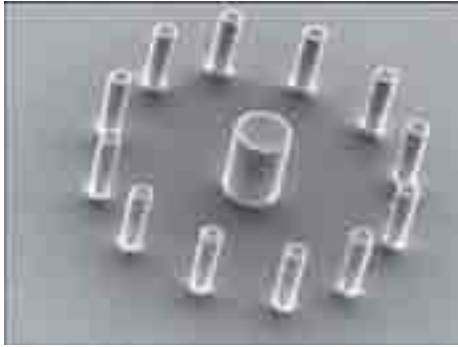


Figure 1: sacrificial pillars surrounding the main pillar-electrode protect the structure from being etched faster at the bottom

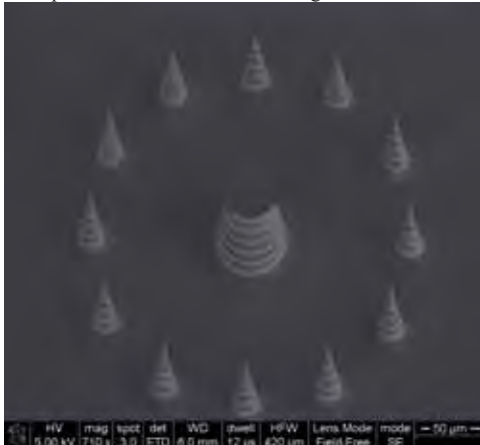


Figure 2: silicon pillars obtained with tapered etching

The scallops formed from switching between different processes can be controlled, as shown by [6]. In a different approach, this report uses the scalloped profile as a way to ease the consequent metallization of the structures to create conductive electrodes

4 Conclusions/summary

The array of scalloped electrodes is intended to be used on brain slice cultures on chip, for long term studies. It is to be seen what effects does have this profile on the recording of the electrical signals. The integration of a culture chamber will follow, and preliminary results with biological samples will be shown.

Acknowledgement

We would like to thank the CellCheck project within the Marie Curie European program for its financial support. Also, thanks to all the Danchip personnel for their technical advice and help in the fabrication process.

References

- [1] Heuschkel, M.O., et al., A three-dimensional multi-electrode array for multi-site stimulation and recording in acute brain slices. *Journal of Neuroscience Methods*, 2002. **114**(2): p. 135-148.
- [2] Gabay, T., et al., Electro-chemical and biological properties of carbon nanotube based multi-electrode arrays. *Nanotechnology*, 2007. **18**(3).
- [3] Hanein, Y., et al., High-aspect ratio submicrometer needles for intracellular applications. *Journal of Micromechanics and Microengineering*, 2003. **13**(4): p. S91-S95.
- [4] Kim, W., et al., Interfacing silicon nanowires with mammalian cells. *Journal of the American Chemical Society*, 2007. **129**(23): p. 7228-+.
- [5] McKnight, T.E., et al., Resident neuroelectrochemical interfacing using carbon nanofiber arrays. *Journal of Physical Chemistry B*, 2006. **110**(31): p. 15317-15327.
- [6] Roxhed, N.G.P.S.G., Reliable in-vivo penetration and transdermal injection using ultra-sharp hollow microneedles. 2005. p. 213.

Solid Silver Microneedle Electrode Arrays for Intracellular Recording Applications

Jochen Held^{1*}, Joao Gaspar¹, Patrick Ruther¹⁺, Matthias Hagner², Andreas Cismak³,
Andreas Heilmann³, and Oliver Paul¹

¹ Department of Microsystems Engineering (IMTEK), University of Freiburg, Freiburg (Germany)

² Department of Physics, University of Konstanz, Konstanz (Germany)

³ Department of Biological Materials and Interfaces, Fraunhofer Institute for Mechanics of Materials Halle, Halle (Germany)

* Corresponding author. E-mail address: ruther@imtek.de

+ On leave to Natural and Medical Sciences Institute (NMI) at the University of Tuebingen, Reutlingen (Germany)

This paper reports on the fabrication of microneedle-based electrodes for the electroporation of adherent cells and intracellular recording applications focussing on the influence of external factors on the cell metabolism. Classical methods such as the patch-clamp method have been mostly applied to single cells in suspension. However, in the human body the majority of cells are adherent cells, which motivates the development of the microneedle-based chip design reported here. The chip comprises an array of 64 microneedles electrodes spread over a total area of around 1 mm². The microneedles are fabricated using dry etching of silver, followed by the deposition of a metallization and a passivation layer using sputtering and chemical vapor deposition, respectively. The passivation layer is locally opened at the needle tip in order to expose the underlying metal required for electroporation and intracellular recording. Various needles with diameters as small as 2 μm and a height around 5 μm were fabricated.

1 Introduction

This paper reports on the fabrication of solid silver (Ag) microneedle electrodes aiming at the electroporation of adherently growing cells enabling intracellular recording applications. The classical approach for intracellular potential measurements is the patch-clamp method using single cells in suspension [1]. Although well-established, this method is time-consuming, restricted to the investigation of a small number of cells per experiment and requires experienced laboratory staff [1]. On the other hand, patch-on-chip systems are limited to the investigation of suspended single cells [2] and do not enable intracellular potential measurements. The fact however that the majority of cells in the human body are adherently growing cells motivated the development of microneedle-based electrode arrays. In the past, silicon-based needle electrode arrays have been presented by our group for this specific application [3]-[6]. The presented systems apply a thin film metallization, i.e. Pt or Ag, deposited onto the silicon microneedles. In contrast, solid Ag microneedle electrodes are presented in this paper. It is expected that the stability of these electrodes in the context of electrochemical measurements is increased.

2 Fabrication

The fabrication process of the microneedle electrodes is schematically shown in Fig. 1. It starts with the deposition of a seed layer (15 nm Cr and

150 nm Ag) and electroplating of a 5-μm-thick Ag layer on a Pyrex wafer {Fig. 1 (a)}. The microneedles are machined using ion beam etching (IBE) with a 7-μm-thick photoresist serving as the etch mask {Fig. 1 (b, c)}. By tilting the substrate by 40° and rotating it during etching around its normal axis, circular mask patterns result in needles with the shape

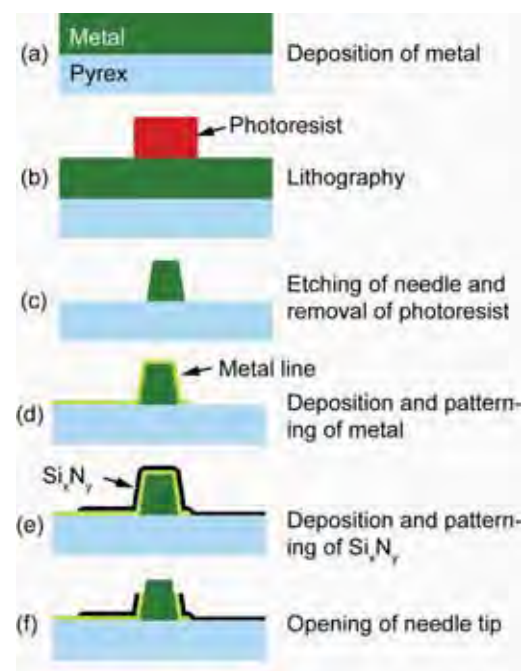


Fig. 1. Fabrication process of metal microneedle electrode arrays based on electroplating and ion beam etching.

of a truncated cone {Fig. 1 (c)}. After etching and mask removal with acetone, a metal layer stack, i.e. 150-nm-thick Cr and gold, interconnecting the needles to contact pads {Fig. 1 (d)} and a silicon nitride passivation layer {Fig. 1 (e)} are deposited and patterned using lift-off and reactive ion etching (RIE), respectively. Finally, the metal and passivation layers are removed from the needle tips using a maskless lithography step, the etch-back of the photoresist, RIE of the passivation layer and IBE of the thin metal layer {Fig. 1 (f)}. Needles with diameters of about 1 μm and a height of around 5 μm have been fabricated. The layout of the 3-mask process used to realize these chips is shown in Fig. 2. Figures 3 (a) and (b) present scanning electron micrographs of a microneedle electrode and the corresponding cross-section realized using focused ion beam (FIB) etching, respectively.

3 Conclusions

This paper focuses on the fabrication of solid Ag microneedle based electrode arrays. Successful electroporation tests with similar needle systems have been demonstrated previously [4, 5]. The application of these solid metal needle electrodes is demonstrated in Ref. 7 measuring action potentials of cardiomyocytes.

Acknowledgement

The authors gratefully acknowledge A. Baur, N. Lehmann and M. Reichel (IMTEK cleanroom

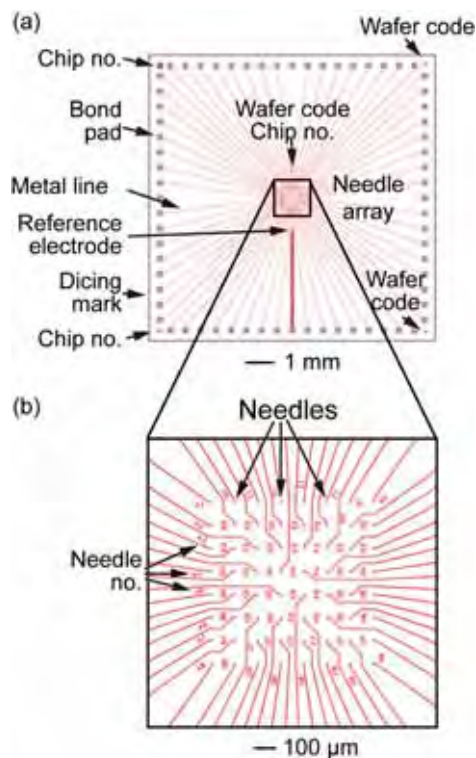


Fig. 2. Chip layout of the structures used for intracellular recording.

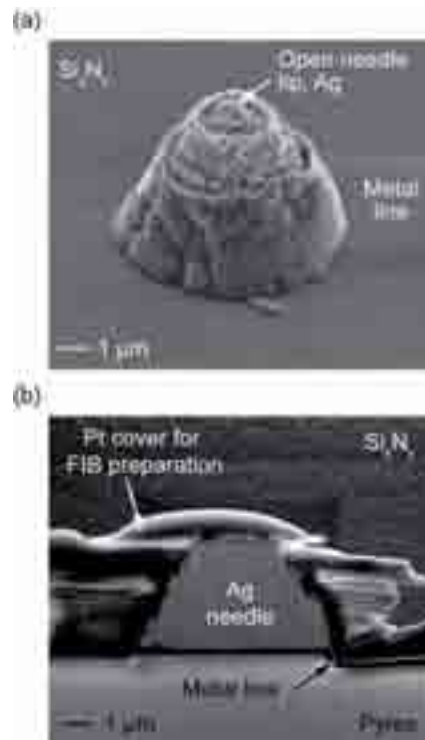


Fig. 3. (a) SEM micrographs of solid metal microneedle with metal leads covered by a Si_3N_4 layer and (b) respective FIB cross-section.

service center) for useful discussions and help in cleanroom fabrication. The authors also thank BMBF/VDI/VDE for funding the project MIBA – Mikrostrukturen und Methoden für die intrazelluläre Bioanalytik (project number 16SV2337).

References

- [1] Hamill, O. P., Marty, A., Neher, E., Sakmann, B., and Sigworth, F. J. (1981) Improved Patch-clamp Techniques for High-resolution Current Recording from Cells and Cell-free Membranes Patches. *Pflügers Arch.* Vol. 391, 85-100.
- [2] van Stiphout P., Knott T., Danker T., Stett A., (2005). 3D Microfluidic Chip for Automated Patch-Clamping. *MST-Kongress*, pp. 435-438.
- [3] Held J., Gaspar J., Ruther P., Hagner M., Cismak A., Heilmann A., Paul O., (2007). Systematic Characterization of DRIE-based Fabrication Process of Silicon Microneedles. *in Mat. Res. Soc. Symp. Proc.* 1052-DD07-07.
- [4] Held J., Gaspar J., Koester P. J., Tautorat C., Cismak A., Heilmann A., Baumann W., Trautmann A., Ruther P., Paul O., (2008). Microneedle Arrays for Intracellular Recording Applications. *in Tech. Dig. IEEE MEMS'08 Conf.*, pp. 268-271.
- [5] Held J., Gaspar J., Koester P. J., Tautorat C., Hagner M., Cismak A., Heilmann A., Baumann W., Ruther P., Paul O. (2009). Hollow Microneedle Electrode Arrays for Intracellular Recording Applications. *in Tech. Digest IEEE MEMS'09 Conf.*, pp. 220-223.
- [6] Held J., Gaspar J., Ruther P., Hagner M., Cismak A., Heilmann A., Paul O., (2010). DoE Characterization of Microneedle Fabrication Processes Based on Dry Silicon Etching. *J. Micromech. Microeng.*, Vol. 20, No. 2, 025024 (11pp).
- [7] Koester P. J., Tautorat C., Held J., Ruther P., Gaspar J., Paul O., Beikirch H., Gimsa J., Baumann W., (2010). GO-Bio 3: PoreGenic® - 2. Cardiomyocyte Action Potential Recordings with a 3D-MEA chip. *7th Int. Meeting on Substrate-Integrated Microelectrodes 2010*, in press.

Biocompatible MWNTs-based MEA for the study emergent activity in the cortical network

G. Gabriel^{1,2*}, I. Martín¹, A. Guimerà^{1,2}, M. Sánchez-Vives^{3,4}, R. Reig³, X. Palomer³, P. Godignon¹, R. Villa^{1,2}

¹ Instituto de Microelectrónica de Barcelona (IMB-CNM), CSIC, Campus UAB, Barcelona, Spain

² CIBER-BBN, Networking Center on Bioengineering, Biomaterials and Nanomedicine.

³ IDIBAPS (Institute of Biomedical Research August Pi y Sunyer), Barcelona, Spain

⁴ ICREA (Institut Català de Recerca i Estudis Avançats), Barcelona, Spain

* Corresponding author. E-mail address: gemma.gabriel@imb-cnm.csic.es

Here it is presented a novel carbon nanotube growth method that has been optimized in order to obtain selective growth and high density multi walled carbon nanotubes (MWNT) on multi electrode arrays systems (MEA). Platinum has been used as electrode substrate and at the same time as metal nanoparticle. The use of platinum ensures the use of biocompatible microelectrode materials for bio applications. These MWNTs modified electrodes enhance the electrode sensitivity and increase the electric charge transfer, by lowering the impedance and improving the electrode-tissue contact. The system was tested for the recording of spontaneous rhythmic activity generated by ferret cortical slices [1] before and after blockade of inhibition.

1 Introduction

1.1 Background

Carbon nanotubes coatings have been demonstrated extensively in the literature that improve neuronal recordings. However usually the catalysts used for the carbon nanotube growth are Fe and Ni. For biomedicine applications is always desirable to avoid any non biocompatible material. Here it is presented the growth of biocompatible carbon nanotubes and their characterization.

1.2 Methods

A custom 16 electrode MEA previously reported [2] has been used for selective growth of the MWNTs at a wafer scale (Fig 1a) [3]. The growth has been implemented in a silicon wafer and was performed in 3 steps. Before depositing the Pt that acts as CNT catalyst, a 15 nm SiO₂ inter-layer was deposited by CVD on the whole wafer aiming, to inhibit the diffusion in between the Pt forming the catalyst layer and the Pt from the electrode. The 4 nm sputtered Pt layer forming the catalyst layer was selectively deposited at the electrodes by means of a lift-off process. CNT growth process was divided in two main steps: the catalyst activation step (800°C; 500 sccm H₂; 5 min) and the CNT growth step (800°C; 1000 sccm CH₄; 5 min).

Ferret cortical slices were prepared and maintained as has been described in previous work [4]. Spontaneous slow oscillations and epileptiform activity induced after the blockade of inhibition were recorded through a MEA connected to amplifiers from Multichannel Systems (Reutlingen, Germany). The recordings were obtained at physiological

temperatures [5] and under conditions close to an interface chamber.

2 Results

The devices (Fig 1a) were characterised by SEM (Fig 1b). It could be verified that they only grow where the catalyst layer has been deposited. TEM images (Fig 1c) show that MWNT diameters are in the range from 5 to 20 nm and length in the order from 1 to 1.5 µm. It can be also seen in detail (dark spots) the platinum catalyst at the top of the nanotubes.

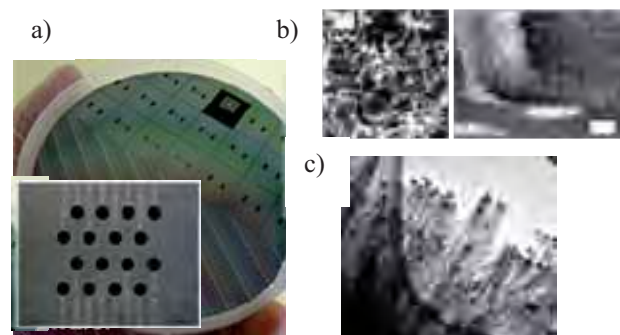


Fig. 1. a) Image of the 4-inch silicon wafer after the MWNT CVD growth process, and the inset is a detail of the 16 microelectrodes. b) SEM images of the MWNTs. c) TEM images of the MWNTs where can be seen the platinum catalyst at the top of the tubes.

Due to their high aspect ratio, the grown MWNTs allow to decrease the electrode impedance as they increase the electrode surface roughness. In order to determine if the CNT coating altered the electrochemical properties, impedance spectroscopy and cyclic voltammetry was done. Impedance spectroscopy (Fig 2a), which measures the frequency

dependent changes in impedance, shows how the MWNT growth led to a 30-fold decrease in impedance. Cyclic voltammetry (Fig 2b), in which changes in current are measured as an applied voltage pulse, shows that the CNT coating led to a 50-fold increase in charge transfer across the electrode surface.

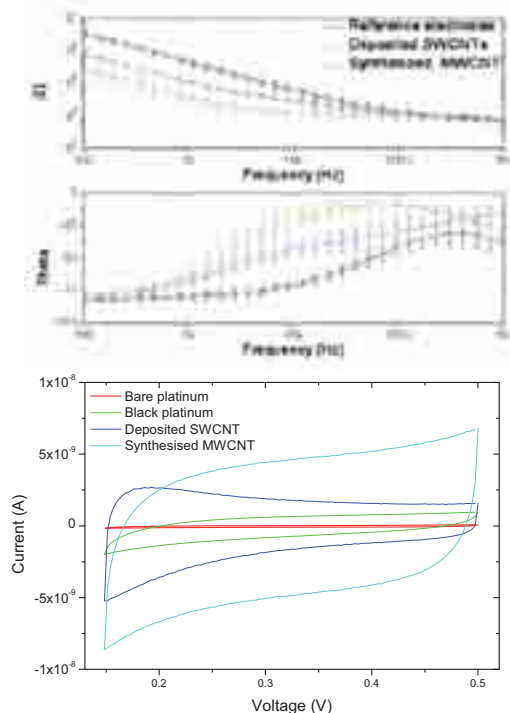


Fig. 2. a) Electrode Impedance and b) cyclic voltammetry (200 mV/s in NaCl 0.9 wt.%) measurements of bare platinum electrodes and synthesized MWNT

The planar electrodes in a MEA often pose the difficulty of a poor tissue-electrode contact. This is particularly evidenced when the electrophysiological activity to be recorded is not electrically evoked but a more sparse, spontaneous activity which generates lower amplitude signals. However, the long carbon nanotubes coatings can be useful for overcoming this problem. Besides, the increased capacitances found for this electrodes increase the charge transfer, which enable the improved signal registering. In our tests recording from oscillating cortical slices we obtained better signal to noise ration, shown in Fig 3, whenever the MEAs were coated with carbon nanotubes.

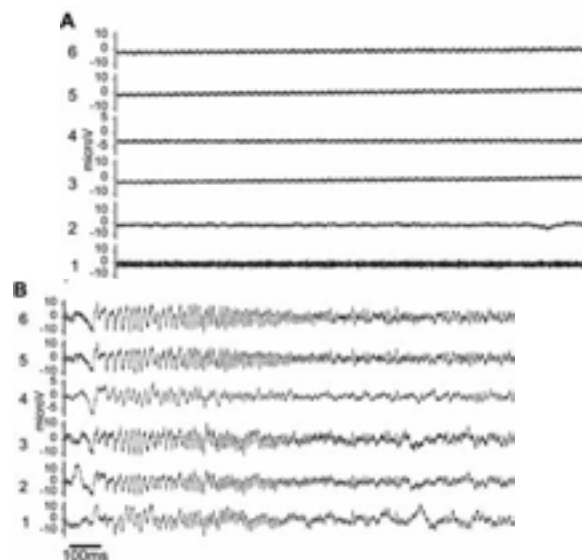


Fig. 3. Action potential monitoring for a) black platinum and b) MWNTs grown, in MEA.

3 Conclusion

The technology for modifying bio-compatible electrodes with directly synthesized CNTs using a bio-compatible CNT catalyst material, platinum, has been demonstrated. We conclude that this treatment results in an improvement in the signal to noise ratio while recording spontaneous activity generated by cortical slices.

Acknowledgement

This work has been founded by the projects TEC2006-14186-CO2-01 and TEC2009-14779-CO2-01 from the Spanish Ministry of Science and Innovation, and RD08-2-0013 from the Autonomous Government of the Generalitat de Catalunya.

1. Sanchez-Vives and McCormick, *Nat Neurosci* 10:1027, 2000
2. G.Gabriel et al., *Biosensors and Bioelectronics* 24 (2009) 1942–1948
3. I. Martin-Fernandez et a., *Microelectronic Engineering* 86 (2009) 806–808
4. Sanchez-Vives, M. V. & McCormick, D. A. - *Nature Neuroscience* (2000) 3, 1027-1034
5. Reig et al., *J Neurophysiology*, 2009 epub

Microelectrode cavity arrays (MECA) for parallel and high resolution ion channel recording

Gerhard Baaken^{1,2}, Srujan Dondapati¹, Jürgen Rühle^{2,3}, Jan C. Behrends^{1,3*}

¹ Laboratory for Electrophysiology and Biotechnology, Department of Physiology, University of Freiburg, Freiburg, Germany

² Laboratory for Chemistry and Physics of Interfaces, Department of Microsystems Engineering – IMTEK, University of Freiburg, Freiburg, Germany

³ Freiburg Materials Research Center (FMF), University of Freiburg, Freiburg, Germany

* Corresponding author. E-mail address: Jan.Behrends@physiologie.uni-freiburg.de

The necessity of an increase in throughput and resolution within electrophysiological experiments to detect conformation dependent ion flows through biological channels and pores is a significant technical challenge. Despite recent developments with automated patch clamp devices, the currently available technology is not capable of covering the experimental needs of the future. Here, an innovative approach based on sub-picoliter-cavities individually addressed with polarizable microelectrodes is presented that is suitable for low-noise as well as highly parallel electrical recording from ion channels and pores.

1 Background/Aims

Highly parallel, low noise electrophysiological recordings of single ion channels in lipid bilayers or cell membranes are of interest for basic research, drug development and other analytical tasks such as mass spectroscopy or DNA-sequencing¹⁻³. We have recently presented a microsystems approach where a lipid bilayer is formed on a microcavity generated within a photochemical dielectric and containing a non-polarizable microelectrode capable of carrying sufficient DC-current to record ionic flux through channels and pores in a lipid bilayer spanning the cavity¹. We here show that this design allows for the generation of an array of functional bilayers on 16 such cavities on one chip in a microarray, and is therefore in principle well suited for highly parallel single channel recordings. Simultaneous recordings of currents mediated by alamethicin are shown as well as PEG induced current fluctuations through a α -hemolysin pore on a 16 electrode device.

2 Methods

Standard MEMS processes followed by a microgalvanic electrodeposition step were used to produce the MECA device. Negative photoresist was spun onto a glass wafer and exposed to UV light through a photolithographic mask (Deltamask, Enschede, Netherlands) containing a contact line pattern. Following deposition of a 20 nm Ti adhesion layer, 200 nm gold was applied using electron beam evaporation and the photoresist removed. Microcavities (6-30 μm diam.) are then defined on the end points of the gold contact lines in a new layer of photoresist (SU8 2010, Microchem Newton, MA) using a second photolithographic step. In order to generate non-polarizable electrodes in the cavities,

silver was electrochemically deposited (0.5 M $\text{NH}_3(\text{aq})$, 0.1 M AgNO_3 , 5 mA cm^{-2} for 150 s) and later chloridized (3M KCl, 5 mA cm^{-2} , 60 s).

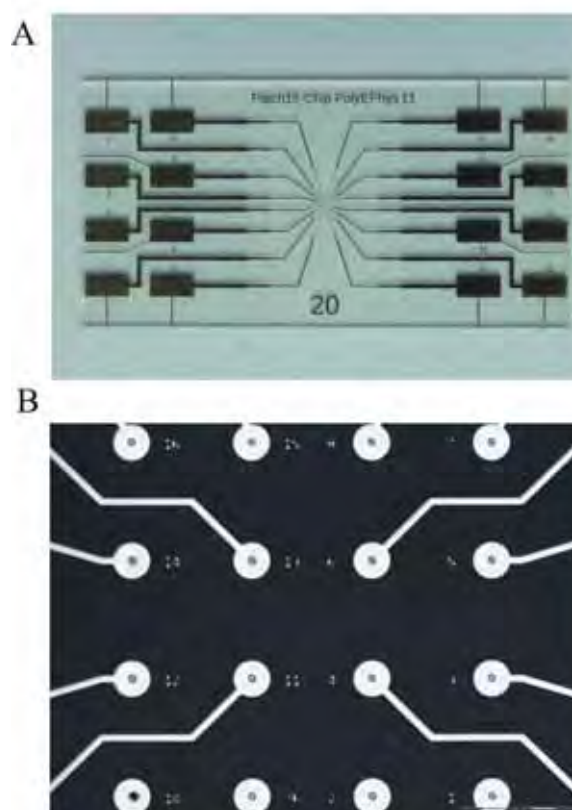


Fig. 1. Images of the MECA device: (A) whole Microchip (2 x 1 cm) with connector pads and connection wires leading to the microelectrodes (B) with sub-picoliter-cavities in the center.

3 Results and Conclusion

Initial functional tests of MECA devices with 4 and 16 cavities (Fig.1) were undertaken using formation of lipid bilayers (DPhPC in octane) to span the cavities by the painting method. We obtained high seal resistances exceeding 10 G Ω s. Using standard reconstitution protocols, we have been able to demonstrate both high-resolution and low-noise (<300 fA @ 10 kHz using an Axopatch 200B amplifier) and parallel (n=16, using a Tecella Jet multichannel amplifier) recordings of both the voltage dependent channel formation by alamethicin and transient blocks of the alpha-Hemolysin pore by mono- and polydisperse poly ethylen glycol (Fig. 2).

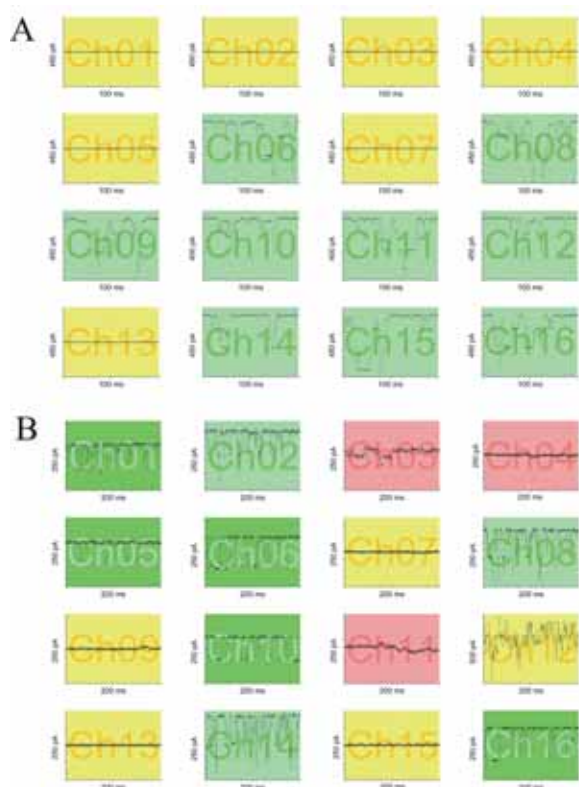


Fig. 2. Parallel recordings of alamethicin state transitions (A) and α -hemolysin blockages by PEG (B) using a 16-channel, low resolution amplifier (Tecella Jet). Colored backgrounds indicate unstable bilayer (red), bilayer with (green) without active pores (yellow).

Thus, the present platform holds promise as a platform for both high-throughput and high-resolution recordings of reconstituted ion channel activity and for nanopore screening applications.

Acknowledgement

Funded by the Federal Ministry of Education and Research (BMBF), Project PolyEPhys (FKZ 0315316B, Projektträger Jülich).

References

- [1] Baaken G., Sondermann M., Schlemmer C., Ruehe, J., Behrends, J.C. (2008) Planar microelectrode-cavity array for high-resolution and parallel electrical recording of membrane ionic currents. *Lab on a Chip*, 8, 938-944.
- [2] Fertig N., Klau M., George M., Blick R. H., Behrends J. C. (2002) Activity of single ion channel proteins detected with a planar microstructure, *Applied Physics Letters*, 81, (25), 4865-4867
- [3] Mahendran K. R., Kreir M., Weingart H., Fertig N., Winterhalter M. (2010) Permeation of Antibiotics through Escherichia coli OmpF and OmpC Porins: Screening for Influx on a Single-Molecule Level, *Journal of Biomolecular Screening*, 15, (3), 302-307.

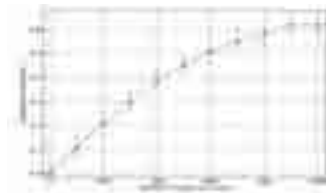


Fig. 3: Irradiance derived from the LED to the object plane (25 mm above the



Fig.4: LED holder which screws into objective current under microscope stage

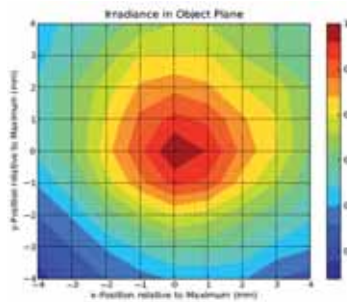


Fig.5: Relative variation on the irradiance respective to the point of maximum power density, measured approximately 25 mm above the bare LED ($1 \text{ mm}^2 \sim 2.3^0$). The active area of the MEA is only $1.2 \times 1.2 \text{ mm}^2$ in size.

We also ruled out the possibility of photoelectrical currents deriving from the metal of the MEA electrodes, thus yielding false signals. The external photoeffect of metals immersed in electrolytes has been studied in detail by Zolotovitskii et al. (2). None of the metals investigated have work functions below 2.7 eV, which make it impossible for the external photoelectric effect to play any part above wavelengths of $\lambda = 450 \text{ nm}$ ($h \cdot c/\lambda = 2.76 \text{ eV}$). Because of the spectral properties of the LEDs employed, basically no photo-electric currents can arise. To directly rule out such effects, we made measurements with Multi Electrode Arrays only filled with the culture medium and up to three fold larger irradiation than used in our current experiments: No signal correlated with the irradiation could be detected.

3 Results

An increase in the average network firing rate (obtained by binning time and counting spikes with $\delta t = 100 \text{ ms}$) was observed during blue light pulses for constant as well as ramped pulses (Fig. 6, Fig. 7):

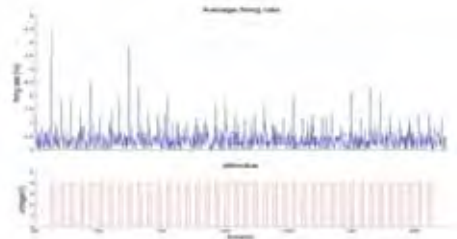


Fig.6: The average firing rate of 60 electrodes upon stimulation (above) with forty 1 s constant light pulses separated by 2 s (below).

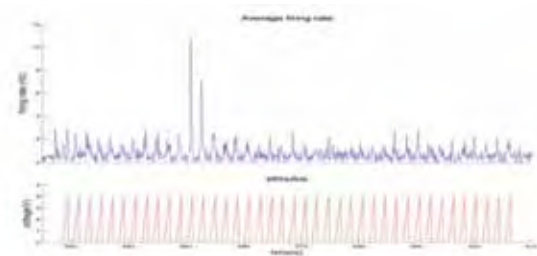


Fig 7: The average firing rate of 60 electrodes upon stimulation (above) with forty ramping (from 0 to 4 V in 1 s) light pulses separated by 2 s.

The difference in the average firing rate increase between constant and ramped blue light photostimulation is depicted in the following figure (Fig 8):

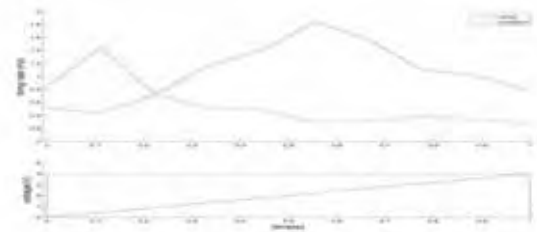


Fig 8: The average firing rate during forty times stimuli of 1 s over 60 electrodes computed for constant (red, below) and ramp (blue, below) blue light stimulation.

4 Conclusion

We presented a proof of concept that upon repetitive whole field light stimulation, an increase of the average firing rate of the network was induced. Moreover, we have shown that the ramping light stimulation gradually increases the firing rate of the network to a higher level than constant illumination as previously reported (3). Subsequent experiments should work out whether we can get a sustained firing rate control of the network using the feedforward or the feedback configuration.

Acknowledgements

We thank Ghazaleh Afshar, Annette Witt & Demian Battaglia for data analysis, Ragnar Fleishmann, Denny Fliegner & Theo Geisel for helpful discussions and the BMBF for funding. Ahmed elHady acknowledges support by a Neurosenses Lichtenberg fellowship.

References

- [1] Boyden ES et al. Millisecond-timescale genetically targeted optical control of neural activity. *Nat Neurosci.* 2005 Sep;8(9):1263-8
- [2] Zolotovitskii, K., Electronic Work Functions from Metals in a Liquid Dielectric, *Izvestiya Akademii Nauk SSSR*, No. 4, pp. 802-806, April 1972
- [3] Adesnik H, Scanziani M. Lateral competition of cortical space by layer specific horizontal circuits. *Nature* 2010 Apr 22;464(7292):1155-60.

Effect of electrode dimensions on nerve fiber signal recordings

Kiran Kumar Sriperumbudur, Philipp Julian Koester, Werner Baumann, and Jan Gimsa*

University of Rostock, Chair for Biophysics, Gertrudenstrasse 11a, 18057 Rostock, Germany

* Corresponding author. E-mail address: jan.gimsa@uni-rostock.de

Many types of MEA-based cell chips exist with different electrode types and dimensions. The interaction of electrically active cells with the MEA is governed by the characteristic dimensions of neurons, axons, dendrites, and the signal recording microelectrodes (diameter, shape, material etc.). In addition, the cell-electrode distance is given by the stochastic distribution of the cells on the MEA surface. We present a way to model the signal amplitude in relation to the microelectrode diameter and the propagating action potential to optimize future MEA cell chips.

1 Introduction

Generation and propagation of action potentials in the nerve fibers (axons) is a much attentive and interesting biological phenomenon. Many laboratory experiments have been done regarding the detection of nerve signals on different electrode structures. However, a mathematical model of an axon coupled with an electrode structure is useful to predict some of the axon-electrode interactions, like dependence of signal strength on the dimensions of electrode.

2 Method

The mathematical model of an axon based on the FitzHugh-Nagumo (FHN) equations [1, 2] was a simple and easy model for simulating the propagation of action potential. We have improved an existing axon model [3] based on FHN equations suitable for the present simulation. The improved model was coupled with different sized electrodes. The simulations were performed in Comsol Multiphysics® (COMSOL Multiphysics GmbH, Göttingen) to establish a mathematical relation between the dimensions of an electrode and the strength of recorded signal on the electrode.

2.1 The FHN equations

The FHN equations for a propagating action potential pulse generation are:

$$\frac{\partial u_1}{\partial t} = \Delta u_1 + (\alpha - u_1)(u_1 - 1)u_1 + (-u_2) + I$$

$$\frac{\partial u_2}{\partial t} = \varepsilon(\beta u_1 - \gamma u_2 - \delta)$$

Where u_1 is the membrane potential, u_2 is a recovery variable, I is the magnitude of stimulus current and α , β , γ , δ , ε are the system parameters. The FHN equations were written in PDE (partial differential equations) mode in Comsol Multiphysics®

to generate a propagating action potential pulse in the axon. The axon was assumed as a long cylinder with a constant diameter of 1 μm and a length of 125 μm . A platinum electrode structure was coupled with the axon in AC/DC mode in Comsol Multiphysics®. The diameters of platinum microelectrodes were varied from 1 to 40 μm . The electrodes were placed at 1.5 μm distance from the geometric centre of the axon. A realistic culture environment (physiological saline medium) was assumed around the axon and the voltage recorded by the microelectrodes was modelled. The parameter values in FHN equations were assumed in accordance with the present model (Table 1). Suitable boundary conditions and material properties (Table 2) were applied and simulated in Comsol Multiphysics®.

Table 1. The parameter values used in the simulation.

Parameter	α	β	γ	δ	ε
Value	0.0001	1000	2540	0	1

Table 2. The material properties and boundary conditions applied to the subdomains in the simulation.

Material	Properties		Boundary conditions
	σ (S/m)	ε_r	
Axon	0.1	2.1	Neumann
Physiological saline	1.2	80	Ground at outer surface
Platinum electrodes.	8.9 e6	7.5	Distributive impedance

3 Results

Simulations were run for six different electrode sizes. A 5 μm electrode was kept as an error console electrode to test the correctness of each simulation result. Figure 1 depicts one of the nine simulation results (run for 10 μm electrode)

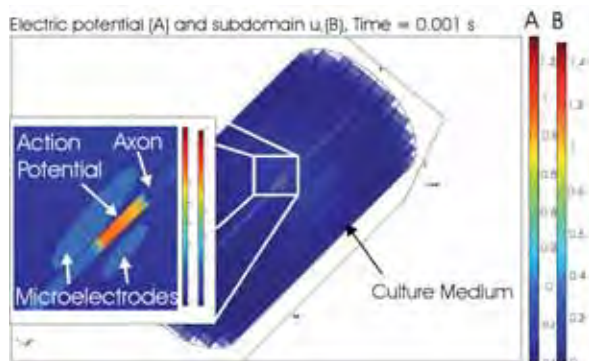


Fig. 1. The subdomain and slice plot of the model showing the action potential in the axon and the electric potential in the surrounding medium respectively. The electrodes shown in zoomed picture were with 10 μm (big), 5 μm (small, an error console electrode) diameters.

The signals obtained on the electrodes from above simulations were given as input signal to the Spice circuit (Figure 2) which represents the combination of filter and impedance converter.

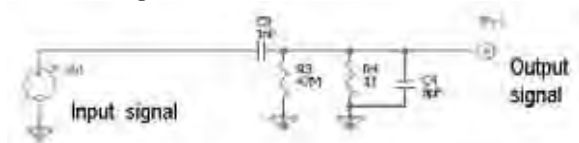


Fig. 2. Schematic picture of Spice model used to get an output signal of the electrode.

The output signals were obtained by the transient analysis of given input signal. A graph was drawn for the different output signals for different electrodes diameters (Figure 3).

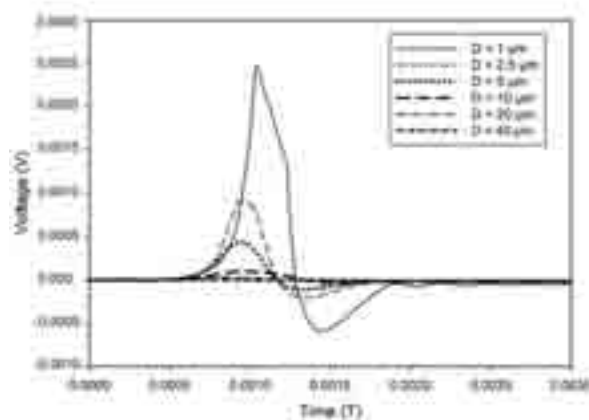


Fig. 3. The graph of different output signals obtained for various diameters (D) of electrodes.

From the graph it can be seen that the signal strength varying inversely to the diameter of the electrode.

4 Conclusion/summary

We could show the theoretical relation between the recorded potentials and the microelectrode diameters. We compared the simulated values with laboratory measurements with a glass neurochip [4, 5] containing 52 microelectrodes ($D = 35 \mu\text{m}$). The recorded neuronal potentials were 0.6 mV at maximum, which is in the range of the presented model.

In the future, we plan to modify the model to predict the distance of a neuron, which fires an action potential, which is recorded by a microelectrode of certain geometry. This model could then be implemented to identify the active neurons in a neuronal network. To mirror the reality, we will improve the above model by embedding the microelectrode into a glass substrate, by considering the amplifier input impedance, and by introducing the voltage divider properties of the electrode/amplifier couple. However, the frequency-dependent voltage divider properties will influence the signal detection.

Acknowledgement

This work was supported by grant 01EZ0911 of the Federal Ministry of Education and Research (BMBF) and grants of Mecklenburg-Western Pomerania (UR09045 of the Ministry of Education, Science and Culture, and V220-630-08-TFMV-F-011 (project part FLUXELL) of the Ministry for Economics, Work and Tourism). We are thankful to Marco Stubbe for his useful discussions.

References

- [1] FitzHugh R. (1961). Impulses and Physiological States in Theoretical Models of Nerve Membrane. *Biophysical Journal*, 1: 445-466.
- [2] Nagumo J., Arimoto S., and Yoshizawa S. (1962). An Active Pulse Transmission Line Simulating Nerve Axon. *Proceedings of the IRE*, 50: 2061-2070.
- [3] Appali R., Petersen S., Gimsa J., and van Rienen U. (2009). 3D-Simulation of Action Potential Propagation in a Squid Giant Axon. *Conference Proceedings of the COMSOL*, Bangalore.
- [4] Koester P. J., Buehler S. M., Tautorat C., Sakowski J., Schrott R., Baumann W., and Gimsa J. (2008). A New Glass Chip System Acquiring Electric Activity And Physiological Parameters of Stem Cell Derived Cells. *Conference Proceedings of the 6th International Meeting on Substrate-Integrated Micro Electrode Arrays*, 315-316.
- [5] Koester P. J., Buehler S. M., Stubbe M., Tautorat C., Niendorf M., Baumann W., and Gimsa J. (2010). Modular glass chip system measuring the electric activity and adhesion of neuronal cells – application and drug testing with sodium valproic acid. *Lab-chip*, DOI: 10.1039/b923687b.

Insect neurons coupled to iridium oxide electrodes

Katrin Göbbels^{1*}, André van Ooyen², Andreas Offenhäusser³, Uwe Schnakenberg², Peter Bräunig¹

¹ Institute of Biology II, RWTH Aachen University, 52074 Aachen, Germany

² Institute of Materials in Electrical Engineering (IWE 1), RWTH Aachen University, 52074 Aachen, Germany

³ Institute of Bio- and Nanosystems (IBN-2), Forschungszentrum Jülich, 52425 Jülich, Germany

* Corresponding author. E-mail address: goebbels@bio2.rwth-aachen.de

We present extracellular single cell stimulation of locust neurons with sputtered iridium oxide film (SIROF-) electrodes. The changes in the membrane potential of the stimulated cells were controlled by intracellular recordings with sharp glass electrodes. The effect of different pulse parameters on the stimulation efficiency and also different electrode designs were investigated. First results of surface modifications for neuronal guiding are shown.

1 Introduction

We are interested in the development of new biohybrid systems, composed of defined neuron populations and semiconductor chips, which allow for simultaneous extracellular stimulation and recording of their activity *in vitro*. Recording electrodes (field-effect transistors (FETs) [1]) are surrounded in the immediate vicinity by sputtered iridium oxide film (SIROF)-electrodes [2] for single cell stimulation. Insect neurons are suitable as a test system for two reasons. First, their somata range in size from 10-120 μm . This means that larger somata are able to completely cover individual electrode combinations which allows to couple single neurons to the microelectrodes in a one-to-one ratio. Second, insect neurons can be cultured at extremely low densities [3]. Thus, it is possible to build networks of only a few nerve cells in which the recorded signals can be assigned to each single neuron. Coating chemicals that provide a means to fix the cells to the electrodes and allow for a directed outgrowth of neurites are of critical importance. Since insect neurons are very unselective regarding the surface material they grow on, it became important to identify suitable cell-adhesive materials for guidance.

2 Materials and Methods

2.1 Cell Culture

Neuron cell culture was made of thoracic ganglia of *Locusta migratoria* and transferred to the MEA surface. The MEA surface was non-modified or pretreated with Concanavalin A (Con A).

2.2 SIROF-MEA

Neurons were plated on in-house fabricated MEAs with SIROF stimulation electrodes exclusively. MEAs equipped with different types of electrodes

(variations in shape and area) were used to investigate the suitability of different designs (Fig. 1). The 12 circular microelectrodes had a diameter of 30 μm (circle-design) or 50 μm (button- and quad-design) with 200 μm inter-electrode distance. The stimulation electrodes were designed to surround recording electrodes in the immediate vicinity. Spikes were detected by intracellular recordings with glass microelectrodes. The effect of different pulse parameters such as amplitude, polarity, and frequency on the stimulation efficiency was investigated.

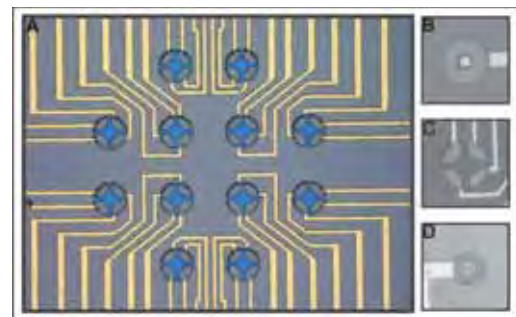


Fig. 1. A) MEA with SIROF-electrodes in quad-design (top view). SIROF-electrodes in B) button-, C) quad-, and D) circle-design.

2.3 Surface Modification

Agarose gel layers were pre-patterned and arranged on glass coverslips. Agarose-free surfaces of the substrate can be coated with growth promoting substance. Substrates modified in this fashion were used as cell culture substrate.

3 Results

3.1 SIROF-MEA

Extracellular stimulation was successful in several experiments. In every experiment the number of excitable neurons located on electrodes was

limited. The available time for analyzing the stimulation varied from cell to cell most likely due to damage caused by intracellular recording. In all stimulation experiments, biphasic rectangular voltage-controlled pulses were used.

Two of three electrode designs - button- and quad-design - turned out to be suitable for stimulation experiments with locust neurons. All measurements confirmed that increasing pulse amplitude enhances the success rate (Fig. 2). However, the threshold values varied from 400 mV to 1 V for individual neurons. We compared the stimulation efficiencies of biphasic pulses with two possible polarity orders, having either anodal phase first or cathodal phase first.

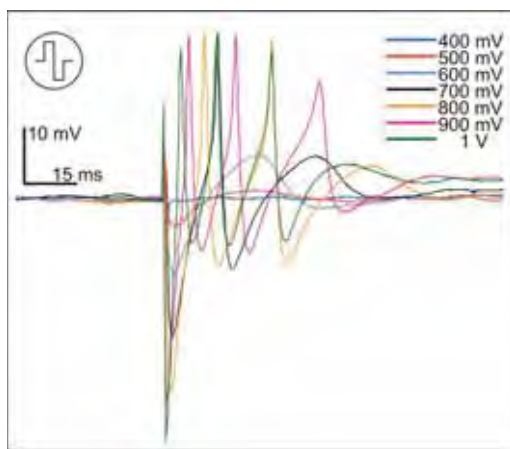


Fig. 2. Effect of varying pulse amplitude. Stimulation experiments with a biphasic anodal phase first rectangular pulse with an amplitude range from 400 mV to 1 V. The onset of the extracellular stimulation pulse can be seen by occurrence of stimulation artefacts. Action potentials were excited for pulses from 700 mV on. In this case, the action potential latency decreased with increasing pulse amplitude.

The results did not provide a clear hint on the dependency between pulse polarity order and stimulation efficiency. Both stimulus configurations seemed to be equally suitable or rather unsuitable for individual neurons. First results showed that using more than one stimulation pulse with constant pulse amplitude led to an increase in stimulation efficiency.

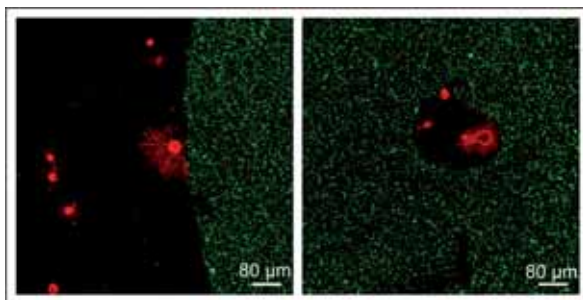


Fig. 3. Locust neurons (red) grown on glass substrate with agarose patterning (green).

3.2 Surface Modification

Agarose gel turned out to be the most promising cell-averse material for neurons. On agarose gel-coated substrates cell growth of locust neurons was inhibited completely while growth on adjacent non-coated areas was not disturbed (Fig. 3).

4 Discussion

The SIROF-electrodes were successfully applied for extracellular stimulation of single locust neurons. In combination with intracellular recordings experiments with different neurons provided general tendencies for the influence of the investigated parameters on the stimulation efficiency. Due to the fact that *Locusta* neurons in vitro can be described according to their electrophysiological response as non-, axon-, and soma-spiker [4], the limited number of excitable neurons in every culture can be explained. As expected, increasing the pulse amplitude also leads to an increase of the stimulation efficiency. The variations in the success rates were presumably the consequence of variations in experimental conditions and were also dependent on the neurons itself. Further measurements have to show if the electrode design has an effect on the success rate. For long-term experiments it is a crucial factor to avoid cell damage. Therefore a good alternative to amplitude increase is the increase of the stimulation pulse frequency.

Techniques to position insect neurons on electrodes and to guide neurite outgrowth patterned substrates provide important steps towards the construction of small defined biohybrid networks. To our knowledge, agarose beside starPEG [5] is the only known aversive chemical surface modification for locust neurons.

Acknowledgement

Financial support was provided by Deutsche Forschungsgemeinschaft (DFG), grants BR 882/6-1, SCHN 587/5-1, and OF 22/7-1.

References

- [1] Sprössler C., Denyer M., Britland S., Knoll W., Offenhäusser A. (1999). Electrical recordings from rat cardiac muscle cells using field-effect transistors. *Physical Review E*, 60, 2171-2176.
- [2] Wessling B., Mokwa W., Schnakenberg U. (2006). RF-sputtering of iridium oxide to be used as stimulation material in functional material medical implants. *Journal of Micromechanics and Microengineering*, 16, S142-S148.
- [3] Kirchof B., Bicker G. (1992). Growth properties of larval and adult locust neurons in primary cell culture. *The Journal of Comparative Neurology*, 323, 411-422.
- [4] Burrows M. (1996). Neurobiology of an insect brain. *Oxford University Press*.
- [5] Reska A., Gasteier P., Schulte P., Moeller M., Offenhäusser A., Groll J. (2008). Ultrathin coatings with change in reactivity over time enable functional in vitro networks of insect neurons. *Advanced Materials*, 20, 2751-2755.

Spike recordings from ganglion cell populations using a new type of carbon nanotubes surface multi-electrodes

Markus Bongard^{1,4,*}, Gemma. Gabriel^{1,2}, Rosa Villa^{1,2}, Rodrigo Gomez², Nuria Benito³, Eduardo Fernandez^{1,4}

1 El Centro de Investigación Biomédica en Red en Bioingeniería, Biomateriales y Nanomedicina (CIBER BBN), Spain

2 Universitat Autònoma de Barcelona, Centre Nacional de Microelectrònica (CNM-CSIC), Spain

3 Cajal Institute (CSIC), Spain

4 Universidad Miguel Hernández, Instituto de Bioingeniería, Spain

* Corresponding author. E-mail address: markus.bongard@umh.es

Due to its modular organization the retina proffers for systematic studies of a neural circuit. Simultaneous recording from a small patch of ganglion cells should allow to sample its full functionality. While multi-electrode array technology is available for about 2 decades the number of ganglion cells usually recorded represents only a small fraction of the cells present in a tissue patch. Here we report the development of a dense multi-electrode array with 54 electrodes special customized for retinal application. Its geometrical design is optimized to the ganglion cell distribution in the peripheral retina by adjusting electrodes of three different diameters on a hexagonal grid (figure 1 A, B). Additionally single-walled carbon nanotubes are deposited on these electrodes (figure 1 C, D). Carbon-Nanotubes (CNTs) have many qualities that make them attractive as a material for use in neurobiological applications. They are electrically conductive, biocompatible, small and flexible yet possess high strength, and can be functionalized with different molecules, properties that may be useful in basic and applied neuroscience. Thus, the combination of high conductivity, strength and flexibility is highly desirable for any neural interface, therefore the possible usefulness of CNTs in neural stimulation and recording has been previously proposed by several authors.

1 Methods

A custom multi-electrode array (figure 1A) optimized for low noise performance and physical compatibility with our acquisition setups (Braingate, USA; MultiChannel Systems, Germany) was fabricated using conventional microsystems technology. The MEAs were built on 500 μm -thick Pyrex 7740 wafers. A Ti/Pt layer (30 + 180 nm) was deposited and patterned following standard techniques as described elsewhere. The device was then passivated using plasma-enhanced chemical vapor deposition (CVD) of standard SiO₂-Si₃N₄ (300 + 700 nm). The MEA consisted of an array of 54 platinum electrodes located in an area with a diameter of 430 μm in the center of the layout (figure 1A). Two bigger electrodes (2500 μm x 1000 μm) were designed and used as reference electrodes. Additionally 4 temperature sensors were integrated. The physical characteristics and geometrical orientation of the design was optimized for conventional cell incubation conditions. Our straightforward and uncomplicated procedure for the modification of the Pt-electrodes with SWNT is depicted in Figure 2D. In the first step 10 mg of pure SWNT were dispersed in 10 ml of dimethyl formamide (DMF) under ultrasonic agitation. The Pt-electrode array was cleaned with ethanol, and in a second step the surface was coated by dropping

the SWNTs/DMF-suspension, followed by a drying process at 90-100° Celsius. In a third and last step, the device was rinsed with distilled water and thoroughly wiped with wet clean-room wipers to ensure that carbon-nanotubes stayed only in the electrode area (Fig 1D) [2].

In order to test the functionality of the MEA systems and to study the usefulness of the SWNTs-multi-electrode arrays to improve electrical signal transfer in neurophysiological experiments, we performed extracellular ganglion cell recordings in isolated superfused rabbit (*Oryctolagus cuniculus*) retinas as reported previously [1]. Briefly, after enucleation of the eye, the eyeball was hemisected with a razor blade, and the cornea and lens were separated from the posterior half. The retina was then isolated from the pigment epithelium and mounted on the SWNTs MEA photoreceptor side down (Fig 1C). Retinas were superfused with bicarbonate-buffered Ames medium at 35°C. The electrode signals were amplified, passed through a bandwidth filter (300-2000 Hz) and digitized with a resolution of 16 Bit at a sampling rate 32kHz using a commercially available acquisition system (Braingate, USA; Multichannel Systems, Germany).

This retina preparations were then visually stimulated using a computer system with a 16-bit

BENQ TFT monitor or a white LED. Neural spike events were detected by comparing the instantaneous electrode signals to level thresholds set for each data channel using standard procedures described elsewhere. When a supra-threshold event occurs, the signal window surrounding the event was time-stamped and stored together with the state of the visual stimulus for later, offline analysis.

2 Results

Our results show that the SWNTs-MEAs are able to record action potentials from large ensembles of ganglion cell types in a bigger proportion than comparable platinum electrodes. Thus on approximately 60-70% of the SWNT-based electrodes isolated, easily classifiable waveforms could be recorded and were later characterized based on the responses and receptive field properties. Phasic responses to e.g. light flashes with 'ON', 'OFF' and 'ON/OFF' components were typically observed. The remaining electrodes registered either no light evoked responses, or allowed only the registration of field potentials from distal units. The number of 'active' electrodes decreased to approximately 30-40% when platinum electrodes with the same geometrical design were used.

There are at least two major requirements which have strong impact on the yield and the quality of the recorded neural signals: an electrode has to be placed close to a neuron, so that the extracellular voltage changes can be registered and information about this given cell and its immediate neighbors can be obtained (figure 1E). Secondly a limiting factor for such electrophysiological recordings is the biological electrical noise present in the system. The average noise recorded with the SWNT-based electrodes was between 10-15 μ V, whereas for the platinum electrodes, manufactured using the same lithographic processes, it was more than twice as high. This noise was larger than the inherent amplifier noise, indicating that the amplifier was not the dominant noise source in the system. This reduction in the noise levels when SWNTs-electrodes were used, facilitated significantly the identification and isolation of extracellular recorded neural signals. Furthermore we encountered a somewhat "velcro-like"-effect when using the SWNT-MEAs, sometimes to such a degree that it was even difficult to detach the retinas from the electrodes after the actual experimental sessions. This effect on the other hand brings the biological specimen and therefore the neurons closer to the recording electrodes and could contribute to minimize the noise.

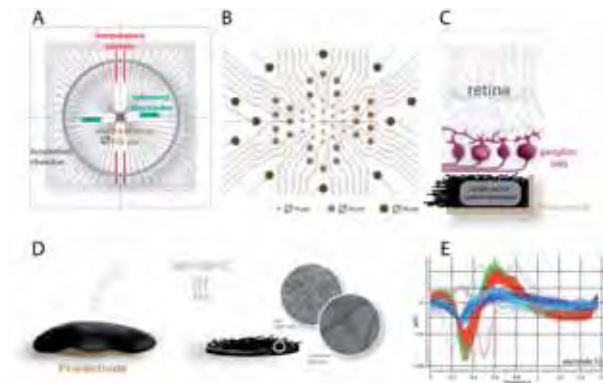


Fig. 1. A - overview custom-designed multi-electrode array geometry, B - central region of the MEA in A showing the electrode layout on a hexagonal grid. The electrode diameter is shrinking from outside to inside. C - schematic representation of the experimental preparation with the ganglion cell layer of the retina placed on top of the SWNT-electrodes. D - procedure to obtain SWNT-electrodes, the round insets show EM-photographs of the carbon nanotubes at different magnifications. E - multi-unit spike recording registered on a single SWNT-electrode ($D=30\mu\text{m}$).

3 Conclusion

We have presented an easy realizable method to fabricate SWNT-covered multi-electrode arrays. The resulting improvements in functionality underline the advantages of the use of carbon-nanotubes in an electrophysiological application. The results from this series of experiments demonstrate the advantages of SWNT-based electrodes over metal electrodes in the same geometrical design and suggest that, although more studies are still needed, such multi-electrode arrays can be used for many different applications, e.g. in extracellular acute slice recordings, or in the long-term monitoring of tissue based neurotoxins in which electrophysiological activity is used to detect and identify toxic and hazardous chemicals, or even for the development of new cortical implants.

References

- [1] Meister M, Pine J, Baylor DA (1994) Multi-neuronal signals from the retina: acquisition and analysis. *J Neurosci Methods* 51: 95-106.
- [2] Gabriel G, Gómez R, Bongard M, Benito N, Fernández E, et al. (2009) Easily made single-walled carbon nanotube surface microelectrodes for neuronal applications. *Biosens Bioelectron* 24: 1942-8.

Transparent NCD microelectrode array for spatially resolved detection in micro-areas of single cells

E. Colombo^{1,2}, C. Pietzka¹, V. Carabelli², Z. Gao¹, P. Herfurth¹, Y. Men¹, M. Schneider³, E. Carbone², E. Kohn¹, A. Pasquarelli^{1*}

¹ Institute of Electron Devices and Circuits, Ulm University, 89069 Ulm, Germany

² Department of Neuroscience, NIS Center, 10125 Torino, Italy

³ Experimental Anesthesiology Department, Ulm University Hospital, 89075 Ulm, Germany

* Corresponding author. E-mail address: alberto.pasquarelli@uni-ulm.de

We present a device consisting in a 3x3 microelectrode array (MEA) of boron-doped nanocrystalline diamond (NCD) on sapphire for the electrochemical detection of molecules released from membrane micro-areas of single excitable and secretory cells. The MEA has been tested in liquid environment containing the standard red-ox couple for diamond testing $\text{Fe}(\text{CN})_6^{4-/3-}$ and with adrenaline, confirming the suitability of the device for high sensitivity and high spatial resolution electrophysiological analysis on single cells.

1 Introduction

Diamond electrodes are gaining increased interest for biochemical and biomedical application due to their biocompatibility, chemical inertness, wide potential window of water dissociation ($\sim 3\text{V}$) and very low background currents [1].

Nanocrystalline diamond (NCD) microelectrodes for the amperometric detection of catecholamines have been extensively studied [2, 3, 4] and the detection of adrenaline in chromaffin cells with a NCD four electrodes planar device is presented in this conference [5].

Moreover, since NCD electrodes can be fabricated on various transparent substrates like glass, quartz or sapphire, they allow the exploitation of the intrinsic transparency of diamond for commonly used investigation techniques in biology such as inverted microscopy and fluorescence detection.

We present here a transparent microelectrode array (MEA) with a total sensing area comparable to the size of a single cell, where nine NCD boron-doped electrodes allow one-cell amperometric detection spatially resolved down to the micrometer scale. In addition, the employment of sapphire as a substrate will allow the integration of GaN-based heterostructures for ion-sensitive field effect transistors (ISFETs) in order to perform with the same device both amperometric and potentiometric measurements [6].

2 Experimental

The NCD thin film layers ($\sim 200\text{ nm}$ intrinsic NCD + 300 nm boron-doped NCD) have been deposited on a double side polished sapphire substrate (Epistone, 2" DSP wafers) by Hot Filament Chemical Vapour Deposition (HFCVD) using a bias-enhanced nucleation (BEN) method which ensures strong

covalent adhesion of the films to the substrate [7]. The substrate treatments before growth, the BEN and the growth parameters have been described in [8]. SEM and AFM characterization of the surface revealed an average grain size of $\sim 70\text{ nm}$ and a $\sim 12\text{ nm}$ rms roughness respectively. The boron concentration estimated by capacitance-voltage measurements in electrolytes is approximately $3 \times 10^{20}\text{ cm}^{-3}$.

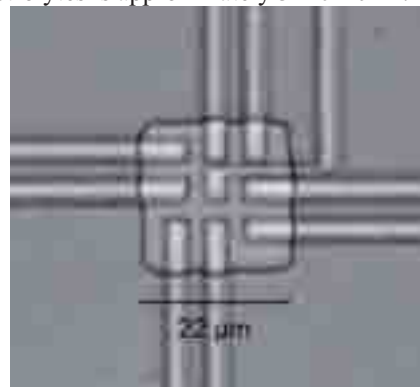


Fig. 1. Top view of the 3x3 MEA: the squared structure is opening in the SU-8 passivation and therefore the active area of the device.

In order to map the area underneath a typical neuroendocrine cell, nine electrodes with an individual area of $\sim 30\text{ }\mu\text{m}^2$ exposed to the electrolyte have been designed to form a 3x3 array extended over a total sensing area of approximately $20\text{ }\mu\text{m}$ in diameter, defined by the epoxy (SU-8 2005) passivation layer (Fig. 1). The patterning of the NCD electrodes has been performed both with optical and e-beam lithography and dry etching. Ohmic contacts were realized by Ti/Au deposition. SU-8 passivation has been performed by optical lithography. Fig. 1 shows a top view of the finished device. The electrochemical characterization has been realized with a three electrodes set-up equipped with a Saturated Calomel reference Electrode (SCE) and a Pt counter electrode.

3 Results and discussion

We tested the 3x3 MEA first by cyclic voltammetry measurements in 0.1M KCl solution, which showed the typical 3 V hydrolysis potential window and background currents smaller than $1 \mu\text{A}/\text{cm}^2$ (Fig. 2).

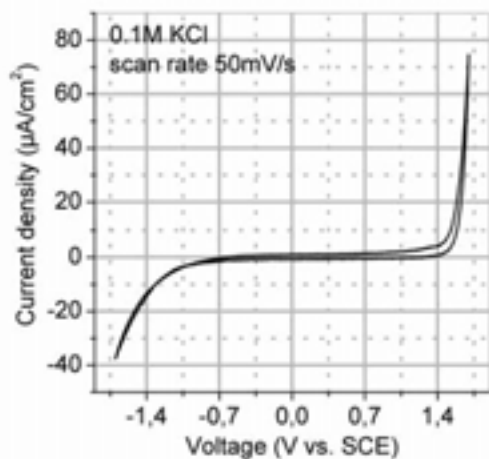


Fig. 2. Typical cyclic voltammetry of one of the electrodes of the 3x3 MEA in 0.1 M KCl solution at 50 mV/s scan rate.

Fig. 3 and 4 show then cyclic voltammetry plots of one of the microelectrodes in 0.1 M KCl + 10 mM $\text{Fe}(\text{CN})_6^{4-/3-}$ and 0.1 M KCl + 15 μM adrenaline at scan rates varying from 20 to 400 mV/s: in the ideal case of a microelectrode the current density should be scan rate-independent due the dominant hemispherical diffusion mass transport. In our case the current density varies by a factor 1.4 and 1.6 respectively for the two tested oxidizing molecules, when the scan rate is changed by a factor of 20. These variations are smaller if compared to the theoretical factor expected for a large-scale electrode ($\sqrt{20} \approx 4.5$). This gives further proof of the improved detection sensitivity of the device.

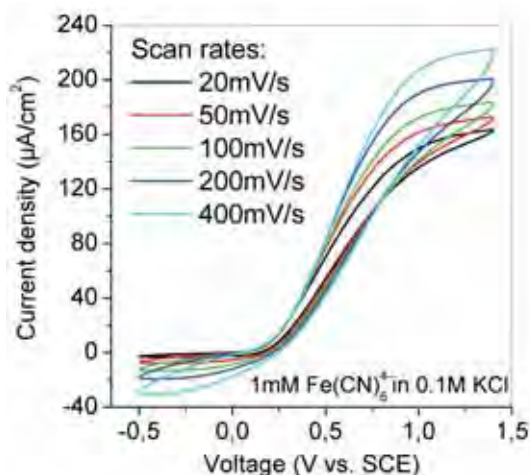


Fig. 3. Cyclic voltammetry of one of the electrodes of the 3x3 MEA with 1mM $\text{Fe}(\text{CN})_6^{4-/3-}$ in 0.1 M KCl solution at different scan rates.

4 Conclusions

We realized a new 3x3 microelectrode array out of boron-doped NCD on sapphire. Due to the transparency of both substrate and electrodes, the electrochemical detection can be easily coupled with inverted microscopy and fluorescence analysis.

The presented device is suitable for electrochemical measurements with subcellular spatial resolution.

We can conclude that the new MEA improves the spatial resolution for amperometric detection preserving a good signal/noise ratio due to the typical hemispherical diffusion microelectrode behavior.

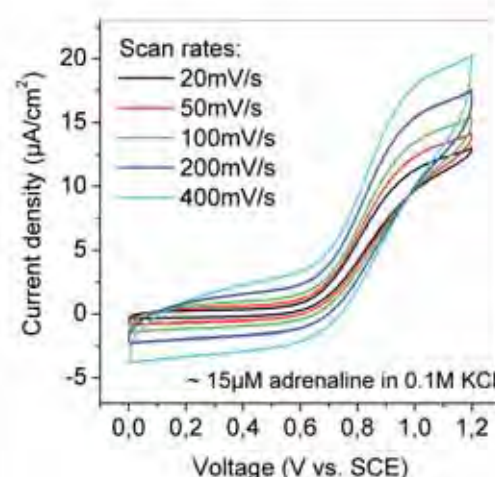


Fig. 4. Cyclic voltammetry of one of the electrodes of the 3x3 MEA with $\sim 15 \mu\text{M}$ adrenaline in 0.1 M KCl solution at different scan rates.

References

- [1] Y. Zhou et al., *Talanta* 79 (2009) 1189.
- [2] J. Park et al., *Diamond and Related Materials* 15 (2006) 761.
- [3] S. Raina et al., *Diamond and Related Materials* 19 (2010) 256.
- [4] V. Carabelli et al., accepted for publication in *Biosensors and Bioelectronics*.
- [5] S. Gosso et al., MEA meeting 2010.
- [6] M. Dipalo et al., *Diamond and Related Materials* 18 (2009) 88.
- [7] K. Janischowsky et al., *Diamond and Related Materials*, 2 (1993) 158.
- [8] Z. Gao et al., in press in *Diamond and Related Materials*.

Accurate validation of extra-cellular neuronal recordings in culture

Nitzan Herzog¹, Mark Shein², Yael Hanein^{2*}

¹ Department of Bio-Medical Engineering,

² School of Electrical Engineering, Faculty of Engineering, Tel Aviv University, Tel Aviv, Israel.

* Corresponding author. E-mail address: hanein@eng.tau.ac.il

Simultaneous in-vitro calcium imaging and extra-cellular recording from cultured cortical rat neurons were performed to elucidate the true nature of extra-cellular recordings using micro electrodes. For the first time, we unambiguously demonstrate the exact number and location of recorded cells by means of correlating the recorded electrical signal at the electrode and the calcium response. We quantify the electrical recording range and show that recording is limited to only a partial subset of the cells residing in this range. Furthermore, we show that even in cases of high SNR coupling, extra-cellular signals may vary in strength only partially reflect the cellular activity.

1 Introduction

The use of extra-cellular electrical recordings from neuronal networks has classically relied on several fundamental paradigms [1]. Primarily, it is widely accepted that the neuron-electrode physical coupling is a primary factor determining the shape and amplitude of the recorded signal. It is additionally accepted that well separated spikes exhibited in extra-cellular (EC) signals are manifestations of single action potentials in recorded neurons, that different neurons are characterized by differing spike shapes allowing for reliable classification and that the electrode homogeneously samples neurons up to a certain fixed radial distance. However, the limiting properties of EC recordings has so far prevented these assumptions from being corroborated and the relative role of the various factors contributing to signal shape has yet to be fully elucidated. Towards this aim, we have built a special setup combining up-right calcium (Ca) imaging [2] microscopy and conventional extracellular MEA recording, allowing visual identification of individual firing neurons through their calcium signal. This setup is also aimed at interrogating aspects of EC driven electrical neuronal stimulation.

2 Results

2.1 Synchronized Recording

Synchronized electro-optical recordings were performed between 10 days to 3 weeks in vitro. Sample simultaneously recorded data are presented in figure 1.

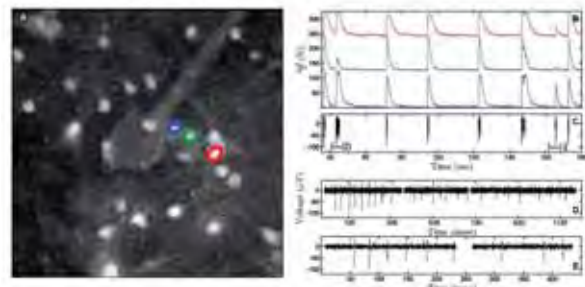


Fig. 1. Synchronized EC recording and Ca Imaging (A, B, C), with expanded view of selected EC events (D, E).

The activity shown is typical to such systems and is characterized by intensive bursting activity in which a large cell population fires in synchrony (figure 1, B). A clear temporal correspondence is apparent between the Ca and the EC data, with small calcium events occurring in conjunction with few or a single EC spike, and large ones registered in concurrence with as many as 70 EC spikes (figure 1, B - E).

2.2 Identification

In order to further corroborate and refine the identity of the recorded neurons, we examined the ability to reconstruct the Ca response from the electrically recorded raster plot.

Calcium events temporally correlated with only a single EC spike were collected, averaged and mean square fitted to a gamma function serving as a kernel for convolution over a spike count vector (figure 2, A, inset).

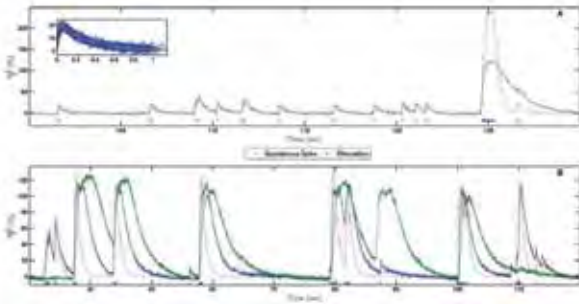


Fig. 2. Convolution of electrical raster plot with averaged single Ca-spike (A, B, red trace, inset in A shows CI-spike kernel) reconstructs isolated events in recorded cells. (A) Single spikes elicited by applying stimulatory voltage at the electrode shown in.

The prediction closely follows the Ca trace throughout the smaller events implying that the EC spikes can indubitably be attributed to the cell selected for convolution. Cells around an examined electrode were manually inspected for occurrences of isolated activity. Presence of such activity closely reproducible by the reconstruction indicates a cell unambiguously recorded by the electrode, whereas a large deviation from the reconstruction indicates a non-recorded cell. In cases where stimulation was employed, single spikes were elicited, allowing reconstruction of spontaneous multi-spike events (figure 2, A).

2.3 Statistics

Amongst the viewed electrodes, cases of picking up EC discharges from neurons located as far as $28\mu\text{m}$ were seen. However, other cases where the electrode had proven blind to neurons as close as $9\mu\text{m}$ were also viewed. Figure 3 displays the spatial view of the obtained statistics around an averaged electrode.

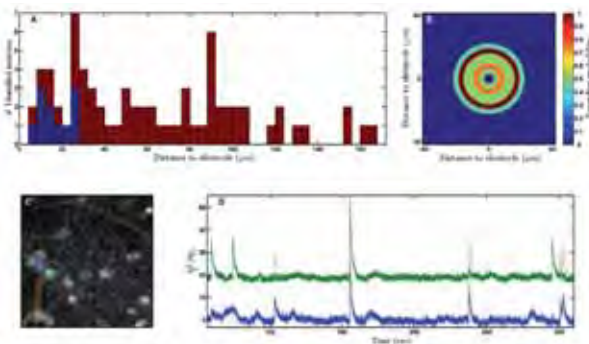


Fig. 3. (A, B) Obtained statistics of recording efficacy throughout examined electrodes. (C,D) Sample case of identified non-recording cells placed directly on top of monitored electrode.

Also presented is the identification of a non-recorded cell. Reconstruction based on the raster plot from the delineated electrode accurately predicts the events in a cell placed next to the electrode whereas characteristic supra-threshold events in a cell placed directly on top of the electrode go un-reflected in the EC raster plot (figure 3, C-D).

3 Discussion

We have proposed using multi-cell-Ca imaging in conjunction with an EC recording system in order to obtain an overview of the true activity pattern around the electrode and thereby assess the degree to which this activity is reflected in the EC signal. Using this approach, we were surprised to observe cases of neuronal somata clearly positioned directly on the electrode and exhibiting neuronal discharges without any manifestation in the electrode's signal. This despite display of high SNR discharges at other time points. Overall, The recording range of a constituent electrode in a neuronal plated MEA is $\sim 25\mu\text{m}$, and even in this range, roughly 50% of the cells are "visible" to the electrode.

Previous modelling and experimental work on other EC recording substrates have addressed possibility for lack of robustness of the EC signal [3].

These findings should be taken into account during work utilizing MEA to make statistical characterizations of network activity.

Looking at the described prediction attempts of larger population events (figure 2, B), it is evident that the convolution falls short at the decay phase of the event, where the convolution suffers faster termination. This difference is a manifestation of known efficacy decrease of EC electrodes during rapid firing events [1]. The presented technique will allow assessment of EC signal characterization in identified cases of single cell in contrast to multi cell electrode coupling and will hold relevance to spike sorting techniques [4].

4 Methods

Dissociated cortical neuronal cultures were used. Cultures were plated on 500-30iR-Ti or HD30-10 MCS-MEAs and recorded at 10-15 DIV using MCS recording system. Optical activity imaging was attained through incubation of cultures in a calcium sensitive fluorescent dye (either Fluo-4 or Oregon Green) and time lapse recordings with an Olympus upright microscope (BX51WI) fitted with an EMCCD camera (Andor Ixon-885) whose clock signal was digitally fed into the recording system so as to achieve synchronization.

References

- [1] Buzsáki, G. (2004). "Large-scale recording of neuronal ensembles." *Nature Neuroscience* 7(5): 446-451.
- [2] Cossart, R., Y. Ikegaya, et al. (2005). "Calcium imaging of cortical networks dynamics." *Cell Calcium* 37(5): 451-457.
- [3] Cohen, A., J. Shappir, et al. (2006). "Experimental and theoretical analysis of neuron-transistor hybrid electrical coupling: the relationships between the electro-anatomy of cultured Aplysia neurons and the recorded field potentials." *Biosensors and Bioelectronics* 22(5): 656-663.
- [4] Lewicki, M. (1998). "A review of methods for spike sorting: the detection and classification of neural action potentials." *Network: Computation in Neural Systems* 9(4): 53-78.

Polystyrene coated MEA

Tomi Ryyänen^{1*}, Ville Kujala², Laura Ylä-Outinen², Erja Kerkelä², Susanna Narkilahti², Jukka Leikkala¹

¹ Department of Automation Science and Engineering, Tampere University of Technology, Tampere, Finland

² Regea – Institute for Regenerative Medicine, University of Tampere and Tampere University Hospital, Tampere, Finland

* Corresponding author. E-mail address: tomi.ryyänen@tut.fi

Inspired by the fact, that polystyrene is the most common material for cell cultivation vessels and well plates, and the majority of experiments on cell culturing are conducted on that material, we have fabricated microelectrode arrays (MEAs) that have polystyrene as insulator layer instead of industry standard silicon nitride (Si_3N_4). The coating has been successfully tested with human embryonic stem cell -derived neuronal cells (hESC-N) and cardiomyocytes (hESC-CM).

1 Introduction

Evidently, the most common insulator layer used both in commercial and research MEAs is Si_3N_4 . However, the available thickness range of Si_3N_4 coating and thus its capability to reduce parasitic capacitances is limited [1]. Based on our experience Si_3N_4 coating also suffers from occasional quality variations and during the time it wears out when MEAs are reused many times. The highest motivation for introducing polystyrene as an alternative insulator layer, however, comes from the fact that vessels made of polystyrene, for example well plates, have been used for decades by cell scientist and thus there exist far more protocols to grow cells on polystyrene than on Si_3N_4 . One more benefit related to polystyrene coating is low capital cost needed to fabricate it as no PECVD kind of expensive processing equipment are needed.

2 Methods

2.1 Fabrication

Polystyrene coated MEAs having 30 μm electrodes (and some bigger electrodes for characterization purposes) in 8x8 format with separation of 200 μm were fabricated in quite a traditional way. A glass wafer was coated with a 300 nm titanium layer, where 60 electrodes, contact pads, and wiring were patterned lithographically. After that, hexamethyldisilazane (HMDS) was applied to improve the polystyrene adhesion on glass. The polystyrene layer was fabricated by dissolving polystyrene grains (BASF Polystyrol 158 K) on toluene and applying that solution on the wafer by spin coating it as thin layer. After curing the polystyrene, openings above electrodes and contact pads were again formed lithographically. The thickness of the polystyrene layer was measured from

the ready made MEAs with an optical profilometer and was found to be only about 230 nm, which was clearly less than expected. Obviously toluene had not evaporated from the polystyrene solution as much as in our earlier bulk experiments. Finally, the fabrication process was concluded with or without oxygen plasma treatment.

2.2 Measurement system

Noise and cell measurements were done with MEA1060-Inv-BC amplifier and MC_Rack software, both from Multi Channel Systems.

2.3 Tests

Noise characterization

Before plating cells on MEAs, we recorded noise from the MEAs for three minutes. From the data we calculated the RMS noise.

Neuronal cells

HESC-Ns were plated onto polyethyleneimine (0.05 % w/v) and laminin (20 $\mu\text{g}/\text{ml}$) coated MEAs as described earlier by Heikkilä et al. [2]. Cells attached onto surface and formed neural networks. The spontaneous activity of the network was measured starting one week after the plating.

Cardiomyocytes

Cardiomyocytes were derived from H7 human embryonic stem cell line as described before [3]. For hESC-CM adhesion, the MEAs were coated with fetal bovine serum (FBS) and 0.1 % gelatine. Spontaneously beating aggregates of hESC-CMs were mechanically excised and plated onto the MEAs. Cardiac field potentials were recorded as electrode raw data for three minutes via all recording electrodes.

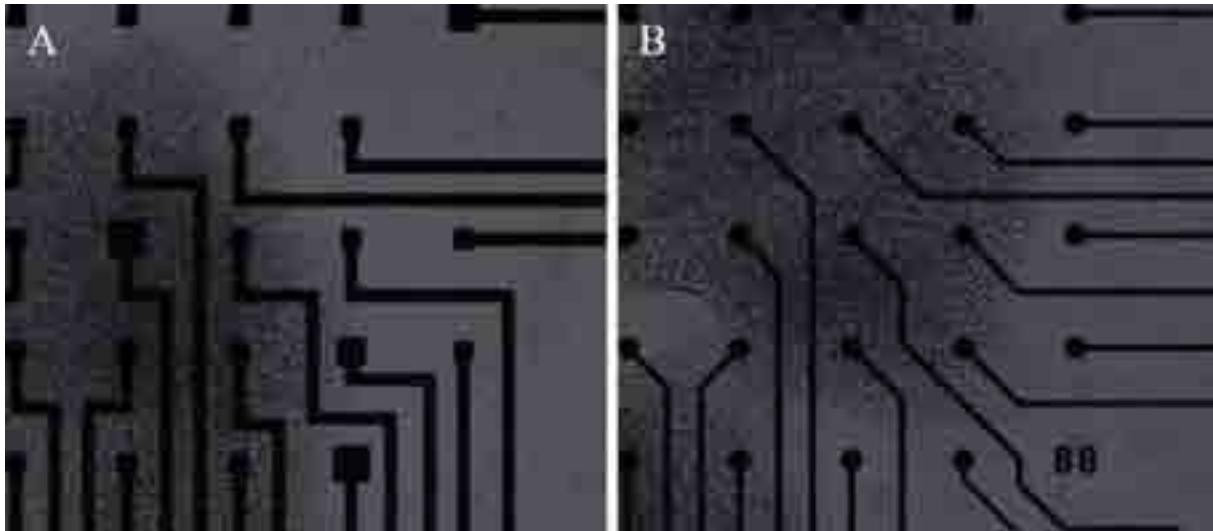


Fig. 1. Neuronal cells (hESC-N) growing on a) polystyrene surface and b) on Si_3N_4 surface after 17 days on the MEAs.

3 Results

The average RMS noise measured from 6 electrodes of three MEAs was $18 \mu\text{V}$, which is about three times the RMS noise of otherwise similar, but Si_3N_4 insulated MEAs we have fabricated. We assume the rather high noise level to originate from the too thin polystyrene layer and expect it to lower to the competitive level when the layer thickness is increased.

Neuronal cells attached well to the non-plasma treated polystyrene surfaces coated with polyethyleneimine and laminin. Fig. 1 shows human embryonic stem cell-derived neuronal cells growing both on polystyrene surface as well as on Si_3N_4 surface of a commercial (Multi Channel Systems) MEA after 17 days on the MEAs. On the both surfaces the cells grew well and formed networks with spontaneous neuronal network activity comparable to each others.

Cardiomyocytes on the contrary preferred the plasma treated polystyrene surface which was coated with FBS and 0.1 % gelatine (Fig. 2). In the absence of the plasma treatment, the polystyrene surface did not promote hESC-CM adhesion. Detected cardiac field potentials were comparable to our earlier experiments with Si_3N_4 insulated MEAs.



Fig. 2. A beating cardiomyocyte aggregate on polystyrene surface.

4 Conclusion

Polystyrene is found to be promising alternative as MEA insulator layer. Our preliminary results indicate that oxygen plasma treated polystyrene surface has good cell adhesion properties with regard to hESC-CM attachment. Also hESC-Ns attached to polystyrene surface and formed functional neuronal networks. No biocompatibility or polystyrene to glass adhesion problems were observed during the test period of three months. Still, more experiments are needed to ensure reliable fabrication process and especially to find the polystyrene layer thickness that lowers the noise level to the same level or even below the noise level of the Si_3N_4 coated counterparts.

Acknowledgement

This work was supported by the Academy of Finland (decision number 123359), CHEMSEM graduate school and Biosensing Competence Centre.

References

- [1] Heuschkel M.O., Wirth C., Steidl E-M., Buisson B. (2006). Development of 3D Multi Electrode Arrays for Use with Acute Tissue Slices. In Taketani M., Baudry M. (Eds.), *Advances in Network Electrophysiology Using Multi-Electrode Arrays*. Springer, 69-111.
- [2] Heikkilä T.J., Ylä-Outinen L., Tanskanen J.M.A., Lappalainen R.S., Skottman H., Suuronen R., Mikkonen J.E., Hyttinen J.A.K., Narkilahti S. (2009). Human embryonic stem cell-derived neuronal cells form spontaneously active neuronal networks in vitro. *Experimental Neurology*, 218, 109-116.
- [3] Mummery C., Ward-van Oostwaard, D., Doevendans, P., Spijker, R., van den Brink, S., Hassink, R., van der Heyden, M., Opthof, T., Pera, M., de la Riviere, A.B., Passier, R., Tertoolen, L. (2003). Differentiation of Human Embryonic Stem Cells to Cardiomyocytes: Role of Coculture With Visceral Endoderm-Like Cells. *Circulation*, 107, 2733-2740.

Integration of Carbon Nanotubes in Microelectrode Arrays by Microcontact Printing and Electropolymerization for Neurostimulation and Biosensing Applications

Kai Fuchsberger^{1*}, Alan Le Goff², Ramona Gerwig¹, Claus Burkhardt¹, Janine Elit¹, Yingjia Li¹, Andreas Scheipers¹, Alfred Stett¹, Martin Stelzle¹

¹ NMI Natural and Medical Sciences Institute at the University of Tuebingen, Reutlingen, Germany

² Department of Pharmaceutical Sciences, University of Trieste, Trieste, Italy

* Corresponding author. E-mail address: kai.fuchsberger@nmi.de

Electrode functionalization by carbon nanotubes (CNT) was achieved by either micro contact printing of CNT layers or deposition of CNT / polymer composites by electropolymerization of poly(3,4-ethylenedioxythiophene). A procedure useful to pre-define thickness of CNT layers was developed. CNT content of suspensions was measured by UV/VIS absorption spectrometry and correlated with layer thickness obtained upon filtering through a nanoporous membrane. Microstamps made from a silicone elastomer were employed to transfer micropatterned layers of CNTs onto various substrate materials such as TiN and Si₃N₄. Electropolymerization of 3,4-ethylenedioxythiophene in the presence of CNT yields porous composites with a fibrous morphology.

1 Introduction

Electrical recording and stimulation of brain tissue *in vitro* and *in vivo* is widely used to gain an understanding of the central nervous system and in the development of neuroimplants for the treatment of central nervous system disorders^[1, 2]. So far, the interface between the electrical device and the brain tissue typically consists of a metal electrode. To decrease impedance and to enhance biocompatibility while maintaining electrode sensitivity new composite electrode coatings are developed.

Neuronal cells have shown exceptional viability and efficient integration with layers comprised of carbon nanotubes (CNT)^[3, 4]. CNT are biocompatible and biostable and layers exhibit a large effective porosity and surface area. This results in very favorable charge transfer capability^[5]. CNT layers are therefore considered an attractive candidate for the fabrication of stimulation electrodes in neuroprostheses. The ultimate goal of this research consists in robust technologies to fabricate mechanically stable, micropatterned layers of CNT and for their integration in neuroprostheses and biosensors.

2 Methods

Microcontact printing (μ CP) can be used to directly deposit CNT onto any surface while by electropolymerization CNT are embedded in a matrix of conductive polymer like polypyrrole or poly(3,4-ethylenedioxythiophene) (PEDOT)^[5]. For μ CP, Micromoulds were fabricated from glass, patterned using photolithography and etched in buffered

hydrofluoric acid. Stamps were fabricated from polydimethylsiloxane (PDMS). Functionalized multiwalled CNT were suspended and filtered to receive a homogeneous film. CNT are transferred to the PDMS stamps and printed onto multielectrode arrays. Electropolymerization of suspensions of ethylenedioxythiophene (EDOT, 0.02 M), Poly(sodium-p-styrenesulfonate) (1%) and carbon nanotubes (0.03%) was performed in a three electrode system under potentiostatic control at $U=1V$ vs. Ag/AgCl. Electrical properties and morphology of electrodes can be controlled by deposition protocols.

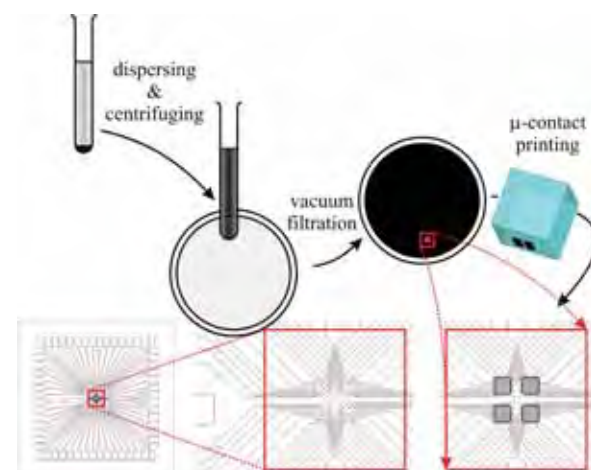


Fig. 1. Procedure for micro-contact printing of MWCNTs onto MEA

3 Results

Micropatterned CNT layers exhibiting a tunable thickness within 100 to 300 nm and were deposited on microelectrode arrays by means of μ CP (Fig. 1, 2). Layer and contact resistance, nanostructure and electrode capacitance were investigated. μ CP in particular allows for the deposition of CNT layers on insulators and on materials with low temperature resistance. Structural and electrochemical properties render these electrodes suitable for electrical stimulation and recording of neurons as well as for electrochemical detection of dopamine. Electropolymerization of electroactive monomers such as pyrrole or EDOT enables the fabrication of conductive CNT / polymer composites on electrodes (Fig. 3) which generally show low impedance when compared to uncoated electrodes.

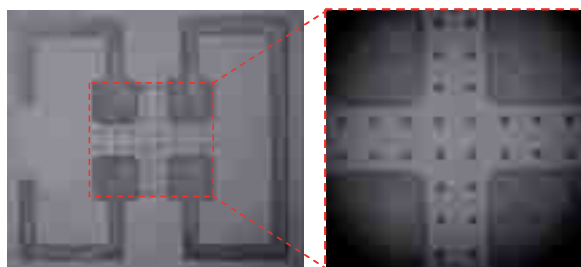


Fig. 2. Micro-patterned CNT layer on micro-electrode array by μ CP

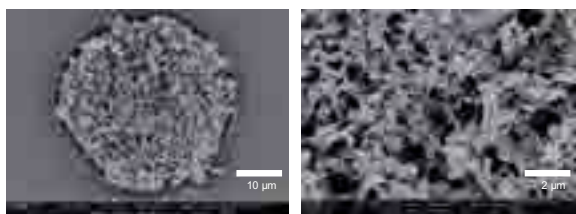


Fig. 3. CNT / PEDOT composite on MEA electrode deposited by electropolymerization from a suspension of CNT and EDOT

4 Conclusion

μ CP and electropolymerization have been used to generate well defined micropatterns of CNTs on MEAs. Thickness, morphology and electrical properties may be controlled by proper choice of deposition parameters. However, achieving sufficient mechanical stability and adhesion remains a critical prerequisite for these systems to be suitable for applications in neuroprosthetics.

Acknowledgement

Funding for this research was in part obtained from Multichannelsystems GmbH, Reutlingen and through grant “Incrimp” by the German Federal Ministry of Education and Research (BMBF), grant no. 16SV3F82.

References

- [1] D. R. Kipke, W. Shain, G. Buzsaki, E. Fetz, J. M. Henderson, J. F. Hetke, G. Schalk, *Journal of Neuroscience* 2008, 28, 11830.
- [2] K. D. Wise, D. J. Anderson, J. F. Hetke, D. R. Kipke, K. Najafi, *Proceedings of the IEEE* 2004, 92, 76.
- [3] V. Lovat, D. Pantarotto, L. Lagostena, B. Cacciari, M. Grandolfo, M. Righi, G. Spalluto, M. Prato, L. Ballerini, *Nano Lett* 2005, 5, 1107.
- [4] A. Mazzatenta, M. Giugliano, S. Campidelli, L. Gambazzi, L. Businaro, H. Markram, M. Prato, L. Ballerini, *J Neurosci* 2007, 27, 6931.
- [5] E. W. Keefer, B. R. Botterman, M. I. Romero, A. F. Rossi, G. W. Gross, *Nat Nanotechnol* 2008, 3, 434.

CNT electrodes for MEAs and neuronal applications

B. Stamm^{1*}, K. Schneider², L. Pastewka³, C. Burkhardt¹, W. Nisch¹, M. Häffner²,
M. Fleischer², M. Moseler³, S. Di Giovanni⁴, D. P. Kern², A. Stett¹

¹ NMI Natural and Medical Sciences Institute at the University of Tübingen, Reutlingen

² Institute of Applied Physics, University of Tübingen

³ Fraunhofer Institute for Mechanics of Materials IWM, Freiburg

⁴ Hertie Institute for Clinical Neuroscience, Tübingen

* Corresponding author. E-mail address: boris.stamm@nmi.de

Aim of this project is the development of electrodes coated by oriented carbon nanotube (CNT) films on microelectrode arrays (MEA) for in vitro and in vivo applications. Due to their low impedance, high charge transfer capacity and the chemically inert properties of carbon, CNT electrodes represent an improvement compared to conventional metal electrodes (e. g. titanium nitride). Low temperature synthesis of CNTs directly on the temperature sensitive substrates for these applications, like polyimide, is an unsolved problem yet.

1 Introduction

In drug discovery and basic research glass based MEAs are a well established in vitro system for recording and stimulating electrical activity of cell tissue like cortical neurons or heart cells [1].

Beyond in vitro systems, electrode arrays on flexible intracranial in vivo implants are used in neurosurgery for recording electrocorticograms (ECoG), e.g. in diagnostics and monitoring of preoperative epilepsy patients. Current intracranial implants can record the electrical activity of neuronal cells for a period of 7 up to 14 days. From a clinical point of view, a long term implantation is favoured, which requires high standards concerning biostability. Furthermore, for recording of electrical activity a low signal-to-noise ratio (SNR) and thus low impedance of the electrodes is desirable. Also an important attribute of electrodes for neuronal applications is their charge transfer capacity in case of stimulating neuronal tissue.

Electrodes made of carbon nanotubes provide high charge transfer capacity, low impedance and chemically inert properties [2, 3]. In particular CNT-electrodes based on flexible and biocompatible polyimide substrates are an appropriate system for neuronal in vivo applications. Due to the fact that CNT synthesis usually requires process temperatures above 500 °C, the fabrication of electrodes from vertically oriented CNTs on temperature sensitive substrates like polyimide still remains a challenge. In this project we aim at developing a low temperature synthesis process for deposition of CNTs on glass and polyimide substrates.

2 Materials and Methods

For CNT synthesis by chemical vapour deposition (CVD) an initial catalyst layer is deposited on the substrate. Established catalysts are cobalt, nickel and iron with a typical thickness of 10 nm. At the beginning of a regular high temperature CVD-process the thin catalyst layer rearranges into small particles from which CNTs start to grow. One possible approach for applying iron catalyst is ferritin: ferritin is a protein shell in which clusters of Fe³⁺ ions are stored. After removing the protein in an O₂-plasma, Fe clusters of nm size remain, consisting of iron-oxide, which is reduced to Fe during growth in an appropriate gas mixture [4].

A 600 nm thick layer of titanium nitride acts as a diffusion barrier between substrate and catalyst. The catalyst and thus the CNT electrodes can be structured in defined patterns ranging from 250 nm to 100 µm using lithography techniques. CVD processes for CNT growth employ a carbon containing gas atmosphere at pressures around 5 mbar. A typical gas mixture for CNT growth is C₂H₂ as carbon source and NH₃ as an etching and reducing agent to avoid catalyst poisoning during growth. In thermal CVD processes, temperatures above 700 °C are typical. In order to obtain vertically aligned CNTs at reduced growth temperatures, plasma enhanced CVD (PECVD) growth processes are established, in which part of the growth energy is supplied by the plasma.

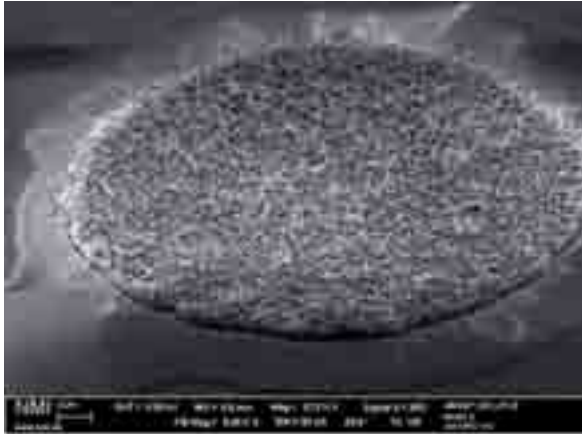


Fig. 1. Prototype of a CNT electrode, grown via thermal CVD. The electrode diameter is 30 micrometers

3 Results

Fig. 1 shows the prototype of a CNT electrode grown via thermal CVD at 700 °C on quartz glass as substrate.

PECVD growth processes applying a DC plasma discharge have been evaluated with respect to low substrate temperatures. On silicon test substrates, optimised CNT growth parameters were found at a pressure of 1.6 mbar, 10 W plasma power, and an NH_3 to C_2H_2 ratio of 8 to 1. Fig. 2 shows the CNT heights achieved with these parameters for different substrate temperatures and growth times.

Normally a 10 nm thick Ni catalyst layer was used. With a reduced Ni thickness of 2 nm, growth with the optimised parameters yielded a total CNT height of 1 μm at 350 °C growth temperature (Fig. 3). The applied DC plasma process is, however, restricted to conductive substrates like silicon. For insulating substrates like glass slides or polyimides, high frequency (RF) plasma will be used in the future.

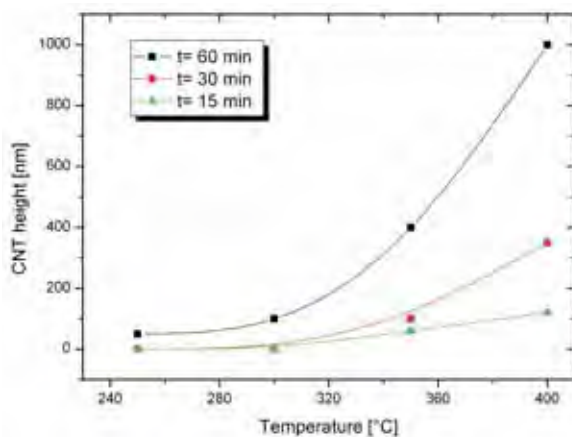


Fig. 2. CNT height vs. process temperature for 3 different growth times at optimised parameters

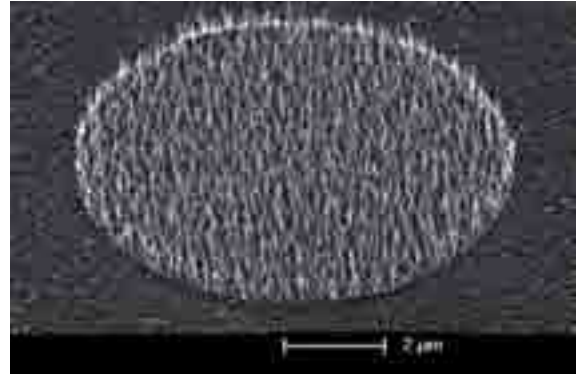


Fig. 3. CNTs grown at 350 °C with a total height of 1 μm

Simultaneously to the experimental work, numerical simulations of the fundamental processes concerning the catalytic growth are performed. In these simulations dewetting of nickel catalyst is studied using molecular dynamics simulations (Fig. 4). In particular, these simulations reproduce the stick-slip events seen in earlier in-situ transmission electron microscopy studies of tip-growth [5]. Overall dewetting occurs through diffusion of nickel atoms at the nickel-CNT interface. These results give insights into catalyst poisoning, and hence hints for an optimisation of the actual processes.



Fig. 4. Simulation of dewetting of nickel atoms (red) along the CNT wall (black)

Acknowledgement

This work is supported by the Baden-Württemberg Stiftung under grant-ID MST II - 12. M.F. gratefully acknowledges support by the European Social Fund and by the Ministry of Science, Research and the Arts Baden-Württemberg.

References

- [1] Stett A., Egert U., Guenther E., Hofmann F., Meyer T., Nisch W., Haemmerle H. (2003). Biological application of microelectrode arrays in drug discovery and basic research. *Analytical and Bioanalytical Chemistry*, 377, 486-495.
- [2] Keefer E.W., Botterman B.R., Romero M.I., Rossi A.F., Gross G.W. (2008). Carbon nanotube coating improves neuronal recordings. *Nature Nanotechnology*, 3, 434-439.
- [3] Lin C.M., Lee Y.T., Yeh S.R., Fang W. (2009). Flexible carbon nanotubes electrode for neural recording. *Biosensors and Bioelectronics*, 24, 2791-2797.
- [4] Häffner M., Schneider K., Schuster B.-E., Stamm B., Lattayer F., Fleischer M., Burkhardt C., Chassé T., Stett A., Kern D.P. (2010). Plasma enhanced chemical vapor deposition grown carbon nanotubes from ferritin catalyst for neural stimulation microelectrodes. *Microelectronic Engineering*, 87, 734-737.
- [5] Helveg S., López-Cartes C., Sehested J., L. Hansen P., S. Clausen B., R. Rostrup-Nielsen J., Abild-Pedersen F., K. Nørskov J. (2004). Atomic-scale imaging of carbon nanofibre growth. *Nature* 427, 423-426.

Microscope Setup For Laser Manipulation And Long-Term Monitoring Of Neuronal Cell Cultures

Torben Harbodt¹, Reinhard Galneder¹, Susann Schröder¹, Karl-Heiz Boven², Christian Hembd³, Alfred Stett^{1*}

¹ NMI Natural and Medical Sciences Institute at the University of Tübingen, Reutlingen, Germany

² Multi Channel System MCS GmbH, Reutlingen, Germany

³ TILL Photonics GmbH, Gräfelfing, Germany

* Corresponding author. E-mail address: stett@nmi.de

To investigate and manipulate developing neural networks we developed a microscope platform that allows long-term optical and electrophysiological monitoring of cell cultures on MEAs and microdissection of neurites using a pulsed UV-Laser (355 nm). We succeeded in selectively disconnect single neurons from a network cultured on a MEA.

1 Introduction

Microelectrode arrays (MEAs) are routinely used for electrophysiological investigation in neurophysiology and cardiovascular research. To allow for electrophysiological and optical long-term monitoring and sterile manipulation of neuronal cell and organotypic tissue cultures we developed a modular setup containing an imaging workstation, a laser for microdissection and a MEA system.

2 Methods

The platform combines the automated microscope iMIC 2000 (TILL Photonics) and the MEA System from Multi Channel Systems MCS. A 355nm diode pumped solid state laser (μ Flare, InnoLight) is coupled into the optical pathway of the microscope via a beam expander (Fig. 1). The energy per pulse is about $5\mu\text{J}$ and pulse repetition rate is 10 kHz. A neutral density filter is used to control deposited laser energy in the cell culture. The diameter of the focussed beam in the object plane is about $1\mu\text{m}$.

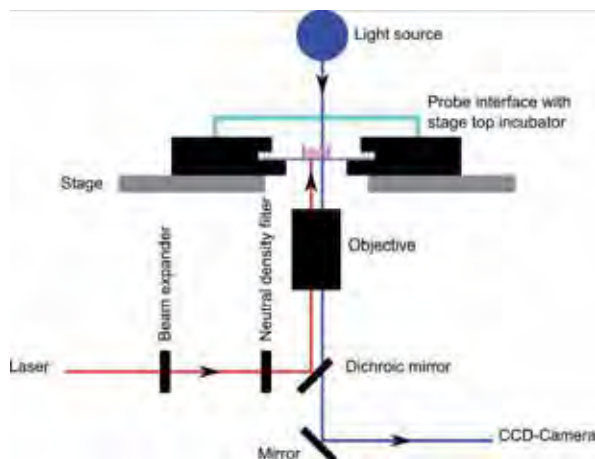


Fig. 1. Schematic drawing of the optical pathway of the microscope.

Neuronal cells from SD-rats cortex were cultured on standard MEAs (MCS, 200/30iR-ITO-w/o). A miniaturized incubator chamber with integrated heating element, temperature sensor and controlled humidity (37°C , 5% CO_2 , 97% rel. humidity) allows for long-term culturing and recording and synchronized time-laps recording.

3 Results

Fig. 2 shows cell clusters growing on a MEA (div 14 days) and corresponding spontaneous network activity (Fig. 3). To isolate a cluster from the network each neurite was cutted by laser irradiation of 2 ms duration. After the manipulation the isolated cluster showed no activity whereas the network activity was undisturbed.

Fig. 4 shows a time-lapsed imaging of cultured neurons on a MEA (div 10 days). The arrow marks a single cell which moves in a period of 25 hours.

4 Conclusion

The proof of principle experiments demonstrated the possibility to isolate single axons and dendrites in a reproducible manner. In combination with long-term signal recording and time-lapse imaging this setup is suitable to investigate plasticity in developing and injured neuronal networks.

Acknowledgement

Supported by German Ministry for Education and Research (BMBF), grant 16SV237.

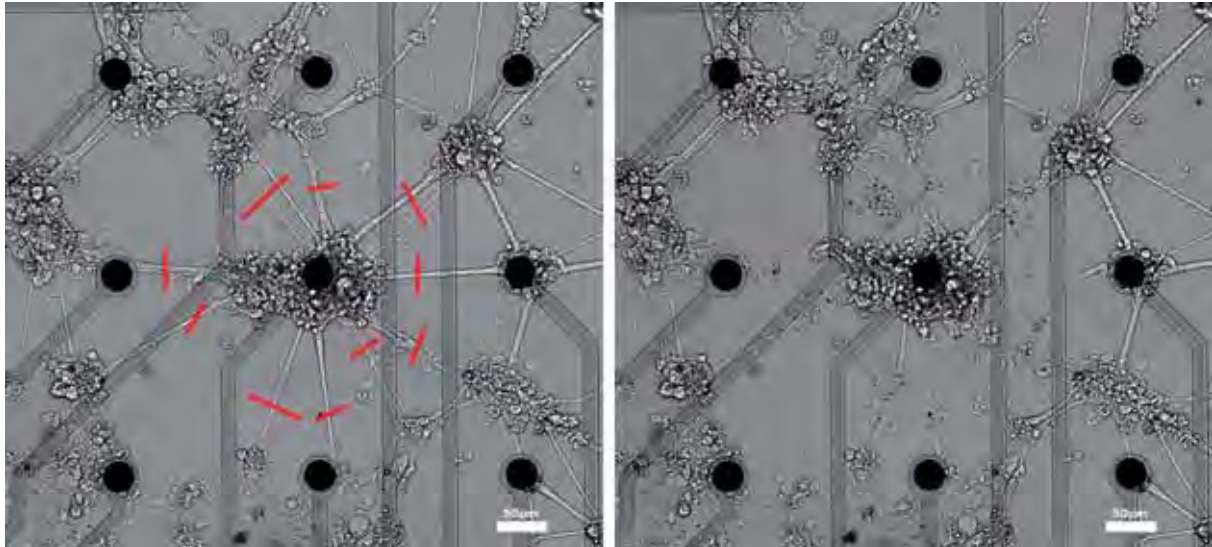


Fig. 2. Isolation of a cell cluster. Left before cutting the neuritis, right after successful cutting. The black lines (left) indicate the cutting positions.

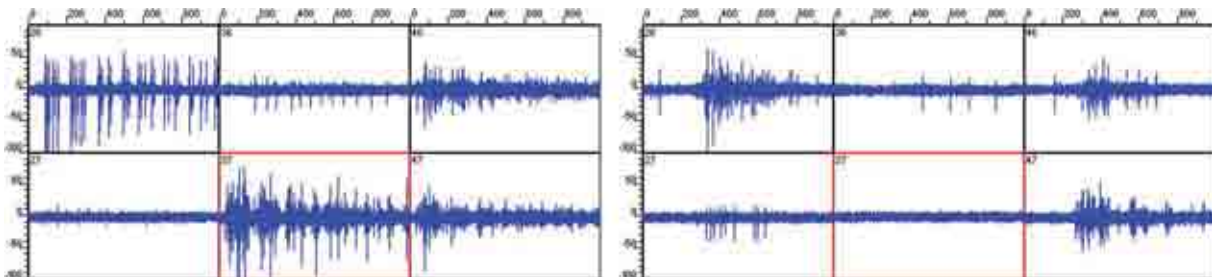


Fig. 3. Recorded signals before and after isolation. The red square indicates the signal from the electrode beneath the isolated cluster (last row, center electrode)

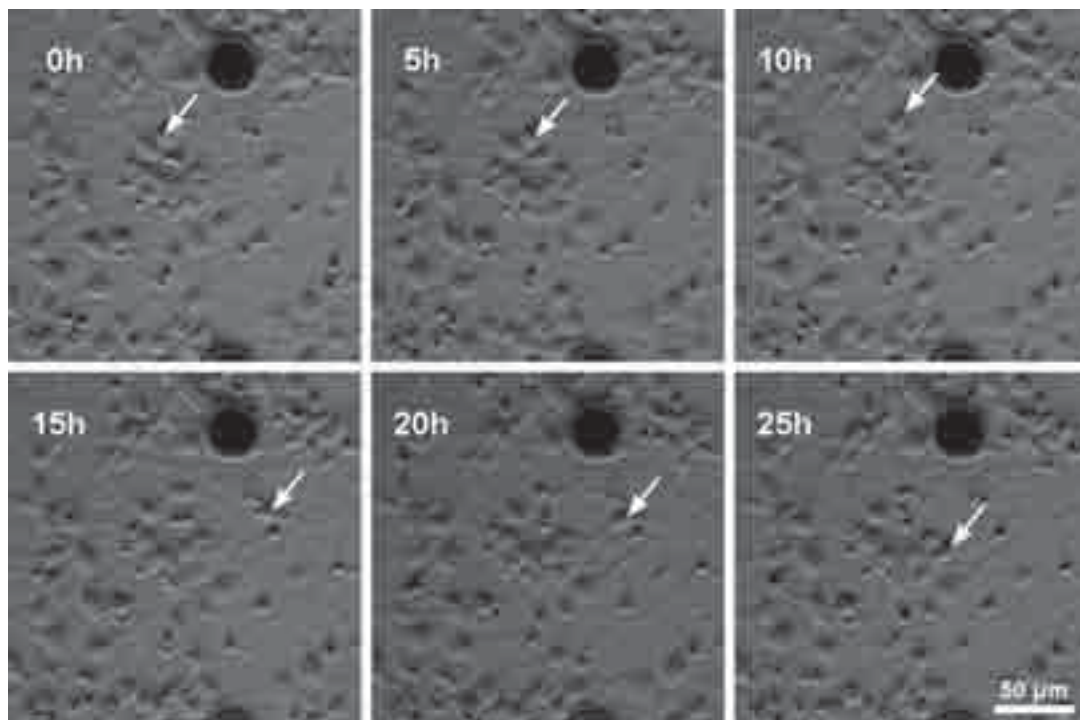


Fig. 4. Time-lapse imaging shows the movement of a single cell cultured on a microelectrode array.

Electrical and Optical Recording of Interactions between Small Neuronal Networks using Needle-Type Microelectrodes

Aki Saito*, Hiroyuki Moriguchi, Miho Goto, Atsushi Saito, Yuzo Takayama, Kiyoshi Kotani, Yasuhiko Jimbo

Graduate School of Frontier Sciences, University of Tokyo, 5-1-5 Kashiwanoha, Kashiwa-shi, Chiba 277-8563, Japan

* Corresponding author. E-mail address: saito@bmpe.k.u-tokyo.ac.jp

We have developed a practical experimental method to mass-produce and maintain a variation of minimal neuronal networks (“small neuronal networks”) consist of a single to several neurons in culture using spray-patterning technique. By using this method, micro neuronal networks of rat hippocampal cells were cultured for more than 4 weeks and the interaction between the networks was investigated by means of calcium imaging. The spontaneous intracellular calcium activity indicated that the small neuronal networks showed synchronized activity even without morphologically observable intercellular connections.

1 Introduction

Recent advances in micro-fabrication and recording techniques enable us to monitor electrical activity in numerous numbers of neurons at the same time, which are significant for investigating the biological information processing. In particular, microelectrode array (MEA) – based electrical recording system for cultured neuronal networks have attracted the broad attentions for studying the developmental and maturation processes of neuronal networks because of its capability of spatio-temporal and non-invasive recording [1-3]. Difficulties in controlling the morphology of dissociated cultured networks, however, have been the significant problem to obtain statistical and reproducible results. This is mainly due to a large number of constitute neurons in networks even in culture system. To address this, we have developed a practical experimental method to mass-produce small neuronal networks consist of a single to several neurons in culture. In this paper, we carried out electrical and optical recording of spontaneous activity in small neuronal networks and considered the morphologically non-connected neuronal networks between them.

2 Methods and Methods

2.1 Micropatterning

The bottom surfaces of 35-mm polystyrene culture dishes were precedently coated with 1 % Agarose L solutions to make a cell - nonadhesive layer. Afterwards, the Poly-D-Lysine (PDL) solutions were randomly sprayed onto the agarose layer in order to form cell – adhesive regions (Fig. 1). Hippocampal neurons were obtained from 17 ~ 19 – day – old

Wistar rat embryos and were plated onto the micropatterned surfaces at a density of 50,000 cells/cm². Cultures were maintained in Neurobasal™ Medium with 2%(v/v) B27, 0.5mM glutamax and 1%(v/v) penicillin-streptomycin. Half of the medium was conditioned by rat astrocyte to keep a steady environment.

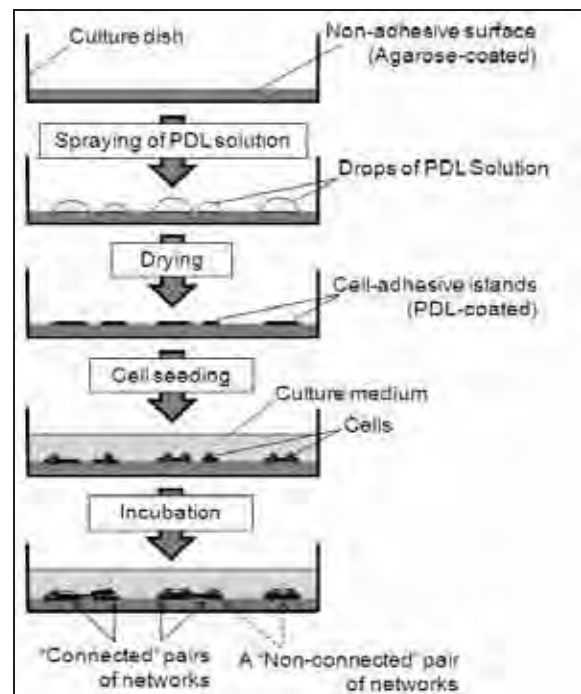


Fig. 1. A schematic diagram of the production process of micro neuronal networks using spray-patterning technique. Distributed PDL microdrops form cell-adhesive islands on the non-adhesive surface of agarose-gel. Distributing PDL solution at random leads to the production of morphologically “connected” and “non-connected” networks at once on a culture surface.

2.2 Measurement

Spontaneous activity in small neuronal networks was monitored by both electrical and optical recording technique. Electrical activity in neurons was extracellularly recorded with custom-made needle-type microelectrode. The needle-type microelectrode was made by referring to the previous study[4]. Briefly, tungsten wires were inserted into fine glass pipeeyes, fixed at the endpoints and coated with platinum-black (Fig. 2). The extracellular recording using these microelectrodes was carried out by handling the tips of the microelectrodes close to the cell bodies of cultured neurons using micromanipulator. Extracellular voltages obtained through the needle-type microelectrode was amplified and recorded using the one channel of 64 channel MEA-based measurement system. And, fluorescence changes in several small networks were simultaneously measured using calcium indicator dye fluo-4.

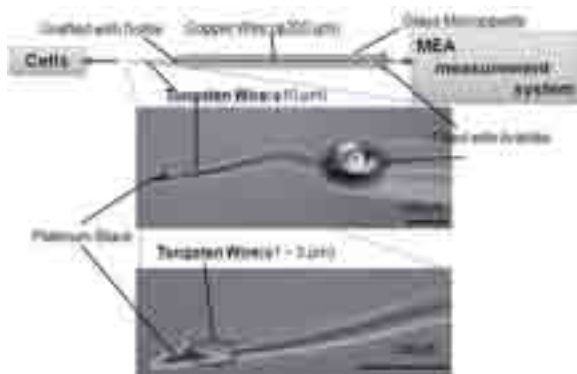


Fig. 2. A schematic of our handmade metal needle-type microelectrode and apical part.

3 Results

By using the spray-patterning method, a large number of cell-adhesive micro regions were formed. The diameters of the micro regions were in the range of 150 – 250 μm . Neurons extended neurites along the edge of the cell-adhesive micro regions and form small neuronal networks. On the average, five neurons were plated in the micro regions at a present cell density. In part of micro regions, some neurite was protruded from the region, and thus small neuronal networks were connected with synapses (Fig. 3A and 4A). In these networks, a single neuron-induced network activity was observed. On the other hand, even in morphologically non-connected neuronal networks, synchronous oscillations between small neuronal networks were observed (Fig. 4).

4 Conclusion

Our micro-patterning methods and results provide the possibility that synchronous activity occurred between morphologically non-connected neuronal networks.

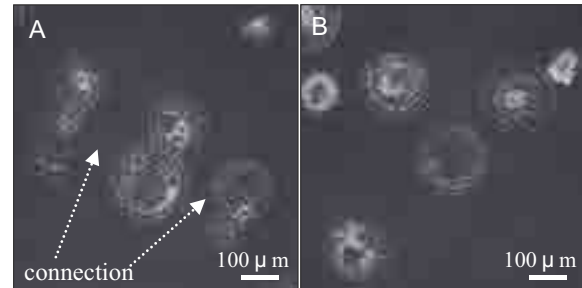


Fig. 3. Phase-contrast images of small neuronal networks at 33 DIV. A : Small networks in each region are connected with sparse neurites. B : Small neuronal networks formed on cell-adhesive regions. Small networks in each region are isolated from each other.

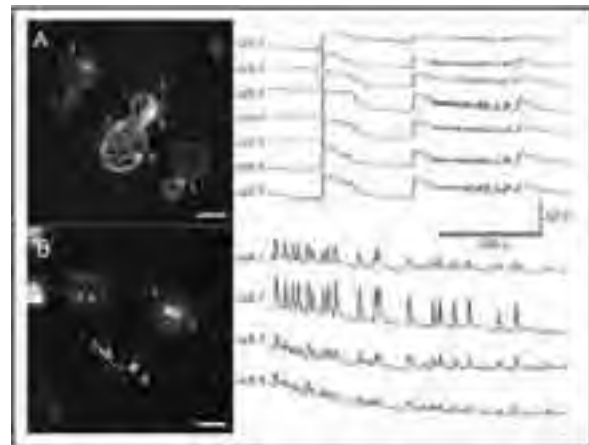


Fig. 4. Time courses of the spontaneous Ca^{2+} changes recorded from morphologically connected (A) and non-connected (B) micro neuronal networks. Left: Fluorescent images of the micro neuronal networks loaded with fluo-4 AM. Right: Traces of intracellular calcium level recorded from cells indicated in the fluorescent micrographs. Synchrony was observed in the transient calcium uptakes between both the morphologically connected and non-connected networks. Scale bar, 100 μm .

References

- [1] G. W. Gross. (1979). Simultaneous single unit recording in vitro with a photoetched laser deinsulated gold multimicroelectrode surface. *IEEE Trans. Biomed. Eng.*, **26**, pp. 273-279
- [2] J. Pine. (1980). Recording action potentials from cultured neurons with extracellular microcircuit electrodes. *J. Neurosci. Methods*, **2**, pp. 19-31
- [3] Y. Jimbo, *et al* (1993): Simultaneous measurement of intracellular calcium and electrical activity from patterned neural networks in culture, *IEEE Trans. Biomed. Eng.*, **40**, pp. 804-810
- [4] H. Moriguchi, *et al* (2008): Extracellular Recording from Mass-produced Small Neuronal Networks using Mobile Metal Microelectrodes, MEA Meeting 2008 Int., pp. 267-270

High-density micro-needles for in vitro neural studies

D.E. Gunning^{1*}, P. Hottowy², W. Dabrowski², J. P. Hobbs³, J.M. Beggs³, A. Sher⁴, A.M. Litke⁴, C.J. Kenney⁵, K. Mathieson¹

¹ Department of Physics and Astronomy, University of Glasgow, Glasgow, UK

² Faculty of Physics and Applied Computer Science, AGH University of Science and Technology, Krakow, Poland

³ Biocomplexity Institute, University of Indiana, Bloomington, IN, USA

⁴ SCIPP, University of California Santa Cruz, Santa Cruz, CA, USA

⁵ SLAC National Accelerator Laboratory, Menlo Park, CA, USA

* Corresponding author. E-mail address: d.gunning@physics.gla.ac.uk

Much information has been discovered about the behaviour of individual neurons. Significantly less, however, is known about the interactions between these neurons in the brain and how they result in meaningful patterns of neural activity. Here, an array of micro-needles capable of penetrating in to slices of neural tissue has been designed and fabricated. In acute slices of brain, surface layers of neurons are damaged and have severed connections. The penetrating action of these micro-needles bypasses this layer to study healthy neurons with their original network structure. A reliable fabrication process for these micro-needle arrays has been developed. Mechanically and electrically, they perform well. With small, biocompatible, low-impedance ($150\text{k}\Omega$ at 1kHz) tips, these needles record extracellular action potentials from ~ 12 individual cortical neurons and with $\sim 20:1$ signal to noise. A state-of-the-art system, in terms of temporal and spatial resolution and area coverage, has been manufactured.

1 Introduction

The brain works through complex interactions of billions of neurons. In order to study these interactions, neurobiologists have, for years, used planar arrays of extracellular microelectrodes to record simultaneously the electrical behaviour of many neurons. The use of such electrode arrays has been incredibly successful in studies with retina [1], cultured neurons [2] and also in vivo studies with planar arrays patterned on to silicon probes [3]. There is a large gap, however, in technologies capable of recording from neurons in acute slices, arguably the closest in vitro model of the working brain. The limiting factor of planar arrays is their ability to record only from neurons lying close to the surface of the array. In preparing acute slices ($\sim 300\mu\text{m}$ thick), the cutting process damages the surface layer of neurons and their connections, effectively forming a resistive layer of tissue between the electrodes and healthy neurons with intact circuitry. Arrays of needle electrodes address this problem by penetrating into the tissue bypassing the damaged layer. Existing devices of this nature have widely spaced needles far larger than typical neuron spacing, resulting in significant sub-sampling of the neuronal population [4] [5]. The array made here has 61 hexagonally close-packed needles with $60\mu\text{m}$ spacing and small conducting tips to record the electrical behaviour of individual neurons in a local network. It has been used successfully to record action potentials from several cortical neurons in a single acute slice preparation

with a signal to noise of up to 20:1 and signal amplitudes of $\sim 100\mu\text{V}$.

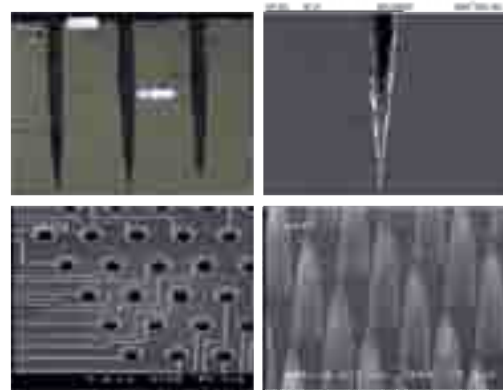


Fig. 1. Top left: Cross section of holes etched in to a silicon wafer. Top right: Cross section of a hole with oxide, tungsten and polysilicon deposited. Bottom left: Surface of silicon wafer with hole openings and aluminium readout. Bottom right: Array of $100\mu\text{m}$ needles with silicon dioxide sidewall insulation.

2 Method

The device is made using a novel combination of semiconductor fabrication techniques. The design is compatible with existing low noise pre-amplification and stimulation circuitry that provides excellent temporal resolution ($50\mu\text{s}$) [6]. The array is comprised of 61 hexagonally close-packed needles with $60\mu\text{m}$ inter-needle spacing and each needle can be engineered to measure up to $200\mu\text{m}$ in height. Etching high aspect ratio holes on the front side of a silicon

wafer is the first step in the process (Fig. 1 top left). A $2\mu\text{m}$ thermal oxide is grown forming the needle sidewall insulation. LPCVD (low pressure chemical vapour deposition) tungsten is deposited ensuring a conformal coating is achieved since the tapered point of a hole becomes the conducting tip of a needle. For strength, the holes are partially filled with polysilicon (Fig. 1 top right). $1\mu\text{m}$ of aluminium is deposited and etched to form conducting tracks connecting each electrode individually to a bond pad for wire bonding to the readout PCB (Fig. 1 bottom left). The bulk silicon, on the backside of the wafer, is etched, using a chemical wet etch (25% TMAH), exposing the needle tips.



Fig. 2. An SEM image of the tip of a single needle. Platinum black has been electroplated on the tip to lower the electrode/electrolyte impedance. This electrode has an impedance of $\sim 150\text{k}\Omega$ at 1kHz .

The size of the conducting tip is controllable in size down to a few microns in diameter and is defined at this stage. The oxide is partially etched using buffered hydrofluoric acid. The remaining silicon is etched as before, defining the length of the needle (Fig. 1 bottom right). A blanket oxide etch thins the sidewall insulation but completely removes the thinner oxide at the needle tip, exposing tungsten. This tungsten is electroplated with platinum black [7] to lower the electrode/electrolyte impedance (see Fig. 2). The result is an array of closely spaced, low impedance, biocompatible electrodes with low noise at high spatial resolution. To quantify this: a typical electrode has, at 1kHz , an impedance of $150\text{k}\Omega$ and $\sim 5\mu\text{V}$ RMS noise.

3 Results

In pilot experiments, acute slices of rat barrel cortex were placed on to an array of needles. Using an artificial cerebrospinal fluid (using 5mM K^+) and precise temperature control (37°C), the slice was kept alive and the spontaneous activity of the cells was recorded. The slices were cut $300\mu\text{m}$ thick to allow perfusion of oxygen to cells throughout the tissue slice. It was observed that both somatic and axonal action potentials of individual neurons could be detected across the whole array of electrodes, with typical action potential amplitudes of $100\mu\text{V}$ and a signal to noise ratio of up to 20:1. Figure 3 is a 3 second sample of data taken from a single electrode

and shows a number of action potentials. This is typical of data taken across the array. On the right, a typical extracellular somatic (from the cell body) action potential recorded from rat cortex is shown. It has the expected duration of 1ms and amplitude $\sim 90\mu\text{V}$. Using a principal components analysis technique, characteristics of each action potential are used to attribute it to a specific neuron and feature of a neuron (axon, soma and dendrites) [8]. These neurons can then be mapped across the array with ~ 12 neurons being recorded from in each preparation.

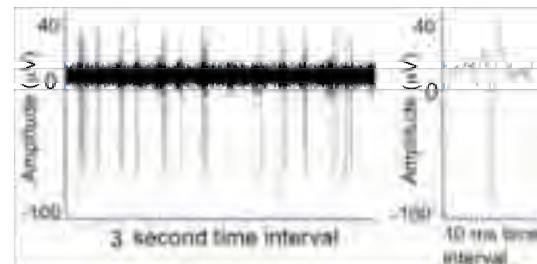


Fig. 3. Example of action potentials recorded from a single electrode from a neuron in rat cortex. Left: A recording of up to $100\mu\text{V}$ action potentials over a 3 second time interval. Right: A single action potential of duration $\sim 1\text{ms}$ and amplitude $90\mu\text{V}$

4 Conclusions

An advanced micro-needle technology, capable of recording action potentials from a population of individual neurons, at high spatial density, has been developed. It is possible to record from a network of tens of neurons from the central region of an acute slice of brain where the network connections are intact. The planned future of this technology is to scale to an order of magnitude more electrodes with multiple needle heights across an array allowing a larger area and volume of tissue to be studied. Combined with the arbitrary patterned electrical stimulation capability of the existing readout electronics [6], this work has important implications for furthering the understanding of network dynamics in slices of brain tissue.

Acknowledgement

We thank the EPSRC for funding, the Queen's University Belfast for LPCVD depositions and the University of Glasgow for technical support.

References

- [1] M. Meister, *J. Neurosci. Meth.* 51 (1994) 95-106.
- [2] J.M. Beggs, *J. Neurosci. Meth.* 35 (2007) 11167-77.
- [3] T.J. Blanche, *J. Neurophysiol.*, 93 (2005) 2987-3000.
- [4] K.D. Wise, *Proc. Of IEEE*, 92 (2004) 76-79.
- [5] M.O. Heuschkel, *J. Neurosci. Meth* 114 (2002) 135-148.
- [6] P. Hottowy, *Proc. of MEA meeting* (2008) 259-262.
- [7] G. Jones, *J. Am. Chem. Soc.* 57 (1935) 280-284.
- [8] A.M. Litke, *IEEE Trans. Nucl. Sci.* 51 (2004) 1434- 1440.

Polymeric Micro Technologies for Flexible Actuator Devices

Rakefet Ofek Almog^{1*}, Yelena Sverdlov¹, Tsvi Shmilovich¹, Slava Krylov¹, Aryeh Taub², Yosi Shacham-Diamand¹

¹ Faculty of Engineering, Tel Aviv University, Tel Aviv, Israel

² Psychobiology Research Unit, Tel Aviv University, Tel Aviv, Israel

* Corresponding author. E-mail address: ofek.almog@gmail.com

A Flexible microelectrode array of devices was fabricated on a polymer substrate, where the metal lines are embedded onto the polymeric structure of PDMS (Polydimethylsiloxane, elastomer-base polymer), using a photolithography process.

Polymeric based micro actuators were fabricated by integration of organic conductors (conductive polymer) on polymeric substrates. A flexible actuators process was developed integrating a polymer substrate and a conductive polymer (polypyrrole) deposited on a thin metal seed. The relatively thick polypyrrole on thin metal seed (e.g. Copper) is flexible enough shunting cracks in the metal, thus increasing the device durability and reliability.

1 Introduction

Over the last two decades, a great deal of research was concerned with patterning of polymer films which can be used as components in molecular electronics, optical devices, etch resists, biosensors and as scaffolds for tissue engineering and fundamental studies in cell biology. In addition to their electrical properties, they offer attractive mechanical properties, such as flexibility and immune to cracking[1].

Among such polymers, conjugated organic polymers are especially attractive since they offer several advantages over the metals and the conventional inorganic semiconductors, such as more facile processing and ease of adjusting the conductivity in a wide range. They can be considered as potential alternatives to the metals and semiconductors as connecting wires and conductive channels, which can be used as active materials in optoelectronics, microelectronics, micro electromechanical systems (MEMS) and sensors [2].

2 Experimental

A Flexible micro electrode array was fabricated on PDMS (Polydimethylsiloxane) substrate, using a photolithography process (Fig.1) Ppy (Polypyrrole, a conductive polymer) was deposited on the micro actuator's copper seed layer by electropolymerization using cyclic voltammetry (CV). Thus, we developed a process for a flexible electrode that integrates a polymer substrate and a conductive polymer.

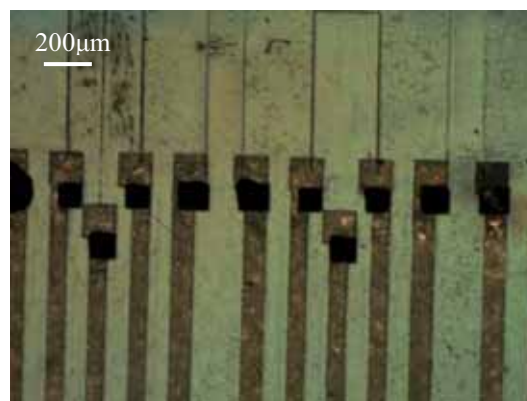


Fig. 1. Electrodeposited PPy –Microscope picture of part of the MEA of Flexible Actuator Devices

3 Results

The thickness of the polypyrrole was measured using a Tencor Alpha Step 500 Profilometer. The thickness of the polypyrrole as a function of the number of cycles is demonstrated in Fig. 2. It can be seen that the thickness increased as the number of CV cycles increased.

We developed a photolithography process for electrodes on organic substrate with conductive polymers. Moreover, selective electrochemical polymerization of polypyrrole was performed: Polypyrrole was embedded in flexible devices configuration that can serve as sensors or actuators. (Fig. 3) Their structure consisted of metal (copper) connectors embedded on a flexible PDMS polymer. Polypyrrole was selectively deposited (using electropolymerization) on the embedded copper “windows”.

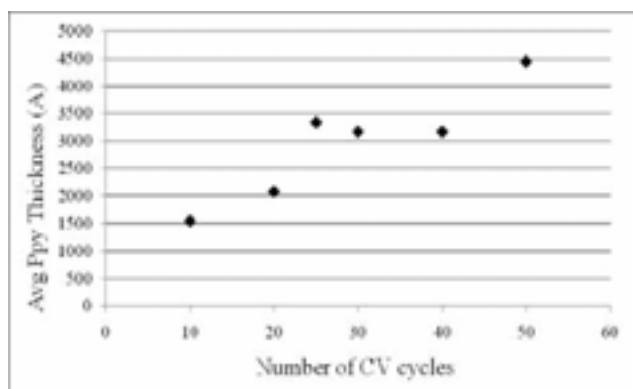


Fig. 2. Thickness of the PPy films, obtained by anodic electropolymerization of pyrrole as a function of the number of cycles.

Acknowledgement

This work was partially supported by the BMP MAGNET program of the Office of the Chief Scientist, Israeli Ministry of Trade and Industry (flexible actuator)

References

- [1] B.A. Weisenberg, D.L. Mooradian. (2002), *J Biomed Mater Res.*, 60, 283–291.
- [2] N.K. Guimard , N Gomez, CE Schmidt, (2007) *.Prog. Polym. Sci.*, 32, 876–921.

4 Conclusions

The polypyrrole is reinforcing the copper wires and electrically shunting the interconnects, increasing thereby the device durability and reliability, especially under stress conditions such as electrode multiple bending.

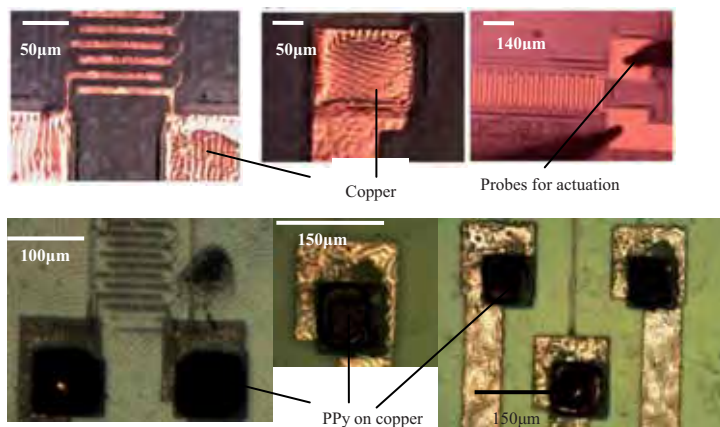


Fig. 3. Microscope picture of Electrodeposited PPy on Flexible Actuator Devices

Mussel-Inspired Polymer Coating for Surface Modification of MEA Applications

Kyungtae Kang¹, Min Jee Jang², Insung S. Choi^{1*}, Yoonkey Nam^{2*}

¹ Molecular-Level Interface Research Center, Department of Chemistry, KAIST, Daejeon 305-701, Korea

² Department of Bio and Brain Engineering, KAIST, Daejeon 305-701, Korea

* Corresponding author. E-mail address: ynam@kaist.ac.kr and ischoi@kaist.ac.kr

To be applied to myriad of surfaces and sophisticated purposes, surface modification methods for neuron-surface interfaces should be independent of the surfaces and versatile for the incorporation of various functionalities. Currently, the methods are yet to be advanced in order to meet the both criteria. Herein, we report a novel and powerful surface chemistry using mussel-inspired polymer for generating effective platforms for dissociated neuronal cultures. We coated polydopamine films to various surfaces which are being frequently used in neuronal applications and subsequently functionalized them with amine-based molecule for the viability of neurons on each surface. The polydopamine films exhibited uniform and reproducible surface properties and also biocompatibility for neurons independent of surface materials. In addition, spontaneous and evoked neural activities were readily recorded from the neurons culture on the polydopamine film coated on the microelectrode array.

1 Introduction

There have been numerous approaches immobilizing amine-containing molecules to MEAs for the generation of cell-adhesive surfaces[1,2]. However, previous reports mainly have used physisorption to modify the surfaces, which could hardly generate long-lasting and uniform surface coatings. In order to overcome these hurdles, there also have been a few approaches using covalent linking[3]. In their reports, covalent linking strategy was able to generate not only stable and uniform surface coatings but also versatile surfaces for the introduction of various functions[2]. However, there is still a need for better surface modification strategy for MEAs, since every covalent linking strategy targets their own specific surface material and MEAs are composed of more than two different surfaces. To this end, it is required that surface modification strategy be independent of the surface material.

Herein, we report the application of mussel-inspired polymer coating strategy for the modification of the MEA surfaces. Recently, mussel-inspired surface chemistry was reported by Messersmith *et al.*[4]. This strategy fit the mentioned requirements quite well, because it is not affected by the surface material, and covalently interacts with amine or thiol containing molecules. In this study, we optimized the mussel-inspired polymer coating strategy to be used in neuron cultures, and demonstrated the successful performance of the optimized strategy, including patterned neuronal growth and recording of neuronal networks after 3 weeks in culture.

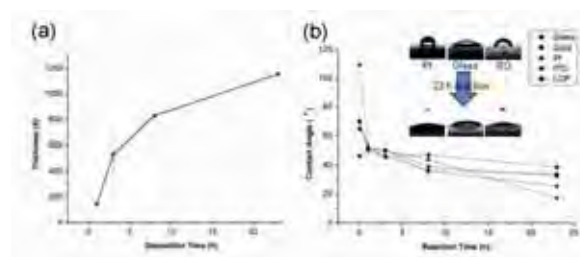


Fig. 1. (a) Thickness of deposited polydopamine films on gold. (b) Change of the water contact angles on the polydopamine films deposited on various surfaces.

2 Methods

Mussel-inspired polymer coating strategy was tested on the surfaces of various materials which have frequently been used for MEAs. We followed published procedures in order to deposit polydopamine films[4]. In addition, we controlled reaction time to optimize the thickness of the polydopamine polymer. For covalent linking of biomolecules, poly-D-lysine (PDL, 0.1 mg/mL) was dissolved in 10 mM Tris-HCl (pH 8.5), and polydopamine-coated substrates were immersed into the solution. After overnight incubation, the substrates were rinsed and dried. Hippocampal neurons were plated onto the PDL-immobilized polydopamine film at the density of 200-1000 cells/mm².

3 Results

The formation of polydopamine coating was confirmed by measuring thickness and water contact angle. According to our result, thickness of

polydopamine film deposited on gold surface was proportional to the reaction time, which was consistent with the previous result[4] (Fig. 1(a)). From the water contact angle measurement, we could conclude that only 1-h reaction was enough to generate effective polydopamine films independent of substrate material, as their water contact angle was converged to the value about 50° (Fig. 1(b)). Hippocampal neurons grown on the PDL-immobilized polydopamine films were healthy and their spontaneous activity was recordable at 17 days in vitro (DIV) (Fig. 2). The mean amplitude of recorded spikes was around 100 μ V and every spike was highly synchronized through all recordable electrodes. Patterned neuronal networks could be obtained by micro-contacting printing PDL on polydopamine film.

4 Conclusion

We demonstrated the successful application of mussel-inspired polymer coating strategy to the surface modification of the MEAs. We expect that this strategy can be adapted to various MEA applications.

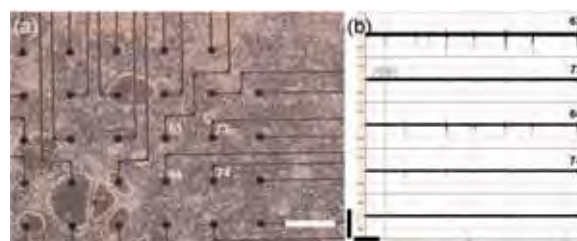


Fig. 2. (a) Neuronal cultures on PDL-linked polydopamine-coated MEA (17 DIV). Scale bar: 200 μ m. (b) Multichannel recording from neuronal cultures on modified electrodes. Scale bar: 5 s, 200 μ V. The numbers (white in (a) and black in (b)) represent the electrodes and the recorded traces responsible for them.

References

- [1] Chang J. C., Brewer G. J., Wheeler B. C. (2000). Microelectrode array recordings of patterned hippocampal neurons for four weeks. *Biomed. Microdevices*, 2, 245-53.
- [2] Branch D. W., Wheeler B. C., Brewer G. J., Leckband D. E. (2000). Long-term maintenance of patterns of hippocampal pyramidal cells on substrates of polyethylene glycol and microstamped polylysine. *IEEE Trans. Biomed. Eng.*, 47, 290-300.
- [3] Nam Y., Branch D. W., Wheeler B. C. (2006). Epoxy-silane linking of biomolecules is simple and effective for patterning neuronal cultures. *Biosense. Bioelectron.*, 22, 589-597.
- [4] Lee H., Dellatore S. M., Miller W. M., Messersmith P. B. (2007). Mussel-inspired surface chemistry for multifunctional coatings. *Science*, 318, 426-430.

All-polymer MEAs: Challenges, Features and Perspectives

Axel Blau^{1*}, Angelika Murr², Sandra Wolff³, Jens Wüsten², Francesco Difato¹, Christiane Ziegler³, Fabio Benfenati¹

1 The Italian Institute of Technology (IIT), Dept. of Neuroscience and Brain Technologies (NBT), Via Morego 30, 16163 Genoa, Italy, www.iit.it, *axel.blau@iit.it

2 Institut für Mikrotechnik Mainz GmbH (IMM), Carl-Zeiss-Str. 18-20, 55129 Mainz, Germany, www.imm-mainz.de

3 Nano+Bio Center (NBC) at the University of Kaiserslautern, Erwin-Schrödinger-Str. 13, 67663 Kaiserslautern, Germany, www.nbc.uni-kl.de

Besides summarizing briefly the overall concept of polymer MEAs, we present a straightforward strategy for translating the layout and performance of passive electrode devices from metal to all-polymer microelectrode arrays with peculiar and promising electrical, optical and mechanical characteristics. We briefly discuss the differences in the wide-frequency band impedances between various types of flexible conductors and common MEAs. We demonstrate that polymer devices with polymer conductors capture membrane potential fluctuations with high fidelity, be it from acute cardiomyocyte preparations [1] or from cultures of neural networks. *PolyMEAs* may thus complement metal-based electrode arrays not only for *in vitro* experiments, but also in *in vivo* scenarios where flexibility, biocompatibility and transparency is of major concern, be it in retinal implants or supracortical recording devices.

1 Introduction

Microelectrode arrays (MEAs) for *in vitro* applications look back at a history of almost four decades [2]. As most of us associate the word electrode with some sort of metal or semiconductor, in recent years organic conductors have matured to be integrated into solar cell panels, batteries, displays and other consumer devices. While they thus opened a new chapter for common day electronics, their integration into biomedical devices is still in its infancy. Two of the main reasons are i) the requirement of resorting to non-standard fabrication processes and ii) their inherently low conductivity, which is comparable to that of semiconductors ($<10^2$ S/m vs. $<10^8$ S/m of metals). We exemplarily demonstrate that organic conductors are nonetheless suitable bioelectrical signal transducers and have features and advantages that outweigh their shortcomings.

2 Methods

polyMEA fabrication

PolyMEAs fabrication by replica-molding from SU-8 or epoxy-masters has been described before [1, 3]. Briefly, in a three step approach, cavities for the electrodes, leads and contact pads were molded into a thin (≤ 500 μm) PDMS top layer. The geometries of these cavities were defined by the two-level molding masters. Electrode and pad features extended through the entire top layer while the interconnection channels for the electrode leads stayed covered by PDMS. The

cured PDMS slab was peeled from the master and hydrophilized by O_2 -plasma treatment (3 min, 60% power, 0.3 mbar, 2.45 GHz, Femto, Diener). Its cavities were filled with one of the conducting polymers (PEDOT:PSS (Baytron CPP105D) with 5% ethylene glycol or graphite in PDMS) and tempered at $> 80^\circ\text{C}$ for ≤ 3 h. The back side of the slab was then electrically insulated by another thin layer of PDMS.

polyMEA characterization

Impedance measurements from 1 Hz to 100 kHz were performed on differently treated and reused *polyMEAs* in saturated KCl using a potentiostat (PARSTAT 2273 with PowerSuite, Princeton Applied Research). An Ag/AgCl wire served as the reference electrode, a Pt sheet as the counter electrode. Noise levels on individual electrodes were evaluated using a 60-channel recording station (MEA60, Multi Channel Systems).

polyMEA recordings

Neural signals were recorded from rat cortical and hippocampal cultures (E18). Biocompatibility and biostability of *polyMEAs* were validated for a period of more than 8 weeks using standard cell culturing protocols.

3 Results

While PEDOT:PSS electrodes are mostly bluish transparent, graphite-PDMS (gPDMS) electrodes are not. However, the stability of the gPDMS composite conductor is notably higher; PEDOT:PSS films tend to

break upon focal pressure or during bending for more than 60° . While gPDMS electrode diameters are $80\ \mu\text{m}$, the PEDOT:PSS electrode areas are smaller and less defined. PEDOT:PSS coats the microchannels of the PDMS-slab as a thin film. Equally, the electrode itself will consist of a thin film. However, this film sometimes peels off in postprocessing steps. Therefore, electrode areas might shrink to a ring, which is defined by the circumference of an electrode channel, having thicknesses as thin as the PEDOT:PSS film.

The impedance of the mostly transparent polymer electrodes with diameters of less $80\ \mu\text{m}$ were almost constant and below $5\ \text{M}\Omega$ over the range of $1\ \text{Hz}$ to $100\ \text{kHz}$ (fig. 1). PEDOT:PSS electrodes behaved mostly resistive at low frequencies, while gPDMS electrodes, being mostly capacitive, resembled standard TiN-coated metal electrodes (fig. 2). Peak-to-peak noise varied between $\pm 10\ \mu\text{V}$ and $\pm 100\ \mu\text{V}$. Variations in electrode characteristics resulted from the manual fabrication of the prototypes. Electrical characteristics were not affected by normal use (autoclavation, several weeks of cell culturing under standard cell culturing conditions: $5\% \text{CO}_2$ in a humidified incubator at 37°C). However, the conductivity of the organic conductor PEDOT:PSS is destroyed by bleach.

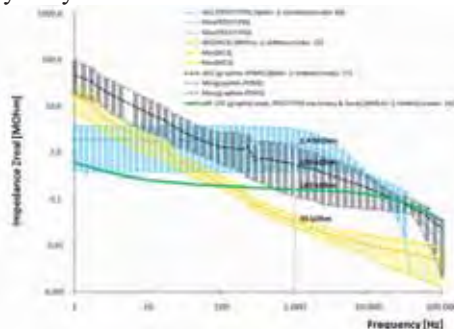


Fig. 1 Comparison of the averaged impedance (real part) of $\text{Ø } 80\ \mu\text{m}$ PEDOT:PSS electrodes (blue; number of devices: $n = 3$ *polyMEAs*; # of electrodes measured: $m = 84$) with that of metal-like $\text{Ø } 80\ \mu\text{m}$ gPDMS electrodes (grey; $n = 3$ *polyMEAs*; $m = 57$) and of $\text{Ø } 30\ \mu\text{m}$ or $10\ \mu\text{m}$ TiN-coated Au or ITO electrodes (yellow; $n = 3$ *MEAs*, $m = 15$ electrodes) on commercial microelectrode arrays (30 or 10/200iR, Multi Channel Systems) measured in saturated KCl versus an Ag/AgCl-reference electrode (Pt counter electrode).

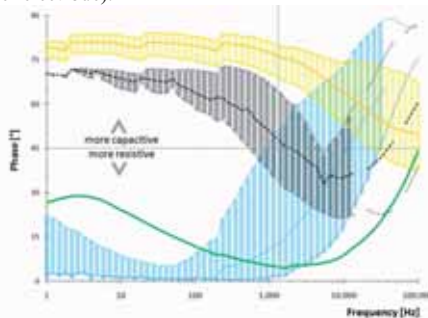


Fig. 2 Comparison of the phase of the same electrodes discussed in figure 1. While PEDOT:PSS electrodes (blue) become merely resistive at low frequencies, gPDMS electrodes (grey) with their inherent elevated surface roughness become as capacitive as TiN-coated Au or ITO electrodes (yellow).

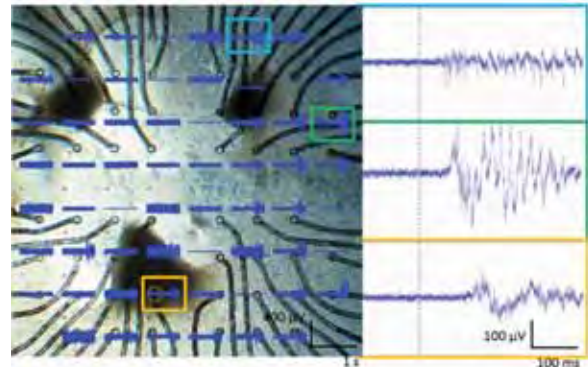


Fig. 3 One-second activity snapshot from 38 of 60 electrodes (22 electrodes were broken and connected to GND) with zoom into the activity on 3 channels that exemplarily reveal the different types of recordable signals from a PEDOT:PSS *polyMEA* with $\text{Ø } 80\ \mu\text{m}$ (nominal value) electrodes: action potentials (top) and bursts (middle) are in most cases overlaid by low-frequency signal components (middle and bottom). Mix of cortical & hippocampal neurons after 38 DIV (rat, E18).

4 Conclusion

Despite their rather large electrode diameters of $\leq \text{Ø } 80\ \mu\text{m}$ (compared to commercial MEAs with electrode diameters $\leq \text{Ø } 30\ \mu\text{m}$), *polyMEAs* made of different types of polymer conductors (PEDOT:PSS or gPDMS) reliably resolve individual action potentials. Furthermore, due to the flat impedance characteristics of PEDOT:PSS electrodes down to $1\ \text{Hz}$, the low-frequency components of bioelectric signals can be captured as well. *polyMEAs* have the potential to become inexpensive and discardable devices for the study of bioelectrical signals from *in vitro* preparations of electrogenic cells. Due to their flexibility and robustness, they may also find application as epicortical or deep brain recording devices, or as retinal implants *in vivo*.

Acknowledgements

Many thanks to Tanja Neumann, Marina Nanni and Francesca Succol for their expert advice and assistance in tissue preparation.

References

- [1] Blau, A., et al. Prototyping all-polymer bioelectrical signal transducers. in Proceedings of the World Congress on Medical Physics and Biomedical Engineering, September 7 - 12, 2009, Munich, Germany. 2009. Munich: Springer.
- [2] Pine, J., A History of MEA Development in Advances in Network Electrophysiology. Using Multi-Electrode Arrays, M. Taketani and M. Baudry, Editors. 2006, Springer: New York. p. 3-23.
- [3] Murr, A., et al. Replica-molded polymer microelectrode arrays (*polyMEAs*) in 6th International Meeting on Substrate-Integrated Micro Electrode Arrays. 2008, July 8-11. Reutlingen, Germany: BIOPRO Baden-Württemberg GmbH, Stuttgart.

Combining MEA and VSD to study cells in a pattern generator

Pieter Laurens Baljon^{1,2*}, John Nagarah¹, Daniel A. Wagenaar¹

¹ Broad Fellows Program and Division of Biology, California Institute of Technology, Pasadena CA, United States

² Department of Biophysical and Electronic Engineering, University of Genova, Genova, Italy

* Corresponding author. E-mail address: pbaljon@caltech.edu. Current address: Department of Experimental Neurophysiology, Vrije Universiteit, Amsterdam, The Netherlands

In this paper we describe a setup for combined recordings with extracellular microelectrodes and voltage sensitive dyes. We apply this technique to the Leech ganglion where the role of many individual cells in a variety of circuits has been established. Individuating cells is a traditional drawback of extracellular recording. We show that the extracellular signal is correlated to individual cells from the optical signal. This shows the possibility to eventually for a large number of spike trains simultaneously, assign them to the respective cells as they participate in a neural circuit such as the Leech pattern generator for swimming.

1 Introduction

While extracellular recordings provide excellent temporal resolution, it is nearly impossible to identify the source of a recorded action potential. In voltage-sensitive dyes (VSD) the source is contained in the recording, but temporal resolution, sensitivity and longevity of the recording are limited. A successful combination of the two could truly give us the best of two worlds. Here we report on our first simultaneous recordings of the cells in the leech ganglion.

2 Methods

Biological preparation

We use the intact nerve cord of the *Hirudo verdana*, the medicinal leech [1]. Firstly, we prepare the tenth ganglion for extracellular and VSD recordings by removing the blood vessel and on the ventral side the ensheathing glial cell. This ganglion is fixated on a sylgard 'transfer slab' to allow positioning

of the preparation over the electrodes (See Panel B of Figure 1). Secondly, we free the dorsal roots of the two posterior nerve roots of the sixteenth ganglion for recording and stimulation with a suction electrode. Though the preparation is spontaneously active, stimulation through the suction electrode increases activity and in some cases evokes the activity pattern associated with swimming [2].

Recording setup

The setup is depicted in Figure 1. We used hexagonal MEAs with ITO electrodes (Multichannel systems) for compatibility with imaging. Inside the MEA ring is a small piece of sylgard that allows fixating the caudal nerve cord for easy access to the nerve root. We used a coumarin/oxonol FRET pair as voltage sensitive dye [3]. Imaging was performed with a 1.0NA, water-immersed 20x objective on an inverted microscope and two high-sensitivity CCD cameras (Photometrics) for the Coumarin and Oxonol fluorescence.



Fig. 1. The setup for combined extracellular and VSD recording. A) The setup inside the microscope. The micromanipulator (MM) is used to precisely position the ganglion over the active area. B) Top-side view of the MEA with the Sylgard carrier to keep the tenth ganglion in place. The suction electrode is placed on the sixteenth ganglion. The nerve cord is fixated to the rim of the dish caudally to ganglion 16. For clarity not all 21 ganglia are drawn. Figure not to scale.

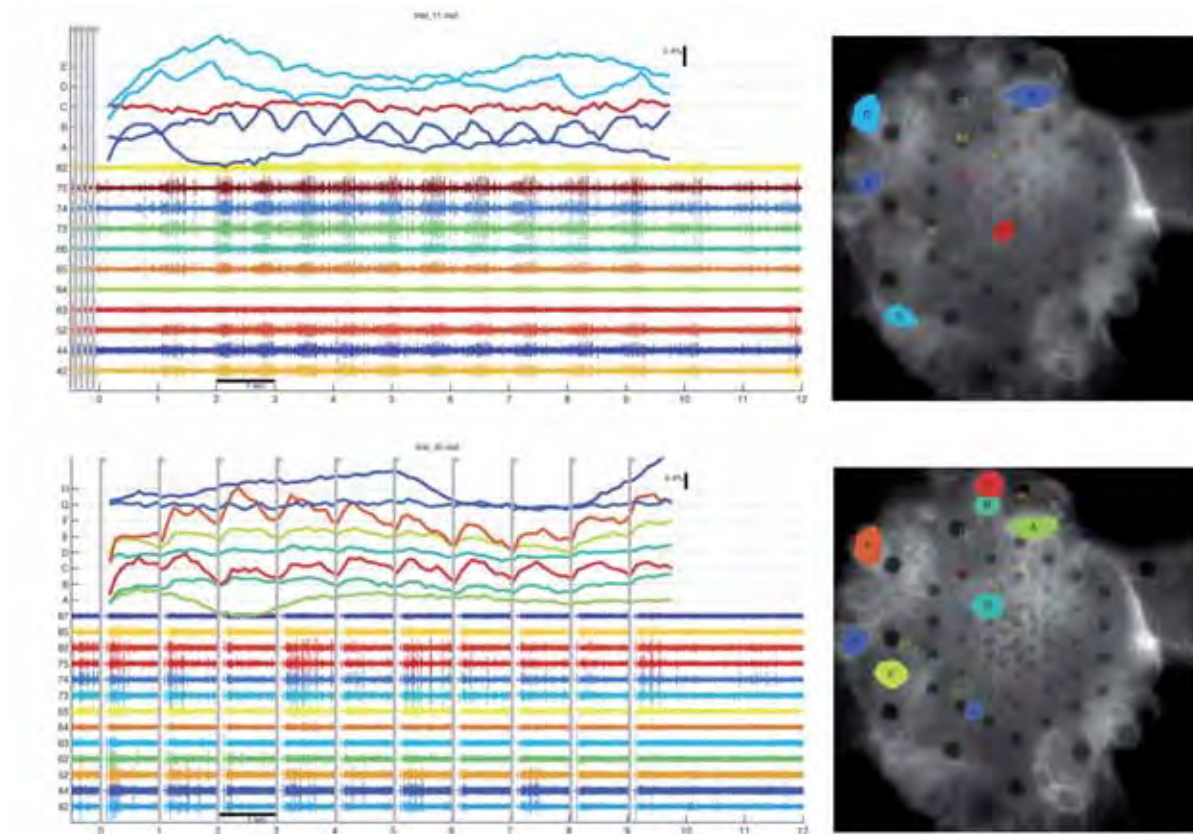


Fig. 2. Simultaneous MEA and VSD recordings. A) Repetitive stimulation. Several neurons show modulations of their membrane potential coherent with the stimulation. B) Single stimulus evoking oscillation. The frequency and activity patterns in the nerve root are consistent with the swimming pattern generator being activated.

The change in fluorescence is analyzed as the ratio in the Coumarin and Oxonol band in regions of interest (ROIs), drawn over the cell bodies readily visible in a single VSD frame. MEA recordings are currently analyzed as multi-unit activity. We are currently developing a method for spike sorting on sixty channels simultaneously to obtain spike trains of individual units to be correlated with the VSD signal.

3 Results

We obtain oscillating signals both from repetitive stimulation (Figure 2, panel B) and from spontaneous swimming (Panel A) [2]. Swimming could be evoked in roughly half the preparations. The other half probably suffered damage during the 2.5-hour preparation. The traces clearly show the relationship between VSD and extracellular potential. The number of units exhibiting oscillations in the VSD is higher in the trial with repetitive stimulation. The MEA recording shows much more activity in response to stimulation. From visual inspection of the waveforms we expect to be able to reliably isolate at least ten units in those recordings.

Electrode 52 in panel A shows a well isolated unit and close by is a cell with an oscillatory VSD signal. However, the VSD has a slow onset, while the large isolated unit starts firing immediately after stimulation.

Acknowledgement

Funding was provided by the Broad Foundations (to DAW). DAW is a recipient of a Career Award at the Scientific Interface from the Burroughs Wellcome Fund.

References

- [1] K J Muller, J G Nicholls, and G S Stent, eds. (1981). "Neurobiology of the leech". Cold Spring Harbor Laboratory Press, Cold Spring Harbor, NY.
- [2] W B Kristan and R L Calabrese (1976). Rhythmic swimming activity in neurons of isolated nerve cord of leech. *J. Exp. Biol.* 65(3), 643-668.
- [3] S M Baca, A Marin-Burgin, D A Wagenaar, and W B Kristan Jr (2008). Widespread inhibition proportional to excitation controls the gain of a leech behavioral circuit. *Neuron* 57(2), 276-289.

Transparent Multisuction Electrode Arrays For Tissue Immobilization And Simultaneous MEA And VSD Measurements

John M. Nagarah¹, Pieter Laurens Baljon², Daniel A. Wagenaar^{1*}

¹ Broad Fellows Program, Division of Biology, California Institute of Technology, Pasadena, CA, USA

² Experimental Neurophysiology, Vrije Universiteit, Amsterdam, Netherlands

* Corresponding author. E-mail address: daw@caltech.edu

We are constructing transparent, multi-suction electrode arrays (MSEAs) to study multisensory integration of prey localization in the medicinal leech (Figure 1) during simultaneous electrophysiology and voltage sensitive dye (VSD) imaging measurements. However, the VSD percent signal change is small, so a shift of even a few micrometers can be detrimental to measurements. Custom-designed multielectrode arrays (MEAs) will be integrated with planar quartz suction devices and microfluidics to immobilize leech ganglia during multisensory integration experiments.

1 Background/Aims

We are constructing devices to study multisensory integration of prey localization in the medicinal leech, an ideal organism to test novel technologies due the unrivaled accessibility to its nervous system and well characterized behavior (Figure 1). For example, we have recently invented a technique that combines multielectrode arrays (MEAs) with voltage sensitive dye (VSD) imaging to sense neuronal signals from the leech ganglion, the putative site of multisensory integration. The high temporal resolution (<1ms) of the MEA measurements when combined with the high spatial resolution of VSD imaging will be a powerful new technique to identify neuronal circuitry and analyze the computations that take place within them. Ultimately, these tools should be amenable to flat tissue systems in higher organisms as well.

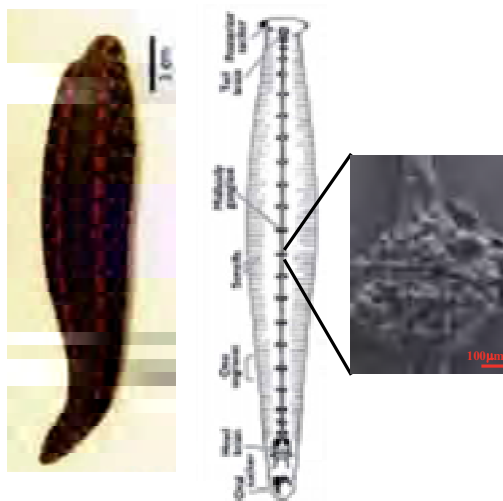


Fig. 1. Photo and schematic of the medicinal leech. Inset: An SEM image of a fixed leech ganglion, the putative site of multisensory integration.

2 Methods

Experiments are being performed on a single ganglion, either isolated or in the intact nerve cord from the leech (*Hirudo medicinalis*). Through-pore arrays in suspended quartz membranes are fabricated into quartz wafers utilizing high density fluorocarbon plasma etching. An array of 10µm wide holes is patterned in the center of the wafer into a suspended membrane while ~200µm wide holes are patterned in the periphery for tissue pinning (Figure 2A). Transparent indium tin oxide MEAs are fabricated utilizing standard lithography techniques. For the integrated MEA immobilization device, MEAs will be patterned over the planar pore suction device so that each electrode fills in and surrounds each pore in the center of the quartz wafer. To apply negative pressure for immobilization, a PDMS microfluidic layer will contact the bottom-side of the device.



Fig. 2. A. A schematic of the planar immobilization device. An array of small pores is located in the center while larger through pores are located in the periphery for tissue pinning. B. A leech ganglion is pinned over a suspended glass membrane, demonstrating mechanical robustness of the device. C. Fabrication of an array of pores through ~20µm thick quartz is indeed possible (design from Figure 2A).

3 Results

A leech ganglion was successfully pinned over a suspended glass membrane, demonstrating mechanical robustness of the planar device (Figure 2B). Also, we

fabricated arrays of pores through a $\sim 20\mu\text{m}$ thick suspended quartz membrane (Figure 2C). Separately, we recorded neuronal signals in the leech ganglion from a custom-built, transparent MEA device (Figure 3A). Signal is clearly discriminated from the baseline. Finally, we have fabricated the PDMS microfluidics to be attached to the underside of the MSEA device.

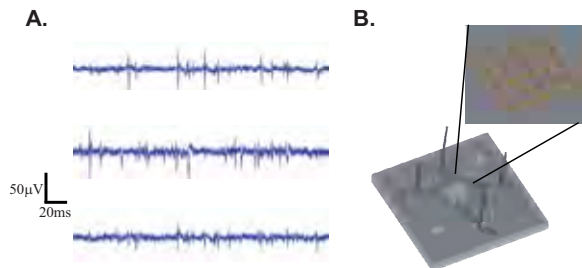


Fig. 3. A. Extracellular measurements from a leech ganglion on a custom-built, transparent MEA. B. Schematic of a planar multi-suction electrode array (MSEA). Electrodes will be fabricated inside and around the through pores.

4 Conclusion

The glass/quartz device fabrication, ganglion pinning on the device, and successful MEA recordings all together give a proof-of-principle for the MSEA (Figure 3B). Integration of the suction device, MEA, and microfluidics will enable not only high quality neuronal measurements, but proper identification of MEA signals to single neurons with the simultaneous VSD measurements. This new technique will enable significant multisensory integration studies in the leech, and should be applicable to other systems as well.

Acknowledgement

This work is a contribution in part from Pieter Laurens Baljon and Daniel A. Wagenaar. This work is funded by the Broad Fellows Program in Brain Circuitry and the Burroughs Wellcome Fund.

Conducting Polymer Coated MEAs for Enhanced Signal Recording and Stimulation

Vini Gautam¹ and K.S. Narayan^{1*}

¹ Molecular Electronics Laboratory, Jawaharlal Nehru Centre for Advanced Scientific Research, Jakkur P.O., Bangalore, India.

* Corresponding author. E-mail address: narayan@jncasr.ac.in

Mechanical interface between tissue and electrodes is an important parameter in extracellular recordings using MEAs. We demonstrate that using a conducting polymer coating on standard MEAs improves tissue adhesion, reduces noise levels and enhances signal recording as well as stimulation properties of standard electrodes.

1 Introduction

Micro-electrode arrays (MEA) are widely used for signal recording and stimulation from cultured neurons or whole tissue mounts like hippocampus and retina. However, reducing the electrode size to microscale for higher spatial sensitivity increases the electrode impedance thereby leading to a lower sensitivity. Moreover, the recording with MEA is extracellular and hence, the signal strength depends directly on the electrode-cell distance, i.e. the mechanical contact of tissues onto the MEA [1]. Various coatings such as lysine, laminin and nitrocellulose are used for better adhesion of tissues and cells on the MEAs. However, these coatings are non-conducting and hence introduce an additional impedance factor.

Conducting polymers such as poly(-pyrrole) (Ppy) and poly-(3,4-ethylenedioxythiophene) (PEDOT) have been considered as bio-electronic interfaces [2]. They have been used as scaffolds to grow neurons and are shown to be biocompatible [3]. PEDOT nanotubes were recently shown to enhance charge injection capabilities of underlying metal electrode sites as well as improve the adhesion and attachment between neurons and electrodes [4,5].

We demonstrate the modification of MEA electrodes by coating PEDOT:PSS in form of a thin film which enhances adhesion of retina whole mount tissues to MEAs and thereby provides improved signal recording and stimulation capabilities.

2 Materials and Methods

TiN array (Hexa MEA from MCS, Germany) and ITO array (MEA60 200-ITO from Ayanda Biosys, Switzerland) were used for the studies. Retina isolation was done from mice (C57Bl/6J) using standard protocols [6]. Ganglion cell side was placed towards the MEA electrodes. Data was recorded using BC1060-Inv amplifier (MCS, Germany) at a sampling rate of 25 kHz using a MC_Card and MC_Rack software (MCS, Germany). PEDOT:PSS dispersion

was procured from Baytron P. About 10 μ l of the filtered dispersion was spin coated on the recording area of the MEAs. The MEAs were heated at 50°C for 30 mins for annealing the polymer film.

Around 6-7 retina whole mounts were tested on bare MEAs and subsequently on PEDOT:PSS modified MEAs. Visual stimulus was 1 Hz full field temporal square wave with 100 ms duration of light-On. White LEDs were used as the light source.

3 Results and Discussions

It was noticed that coating PEDOT:PSS reduces background noise prevailing in the MEAs (fig.1). Typical micro ERGs were observed on both bare and PEDOT:PSS coated MEAs upon photo-stimulation. Additionally, the light induced signals from the polymer coated electrodes were more appreciable in magnitude as well as features (fig. 2). The magnitude of ERGs increased by about 75% after PEDOT:PSS coating on the MEAs.

PEDOT:PSS intermediate layer improves the adhesion of retinal tissue onto the standard MEAs. PEDOT film has a 'softer' modulus than the metal electrodes. This allows it to get slightly deformed when it comes in contact with a tissue and hence it provides a better mechanical contact between the tissue and the bottom surface.

PEDOT:PSS also improves the work function of the underlying metal electrodes and lowers the interface barrier between metal electrodes and the tissue.

The signal enhancement therefore arises from the close electrical contact for signal transmission as well as better charge injection property of the PEDOT:PSS conducting layer.

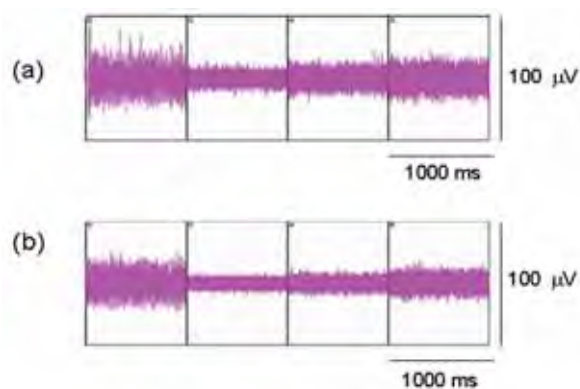


Fig. 1. Baseline noise level on four randomly selected windows from TiN array with Ames' buffer medium. (a) Without PEDOT:PSS coating (b) After modification with PEDOT:PSS.

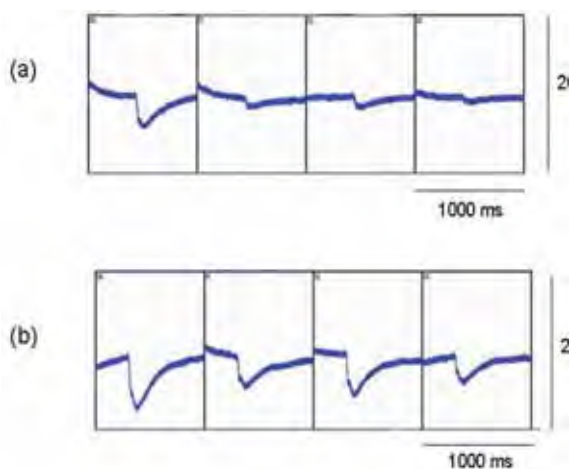


Fig. 2. ERGs obtained with filter settings 0.3-300 Hz. (a) Without PEDOT:PSS coating (b) After modification with PEDOT:PSS.

4 Conclusion

PEDOT:PSS is optically transparent and can be patterned. It has also been shown recently that the conductivity of PEDOT:PSS films can be improved to up to 250 kS/s using specific post annealing solvent treatments [7]. We speculate that it is possible to conceive PEDOT:PSS based MEAs with better recording and stimulation properties that can replace the existing metal and metal-oxides based MEAs. Further, the glass chips can be replaced by directly patterning PEDOT:PSS electrodes on flexible substrates. This would be useful for in-vivo extracellular recordings.

We propose the use of PEDOT:PSS as transparent, metal-free electrodes on flexible MEAs which do not need any additional adhesive and biocompatible coatings.

References

- [1] Stett A., Egert U., Guenther E., Hofmann F., Meyer T., Nisch W., Haemmerle, H. (2003). Biological application of microelectrode arrays in drug discovery and basic research. *Analytical and Bioanalytical Chemistry*, 377, 486-495.
- [2] Berggren M., Dahlfors A. R. (2007). Organic Bioelectronics, *Advanced Materials*, 19, 3201-3213.
- [3] Burns S.M.R, Hendricks J.R., Foster B., Povlich K.L., Kim D.H. and Martin D.C. (2007). Polymerization of conducting polymer PEDOT around living neural cells. *Biomaterials*, 28, 1539-1552.
- [4] Abidian M.R., Ludwig K. A., Marzullo T.C., Martin D.C. and Kipke D.R. (2009). Interfacing conducting polymer nanotubes with the central nervous system: Chronic Neural Recording using PEDOT Nanotubes. *Advanced Materials*, 21, 3764-3770.
- [5] Abidian M.R., Corey J. M., Kipke D. R. and Martin D.C (2010). Conducting polymer nanotubes improve electrical properties, mechanical adhesion, neural attachment and neural outgrowth of neural electrodes. *Small*, 6(3), 431-429.
- [6] Guenther E, Herrmann T. and Stett A.(2006). The Retinasensor. *Advances in Network Electrophysiology* (Springer).
- [7] Yoo J.E., Leeb K.S., Garcias A., Tarvera J., Gomez E.D., Baldwin K., Sumb Y., Meng H. and Loo Y.H. (2010). Directly patternable, highly conducting polymers for broad applications in organic electronics, *PNAS*, 107(13), 5712-5717.

Gold Shark Teeth Structures on MEAs - Electroplating of Nano-Structures on Metallic Microelectrodes

Philipp Julian Koester¹, Carsten Tautorat¹, Tom Reimer¹, Michael Zwanzig², Werner Baumann¹, and Jan Gimsa^{1*}

¹ University of Rostock, Chair for Biophysics, Gertrudenstrasse 11a, 18057 Rostock, Germany.

² Fraunhofer Institute for Reliability and Microintegration (IZM), Gustav-Meyer-Allee 25, 13355 Berlin

* Corresponding author: jan.gimsa@uni-rostock.de

To improve the signal quality of MEA chips, we enlarged the electrode surfaces of two different chip types: a glass neurochip with 52 Pt-electrodes and a silicon neurochip with 58 Pd/poly-silicon electrodes. The electrodes were electroplated with gold particles. First results regarding test signal transmission are given in this report.

1 Introduction

Biosignal recording from electrically active cells such as neurons or muscle cells does strongly depend on (i) the electrode metal, e.g. palladium (Pd), platinum (Pt), silver (Ag) or gold (Au) on (ii) the electrode surface [1-3] and (iii) the electrode surface area properties. MEA chip properties may change due to electrode processes caused by biological activity of adherent cells. Very low pH-values in the space between the cells and the electrode result in erosion and a reduced electrode quality. This process may lead to low biosignal amplitudes and unsuccessful experiments. Oxidative processes producing oxide layers on the recording electrodes may also lead to reduced biosignals quality. To improve the signal quality of MEA chips, we enlarged the electrode surfaces of two different chip types: a glass neurochip with 52 Pt-electrodes and a silicon neurochip with 58 Pd/poly-silicon electrodes. The electrodes were electroplated with gold particles.

In this short report, we present first results this new method on electrodes of our new glass neurochip [4] (Fig. 1). The effect on neuronal recording will be published elsewhere.

2 Material and Methods

Chips were filled with a gold solution and different electroplating processes were conducted. In any case, a ground gold layer of 1 μm thickness was electroplated before structured gold was disposed. The processes were controlled in such a way that two different gold structures were obtained on the chips. For control, half of the electrodes were not electroplated. After electroplating, the chips were thoroughly rinsed to remove toxic residues. Afterwards, electrode transmission tests were done with a signal generator connected with the chip medium to measure the obtain signal yield. A sine shaped signal (1 mV, 1 kHz) was used to simulate an

active neuron. The signal was recorded with the electroplated and the control electrodes.

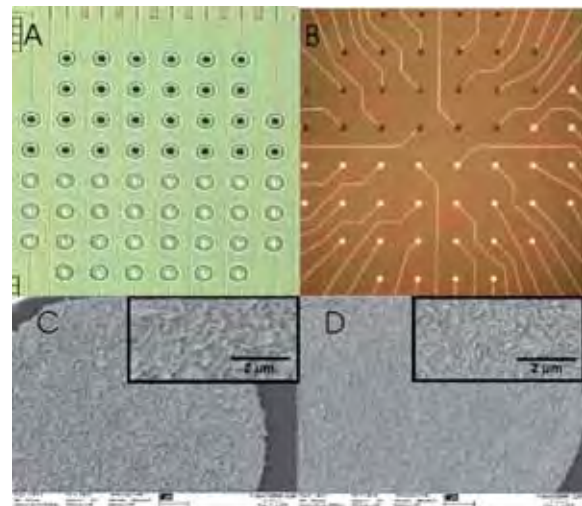


Fig. 1: Gold-electroplated Pd/Pt electrodes (black spots). A: Pd-electrodes, $\varnothing = 25 \mu\text{m}$; B: Pt-electrodes, $\varnothing = 20 \mu\text{m}$; C: rough Au-structures on Pd-electrode; D: fine Au-structure on Pd-electrode.

3 Results

Electroplating was microscopically examined by SEM. Fig. 1 shows the resulting shark teeth-shaped gold formations on the Pd-electrodes. After electroplating, fine and rough structured gold layers were found on the electrodes with 1 μm and 2 μm wide gold structures, respectively. Of four chips, two chips showed fine or rough structures, respectively. The signals recorded with the control electrodes were approx. 0.87 mV (controls for fine structures) and 0.82 mV (controls for rough structures). The signals recorded with the electroplated electrodes were higher, i.e. 5 % for fine gold surface (0.91 mV) and 13 % for rough surfaces (0.92 mV). The signals recorded with the control Pt-electrodes were approx. 0.59 mV. With Pt-electrodes, only one structure type (rough) was electroplated. The signals recorded with the

electroplated electrodes were approx. 36 % higher (0.80 mV).

4 Conclusion

The surface enlargement by shark-teeth electroplating led to an increase of the signal amplitude and signal/noise-ratio. Electroplating can be applied subsequently to the chip production with ready-to- biochips. In addition, our methods allows for a subsequent refurbishment of aged or used MEA chips.

Acknowledgement

This work was supported by grants of Mecklenburg-Western Pomerania (UR09045 of the Ministry of Education, Science and Culture, and V220-630-08-TFMV-F-011 (project part FLUXELL) of the Ministry for Economics, Work and Tourism).

References

- [1] Ross, J. D., O'Connor, S. M., Blum, R. A., Brown, E. A., and DeWeerth, S. P. 2004. Multielectrode impedance tuning: reducing noise and improving stimulation efficacy. *Proceedings of the 26th Annual International Conference of the IEEE EMBS*, 4115-4117.
- [2] Marrese, C. A. 1987. Preparation of strongly adherent platinum black coatings. *Analytical Chemistry*, 59: 217-218.
- [3] Chu, H. Y., Kuo, T. Y., Chang, B., Lu, S. W., Chiao, C. C., and Fang, W. 2006. Design and fabrication of novel three dimensional multi-electrode array using SOI wafer. *Sensors and Actuators A: Physical*, 130-131: 254-261.
- [4] Koester, P.J., Buehler, S.M., Stubbe, M., Tautorat, C., Niendorf, M., Baumann, W. and J. Gimsa (2010). Modular glass chip system measuring the electric activity and adhesion of neuronal cells – application and drug testing with sodium valproic acid. *Lab-Chip*, DOI: 10.1039/b923687b

GO-Bio 3: PoreGenic[®] - 1. Whole-Cell Patch Clamp Recordings with a 3D-MEA chip.

Philipp Julian Koester^{1*}, Carsten Tautorat¹, Jochen Held², Patrick Ruther², João Gaspar², Oliver Paul², Helmut Beikirch³, Jan Gimsa¹, and Werner Baumann¹

¹ University of Rostock, Chair for Biophysics, Gertrudenstrasse 11a, 18057 Rostock, Germany.

² University of Freiburg, Department of Microsystems Engineering (IMTEK), Georges-Köhler-Allee 103, 79110 Freiburg, Germany

³ University of Rostock, Faculty of Computer Science and Electrical Engineering, Institute of Electronic Appliances and Circuits, Albert-Einstein-Strasse 2, 18059 Rostock, Germany

* Corresponding author: philipp.koester@uni-rostock.de

We present the first intracellular measurements with our new PoreGenic[®] microneedle chip prototype providing a new 3D-MEA. These are the first steps towards the analysis of adherent cells with our patch-on-chip system PoreGenic[®]. In future, it will allow for drug screening measurements during stable intracellular contact.

1 Introduction

Existing classical methods for intracellular measurements are time-consuming and complex [1, 2]. Present Patch-on-chip systems are limited to the investigation of single cells in suspension [3-6]. Nevertheless, the most part of the cells of the human body is adherently growing. Therefore, we develop the new chip system PoreGenic[®] for adherent cells. With this analytical chip, the intracellular investigation of electrochemical changes and processes in adherently growing cells will become possible in the near future as reported at MEA Meeting 2008 [7,8].

This short report is about the innovative method of the local micro-invasive needle electroporation (LOMINE) of single cells. The investigation of cellular reactions in living cell cultures represents a fundamental method e.g. for drug development and environmental monitoring. As a new step, we present the first intracellular measurements with our new PoreGenic[®] microneedle chip prototype providing a new 3D-MEA.

2 Material and Methods

64 micro-structured needle electrodes as well as 128 dielectrophoretic electrodes located within a measuring area of 1 mm² were processed on a silicon as well as Pyrex[®] substrate (Fig. 1). The system is in detail described elsewhere [9-11]. L929 tumour cells and human skin fibroblasts were positioned in the proximity of the electrodes using the DEP electrodes. After their adherence, electroporation experiments were done and the membrane potential was measured.

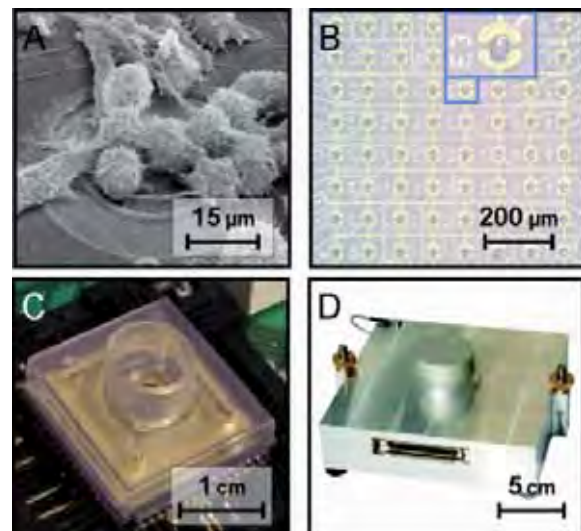


Fig.1. The PoreGenic[®] chip provides a micro needle array with integrated dielectrophoretic electrodes (A & B). In (A), the array is overgrown by a L929 tumor cell. The chip and the hardware setup is shown in (C) and (D).

3 Results

Cultures of L929 tumor cells were electroporated with low voltages under 2 V (relative to the cell culture medium in the chip trough) with a certain frequency at the electrodes tips. Cell free electrodes react to these pulses with a voltage increase of approx. +10 mV or higher which exponentially converge against the output voltage (data not shown). After the step, the typical voltage drops for overgrown electrodes are clearly recognizable. In general, overgrown electrodes react with a negative voltage drop. The voltage drop amounted to approximately -30 mV (Fig. 2).

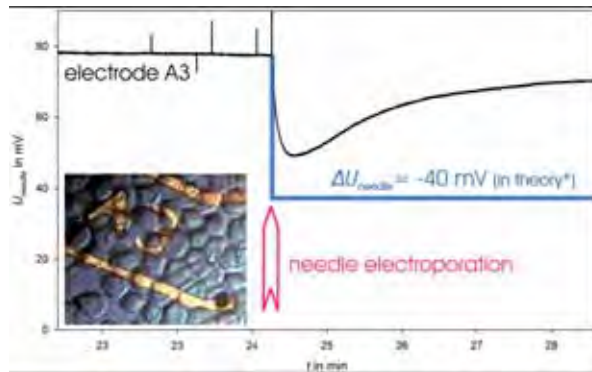


Fig.2: Potential measurement of the electrode A3 overgrown with a L929-tumour cell (see insert, bottom left) after electroporation pulse, see text for further information.

4 Conclusion

Comparisons with literature values result in similar potentials for this cell type [12]. This depends on the physiological situation of the individual cells (reproduction status, age of the medium etc.). The longer the measured voltage drop can be held, the more probable is that one performed an intracellular measurement. However, the last-finite proof for these intracellular measurements is still missing. These are the first steps towards the analysis of adherent cells with our patch-on-chip system PoreGenic[®]. It will allow for drug screening measurements during stable intracellular contact. Recently, we found that it is also suitable for the extracellular detection of action potentials from primary cardiomyocytes.

Acknowledgement

The authors also thank the Federal Ministry of Education and Research (BMBF) for funding the project MIBA – *Mikrostrukturen und Methoden für die intrazelluläre Bioanalytik* (grant 16SV2337) and the project PoreGenic (GO-Bio grant 0315809). This work was also supported by grants of Mecklenburg-Western Pomerania (UR09045 of the Ministry of Education, Science and Culture, and V220-630-08-TFMV-F-011 (project part FLUXELL) of the Ministry for Economics, Work and Tourism).

References

- [1] Neher, E. and Sakmann, B. 1976. Single-channel currents recorded from membrane of denervated frog muscle fibers. *Nature*, 260: 799-802.
- [2] Hamill, O.P., Marty, A., Neher, E., Sakmann, B., and Sigworth, F.J. 1981. Improved patch-clamp techniques for high-resolution current recording from cells and cell-free membrane patches. *Pfluegers Archiv*, 391: 85-100.
- [3] Stett, A., Burckhardt, C., Weber, U., van Stiphout, P., and Knott, T. 2003. CYTOCENTERING: A novel technique enabling automated cell-by-cell patch clamping with the CYTOPATCH chip. *Receptors and Channels*, 9: 59-66.
- [4] van Stiphout, P., Knott, T., Danker, T., and Stett, A. 2005. 3D Microfluidic Chip for Automated Patch-Clamping. *Proceedings of the MST-Congress 2005*, 435-438.
- [5] Kiss, L., Bennett, P.B., Uebele, V.N., Koblan, K.S., Kane, S.A., and Neagle, B.S.K. 2003. High throughput ion-channel pharmacology: planar-array-based voltage clamp. *Assay Drug Development Technologies*, 1: 127-135.
- [6] Farre, C., Haythornthwaite, A., Stoelzle, S., Kreir, M., George, M., Brueggemann, A., and Fertig, N. 2009. Port-a-patch and patchliner: high fidelity electrophysiology for secondary screening and safety pharmacology. *Combinatorial Chemistry & High Throughput Screening*, 12: 24-37.2.
- [7] Held, J., Gaspar, J., Ruther, P., and Paul, O. 2008. Microneedle Arrays Electrode With Dielectrophoretic Electrodes For Intracellular Recording Applications. *Conference Proceedings of the 6th International Meeting on Substrate-Integrated Micro Electrode Arrays*, 295-296.
- [8] Koester, P.J., Tautorat, C., Podssun, A., Gimsa, J., Jonas, L., and Baumann, W. 2008. A new Principle for intracellular Potential Measurements of adherently growing Cells. *Conference Proceedings of the 6th International Meeting on Substrate-Integrated Micro Electrode Arrays*, 271-274.
- [9] Tautorat, C., Koester, P.J., Held, J., Gaspar, J., Ruther, P., Paul, O., Cismak, A., Heilmann, A., Gimsa, J., Beikirch, H., Jonas, L., and Baumann, W. 2008a. Intracellular potential measurements of adherently growing cells using micro-needle arrays. *The Proceedings of μTAS 2008 Conference*, 1777-1780.
- [10] Tautorat, C., Koester, P.J., Podssun, A., Beikirch, H., Gimsa, J., Jonas, L., and Baumann, W. 2008b. Local Micro-Invasive Needle Electroporation - A Technical Challenge. *Conference Proceedings of the 6th International Meeting on Substrate-Integrated Micro Electrode Arrays*, 340-341.
- [11] Held, J., Gaspar, J., Ruther, P., Hagner, M., Cismak, A., Heilmann, A., and Paul, O. 2010. Design of experiment characterization of microneedle fabrication processes based on dry silicon etching. *Journal of Micromechanics and Microengineering*, 20: 025024-
- [12] Osipenko, O.N., Tate, R.J., and Gurney, A.M. 2000. Potential Role for Kv3.1b Channels as Oxygen Sensors. *Circulation Research*, 86: 534-540.

GO-Bio 3: PoreGenic[®] - 2. Cardiomyocyte Action Potential Recordings with a 3D-MEA chip

Philipp Julian Koester^{1*}, Carsten Tautorat¹, Jochen Held², Patrick Ruther², João Gaspar², Oliver Paul², Helmut Beikirch³, Jan Gimsa¹, and Werner Baumann¹

¹ University of Rostock, Chair for Biophysics, Gertrudenstrasse 11a, 18057 Rostock, Germany.

² University of Freiburg, Department of Microsystems Engineering (IMTEK), Georges-Köhler-Allee 103, 79110 Freiburg, Germany

³ University of Rostock, Faculty of Computer Science and Electrical Engineering, Institute of Electronic Appliances and Circuits, Albert-Einstein-Strasse 2, 18059 Rostock, Germany

* Corresponding author: philipp.koester@uni-rostock.de

We present our new PoreGenic[®] microneedle chip prototype providing a new 3D-MEA chip. This chips allows for the detection of intracellular whole cell potentials. First results are given in this report.

1 Introduction

In vitro studies of extracellular cardiac action potentials of primary cardiomyocytes (PCMs) on MEAs have a long tradition [1, 2]. *In vivo* intracellular cardiac potential measurements can be accomplished with microelectrodes [3]. CMOS based systems were recently developed [4]. Channel properties of single PCMs can be examined with patch-on-chip systems [5-7]. Nowadays, automated systems are used for the mandatory tests of drug candidates for their hERG-activity on suspended cells [8-10, 7]. The same systems are used in the research on cardiovascular diseases [11]. Nevertheless, their throughput rates are not sufficient for the current demands in drug development [9]. Moreover, no such systems exist for adherent cells.

In this short report, we present our new PoreGenic[®] microneedle chip prototype providing a new 3D-MEA chip (Fig. 1). Recently, we found that it is also utilizable for the extracellular detection of action potentials from adherent primary cardiomyocyte cultures. Here, we present first results.

2 Material and Methods

We apply the new system in extracellular recordings of action potentials from PCMs of rat pups. The system as well as the microneedle electrodes (MNEs) are described elsewhere [12].

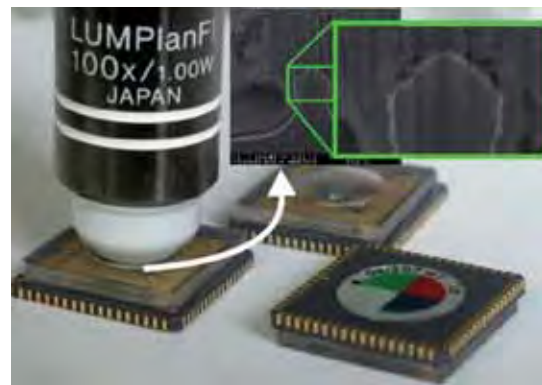


Fig.1. The PoreGenic[®] chip provides a micro needle array with integrated dielectrophoretic electrodes. The inserts show the micro needle and a focussed ion beam (FIB) cut -SEM of a needle overgrown by a cell.

3 Results

Amplitudes of up to tens of mV were recorded with solid metal microelectrodes based on solid silicon microneedles with a platinum seed layer. Besides the amplitude, the detected signal shows a significant similarity to an actual intracellular cardiac action potential shape (Fig. 2). However, the action potential amplitude decreases rapidly over minutes as can be seen in the four phases reflected by Fig. 2A2 as well as Fig. 2B. This effect can only be explained by poisoned electrodes.

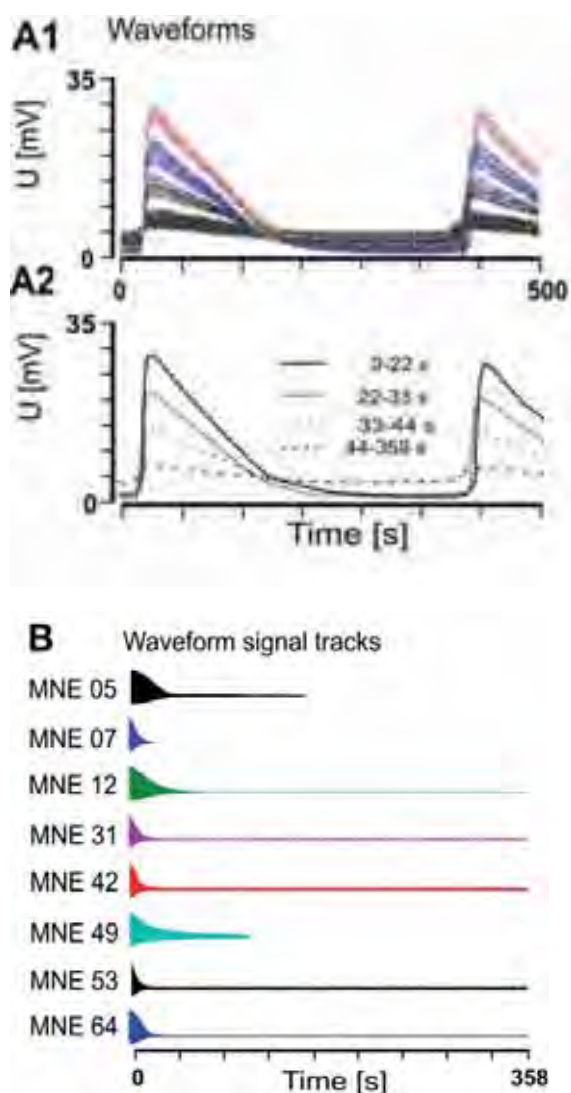


Fig.2: Electrical signal recordings from PCMs of embryonic rats with solid metal MNEs. (A) A1: 30 superimposed cardiac signals from MNE 12 subdivided into four time phases; A2: average waveforms of the four phases; (B) beating tracks of eight uniformly beating cells with rapidly decreasing amplitudes.

4 Conclusion

We think that the high signal quality is due to the improved electrochemical properties of the metal electrodes. Nevertheless, the signal amplitudes decreased within a few minutes after the detection was started. Probably, the decrease is caused by electrode poisoning. In future, the new PoreGenic[®] chip will also allow for intracellular whole-cell patch clamp recordings after penetration of the cell membrane by electroporation.

Acknowledgement

The authors also thank the Federal Ministry of Education and Research (BMBF) for funding the project MIBA – *Mikrostrukturen und Methoden für die intrazelluläre Bioanalytik* (grant 16SV2337) and the project PoreGenic (GO-Bio grant 0315809). This

work was also supported by grants of Mecklenburg-Western Pomerania (UR09045 of the Ministry of Education, Science and Culture, and V220-630-08-TFMV-F-011 (project part FLUXELL) of the Ministry for Economics, Work and Tourism).

References

- [1] Thomas Jr., C.A., Springer, P.A., Loeb, G.E., Berwald-Netter, Y., and Okun, L.M. 1972. A miniature microelectrode array to monitor the bioelectric activity of cultured cells. *Experimental Cell Research*, 74: 61-66.
- [2] Jongsam, H.J. and Schoonlingen, C.C. 1970. Electronic spread of current in monolayers of cultured heart cells. *Pfluegers Archiv*, 314: 144-145.
- [3] Gintant, G.A., Limberis, J.T., McDermott, J.S., Wegner, C., and Cox, B.F. 2001. The canine Purkinje fiber: An in vitro model system for acquired long QT syndrome and drug-induced arrhythmogenesis. *Journal of Cardiovascular Pharmacology*, 37: 607-618.
- [4] Pancrazio, J.J., Bey, J., Loloee, A., SubbaRao, M., Chao, H.C., Howard, L., Milton Gosney, W., Borkholder, D.A., Kovacs, T.A., Manos, P., Cuttino, D.S., and Stenger, A. 1998. Description and demonstration of a CMOS amplifier-based-system with measurement and stimulation capability for bioelectrical signal transduction. *Biosensors and Bioelectronics*, 13: 971-979.
- [5] Kutchinsky, J., Friis, S., Asmild, M., Taborski, R., Pedersen, S., Vestergaard, R.K., Jacobson, R.B., Krzywkowski, K., Schröder, R.L., Ljungström, T., Hélix, N., Sørensen, C.B., Bech, M., and Willumsen, N.J. 2003. Characterization of potassium channel modulators with QPatch automated patch-clamp technology: system characteristics and performance. *Assay and Drug Development Technologies*, 1: 685-693.
- [6] Guthrie, H., Livingston, F.S., Gubler, U., and Garippa, R. 2005. A place for high-throughput electrophysiology in cardiac safety: screening hERG cell lines and novel compounds with the Ion works HTTM system. *Journal of Biomolecular Screening*, 10: 832-840.
- [7] Farre, C., Haythornthwaite, A., Stoelzle, S., Kreir, M., George, M., Brueggemann, A., and Fertig, N. 2009. Port-a-patch and patchliner: high fidelity electrophysiology for secondary screening and safety pharmacology. *Combinatorial Chemistry & High Throughput Screening*, 12: 24-37.
- [8] Kiss, L., Bennett, P.B., Uebele, V.N., Koblan, K.S., Kane, S.A., and Neagle, B.S.K. 2003. High throughput ion-channel pharmacology: planar-array-based voltage clamp. *Assay and Drug Development Technologies*, 1: 127-135.
- [9] Brown, A.M. 2004. Drugs, hERG and sudden death. *Cell Calcium*, 35: 543-547.
- [10] Wible, B.A., Hawryluk, P., Ficker, E., Kuryshew, Y.A., Kirsch, G., and Brown, A.M. 2005. hERG-Lite: a novel comprehensive high-throughput screen for drug-induced hERG. *Journal of Pharmacological and Toxicological Methods*, 52: 136-145.
- [11] Krinke, D., Jahnke, H.G., Paenke, P.O., and Robitzki, A.A. 2009. A microelectrode-based sensor for label-free in vitro detection of ischemic effects on cardiomyocytes. *Biosensors and Bioelectronics*, 24: 2798-2803.
- [10] Tautorat, C., Koester, P.J., Held, J., Gaspar, J., Ruther, P., Paul, O., Cismak, A., Heilmann, A., Gimsa, J., Beikirch, H., Jonas, L., and Baumann, W. 2008. Intracellular potential measurements of adherently growing cells using micro-needle arrays. *The Proceedings of μTAS 2008 Conference*, 1777-1780.

High-Resolution Amperometric Spikes From Chromaffin Cells Revealed By Boron-Doped Nanocrystalline Diamond Microelectrode Arrays

Sara Gosso¹, Andrea Marcantoni¹, Yanlin Xu², Elisabetta Colombo^{1,2}, Zi-yao Gao², Erhard Kohn², Alberto Pasquarelli², Emilio Carbone¹, Valentina Carabelli^{1,*}

¹ Department of Neuroscience, NIS Center, 10125 Torino, Italy

² Institute of Electron Devices and Circuits, Ulm University, 89069 Ulm, Germany

* Corresponding author. E-mail address: valentina.carabelli@unito.it

Exocytosis is a Ca^{2+} -dependent process at the basis of synaptic transmission occurring through quantal release of neurotransmitter molecules into the synaptic cleft. Single secretory events of oxidizable molecules can be conventionally detected by means of carbon fiber microelectrodes (CFEs) [1], with submillisecond time resolution but limited to single cells. Here we radically changed the approach of recording by adopting a planar microelectrode configuration, with the aim of detecting secretory events from different chromaffin cells simultaneously. We describe the construction of a planar nanocrystalline diamond microelectrode array for recording quantal secretory events of oxidizable neurotransmitters from living cells.

1 Materials and methods

1.1 Chip realization

Our prototype is realized in nanocrystalline diamond (NCD) thin-film technology [2]. Diamond has been chosen because of its optical transparency, high biocompatibility, chemical inertness and a quasi-metallic conductivity, if properly doped. Moreover, the high corrosion resistance of the NCD electrodes ensures a long-term reliability not easily achievable with other electrode materials. Starting from a sapphire wafer, a 200 nm layer of intrinsic diamond was thus deposited using HF-CVD technique followed by 350 nm of boron-doped diamond (boron concentration was 10^{20} cm^{-3}) [3]. As an initial prototype, the array has been patterned with four circular microelectrodes ($20 \mu\text{m}$

diameter, Fig.1) using photolytographic methods, even though a more complex geometry is under construction [4].

1.2 Cell preparation

Isolated chromaffin cells were obtained from adrenal glands of adult mice [5] and positioned onto the NCD microelectrodes by means of a patch-clamp micromanipulator.

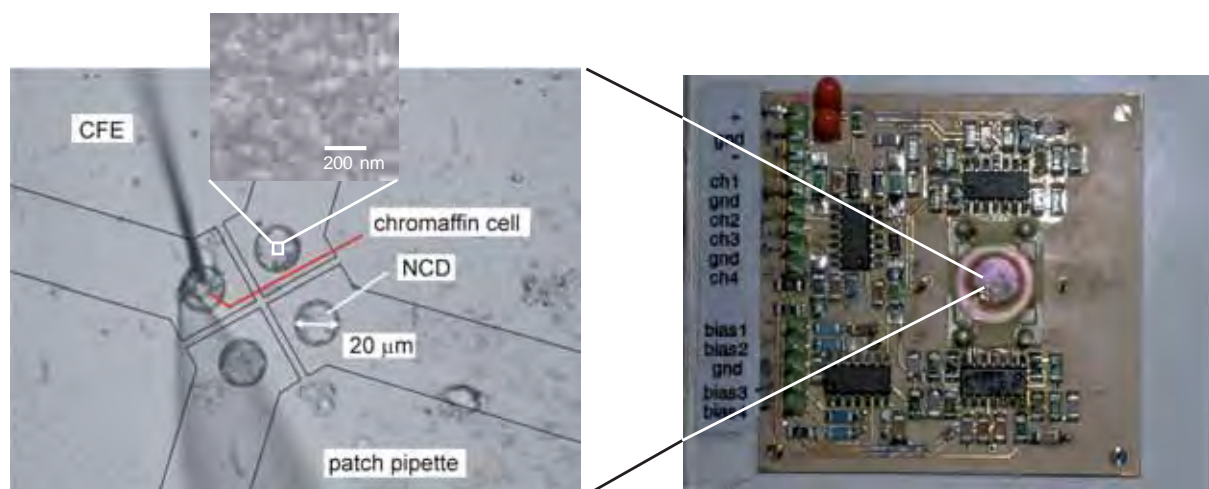


Fig. 1. (Left) A mouse chromaffin cells has been positioned on one of the detecting electrodes by means of a patch-clamp glass pipette inserted on a micromanipulator system [2]. A carbon fibre electrode (CFE) has been placed adjacent to the cell membrane. This configuration allowed the simultaneous detection of catecholamine secretion from planar and classical CFE. (Right) The electronic circuitry.

2 Results

To assay the feature of the amperometric recordings on the NCD device, we compared the spikes simultaneously recorded by the planar NCD and the CFEs. We found that maximal current amplitude as well as quantity of charge of the spikes were not significantly different in the two conditions, suggesting that the NCD microelectrode has the same amplitude resolution and signal-to-noise ratio of the classical CFEs.

Subsequently, we concurrently tested the responsiveness of all four NCD channels by positioning the chromaffin cells on each electrode. Quantal amperometric events could be independently detected on all channels with no time correlation between the recorded signals, excluding crosstalks between the four detecting NCD microelectrodes.

Finally, by combining patch-clamp and amperometric recordings, we simultaneously measured *i)* the Ca^{2+} currents evoked by 100 ms depolarizing pulses to +10 mV, from a resting potential of -70 mV (blue traces in Fig. 2), *ii)* the corresponding capacitance increases, representing the overall secretion from the cell (red traces), and *iii)* the amperometric spikes from the planar NCD.

3 Conclusion

The planar boron-doped NCD microarray can detect quantal secretory events of released catecholamines from adrenal chromaffin cells, with time and amplitude resolution comparable to the

conventional CFEs. Main advantages with respect to the classical carbon fibers are the patterned planar configuration of the NCD and the possibility of measuring neurotransmitter release from networks of cells or tissues and detecting other molecular species in cathodic and anodic regime besides catecholamines.

References

- [1] Wightman, R.M., Jankowski, J.A., Kennedy, R.T., Kawagoe, K.T., Schroeder, T.J., Leszczyszyn, D.J., Near, J.A., Diliberto, E.J. Jr, Viveros, O.H., (1991). Temporally resolved catecholamine spikes correspond to single vesicle release from individual chromaffin cells. *Proc Natl Acad Sci USA*. 88(23), 10754-10758.
- [2] Carabelli V, Gosso S, Marcantoni A, Xu Y, Colombo E, Gao Z, Vittone E, Kohn E, Pasquarelli A, Carbone E. Nanocrystalline diamond microelectrode arrays fabricated on sapphire technology for high-time resolution of quantal catecholamine secretion from chromaffin cells. *Biosensors and Bioelectronics*, in press.
- [3] Gao Z., Carabelli V., Carbone E., Colombo E., Demaria F., Dipalo M., Gosso S., Manfredotti Ch., Pasquarelli A., Rossi S., Xu Y., Vittone E., Kohn E., 2010. Transparent diamond microelectrodes for biochemical application, *Diamond & Related Materials*, (in press doi: 10.1016/j.diamond.2010.03.014)
- [4] Colombo E., Carabelli V., Carbone E., Gao Z., Herfurth P., Kohn E., Men Y., Pasquarelli A., Pietzka C. MEAmeeting 2010. Transparent NCD microelectrode array for spatially resolved detection in micro-areas of single cells (this volume)
- [5] Marcantoni, A., Carabelli, V., Vandael, D.H., Comunanza, V., Carbone, E., (2009). PDE type-4 inhibition increases L-type Ca^{2+} currents, action potential firing, and quantal size of exocytosis in mouse chromaffin cells. *Pflugers Arch-Eur J Physiol*. 457, 1093-1110.

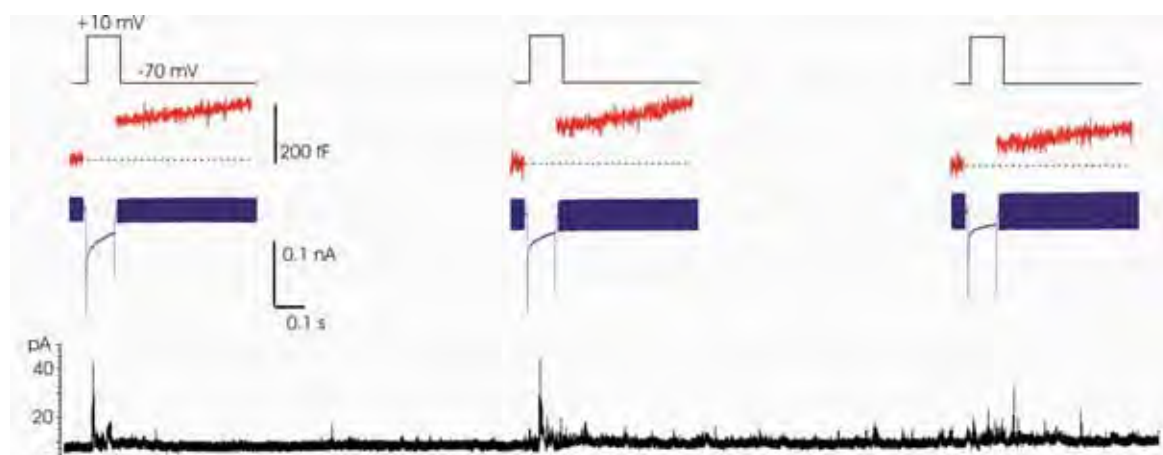


Fig. 2. Top) Three consecutive depolarizations to +10 mV applied every 45 seconds. Middle) Depolarization-evoked Ca^{2+} currents (blue traces) caused massive secretion from the whole cell, measured as capacitance increase (red traces). Bottom) Bursts of amperometric spikes detected by means of the planar NCD soon after the beginning of Ca^{2+} entry.

Cell-a-V, a novel multi-well MEA for multi brain-structures research

Taub Aryeh^{1*}, Rabner Arthur², Shacham-Diamand Yosi²

¹ Psychobiology Research Unity, Department of Psychology, Tel Aviv University, Tel Aviv, Israel

² Faculty of Engineering, Tel Aviv University, Tel Aviv, Israel

* Corresponding author. E-mail address: aryataub@post.tau.ac.il

Despite the benefits in using traditional methods for neuronal-network research, such as MEAs, it is still tricky to mimic the interaction between cell populations in-vitro. This disadvantage does not allow scholars to reliably mimic and study the interaction between several brain structures. Additionally, while developing brain-computer interfaces, functional examination of the electrode's size, structure, configuration and surface-functionalization should be done in-vitro rather than the present convention to examine it in-vivo. The focus of the present project was to develop a novel multi-wells MEA, which allows studying the interaction of up to 8 different cell types and/or different structures of electrodes, while sharing the same experimental environment.

1 The MEA chip

1.1 Chip development

A MEA chip was manufactured on Si-based wafers. The design consists of 8 wells (8 MEAs of 48 Au/TiN electrodes each; total of 384 electrodes on each Si chip). In the 1st generation we produced 4 wells with 25 μm X 25 μm electrodes and 4 wells with 30 μm X 30 μm electrodes (Fig. 1 & 2). For each well, a reference electrode was designed to almost surround the edge of the well. Four large ground electrodes were positioned at the centre of the chip.

1.2 The acquisition system

The Cell-a-v data acquisition system was designed by g.tec (Austria). Using multiplexers allows using each electrode for recording (passive) or stimulating (active). Each recording channel can be sampled with A2D rate of < 15k and bandpass filter can be applied on line or retrospectively. Each recording channel can be sampled in reference to its well's reference, reference electrode of a selected well or in reference to one of the ground electrodes.

1.2 Stand-alone system

The Cell-a-V system was designed as a stand-alone system with controllable autonomous temperature and nutrition system.

2 Results

A manufacturing procedure for the MEAs chip was developed. A chip of 384 electrodes was fabricated (Fig. 1), with 8 MEAs of 48 electrodes each (Fig. 2).

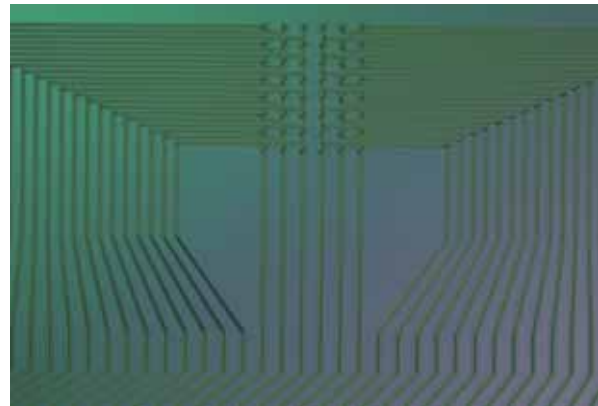


Fig. 1. Microscope image of the Cell-a-V wafer. A marks a 48 electrodes MEA.

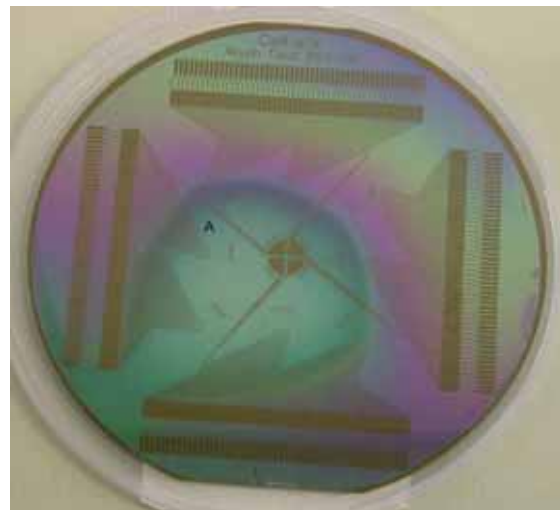


Fig. 2. Microscope image of 1 well (1 MEA) with 48 TiN electrodes.

3 Conclusion/Summary

We have developed a multi micro electrode arrays platform designed for multi brain structures network study. The Cell-a-V platform allows studying the interaction between multiple afferent and efferent cells converging to defined tissue and plasticity processes in the tissue and between the afferents.

Acknowledgement

We would like to thank Almog R. for her help during the study. The research leading to these results was supported by the European Community's Seventh Framework Program (FP7) under grant agreement # 216809.

Electrical Stimulation, Implants and Robotics

Subretinal electrical stimulation of isolated RCS rat retina with pulse trains and paired pulses

Thoralf Herrmann, Alfred Stett*

NMI Natural and Medical Sciences Institute at the University of Tübingen, Reutlingen, (Germany)

* Corresponding author. E-mail address: stett@nmi.de

Retina samples from blind RCS rat were electrically stimulated with temporally and spatially separated paired pulses to investigate network response to continuous stimulation. Repetitive stimulation by paired pulses and pulse trains with interpulse intervals of 250 ms and shorter resulted in local depression of ganglion cell activity within a retinal patch with a diameter of about 180 μm .

1 Background

Subretinal neuroprostheses aim at restitution of lost visual function by continuous electrical multi-site stimulation of the degenerated retina in blind people [1]. Repetitive, focal stimulation of the retinal network with electrical pulses causes, however, a frequency dependent attenuation of ganglion cell response [2]. This may affect the temporal resolution obtainable by continuous stimulation by a subretinal implant. Using pulse trains and paired pulses applied to one and two spatially separated electrodes, respectively, at different interpulse intervals we investigated the temporal and spatial extension of the retinal patch in which response depression occurs after local stimulation.

2 Methods

Retina pieces from blind RCS rats (50 to 177 days old) were placed ganglion cell layer down on microelectrode arrays (MEAs). An 8-channel comb electrode array (pitch 80 μm , Thomas Recordings) was used for electrical stimulation of the distal retina (Fig. 1). Paired voltage pulses were delivered through an 8-channel stimulus generator. We varied both the spatial and the temporal distance between the first and the second pulse. Ganglion cell activity was recorded with the MEA system (Multi Channel Systems). The extracted timestamps were averaged over 20 sweeps, binned and plotted as PSTH and activity patterns.

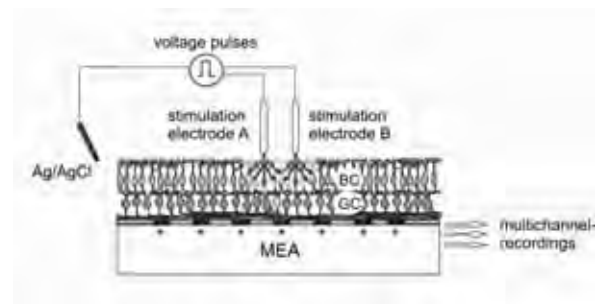


Fig. 1. Arrangement for multifocal electrical stimulation of degenerated retina (BC = bipolar cells, GC = ganglion cells) with paired pulses. Activity patterns are recorded with the MEA electrodes.

3 Results

3.1 Repetitive stimulation with pulse trains

In the degenerated retina from RCS rat, the local stimulation by pulse trains with interpulse intervals of 250 ms and shorter resulted in local depression of ganglion cell activity after the preceding pulse (Fig. 2). The activity evoked by the first pulse within a train was undisturbed by successive pulses. When a train of stimulus pulses was applied, a steady depression was observed after the first pulse.

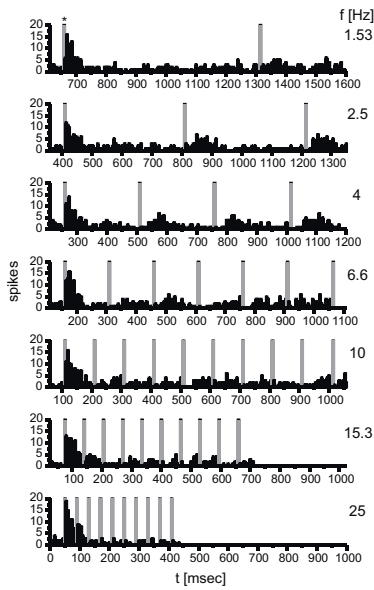


Fig. 2. Response analysis from repetitive stimulation experiments with trains of 10 pulses and variable frequency. PSTH from 20 trials, bin width 5 ms, gray bars (*) marks stimulation artifact.

3.2 Paired-pulse stimulation

Using a paired-pulse protocol (Fig. 3), we observed almost undisturbed activity after the second pulse when the first pulse was applied by an electrode with a distance $> 80 \mu\text{m}$ to the recording site (Fig. 4). This was nearly independent of the interpulse interval and stimulation strength (data not shown).

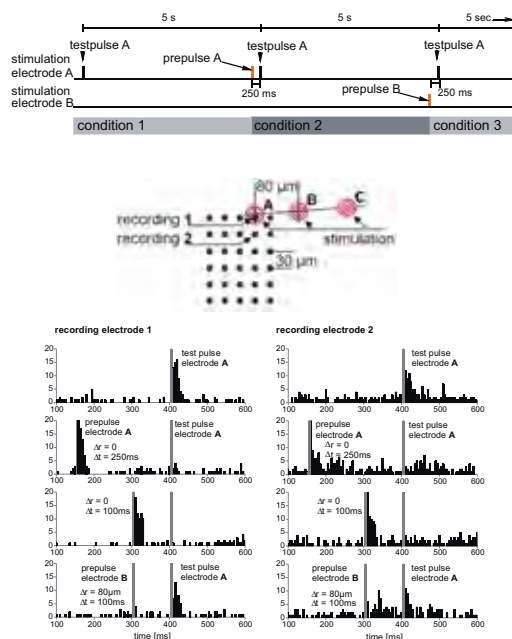


Fig. 3. Paired-pulse stimulation with temporal and spatial displacement between prepulse and test pulse (unsorted spike activity). Top: stimulation protocol, center: location of stimulation (A, B, C) and recording electrodes. Bottom: PSTHs of recordings on electrode 1 and 2 at stimulation with electrode A and B.

4 Conclusion / Summary

Local electrical stimulation of the retina leads to temporary and spatially confined inhibition of the signal transmission. We suppose that the inhibition is located in the vertical retinal pathway, presumably at the synapses at the axon terminal of bipolar cells. Whether the lateral pathway including amacrine cells is inhibited or not has to be shown in further experiments.

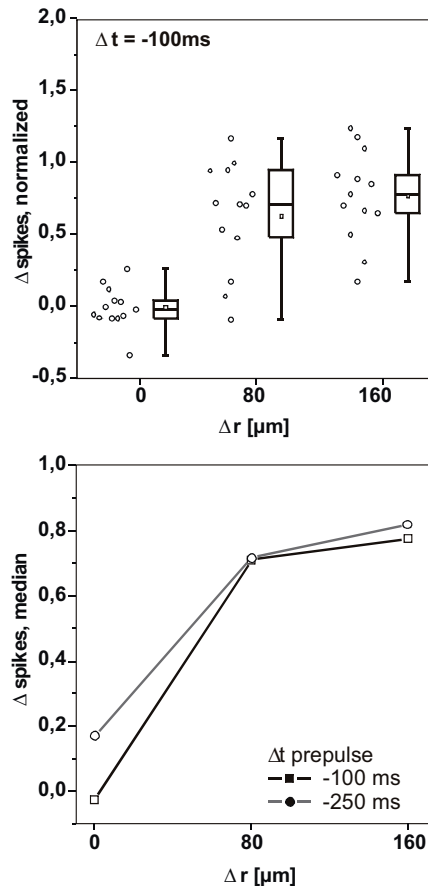


Fig. 4. Paired-pulse depression of RGC response amplitudes as a function of spatial displacement of the prepulse. For each RGC ($n=13$), the responses to the test pulses were averaged for 20 trials at each interpulse interval, and normalized to the activity evoked by the test pulse under condition 1 (see Fig. 3).

Acknowledgement

Supported by German Ministry for Education and Research (BMBF), grant 0315113 to Retina Implant AG.

References

- [1] Stett A., Mai A., Herrmann T. (2007). Retinal charge sensitivity and spatial discrimination obtainable by subretinal implants: key lessons learned from isolated chicken retina. *Journal of Neural Engineering* 4, S7-S16
- [2] Jensen R., Rizzo III J. (2007). Responses of ganglion cells to repetitive electrical stimulation of the retina. *J. Neural Eng.*, 4, 1-6.

Real-time Characterization of Neuronal Response for Selective Stimulation

Michelle L. Kuykendal¹, Gareth S. Guvanasen¹, Martha A. Grover², Steve M. Potter¹, Stephen P. DeWeerth^{1*}

¹ Laboratory for Neuroengineering, Coulter Department of Biomedical Engineering, Georgia Institute of Technology, Atlanta, Georgia, USA

² School of Chemical & Biomolecular Engineering, Georgia Institute of Technology, Atlanta, Georgia, USA

* Corresponding author. E-mail address: steve.deweerth@gatech.edu

Spatiotemporal selectivity of extracellular stimuli is a significant challenge in the development of neural interfacing devices. Although models have previously been used to investigate responses to various stimulus waveforms, it is of significant interest to experimentally validate the stimulus-evoked cellular response and use that information to optimize the stimulus patterns. To address these challenges, we have developed a high-throughput closed-loop system of multisite stimulation and recording that facilitates the characterization of the cellular activity evoked by extracellular stimulation. We explore excitatory waveforms applied to cortical networks at multiple sites in a multi-electrode array (MEA) to achieve increased precision and localization of extracellular stimuli. We measure the response of all individual neurons using fluorescent calcium-sensitive dyes in conjunction with novel real-time optical processing algorithms and an automated data acquisition platform. Using this system, we have characterized waveforms that excite neural activity within a 400 μ m X 400 μ m field of view, and in this work we investigate the use of such waveforms to explicitly direct the focus of an extracellular stimulus.

1 Introduction

Extracellular stimulation of neural tissue is essential for the enhancement of neuroprostheses, including retinal and cochlear implants, and the treatment of complex diseases, ranging from Parkinson's Disease to epilepsy and depression. If we could target our stimulation to only those cells and networks that are essential to the system, we could significantly increase our efficacy and eliminate side effects due to diffuse stimulation. Future clinical implementations of this technology will use systems that optimize their outputs based on real-time closed-loop processing of the evoked neuronal responses [1].

Our system enables the real-time processing of optical signals to measure the stimulus-evoked responses in the tissue so that we can automatically home in on the optimal stimulus. First we must study the excitatory aspects of neuronal tissue, and then we can explore the potential to inhibit certain cells while stimulating others, using the spatial precision that MEAs afford.

2 Methods

2.1 Cell Culture

Cortical neurons from embryonic day-18 rat were enzymatically and mechanically dissociated using papain and a vortex mixer, respectively. The neurons were then grown in DMEM with 10% horse serum on

multi-electrode arrays (200/30-TiN, Multichannel Systems) coated in polyethylene amine and laminin to encourage cell adhesion [4].

2.2 Fluorescence Imaging

Cultures were bathed in an acetoxymethyl-ester calcium-sensitive fluorescent dye, Fluo-5F-AM [3], which was combined with pluronic F-127 and DMSO to enhance cell-loading. All synaptic communication in the network was then blocked using receptor antagonists APV (100 μ M), bicuculine (50 μ M) and CNQX (10 μ M), which bind NMDA, GABA_A and AMPA receptors, respectively [2]. All optical recording was performed using an electron multiplication CCD camera (QuantEM, Photometrics) while electrical stimulation was conducted with an STG2004 and electrical recording utilized the MCRack software (Multichannel Systems). All other software was developed in-house using MATLAB.

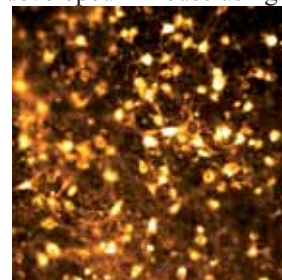


Fig. 1. Fluorescence image of integrated spontaneous activity across time (10 min) in a 2-D neuronal network. Post-processing includes frame averaging, median filter and coloring (ImageJ).

3 Results

Trains of five excitatory cathodic pulses were delivered 50ms apart to provide fluorescence summation improving signal-to-noise ratio in the optical recording. All stimulus trains were repeated three times in random order for averaging.

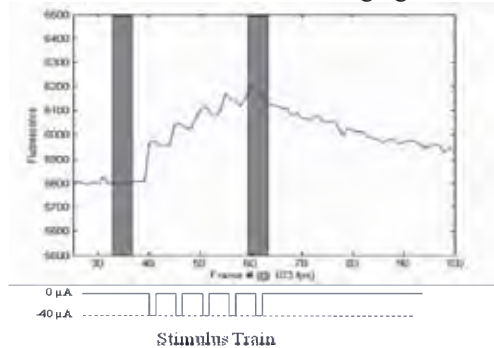


Fig. 2. Example of a stimulus train (bottom) applied to the culture via one electrode, and resulting fluorescence recording (top). Gray bars indicate regions of peak and baseline fluorescence for averaging.

3.1 Current Sweep

While holding the stimulus duration constant, we varied the current amplitude and analyzed the resulting neuronal response. Increasing current activated more cells within any given radius, and this activation falls off with distance from the electrode similarly in each stimulus condition. Radii that produced the same incremental area were used to divide the cells into quartiles moving away from the center electrode.

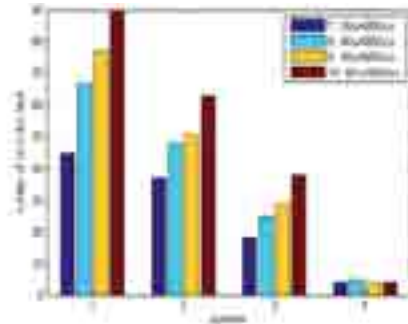


Fig. 3. Activation of neurons versus distance from the stimulating electrode under four stimulus amplitude conditions. Quartile radii are as follows: 181.0 μm , 256.0 μm , 313.5 μm and 362.0 μm .

3.2 Equal Charge Delivery

The same total charge was delivered in each stimulus; however, the amplitude and duration were varied. From these data we see that at the lowest stimulus amplitude we may be approaching the limits defined in a chronaxie curve because the evoked response is consistently less than that of the others. However, all other stimuli produce similar responses. This is consistent with the theory that the total stimulus charge dictates the cellular response, independent of amplitude and duration, once the total stimulus charge is above threshold.

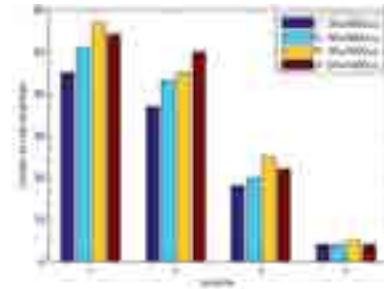


Fig. 4. Activation of neurons versus distance from the stimulating electrode for four stimulus waveforms of equal charge delivery. Quartile radii are as follows: 181.0 μm , 256.0 μm , 313.5 μm and 362.0 μm .

4 Conclusions

Experimentation has previously demonstrated the potentially inhibitory effects of below-threshold excitatory stimulation [5]. If we simultaneously combine these waveforms on multiple electrodes with our excitatory stimuli, we may be able to further localize our stimuli in both space and time. Because data collection and analysis are fully automated in our system, future work will use feedback of neuronal activation to optimize our stimuli and spatiotemporally target a population of cells. Furthermore, the use of optical imaging provides us with a ground truth of the activity both at and in between electrodes so that we can calibrate our simultaneous electrical recording to what we know is actually happening in the network. This could ultimately allow us to electrically stimulate *in vivo*, without the need for optics, while still maintaining the ability to focus our stimulus.

The ability to selectively stimulate neurons will help us to improve the development of neural interfacing devices, including motor prostheses and deep brain stimulators that are free from side effects.

Acknowledgement

We thank the NSF for supporting our work through NSF EFRI grant #0836017 and the NSF Graduate Research Fellowship Program.

References

- [1] M. Arsiero, H. Luscher, et al. (2007). "Real-time closed-loop electrophysiology: towards new frontiers in *in vitro* investigations in the neurosciences." *Arch Ital Biol* 145(3-4): 193-209.
- [2] D. J. Bakkum, Z. C. Chao, S. M. Potter (2008). "Long-Term Activity-Dependent Plasticity of Action Potential Propagation Delay and Amplitude in Cortical Networks." *PLoS ONE* 3(5): e2088.
- [3] A. Minta, J. P. Y. Kao, and R. Y. Tsien (1989). "Fluorescent Indicators for Cytosolic Calcium Based on Rhodamine and Fluorescein Chromophores." *Journal of Biological Chemistry*, vol. 264, pp. 8171-8178.
- [4] S. M. Potter and T. B. DeMarse (2001). "A new approach to neural cell culture for long-term studies." *Journal of Neuroscience Methods*, vol. 110, pp. 17-24.
- [5] J. D. Ross, N. E. Reddy, D. J. Bakkum, S. M. Potter, and S. P. DeWeerth (2007). "Experimental Platform for the Study of Region Specific Excitation and Inhibition in Neural Tissue" *Proceedings of the 29th Annual International Conference of the IEEE EMBS*. pg:4759.

Voltage-controlled Stimulation Pulses May Be Lethal

Jonathan C. Erickson^{1*}¹ Washington and Lee University, Department of Physics-Engineering, Lexington, VA, USA

* Corresponding author. E-mail address: ericksonj@wlu.edu

Biphasic controlled-voltage pulses are commonly used to evoke action potentials (APs) in neural cultures grown on MEAs. Responses of individual neurons to such pulses were studied using the caged-neuron MEA system, in tandem with voltage-sensitive fluorescence imaging. The results indicated that controlled-voltage pulses are often lethal to a neuron adjacent to the platinum black electrode. Controlled-current pulses, on the other hand, were observed to reliably evoke APs without any deleterious effect. MEA users, therefore, should carefully consider the type of stimulus used to study cultured neural network dynamics.

1 Introduction

Dissociated neuronal cultures grown on MEAs are commonly studied using biphasic controlled-voltage pulses (e.g., [1], [2], [3]), with amplitudes up to 900 mV, and durations of 200–400 μsec . A previous study concluded that voltage-controlled pulses are highly effective at eliciting APs in dense (5000/ mm^2) cortical cultures [4]. However, studying responses of individual neurons to electrical stimuli in the caged neuron MEA system [5] led to a different conclusion: voltage-controlled pulses are less effective at evoking APs than current-controlled pulses; moreover, they appear to often be lethal.

2 Methods

2.1 Cell Culture

Dissociated E18 hippocampal cultures were grown, and single neurons were loaded into neurocages, which confines the soma to be adjacent to a 12 μm diameter, platinum black electrode, as described in [5].

2.2 Voltage-sensitive Fluorescence Imaging

Voltage-sensitive fluorescence imaging was used to study the response of neurons to electrical stimuli, as patching to directly measure the membrane potential (V_m) was not technically feasible. Cultures 6–31 DIV were stained with di-4-ANEPPDHQ, a fast responding, linear potentiometric dye [6] (Fig. 1). The change in fluorescence intensity ($\Delta F/F$) of membrane-bound dye molecules is about -1 % for every +100 mV change in V_m (depolarization leads to a decrease in $\Delta F/F$, and vice-versa).

Stained, caged neurons were illuminated with the Hg green line ($\lambda = 546 \text{ nm}$). To prevent photobleaching and phototoxicity, exposure times were minimized to 100 msec using a mechanical shutter synced to the stimulus. The *RedShirt* NeuroCCD camera (frame rate

= 2 kHz; 80 x 80 pixels/frame) measured $\Delta F/F$ versus time in response to electrical stimuli.

2.3. Electrical Stimuli

Responses to charge-balanced, biphasic (400 $\mu\text{s}/\text{phase}$), both positive- and negative first, voltage-controlled pulses (0–800 mV) were examined in 21 neurons. Responses to biphasic (400 $\mu\text{s}/\text{phase}$), current-controlled pulses (0–20 μA) were similarly examined in 66 neurons.

It is important to note that a voltage-controlled pulse produces a large ($\approx 100 \mu\text{A}$) RC current transient—therefore a large voltage gradient—in the cell culture medium, with a time constant ($\approx 100 \mu\text{s}$) that depends on the electrode capacitance ($\approx 5000 \text{ pF}$) and the bath resistance ($\approx 20 \text{ k}\Omega$). The maximum voltage gradient occurs on the mid-stimulus pulse transition (negative-to-positive, or vice-versa).

2.4 Signal Processing: Response Detection

$\Delta F/F$ signals were spatially averaged over the entire soma, photobleach corrected, and digitally high-pass filtered (2nd order Butterworth; 30 Hz cutoff). “Significant” $\Delta F/F$ responses were defined to occur when $\Delta F/F > 5*\sigma$, where σ is the noise estimated using the median of the absolute deviation [7].



Fig. 1. Caged neuron DIC (left), voltage sensitive dye-stained (center), and NeuroCCD (right) images. The soma is adjacent to the lower-right side of the platinum black electrode.

3 Results

Fast ($\leq 1 \text{ ms}$) transients in $\Delta F/F$ with a magnitude proportional to the size of the stimulus (Fig. 2) were

commonly observed in response to voltage-controlled stimuli. Importantly, the direction of the major deflection in $\Delta F/F$ depended on whether the stimulus was positive- or negative-first. A positive-first pulse (negative-going RC current transient) resulted in an upward deflection; a negative-first pulse (positive-going RC current transient) resulted in a downward deflection. Recalling the -1% per +100 mV calibration of the dye, these results suggest that the cell membrane was being directly driven according to the direction and strength of the RC current transient.

In addition, the resting light intensity (RLI) was often noted to suddenly increase after a large enough magnitude pulse (typically > 600 mV), indicating that more dye molecules implanted in the cell membrane. 14 of 21 cells responded in this manner.

Taken together, these observations suggest that voltage pulses can severely and irreversibly disrupt the integrity of the cell membrane, thus leading to cell death.

By contrast, neurons responded to current-controlled pulses in an all-or-nothing manner, with the main stroke in $\Delta F/F$ always downward, usually on the order of -1%, and lasting for a longer a time (3–5 ms), indicating APs were evoked. 59 of 66 neurons responded in this manner to current-controlled pulses.

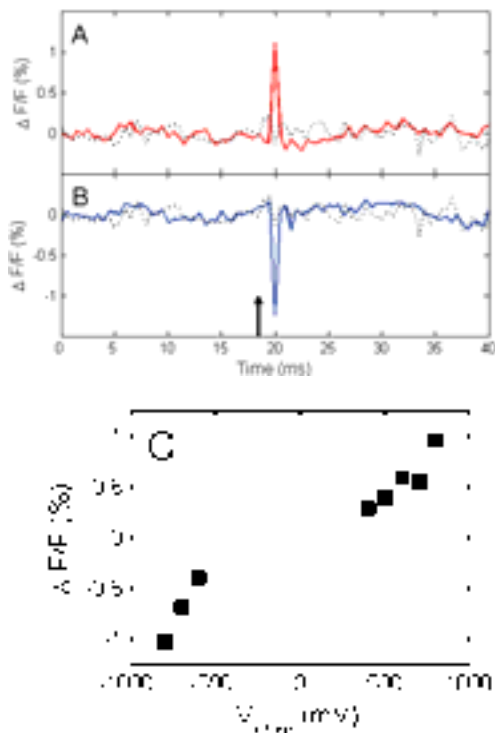


Fig. 2. Fluorescence intensity responses to a positive-first (A, red) and negative-first (B, blue) biphasic (400 μ s/phase) 800 mV voltage pulse. A control trace is overlaid (black, dotted). The arrow marks the onset timing of the stimulus. (C) Maximal fluorescence response versus stimulus strength (negative amplitude indicates negative-first stimuli, and vice-versa). The response to small stimuli (< 400 mV) was lost in the noise, hence no response marked.

4 Discussion

Due to the linearity di-4-ANEPPDHQ, the charge injection signal should (ideally) be zero, if the cell is being stimulated symmetrically. Therefore, it is highly unlikely that the linearly proportional transients observed during voltage pulse stimulation correspond to a charge injection failing to subsequently evoke an AP. Furthermore, voltage gradients >100 mV/ μ m are known to create large electroporative holes in cell membranes leading to cell death [8]. The gradient near the cage electrode during the mid-voltage-pulse transition is known to exceed this level (Fig. 3), which explains why voltage pulses can be lethal.

Voltage pulses may be effective at eliciting more APs in large, dense cultures as their “sphere of influence” is larger than that of current pulses. However, caution is advised when choosing the type of stimulus because voltage pulses appear to be lethal to cells adjacent to an electrode. If an investigator does not account for this deleterious effect, then the results of a plasticity or connectivity experiment may be confounding, or misinterpreted. Current pulses, by contrast, have not been observed to be harmful.

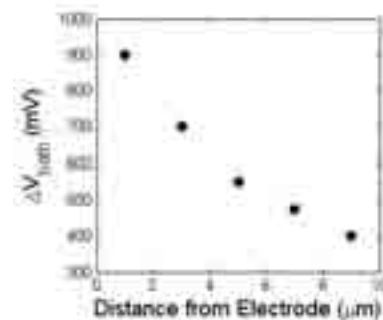


Fig. 3. Voltage gradient in the cell-culture medium bath generated by voltage-controlled pulse, as a function of distance from the electrode (measured along the vertical axis of the cage). ΔV_{bath} indicates the electric potential between a position in the cage near the electrode and the bath ground. It was measured by positioning a patch micropipette near the base of the cage, moving upward in 2 μ m increments.

Acknowledgement

The author would like to thank Dr. Jerry Pine at the California Institute of Technology for helpful discussion related to the work presented in this manuscript.

References

- [1] Jimbo (1999), *Biophys. J.* **76**: 670–678.
- [2] Ruaro (2005), *IEEE Trans Biomed. Eng.* **52**(3): 371–383.
- [3] Wagenaar et al. (2005), *J. Neurosci.*, **25**(3): 680–688.
- [4] Wagenaar and Potter, *J Neurosci Meth.* **138**(1–2): 27–37.
- [5] Erickson and Pine (2008), *J. Neurosci Meth.*, **175**: 1–16.
- [6] Obaid et al. (2004), *J Neurosci Meth.*, **134**: 179–190.
- [7] Nenadic (2005), *IEEE Trans. Biomed. Eng.*, **52**(1): 74–87.
- [8] Chu et al. (1987), *Nucl. Acid Res.*, **15**: 1311–26.

Wireless Stimulation of MEAs Inside the Incubator

Chinmay Joag, Bruce Wheeler, Thomas DeMarse*

1 J. Crayton Pruitt Department of Biomedical Engineering, University of Florida, Gainesville, FL, USA

* Corresponding author. E-mail address: tdemarse@bme.ufl.edu

Background Stimulation of neurons on MEAs usually requires removal from the incubator so as to utilize the amplifier/stimulator electrode array holder. Alternatively, cabling can be run into the incubator, with the potential for disruption of the integrity of the incubator. In either case the amplifier system, whose cost precludes large-scale purchase, is tied up during the process, limiting the number of cultures for which long-term stimulation is possible. We report here a prototype of a low cost, programmable, wireless 60 channel stimulator enabling investigations involving long term chronic stimulation within the incubator environment.

1 Introduction

With the advent of hi-resolution multichannel recording methods a parallel need for multichannel stimulation has emerged. Commercially available systems are often limited to only a small subset of those channels (e.g. Mutichannel Systems STG1004 and 1008 series) offering pre-programmable stimulation trains. A number of custom built hardware alternatives by individual labs have been created to provide more dynamic stimulation needs (Nam et al., 2009; Potter et al., 2006; Wagenaar et al., 2004).

In this paper we describe a neural stimulator for Multichannel Systems MEAs engineered for independent multichannel stimulation within an incubator environment and WiFi stimulation control.

2 Design

- Continuous in incubator operation
- Wireless communication for remote programming of stimulation protocols
- Minimum two week battery operation under continuous stimulation load for realistic long term stimulation
- Voltage stimulation with simultaneous-capable independently programmed levels for each MEA electrode
- Hi resolution timing of pulse waveform and inter-stimulus delivery

2.1 Power

The board shown in Fig. 1 was powered by two standard 9V Li-On batteries which have a power output of 2200mAh. Estimated battery life under continuous operation is several weeks.

2.2 Wireless Communication

A 2.4GHz Xbee Pro WiFi module was employed for wireless communication between a host computer and the stimulation board. This communication channel has a straight-line transceiver capacity of 1 mile with 60 mW power consumption (ideal for battery powered hardware) and operated without problem within an incubator environment.

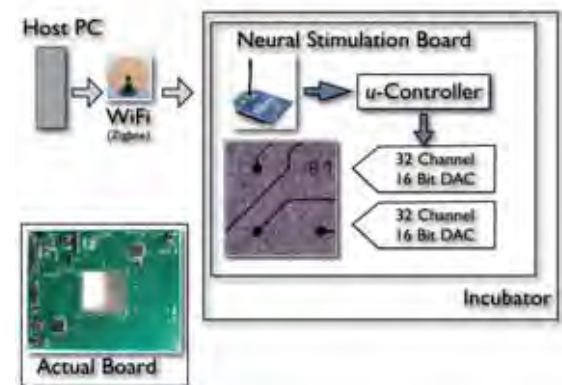


Fig. 1. Neural stimulation board featuring wireless communication, independent electrode voltage stimulation and in incubator battery operation.

2.3 Microcontroller and Stimulation Programming

An ATmega1281™ microcontroller with 128K flash memory handled stimulation pulse timing, and scheduled pulses according to programming received from the wireless communication channel.

User designed trains of stimuli are first created on a host computer (PC- C# Interface), compiled into ATmega assembly code generated by the freely available AVR GNU gcc compiler, and then flashed onto the microcontroller via the wireless interface for stand alone operation. Alternatively, for

situations in which dynamic stimulation is required the device can be flashed with a small operating system to handle an asynchronous communications link via Wi-Fi (Zigbee) scheduling stimulation on the fly (e.g., real-time stimulation feedback control).

2.4 Stimulation Specifications

To implement asynchronous independent voltage control a pair of output buffered 32 channel 16 bit digital-to-analog converters (DAC) (AD5372) were used. The board delivered program adjustable (± 2 V) square-wave charge-balanced voltage pulses. Voltage step resolution is 0.1 mV with single channel programmable gain and zero offset adjustment. Resolution of pulse width timing is 10 μ s due to timing constraints from SPI control via the microcontroller. These specifications are well within the range needed for typical stimulation of dissociated neural culture (The board design could quickly be modified to expand that range to ± 8.6 V for stimulation of acute brain slice but we did not implement that feature).

2.5 Board Design

Spring loaded gold-plated pins interface the board to contacts on the periphery of the MEA (ED8186-ND from MILL-MAX Manufacturing). Each board measures 12.5 x 10 cm and was placed in a plastic enclosure to isolate the PCB and components from the high humidity environment within the incubator.

3 Conclusion

Long term stimulation protocols delivered within the stable incubator environment are increasingly being used to study developmental processes within dissociated neural networks on MEAs (e.g., Brewer, et al. 2009). In this paper we describe a stimulation device that operates wirelessly within the incubator to deliver relatively complex stimulation pulse trains and can do so for long periods (> 2 weeks). Further, the board employs independent voltage values on a per electrode basis when stimulation is simultaneous and can be programmed in a stand-alone configuration or in a real-time interactive input scheme if needed.

Acknowledgement

This work was partly supported by NIH grant NS052233.

References

- [1] Brewer, G., Boehler, M., Ide, A., & Wheeler, B. (2009). Chronic electrical stimulation of cultured hippocampal networks increased spontaneous spike rates. *J Neurosci Methods*, 184, 104-109.
- [2] Nam, Y., Brown, E. A., Ross, J. D., Blum, R. A., Wheeler, B. C., & DeWeerth, S. P. (2009). A retrofitted neural recording system with a novel stimulation IC to monitor early neural responses from a stimulating electrode. *J Neurosci Methods*, 178, 99-102.
- [3] Potter, S. M., Wageenar, D. W., & DeMarse, T. B. (2006). Closing the loop: Stimulation Feedback Systems for Embodied MEA Cultures. In M. Taketani, & M. Baudry (Eds.), *Advances in Network Electrophysiology Using Multi-Electrode Arrays* (pp. 215-42). New York: New York: Springer.
- [4] Wagenaar, D. A., & Potter, S. M. (2004). A versatile all-channel stimulator for electrode arrays, with real-time control. *J Neural Eng*, 1, 39-45.

Ex ovo culture: An *in vivo* model for microsensor implants

Massimo Kubon^{1*}, Meike Moschallski¹, Gorden Link¹, Simon Werner¹, Claus Burkhardt¹, Wilfried Nisch¹, Beate Scholz¹, Burkhard Schlosshauer¹, Gerald Urban² and Martin Stelzle¹

¹ NMI Natural and Medical Science Institute at the University of Tuebingen, Reutlingen, Germany

² University of Freiburg, IMTEK, Laboratory of Sensors, Freiburg, Germany

* Corresponding author. E-mail address: massimo.kubon@nmi.de

Microsensors for medical applications have been under research for decades. For *in vivo* applications longterm stability is a critical prerequisite, mainly due to host response towards the micro implant. Currently, biological evaluation of implants relies on the implantation of test samples into animal models for different durations followed by histological examination of explanted specimens. In order to assess tissue response towards implants and biomaterial coatings, we propose continuous measurements at the implant/tissue interface employing a microsensor device placed in contact with the chorioallantoic membrane (CAM) of the avian embryo.

We introduce an electrochemical microsensor array and a miniaturized potentiostat unit ("MiniPot") to measure oxygen, pH and electrical impedance *in situ*. As an *in vivo* test environment we established avian *ex ovo* cultures as an immune-active and -deficient *in vivo* model, enabling comparison between either weak or strong immune responses in the same organism, respectively. Measurements were performed in an incubated biological environment. We consider this model to be a useful tool to evaluate future developments of biofunctional coatings and implants in a quasi-*in vivo* environment to promote research of implantable active micro devices.

1 Introduction

For *in vivo* applications longterm stability of microsensors is a critical prerequisite. Coatings are under research to enhance microimplant performance and to enable continuous longterm measurements. These coatings either improve biofunctionality or biocompatibility in terms of decreased fibrous capsule formation around the implant [1]. Lately, Nanotechnology implies potential to decrease foreign body responses [2]. But up to present, biomaterials to enhance *in vivo* performance over longer periods are still under development. Due to higher validity towards *in vitro* systems, evaluation of biomaterials and -coatings towards foreign body responses is still performed using animal models [3]. Tissue reactions appearing at the interface between implant and active tissue are indicative of the biocompatibility of such implant. Hence, an in depth understanding of these processes is critical.

In order to assess tissue response towards implanted biomaterials in a quantitative and continuous fashion, we propose measurements of oxygen, pH and electrical impedance at the implant/tissue interface employing a planar microsensor device placed in contact with the chorioallantoic membrane (CAM) of the avian embryo. These values are indicative of the tissue properties and can then be correlated to results obtained from histology.

The CAM is a highly vascularized cortical membrane of the avian embryo. It serves as an area

for respiratory gas exchange, ionic and molecule transport through the nano-porous egg shell. It has been used as an active tissue assay in several studies in biology [4]. Its attractiveness is founded in its low cost, simple preparation, the feasibility of optical observation of the operation area and minor ethical concerns when compared to conventional animal testing. Avian embryos may be cultured shell less (*ex ovo*) in a separate container, making it relatively convenient to handle in combination with external equipment. While it has been used as an active tissue model to evaluate biosensor function [5], to our knowledge the development of the foreign body response has not previously been investigated. In this work we discuss its use as an immune-inactive/active model.

2 Methods

We fabricated a microsensorarray (MSA) comprising sensors for dissolved oxygen, pH and electrical impedance. The MSA was realized using standard thin film techniques. Ti/Pt electrodes were deposited on PET (Acos GmbH, Tesa AG), Kapton® (DuPont®) or glass wafers (Menzel GmbH & Co. KG) and functionalized by electrodeposition techniques [6].

Avian *ex ovo* culture was prepared by standard protocols obtained from literature [7] as well as through in-house expertise. Avian eggs were purchased from a local vendor and pre-incubated (3 days) prior to use (37,5°C; 80% r.h.). We used

hydrophobic sterile cultures dishes (Corning® Inc.) after priming with 5ml of Ringer-Lactate solution (Serag-Wiessner KG) containing 0,02 mg/ml Gentamicin. Specimens with ruptured yolk were discarded. Cultured embryos were then post-incubated *ex ovo* until embryonic day (ED) 8 (37,5°C; 80% r.h.) (Fig.1).

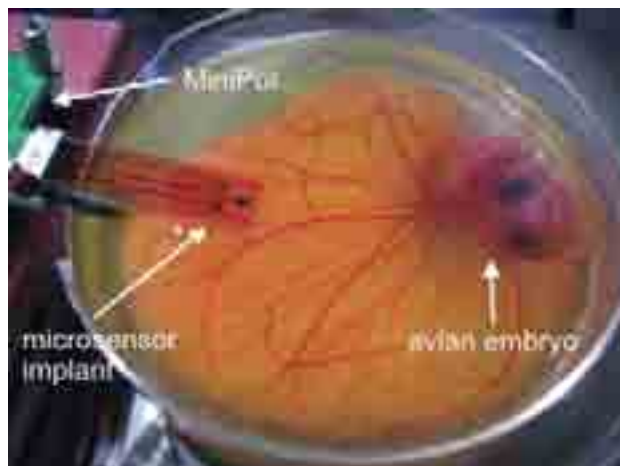


Fig. 1. *Ex ovo* cultured avian embryo with spread chorioallantoic membrane in contact with the MSA.

3 Results & Discussion

We determined the formation of immune responses from ED 8 to ED 17. Substrates (5mm x 5mm) cut from PET and Kapton® foils (materials used with the microsensor device) were prepared and sterilized with 70% ethanol. n=5 avian cultures were used for each day (ED) to implant both specimen materials. At ED 17 the CAM of all specimens was fixed with 4% PFA and explanted after 3 hours. We found that the capsule has auto-fluorescence capabilities due to PFA fixation. Hence, we could measure the average thickness of the encapsulation around the substrates (Fig. 2A & 2B). Additional histological data showed cell proliferation and collagen expression, confirming the capsule observed being due to a foreign body response. We found that after ED 13 the capsule formation significantly increases by 500% when compared to specimens implanted at ED 8 (Fig. 3). This indicates development of the immune system after ED 13.

The MSA obtained a pH of 8,3 and a dissolved oxygen level of 3,5 mg/l in contact with the CAM. Avian embryos develop in both alkaline (albumen) and acidic (yolk) environments caused by carbonic anhydrase processes [8]. Therefore the physiological pH of the embryo can differ from the pH of the culture environment. The optimal culture environment is considered at pH = 8,2 [8]. The dissolved oxygen level in developing organisms is extremely hypoxic and can therefore drop below 50% (< 4 mg/l) [9].

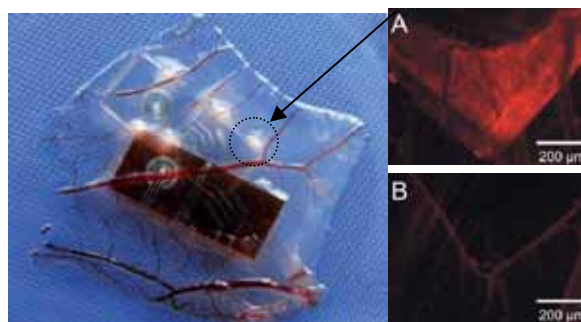


Fig. 2. Explant of the CAM fixed with 4% PFA at ED 17. PET and Kapton® implants exhibit surrounding white capsule formation (left). Autofluorescence of proteins in tissue capsule at the implant periphery implanted at ED 16 (A) and ED 9 (B), both explanted at ED 17.

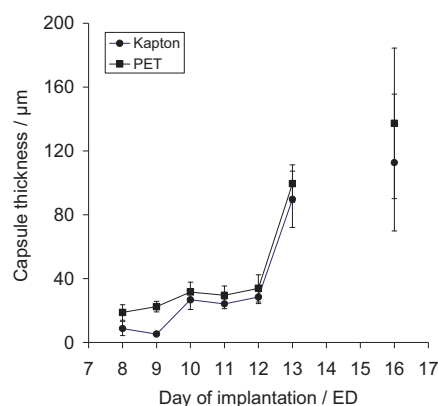


Fig. 3. Thickness of capsules formed around PET and Kapton® implants (n=5) as function of embryonic development.

4 Conclusion & Outlook

We evaluated the capability of avian *ex ovo* cultures to be used as an immune active model showing weak and high immune responses in the same organism depending on time of implantation. After a longterm continuous data acquisition at the implant/CAM interface, we attempt to correlate data obtained from the MSA with histological observations of immune responses.

References

1. Frost, M. and M.E. Meyerhoff, *Anal Chem*, 2006. **78**(21): p. 7370-7.
2. Vaddiraju, S., et al., *Biosensors and Bioelectronics*, 2010. **25**(7): p. 1553-1565.
3. Ratner, B.D., et al., *Biomaterial Science*, S.f. Biomaterials, Editor. 2004, Elsevier Academic Press.
4. Dreesmann, L., M. Ahlers, and B. Schlosshauer, *Biomaterials*, 2007. **28**(36): p. 5536-43.
5. Valdes, T.I., Klueh, U., Kreutzer, D., Moussy, F., *J Biomed Mater Res A*, 2003. **67**: p. 215 - 223.
6. Kubon, M., et al. in *Proceedings of 6. Deutsches BioSensor Symposium*. 2009, Freiburg.
7. Dohle, D.S., et al., *J Vis Exp*, 2009(33).
8. Reijrink, I.A.M., et al., *World's Poultry Science Journal*, 2008. **64**(04): p. 581-598.
9. Rowlett, K. and K. Simkiss, *J Exp Biol*, 1989. **143**(1): p. 529-536.

Electric Stimulation Of Explanted Retina Using A Subretinal Implant Chip In A Video Projector Setup

Andreas Padberg^{1,2*}, Steffen Kibbel³, Thoralf Herrmann¹, Ulrich Egert², Alfred Stett¹

1 NMI Natural and Medical Sciences Institute at the University of Tuebingen, Reutlingen, (Germany)

2 IMTEK, Biomicrotechnology, Albert-Ludwigs-Universität Freiburg, Freiburg, (Germany)

3 Retina Implant AG, Reutlingen, (Germany)

* Corresponding author. E-mail address: Andreas.Padberg@NMI.de

A light-sensitive stimulation chip from a subretinal implant system was used for electric stimulation of degenerated retinal tissue. The constructed setup mimics the clinical implant situation. Ganglion cell response upon stimulation was recorded. Results indicate functional lateral interactions within the degenerated retina.

1 Introduction

Retinitis pigmentosa (RP) leads to gradual degeneration of photoreceptor cells in human retina, ultimately causing blindness. Despite loss of photoreceptor- and horizontal cells, remaining bipolar and ganglion cell populations show little decay. The subretinal implant (Retina Implant AG) contains a light sensitive photodiode-array with corresponding stimulation electrodes. Subretinally implanted between pigment epithelia and neural retina, the implant resumes the function of photoreceptor cells by electrical stimulation of bipolar cells [1, 2]. Electric stimulation of bipolar cells causes correlated activity in ganglion cells, and evokes perception of phosphenes in humans with advanced RP. Patients with a subretinally implanted chip perceived phosphenes in an orderly fashion, reflecting shapes and sizes of objects in their environment, one patient even regained the ability of reading large letters [3].

We developed a setup for conducting electrophysiological research on underlying biological mechanisms (Fig.1). The retinal implant chips were used for continuous electrical stimulation of degenerated retinal tissue from an RP-model (RCS-Rat) with a fixed frequency of 5 Hz and pulse duration of 500 μ s.

2 Materials and Methods

Visual patterns are generated, using a PC and the psychologist toolbox for Matlab [4, 5]. Patterns are presented via a LCD-projector focused and coupled through a binocular. Focal planes of binocular and video projector are adjusted to match the chip's surface. The chip contains 40 x 40 pixels with a pitch of 70 μ m covering an area of 3 x 3 mm. Each pixel contains a micro-photodiode to detect light-intensity, a circuit to convert the detector signal into a stimulating voltage and a 50x50 μ m² TiN stimulation electrode. The sensitivity and gain of the chip can be adjusted. The chip is mounted on a carrier providing electric

connection, allowing application, perfusion and tempering of retinal tissue. Adjustment of the chip to illumination levels of patterns, frequency and pulse duration are set with the chip's stimulus generator.

Samples from explanted retinas are placed ganglion cell up on the chip surface (Fig. 2). For proper handling, the retina was mounted on a nitrocellulose filter with a punched opening with 2 mm diameter. Extracellular recording of ganglion cell activity is conducted with a needle electrode, mounted to a micromanipulator and lowered onto the ganglion cell layer under visual control. Signals are amplified and recorded, together with timestamps of chip's stimulation pulses, and timing of light stimulus on- and offset. Spike activity is extracted and correlated to the stimulus using Matlab.

3 Results

Ganglion cell activity from retina samples placed on a chip could be recorded for up to 7 hours. Visual patterns are converted to electric stimulation patterns via the chip. Cell activity can be modulated with different levels of brightness. Activity was correlated to temporal and spatial change of illumination only when the chip was activated (Fig. 3). Ganglion cells increased or decreased spiking activity upon electric stimulation. Response to both on- and offset of stimulus and on-/off- receptive field structures were observed (Fig. 4).

4 Discussion

Functionality of the setup for electric stimulation of degenerated retinal tissue with visual patterns was shown. Different types of response were recorded. Results indicate functional lateral interactions within the degenerated retina. The setup is advantageous for experiments with moving patterns. However, chip electrode spacing and binocular magnification limits spatial resolution. Further experiments will investigate functionality of remaining lateral amacrine network,

and pathways of synaptic transmission upon electric stimulation, with a pharmacological approach.

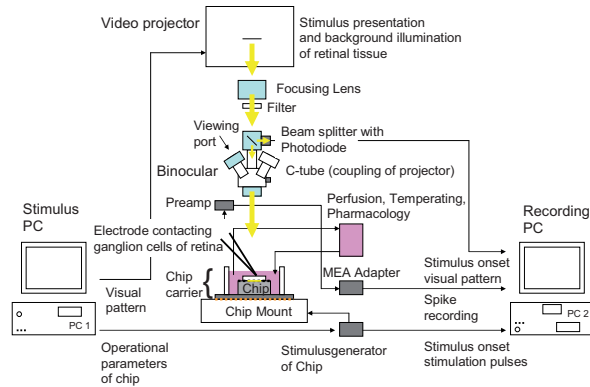


Fig. 1. Main components of the setup for stimulation of retinal samples attached to light-sensitive stimulation chip.

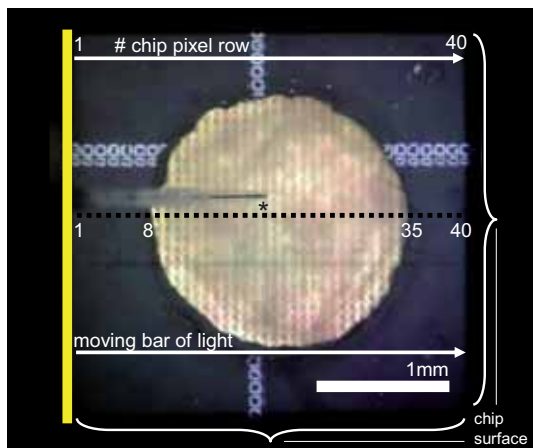


Fig. 2. Top view on chip with attached retina (see text). For experiments in Fig.4., a light bar presented on dark background moved with constant motion from left to right across all 40 chip pixel rows. * Position of needle electrode for spike recording.

Acknowledgement

This work was supported by the German Ministry for Education and Research (BMBF), grant 0315113 to Retina Implant AG.

References

- [1] Stett A., Mai A., Herrmann T. (2007). Retinal charge sensitivity and spatial discrimination obtainable by subretinal implants: key lessons learned from isolated chicken retina. *Journal of Neural Engineering* 4, S7-S16
- [2] Gerhardt M, Alderman J, Stett A. (2010). Electric field stimulation of bipolar cells in a degenerated retina - a theoretical study. *IEEE Trans Neural Syst Rehabil Eng.* 18(1):1-10.
- [3] Zrenner E, et al. (2009) Subretinal Microelectrode Arrays Allow Blind Retinitis Pigmentosa Patients to Recognize Letters and Combine them to Words. *Biomedical Engineering and Informatics* 2, 1-4.
- [4] Brainard, D. H. (1997) The Psychophysics Toolbox, *Spatial Vision* 10: 433-436.
- [5] Pelli, D. G. (1997) The VideoToolbox software for visual psychophysics: Transforming numbers into movies, *Spatial Vision* 10: 437-442.

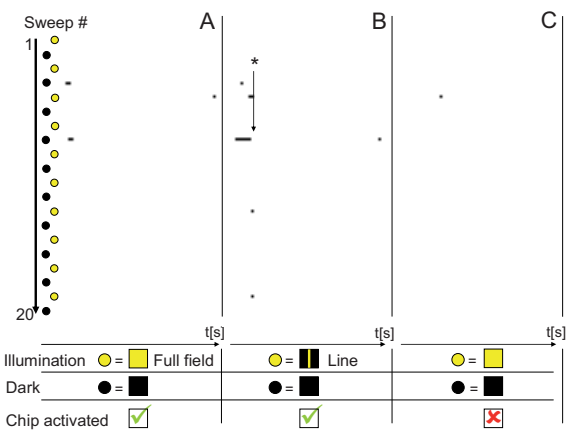


Fig. 3. Rasterplot of a ganglion cell's activity (on/off type). Two seconds of spike events are shown in each line. Light condition switched from dark to bright illumination every 5 seconds with 20 repetitions. **A)** Full field illumination: Transient increase of activity to stimulus offset. **B)** Stationary line illumination (70 μm bar of light at central position of chip): Additional, short and delayed increase of activity to stimulus onset. *Differences between A and B indicate retinal network activity. Additional response to stimulus onset in B might appear due to lacking inhibition from lateral areas, with less retinal surface being stimulated than in A. **C)** Control with deactivated chip.

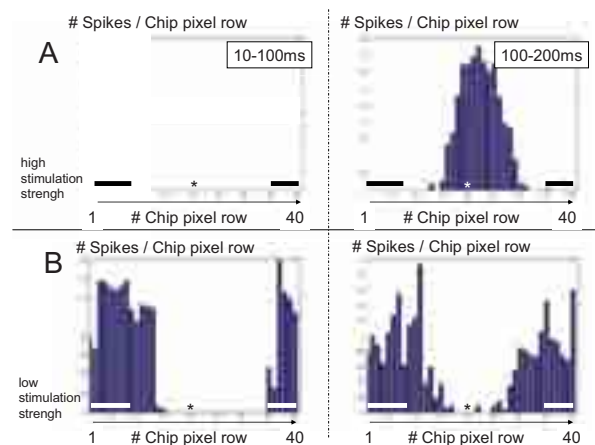


Fig. 4. Stimulation-strength-dependent on/off-response of a ganglion cell. A light bar moved from left to right across a retina attached on the chip (see Fig.2.). Bar velocity 250 $\mu\text{m}/\text{s}$, bar diameter 70 μm . Spike rates are calculated for the time windows 10-100 ms and 100-200 ms after the electric stimulation pulses. Spike rates are plotted against the position of the light bar on the chip, and averaged for 15 repetitions of bar movement across the chips surface. The histogram column for a chip pixel row shows the number of average spike events that occurred within the timeframe the light bar took to move across that row. Thus a map of the activity induced from each of the 40 chip electrode rows is generated, and displays the cells receptive field upon electric stimulation in direction of the x axis. **A)** High stimulation strength / On-component: Spontaneous activity is actively suppressed by charge that is delivered by chip under dark condition (dark background illumination). Increase of charge transfer as light bar enters area of exposed photodiodes elicits central on-response. **B)** Low stimulation strength / Off-component: Spontaneous activity is actively suppressed when the light bar enters receptive field area, but charge is insufficient to elicit on-response. Gap between black bars (A) and white bars (B) indicates area of exposed photodiodes. * Position of recording electrode.

Epiretinal stimulation of retina with CMOS Multi-Capacitor-Array

Max Eickenscheidt¹, Günther Zeck², Peter Fromherz^{1*}

¹ Max Planck Institute for Biochemistry, Department of Membrane and Neurophysics, Martinsried, Germany

² NMI Natural and Medical Science Institute, Reutlingen, Germany

* Corresponding author. E-mail address: fromherz@biochem.mpg.de

1 Methods

We studied the stimulation of adult rabbit retina in epiretinal configuration using a 20x20 multi-capacitor array. Each capacitor measures 50x50 μm with 1 μm spacing in between and insulated by a thin layer of TiO₂/ZrO₂ with a capacitance of 2.7 $\mu\text{F}/\text{cm}^2$. The stimulation device fabricated on the basis of CMOS technology allows addressing subsets of the array by an external voltage source. We applied falling voltage ramps with amplitude up to -1 V and duration of 0.05 – 10 ms. The capacitive current density ranged between 0.027 and 54 mA/cm^2 . This method of stimulation avoided a faradaic current and a perturbation of stimulation by electrochemical side effects.

2 Results

The electrical response of individual ganglion cells was recorded with a tungsten electrode. Single action potentials were elicited within the first millisecond after the onset of a stimulus. They are assigned to a direct stimulation of retinal ganglion cells. The threshold is described by a rheobase of 1.1 mA/cm^2 and a chronaxie of 0.7 ms. In addition, bursts of action potentials are observed 5-10 ms after the onset of the stimulus. The threshold of the late response is described by a rheobase of 0.2 mA/cm^2 and a chronaxie of 4.5 ms. These responses disappear when the glutamate receptors are blocked. They are attributed to a capacitive stimulation of the presynaptic ganglion cell circuitry. Early and late spikes have been measured in a previous study using metal electrode stimulation [1].

Using single stripes of the capacitor array we investigated the spatial sensitivity of the early and late response. The threshold of the early response depends strongly on the position and orientation of the capacitor strip. The lowest threshold was found about 100 μm from the cell soma. These observations indicate that the early spike is elicited in a high sensitive 'axon band' region of the retinal ganglion cell [2].

The late response could be elicited up to a distance of 400 μm around the ganglion cell soma. This is in agreement with stimulation of the presynaptic circuitry and thus of the cell's receptive field.

3 Conclusion

In summary we demonstrate capacitive stimulation of retinal neurons using low current densities. Appropriate parameter values allow for the stimulation of either the retinal ganglion cell alone, the presynaptic circuitry or of both.

References

- [1] Jensen RJ et al. (2005). Thresholds for activation of rabbit retinal ganglion cells with relatively large, extracellular microelectrodes. *IOVS. Vol 46 No. 4*
- [2] Fried S. et al. (2009). Axonal sodium-channel bands shape the response to electric stimulation in retinal ganglion cells. *J.Neurophysiol, 101, 1972-1987*

Tetanization Dynamics in Human Neuroblastoma Cultures

Ferrández J. M.^{1,2,*}, Lorente V.², Bongard M.^{1,3}, Díaz G.^{1,3}, de la Paz F.⁴, Fernández E.^{1,3}

1 Instituto de Bioingeniería, Universidad Miguel Hernández, Alicante

2 Dpto. Electrónica, Tecnología de Computadoras, Univ. Politécnica de Cartagena,

3 CIBER-BBN, Spain

4 Departamento de Inteligencia Artificial, UNED, Spain

* Corresponding author: jm.ferrandez@upct.es

The main objective of this work is to analyze the computing capabilities of human neuroblastoma cultured cells and to define stimulation patterns able to modulate the neural activity in response to external stimuli for controlling an autonomous robot. Multielectrode Arrays Setups have been designed for direct culturing neural cells over silicon or glass substrates, providing the capability to stimulate and record simultaneously populations of neural cells. This paper tries to modulate the natural physiologic responses of human neural cells by tetanic stimulation of the culture. We show that the large neuroblastoma networks developed in cultured MEAs are capable of learning: establishing numerous and dynamic connections, with modifiability induced by external stimuli.

1 Introduction

Learning is a natural process that needs the creation and modulation of sets of associations between stimuli and responses. Our learning experiments were performed in neural cultures containing 120.000 human neuroblastoma SY-5Y, under the assumption that this kind of cells are able to respond electrically to external stimuli and modulate their neural firing by changing the stimulation parameters.

This paper describes the process of growing human neuroblastoma cells over MEA substrates and tries to change the natural physiologic responses of these cells by external stimulation of the culture.

2 Methods

A human neuroblastoma SY5Y cell line, that express clonal specific human dopamine receptors, and also NMDA receptors, will be the biological platform for studying learning in cultured cells.

Neuroblastoma SH-SY5Y cells are known to be dopaminergic, acetylcholinergic, glutamatergic and adenosinergic, so in this line they respond to different neurotransmitters. Neuroblastoma culture cells show electrophysiological responses similar to standart neurons, as potential actions generation sensible to tetrodotoxin (TTX) and acetylcholin. They have neurotransmitters synthesis process and are able to neuritic growth in culture medium. (Figure 1).

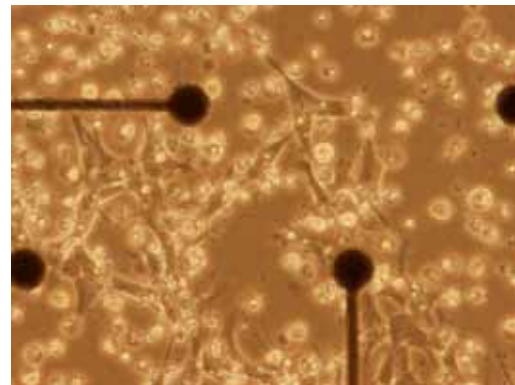


Fig. 1. Neuroblastoma cultures over MEA

3 Results

The electrophysiological properties of the neuroblastoma cultures were analyzed by recording the spontaneous activity of the network. Time course of experiments was over 15 days; recordings were done using two MCS-Meas with two neuroblastoma cell cultures (but only in one the cells survived till day 15). In vitro neuroblastoma networks show spontaneously firing. This firing rates change during the culture development with marked day differences and the global rate is closely related to the age of the network. The physiological recordings correspond to neuroblastoma cultures in the range of 1-7 div. They show bursting and spiking activity, with usually negative depolarisations. Figure 2 show the spiking activity of the neural population with an automatic detection level for each electrode.

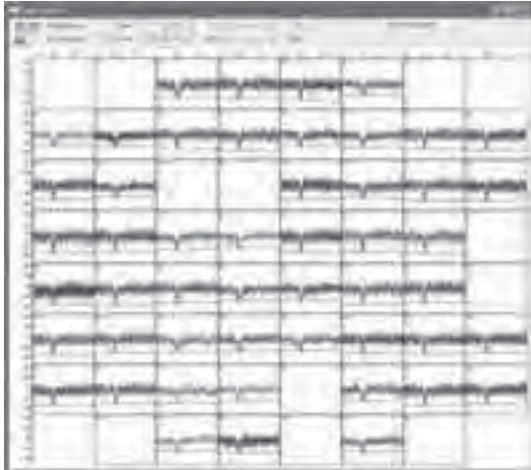


Fig. 2. Spontaneous neural activity detected by the multielectrode array

During the neuroblastoma development, a wide range of population bursting or synchronized activity has been observed, according to some studies in neural cultures preparations (Wagenaar, Pine, and Potter, 2006). The burst usually contains a large number of spikes at many channels, with variable duration, from milliseconds to seconds.

Tetanic Stimulation

Spontaneous activity was recorded for intervals of 3 minutes before stimulation (PRE-data), and the total number of spikes extracted was counted. The biphasic stimulus consists in a 10 trains of a 100 anodic-first waveform with 1 Volt amplitude delivered to all 60 electrodes in order to propagate a tetanization stimulus to the neuroblastoma culture. Once the tetanization stimulus was applied to the whole population 5 minutes after the stimulation a 3 minutes interval was recorded (POST-data). Only neuronal signals which had at least a 2:1 signal:noise ration were valued as "spikes". Again, the total number of spikes extracted was counted. This process was made for cultures at 1 day in vitro (div), 5 div and 16 div.

Figure 3 represents the counted spikes with bar charts for the different recordings. The conclusion from this Figure is:

- 1) While the neuroblastoma culture is growing new connections are created, and the number of spikes increases as the culture expands over the MEA.
- 2) After a tetanic stimulation the cells continue with their increased spiking rate, providing a persistent change in the culture behaviour.

In all the experimentation performed, tetanic stimulation got a potentiation effect on the spontaneous firing, modulating in this way the culture neural activity.

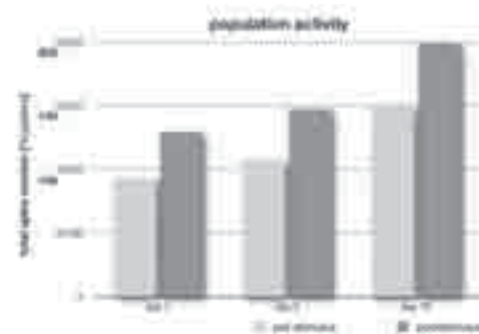


Fig 3: Induced neural activity by tetanization

4 Discussion

Tetanization consists in high-frequency stimulation to the culture, in order to cause an increase in transmitter release called post-tetanic potentiation. The results illustrate the existence of qualitatively different responses to stimulation. Our results indicate the existence of a clear facilitation mechanism in response to the tetanization stimuli at different stages of cell development. Since this kind of stimulation has been used in attempts to induce plasticity in neuroblastoma, refining some crucial aspects of the stimulation is still indispensable.

References

- [1] Bading H. and Greenberg M.E., 1991. "Stimulation of protein tyrosine phosphorylation by NMDA receptor activation", *Science*, 253, Issue 5022, pp. 912-914.
- [2] Wagenaar, D. A., Pine, J. and Potter, S. M., 2006. "An extremely rich repertoire of bursting patterns during the development of cortical cultures.", *BMC Neuro-science*, 7:11.
- [3] Antonov I., Antonova I., Kandel E.R., 2003. "Activity-Dependent Presynaptic Facilitation and Hebbian LTP Are Both Required and Interact during Classical Conditioning in Aplysia", *Neuron*, Volume 37(1), pp. 135-147.

A Closed-Loop System for Robotic Control using Human Neuroblastoma Cultures

Ferrández J. M.^{1,2,*}, Lorente V.², Bongard M.^{1,3}, Díaz G.^{1,3}, delaPaz F.⁴, Fernández E.^{1,3}

¹ Instituto de Bioingeniería, Universidad Miguel Hernández, Alicante

² Dpto. Electrónica, Tecnología de Computadoras, Univ. Politécnica de Cartagena,

³ CIBER-BBN, Spain

⁴ Departamento de Inteligencia Artificial, UNED, Spain

* Corresponding author: jm.ferrandez@upct.es

This paper introduces an open-source real-time system that controls remotely a robot using Human Neuroblastoma cultures and basic Braitenberg principles. Multielectrode Arrays Setups have been designed for direct culturing neural cells over silicon or glass substrates, providing the capability to stimulate and record simultaneously populations of neural cells. The main objective of this research is to modulate the natural physiologic responses of human neural cells by tetanic stimulation of the culture. If the system is able to modify the selective responses of some cells with an external pattern stimuli provided by a robot over different time scales, the neuroblastoma-cultured structure could be trained to process pre-programmed spatio-temporal patterns, controlling in this way the robotic behaviour.

1 Introduction

Using neural cultures as conventional computer elements is an emerging field that permits the hybridation between Neuroscience and Computer Science. This fascinating approach can provide a deeper understanding of natural processing and may be used for the design of new computing devices based on natural computational paradigms. A real biological neuroprocessor with millions of interconnections, would provide much more computational power instead of their low transition rates due to high number of computing elements and the extraordinary network capability of adaptation and reconfiguration to unknown environments.

Our learning experiments were performed in neural cultures containing 120.000 human neuroblastoma SY-5Y, under the assumption that this kind of cells are able to respond electrically to external stimuli and modulate their neural firing by changing the stimulation parameters. This paper introduces an open-source real-time system that controls remotely a robot using Human Neuroblastoma cultures and basic Braitenberg principles. The main objective of this work will be to control a robot using this biological neuroprocessor and a simple Braitenberg [2] learning scheme.

2 Methods

A human neuroblastoma SY5Y cell line, that express clonal specific human dopamine receptors, and also NMDA receptors, will be the biological platform for studying learning in cultured cells.

Neuroblastoma culture cells show electrophysiological responses similar to standard neurons, as potential actions generation sensible to tetrodotoxin (TTX) and acetylcholin. They have neurotransmitters synthesis process and are able to neuritic growth in culture medium. Human neuroblastoma cultures were produced using the commercial line SH/SY5Y. Cell culture of SH SY5Y was grown in DMEM (Gibco) completed with 10% of fetal bovine serum at 37 oC in 5% CO₂ and humidify atmosphere. On each MEA 100 000 cell/ml where placed in a volume of 2 ml and maintained on the mentioned conditions until experimentation on different days in vitro (div). They begin to diferenciate as neural units at day two.

The neuro-physiology setup provides a complete solution for stimulation, heating, recording, and data acquisition from 64 channels.

The basic components of the proposed system are shown in Figure 1.



Figure 1: Experimental Setup

Culture Data Acquisition Systems

Recording from large numbers of electrodes has become increasingly common in neuroscience over the last 30 years. For electrophysiological data

acquisition and analysis there exist several tools available, but two of them are more frequently used: MC_RACK (MultiChannel Systems, Reutlingen, Germany) and MEABENCH (Daniel Wagenaar, California Institute of Technology). MEABENCH is a free, open-source, set of programs designed primarily for Linux for multi-electrode data acquisition (DAQ) and online analysis [3]. MEABENCH directly communicates with DAQ hardware as well as providing real-time visualization. Thanks to its ability to communicate in real-time with stimulator hardware it can be used in closed-loop stimulation experiments.

Robotic Control

For controlling the direction of the robot we propose to compute the vector resulting from neural activity recorded in the human neuroblastoma culture. This vector will be provided to the robot in order to guide his movement. The sensors will detect the obstacles, and the information will be passed to the computer in order to induce a selective tetanization of the biological neural network for changing the resulting direction vector. When the robot detects an obstacle in his *left* path, a stimulation signal will be sent to the system for tetanizing the *right* tissue. By tetanization the electrodes of the right part of the array, an increase in the firing rate of the neural cells that lie in the part of the culture will be achieved, and the direction vector will point to the right in this particular case. We expect to apply some basic Braitenberg principles to the system in order to study the biological neural network behaviour induced by a tetanization-learning scheme.

Robotic Control System

We have developed a system that provides a complete robotic control platform over neuroblastoma cultures. The system includes five free, open-source, console-based programs written in C/C++ for real-time robotic applications with embodied cultures. All of this software has been developed for the Linux Operating System and MCS hardware (MultiChannel Systems, Reutlingen, Germany). Using this software in conjunction with MEABENCH is specially intended for close-loop experiments.

The software developed consists of the following programs:

- *Cult2Robot*: The main program. It has been developed as a MEABENCH module, so it can read spikes information from MEABENCH spike detector and compute a direction vector based on MEA neural activity. The direction vector is calculated based on the number of spikes per electrode in t seconds and it can be weighted by the height and width of the spikes. This direction

vector could be sent to a robot to control its movement.

- *Stg_control*: This program controls a general-purpose stimulus generator for current and voltage-driven electrical stimulation, STG 1000 series (MultiChannel Systems, Reutlingen, Germany).
- *Electrode_select*: This module allows configuring the MEA1060BC amplifier following the MEA protocol from MCS [4].
- *BT_server*: Non-blocking Bluetooth server that uses RFCOMM protocol to receive characters from a specific MAC, process the information and do some action, e.g. it can be used to call another program when an obstacle is detected (An 'O' has been received).
- *BT_client*: Sends ASCII characters via Bluetooth using RFCOMM protocol. In our research *BT_client* sends the direction vector calculated by *Cult2Robot* to change the movement of the robot.

3 Results

The system has been validated using a MCS Signal Generator in the MEA1060BC preamplifier and neuroblastoma cultures. *Cult2robot* has been tested with some different cultures showing that it can get a vector direction successfully. *Electrode_select* and *Stg_control* have been monitored using MEABENCH data acquisition system. Bluetooth client and server have been used with a humanoid robot (Robonova, Hitec Robotics) to send and receive information about obstacles.

4 Conclusion

Learning in cultured neuroblastoma networks by a stimulation process controlled by robot sensors requires identifying the correct stimuli to provide to the neurons maintained *ex vivo*. These neuroblastoma networks form a large culture covering the whole electrode array and generating a rich dendritic configuration. It is needed an open neural acquisition and stimulation system that responds in real time to the information provided by the robot sensors controlling its behaviour. At the moment, we are developing a GUI program for doing *remote close-loop* experiments that involves data acquisition, stimulation and robot controls. Also, some new utilities are being designed to add more features to this set of software, such as different learning procedures.

References

- [1] Anderson J.A., and Rosenfeld E.. "Neurocomputing: Foundations of research", MIT Press Cambridge, MA, USA, 1998.
- [2] Braitenberg, V. Vehicles: Experiments in synthetic psychology. Cambridge, MA: MIT Press, 1984.

Chronic Network Stimulation Enhances Evoked Action Potentials

A. N. Ide¹, A. Andruska¹, M. Boehler¹, B. C. Wheeler³, G. J. Brewer^{1,2*}

¹ Department of Medical Microbiology, Immunology and Cell Biology, Southern Illinois University, School of Medicine, Springfield, IL 62794-9626, USA.

² Department of Neurology, Pharmacology, Southern Illinois University, School of Medicine, Springfield, IL 62794-9626, USA.

³ J. Crayton Pruitt Family Department of Biomedical Engineering, University of Florida, Gainesville, FL 32611-6131, USA.

* Corresponding author. E-mail address: gbrewer@siumed.edu

Neurons cultured on multielectrode arrays almost always lack external stimulation except during the acute experimental phase. We have investigated the effects of chronic stimulation during the course of development in cultured hippocampal neural networks by applying paired pulses at half of the electrodes for 0, 1, or 3 hr/day for 8 days. Spike latencies increased from 4 to 16 ms as the distance from the stimulus increased 200-1700 μm , suggesting an average of 4 synapses over this distance. Compared to no chronic stimulation, our results indicate that, chronic stimulation increased evoked spike counts per stimulus by 50% at recording sites near the stimulating electrode and increased the instantaneous firing rate. On trials where both pulses elicited responses, spike count was 40-80% higher than when only one of the pulses elicited a response. In attempts to identify spike amplitude plasticity, we found mainly amplitude variation with different latencies suggesting recordings from neurons with different identities. These data suggest plastic network changes induced by chronic stimulation that enhance the reliability of information transmission and the efficiency of multisynaptic network communication

1 Introduction

We chronically stimulated arrays for 0, 1 and 3 hr/day, during 8 days before the recording day in order to investigate the long-term effects that external inputs can provide to the network compared to the standard unstimulated condition. In order to increase the probability of excitation without overstimulation, we applied a paired-pulse stimulation paradigm. We determine whether this stimulus paradigm has an additional effect on action potential amplitude as it has been demonstrated for tetanic stimulation. We were also interested in the larger effect on the network to determine how chronic stimulation affected network elements at a distance. For this reason, we stimulated only half of the array to be able to detect responses as an explicit effect of distance from the stimulation site. We have extended Potter's concept of acute stimulation of the network on one day (Bakkum et al 2008) to 8 days to determine longer term effects of chronic stimulation on the efficiency of communication in the network.

2 Methods

E18 rat hippocampal neurons were plated at 500 live cells/ mm^2 on poly-D-lysine coated MEA's in NbActiv4TM medium (BrainBits, Springfield, IL). Stimulation trains included two groups of 30 μA constant current paired-pulses (biphasic, 100 μs /phase duration beginning positive; 50 ms ISI between individual stimuli). An automatic stimulation program was created to stimulate the entire top half (30 electrodes) of the MEA in a pseudorandom sequence. The bottom half of the array was never stimulated to

serve as a within-array control for recording sites more than 400 μm from a stimulating electrode. Arrays were chronically stimulated for 1 (n=8) and 3 (n=12) hour(s)/day at 7, 11, 12, 14, 18, 19, and 21 days in vitro (DIV). Thus, each of 30 electrodes received 0, 2100 or 6300 stimuli/day x 8 days. Since stimulation began at 7 days in culture, before much activity, sites were stimulated without regard to active or non-active electrodes.

3 Results

Effects of chronic stimulation and distance from stimulus on active channels.

An average of 2.7 channels per stimulus was activated for each distance (200-1721 μm), which suggests that 16 channels on average were activated every time a stimulus was delivered, averaged over all chronic stimulation conditions. Based on all arrays tested, the fraction of channels recording any evoked activity during the entire probe recording (~17 min) was 45-50% with no significant increase due to chronic stimulation. In contrast, this response rate was two-fold higher than spontaneous activity without chronic stimulation and 30% higher than spontaneous activity with chronic stimulation (Brewer et al 2009). The percent active electrodes could surely be increased by increasing the density of plated neurons or by addition of extra astroglia (Boehler et al 2007).

Effects of chronic stimulation and distance from stimulus on evoked activity.

We first determined how the Euclidian distance from a recording to a stimulating electrode affects the

probability of a response to the stimulus. Note that the distances between closest, diagonally adjacent and most widely separated pairs of electrodes are 200 μm , 283 μm and 1721 μm , respectively. Chronic stimulation (1 or 3 h) led to higher response rates (50% or 35% versus no chronic stimulation) at recording electrodes near the probe electrode (283 μm away). Response rates decreased threefold and monotonically with distance to the furthest electrode. Electrodes in close proximity to the stimulus (283 μm) recorded threefold more spike responses than the ones at the longest distance (1721 μm). During 1 h/day chronic stimulation, the number of spikes per stimulus, for all distances, was 10–15% higher than with no chronic stimulation, with the values for 3 h/day stimulation falling in between. The results show both enhancements due to chronic stimulation and connectivity that decline with distance.

Effects of chronic stimulation and distance from stimulus on first spike latency.

Near the stimulating electrode, it is common to record spikes at short latency and uniform amplitude, suggesting reliable, direct or at most monosynaptic excitation of the same neuron. In contrast, at maximal distance, shows a variety of spike latencies and amplitudes, suggesting activation of different paths and recorded neurons. The coefficient of variation of the latency (mean/SD) increases with distance (from 0.8 to 1.6), largely independent of time of chronic stimulation, indicating greater dispersion with distance from the stimulus site. The latencies variation suggest near linear propagation with distance, equivalent to a speed of 0.1 mm ms^{-1} . If one extrapolates to zero distance, the latency is 1.2 ms, which may be the time to activation of a directly stimulated neuron. Alternatively, the graph appears to asymptote at 4 ms, the same as might be inferred as the time to activation of a directly responding neuron (Bakkum et al 2008). Therefore, at maximum distance of 1721 μm , an average delay of 16 ms suggests either three or four synapses.

Effects of chronic stimulation and distance from stimulus on spike amplitude evoked by the second pulse.

Even if extracellular recordings are not the best choice to assess changes in amplitude, we examined evidence for spike amplitude plasticity because the developmental accumulation of sodium channels at the axon initial segment might be influenced by chronic stimulation. We also know that our recordings come from multiple neurons, so any change in amplitude could be from neurons with different identities. Spike sorting was considered problematic due to the huge variety of spike shapes observed in our cultures, especially for overlapping waveforms during bursts, as pointed out also by others (Eytan and

Marom 2006, Rolston et al 2007, Chiappalone et al 2008). To test for spike amplitude plasticity caused by paired pulse or chronic stimulation, we compared first spike latency and amplitude responses from the first to those from the second pulse. We found no differences in the probability of the number of responses or spike latency. However, a remarkable fourfold increase in the evoked spike amplitude of the second pulse minus that evoked by the first pulse. Several possible mechanisms could explain the enhancement in spike amplitude by the 2nd pulse: a) spillover of a burst elicited by the 1st pulse into the recorded response to the 2nd stimulus; b) different neurons being recruited each time; c) compound action potentials; or d) spike amplitude plasticity.

Pulse order effects on evoked spikes.

We found no difference in the number of responses evoked by the 1st or 2nd pulses. However, there were notable differences in the statistics for records in which there were evoked responses to both pulses (50%) or to only one of the pulses (50%). When both pulses were effective, more spikes were elicited (2.5 spikes/stimulus) than when only one of the pulses elicited spikes (1.5 spikes/stimulus). The 3 hr/day chronic stimulation further increased these rates. In addition, spike amplitudes were 40–80% higher for responses to both pulses of the paired stimulus compared to responses to only one of the stimuli.

4 Conclusions

In conclusion, paired-pulse chronic stimulation of hippocampal networks cultured on MEAs results in an enhancement of the probability of evoked spikes at short distances and a higher spike rate for 3 h/day chronic stimulation for the entire network. Apparent increases in spike amplitudes could be accounted for by incommensurate neuron identities, overlapping spikes and burst activity. Burst activity is of higher amplitude than isolated spikes and is associated with higher response probabilities to both pulses in the paired stimulus. These data suggest plastic network changes induced by chronic stimulation that enhance the reliability of information transmission and the efficiency of multisynaptic network communication.

Acknowledgement.

This work was supported in part by NIH NS052233 from the National Institute of Neurological Sciences. The authors would like to thank Professor S Martinoia's Lab for providing the spike detection algorithm, R Pearson for the pseudo-random stimulus pattern design and D Khatami for the looping stimulus program on multiple electrodes.

Published Reference.

- [1] Ide AN, Andruska A, Boehler M, Wheeler BC and Brewer GJ. 2010. Chronic network stimulation enhances evoked action potentials. *J Neural Eng* 7(1):16008.

Highly Stretchable PDMS-Based Multi-Electrode Array For Epidural Electrical Stimulation To Regain Motor Function After Spinal Cord Injury

Alexandre Larmagnac^{1, 2*}, Pavel Musienko², Janos Vörös¹, Grégoire Courtine²

¹ Laboratory of Biosensors and Bioelectronics, ETH Zurich, Switzerland

² Experimental Neurorehabilitation Laboratory, Department of Neurology, University of Zurich, Switzerland

*Corresponding author. E-mail address: larmagnac@biomed.ee.ethz.ch

We present a skin-like multi-electrode array for in-vivo epidural electrical stimulation of the spinal cord. This is the first reported implantable electrode array using conductive PDMS as a material for stretchable conductive leads. This all-elastomeric technology provides high flexibility and stretchability to the implant thus making it possible to fix it as a second skin on the spinal cord. We also report preliminary results of the clinical studies.

1 Background

Traumatic injuries of the spinal cord have long-term health, economic and social consequences, giving a sense of the urgency to the development of ways to treat them. Worldwide, an estimated 2.5 million people live with a chronic spinal cord injury (SCI). Individuals who remain permanently paralyzed after a SCI represent 50% of the total human disabled population. Consequently, there is a critical need to improve rehabilitative strategies to help these patients to regain the ability to stand or step. We recently demonstrated the impressive capacity of pharmacological and electrical spinal cord stimulations to promote full weight bearing walking in paralyzed rats when combined with rehabilitation [1]. Specifically, we showed that epidural electrical stimulation (EES) applied at S1, L4, or L2 spinal segments could each promote unique patterns of locomotion, which were biased toward flexion when stimulating upper lumbar segments and toward extension when stimulating the sacral level. Next, we revealed that the combination of two, and even more efficiently three, sites of EES promoted clear synergistic facilitation of stepping in paralyzed rats [2]. Together, these results suggest that multi-site EES strategies would enable a finer control of locomotion after a SCI than currently possible with existing stimulation paradigms. However, no systematic studies on the potential benefit of multi-site EES have been conducted so far, largely because of the lack of interfaces for simultaneously delivering stimulation at multiple spinal cord locations. Here, we present a novel neuroprosthetic multi-electrode array (MEA) for multi-site EES *in vivo*.

2 Methods

Our MEAs have been designed to meet the following requirements: i) stable implantation over the dura for extended periods of time, ii) high flexibility, i.e. act as a second skin that bends with the spinal cord, iii) impermeability to body fluids to prevent short-circuits due to water absorption, iv) biocompatibility, v) capacity to deliver sufficient electrical charges to recruit neural structures while avoiding tissue damage, and vi) high spatial selectivity without overlapping stimulating fields.

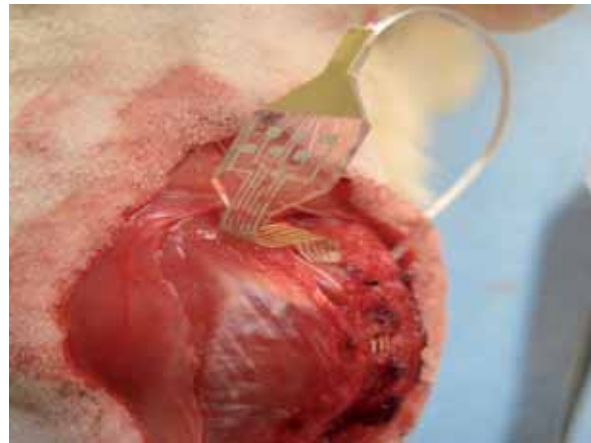


Fig. 1. Picture of our first flexible MEA with 6 electrodes during implantation in rats. The square-shaped contact pads are visible on the left and connected to the electrodes via conductive PDMS tracks that provide greater stretchability than sputtered gold tracks.

3 Results

Our first MEA prototype shows adequate stretchability, conductivity and biocompatibility (Figure 1). The monolithic PDMS structure contains conductive PDMS tracks, gold electrodes and contact pads connected to a head connector via a micro ribbon cable. The elastic properties of conductive silver-

PDMS promote stretchability to the implant. Such MEAs can be deformed to high strain while maintaining electrical conductivity. Preliminary testing in rats with chronically implanted MEA over lumbosacral segments showed no sign of inflammation and preserved implant integrity 2 weeks after surgery. As early as 1 week after a complete spinal cord transection, EES applied at the various electrodes of the MEA could encourage continuous locomotion on the treadmill. The materials do not adversely affect the integrity of tissue culture. Recently, we found how to parameter pulsed currents in order to avoid tissue damage *in vitro* [3].

4 Conclusion

Using this expertise and our first MEA, we will investigate the potential of multi-site EES to encourage weight bearing locomotion in paralyzed spinal rats, and to improve the functional outcomes of neurorehabilitative locomotor training.

Acknowledgement

We thank the ETH Zurich and the European Union for funding.

References

- [1] Courtine et al. (2009). Transformation of nonfunctional spinal circuits into functional states after the loss of brain input. *Nature Neuroscience*, 12, 10, 1333-U167.
- [2] Musienko et al. (2009). Combinatory Electrical and Pharmacological Neuroprosthetic Interfaces to Regain Motor Function After Spinal Cord Injury. *IEEE Transactions on Biomedical Engineering*, 56, 11, 2707-2711.
- [3] Gabi et al. (2009). Influence of applied currents on the viability of cells close to microelectrodes. *Integrative Biology*, 1, 1, 108-115.

Neuro-Robot Vitroid, with simple coupling approach.

Suguru N. Kudoh^{1*}, Naohiko Fujiwara¹, Hidekatsu Ito¹, Minori Tokuda and Ai Kiyohara¹

¹ Department of Human System Interaction, School of Science and Technology, Kwansai Gakuin University, Sanda, Hyogo, Japan

* Corresponding author. E-mail address: snkudoh@kwansai.ac.jp

Autonomous activity is observed in dissociated hippocampal neurons on multielectrode array (MEA) dish. Interaction between neuronal circuit and outer objects gives meanings to the pattern of autonomous electrical activity in the circuits. Our purpose of making the neuro-robot "Vitroid" is to make a model system for the network activity with I/O interaction with outer world. For this purpose, the simple coupling between neuronal circuit and robot body is suitable and we succeeded in the making robot behavior of the collision avoidance by template-matching algorithm. In addition, we propose the auto-tuning type of Vitroid, utilizing the dynamics of the living neuronal network.

1 Introduction

For elucidation of the mechanism of information processing of organism, it is important that analyzing dynamics of cultured simple neuronal networks. We cultured rat hippocampal neurons on a multielectrode array (MEA) dish which allow us to make electrical stimuli and recordings to/from the neuronal network, which formed on the dish [1,2]. Interaction between neuronal circuit and outer objects gives meanings to the pattern of autonomous electrical activity in the circuits. I/O system of the neuronal circuit is critical in the view point [3,4]. In previous study, we developed the "Vitroid" neuro-robot system in which the neurons were connected to a robot body and interacted with outer world. Our purpose of making the neuro-robot Vitroid is to make a model system for investigation of the effects of interaction between the neuronal circuit and outer environment on the network activity. For this purpose, the simple coupling between neuronal circuit and robot body is suitable, because it makes analysis of the network activity modified by the coupling between neuronal circuit and embodiment. We tried such simple couplings and succeeded in the making robot behavior of the collision avoidance. The autonomous activity in LNN is not completely random but has some periodicity, and these features were fundamental property of information processing. In this study, we analyzed the temporal structure of spontaneous and evoked network activity, and discussed about the overview of stability of the network. In addition, we propose the neuro-robot system, which utilize the dynamics of the living neuronal network.

2 Vitroid with simple coupling

2.1 Rat hippocampal dissociated culture

The brain of Vitroid is LNN, consists of rat hippocampal neurons (Fig.1). The hippocampal region

was cut off from E18 embryo of Wistar rats, and neurons were cultured on the MEA dish, coated with 0.02% polyethylene imine. The cloning ring, which the inner diameter is 7 mm was put on the center of a culture dish. The dissociated cells were plated inside the ring. In this case, the cell density was 7800 cells/mm². Culture medium was DMEM-F12 containing 5% horse serum, 5% fetal bovine serum, 100U/100 μ g/ml Penicillin-Streptomycin, and 0.2% insulin.



Fig. 1. Living Neuronal Network (LNN). Rat hippocampal neurons (E18D13)

2.2 Robot body and coupling methods

The embodiment of the neuronal circuit was implemented by the robot body constructed by MindStorm NXT kit (Fig.2). The robot equipped with infra-red (IR) sensors and can detect the obstacles. Stimulating electrodes were selected according to the location of the obstacles. Certain spatiotemporal patterns of activity evoked by the selected electrodes was stored as templates. After the making of templates, correlation coefficients between templates and spatio-temporal pattern of the activity were calculated. Motor speeds of the robot were determined as multiple of the correlation coefficients. This simple coupling between the neuronal activity and motor

speed was enough to succeed in the avoidance of collision.



Fig. 2. Robot body constructed by Mind storm NXT kit.

Even though there were only small differences between the evoked activity patterns according to the different sensor value, the probability of which system selected a correct template was higher than the probability of the wrong selection (Fig.3). The activity pattern of the neuronal circuit was stable during the test run for 1 hours.

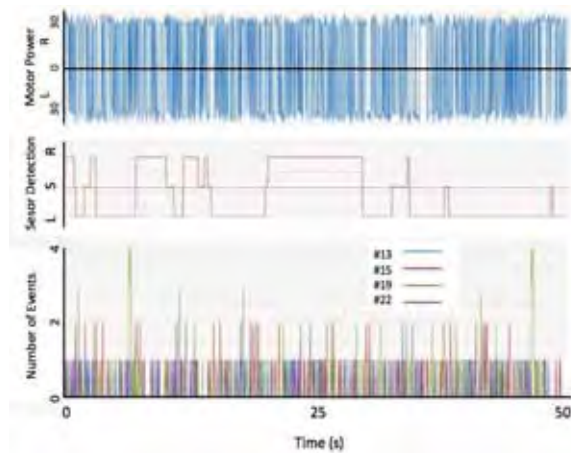


Fig. 3. Template selection and activity pattern of representative 4 neurons during test run.

2.3 The self-tuning type of Neuro-Robot

In this Vitroid system, LNN itself "does not know" the suitable responses to inputs, previously. In this self-tuning type of neuro-robot system, instead of giving an explicit teacher signal, a teacher signal is expressed by the relationship between sensors and motors, and it is embedded into "embodiment" of the robot (Fig. 4). Node of a neuron layer of the Artificial Neural Network (ANN) has inputs from a neural network. At the beginning, each node of an output layer and a neuron layer is all connected equally, a specific combination is selectively reinforced with the weight of the combination being tuned by the Hebbian rule. After this learning of ANN, when connections between an output layer and sensors are intercepted and the system is switched so that an output layer may be activated only by the input from a neuron layer, the behavior of robot will be determined depending only

on activity of a neural network, independently the direct inputs from sensor inputs.

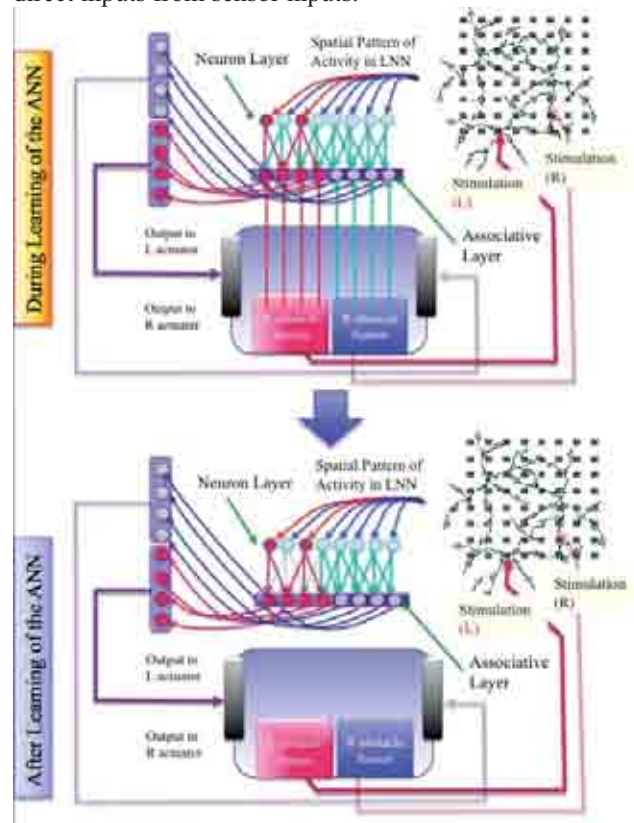


Fig. 4. The self-tuning type of Neuro-Robot

3 Conclusion/Summary

We composed the neuro-robot with simple coupling between motors and the activity of the neuronal circuit and the robot succeeded in collision avoidance.

Acknowledgement

This research is supported by the Ministry of Education, Culture, Sports, Science, and Technology of Japan under Grant-in-Aid for Scientific Research 19200018..

References

- [1] Gross G.W., Rieske E., Kreutzberg G.W. and Meyer A. :A new fixed-array multimicroelectrode system designed for long-term recording of long-term recording. *Neurosci Lett*, Vol.6, pp.101–105, 1977.
- [2] Pine J.: Recording action potentials from cultured neurons with extracellular microcircuit electrodes. *J Neurosci Methods*, Vol. 2, pp. 19–31, 1980.
- [3] Bakkum D.J., Shkolnik A.C., Ben-Ary G., Gamblen P., De-Marse T.B. and Potter S.M. (2004) : Removing some 'A' from AI: Embodied Cultured Networks. In *Embodied Artificial Intelligence*. Edited by Iida F., Pfeifer R., Steels L. and Kuniyoshi, Y. New York, Springer. 3139 , 130–145
- [4] Suguru N. Kudoh, Minori Tokuda, Ai Kiyohara, Chie Hosokawa Takahisa Taguchi and Isao Hayashi: Vitroid - the robot system with an interface between a living neuronal network and outer world, *International Journal of Mechatronics and Manufacturing Systems (IJMMS)*, in press, 2010.

Signal Analysis, Statistics and Software

Modeling of extracellular potentials recorded with multicontact microelectrodes

Gaute T. Einevoll

Norwegian University of Life Sciences, 1432 Aas, Norway
E-mail address: gaute.einevoll@umb.no, web: <http://compneuro.umb.no/>

Keynote Lecture

Large-scale extracellular electrical recordings using various types of multicontact microelectrodes have become a common tool for investigating neural activity at the population level. Here we present results from several projects in our group aimed at elucidating the link between recorded extracellular potentials and the underlying neural activity. We further present several new methods for analysis of such multielectrode data including the *inverse current source-density (iCSD)* method and *laminar population analysis (LPA)*.

1 Introduction

Mathematical modeling relies on experimental data to make progress, both to constrain and to test the models. For neural network models the dominant experimental method *in vivo* has so far been single-unit extracellular recordings: when a sharp electrode is placed sufficiently close to the soma of a particular neuron, the recorded potential reliably measures the firing of individual action potentials in this neuron. This information is contained in the high-frequency part of the recorded potentials. The low-frequency part, that is, the local field potentials (LFP), has proved much more difficult to interpret and has typically been discarded.

Other experimental methods, particularly methods that measure population-level activity *in vivo*, are needed to facilitate development of biologically relevant cortical network models, cf. Fig. 1. Large-scale electrical recordings using various types of multielectrodes, i.e., electrodes with many closely spaced contacts, are one such option. As techniques for such recordings are rapidly improving, there is a need for new methods for extraction of relevant information from such data. Several projects in our group have been aimed at elucidating this link between recorded extracellular potentials and the underlying neural activity. Some of them are briefly outlined here.

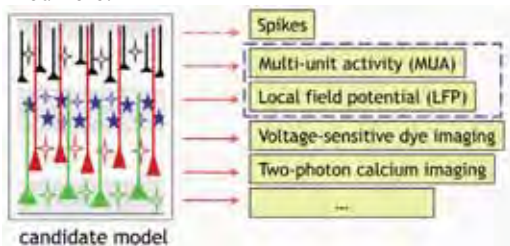


Fig. 1. Illustration of the concept of multimodal modelling: predictions from a candidate model should be tested against several types of measurement modalities. Here we focus on the link between neural activity and extracellularly recorded potentials, both the high-frequency (MUA) and the low-frequency parts (LFP).

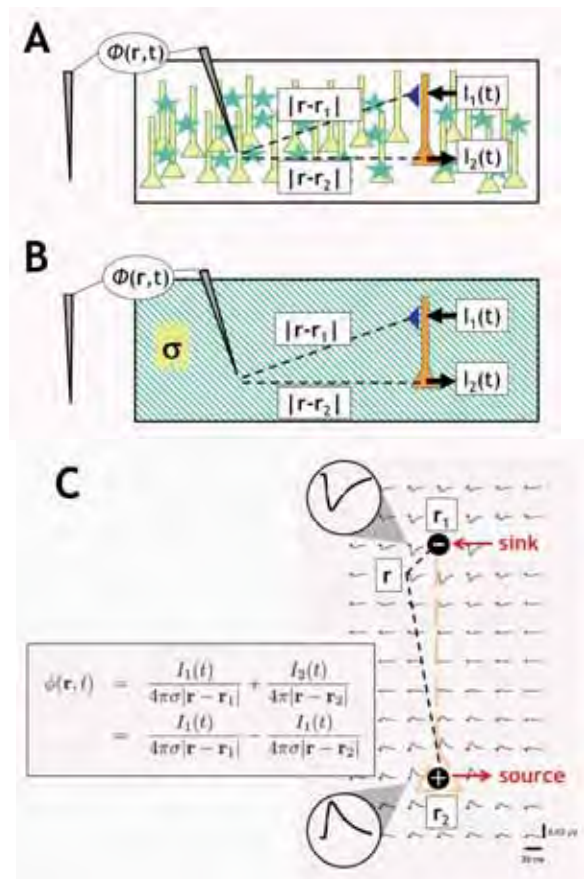


Fig. 2. Illustration of forward-modeling scheme for the simple situation with a current dipole stemming from excitatory synaptic activation of a single neuron at an apical synapse (dark triangle in A). The synaptic transmembrane current ($I_1(t)$) at the position r_1 corresponds to a “sink”. The equally sized return current ($I_2(t) = -I_1(t)$), corresponding to a “source”, is here for simplicity assumed to go through the soma membrane positioned at r_2 . In the forward-modeling scheme the electrical properties of the extracellular medium is represented by the *electrical conductivity* σ (panel B), and the extracellular potential at a position r is given by the simple formula shown in panel C. Panel C further illustrates the extracellular potential generated by such a sink-source pair at various spatial positions following an example activation of an excitatory synapse.

2 Modeling of extracellular potentials

Extracellular potentials in the brain are in general due to complicated weighted sums of contributions from transmembrane currents, and the potentials can be calculated by a combination of compartmental modeling providing the transmembrane currents following neural activity and electrostatic forward modeling using the quasistatic version of Maxwell's equations [1-5]. In Fig. 2 this forward-modeling scheme is illustrated for the simplest possible situation giving a non-zero extracellular potential: If, say, a pyramidal neuron receives synaptic input current through an apical synapse and all current is assumed to leave the neuron through the soma, one is left with a neuronal sink-source pair. From charge conservation it follows that all current that enters a neuron, must leave it as well, so the sink and source currents must have equal magnitudes at all times. Together they constitute a *current dipole*. In general, the return currents following activation of a single synapse will be more spatially distributed. However, the scheme generalizes straightforwardly to the case of a multicompartment neuron, cf. Fig. 3, or a population of such neurons [3].

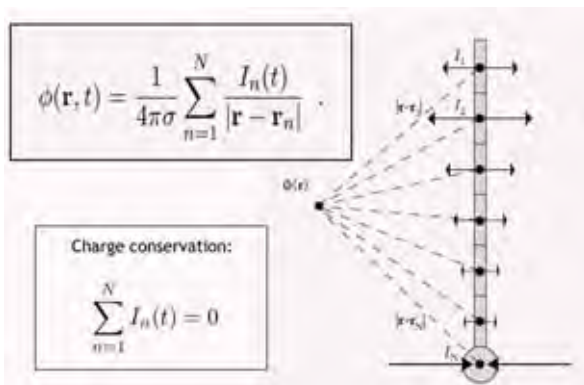


Fig. 3. Illustration of forward modelling scheme for a multicompartment neuron with N compartments. In our projects we have used the simulation tool Neuron (<http://www.neuron.yale.edu/>) to calculate the transmembrane currents $I_n(t)$ and then evaluated the formula for the extracellular potential in MATLAB or Python (<http://www.python.org/>).

3 Extracellular signatures of neural activity

In Fig. 4 we show as a first modeling example the calculated extracellular signature of an action potential. We observe that both the magnitude and shape of the extracellular spike vary strongly with position (note the varying scales used for positions close to and far away from the soma). For example, at the position of the illustrated sharp electrode, 100 μm left from the soma center, a characteristic waveform with a sharp downward “sodium peak” followed by a slower upward “potassium peak” would be recorded. Far above the soma an opposite waveform would be

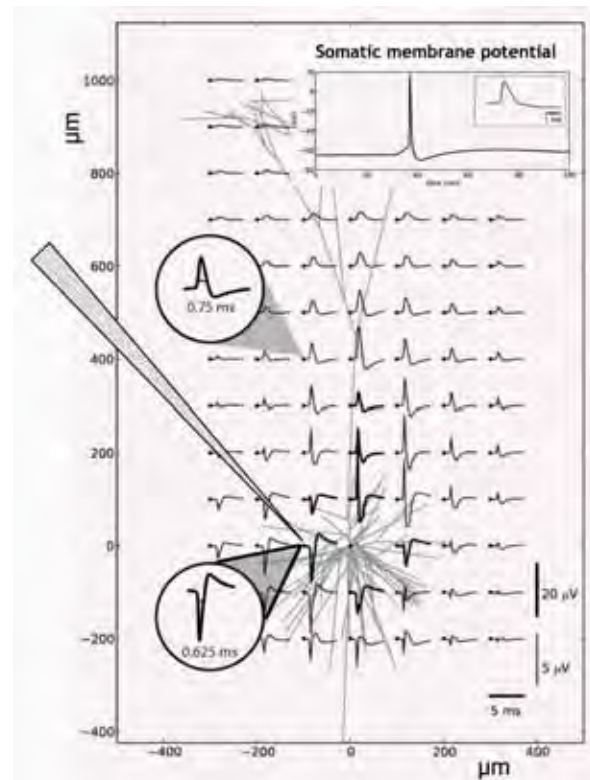


Fig. 4. Example of calculated extracellular signature of an action potential generated by a layer-5 pyramidal neuron. Traces show extracellular potentials in 5 ms windows around the time of spiking at various positions in the vicinity of the neuron. Upper inset shows corresponding intracellular action potential recorded in the soma. Extracellular conductivity σ has been set to 0.3 S/m. A sharp electrode positioned as illustrated would measure the extracellular potential depicted in the lowest inset circle. The numbers in the circular insets refer to the depicted measured spike widths. Adapted from [5].

recorded, a positive peak followed by a shallower negative peak. Another important qualitative feature immediately apparent from Fig. 4 is the inherent high-frequency attenuation of the extracellular spike with distance from the soma, i.e., spikes far away from the soma are blunter than spikes recorded close to soma. The spike in the lower circular inset are, for example, narrower than the spike in the upper circular inset. This low-pass filtering effect follows from the passive electrical properties of the neuronal membrane.

In [2] we investigated in detail how neural morphology and electrical parameters affect the shape and size of extracellular action potentials. This is important as it determines how easy it is to record spikes from different types of neurons with extracellular electrodes.

In another study [4] we correspondingly investigated the LFP, i.e., the low-frequency part of the extracellular potential, generated by synaptic activation of single pyramidal and stellate neurons. The resulting shape and size of the LFP waveforms were essentially found to depend on everything, e.g., neuronal morphology, position of active synapse, and position of recording electrode. Also the LFP is found

to be low-pass filtered due to the *intrinsic dendritic filtering effect* described above for the extracellular spike. Any theory aiming to explain the apparent power laws seen in LFP or EEG signals must thus include this effect [4].

4 New analysis methods

4.1 iCSD method for estimation of current-source density

The forward modeling scheme described above has also allowed for the development of new methods for analysis of multielectrode data. One example is the *inverse current-source density (iCSD)* method [6-8], a method for estimation of the current-source density (CSD), i.e., the net density of transmembrane current entering or leaving the extracellular medium, based on LFP recordings. The principle behind CSD estimation is illustrated in Fig. 5.

In the traditional CSD method with laminar LFP recordings, the CSD is estimated as the double spatial derivative of the LFP in the vertical direction [6]. This inherently assumes the CSD to be constant in the two horizontal directions, a requirement not fulfilled for, e.g., the cylindrical CSD distribution shown in the middle panel of Fig. 5. In the iCSD method prior knowledge about, e.g., the horizontal spread of the activation or spatially varying extracellular conductivities can be built into the estimator. The

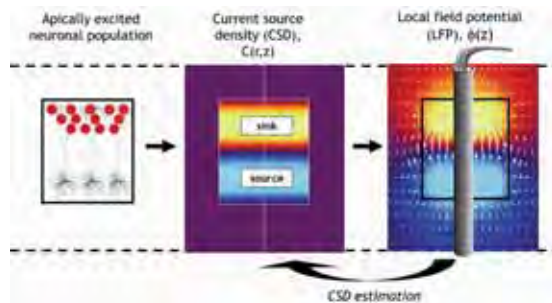


Fig. 5. Illustration of principle behind current-source density (CSD) estimation. An apically excited columnar population of cortical pyramidal neurons (left) will give a characteristic CSD pattern with an approximately cylindrical sink positioned above a cylindrical source (middle). This CSD distribution sets up an LFP that is measured by, in this case, a linear-array (laminar) multielectrode inserted perpendicular through the column. The challenge of CSD estimation is then to infer the true underlying CSD distribution as accurately as possible.

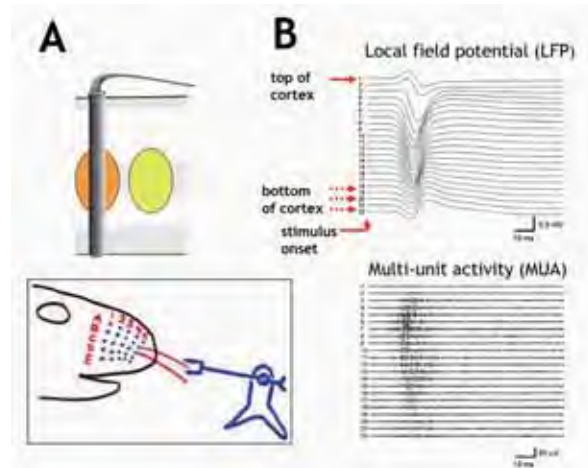


Fig. 6. Illustration of origin of stimulus-evoked laminar electrode data analysed by use of *laminar population analysis (LPA)* [9]. A laminar electrode is inserted into a barrel column and the appropriate whisker is flicked (panel A). Characteristic single-trial results for the low frequency band (LFP; < 500 Hz) and the high-frequency band (MUA; > 750 Hz) are shown in panel B. Adapted from [9]

superiority of this approach under the condition of columnar activation was demonstrated in a comprehensive forward modeling study [3]. Here a synaptically activated population of about 1000 layer-5 pyramidal neurons, mimicking an infragranular population in the barrel column, was investigated. The traditional CSD method was, unlike the appropriate designed iCSD method, found to predict spurious sinks and sources.

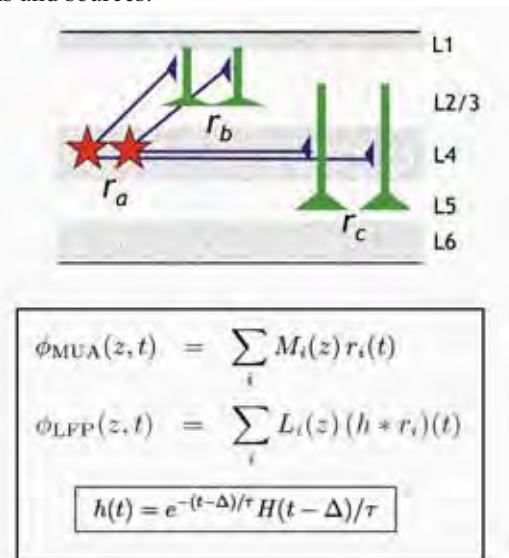


Fig. 7. Illustration of principle behind laminar population analysis (LPA) [9]. Firing of action potentials in population *a* (see upper panel) is reflected in the MUA signal via $M_a(z)r_a(t)$ where $M_a(z)$ is a characteristic MUA depth profile, and $r_a(t)$ is the population firing rate. This firing rate also gives a contribution to the LFP signal given by $L_a(z)(h * r_a(t))$ where $L_a(z)$ is a characteristic LFP depth profile, h is an exponentially decaying temporal kernel with a delay term (see bottom equation), and “*” represents a temporal convolution. $L_a(z)$ reflects the morphologies and positions of the neurons in the populations that population *a* project to. The full mathematical expansion of the MUA and LFP signals in terms of contributions from laminar populations are shown in the rectangular frame.

4.2 Laminar Population Analysis (LPA)

The CSD is easier to interpret than the LFP, but this measure cannot distinguish between contributions from different neuronal populations. We thus developed the so called *laminar population analysis (LPA)* to interpret stimulus-evoked laminar-electrode data recorded from rat barrel cortex in terms of contributions from a set of laminar neuronal populations [9]. See Fig. 6 for a brief description of the experiments.

In LPA the trial-averaged MUA and LFP signals are jointly modeled using a physiological constraint: the MUA is assumed to reflect the firing rates of the laminar populations while the LFP is assumed to be due to postsynaptic activation following the observed population firing, see Fig. 7. (The applicability of these assumptions was later supported by the model study reported in [3]). As illustrated in Fig. 8 the direct outcome of an LPA analysis of a data set is MUA (panel A) and LFP (panel B) population profiles, as well as population firing rates (panel C). In [9] we also introduced a *template-fitting analysis* of the estimated LFP population profiles allowing for estimation of the synaptic connection pattern between the identified laminar populations (panel D).

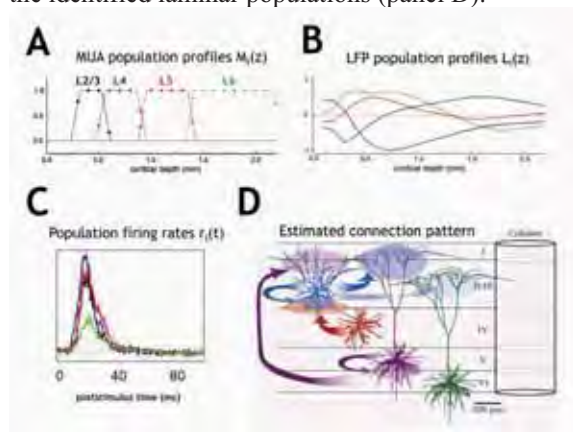


Fig. 8. Results from LPA: MUA (A) and LFP (B) population profiles, and population firing-rates (C). In combination with a template-fitting analysis, the synaptic connection pattern between the populations can also be inferred (D). Example data from [9].

4.3 Extraction of population rate models

As illustrated in Fig. 9 the extracted population firing rates using LPA can in turn be used to identify intracortical and thalamocortical network models [10], the latter also requiring simultaneous recordings of thalamic firing activity recorded in the homologous barreloid. This is important as network models with demonstrated biological relevance are scarce.

Acknowledgements

I thank Klas Pettersen and Henrik Lindén for help with the figures. Projects supported by Research Council of Norway (eScience, NOTUR, NevroNor).

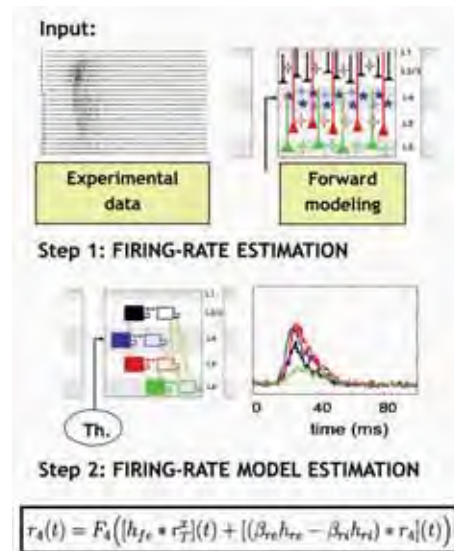


Fig. 9. Illustration of principle behind population firing-rate model extraction from multielectrode recordings [10]. Step 1: Population firing-rates are estimated from MUA data using insights from forward modelling [2,3]. Step 2: Firing-rate models are estimated by fitting with extracted population firing rates.

References

- [1] Holt G.R., Koch C. (1999). Electrical interactions via the extracellular potential near cell bodies, *Journal of Computational Neuroscience*, 6, 169-184
- [2] Pettersen K.H., Einevoll G.T. (2008). Amplitude variability and extracellular low-pass filtering of neuronal spikes, *Biophysical Journal*, 94, 784-802
- [3] Pettersen K.H., Hagen E., Einevoll G.T. (2008). Estimation of population firing rates and current source densities from laminar electrode recordings, *Journal of Computational Neuroscience*, 24, 291-313
- [4] Lindén H., Pettersen K.H., Einevoll G.T. Intrinsic dendritic filtering gives low-pass power spectra of local field potentials, *Journal of Computational Neuroscience*, to appear
- [5] Pettersen K.H., Lindén H., Dale A.M., Einevoll G.T. Extracellular spikes and current-source density. In R. Brette & A. Destexhe (eds.), *Handbook of neural activity measurements*, Cambridge University Press, Cambridge, UK, to appear
- [6] Pettersen K.H., Devor A., Ulbert I., Dale A.M., Einevoll G.T. (2006). Current-source density estimation based on inversion of electrostatic forward solution: Effects of finite extent of neuronal activity and conductivity discontinuities, *Journal of Neuroscience Methods*, 154, 116-133
- [7] Leski S., Wojcik D.K., Tereszczuk J., Swiejkowski D.A., Kublik E., Wrobel A. (2007). Inverse current-source density method in 3D: reconstruction fidelity, boundary effects, and influence of distant sources, *Neuroinformatics*, 5, 207-222
- [8] Leski S., Pettersen K.H., Tunstall B., Einevoll G.T., Gigg J.G., Wojcik D.K.. Inverse Current Source Density method in two dimensions: Inferring neural activation from multielectrode recordings, *submitted*
- [9] Einevoll G.T., Pettersen K., Devor A., Ulbert I., Halgren E., Dale A.M. (2007). Laminar Population Analysis: Estimating firing rates and evoked synaptic activity from multielectrode recordings in rat barrel cortex, *Journal of Neurophysiology*, 97, 2174-2190
- [10] Blomquist P., Devor A., Indahl, U.G., Ulbert I., Einevoll G.T., Dale A.M. (2009). Estimation of thalamocortical and intracortical network models from joint thalamic single-electrode and cortical laminar-electrode recordings in the rat barrel system, *PLoS Computational Biology* 5, e1000328

Identifying Electrically Active Cells In Neuronal Culture And Tissue Using CMOS Based Multi-Transistor Arrays (MTAs)

Lambacher Armin¹, Vitzthum Veronika¹, Zeck Günther², Fromherz Peter¹

¹ Membrane and Neurophysics, MPI for Biochemistry, Martinsried/Munich, Germany

² Systems and Computational Neurobiology, MPI of Neurobiology, Martinsried/Munich, Germany

A unique feature of CMOS based Multi-Transistor Arrays (MTAs) compared to Metal-Electrode Arrays (MEA) is the high density of the sensor pixels over a large sensor array [1-3]. Key parameters for MTAs are a spatial resolution of 7.8µm, a temporal resolution of 6 kHz (full frame readout) and a size of 1mm² (16384 sensors in total).

When using these chips for measuring the electrical activity of neurons in culture or tissue, usually the signal of one neuron is detected on several transistors. We make use of this feature to automatically identify action potentials and individual neurons in recorded data, even if the coupling area of neighboring cells overlap and therefore a sensor transistor records activity of different cells.

In a first step we detect statistically significant data by examining the combined deviation of the signal from its average on the considered transistor and its neighbors in space and time. This results in a map of data points in space and time for each action potential of all electrically active cells. By grouping signals that form cohesive neighborhoods in space and time we can identify action potentials. By examination of the cross correlation between pairs of action potentials it is possible to identify single cells, even if the coupling area of neighboring cells overlap and therefore a sensor transistor records activity of different cells. We show an application of this method to dissociated cultures of hippocampal rat neurons, to cerebellar slices of the rat brain and to rabbit retina.

References

- [1] Eversmann, B. et al. (2003) *IEEE J. Solid State Circ.* 38, 2306
- [2] Lambacher, A. et al (2004) *Appl. Phys. A* 79, 1607
- [3] Hutzler, M. et al (2006) *J. Neurophysiol.*, 96, 1638

Investigating neuronal networks dynamics in hippocampal cultures by means of high-density CMOS-MEAs

Mauro Gandolfo^{1*}, Alessandro Maccione², Mariateresa Tedesco¹, Thierry Nieuws², Kilian Imfeld³, Sergio Martinoia^{1,2}, Luca Berdondini²

¹ Department of Biophysical and Electronic Engineering, University of Genova, Genova, Italy

² Department of Neuroscience and Brain Technology, Italian Institute of Technology, Genova, Italy

³ Nanomedicine, Centre Suisse d'Electronique et de Microtecqnie, Landquart (Switzerland)

* Corresponding author. E-mail address: mauro.gandolfo@unige.it

Microelectronic CMOS technology was recently introduced for realizing advanced micro electrode arrays (MEAs) integrating thousand of electrodes, densely packed over large recording area. Here, we adopt a CMOS-MEA platform (i.e. BioCam₄₀₉₆ from 3Brain) to investigate networks of dissociated hippocampal neurons and we evaluate the benefits of this technology from two viewpoints: (i) the capability of high spatial resolution to provide reliability in the evaluation of conventional rate-based statistics; (ii) the opportunity given by high-density large-scale recordings of spontaneous activity to finely track propagating and oscillatory spatial-temporal patterns (i.e. network bursts). Results highlight that basic statistics are influenced by the spatial resolution and that higher electrode densities allow improving the reliability of the statistics. Moreover, this high spatial resolution enhances the current capability to study network dynamics, also by introducing new analysis approaches.

1 Introduction

MEAs give the unique possibility to directly interface with different types of neuronal preparations. This model is used to investigate several properties of neural assemblies (e.g., learning, plasticity, encoding strategies, information processing) usually by starting from the identification of spiking and bursting activities and by proceeding with basic rate analysis (e.g., Mean Firing Rate – MFR and Mean Bursting Rate - MBR) or with high-order statistics that consider also the time occurrence (e.g. cross-correlation, mutual information, phase relationship). One of the main issues affecting this kind of analysis on dissociated neuronal networks is the relatively large variability and complexity of spatial-temporal patterns. This often requires large number of experiments and/or long-term recordings to achieve reliable rate-based statistics. On the other hand, a precise identification of complex firing dynamics with conventional MEAs, due to the spatial under-sampling (i.e., typical pitch is 100-200 μm for typically 60-250 electrodes) [1], is indeed partly impaired.

The access to a more detailed spatial-temporal view of the global network activity has become feasible only recently with the development of MEAs based on CMOS technology [2, 3]. In this work we report our results on a recently presented CMOS-MEA platform [4] that provides on a large active area ($\sim 7 \text{ mm}^2$) the simultaneous recording from 4096 electrodes at 7.7 kHz/channel and at high spatial resolutions (inter-electrode separation of 21 μm). At

first, we focus on the evaluation of how spatial resolution can affect statistical parameters commonly used on the MEA field. Successively, we evaluate the capability of this technology to describe activity dynamics during network burst (NB) events.

2 Materials and methods

2.1 High density MEA platform

The high resolution MEA platform is based on the Active Pixel Sensor (APS) technology originally developed for image-sensors and adapted to electrophysiological recordings. The system acquires electrophysiological signals at high enough sampling rate (7.7 KHz) to detect spikes reliably, from 4096 electrodes/pixels (21 μm x 21 μm electrodes, 21 μm inter-electrode separation) arranged in a 64 x 64 grid.

2.2 Hippocampal neuronal cultures

Neuronal cultures were prepared by adopting a protocol described in [5]. Briefly, the APS-MEA devices were first sterilized and then coated with laminin and poly-d-lysine. Primary hippocampal neurons were obtained from Sprague Dawley rat embryos (E18). Dissociated neurons were plated onto MEAs and 2 hours later the Neurobasal Medium (Invitrogen) supplemented with 1% Glutamax, 2% B-27 was added. Cultures were maintained in incubator (5% CO₂, 37° C). Half of the medium was renewed every week.

2.2 Data analysis

Event detection

Acquired data were firstly processed by the spike detection algorithm presented in [6]. Successively, spike arrays were searched for organized activities by looking at the inter-spike interval (ISI). Channel bursts (number of spikes ≥ 5 with ISI ≤ 30 ms) were identified on single spike trains, while network bursts (number of recruited channels $\geq 10\%$ of active channels with ISI ≤ 50 ms) on the whole spike train derived by summing the activity of all channels.

Statistical stability analysis

In order to compare analysis results at different spatial resolutions, we extracted from the original full resolution recording, subsets of electrodes at different spatial densities over an active area of $1.7 \times 1.7 \text{ mm}^2$ (lower than the full CMOS-MEA area of $2.7 \times 2.7 \text{ mm}^2$). Starting with a subset of 60 electrodes (inter electrode distance of $189 \mu\text{m}$, electrode density of 19 electrode/ mm^2), we gradually increased the number of electrodes (and thus the electrode densities) up to the full resolution provided by the APS-MEA chip (1849 electrodes and electrode density of 580 electrode/ mm^2). These data were then analyzed as they were distinct MEA layouts by computing for each one the MBR and the MFR. In order to obtain a distribution for each layout, the size of the datasets was increased by moving the original layout by one electrode above, below to the right and to the left. Hence, in order to quantitatively assess the differences across pair-wise layout distributions we adopted the Kullback-Leibler distance [7] defined as:

$$KL_d(p_i, p_{i+1}) = \frac{KL_m(p_i, p_{i+1}) + KL_m(p_{i+1}, p_i)}{2},$$

$$KL_m(p_i, p_{i+1}) = \sum_f p_i(f) \cdot \log \left(\frac{p_i(f)}{p_{i+1}(f)} \right)$$

where $p_i(f)$ and $p_{i+1}(f)$ are result distributions for layout i and neighbor layout $i+1$ respectively ($KL_m = 0$ for identical neighbor distributions).

Activity pattern analysis

With the aim to reduce the computational costs and to exploit the frame sequence generated by the APS-MEA system, we introduced activity movies as a representation of the raw data in a false color map. Upon inspection of the raw signals along small time windows (TW_s), activity movies can be defined by color-coding the voltage values $P_{TW}(k)$ obtained at each pixel k as:

$$P_{TW}(k) = \frac{\exp(\text{diff}_{TW}^{LT}(k) / c)}{\exp(M / c)} \cdot M,$$

where M is the full scale value chosen, $\text{diff}_{TW}^{LT}(k)$ is the highest max-min difference of the signal computed in TW at the channel k and ranging between a low threshold (LT) and M , c is a constant experimentally fixed to $1/5$ of M .

Hence, for tracking activity propagation during the onsets (first tens of ms) of network bursts, we computed the Center of Activity Trajectory (CAT), directly on activity movies, according to:

$$\vec{CAT}(t_0, t_1) = [\vec{CA}(t_0), \vec{CA}(t_0 + \Delta t), \dots, \vec{CA}(t_1)];$$

$$\vec{CA} = \frac{\sum_k P_{TW}(k) \cdot \vec{\rho}_k}{\sum_k P_{TW}(k)},$$

where $\vec{\rho}_k$ is the position from the reference point of the channel k .

The trajectories were then classified using an automated k -means algorithm in order to assess the repeatability of the activity patterns.

3 Results

Spontaneous activity was recorded up to 40 minutes at high resolution from 7 hippocampal cultures between 18 and 32 DIVs. At this age all preparations showed both random (spikes) and quasi-synchronized (network bursts; NBs) activities.

3.1 Spatial resolution

Results achieved by evaluating the MFR and the MBR on the spatially under sampled layouts are reported in Fig. 1a and 1b respectively. As shown by these plots, by increasing the electrode density a stable MFR and MBR is reached especially for experiments 2, 3 and 7.

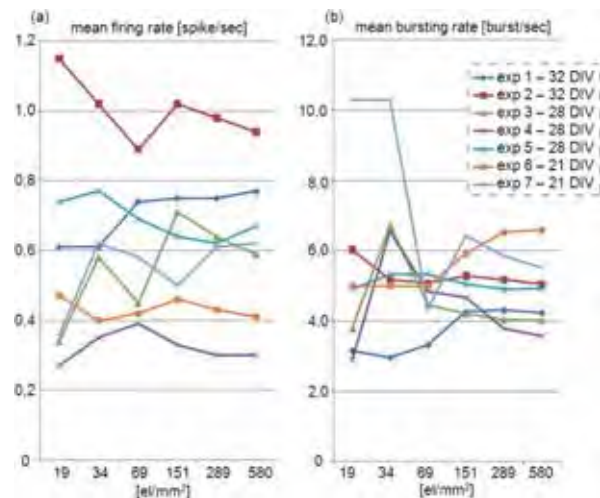


Fig. 1. MFR (A) and MBR (B) values on 7 experiments plotted against the electrode density.

Looking at the standard deviation obtained on the full data set distribution (Fig. 2a), a plateau can be noticed for electrode densities higher than 151 el/mm². Similarly, box-plots for the highest electrode densities tend to resemble (Fig. 2a). As a further confirmation, the KL distances show a change of three orders of magnitude passing from $\sim 10^{-1}$ for lower electrode density pair-wise distributions to $\sim 10^{-4}$ when comparing the two highest electrode density distributions. In addition, the latter distance is considered statistically significant ($p < 0.05$), thus demonstrating that the firing rate evaluation is stable for electrode densities higher than 298 el/mm².

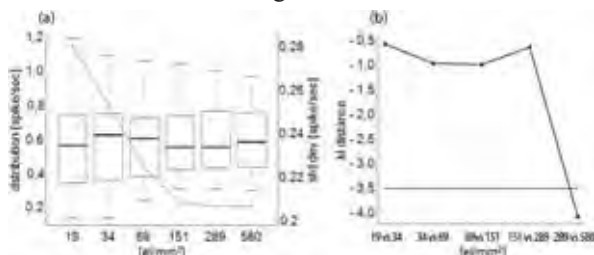


Fig. 2. (A) Box-plots representation of the firing rate distribution (left axis) superimposed to the StdDev (right axis) at different electrode densities. (B) Kullback-Leibler distances in logarithmic scale against pair-wise firing distribution. The grey dashed line represents the threshold for considering two distributions significantly close to each other ($p < 0.05$).

3.2 Activity propagation

Fig. 3 shows first tens of milliseconds of a network burst by means of a subset of frames extracted from an activity movie. As it can be noticed, the high resolution offered by the CMOS-MEA enables to finely represent the NB propagation.

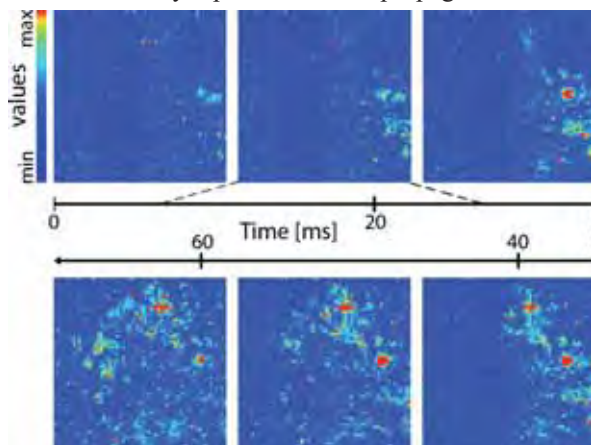


Fig. 3. NB onset (68 ms) visualization by means of voltage values coded in an exponential false color map (activity movie).

Successively, the CATs were computed over each NB onset by using a time window of 20 ms and a time step (Δt) of 4 ms. The trajectories were then classified with an automated algorithm. Interestingly, the clustering procedure resulted only in a few network burst classes. In fact, the majority of the experiments showed typically 2 classes, while only

two cultures (Fig. 4) revealed three different propagation patterns, thus indicating a high degree of the activity pattern repeatability during the onset. Conversely, after the NB onsets, the successive activations show more differences in terms of duration, firing intensities and spatial-temporal dynamics (data not shown).

As a preliminary result, the repeatability was further investigated within classes. Fig. 5 shows such an example for NBs belonging to class 3 in the first experiment of Fig. 4. The increased resolution of CMOS-MEAs reveals fine differences between grouped NBs. In particular, the red dotted boxes in Fig. 5 highlight substantially different activity pattern for the lower channels. Such intra-class differences could lead to identify sub-classes of NBs as reported by the labels 'a' and 'b'.

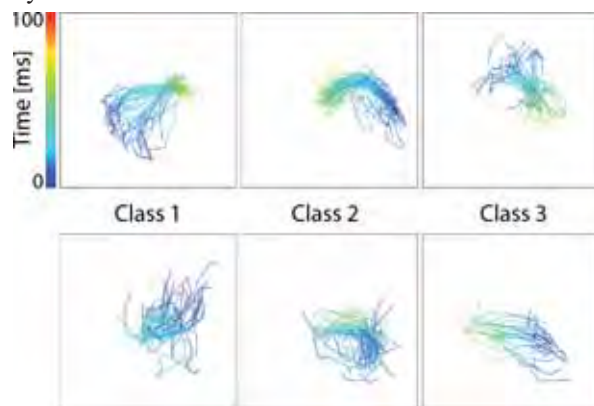


Fig. 4. Classification of CATs from NBs expressed by two (above and below) hippocampal cultures.

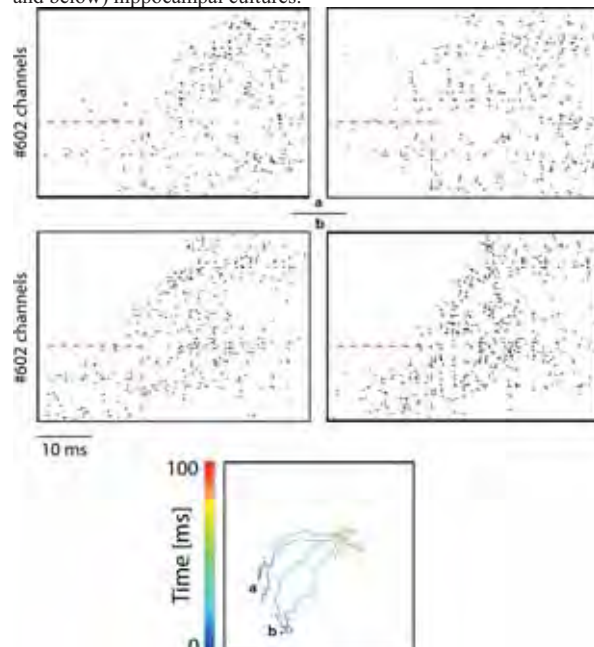


Fig. 5. Raster plots (above) showing 4 NB onsets (50 ms), belonging to the same class (class 1 of Fig. 4), and corresponding CATs (below). Pronounced intra-class differences are observed (e.g., within red dotted boxes) highlighting further segmentation in the two subgroups ('a' and 'b').

4 Conclusions

Our results point out that high resolution large-scale MEAs allow: (i) to improve the reliability and stability of standard statistical parameters such as MFR and MBR; (ii) tracking NBs with CATs directly computed on raw data (activity movies), without needing any spike detection and thus reducing computational costs; (iii) to describe in detail classes of activity patterns. In particular, results on classes' classification support the hypothesis that the same information (NB class) can be transmitted by different patterns of activity as it would be expected for a fault tolerant mechanism [8]. Finally, the achieved significance of the statistical parameters might contribute in the development of MEA-based application such as for pharmacological screenings.

Acknowledgement

This work was supported by a grant from the European Community in the New and Emerging Science and Technology program (IDEA project, FP6-NEST, contract No. 516432).

References

- [1] van Pelt, J., Vajda, I., Wolters, P. S., Corner, M. A., and Ramakers, G. J. A. (2005) Dynamics and plasticity in developing neural networks in vitro. *Progress in Brain Research*, 147, 171-88.
- [2] Berdondini, L., Overstolz, T., de Rooij, N. F., Koudelka-Hep, M., Martinoia, S., Seitz, P., Wány, M., and Blanc, N. (2002). High resolution electrophysiological activity imaging of in vitro neuronal networks. *IEEE-EMBS* (Madison, WI, USA) 241-44.
- [3] Eversmann, B., Jenkner, M., Hofmann, F., Paulus, C., Brederlow, R., Holzapfl, B., Fromherz, P., Merz, M., Brenner, M., Schreiter, M., Gabl, R., Plehnert, K., Steinhauser, M., Eckstein, G., Schmitt-Landsiedel, D., and Thewes, R. (2003). A 128 x 128 CMOS biosensor array for extracellular recording of neural activity. *IEEE J. Solid-State Circuits* 38, 2306-17.
- [4] Berdondini, L., Imfeld, K., Maccione, A., Tedesco, M., Neukom, S., Koudelka-Hep, M., and Martinoia, S. (2009). Active pixel sensor array for high spatio-temporal resolution electrophysiological recordings from single cell to large scale neuronal networks. *Lab on a Chip*, 9, 2644-51.
- [5] Maccione, A., Gandolfo, M., Tedesco, M., Nieuw, T., Imfeld, K., Martinoia, S., and Berdondini, L. (2010). Experimental investigation on spontaneously active hippocampal cultures recorded by means of high-density MEAs: analysis of the spatial resolution effects. *Frontiers in Neuroengineering*, doi: 10.3389/fneng.2010.00004.
- [6] Maccione, A., Gandolfo, M., Massobrio, P., Novellino, A., Martinoia, S., and Chiappalone, M. (2009). A novel algorithm for precise identification of spikes in extracellularly recorded neuronal signals. *Journal of Neuroscience Methods*, 177, 241-9.
- [7] Duda, R. O., Hart, P. E., and Stork, D. G. (2000). *Pattern Classification*, 2nd ed., Wiley.
- [8] Raichman, N., and Ben-Jacob, E. (2008) Identifying repeating motifs in the activation of synchronized bursts in cultured neuronal networks. *Journal of Neuroscience Methods*, 170, 96-110.

Frame work for Comparing Spike Detection Algorithms for Real-Time Applications

Pini Tandeitnik^{1*}, Hugo Guterman¹

¹ Ben-Gurion University, Beer-Sheva, Israel

* Corresponding author email address: pinit@ee.bgu.ac.il

Microelectrode array systems are commonly used in various neural prosthetic devices. The recorded multi channel and multi-units signals should be detected prior to activations of various strategies for data analysis and interpretation. The goal of this work is to compare the performance of various techniques for spike detection. The performance of the various spike detectors may be used for designing real-time and closed loop neural prosthetic application.

1 Introduction

Neural prosthetic device require reliable real-time interpretation of extra-cellular multi-channel and multi-unit recordings. Interpretation of neural activity is a challenging task. It consists of three major stages: Spike detection which discerns the presence of spikes in the channel. The second step is spike counting or spike sorting for more advanced applications (in multi unit recordings spike sorting adds a label to the spike prior to spike counting). The last phase is mapping the multi-channel neural activity to physical tasks, such as arm movement to a new position by linear filtering or by artificial neural networks techniques. To get better performance of the neural device one must detect all spikes. The focus of this work is on the performance of spike detection algorithms.

Prior to spike detection one should estimate the channel background activity during the channel learning phase. The estimated noise level is a parameter for setting the thresholds of the spike detectors.

2 Methods

Analyzing neural activity of a single channel requires settings of the detection parameters, such as the sampling rate and the threshold in terms of number of standard deviation of the noise level.

Detection of signal activity above the threshold is not a real spike for sure; additional criteria such as the spike minimum and maximum pulse width and the refractory period are used. Typical spike duration is about 1msec. The spike width should be less then 0.5msec and more then 0.1 msec.

The following spike detection algorithms were evaluated : Steady Threshold[1], Upper – Lower Threshold[1], Adaptive Threshold[2], Peak To Peak Threshold[3], NEO[4], SNEO[4,5]. The detection algorithms performance was evaluated based on the neural activity simulator of Smith[6] with various sample rates SNR and threshold.

3 Results and discussion

The performance of the above parameters was evaluated by the following criteria's : True Positive and False Negative rates, the accuracy of the spike onset and run time.

A comprehensive presentation of the overall performance is visualized in 3D graphs. The spike onset is a crucial parameter in close loop applications, where the post synaptic potentials are induced for 1-2msec. In this time windows the provided stimuli may induce changes in the synaptic coupling.

The Upper – Lower threshold algorithm has the best performance over a large range of SNR and thresholds. The True Positive and False Negative performance are shown in the next figure, the x-axis is the detector threshold in terms of the channel standard deviation , the y-axis is the channel noise level (linear and logarithmic scale , the z-axis is the channel sampling rate. The color in of the surface represents the performance rate as shown in the toolbar on the right.

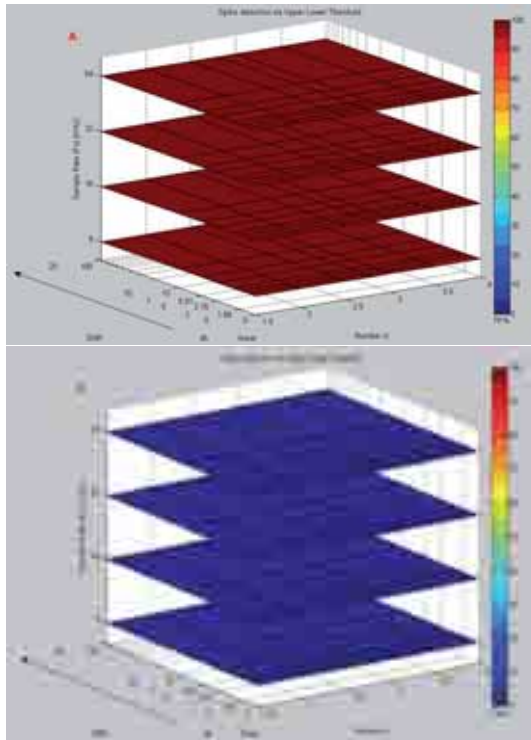


Fig. 1. True Positive (A) and False Negative (B) of the Upper – Lower detection threshold algorithm

As one can see the TP is almost 100% and the FN is very close to zero.

A complete comparison between the six different algorithms is presented (Fig 2). The x-axis is the detector threshold in terms of the channel standard deviation, the y-axis is the channel noise level (linear and logarithmic scale), the z-axis is the selected algorithm at sampling rate of 16Khz.

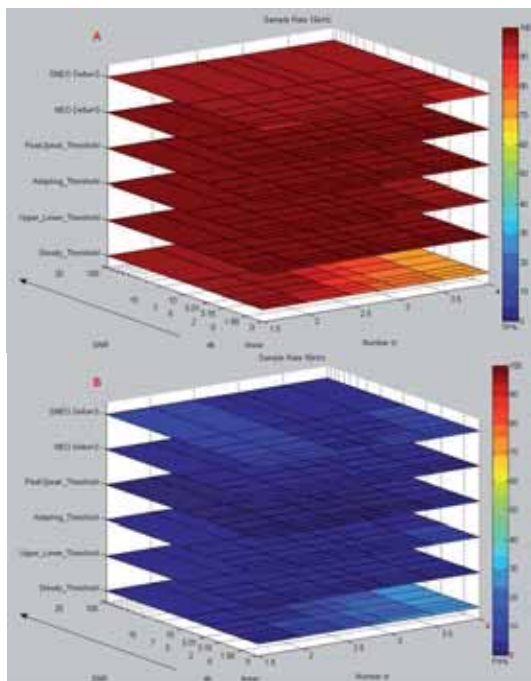


Fig. 2. Sampling rate of 16KHz, True Positive (A) and False Negative (B) of the Upper – Lower detection threshold algorithm

The preferred sampling rate is 16KHz since in lower sampling rate and for narrow spikes width large noise level can lead to TP spike detection and increase the FP detection rate.

4 Summary

The NEO and the Upper – Lower Threshold detector have the overall best performance in criteria of high true positive rate and low false negative rate and run time. The NEO detector has a better accuracy over wider range of SNR levels while the Upper – Lower Threshold detector has better performance for higher SNR levels.

Since both algorithms require low computational power they are appropriate candidates for real time applications.

Acknowledgment

We wish to thank Evgenia Goldshtein for her excellent matlab programming.

References

- [1] Schmidt E.M., 1984. Instruments for sorting neuroelectric data: a review. *J. Neurosci. Methods* **12**, pp. 1–24
- [2] Watkins, H., Validation of Adaptive Threshold Spike Detector For Neural Recording, in *Proceeding of the 26th Annual Conference of the IEEE EMBS*. 2004: San Francisco, USA. p. 4079-4082
- [3] A. Novellino, A. Maccione, M. Gandolfo, M. Chiappalone, P. Massobrio, and S. Martinoia, "A novel spike detection algorithm for real-time applications," in *Mea Meeting 2006*, Reutlingen, 2006, pp. 73-74.
- [4] S. Mukhopadhyay and G. C. Ray, "A new interpretation of nonlinear energy operator and its efficacy in spike detection," *IEEE Trans. Biomed. Eng.*, vol. 45, pp. 180–187, Feb. 1998.
- [5] Obeid I., Wolf P., "Evaluation of Spike-Detection Algorithms for a Brain-Machine Interface Application", *IEEE Trans. Biomed. Eng.*, 51:905-911, 2004
- [6] Smith L.S., Mtetwa N., A tool for synthesizing spike trains with realistic interference, *Journal of Neuroscience Methods*, vol. 159, pp. 170–180, 2007

Signal and Noise Analysis of Low S/N Data Recorded from MEA

V. Gautam¹ and K.S. Narayan^{1*}

¹ Molecular Electronics Laboratory, Jawaharlal Nehru Centre for Advanced Scientific Research, Jakkur P.O., Bangalore, India.

* Corresponding author. E-mail address: narayan@jnrcasr.ac.in

We demonstrate the method of Fast Fourier Transformation for detection of fast events like action potentials in low S/N data recorded from MEAs.

1 Introduction

Detection of fast events like action potentials in extracellular MEA recordings is quite challenging. Existing spike detection techniques usually involve amplitude thresholds to discriminate spike events [1-3]. However, when signal to noise (S/N) ratio is low, the requirement of amplitude thresholds may not be sufficient.

We adopt a procedure to extract information from noisy signals recorded from MEAs. In this study, we show that detection of spikes from the ganglion cells of the retina using MEAs is possible by doing *Fourier transform* of the real time noisy signals into the frequency domain. Further noise analysis can be done by analyzing the Fourier transform of the auto-correlation function.

2 Materials and Methods

Retina whole mounts were prepared using standard protocols [4]. TiN arrays (Hexa MEA from MCS, Germany) were used for the extracellular recording of light evoked activity from the ganglion cells. Whole field stimulation was done using pulsed white LED for an ON time of 60 ms and off time of around 2 s. Data was recorded from BC1060-Inv Amplifier using MC Card and MC rack software (MCS, Germany) at a sampling rate of 25 kHz.

For data analysis, one raw data stream corresponding to no stimulus (light OFF) and one for stimulus (light ON) period were extracted from the same recorded .mcd file using MC_datatool. These were converted to .dat files and simultaneously fed into the Matlab code written for the discrete Fourier transformation (FFT). Before the transformation, the slow field potential (ERG) was eliminated by subtracting the original data from its running average. The FFT code was then used to transform the real time data to frequency domain (ω) as per the expression:

$$X(\omega) = \sum_{t=0}^{N-1} x(t) e^{-i2\pi \frac{kt}{N}}, \text{ where } k=0,1,\dots,N-1.$$

Usually, 4096-point FFT was done. The respective frequency spectra of the two data sets were compared to obtain specific features.

3 Results and Discussions

It was observed that the Fourier transformation of real time signals from non-stimulated ganglions was featureless with a general trend of $I(\omega)$ decreasing in with increasing ω . However, the spectrum obtained from the data collected from the stimulated ganglion cells consisted of additional features which included characteristic frequencies in the range 500 Hz-1.5 kHz (Fig.1). This signature can be interpreted to correspond to action potentials of 0.5 ms-5 ms duration.

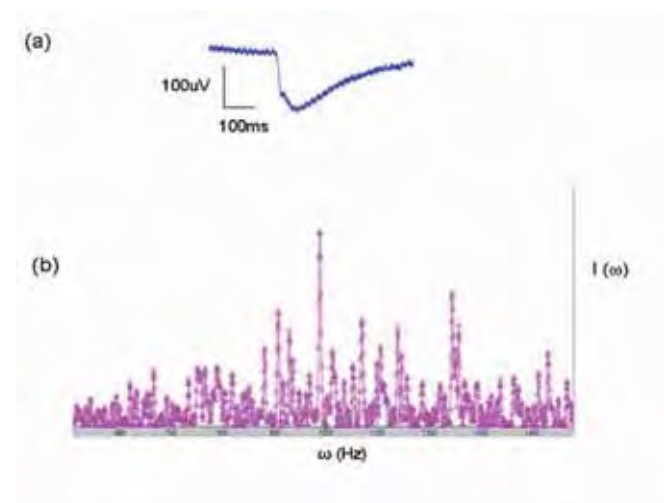


Fig.1. (a) Raw data stream recorded from Hexa MEA (TiN) and (b) Corresponding frequency spectrum exhibiting characteristic frequencies.

Moreover, S/N ratio can be improved by modifying the electrode array and better interfacing the retina tissue with the substrate [5]. Our present efforts are directed towards verifying our analysis procedure and interpretation with such enhanced signals.

4 Conclusion

We have shown that Fourier transformation is a useful method of data mining from the MEA data when the S/N ratio is quite low. The noise levels of MEAs usually increases with prolonged use and S/N level drops. This method can probe nervous tissue activity which otherwise gets suppressed due to high noise levels.

We also propose that to analyze noise in such data, the power spectrum obtained from Fourier transform of the autocorrelation function taken with appropriate time lags would provide additional information.

We propose that this procedure should be incorporated in existing large band-width MEA data measurements.

References

- [1] MEA application notes, Multichannel Systems, Germany.
- [2] Shahid S. and Smith L.S. (2008), Assessing New Techniques for Spike Detection on MEA Data, *Proceedings of 6th Int. Meeting on substrate integrated microelectrode arrays*, 133-134.
- [3] K. Kim and S. Kim (2000). Neural spike sorting under nearly 0-dB signal-to-noise ratio using nonlinear energy operator and artificial neural-network classifier, *IEEE Trans. Biomed. Eng.*, 47(10):1406–1411.
- [4] Guenther E, Herrmann T. and Stett A.(2006). The Retinasensor. *Advances in Network Electrophysiology* (Springer).
- [5] Gautam V. and Narayan K.S. (2010). Conducting Polymer Coated MEAs for Enhanced Signal Recording and Stimulation, *Proceedings of 7th Int.Meeting on substrate integrated microelectrode arrays*.

Where are the barrels? A signal based approach

Rembrandt Bakker, Martijn Selten, Rolf Kötter, Dirk Schubert¹

¹ Donders Institute for Brain and Cognition, University Medical Centre St. Radboud, Nijmegen, Netherlands

* Corresponding author. E-mail address: D.Schubert@donders.ru.nl

The stimulus-response behavior of acute slice preparations of the rat barrel cortex provides valuable insights in the organization, plasticity and fault-tolerance of the primary somatosensory (barrel) cortex. For these experiments, it is crucial to know the correct position of the barrels and associated cortical columns. In the unstained tissue, a well trained observer can see the barrel-shaped areas in cortical layer IV under a light microscope. However, after placing the tissue on a MEA chip and placing a nylon holding grid, this task becomes increasingly error-prone. The question we pose is whether the MEA chip itself can be used to reveal the position of the barrels, by comparing the stimulus-response patterns of all electrodes within the grid. We explore two discriminating features: 1) the amplitude of the negative LFP in the electrode above the stimulated electrode; and 2) the paired pulse ratio taken from the electrode two rows up from the stimulated electrode. The first results indicate that the approach can reveal barrel-associated columns, but only under certain conditions: the holding grid must be fine-grained, applying a uniform pressure on the tissue.

1 Introduction

This analysis approach is part of a larger study on the cortical microcircuits within the rat barrel cortex, using thalamo-cortical slice preparations [1] placed on a micro electrode array chip (MEA: 60 electrodes, 8x8 with empty corners; Multi Channel Systems, Reutlingen, Germany). Assigning electrodes to cortical layers is relatively easy, based on dark and light bands of tissue seen under a light microscope. It is much more difficult to assign the layer IV electrodes to 'within a barrel' or 'in between' (septum), in particular after the slice has been placed on top of the electrode and is held in place using a nylon holding grid. This information is important, since the septa are believed to play a distinct role in thalamo-cortical signalling [2]. The long route to detect barrel positions is to fixate the slices post experiment and apply cytochrome oxidase staining. Then, a manual, landmark-based alignment of photomicrographs taken during the experiment is needed to reconstruct the electrode positions. It would be of great help if barrel positions can be derived directly from data recorded by the MEA chip, at the start of an experimental session. The amplitude of the stimulus-response signal has been shown to be a good indicator for the barrel position [3]. Here we present a case study in which we stimulate all electrodes one by one to reveal the barrel position.

2 Methods

An automated stimulus sequence is designed to capture the stimulus-response behavior of the slice to a maximum extent, within a ten minute time frame. It stimulates electrodes one by one with 10s intervals, in such an order that subsequent stimulations are

spatially as far apart as possible. We slightly varied the stimulus shape between experiments, good results were obtained with a -800mV/+400mV 2x 300 μ s bipolar square pulse. The pulse is repeated after a 50ms interval to observe short-time plasticity. Responses are measured 50 ms pre-stimulus, and 250 ms post-stimulus, at 0.1 ms resolution.

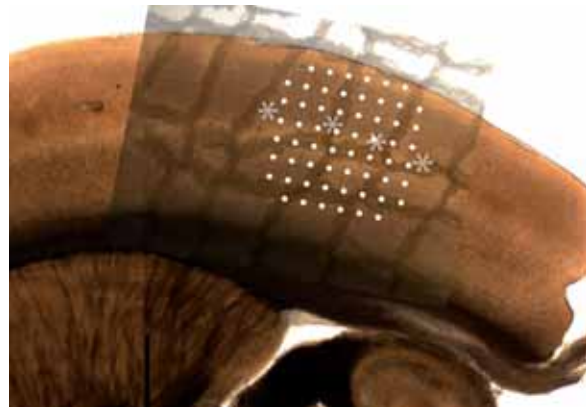


Fig. 1. Fixed thalamo-cortical slice of a P22 wistar rat, stained with cytochrome oxidase. Asterisks denote expert-assigned barrel positions. Superimposed at 50% transparency is the photomicrograph taken during the recordings. White dots are (enlarged) MEA electrode positions. The electrodes have a 30 μ m diameter, and are spaced 200 μ m apart.

Analysis

A single run of the stimulus protocol produces 60 datasets, each containing 1 stimulus channel and 59 response channels. To reduce this vast dataset to an 8x8 matrix revealing barrels, we compute two simple statistics. The first is the amplitude of the signal two rows up from the stimulated electrode: we take the 10th-percentile of the first 50 ms after stimulus as a

robust estimate of the LFP depth. The second statistic is the paired pulse ratio (PPR), the ratio of the 10th-percentile values of the first 10 ms after the paired stimuli. Again we choose the electrode two rows up from the stimulation site.

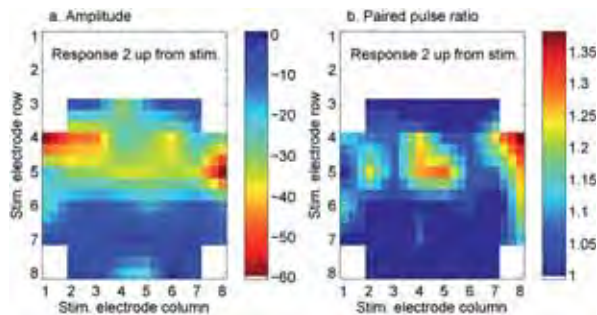


Fig. 2. Amplitude (a) and PPR (b), measured at two electrodes above the stimulation electrode. Every third row/column in the colorplot is a data value, in between are interpolated values to guide the eye.

3 Results and Discussion

Figure 1 shows the slice after staining with cytochrome oxidase. Barrel positions are indicated by a trained expert, and electrode positions are reconstructed from a picture taken during the experiment. Figure 2 shows the two statistics computed for this case study. In Fig. 2a, the yellow-red patches mark the location of electrodes which respond strongly to stimulation. In Fig. 2b, similar patches highlight the location of strong paired-pulse facilitation. In both cases, most activity is seen after stimulation of electrode rows 4-5; the displayed responses are from rows 2-3 (two rows up). These correspond to cortical layers II-III. This is in agreement with Bakker et al. [4], who report that neurons in layers II/III strongly and robustly respond to stimulation of deeper layers. Both plots seem to indicate barrels with the correct inter-barrel distance (400-500 μm , or 2-2.5 electrode distances). The correspondence to the barrels indicated in Fig. 1 is quite reasonable, but the resolution is coarse, limited by the 200 μm grid spacing. The amplitude result suggests there is an additional barrel which is not visible in the stained tissue. The PPR plot clearly reveals patches of high PPR in layer II/III, but further experiments are necessary to see whether they are indicative for the barrel position.

Holding grids

The pattern of Figs. 2a and 2b are not correlated with the mesh wires shown in Fig. 1. We did test however the effect of coarser, parallel wire based grids on the data. They have the big advantage of not blocking the view of the slice, and leaving space for combined single cell electrophysiology. The test showed that local compression of the tissue does amplify the response to stimulation, so that the automated barrel finding procedure can't be used. The paired pulse ratio statistic is a first attempt to find an amplitude-independent parameter.

Future work

This case-study is a work in progress. The all-electrode stimulation has become a routine procedure in our lab, and we are collecting a large number of datasets to validate the automated barrel locator and various, amplitude-independent variants thereof.

Acknowledgement

We thank Moritz Negwer for the histochemical processing of the slices.

References

- [1] Land P.W., Kandler K. (2002). Somatotopic organization of rat thalamocortical slices. *Journal of Neuroscience Methods*, 119 (1), 15-21.
- [2] Alloway, K.D. (2007). Information Processing Streams in Rodent Barrel Cortex: The Differential Functions of Barrel and Septal Circuits. *Cerebral Cortex*, 18(5), 979-989.
- [3] Wirth C., Lüscher, H-R. (2004). Spatiotemporal Evolution of Excitation and Inhibition in the Rat Barrel Cortex Investigated With Multielectrode Arrays, *J Neurophysiol.* 91, 1635-1647.
- [4] Bakker R., Schubert D., Levels K., Bezgin G., Bojak, I., Kötter, R. (2009). Classification of cortical microcircuits based on micro-electrode-array data from slices of rat barrel cortex. *Neural Networks*, 22(8), 1159-68.

NeuVision: a New Simulation Environment to Model Large-Scale Neuronal Networks Coupled to Micro-Electrode Arrays

Marcello Mulas^{1,2*}, Paolo Massobrio¹, and Sergio Martinoia^{1,2}

¹ Neuroengineering and Bio-nanoTechnology Group, Department of Biophysical and Electronic Engineering (DIBE), University of Genova, Genova (Italy)

² Neuroscience and Brain Technology Department, Italian Institute of Technology, Genova, (Italy)

* Corresponding author. E-mail address: marcello.mulas@gmail.com

NEUVISION is a novel simulation environment tailored to simulate the dynamics of large-scale neuronal networks coupled to Micro-Electrode Arrays (MEAs). Such simulator has been developed by using programming languages supported by the .NET framework and allows the user to implement networks of neurons made up of thousands of synaptically connected elements. The main features of this simulator are related to the efficient visualization of the neural activity, as well as the possibility to define different connectivity rules and electrical stimulation protocols. Finally, also the integration of statistical analysis tools for fast neural dynamics characterization was implemented. In this work we present some preliminary validation results obtained simulating large-scale neuronal networks made up of 1024 neurons. In particular we show analyses of both spontaneous and stimulus-evoked activities.

1 Background

Micro-Electrode Arrays (MEAs) are a widespread and recognized technology to study the electrophysiological activity of neural cultures. [1] However, the number of available recording electrodes is still much smaller than the number of neurons for large-scale networks. This spatial undersampling results in a lack of information. The development of a new simulation environment able to reproduce the electrophysiological behavior typically found in these preparations offers a valid support for a better understanding of the actual dynamics. In this work, we present the main features of our software showing simulation results of both spontaneous and stimulus-evoked activity of a high-connected network.

topology of a network (e.g., random, small-world, scale-free, etc.) by changing the parameters that modify the probability to have a link between two neurons. It is also possible to define different stimulation position in the network in order to simulate the evoked activity. The user can also take advantage of a detailed visual representation of the simulated electrophysiological activity (raster plots, shown in Figure 1, membrane potential levels, etc.) and of the connectivity of the network (links, false color map of the synaptic weights, etc.). Finally, some classic analysis tools (mean firing rate, inter-spike-interval, inter-burst-interval, ...) are integrated in the environment to allow a fast characterization of the neural dynamics.

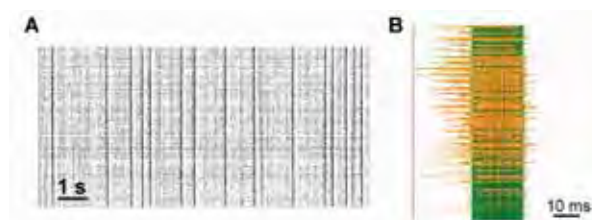


Fig. 1. Raster plot. (A) Spiking and bursting activity. (B) Particular of an evoked network burst.

2 Methods

The simulation environment is developed in C#, the last generation object-oriented language by Microsoft®, particularly suitable to build graphical user interfaces. The available neural network models are written in C++/CLI in order to optimize code performance and allow the user to define the initial

3 Results

We simulated a neuronal network model made up of 1024 point neurons, each modeled according to the Izhikevich equations [2]. In particular, we considered two different types of neuron to model excitatory and inhibitory populations of neurons, respectively: the former belongs to the family of regular spiking neurons while the latter to the family of fast spiking neurons. To preserve some characteristics of the structure of in vitro cortical neurons, we set the ratio between excitatory and inhibitory neurons to 4:1 [3, 4]. We first simulated the spontaneous activity observing the typical behavior found experimentally: a mix of spiking and bursting activity with two well-defined characteristic ISI shapes (Fig. 2A). In addition, we also simulated the evoked activity elicited by a low frequency electrical stimulation (0.2 Hz), finding that the spiking and the bursting activities are modulated by the number and the type of the

stimulated neurons as shown in Fig. 2B. The stimulation of excitatory neurons promotes bursting activity to the detriment of spiking activity, whereas the opposite occurs when we stimulate inhibitory neurons.

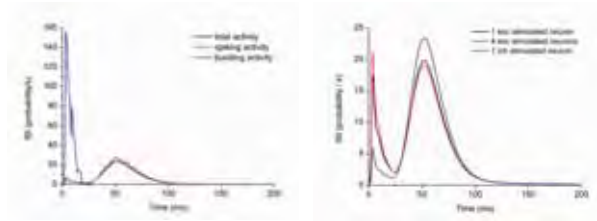


Fig. 2. General statistics used to characterize spontaneous and evoked activity of the simulated network. (A) Inter spike interval (ISI) of the spontaneous activity considering the total network activity (black line), only the spiking activity (red) and the bursting activity (blue). (B) ISI of the evoked activity.

The analysis of the PSTH highlights a relevant peak of activity about 60 ms after stimulating one excitatory neuron as shown in Fig. 3 (black line). This peak is due to the network burst that the stimulation evokes. In general, increasing the number of stimulated neurons the latency response decreases. As a matter of fact the PSTH obtained stimulating four excitatory neurons shows a peak at 48 ms (red line).

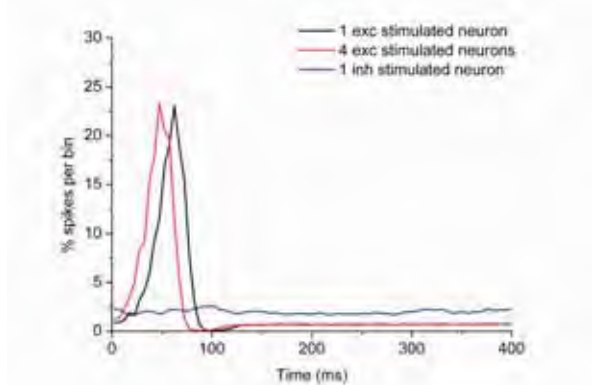


Fig. 3. Post-stimulus time histogram (PSTH) of the network when only one excitatory neuron (black), 4 excitatory neurons (red) and one inhibitory neuron (blue) are stimulated.

After about 30 ms starting from the peak of activity the PSTHs show a silent period, during which no spikes are generated. This is due to the fast discharge of the evoked network burst that leaves all the neurons in a refractory period almost at the same time. Therefore, it is necessary a few milliseconds for the background stimulation current to bring other neurons to fire again. The PSTH concerning the stimulation of the inhibitory neuron (blue line), is very different from the previously analyzed, because it does not show any peak of activity and any silent period. The effect of the stimulation is completely negligible. The low activity is mainly due to the spontaneous one, and is uniformly distributed over the time with no reference to the stimulation time instant.

4 Conclusion

In this work we presented a new simulation environment, designed as a support tool for electrophysiological experiments with neuronal cultures coupled to MEA. The main strengths of this simulator are the efficient visualization of the neural activity, the possibility to define different connectivity rules and stimulation points and the integration of classic analysis algorithms for fast neural dynamics characterization. Our preliminary simulations show that we are able to reproduce both the spontaneous and evoked activity of cultured networks.

References

- [1] Taketani M. and Baudry M. (2006). Advances in network electrophysiology: using Multi-Electrode Arrays. Springer2006.
- [2] Izhikevich E. M. (2003). Simple model of spiking neurons. IEEE Transactions on Neural Networks, 6, 1569-1572.
- [3] Braitenberg V. and Schultz A. (1991). Anatomy of the cortex: statistics and geometry. Springer-Verlag Berlin 1991.
- [4] Marom S. and Shahaf G. (2002). Development, learning and memory in large random networks of cortical neurons: lessons beyond anatomy. Quarterly Reviews of Biophysics, 35,1, 63-87.

Assessment of functionality modulation of in-vitro networks using an intra network burst correlation algorithm

E. Biffi^{1*}, A. Menegon², G. Regalia¹, S. Maida², A. Pedrocchi¹, G. Ferrigno¹

¹ Politecnico di Milano, Bioengineering Department, Neuroengineering and Medical Robotics Laboratory, p.zza Leonardo da Vinci 32, 20133 Milano, Italy

² R&D Laboratory, Alembic, San Raffaele Scientific Institute, via Olgettina 60, 20132 Milano, Italy

* Corresponding author. E-mail address: emilia.biffi@mail.polimi.it

Pharmacological modulation of neuronal electrical activity can provide information about networks' mechanism and dynamics. Moreover, it's possible to argue about functional interaction coupling pharmacological approach with correlation analysis and interpreting cross-correlation measures in terms of the underlying physiological mechanisms. Here an intra network burst correlation algorithm is presented to obtain a quantitative synthetic index of the global level of network activity, called *Total Corr*, with the specific goal of high resolution discrimination in network functionalities. *Total Corr* was able to distinguish the effect induced by bicuculline sub-maximal concentration on neuronal electrical activity and to consistently represent the network response during GABA increasing concentrations adding.

1 Introduction

The inability to record intracellular signals from many neurons in-vitro makes the cross-correlation analysis (CC) a useful tool for assessing internal parameters of a neuronal system using extracellular electrical activity recordings [1]. During the last years, important results in neurobiology were obtained exploiting pharmacological neuronal activity modulation [2, 3]. Coupling correlative and pharmacological analysis, networks' maturation mechanism were explored [4, 5], spontaneous and evoked neuronal activity features were deepened [6] and neuronal information processing was studied [7, 8]. Thus, cross-correlation, computed on the whole spike train sequence, is widely used in literature. What is missing in previous works is the definition of a brief parameter summarizing the behaviour of the whole network. Moreover, resumming the effect of a drug addition on cultures, the index should be able to identify, with high resolution, differences in the drug concentration, so as to be adopted in concentration-response curves. The aim of this work is to provide a quantitative unitary index of the global level of network activity by a correlation analysis, using, as testing platform, changes induced by substances modulating the balance between excitatory and inhibitory network level. Specifically, cultures were processed in presence of γ -aminobutyric acid (GABA), the chief inhibitory neurotransmitter in the Central Nervous System, and its competitive antagonist, bicuculline (BIC). As reported in other experiments [2], GABA_A receptor blockade by BIC induces a transition from a native pattern into a

coordinated, rhythmic activity with an increase of firing and burst rates on all units [9].

2 Methods

Neuronal cultures and experimental setup

Cortical neuronal cultures were prepared from mouse embryos at E17. Cortices were mechanically dissociated and plated on MEA biochips (electrode spacing 200 μ m, electrode diameter 30 μ m), treated with poly-L-lysine (1mg/ml). Extracellular recordings were carried out with a MEA1060 signal amplification and data acquisition system (Multi Channel Systems MCS GmbH) at 25kHz. Two pharmacological protocols were developed: in the first one the electrical activity of 10 cortical cultures was recorded at 13 Days in Vitro (DIV). Three sequential 5 minutes recordings of electrical activity were performed for each biochip: the first one was carried out in absence of BIC; then, BIC 1 μ M (sub-maximal concentration; EC50: 0.03-3 μ M) was added. Finally, neuronal activity was recorded in the presence of BIC 20 μ M, a concentration able to induce the maximal unbalancing of the network. The second pharmacological protocol was aimed at production of concentration-response curves, processing one biochip. GABA was added in 7 increasing concentrations and electrical activity was recorded.

Data analysis

Differently from literature, spike train CC analysis was restricted to network bursts (NB), i.e. recurrent events of strong neuronal interaction.

Indeed, during these periods of synchronized firing, neuronal interactions within connected networks become especially apparent [10]. The presented correlation method computes CC first identifying NB sequences as described in [10, 11], then convolving NB spike trains with a Gaussian ($\sigma=0.2$), and finally computing the continuous CC values in $\tau=0$ (a measure of synchronization). To compare correctly the obtained results, CC was computed on surrogates data, for each experimental condition. Surrogates, were generated simulating random NB sharing, with the corresponding experimental data, the number of spikes, but with shuffled interspike interval distribution [12]. *Total Corr*, defined as the median, computed on NB, of the integral of correlation matrix values, normalized by the number of active channels, was selected to be the single parameter representing the global network activity. Two data validation steps followed: first, *Total Corr* values obtained from neuronal recordings, were compared to surrogates using a Mann-Whitney test to corroborate data, as suggested by [13]. Second, non-parametric statistical analysis was performed on the actual values, refined subtracting surrogates CC, to determine the parameter resolution, comparing the three experimental conditions, even in the case of sub-maximal drug concentration. Finally, utilizing *Total Corr* values, a GABA concentration-response curve was realized and non-linear regression was used to fit data in a “variable slope sigmoidal model”. The goodness-of-fit was assessed using the *Coefficient of Determination* R^2 .

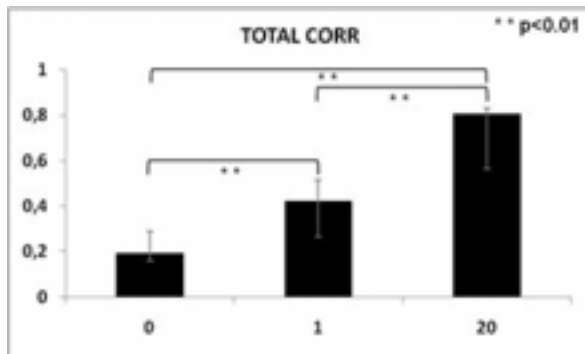


Fig. 1. *Total Corr* values in nominal, BIC 1 μ M and BIC 20 μ M settings: median on 10 cortical cultures.

3 Results

First, Mann-Whitney test recognized significant differences between neuronal and surrogates data ($p<0.01$ for each experimental condition). Second, the method identified differences ($p<0.01$) between the control and the BIC 20 μ M conditions, as in literature [4]. Moreover, it was able to distinguish the 1 μ M setting ($p<0.01$), both from the nominal and the pathological condition (Fig. 1). Finally, Fig. 2 shows

the GABA concentration-response curve obtained with *Total Corr* ($R^2=0.9846$).

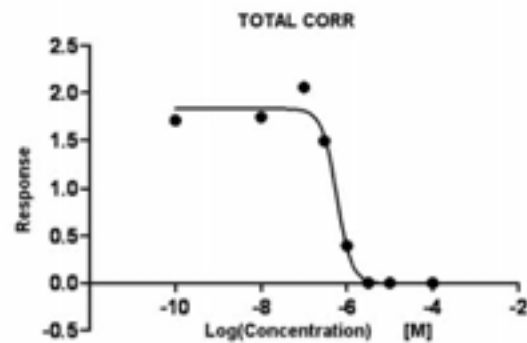


Fig. 2. GABA concentration-response curve ($R^2=0.9846$).

4 Discussion and Conclusion

Results of this work show that an intra NB CC analysis should be a useful method for controlling changes in the correlation structure of a neuronal circuit which reflect changes in its functional connectivity. The defined parameter *Total Corr* showed high statistical significance compared to surrogates data, confirming its reliability. Furthermore, *Total Corr* was able to distinguish the effect induced by pharmacological sub-maximal concentration on neuronal electrical activity. Finally, it was able to consistently represent the network response during GABA increasing concentrations adding.

Acknowledgement

Authors would like to thank dr. Luca Muzio for the critical discussions. The work was developed within the research line - Biosensors and artificial bio-systems – of the convention between the Italian Institute of Technology and Politecnico di Milano.

References

- [1] Knox C.K. (1974). *Biophys. J.*, 14, 567-582.
- [2] Khatami D.B. et al. (2004). *Proc. of the 26th Int. Conf. IEEE EMBS*, 4059-4062.
- [3] Jimbo Y. et al. (2000). *Biol. Cybern.*, 83, 1-20.
- [4] Li X. et al. (2007). *Biosensors and Bioelectronics*, 22, 1538–1543.
- [5] Chiappalone M. et al. (2006). *Brain Res.*, 1093,41-53.
- [6] Eytan D. et al. (2004). *J Neurophysiol.*, 92, 1817–1824.
- [7] Bonifazi P. et al. (2005). *Eur. J. Neurosci.*, 22, 2953–2964.
- [8] Segev R. et al. (2004). *Phys. Rev. Lett.*, 92 (11).
- [9] Gramowski A. et al. (2006). *Eur. J. Neurosci.*, 24, 455–465.
- [10] van Pelt J. et al. (2005). *Prog. Brain Res.*, 147, 173-173-188.
- [11] Chiappalone M. et al. (2005). *Neurocomputing*, 65–66, 653–662.
- [12] Perkel D.H. et al. (1967). *Biophys. J.*, 7, 391-407.
- [13] Theiler J. et al. (1992). *Physica D*, 58, 77-94.

On The Statistics Of Biological Noise And Instrumentation Noise in Active and Inactive Cultures

J.B. Destro-Filho^{1*}, Sergio Martinoia²

¹ School of Electrical Engineering, Federal University of Uberlandia, Brazil.

² Department of Biophysical and Electrical Engineering (DIBE), University of Genoa (UniGe), Genoa, Italy

* Corresponding author. E-mail address: jbdestrof@yahoo.com

MEA signals are composed of instrumentation noise, biological noise, spikes and bursts. These components are present at data arising from active cultures. However, very few is known regarding biological noise and inactive cultures. This paper provides an experimental framework for the statistical characterization and comparison among the four components.

1 Background / Aims

Signals recorded by MEAs are composed of four components: spikes, bursts, biological noise and instrumentation noise. The first and second components are considered the most relevant biological information, so that most of signal processing is devoted to their detection. For this reason, few works in the literature discusses the two other components, especially because their amplitudes are quite low. However, both biological and instrumentation noise influence spike detection, particularly in the context of high-dense MEAs, wherein signal-to-noise ratio decreases dramatically.

The underlying process leading to functional connections between cultured neurons and microelectrodes is not completely clear. Just after the tissue deposition on the planar MEA surface, the ensemble is stored in an incubator. In general, ten days after the deposition, which are labeled as 10th DIV (“Day *In Vitro*”), the culture is connected to the acquisition system, in order to check if functional or anatomical connections between the cells and the microelectrodes have taken place. In this case, signal amplitudes may attain at least 100 μ V during spike activity, firing rates are at least greater than 0.1 spikes/second, and the culture is called “active”. Otherwise, it is called “inactive”.

This abstract aims at establishing differences among the three components of MEA signals, so that to take them into account as spike detection is performed, in the context of both active and inactive cultures.

2 Methods

Primary cultures of rat cortical neurons were prepared based on eighteen-day-embryo tissue extraction, in compliance with the regulations established by the Bioethical Animal Committee of

University of Genoa. Planar sixty-electrode multielectrode arrays (MEAs) were used (*MultichannelSystems, Reutlingen, Germany*). Two different cultures were considered: C1, 41st day in vitro (DIV); C2, 10th DIV. The first one is considered “active”, whereas the second one is “inactive”. Notice that no special procedure was performed to assure the inactive state, since it was an outcome of a natural process.

Four sets of different signals were recorded from these cultures, each of them during 20 minutes, considering a sampling frequency of 10 kHz.

The first set of signals (which will be abbreviated by “S1 – Active”) involves spontaneous electrical activity that normally arises from the culture C1, including spikes and several bursts. The second set of signals (“S2 – Inactive”), are obtained from the inactive culture C2. The third set (“S3 – TTX”) results from recording the same culture as for set S1, but previously adding tetrodotoxin (TTX) to it, so that to minimize spikes and bursts (in fact, almost no bursts were detected for these data). In consequence, this signal just contains biological and instrumentation noise. Finally, the fourth set of signals (“S4 – NoNeurons”) was obtained by turning on all the devices attached to the MEA, which contained no culture at all. In consequence, this last data set contains just instrumentation noise due to the MEA amplifiers.

Each channel signal was segmented based on a one-second rectangular window. For each window, an estimator of the probability density function (PDF) was calculated, considering the signal amplitude [microVolts] as the main random variable. This estimator supposes about $Q = 30$ (thirty) bins, involving amplitudes ranging from -200 microVolts to +200 microVolts, for all the segments. All the histograms were then averaged, leading to the PDF

associated to one single channel (SCPDF). The same procedure was applied to all the other 59 channels, and all the sixty SCPDFs were finally averaged, leading to the “average PDF” (APDF) of the signal set.

Each signal set was then characterized by its average probability density function (APDF), considering all the sixty channels and all the twenty-minute recording length, from which moments of orders one (abbreviated M1x), two (abbreviated M2x), three and four; skewness (Sk) and kurtosis (K) were derived.

3 Results

See Tables 1 and 2

Table 1 – Mean value of the estimated high-order moments associated with the several data sets

	- M1x [μV]	M2x [$(\mu\text{V})^2$]	Sk	K
S1	0.070832	731.1289	-0.1685	1.444644
S2	0.4981	12.6993	-0.0213	0.3903
S3	-0.00332	649.5649	0.001222	-0.01328
S4	0.7709	5.9063	0.0009	0.0167

Table 2 – Variance of the estimated high-order moments associated with the several data sets

	- M1x [μV]	M2x [$(\mu\text{V})^2$]	Sk	K
S1	0,139398	18785,6	0,192724	19,39495
S2	$9,4300 \times 10^{-5}$	3,9151	$5,152 \times 10^{-4}$	0,0374
S3	0,2229	9444,058	8,65E-06	2,61E-05
S4 -	0,0009	0,7709	1,34564E-05	5E-05

Remark: “Variance” written in the first column, regarding lines 3, 5 and 7, regards the variance estimated from the respective high-order moment considering the sixty channels of each recording.

3 Discussions and Conclusions

Amplification noise and biological-noise signal statistics are very close to gaussianity, whereas spikes and bursts present a remarkable non-gaussian character. Signal statistics from inactive cultures may be associated with densities that are neither completely gaussian (as for instrumentation and biological noise), nor non-gaussian (as for spike and bursts). Notice also that the differences between biological and instrumentation noise are very slight, mainly due to the variance of the estimated high-order moments.

In consequence, future work involves the use of more accurate statistical tools, such as high-order correlations and multispectra, to establish differences between the several signals under analysis.

Acknowledgement

We thank CNPq and CAPES for the fellowships funding this project.

References

- [1] Akay, M (2007). *Handbook of neural engineering*. Hoboken, NJ: Wiley Press, 662 p.
- [2] Marom, S.; Shahaf, G. (2002) Development, learning and memory in large random networks of cortical neurons: lessons beyond anatomy. *Quarterly Reviews of Biophysics*, v.35, p.63-87. 2002.
- [3] Taketani, M.; Baudry, M. (2006) *Advances in Network Electrophysiology - Using Multi Electrode Arrays*. New York: Springer Press, 478 p.

Exploring Granger Causality As A Tool For Understanding Connectivity In Patterned Networks

Sankaraleengam Alagapan¹, Liangbin Pan¹, Eric Franca¹, Bruce Wheeler¹, Thomas Demarse^{1*}

¹ J. Crayton Pruitt Family Department of Biomedical Engineering, University of Florida, Gainesville, FL, USA

* Corresponding author. E-mail address: tdemarse@bme.ufl.edu

Granger Causality (GC) has recently been gaining interest in the neuroscience community for its ability to identify functional connectivity primarily in both in vivo and simulated neural systems. However its effectiveness has not been validated due to a lack of unambiguous testable neural system in which connections are known a priori. Here we present an in vitro neural system capitalizing on MEA technology combined with neuronal patterning of cortical neurons to create biological networks with known network topologies. We then validate and refine the Granger Causality metric as a method for determining network's architecture from spike train data.

1 Introduction

In recent years the ever increasing amount of raw neural data has led to the next major challenge facing neuroscience. That is, elucidating the underlying functional connectivity in highly complex networks to understand the relationship between structure and function. This is in part driven by incomplete measures that might clearly identify functional connections from patterns of electrical activity. Granger Causality, a statistical approach originally developed for applications in economics, is one measure that has become popular for identifying both the strength and direction of connections among brain areas implied, for example, by EEG (1), local field potentials (2) (3), and recently from spike trains on MEAs (4). Unfortunately, validation of this metric has primarily been accomplished by comparison to gross anatomical features or via simulated networks. Hence a model of the brain in which the connections and the direction of the connections are known a priori would be a useful tool for evaluating and perhaps improving this measure.

Patterned neuronal networks are one system that partially meets the need for the creation of network topologies whose architecture is known. These are networks in which neurons are constrained to grow in predefined structural patterns on multielectrode arrays(5) for simultaneous measurement of neural activity. These defined networks can be further refined by the addition of microtunnel technology (6) resulting in an overall system in which a complete network topology can be created, and measured.

Here, we report an experiment in which these technologies are combined and then used as test bed to evaluate the accuracy and effectiveness of Granger as a tool to measure functional connectivity. The results of this analysis are compared to traditional correlation methods.

2 Methods

2.1 Conditional Granger Causality and Cross Correlograms

Granger Causality (GC) is a measure to determine the strength and directional influence between two time series. Briefly, if X and Y are 2 time series modeled as autoregressive processes, Y causes X if past observations of Y increases the certainty of prediction of X (7). Furthermore, a technique known as Conditional Granger Causality (CGC) refines structural estimates from GC by removing the contributions from non-causal mediating influences (which cross-correlation methods fail to account for).

2.2 Cell Culture

Microtunnel devices were fabricated from PDMS and consisted of two microwells connected by microtunnels (Fig 1.b.) . These devices were then aligned over MEAs (MCS, Germany) with 60 TiN electrodes such that the entirety of rows 4 and 5 of the MEA were under the microtunnels and the rest under the larger microwells. Cortical cells from E18 Sprague Dawley rats (Brainbits Inc., USA) were first seeded in the bottom microwell and once axons had passed through the microtunnels (10 days), more cortical cells were added to the top well to establish directional connectivity through the tunnels. Network activity was then recorded 10 days later.

2.3 Data Analysis

Spontaneous activity from 5 cultures were recorded using the MEA-1060 BC (MCS Germany). Spikes were detected by threshold crossing (5σ noise). Cross-correlograms were computed between each electrode under the microtunnel as a measure to observe the directionality for comparison to the results from CGC. In the Granger analysis, spike

times were binned at 1ms, smoothed using an exponential function ($\tau = 4$ ms) to produce a continuous waveform, and analyzed using the GCCA toolbox (8). Only the data from the 14 electrodes under the microtunnels are reported in this paper but more results including within well and across well interactions are reported in the poster. *If CGC adequately identifies connectivity, it should be able to detect the directionality along each tunnel, detect connections between the input side and the output side, and unlike cross correlation, eliminate erroneous connections that appear as cross talk between tunnels.*

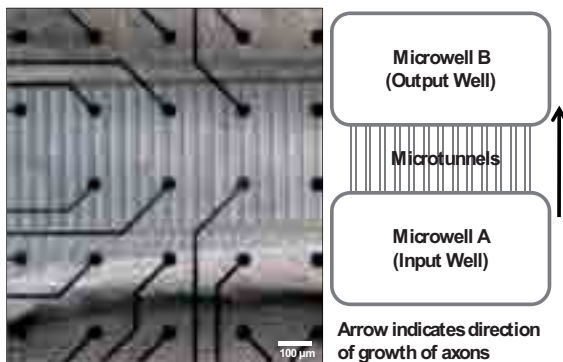


Fig 1. (a) Micrograph of a part of the microtunnel device showing tunnels at the center with neurons in opposing wells; (b) Schematic of the microtunnel device

3 Results

Fig 2a depicts the Granger causality values (colorized) with source and target along the horizontal and vertical axis, respectively. It can be seen that the causal values from electrodes in row 5 to electrodes in row 4 are generally high compared to those from electrodes in row 4 to electrodes in row 5. Fig 2b shows an example to two cross-correlograms along the tunnels over column 8 and 5. In each case a significant peak is seen at positive delays indicating propagation from electrodes in row 5 to electrodes in row 4 under each tunnel consistent with CGC's estimate. There were some cases (about 10%) where propagation was from the top to bottom that was revealed in both cross correlogram analysis (Fig 2b Right) and CGC values (Electrode 84 and Electrode 85 in Fig 2a).

4 Conclusions

Granger analysis on the data from microtunnels shows that GC is effective in determining directionality from neuronal data. Also, CGC is robust to cross talk (data not shown) and eliminates the mediating effect of other external sources which conventional cross-correlogram methods fail to account for. Thus Granger Causality provides a measure to determine the direction of connectivity in neural systems.

Conditional Granger Values Between Electrodes Under Microtunnels

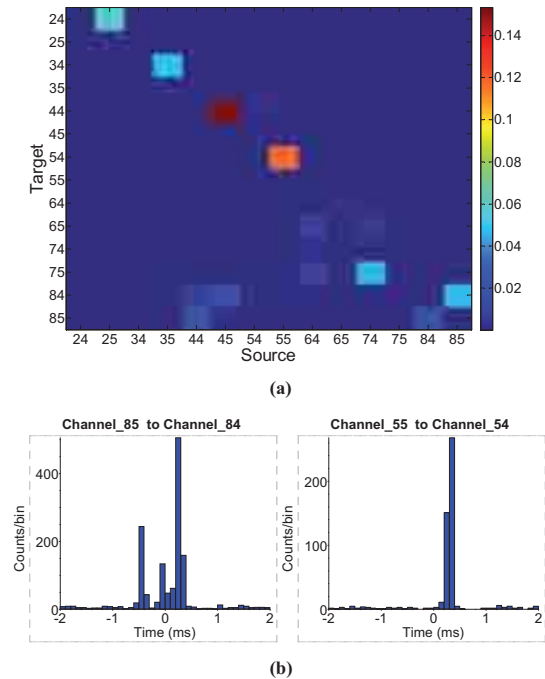


Fig 2. (a) CGC Values between electrodes. Each square represents the G-Causal value between the source electrode denoted (x-axis) to the target location (y-axis). (b) Cross-correlograms for two pairs of electrodes (bin size 0.1 ms). The right graph shows a peak in the negative time indicating propagation in opposite direction

Acknowledgement

This work was partly supported by NIH grant NS052233-05

References

- [1] The use of time-variant EEG Granger causality for inspecting directed interdependencies of neural assemblies. **Hesse W, Möller E, Arnold M, Schack B.** 124, 2003, Journal of Neuroscience Methods, S. 27-44.
- [2] On the directionality of cortical interactions studied by structural analysis of electrophysiological recordings. **Bernasconi, C. & König, P.** 81, 1999, Biological Cybernetics, S. 199-210.
- [3] Beta oscillations in a large-scale sensorimotor cortical network: directional influences revealed by Granger causality. **Brovelli, A., Ding, M., Ledberg, A., Chen, Y., Nakamura, R. & Bressler, S. L.** 101, 2004, Proc Natl Acad Sci U S A, S. 9849-54.
- [4] Causal Measures of Structure and Plasticity in Simulated and Living Neural Networks. **Cadotte AC, DeMarse TD, He PH, Ding MD.** 3:e3355, 2008, PLOS: One.
- [5] Modulation of neural network activity by patterning. **Chang, J.C., Brewer, G.J., and Wheeler, B.C.** 2001, Biosensors and Bioelectronics, Bd. 16, S. 527-533.
- [6] Novel MEA platform with PDMS microtunnels enables the detection of action potential propagation from isolated axons in culture. **Dworak, B.J., Wheeler, B.C.** 2009, Lab on a chip, Bd. 9, S. 404-410.
- [7] **Ding, M., Chen, Y., & Bressler, S.L.** Granger causality: Basic theory and application to neuroscience. [Buchverf.] Winterhalder, N., & Timmer, J. Schelter. S. Handbook of Time Series Analysis. Wienheim : Wiley, 2006.
- [8] *A MATLAB toolbox for Granger causal connectivity analysis.* **Seth, A.K.** 2010, Journal of Neuroscience Methods, Bd. 186, S. 262-273.

Functional Connectivity Maps In Hippocampal Cultures Coupled To High Resolutions MEAs Underlie Structural Connectivity

Alessandro Maccione^{1,*}, Matteo Garofalo¹, Thierry Nieuws¹, Maria Teresa Tedesco², Enrico Commisso², Sergio Martinoia^{1,2} and Luca Berdondini¹

¹ Neuroscience and Brain Technology Department, Italian Institute of Technology, Genova – Italy

² Neuroengineering and Bio-nano Technology Group (NBT), Department of Biophysical and Electronic Engineering (DIBE), University of Genova, Genova – Italy

* Corresponding author. E-mail address: alessandro.maccione@iit.it

Statistical analysis methods applied to electrophysiological signals allow to quantify the information flow through large neuronal assemblies or local micro circuits, providing an estimation of the functional connectivity maps. We applied two methods to low density hippocampal cultures recorded by means of high spatial density Active Pixel Sensor MEAs (APS-MEAs) in order to extract functional links among neurons. We compared these maps with the structure of the networks obtained by immunofluorescence staining techniques.

1 Materials and Methods

1.1 Experimental protocol

Dissociated hippocampal neurons from rat embryos were cultured at a final low cell density ranging from about 100 to 250 cells/mm². Spontaneous spiking activity was recorded after the cultures reached the mature phase (16-20 Days In Vitro) by using APS-MEAs. These high spatial density MEAs [1, 2] enable full-frame acquisitions from 4096 micro-electrodes arranged in a 64 x 64 layout at a spatial resolution of 21 μ m, with a sample rate of 7.8 kHz/channel. After recordings, cultures were fixed and stained with immunofluorescence techniques obtaining topological maps of the network.

1.2 Functional connectivity analysis

Functional Connectivity (FC) maps were extracted by using two approaches previously validated [3]. In addition to the standard Cross-correlation (CC), we applied a dependency-measure across electrodes based on the cross-inter-spike-interval (cISI): the Joint-Entropy (JE). The CC (JE) values were ranked in decreasing (increasing) order to reflect the strongest connections. Spurious connections (false positives) were filtered out by a space-time filter (c.f., Fig.1A) which removed implausible fast connections, i.e. faster than the time delay expected by the maximum propagation velocity (400 mm/s, [4]).

The connectivity maps were built by selecting the strongest causal-relationships inferred by the methods. The estimated functional connectivity maps were superimposed to the fluorescent images (e.g. Fig.2).

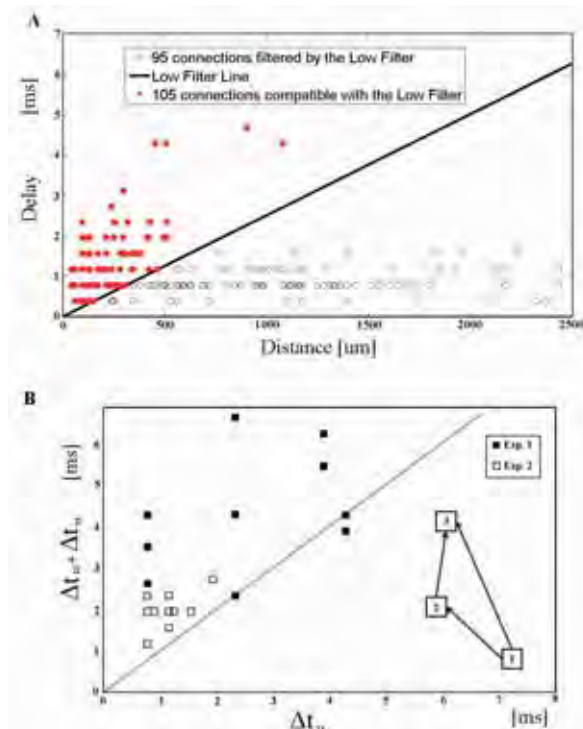


Fig. 1. JE analysis: (A) delay-distance scatter plot of the strongest 200 links. Links compatible with the maximum velocity, i.e. black line, correspond to the red scatter points. (B) Time delay scatter plot. Almost all direct links of the considered microcircuits are causally plausible.

2 Results and Conclusions

2.1 Results

The relationship occurring among the length of the connections, the CC/JE peaks and their delays

provided useful information to refine the FC maps. A spatio-temporal filter (i.e., a Delay-Distance Filter, DDF, Fig.1A) was introduced to select the links compatible with the maximum propagation velocity. The quality of the connectivity maps was tested against the false positive links detected in microcircuits. We focused on the simplest microcircuits (Fig.1B, inset) comprising two direct (1-2, 2-3) and one potential 'indirect' link (1-3). The analysis confirmed that almost all 'indirect' links rather reflected actual direct links. In addition a good correspondence between functional and structural connectivity was found in many situations. Outstandingly, maps reveal a spatial resolution scale not allowed by commercial MEAs and, taking advantage from this evidence, they allow to focus on microcircuits almost at the single cell precision.

2.2 Conclusion and Summary

The use of APS-MEAs coupled with low density culture showed to represent a suitable experimental model to investigate the interplay between FC and structure of the networks (immunofluorescence image). A qualitative comparison of functional and morphological (i.e. structural) connections can be made, underlined by the detection of many microcircuits as well as more global macro-circuits. An example of the effect of the DDF is shown in Fig.2A,B. A close-up on a microcircuit is shown in Fig.2C. The analysis showed that FC methods are able to identify microcircuits which are physiologically plausible based on the estimated time delays.

References

- [1] Imfeld K., Garenne A., Neukom S., Maccione A., Martinoia S., Koudelka-Hep M. and Berdondini L. (2007). High-resolution MEA platform for in-vitro electrogenic cell networks imaging. *Conf Proc IEEE Eng Med Biol Soc*, 2007, 6086-9.
- [2] Berdondini L., Imfeld K., Maccione A., Tedesco M., Neukom S., Koudelka-Hep M. and Martinoia S. (2009). Active pixel sensor array for high spatio-temporal resolution electrophysiological recordings from single cell to large scale neuronal networks. *Lab Chip*, 9,18, 2644-51.
- [3] Garofalo M., Nieuw T., Massobrio P. and Martinoia S. (2009). Evaluation of the performance of information theory-based methods and cross-correlation to estimate the functional connectivity in cortical networks. *PLoS One*, 4,8, e6482.
- [4] Bonifazi P., Ruaro M. E. and Torre V. (2005). Statistical properties of information processing in neuronal networks. *European Journal of Neuroscience*, 22, 12.

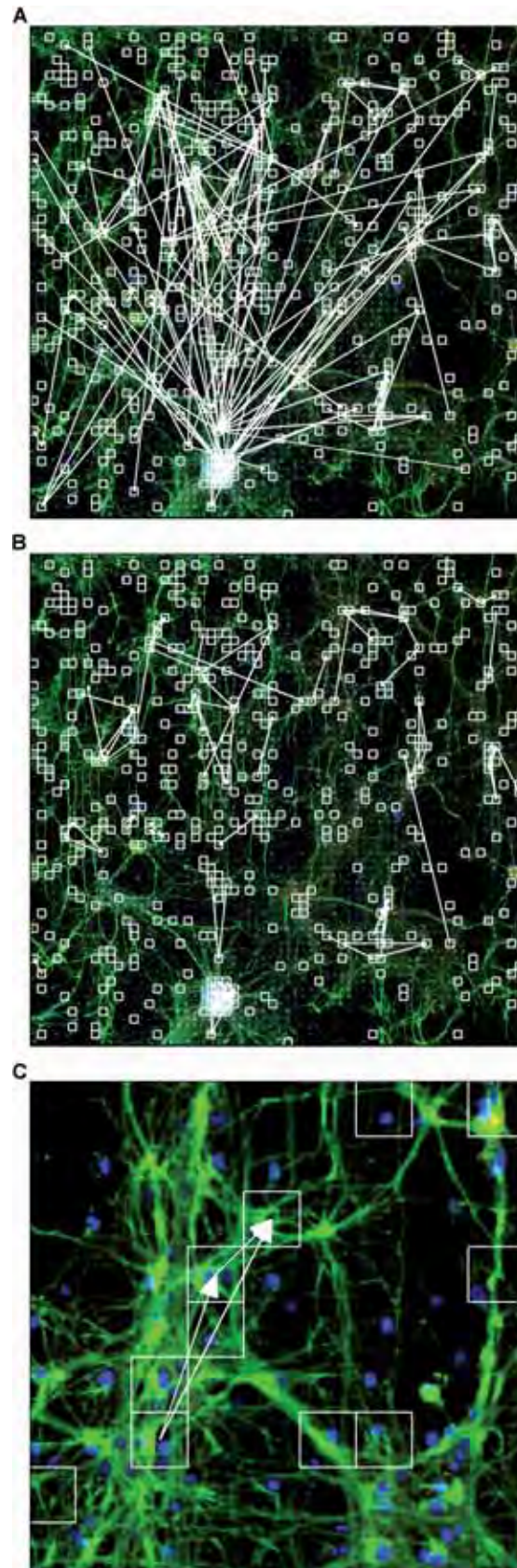


Fig. 2. FC-maps obtained by JE superimposed to the immunofluorescence map. (A) The 200 strongest link, (B) the 105 links compatible with the DDF, (C) close-up on a microcircuit. White squares represent active electrodes.

Investigating neuronal activity by SPYCODE data analyzer

Luca Leonardo Bologna¹, Valentina Pasquale¹, Matteo Garofalo¹, Mauro Gandolfo², Pieter Laurens Baljon², Alessandro Maccione¹, Sergio Martinoia^{2,1}, and Michela Chiappalone^{1*}

¹ Department of Neuroscience and Brain Technology, Italian Institute of Technologies, Genova (Italy)

² Department of Biophysical and Electronic Engineering, University of Genova, Genova (Italy)

* Corresponding author. E-mail address: michela.chiappalone@iit.it

Multichannel acquisition from neuronal networks, either *in vivo* or *in vitro*, is becoming a standard in modern neuroscience in order to infer how cell assemblies communicate. In spite of the large diffusion of Micro-Electrode Array-based systems, researchers usually find it difficult to manage the huge quantity of data routinely recorded during the experimental sessions. In fact, many of the available toolboxes still lack in two fundamental requirements for treating multichannel recordings: (i) a rich repertoire of algorithms for extracting information both at a single channel and at the whole network level; (ii) the capability of autonomously repeat the same set of computational operations to multiple recording streams and without a manual intervention (i.e. 'multiple analysis' approach). Our software package, named SPYCODE, was mainly developed to respond to the above constraints and generally to offer to the scientific community a 'smart' tool for multichannel data processing.

1 Introduction

MEA-based devices are now a well-accepted electrophysiological technique for both *in vivo* and *in vitro* measurements [1-3]. Tens of microelectrodes permanently in contact with electrogenic cells allow monitoring the electrophysiological activity of a cell population for long periods of time. Such a system represents a perfect candidate to routinely record and evaluate the patterns of spontaneous as well as stimulated network behavior. Notwithstanding the widespread use of this technique, there is still a lack of efficient software to manage the large amount of electrophysiological data produced by such multisite recordings.

Among the general-purpose commercially available processing tools (e.g. MC_Rack by Multi Channel Systems, NeuroExplorer and Offline Sorter by Plexon, Conductor and Mobius by Alphamed), there are still no automated tools suitable to manage and support such a large amount of data and with the possibility to easily extend their functionalities. Even if recently a number of scientists have started developing custom-made tools capable to analyze multi electrode data, these tools do not provide the users with a large number of algorithms and they are not able to manage massive quantities of data at a time. These are the main motivations that induced us to develop a new and innovative software package, named SPYCODE which aims at overcoming such limitations. SPYCODE provides a working environment able to perform efficient data management and processing since it incorporates a very rich repertoire of standard and advanced signal analysis tools.

2 Materials and Methods

SPYCODE was written in MATLAB 6.5 and it is compatible with all the following Matlab releases (up to R2008b). Although we have tested it on Microsoft (XP, Vista) and Linux (Ubuntu Jaunty Jackalope 9.04), the software is expected to be compatible with other operating systems within the framework of MATLAB.

3 Results

The SPYCODE software package has been developed through a user-friendly Graphical User Interface (GUI) in which also a non-experienced MATLAB user is able to perform data analysis without knowing the details of the source code [4]. Fig. 1 shows a screen capture of a SPYCODE working session with the GUI running under Windows.

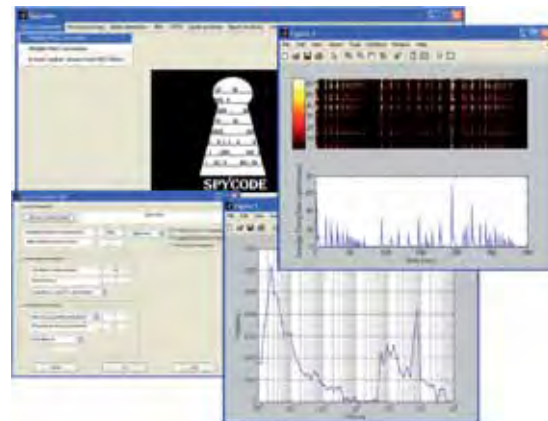


Fig. 1. Running SPYCODE. The main Graphical User Interface (GUI) is depicted during a working session of the software.

The GUI is organized by means of a menu bar, whose detailed structure is reported in Fig. 2. This choice was taken in order to allow the developers to add new functionalities to the software simply by adding new voices or sub-voices to the menu structure. In this way, SPYCODE is a dynamic tool which can easily integrate additional algorithms or modify existing ones, without upsetting the general scheme. The GUI menu is split into sections oriented by function type. The first level consists of eleven menus, namely, ‘Data Conversion’, ‘Pre-processing’, ‘Spike Detection’, ‘Plot’, ‘PSTH’, ‘Spike Analysis’, ‘Burst Analysis’, ‘Cross Correlation’, ‘Additional Tools’, ‘Multiple Analysis’ and ‘Help’. This last one contains a brief documentation on how to use the software.



Fig. 2. The complete structure of the SPYCODE menu.

The ‘Data Conversion’ menu is responsible for data format conversion starting from files recorded by MCS or MED64 system (up to now). The ‘Pre-processing’ menu opens a GUI for selecting the desired filtering option to be applied to the raw data in .mat format. The threshold computation and the shortcuts to two different spike detection procedures are available under the ‘Spike Detection’ voice [5]. The ‘Plot’ menu offers the possibility to plot raw data and raster plot, with the option to add the Average Firing Rate (AFR) profile to the raster. The ‘PSTH’ contains all the voices for calculating the histogram profile, the latencies of the first evoked spikes (for each channel), the area of the histogram and the plot options, including the raster plot in a defined window after the stimulation (i.e. stim raster). In the ‘Spike Analysis’ menu the three functions for analyzing the spike train are provided, while in the ‘Burst Analysis’ two detection methods (i.e. v1 and v2) and the analysis tools are implemented [6]. The ‘Burst Detection v2’ voice offers three additional submenus for the actual detection of bursts by following a new approach, the Inter Burst event Interval (i.e. ‘IBel’) analysis and the Network Burst Detection computation, starting from the burst events. The ‘Cross Correlation’ voice is responsible for the correlogram computation and the plot tools to

visualize the computed histograms. The ‘Additional Tools’ contains the shortcuts to the GUI for the Avalanche Detection and Analysis, the Information Theory Methods and the Shuffling Methods. Finally, the last voice ‘Multiple Analysis’ is responsible of the GUI for selecting the experiments on which the user wants to performs the same set of analysis (Fig. 3).

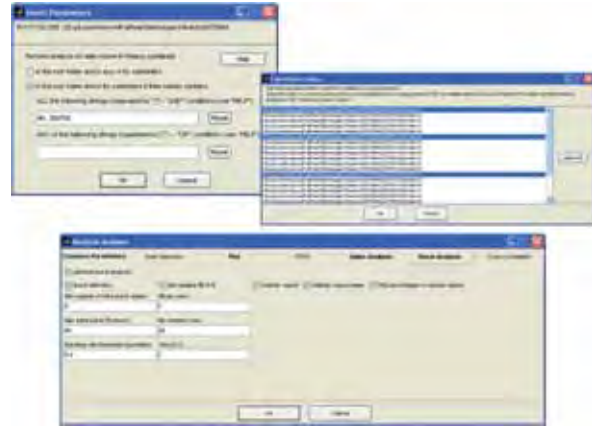


Fig. 3. Multiple analysis GUIs.

4 Conclusions

SPYCODE provides a working environment able to perform efficient data management and processing since it incorporates a very rich repertoire of standard and advanced signal analysis tools, such as burst detection, network burst detection, cross-correlation analysis, information theory methods, connectivity maps and avalanche detection and analysis.

Acknowledgement

The authors would like to thank all the people that, in the course of the years, have given a significant help in inspiring and developing the actual version of the proposed software: Massimo Grattarola, Marco Bove, Giovanni Verreschi, Alessandro Vato, Laura Cozzi, Nicola Rosso and Antonio Novellino.

References

- [1] G. Buzsaki, (2004): Large-scale recording of neuronal ensembles, *Nature Neuroscience*, 7, 446-451.
- [2] T. J. Blanche, M. A. Spacek, J. F. Hetke *et al.*, (2005): Polytrodes: high-density silicon electrode arrays for large-scale multiunit recording, *Journal of Neurophysiology*, 93, 2987-3000.
- [3] A. Minerbi, R. Kahana, L. Goldfeld *et al.*, (2009): Long-term relationship between synaptic tenacity, synaptic remodeling, and network activity, *PLoS Biology*, 7.
- [4] L. L. Bologna, V. Pasquale, M. Garofalo *et al.*, (2010): Investigating neuronal activity by SPYCODE multichannel data analyzer, *Neural Networks* (10.1016/j.neunet.2010.05.002)
- [5] A. Maccione, M. Gandolfo, P. Massobrio *et al.*, (2009): A novel spike detection algorithm for real time applications, *Journal of Neuroscience Methods*, 177, 241-249.
- [6] V. Pasquale, S. Martinoia, and M. Chiappalone, (2009): A self-adapting approach for the detection of bursts and network bursts in neuronal cultures, *Journal of Computational Neuroscience* (10.1007/s10827-009-0175-1).

Adaptive algorithms for burst and network burst detection

Valentina Pasquale^{1*}, Sergio Martinoia^{2,1} and Michela Chiappalone¹

¹ Department of Neuroscience and Brain Technologies, Italian Institute of Technology, Genova (Italy)

² Department of Biophysical and Electronic Engineering, University of Genova, Genova (Italy)

* Corresponding author. E-mail address: valentina.pasquale@iit.it

To study bursting patterns, propagation and synchronicity in neuronal networks cultured *in vitro* it is an essential pre-requisite to have efficient and reliable burst and network burst detection methods. The study presented here aimed at designing adaptive algorithms capable of revealing changes in the bursts' and network bursts' features due to different experimental conditions.

1 Introduction

Neurons dissociated from the original tissue, cultured *ex vivo* and coupled to Micro-Electrode Array (MEA) devices represent a good experimental model for studying basic electrophysiological properties of the nervous system. Generally, the spontaneous activity emerging from such cultured networks ranges from stochastic spiking to organized bursting and this activity pattern is modulated during the *in vitro* development or by pharmacological as well as electrical manipulation.

Bursting is a peculiar feature of isolated neural systems (i.e. systems that lack sensory inputs). A *burst* consists of a fast sequence of spikes recorded by a single electrode of the array; in *in vitro* neural preparations bursts usually appear at all channels at the same time, a phenomenon described in the literature with the name of *network burst* [1]. Several methods have been proposed in the literature for burst detection and analysis, either for *in vitro* or *in vivo* recordings [2-5]. Unfortunately most of them are largely user-dependent and require to set a number of parameters. For these reasons, we developed new algorithms able to automatically detect the best parameters to achieve optimal detection of bursts and network bursts in different experimental conditions.

We validated our algorithms on recordings from primary cultures of rat cortical neurons either spontaneously active or chemically stimulated with bicuculline or APV.

2 Materials and Methods

2.1 Culture preparation

Cortical neurons extracted from rat embryos (E18) were cultured on planar arrays of 60 TiN/SiN electrodes (MultiChannel Systems, Reutlingen,

Germany), pre-treated with adhesion factors (Poli-D-Lysine and Laminin). In two cultures, we applied either bicuculline (BIC, 30 μ M) or *D*-2-amino-5-phosphonopentanoic acid (APV, 25 μ M).

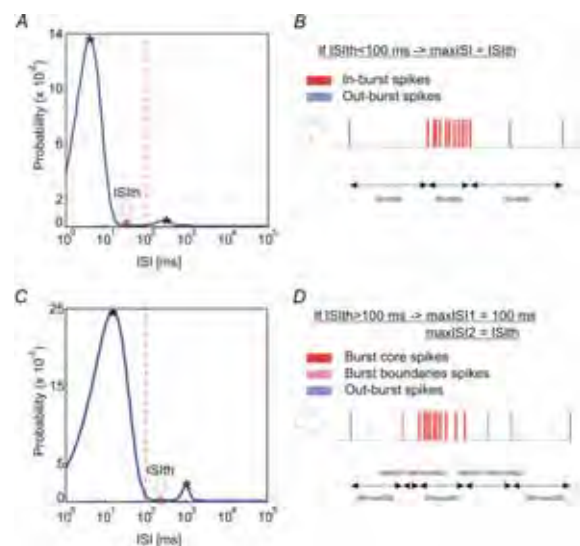


Fig. 1. Sketch illustrating the BD method: the parameters of the algorithm are chosen according to the logISIh, independently for each recording channel.

2.2 Algorithms' description

Burst detection (BD)

The new BD method exploits the logarithmic inter-spoke interval histogram (logISIh) to extract the parameters needed for the analysis independently for each recording channel (see Fig. 1).

In the logISIh data are binned in equally spaced windows of $\log_{10}(\text{ISI})$. The identification of the two principal peaks in the ISI histogram and the minimum value between them provides a simple way to define the ISI threshold (ISIth) that best separates intra-burst ISI from inter-burst [2]. Unfortunately, the frequent

presence of more than two peaks in the logISIH makes it difficult to correctly identify the IS_Ith, even for an expert observer. Hence, we devised a procedure able to deal with *noisy* logISIH, in order to separate different firing modalities.

According to previously developed BD methods [3], spike bursts are defined as sequences of at least n consecutive spikes (usually $n = 5$) spaced less than a convenient time threshold. Our new algorithm estimates the best threshold from the logISIH, independently for each channel, and distinguishes between different cases (see Fig. 1), in order to optimally handle different bursting patterns (e.g. very short and compact bursts, or long-tailed and spread bursts) [6].

Network burst detection (NBD)

To detect network bursts, we considered the *cumulative burst event train*, namely the sequence of all the initial spikes of each burst in the array and we computed the logarithmic inter-burst event interval histogram (logIBeIH). In this way, we are able to highlight the presence of two distinct peaks, the former corresponding to short intervals within network bursts and the latter to long intervals between network bursts.

Hence, the same approach developed for the detection of spike bursts can be potentially applied to the NBD, starting from the cumulative burst event train: we have only to set two thresholds, first the maximum inter-burst event interval for burst events within a network burst (maxIBeI) and second the minimum percentage of recording electrodes involved in a network burst. The maxIBeI is set according to the IBeI threshold extracted from the logIBeIH.

3 Results

We evaluated the performance of our BD algorithm by comparing it with several other methods, either proposed for *in vitro* or *in vivo* recordings, namely the Gourévitch-Eggermont (GE) algorithm [5], the Wagenaar (WA) one [4], the Chiappalone (CH) one [3], and, finally, the Selinger (SE) one [2] (Fig.2). Moreover, we compared our NBD algorithm with the one proposed by van Pelt and collaborators [1] (data not shown). For this purpose we took into consideration two chemical stimulation experiments (i.e. BIC and APV), in which the variations in the bursting pattern are strongly evident, and we measured mean bursting rate and burst duration (mean±S.E.M.).

Our method, when compared to visual inspection and also to other methods, allowed to correctly detect both very long and spread bursts induced by BIC stimulation and short and compact bursts, as present during APV administration.

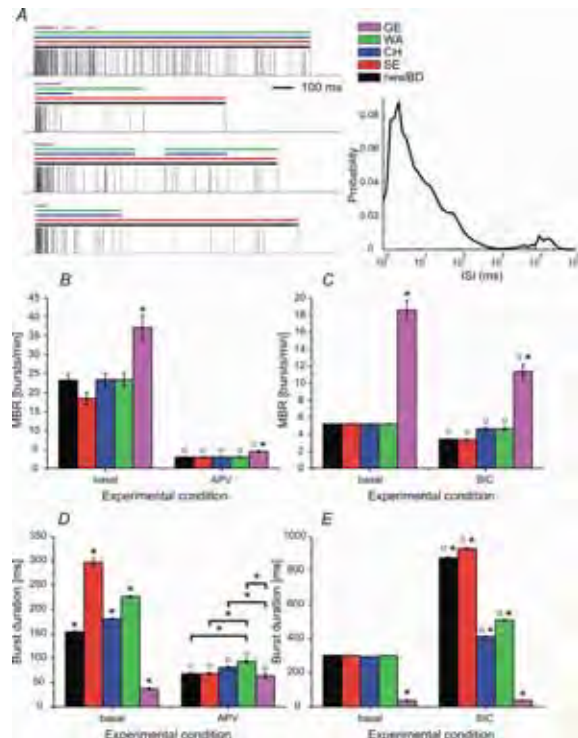


Fig. 2. Testing the new BD algorithm on chemical stimulation experiments A, Visual comparison of the output of different BD algorithms on the BIC experiment. B, C, Mean bursting rate. D, E, Burst duration.

4 Conclusions

We designed new algorithms to optimally detect bursts and network bursts in *in vitro* recordings from MEAs by automatically adapting the parameters to different bursting patterns, e.g. induced by chemical stimulation. Moreover, these algorithms are fully automated and able to manage a large amount of data.

References

- [1] van Pelt J., Corner M.A., Wolters P.S., Rutten W.L.C., Ramakers G.J.A. (2004). Long-term stability and developmental changes in spontaneous network burst firing patterns in dissociated rat cerebral cortex cell cultures on multi-electrode arrays. *Neuroscience Letters*, 361,1-3, 86-89.
- [2] Selinger J.V., Kulagina N.V., O'Shaughnessy T.J., Ma W., Pancrazio J.J. (2007). Methods for characterizing interspike intervals and identifying bursts in neuronal activity. *Journal of Neuroscience Methods*, 162, 64-71.
- [3] Chiappalone M., Novellino A., Vajda I., Vato A., Martinoia S., van Pelt J. (2005). Burst detection algorithms for the analysis of spatio-temporal patterns in cortical networks of neurons. *Neurocomputing*, 65-66, 653-662.
- [4] Wagenaar D.A., DeMarse T.B., Potter S.M. (2005). MeaBench: A toolset for multi-electrode data acquisition and on-line analysis. 2nd Intl. IEEE EMBS Conference on Neural Engineering, Washington, D.C., USA.
- [5] Gourevitch B., Eggermont J.J. (2007). A nonparametric approach for detection of bursts in spike trains. *Journal of Neuroscience Methods*, 160, 349-358.
- [6] Pasquale V., Chiappalone M., Martinoia S. (2009). A self-adapting approach for the detection of bursts and network bursts in cortical cultures *in vitro*. *Journal of Computational Neuroscience*, DOI: 10.1007/s10827-009-0175-1.

Simple Model of a Neuronal Network Reproducing Synchronous Bursts

Masaki Nomura^{1,2*}, Daisuke Ito³, Kazutoshi Gohara³, Toshio Aoyagi^{2,4}

¹ Department of Mathematics, Kyoto University, Kyoto (Japan)

² JST, CREST, Tokyo (Japan)

³ Division of Applied Physics, Hokkaido University, Sapporo (Japan)

⁴ Department of Applied Analysis and Complex Dynamical Systems, Kyoto University, Kyoto (Japan)

* Corresponding author. E-mail address: mnomura@math.kyoto-u.ac.jp

We give a simple neuronal network model that can produce synchronous burst activities. In the model, synaptic weights come from a Bayesian estimation applied to burst activities recorded from cultured neurons. The weight matrix is well balanced between excitation and inhibition. By simulating the system, we found that the synchronous burst activities can emerge stochastically in some parameter ranges, but hardly emerge if the connection matrix is shuffled. Our modelling study suggests that the network structure, the balance between excitation and inhibition, and the signal integration in the synaptic time window and/or in the dendrite are important factors in emerging the synchronous burst activities.

1 Introduction

Synchronous bursts in the early developing stage have received wide attention. They have been observed both in *in-vivo* and *in-vitro* experiments, and discussed about their functional roles [1][2][3][4]. Indeed they can play important roles in organizing a local neuronal network by so-called spike-timing dependent plasticity. Synchrony between neuronal activities has been considered as a candidate for encoding behavioral information. And then, understanding network structure that causes synchronous activities is essential to get to know information processing in brain. Interestingly, self-organized spindle oscillations are observed in a developing somatosensory cortex, and it is suggested that they are required for forming a somatotopic cortical map [2]. Although it is difficult to investigate a network structure that causes such a burst activity *in-vivo*, synchronous bursts are frequently observed on developing cultured neurons, and we hope that some insights can be obtained from *in-vitro*. In this paper, we present a simple model that can produce synchronous bursts whose network structure was estimated from data recorded on cultured neurons while they fired synchronously by using a dynamic Bayesian method [3].

2 Methods

Population spike trains were recorded from cultured dissociated neurons derived from rat cortex (17-day old embryos, SUMITOMO BAKELITE Co., LTD., Tokyo, Japan) on poly (ethyleneimine)-coated multi-electrode arrays (MEAs), where the distance between adjacent electrodes is 150 μm . The dissociated cells were plated on 64 electrode planar

MEAs (Alpha MED Scientific, Osaka, Japan) at a density of 500 cells/mm². The cells were maintained at 37°C in a humidified atmosphere of 5% CO₂ and cultured for 35 days in Neuron Culture Medium (SUMITOMO BAKELITE Co., Tokyo, Japan). Half of the culture medium was changed once a week. Spontaneous electrical activity was recorded at 35 days *in-vitro* (DIV) for 5 minutes with a sampling rate of 20 kHz using MED 64 system (Alpha MED Scientific).

Spikes were detected at each electrode by thresholding based on noise level. Even in the low density culture condition, the network seemed to form very complicated structures, and showed synchronous burst activities (Fig. 1). This result suggests that the intrinsic features of the neurons are retained in low-density culture.

To clarify the morphological properties of the network in detail, after recording neuronal activities, we performed immunocytochemistry of the neurons. Cells were fixed with 4% formaldehyde in a PBS and permeabilized with 0.5% TritonX-100 in a PBS. The cells were then incubated with 5% goat serum (GS)/PBS and with primary antibodies overnight. After washing with PBS, the cells were incubated with secondary antibodies for 1 hour and washed again. The network was visualized with staining the cells with antibodies to MAP2 and to neurofilament 200 (NF200) to identify neuronal cell bodies, and dendrites and axons, respectively. Fluorescence images were taken using a PhC microscope (Olympus IX-71) that was used for fluorescence observations. The network structure was visible by low-density cultivation (Figs. 2).

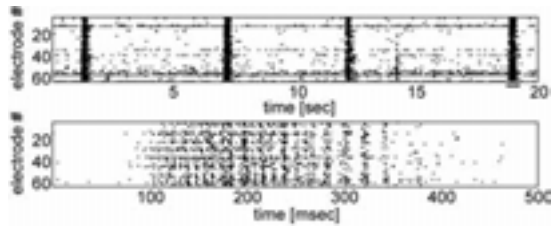


Fig. 1. Raster plots of synchronous burst activities. The last burst is enlarged in the lower figure. Using the last burst data we estimated the synaptic weight matrix.

Because there were only a small number of neurons on a single electrode, and we were considering only the rough architecture of the cultured network, we confined the connectivity to between electrodes. We estimated the intrinsic firing rate of the i -th electrode, θ_i , and the weight of the connection from the electrodes j to i , β_{ij} , with applying a dynamic Bayesian method to the last burst data [3].

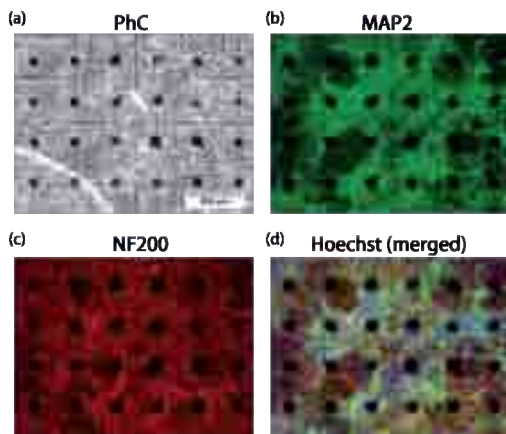


Fig. 2. Immunocytochemistry micrograph of neuronal network on MEAs. (a) Somata and dendrites were stained with antibodies to MAP2: 5 $\mu\text{g}/\text{mL}$ anti-MAP2 mouse IgG (Sigma). 0.4% Alexa Fluor 488 anti-mouse IgG (molecular probes). (b) Axons were stained with Neurofilament 200 (NF200): 5 $\mu\text{g}/\text{mL}$ anti-Neurofilament 200 rabbit IgG (Sigma). 0.4% Alexa Fluor 546 anti-rabbit IgG (molecular probes). (c) Cell nuclei were stained with Hoechst 33342: 2 $\mu\text{g}/\text{mL}$ Hoechst 33342.

3 Results

The estimated parameters are shown in Fig. 3. Using these parameter values except that we strengthened the excitatory weight by a factor of 1.12 times, we evolved the network from an initial condition where all the electrodes are silent. At first, the electrodes fired by themselves according to their intrinsic firing rates. Then, they fired synchronously at times (Fig. 4). Next, we prepared weight matrices by shuffling the estimated one, and evolved the network with them. In these trials, we hardly observed the clear synchronous bursts. We also found that increasing the intrinsic firing rate can cause synchronous burst activities, but whose characteristic is different from one induced by modifying the

connection strength. Finally, we confirmed that when signal integration in time was removed from the model, synchronous bursts never occurred. Our modelling study suggests that the network structure, the balance between excitation and inhibition, the intrinsic firing rate and the signal integration in the synaptic and/or membrane time window are important factors in emerging the synchronous burst activities.

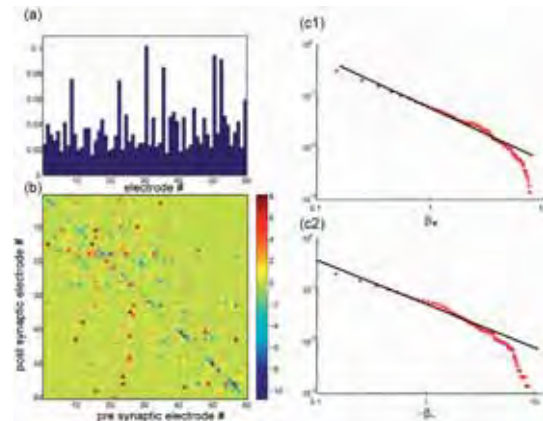


Fig. 3. (a) Intrinsic firing probability of electrodes. (b) Weight matrix between electrodes. (c1)(c2) Cumulative distribution of excitatory (c1) and inhibitory (c2) weights. The red dots are calculated from weight matrix β , and the black lines indicate power law distributions fitted to the data by using the Hill's estimation.

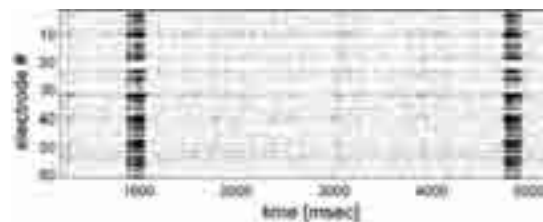


Fig. 4. Synchronous burst activities obtained by simulating the model. Here, we strengthened the excitatory connection by a factor of 1.12 times from the estimated value.

Acknowledgement

This work was supported by KAKENHI (22700321).

References

- [1] Maeda, E., Robinson, H. P. & Kawana, A. (1995) The Mechanisms of Generation and Propagation of Synchronized Bursting in Developing Networks of Cortical Neurons, *J. Neurosci.* **15**(10), 6834-6845.
- [2] Khazipov, R. & Luhmann, H. J. (2006) Early patterns of electrical activity in the developing cerebral cortex of humans and rodents, *Trends in Neurosciences* **29**(7), 414-418.
- [3] Rigat, F., de Gunst, M. & van Pelt, J. (2006) Bayesian Modelling and Analysis of Spatio-Temporal Neuronal Networks, *Bayesian Analysis* **1**(4), 733-764.
- [4] Bettencourt, L. M., Stephens, G. J., Ham, M. I. & Gross, G. W. (2007) Functional structure of cortical neuronal networks grown *in vitro*, *Phys. Rev. E* **75**(2), 021915.

Online Spike Extraction for Bidirectional High-Density Microelectrode Arrays using Optimal Filters

David Jäckel¹, Urs Frey², Jan Müller¹, Ian Jones¹, Muhammad Usman Khalid¹, Jan Sedivy³, Andreas Hierlemann¹

¹ ETH Zurich, Department Biosystems Science and Engineering, 4058 Basel, Switzerland.

² Bio ETH Zurich, Department Biosystems Science and Engineering, 4058 Basel, Switzerland. now at IBM Research, Zurich, Switzerland.

³ Department of Measurement, Czech Technical University, Prague, Czech Republic.

Optimal filtering is an established method for the simultaneous detection and classification of neuronal action potentials. In this paper we demonstrate the potential of this method, in combination with a bidirectional high-density microelectrode array, for real-time spike sorting also in presence for overlapping spikes. The high spatial density allows for selecting the electrodes that provide the best filtering performance.

1 Background

The CMOS-based high-density microelectrode array (HD-MEA) [1] is a highly suitable device for analyzing neuronal networks in vitro, since it allows to arbitrarily select electrodes from a large array for recording and stimulation.

Closed-loop experiments, where a feedback stimulus can be applied in response to specific activity patterns, are crucial to study behaviour, learning and memory in neuronal networks. The closed-loop approach requires real-time sorting techniques, where spike trains are available within milliseconds and where the maximum delays are exactly known and defined.

2 Methods

2.1 HD-MEA System

The HD-MEA features 11'011 metal electrodes on an area of 1.75 x 2.0 mm², up to 126 of which can be simultaneously accessed through bidirectional on-chip circuitry channels. A flexible switch matrix underneath the array connects the channel circuitry units with the electrodes. The data are pre-processed on an FPGA before being stored on a PC.

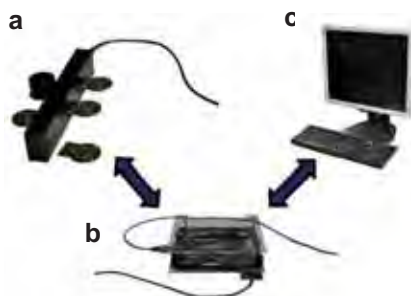


Fig. 1. Main components of the HD-MEA system: (a) Recording MEA chips (b) FPGA (c) Computer.

2.2 Optimal Filtering

Spike extraction is performed using optimal linear filters (OFs). These filters maximize the output for desired signals (spikes of the targeted neuron) and minimize it for undesired signals, which include spikes from other neurons and noise. The problem of spike detection is thereby reduced to simple threshold detection of the filter outputs.

The spike-triggered average waveforms (Figures 2a and 4a) are used as templates to calculate a multi-channel OF for every neuron. The filter coefficients are derived in the frequency domain (see [2, 3]).

As the number of recording channels is limited, the best electrodes for differentiating between certain cells are selected considering the following factors:

1. The energy of the neuron's template on that electrode.
2. Linear dependence between the templates implicates that non-matching templates cannot be completely suppressed, which leads to undesired peaks in the filter response (Figure 2c). The ratio between the first and the second (unwanted) peak value can be seen as a measure of separation quality and as a measure of non-linearity between the templates.

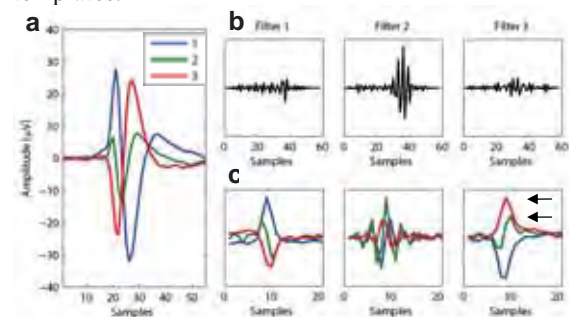


Fig. 2. (a) Templates of three neurons on one electrode (b) Corresponding OFs (c) Normalized responses of the respective filters to the templates. The blue line represents the response to the blue, the green line the response to the green and the red line the response to the red neuronal signal template. The arrows indicate the 1st and 2nd (undesired) peak.

2.3 Overall Sorting Process

The overall spike sorting process is divided into two steps (Figure 3), a first detection step, where the array is scanned at highest spatial resolution and the neurons are identified with an offline spike sorting algorithm. The OFs are calculated, and the electrodes with the best discrimination performance are selected for further read-out. The second step then consists of filtering the data and performing event detection on the filter outputs.

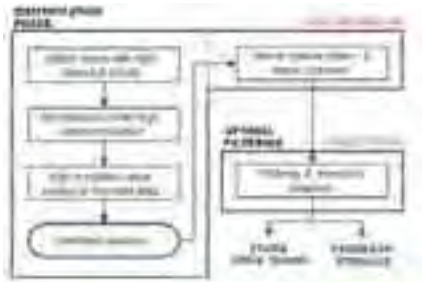


Fig. 3. Proposed algorithm for neuron identification and online spike extraction.

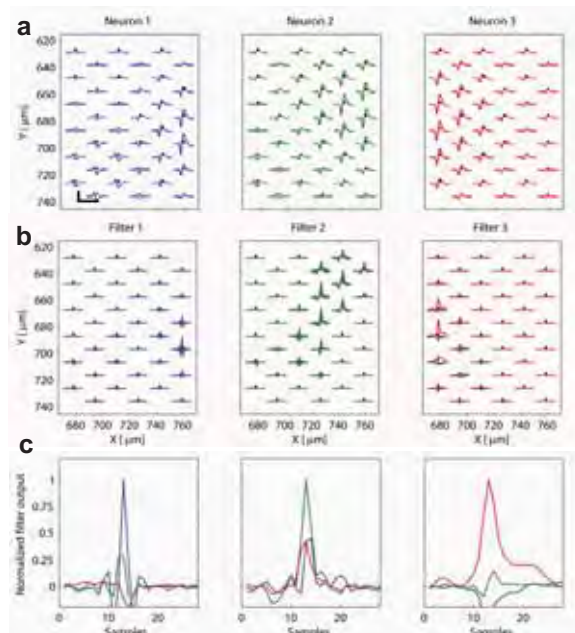


Fig. 4. (a) Spatial distribution of the templates of three identified neurons, which exhibit characteristic cell-specific signatures. Scale bar $80\mu\text{V}$, 1.9ms . (b) Responses of the OFs to the templates, shown for the individual electrodes. The coefficients of ‘low quality’ filters were set to zero. (c) Overall filter responses to the templates. Due to the linear dependence of the templates, the output of, e.g., Filter 2 to the blue neuron is not zero. This crosstalk can be reduced by decorrelation of the filter outputs.

3 Results

3.1 Data Example

We identified three neuronal units by spike sorting of high-density recordings from acute cerebellar slices of rats (Figure 4a). The responses of the OF to the templates demonstrate the filter

efficiency (Figures 4b and 4c). The spatial distributions of the filter responses indicate that some electrodes contribute significantly more to the output peak than others.

3.2 Evaluation with simulated data

A simulated data set featuring four neurons in an electrode block was generated in order to evaluate the OF performance for overlapping spikes. Even though the waveforms of the neurons change due to the overlaps (Figure 5a), the OF are capable of reliably extracting the spike trains (Figure 5b).

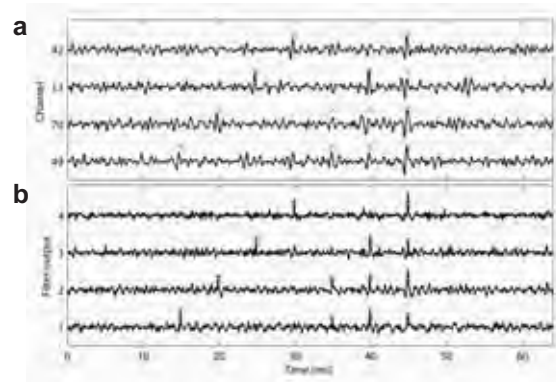


Fig. 5. Overlap detection for a set of four simulated neurons. The four signals in (a) and (b) correspond to the four neurons, the red cross indicates that the particular neuron produced a spike. (a) Raw (simulated) signal at the electrode with the highest amplitude for every neuron. It can be seen that the overlaps cause a change in the spike shape. (b) Output after optimal filtering for every neuron. Even if all four neurons fire simultaneously, the outputs show clear peaks.

4 Conclusions

OF in combination with HD-MEAs present a reliable and promising method for online spike extraction, also in the presence of overlapping spikes. The flexibility of the HD-MEA allows for optimizing the filtering performance by selecting the electrodes that produce the best filter output. Only a fraction of the electrodes produce high peak responses, which underlines the importance of high spatial resolution.

The filters will be implemented into the FPGA to exploit the parallel nature of the FPGA, with the aim to obtain real-time spike extraction with minimal latencies for closed-loop experiments.

References

- [1] Frey, U., et al., *Microelectronic system for high-resolution mapping of extracellular electric fields applied to brain slices*. *Biosensors and Bioelectronics*, 2009. 24(7): p. 2191-8.
- [2] Daniel K. Hartline William M. Roberts. *Separation of multi-unit nerve impulse trains by a multi-channel linear filter algorithm*. *Brain Research*, 1975. 94(1): p.141-149.
- [3] S. N. Gozani and J. P. Miller. *Optimal discrimination and classification of neuronal action potential waveforms from multiunit, multichannel recordings using software-based linear filters*. *Biomedical Engineering, IEEE Transactions on*, 1994. 41(4):358-372.

A Comprehensive and Efficient Python-based Framework for the Processing of Spiking Activity Data in MEA recordings

Maffezzoli Andrea^{1*}, Wanke Enzo¹

¹ Department of Biotechnologies and Biosciences, University of Milano-Bicocca, Milan (Italy)

* Corresponding author. E-mail address: andrea.maffezzoli@unimib.it

Nowadays the need of a dedicated and efficient framework to process MEA recordings data, storing the dynamics of neuronal networks following a precise multi-channel structure in often huge dimension files, became more than ever stringent, especially if taking in account the arrival of the very promising technology with 256, or more in the next, electrodes. In this contest we introduce our work, consisting in the active development of a software written in the Python programming language able to perform and furnish to neuroscientists a comprehensive MEA data processing framework.

1 Background/Aims

We pursued the development of a software not only able to work on the various formats in which commercial MEA instrumentation companies store experimental recordings data, but which also implements without the need of external libraries a number of quantitative methods for the statistical analysis and pattern recognition, finally resulting in a simple-to-use, complete, and at the present time almost unique as far as authors know, toolkit which researchers can readily apply on MEA recordings of spikes timestamps or Local Field Potential (LFP), in order to extract new meaningful information about the concerted activity of in-vitro neurons populations.

2 Methods/Statistics

We start by a file import stage: actually we can read properly files in Plexon® or Neuroexplorer® formats, where timestamps data of spiking activity are stored, and, if in the second format, also the channels voltage traces of LFP recordings, both from 64 or 256 channels acquisitions. Then we continue with data processing: our attention has been focused to the analysis of bursts patterns, in single neurons or the entire population, where in the latter bursts are considered as network-wide phenomena. We can do burst detection in two different flavors: for single neurons as in Neuroexplorer®, for network bursts following (Ham, et al., 2008). Statistical analyses on burst patterns consists of descriptive statistical information, e.g. various orders moments, spike rate (SR), Inter Burst Spike Rate (IBSR), Fano Factor (FF) or Coefficient-of-Variation (CV), Auto-Correlation (AC) of single spiking traces, time of half AC when in its decaying phase (ACHL), also applying on these a dimensional reduction techniques, as Principal Component Analysis (PCA). Such methods extract a

rich set of common features about bursts patterns, which we use to group neurons based on some similarity criterion: at present, after having found a sub-space of most significant burst features via PCA, we classify neurons via a k-means clustering algorithm, given a previously user-defined number of classes. We note that, apart bursts, such techniques can be extended to a wider range of spikes patterns without much of efforts. Parallel to the single neurons approach, we can do an analysis where bursts are intended as a network phenomenon generated from the • simultaneous neurons concerted activity. Here the burst structure is extracted as in (Ham, et al., 2008) with a scanning window searching for the start and the end of each burst, collecting the timestamps counting function of all spikes fired during such event: from this histogram function we derive the SR of all the neurons (cSR), the number of spikes as a function of delay from the burst start ($N(t)$), and all such measures can be distinguished for each cluster found through the previous k-means procedure, so linking the two different burst analysis approaches. Finally when studying LFP data, we usually perform sub-sampling and filtering operations in order to extract only the most meaningful information from data and focus on the neurophysiological processes of our interest. Then we proceed with a Cross-Correlation (CC) analysis on all the pairs of traces from adjacent channels, at the same time reconstructing for each channel the spikes counting function during each LFP.

3 Results

The unsupervised classification learnt via the clustering procedure is well suited to be tested versus physiological knowledge: at the top of hierarchy obtained we discerned excitatory neurons from inhibitory ones, and further we clearly recognized

classes distinguished by other biological characteristics, experimental stimuli or drug applications responses, as properly discussed in (Gullo, et al., 2009). Not only, but when applying the same classification on results from data collected from burst patterns studied in the network approach, and comparing them, we gained new hints about the different response to stimuli and variability in behavior of excitatory versus inhibitory neurons. In particular the last analysis confirms the role of population bursts as being at the basis of mechanisms of membrane excitability and neurons population synchronization, as thoroughly explained on (Gullo, et al., 2010).

4 Conclusion/Summary

Thanks to our framework with its set of statistics techniques applied on temporal patterns of bursts, we can discern classes of neurons well matching various biological families, starting from ensemble activity recorded on MEA. We are so able to extract very significant, but previously hidden, features from the visible spiking activity of single neurons, from the bursts considered as unitary network events and from the LFP voltage traces, so furnishing a comprehensive and valid tools towards a better understanding of the rich facets of neuronal activities. Finally we like to remark that, as confirmed by the very widespread use of Python in scientific programming and in Neuroscience, see (Spacek, et al, 2009), the choice of this language returned us not only appreciable processing performances and efficiencies, but also make usual jobs as refactoring, expansion to new modules or interfacing to external ones an easy and no time-consuming operation.

References

- [1] Ham MI, Bettencourt LM, McDaniel FD, Gross GW. Spontaneous coordinated activity in cultured networks: analysis of multiple ignition sites, primary circuits, and burst phase delay distributions. *J Comput Neurosci.* 2008 Jun; 24(3): 346-57.
- [2] Gullo F, Maffezzoli A, Dossi E, Wanke E. Short-latency cross- and autocorrelation identify clusters of interacting cortical neurons recorded from multi-electrode array. *Journal of Neuroscience Methods* 181 (2009), pp. 186-198.
- [3] Gullo F, Mazzetti S, Maffezzoli A, et al. Orchestration of “presto” and “largo” synchrony in up-down activity of cortical networks. *Frontiers in Neural Circuits*, 2010, Vol. 4, No. 11.
- [4] Spacek MA, Blanche TJ, Swindale NV. Python for large-scale electrophysiology, *Front. Neuroinform.* 2 (9), 2009.

Epileptiform Firing Characteristics in Hippocampal Slices

Zhang Pu-Ming^{1*}, Gong Xin-Wei¹, Yang Fan², Liu Jian-Sheng², Lu Qin-Chi², Gong Hai-Qing¹, Liang Pei-Ji¹

¹ School of Life Sciences and Biotechnology, Shanghai Jiao Tong University, Shanghai, China

² School of Medicine, Shanghai Jiao Tong University, Shanghai, China

* Corresponding author. E-mail address: pmzhang@sjtu.edu.cn

Understanding the initiation site of epileptiform discharges in hippocampus is of important physiological significance. Here the question was investigated in low-Mg²⁺ artificial cerebrospinal fluid (ACSF) perfused hippocampal slices of Sprague Dawley rat using microelectrode arrays. Initiation site of epileptiform discharges was determined by comparing the onset time of field potentials. The result indicates that epileptiform discharges originate from CA3b region in the low-Mg²⁺ ACSF perfused hippocampal slices.

1 Background

Epilepsy is a disorder condition of brain function characterized by recurrent, excessive discharges in large aggregates of neurons. Hippocampus is a common site of focal epileptic activity's initiation. The study of verifying the unambiguous site of the origin and propagation of epileptiform discharges in hippocampal slices are of much significance. Microelectrode array (MEA) facilitates noninvasive stimulations and recordings from cells and network over long time. It is worth investigating the initiation site and propagation of epileptiform discharges in hippocampal slices using MEA technique.

2 Method

Transverse hippocampal slices were prepared from Sprague Dawley (SD) rats (male, postnatal 2 weeks), and low-Mg²⁺ artificial cerebrospinal fluid (ACSF) was applied to induce epileptiform activity. Electric activities were simultaneously recorded by 60 substrate-embedded titanium nitride electrodes with 30 μm diameter, 200 μm spacing, arranged in 8×8 matrix (Multi Channel System, MCS GmbH, Germany).

3 Results

All the results given here are from one hippocampal slice and similar results were observed in other five slices.

The hippocampal slice of SD rat was transferred onto MEA after 1.5-2 h incubation (Fig. 1). After about 15 min low-Mg²⁺ ACSF perfusion, epileptiform discharges occurred in the entire Cornu Ammonis (CA) but rarely in dentate gyrus (DG). Epileptiform discharges in stratum pyramidale and stratum oriens exhibited field potentials of negative-positive waveforms with multiple unit activities

(MUAs) superposed on, while field potentials of stratum radiatum and stratum lacunosum-moleculare displayed positive-negative waveforms (Fig. 2). MUAs of stratum pyramidale were larger in amplitude and more in number than those in the other stratum. (An example is shown in Fig. 2, 3, and 4).

To investigate the initiation site and propagation of epileptiform discharges, short period time of field potentials at about 40 min low-Mg²⁺ perfusion recorded from electrodes whose positions scattered along stratum pyramidale of hippocampal slice were compared. As shown in Fig. 5, the onset time of field potential recorded by electrode No. 75 corresponding to CA3b region was ahead of the onset time of field potentials recorded by the other electrodes in stratum pyramidale. As a consequence, epileptiform discharges of stratum pyramidale originated from CA3b region and propagated to CA3c and CA1 respectively.

4 Conclusion

From our research results, we can see the advantages using MEA to investigate the initiation and propagation of epileptiform discharges in hippocampal slices. The results showed that the CA3b region is epileptiform discharges initiation site of low-Mg²⁺ epilepsy model in SD rat hippocampal slices and epileptiform discharges propagate from CA3b to CA1 and CA3c respectively. However, due to the complexity of epileptiform discharges propagation, the exact pathway of propagation in hippocampal slice is still unknown.

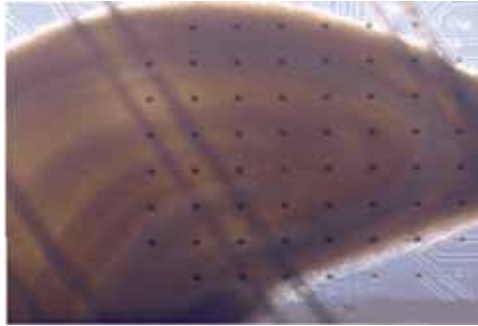


Fig. 1. One hippocampal slice of 2-week SD rat laying on 8 × 8 MEA.



Fig. 2. Low-Mg²⁺-induced signals after 30 min low-Mg²⁺ ACSF perfusion on MEA. No. of each electrode is labeled at its top right corner. Approximate position of stratum pyramidale in CA region and granule cell layer in DG region is indicated by dotted lines.

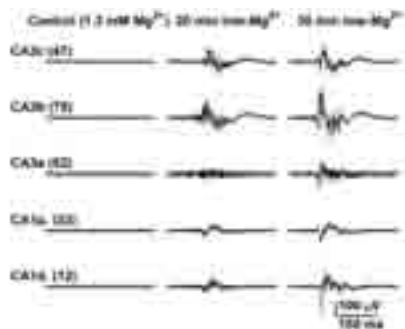


Fig. 3. Simultaneous extracellular recording in the stratum pyramidale of the CA3c, CA3b, CA3a, proximal and distal CA1 subregions under control, 20 min and 30 min perfusion of low-Mg²⁺ ACSF. Numbers in parenthesis are electrode Nos. corresponding to Fig. 2.

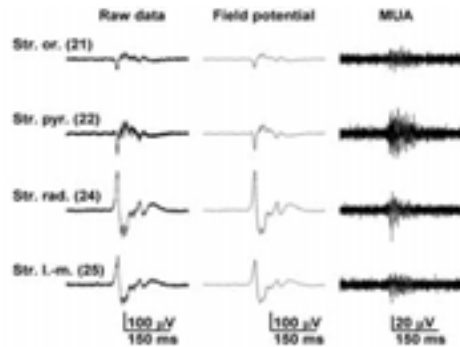


Fig. 4. Simultaneous extracellular recording at about 30 min after low-Mg²⁺ ACSF perfusion (left, 1-4000 Hz band-pass), field potentials (middle, 1-100 Hz) and MUAs (right, 200-4000 Hz) in the CA1 stratum oriens, stratum pyramidale, stratum radiatum, stratum lacunosum-moleculare layers. Numbers in parenthesis are electrode Nos. corresponding to Fig. 2.

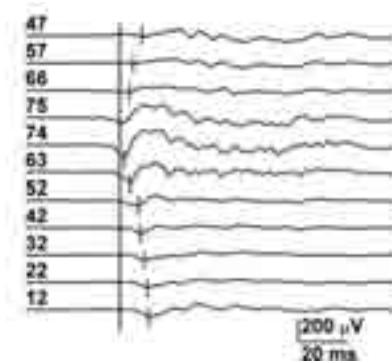


Fig. 5. The initiation of synchronous field potentials at recording sites along stratum pyramidale from CA3c to CA1 distal region. Leftmost vertical bar which shows up first denotes the onset time of field potential recorded by the electrode No. 75 and each little vertical bars which appear subsequently depict the onset times of field potentials recorded by the other electrodes. The numbers in each top left corner of field potentials are electrode Nos. as shown in Fig. 2.

Acknowledgement

This work was supported by grants from the National Natural Science Foundation of China under Grant No. 60775034, and Shanghai Jiao Tong University Fund for Interdisciplinary Research for Medical Applications under Grant YG2007MS07.

Unfolding the Properties of Biological Neural Networks with Multidimensional Reduction Techniques and Graph Theory

Carrillo-Reid Luis, Garcia-Munoz Marianela, Arbutnott Gordon

Okinawa Institute of Science and Technology, Okinawa, Japan

We used MEA recordings and functional multi-cell calcium imaging to investigate cell assembly properties in networks of cultured cortical cells. The overall activity of the neurons can be represented as an array of multidimensional vectors where the dimensionality of the system is given by the number of active elements. The multidimensional reduction of the vectors revealed specific groups of cells firing in synchrony; each group defines a network state. Graph theory techniques applied to the transitions between network states revealed recurrent closed cycles that could explain the compositional properties of neural networks, such as modular architecture and hierarchical organization.

1 Introduction

The ability of neural networks to build complex representations from basic parts is a central issue to understand memory formation [1-2]. Indeed, we continually deal with complex structures, such as language, motor procedures, or action planning [2]. Nevertheless, the rules that support the formation of composite structures have been elusive to examine [3]. We combined MEA recordings and functional multi-cell calcium imaging to study the network properties of cortical neurons with single cell resolution and millisecond precision.

2 Method

Cryopreserved primary mouse cortical neurons (QBMCCellScience) were plated onto MEA. Signals were sampled at 25 kHz using a commercial card (Multichannel Systems, Reutlingen, Germany). Cultures were loaded with the calcium indicator fluo-5 AM. Optical recordings were made with a high resolution cooled digital camera. Images were acquired with a sample rate of 150 ms/frame using commercial software (Photometrics, Roper Scientific). To study the properties of neural networks we constructed different vectors that represent the synchronous activity of neuronal pools within 150 ms time windows. Each vector represents the activation onset of a group of cells. The set of all vectors defines a $N \times V$ binary matrix where N denotes the total number of active elements of the network (dimension of the system), and V represents the total number of vectors (elements of the system). We compared all the possible vector pairs to construct similarity maps [3-5]. The similarity index between a pair of vectors is defined by their normalized inner product. To visualize the network states we reduced the

dimensionality of the vectors with locally linear embedding (LLE) [6]. A cluster of vectors defines each network state [3-4, 7]. Finally we used graph theory to follow the state transitions of the network [3].

3 Results

We performed electrical or optical recordings of many neurons simultaneously to study the properties of biological neural networks (Fig. 1). The analytical tools used here allow the identification of groups of neurons firing in synchrony. The vectorization of the network dynamics is useful to find specific patterns of activity repeated in different times. Similar patterns are represented by geometric structures in the similarity maps. The multidimensional reduction of the vectors allows the visualization of the network states. The transitions between network states can be represented by directed graphs making possible the study of the mathematical properties that underlie the network state transitions. Graph theory techniques could be useful to study the compositional rules that allow the formation of complex activity patterns from basic parts.

4 Discussion

Sequential activity patterns could represent different memories imprinted in neural networks [8-9]. During learning, sequences could be dictated by external events, whereas during recall, imagination, or action planning, the rules governing sequences could be determined by the intrinsic properties of the network [10]. In order to understand the fundamental properties of biological neural networks that give rise to memories, we developed different analytical tools that allow the identification of groups of neurons

firing in synchrony with recurrent activity. Our approaches could be useful to identify different network states from *in vivo* experiments.

Acknowledgement

This work was supported by the Okinawa Institute of Science and Technology.

References

[1] Bienenstock, E. and S. Geman, *Compositionality*, in *The Handbook of Brain Theory and Neural Networks*, M.A. Arbib, Editor. 1995, The MIT press: Cambridge, MA. p. 223-226.
 [2] Hammer, B., *Compositionality in neural systems*, in *The Handbook of Brain Theory and Neural Networks*, M.A. Arbib, Editor. 2003, The MIT Press: Cambridge, MA.
 [3] Carrillo-Reid, L., et al., *Activation of the cholinergic system endows compositional properties to striatal cell assemblies*. *J Neurophysiol*, 2009. **101**(2): p. 737-49.

[4] Carrillo-Reid, L., et al., *Encoding network states by striatal cell assemblies*. *J Neurophysiol*, 2008. **99**(3): p. 1435-50.
 [5] Sasaki, T., N. Matsuki, and Y. Ikegaya, *Metastability of active CA3 networks*. *J Neurosci*, 2007. **27**(3): p. 517-28.
 [6] Roweis, S.T. and L.K. Saul, *Nonlinear dimensionality reduction by locally linear embedding*. *Science*, 2000. **290**(5500): p. 2323-6.
 [7] Stopfer, M., V. Jayaraman, and G. Laurent, *Intensity versus identity coding in an olfactory system*. *Neuron*, 2003. **39**(6): p. 991-1004.
 [8] Baruchi, I. and E. Ben-Jacob, *Towards neuro-memory-chip: imprinting multiple memories in cultured neural networks*. *Phys Rev E Stat Nonlin Soft Matter Phys*, 2007. **75**(5 Pt 1): p. 050901.
 [9] Wagenaar, D.A., et al., *Controlling bursting in cortical cultures with closed-loop multi-electrode stimulation*. *J Neurosci*, 2005. **25**(3): p. 680-8.
 [10] Pastalkova, E., et al., *Internally generated cell assembly sequences in the rat hippocampus*. *Science*, 2008. **321**(5894): p. 1322-7.

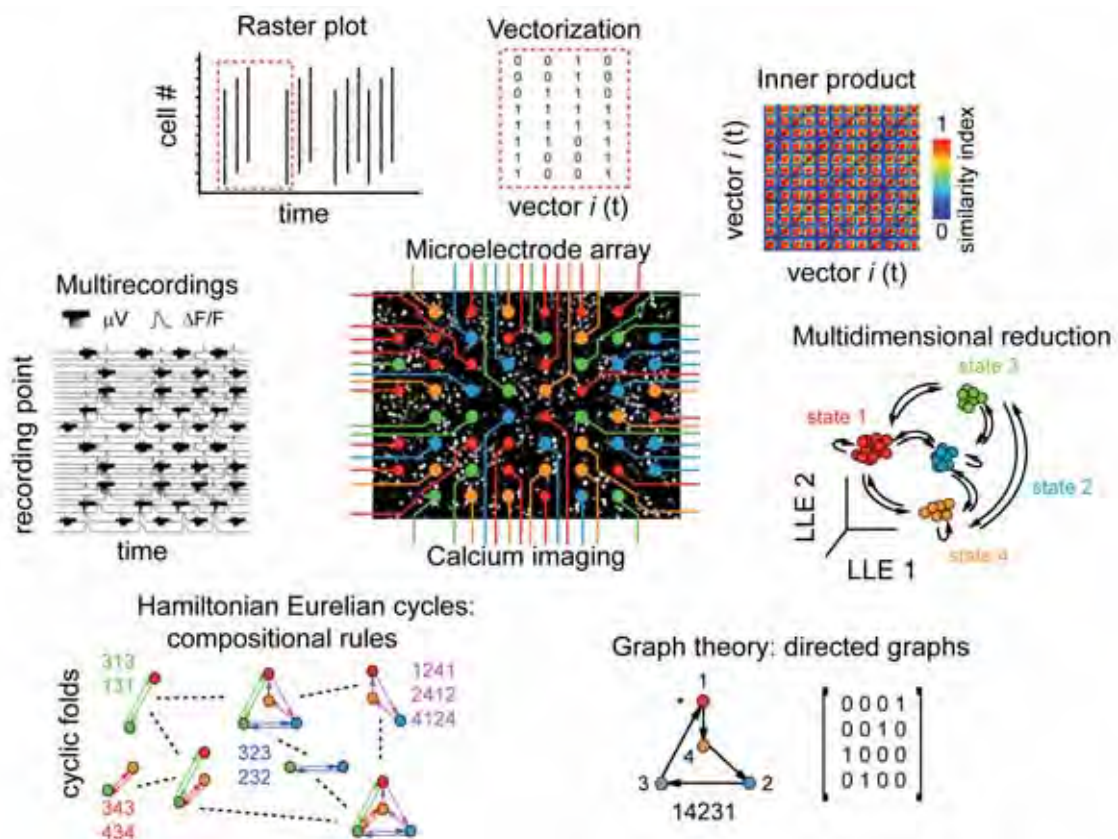


Figure 1. Schematic representation of the different steps used to analyze the network activity.

Multi electrode array recordings and calcium imaging were used to investigate the properties of biological neural networks. Calcium transients representing bursting activity and spike recordings were recorded from multiple sites. Raster plots represent the overall activity of the network, each row represents an active cell, and dots denote the onset of bursting activity. Vectorization of the network activity allows the rigorous comparison of different time points. 0's denote silent cells and 1's denote active cells. The inner product of all possible vector pairs allowed the identification of similar patterned structures along time. Multidimensional reduction of the vectors into a two dimensional space depicted the trajectories between the different states of the network. Graph theory applied to the transitions between network states revealed closed cycles of activity that are repeated over time. Hamiltonian and Eulerian cycles represent the trajectories of the network.

Pharmacology, Toxicology and Drug Screening

Perforated Multielectrode Array in Drug Discovery

Jonathan M. Levenson*, Helen E. Gibson, David Gerber, Margaret Levin

Target Validation, Galenea, Corp., Cambridge, MA, USA

* Corresponding author. E-mail address: jlevenson@galenea.com

Keynote Lecture

A major limiting factor in CNS drug discovery is the lack of robust, predictive *in vitro* correlates of cognitive status that enable reliable translation from target validation and compound evaluation to achievement of *in vivo* efficacy in behavioural pharmacology models. To fill this void, we implemented perforated multielectrode array technology (pMEA) at various stages of our drug discovery process. This new technology has permitted interrogation of neural network activity at multiple functional and anatomical levels, and at a higher throughput relative to conventional electrophysiology methodology. Using pMEA, we have rapidly identified compounds that exhibit disease-modifying effects *in vivo*.

1 The Trouble with Drug Screening

1.1 Target-centric drug discovery

The molecular genetics revolution sparked a new era in drug discovery that promised shorter development cycles and less risk in translating disease hypotheses into viable therapeutics. For the first time, researchers could clone and express precise targets, facilitating the design and execution of high-throughput screens for small molecules that potently and specifically interact with and/or modulate the activity of the target. This “rational” approach to drug discovery (Fig. 1) has proven effective at identifying novel, potent and specific therapeutic candidates for diseases such as diabetes or cancer that can result from dysfunction of one or a small set of targets.



Fig. 1. The conventional drug discovery pipeline.

1.2 Target-centric discovery in the CNS

Development of therapeutics for diseases of cognition is inherently more difficult than for other indications owing to the complexity of the brain. Cognitive disorders, even if resulting from disruption of one gene, often involve pleiotropic effects stemming from aberrant neurodevelopment, disruptions in signalling pathways, functional compensation or neurodegeneration. The consequences of phenotypic pleiotropy on target-centric approaches to drug discovery are two-fold: the difficulty of target selection is magnified, since potential therapeutic targets may not represent the primary cause of the disease state, and any potential therapeutic must restore normal function to the entirety of the brain and not just a single functional

pathway. This highlights the fundamental challenge of target-centric approaches to CNS drug discovery: therapeutics optimized for activity against highly specific targets must restore normal function at multiple levels of the brain in order to be effective. The difficulty of translating basic discoveries on CNS disorders into tangible therapies is borne out in the statistics; less than 1% of clinical candidates for neurotherapeutics become marketed drugs [1]. Clearly, the target-centric approach to CNS drug discovery needs to be revisited in order to improve the success rate for identification of new medicines for CNS disorders

2 Hypothesis-driven Drug Discovery

2.1 Functional Screens

As optical screening technologies have evolved, high-throughput cellular assays have been implemented as a way to monitor compound structure-activity relationships (SAR) regarding functional modulation of a target. This has facilitated discovery of new classes of neurotherapeutics, such as the 5-HT_{2C} receptor agonist vabicaserin [2]. The benefit of function-based screens is that they quantify the effects of compounds on the function of a particular target in the context of a cell, providing more predictive measures of *in vivo* efficacy relative to assays of enzymatic activity or binding.

2.2 The Challenge of Neural Networks

Neurons and glial cells represent the cellular building blocks of the brain. However, while other organs are composed of defined cell types that utilize relatively simple mechanisms for intercellular communication and synchronization; by comparison, the brain is a highly complex web of numerous subtypes of neurons and glia that rely on sophisticated mechanisms for intercellular communication and form

elaborate, higher order functional networks. Therefore, despite their utility in reflecting target actions, cellular functional screens can not capture the complexity of neural networks that give rise to cognitive processes. Herein lies the challenge of current CNS drug discovery: how does one model the complexity of the brain in a manner amenable to preclinical drug discovery?

2.3 The Acute Brain Slice

The biophysical signals that result from single cell and ensemble network activity represent the most direct and convenient measure of neuronal function. These signals are a composite measure of the status of a wide array of processes including signalling, metabolic, and transcriptional pathways. Electrophysiological techniques have been developed to measure a variety of parameters including activity of channels, cells and networks. Moreover, a number of preparations have been developed in which to study neurons including acute and chronic cultures of individual neurons and semi-intact slice preparations. Unfortunately, many of the electrophysiological techniques commonly employed in research laboratories are ill-suited for drug discovery applications as they are characterized by low throughput and high failure rates. Any technology supporting a robust CNS drug discovery process must have the capacity to quantify neural processes that are relevant to higher order brain function using a system that permits the higher throughput demands of compound optimization.

Since the pioneering work of Richards and Sercombe in 1968 [3], acute brain slice preparations have provided a vital tool for characterizing the electrophysiological properties of the adult nervous system. The advantage of the acute brain slice over cell culture preparations is the preservation of CNS microcircuitry and anatomy in a robust preparation easily amenable to pharmacological manipulation. Moreover, the advent of rodent genetic manipulation has permitted dissection of neurophysiological phenomena with molecular precision. Thus, acute brain slices represent an experimental preparation that closely approximates the complex microcircuitry of the intact brain involved in cognitive processes in a manner that is applicable to compound screening.

2.4 Multielectrode Array

The obstacles for implementation of brain slice assays as a drug discovery platform are mainly technical in nature. The conventional methods available to monitor electrophysiological signals from a brain slice rely on amplification of signals using discrete microelectrodes. Thus, the complex responses of self-contained circuits within a brain slice are reduced to one or a few measures. Moreover, the time and technical skill required to record from individual

slices combined with the multitude of equipment that must perform flawlessly for each experiment has created barriers that have prevented many institutions from seriously considering the acute brain slice as a vital part of the drug discovery process.

The commercialization of multielectrode array (MEA) technology for *in vitro* applications addressed many of the shortcomings of the acute brain slice as a potential basis for *in vitro* functional drug discovery assays [4]. Integration of the microelectrodes into the floor of the recording chamber eliminated the need for the experimenter to fabricate or place microelectrodes in order to obtain stable recordings. Moreover, any individual microelectrode within a modern MEA can be used in either a recording or stimulating mode. While seemingly simple, this ability affords the experimenter a degree of freedom in experimental design and execution that is simply not available using standard electrophysiological techniques. Another consequence of MEAs was the miniaturization and consolidation of the electronics needed for amplification, filtering and digitization of signals for subsequent analysis. Thus, for the first time multisite recordings in brain slices could be conducted with higher throughput due to the streamlined experimental workflow that MEA technology permits.

2.5 Perforated Multielectrode Array

The biggest drawback to implementing a MEA workflow for interrogating electrophysiology in acute brain slices is the reliance on a submerged recording chamber. While submerged chambers permit excellent control of the constituents of the recording solution, exchange of gases and metabolites is extremely poor at the bottom of the tissue, precisely where the microelectrodes are situated. Even small changes in pO_2 , pH or metabolite levels can have profound effects on the evoked or spontaneous activity recorded in acute brain slices [5, 6]. Early attempts to mitigate this apparent limitation of MEA electrophysiology in which recordings are made from the least viable surface of the tissue resulted in creation of 3-dimensional MEAs whereby the electrodes pierced the tissue and recorded from layers of cells that had better perfusion. Unfortunately, these arrays did not permit repositioning of tissue if the initial placement on the array was suboptimal and the recorded physiology was still in the context of a slice with suboptimal perfusion.

An elegant solution to the problem of brain slice perfusion came with the advent of perforated MEA technology (pMEA). In pMEA, small holes are plasma etched into the floor of the recording chamber in a regular pattern [7]. Gentle suction is applied such that the perfusate is actively drawn through the slice. Early tests indicate that use of pMEA results in significantly higher pO_2 and signal:noise at the bottom of the slice relative to conventional MEAs [7],

suggesting that pMEA dramatically improves the uniformity of the perfusion of gases, metabolites and even small molecules throughout a slice. Thus, pMEA lowers the technical and logistical barriers to implementation of acute brain slice electrophysiological assays in the drug discovery process by providing the convenience of a submerged recording environment and the cost, time and space efficiencies afforded by equipment consolidation, superior slice health and a streamlined workflow.

2.6 pMEA and Hypothesis-driven Discovery

For the first time researchers now have the capability, through the use of pMEA, to incorporate measures of intact, adult neural network function into the CNS drug discovery process in a manner that is amenable to the higher throughput demands of these projects (Fig. 2). Shifting the focus of drug discovery from target-based analyses to encompass measures of adult neural network activity effectively transforms the process into a more hypothesis-driven approach. New compounds must not only modify the function of a specific target, but also restore normal network function in a disease model. Moreover, pMEA can be used to identify and validate potential molecular targets and processes underlying the disease condition, increasing the likelihood that modulators of these targets will modify the disease condition.



Fig. 2. Galenea's drug discovery pipeline.

Measures of neural network function may also mitigate some of the risk in translating compounds with attractive *in vitro* efficacy profiles into development candidates with good efficacy in disease-relevant behavioural pharmacology models. During the optimization of small molecule therapeutics, early-stage compounds often lack the drug-like properties required for *in vivo* testing. Careful selection of the brain region monitored *in vitro* greatly increases the probability for activity against the targeted network processes *in vivo*. Thus, use of pMEA reduces the major obstacles for achieving *in vivo* efficacy to optimization of pharmacokinetic properties including brain penetration. Collectively, implementation of functional neural network measures during the early stages of CNS drug discovery shifts the focus toward a hypothesis-driven approach that can mitigate much of the risk in translating early stage discoveries into identification of clinical development candidates.

3 Assays for CNS Drug Discovery

3.1 Extracellular Electrophysiology

When designing experiments incorporating measures obtained from pMEA, one must consider that electrical stimulation of tissue and recording of neural activity is performed using extracellular electrodes. The resulting field potentials (Fig. 3A) reflect bulk changes in electrical potential around each electrode and not necessarily the activity of single cells. Therefore, experiments quantifying field potentials must be conceived and interpreted in the context of ensemble neural networks and not the activity of single cells or processes. The following section will highlight some of the assays we use to monitor compound efficacy and detection of off-target effects.

3.2 Synaptic Transmission

The fundamental mechanism for intercellular communication in the CNS is chemical synaptic transmission. Measures of excitatory synaptic transmission can be made by stimulating populations of excitatory fibers and measuring the resulting synchronous synaptic activity as an ensemble field potential (i.e., Fig. 3A). By manipulating the patterns of electrical stimulation, one can monitor different aspects of synaptic transmission. For example, by varying the strength of a single stimulus and determining the ratio of fiber volley amplitude, a measure correlated with the number of presynaptic fibers activated by the stimulus, to the slope of the resulting field excitatory post-synaptic potential (fEPSP), a measure correlating with the number of post-synaptic receptors activated by the stimulus, one can comprehensively quantify the pre- and post-synaptic contributions to overall synaptic transmission (Fig. 3A).

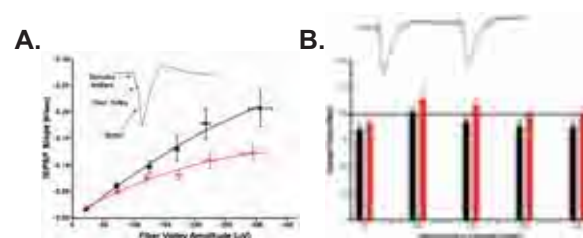


Fig. 3. Input: Output curves and paired pulse ratios.

Likewise, varying the interval between two constant stimuli provides a measure of paired pulse ratios (Fig. 3B). These ratios are inversely correlated with levels of presynaptic neurotransmitter release. Higher ratios suggest low probability of transmitter release while lower ratios suggest higher probability of transmitter release.

3.3 Synaptic Plasticity

The ability of synapses to modulate the efficacy of transmission in response to different patterns of activity, referred to as synaptic plasticity, is thought to be involved in higher cognitive processes such as learning and memory. Synaptic strength can either increase or decrease in response to previous patterns of stimulation. Two robust forms of synaptic plasticity are long-term potentiation (LTP), which refers to an increase in synaptic strength usually observed after high-frequency patterns of afferent activity, and depotentiation, which refers to a loss of LTP following low frequency patterns of afferent activity. Both forms of synaptic plasticity can be evoked and measured in hippocampal area CA1 using pMEA (Fig. 4).

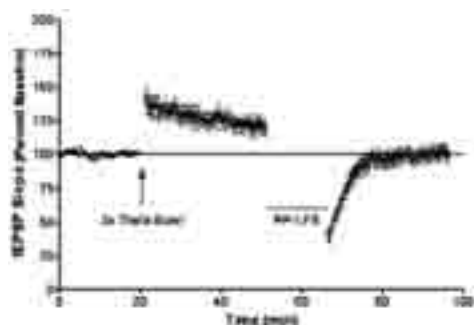


Fig. 4. LTP and depotentiation in area CA1 with pMEA.

3.4 Neural Network Oscillations

The brain is organized into discrete, interconnected networks of neurons. An emergent property of these complex neural networks is their ability to synchronize activity and generate robust oscillations. Neural oscillations have been implicated in various aspects of cognitive processing, including information binding, sensory processing and memory storage and retrieval [8]. These oscillations are induced by afferent activity into the local network and are generated and sustained by local microcircuitry [9]. Since the cellular constituents required for generation of neural oscillations are contained within definable brain regions, they can be reconstituted in acute brain slice preparations for study.

We have recorded neural oscillations, evoked using the nonspecific cholinergic agonist carbachol, from acute mouse brain slices containing the prefrontal cortex (Fig. 5). It should be noted that recording carbachol-evoked oscillations is particularly difficult and requires optimal slice health and oxygenation [6]. Therefore, the ability to evoke robust neural oscillations with carbachol is both a useful tool for interrogating neural network function *in vitro* and further confirmation of the superior recording conditions afforded by pMEA.

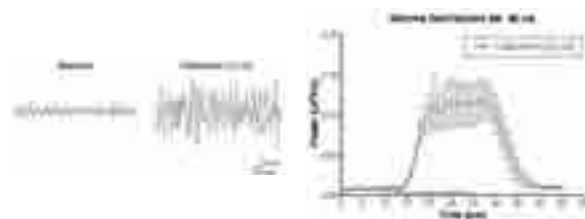


Fig. 5. Carbachol-evoked oscillations in PFC recorded with pMEA.

4 Summary

CNS drug discovery by nature is difficult to successfully conduct using target-based strategies alone. Increasingly, researchers will have to implement tools that provide the flexibility of hypothesis-based drug discovery and that also support the bandwidth required for a robust drug discovery process. At Galenea, we have chosen pMEA as one of our new platforms for target discovery and compound screening. Using pMEA, we have identified novel disease mechanisms and therapeutic compounds with robust *in vivo* efficacy.

Acknowledgement

We thank A. Heynen (MIT) and M. Oza (ALA Scientific) for invaluable support during implementation of pMEA at Galenea.

References

- [1] C. C. Gallen, "Strategic challenges in neurotherapeutic pharmaceutical development," *NeuroRx*, vol. 1, pp. 165-80, 2004.
- [2] S. Rosenzweig-Lipson, J. Dunlop, and K. L. Marquis, "5-HT_{2C} receptor agonists as an innovative approach for psychiatric disorders," *Drug News Perspect*, vol. 20, pp. 565-71, 2007.
- [3] C. D. Richards and R. Sercombe, "Electrical activity observed in guinea-pig olfactory cortex maintained *in vitro*," *J Physiol*, vol. 197, pp. 667-83, 1968.
- [4] H. Oka, K. Shimono, R. Ogawa, H. Sugihara, and M. Taketani, "A new planar multielectrode array for extracellular recording: application to hippocampal acute slice," *J Neurosci Methods*, vol. 93, pp. 61-7, 1999.
- [5] A. Schurr, C. A. West, and B. M. Rigor, "Electrophysiology of energy metabolism and neuronal function in the hippocampal slice preparation," *J Neurosci Methods*, vol. 28, pp. 7-13, 1989.
- [6] C. Huchzermeyer, K. Albus, H. J. Gabriel, J. Otahal, N. Taubenberger, U. Heinemann, R. Kovacs, and O. Kann, "Gamma oscillations and spontaneous network activity in the hippocampus are highly sensitive to decreases in pO₂ and concomitant changes in mitochondrial redox state," *J Neurosci*, vol. 28, pp. 1153-62, 2008.
- [7] U. Egert, S. Okujeni, W. Nisch, K.-H. Boven, R. Rudolf, and N. Gottschlich, "Perforated Microelectrode Arrays Optimize Oxygen Availability and Signal-to-Noise Ratio in Brain Slice Recordings," presented at Mikrosystemtechnologie Kongress, Freiburg, 2005.
- [8] P. J. Uhlhaas, C. Haenschel, D. Nikolic, and W. Singer, "The role of oscillations and synchrony in cortical networks and their putative relevance for the pathophysiology of schizophrenia," *Schizophr Bull*, vol. 34, pp. 927-43, 2008.
- [9] M. Bartos, I. Vida, and P. Jonas, "Synaptic mechanisms of synchronized gamma oscillations in inhibitory interneuron networks," *Nat Rev Neurosci*, vol. 8, pp. 45-56, 2007.

Cerebrospinal fluid of brain-trauma patients suppresses functional neuronal network activity

Marcel Dihné^{1,2}, Sebastian Illes¹, Stephan Theiss³, Alfons Schnitzler^{1,2}

1 Department of Neurology, Heinrich-Heine University, Moorenstr. 5, 40225 Düsseldorf, Germany

2 Institute of Clinical Neuroscience and Medical Psychology, Heinrich-Heine University, Universitätsstr.1, 40225 Düsseldorf, Germany

3 Result Medical, Friedenstraße 39, D-40219 Düsseldorf

In clinical routine, cerebrospinal fluid (CSF) is predominantly used for diagnostic purpose as different neurological diseases influence the composition of the CSF. If CSF itself might functionally influence neuronal network activity was not known. In a proof-of-principle experiment, we collected CSF specimens from patients suffering from severe traumatic brain injury (TBI) or from control patients and investigated their impact on *in vitro* neuronal network activity recorded by the microelectrode array (MEA) technology. We found that CSF specimens of TBI patients with considerably reduced values in Glasgow-Coma-Scale suppressed synchronous network activity of neural populations while control CSF supported network activity. Network suppression was mediated by a CSF fraction containing small molecules, in particular small amino acids like glutamate, glycine, serine or alanine. We found that enhanced N-methyl-D-aspartate (NMDA) receptor activity was involved in network suppression as NMDA antagonists were able to recover functional network activity.

Thus, for the first time, functional consequences of pathological CSF specimens were visualized by means of the MEA technology. We plan to expand this system towards the generation of individual, human functional neuronal networks based on induced, pluripotent stem cells in order to increase the validity of future investigations.

1 Introduction

Next to brain protective functions, cerebrospinal fluid (CSF) also represents a carrier system that transports neuroactive substances like neuropeptides, neurohormones and neurotransmitters across the ventricular ependyma or pia-gial membranes into the interstitial fluid (ISF) of the brain parenchyma^{1,2}. This process allows to widely distributing information within the brain by influencing parasynaptic signal transmission³. Additionally, CSF non-synaptically influences cerebrospinal fluid-contacting neurons acting as sensory cells of chemoreceptor-type that send their dendritic processes into the brain ventricles and their axons into various brain areas. Also, axons contact the CSF and release various bioactive substances. Electrophysiological experiments show that, for instance, paraventricular hypothalamic neurons are highly sensitive to the composition of the ventricular CSF and transport information towards tel-, mes- and rhombencephalic brain nuclei^{4,5}. It is also known that cerebellar Purkinje neurons can extract small and large molecules from the cerebrospinal fluid which is associated with behavioral abnormalities⁶. These anatomical conditions illustrate that the composition of the CSF influences brain activity. As virtually all brain diseases are going ahead with changes in CSF composition, it appeared to be interesting how disease-related CSF changes might secondarily influence brain activity.

Rodent functional neuronal networks on microelectrode arrays (MEAs) served as a simplified *in vitro* model for brain activity. Neural populations were derived either from primary cortical preparations or from embryonic stem cell-derived neural populations whose synchronous burst activity is known to be highly sensitive to chemical changes in the extracellular milieu^{7,8}.

We obtained CSF specimens from patients suffering from severe traumatic brain injury (TBI) or human controls. TBI patients were treated on intensive care unit without, for instance, administration of medicine with effects on consciousness or epileptic seizures at the time, CSF was obtained. In fact, it was tried to awake them, a process which is often prolonged although findings in cranial magnetic resonance imaging did not always conclusively explain dramatically reduced values in Glasgow-Coma-Scale (GCS). Thus, toxic or metabolic disturbances are suspected to additionally play a role in states of reduced levels of consciousness after TBI. We therefore collected CSF specimens from TBI and control patients and investigated their impact on neuronal network activity.

2 Material and Methods

2.1 Collection of CSF

CSF specimens from TBI patients were obtained within the 1st week after the injury and were immediately centrifuged, divided into aliquots, and stored at minus 35°C. Ethics approval for the use of human CSF was obtained from the institutional ethics committee. A total of 12 specimens from inpatients with normal CSF analyses and 12 specimens from TBI inpatients were used for this study. Prior to analyses, CSF was thawed, and the pH was adjusted to 7.4. All CSF specimens were sterile.

Traumatic CSF specimens were used for the generation of low molecular fractions (<3.5kDa) and high molecular fractions (>1kDa) by means of ultracentrifugation, ultrafiltration or dialyses.

To analyze concentrations of single amino acids, an automated amino acid analyzer (LC3001, Biotronik, Munich, Germany) was used. For determination of concentrations of proteins, lactate, glucose, and ions within CSF specimens, standard procedures were applied according to the manufacturer's instructions (all kits and equipment were from Roche Diagnostics/Hitachi, Mannheim, Germany).

2.2 Cell culture

Differentiation of embryonic stem (ES) cells is described elsewhere⁸ with minor modifications. After formation of embryoid bodies, neural differentiation was induced, resulting in neural-induced, serum-free, floating cultures of embryoid body-like aggregates (SFEBs). Neural-induced SFEBs were propagated by adding fibroblast growth factor-2 (PeproTech, Rocky Hill, NJ) for a further 6 days and then seeded and propagated on poly-L-ornithine and laminin-coated dishes or MEAs. Three weeks after seeding, ES cell-derived neurons developed synchronously oscillating networks, which were used to characterize CSF specimens. To compare the functional aspects of ES cell-derived networks with those of conventionally used primary neural cell populations, we additionally performed experiments with cryo-preserved embryonic day 18 primary rat cortical cell-derived networks (QBM Cell Science, Ottawa, Canada).

2.3 Electrophysiological Recordings and Analyses

Extracellular potentials were recorded simultaneously on microelectrode arrays (MEAs) with a square grid of 60 planar Ti/TiN microelectrodes (30µm diameter, 200µm spacing) as described elsewhere⁹. All spike waveforms were stored separately and visually inspected for artifacts. The burst detection relied on an entropy-based algorithm. Interburst intervals were determined as time

differences between the first spikes of subsequent bursts. Bursts were also checked by visual inspection for plausibility.

3 Results

Traumatic CSF (tCSF) specimens significantly modulated neuronal network activity of both rat primary cortical (rPC) and ES cell-derived neuronal populations in comparison with hCSF by means of inhibition and desynchronization, as illustrated by reduced spike rates and kappa values (Fig 1). Thereby, similar changes in network activity of 2 different neuronal populations following tCSF application considerably consolidate the observed effects. Thus, rPC or ES cell-derived neuronal networks on MEAs for the first time allowed direct visualization and measurement of the functional impact of pathologically altered CSF specimens on neuronal network activity without the use of sharp or patch-clamp electrodes.

To directly verify the network suppressive role of amino acids, we generated 2 separate tCSF fractions containing either molecules <3.5kD (tCSF-low) or >1kD (tCSF-high). tCSF-low predominantly contained amino acids such as glycine, serine, alanine, or glutamate, whereas total protein content was low, and vice versa (Fig 2A). Concentrations of glucose, lactate, and different ions were reconstituted in different groups to normal levels of aCSF. Whereas neuronal network function did not significantly deviate under the influence of tCSF-high in comparison to aCSF, tCSF-low significantly suppressed different network parameters (Fig 2b). These data unambiguously identified the tCSF-low fraction containing elevated concentrations of amino acids as responsible for the network suppressive effects of tCSF. The functional relevance is substantiated in that Spearman's rho indicates a correlation between the degree of network synchrony (kappa values) and associated GCS values, although there was no linear relationship (Fig 2C).

By experiments using *N*-methyl-*D*-aspartate (NMDA) or glycine as well as their specific antagonists at the NMDA receptor, 2*R*-amino-5-phosphonovaleric acid (APV) and kynurenic acid, we demonstrated that the NMDA receptor and its agonists are involved in network suppression or recovery (data not shown).

4 Discussion and Conclusion

We might now be able to visualize the impact of clinically important molecules or CSF specimens obtained from patients that suffer from metabolic or toxic encephalopathies on neuronal network activity. By fractionating CSF contents and biochemically antagonizing pathological effects of CSF specimens on neuronal network activity, we might clarify

mechanisms of metabolic encephalopathies and develop new therapeutic strategies which could even be individually adjusted. The use of murine embryonic stem cell-derived neural populations paves the way to the development of brain region-specific neuronal networks and the application of individual human induced pluripotent stem cells that would provide homologous, standardized and defined platforms with increased validity and predictability regarding the human situation.

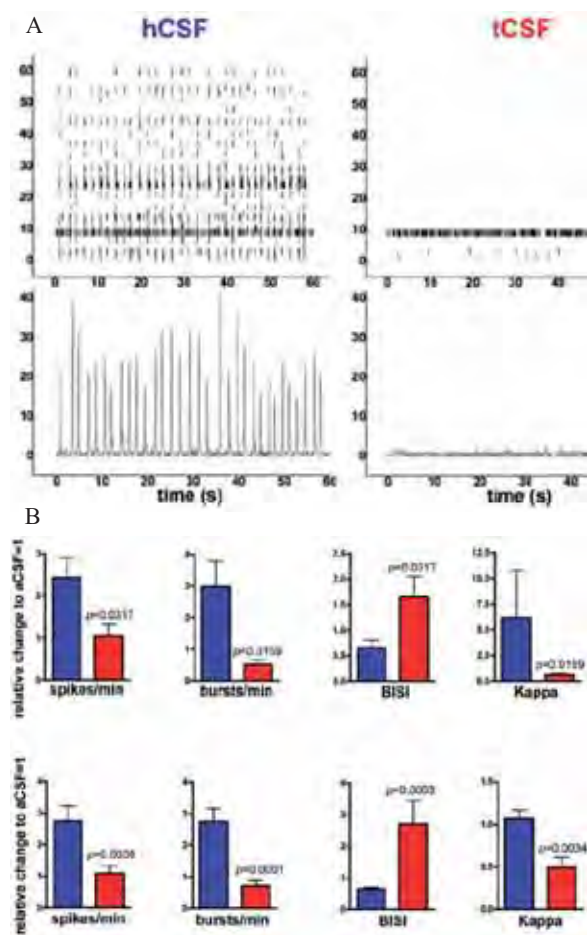


Fig. 1 (A) Representative spike raster plots (upper panel) and frequency counts (lower panel) of embryonic stem (ES) cell-derived networks in human CSF (hCSF) or traumatic CSF (tCSF). Spike raster plots illustrate the spike activity on all 60 microelectrode array electrodes (y axis) during a time interval of 60 seconds (x axis). Frequency counts visualize the synchrony of neuronal networks, as amplitudes represent the total number of spikes within a short time interval of 100 milliseconds (bin). Note the synchronous activity in hCSF and the decreased activity in tCSF. (B, upper row) Different electrophysiological parameters of ES cell-derived networks are shown illustrating values of electrophysiological parameters of hCSF (n= 5, blue) versus tCSF (n=5, red) in relation to artificial CSF (aCSF, y axis) on ES cell-derived networks. (B, lower row) Same parameters as B, upper row, illustrating values of electrophysiological parameters of hCSF (n=12, blue) versus tCSF (n=12, red) in relation to aCSF (y axis) on primary rat cortical cells. Values are presented as mean + SEM, individual p values are given, and the 2-tailed Mann-Whitney U test is used (from *Ann Neurol* 2009;66:546–555)².

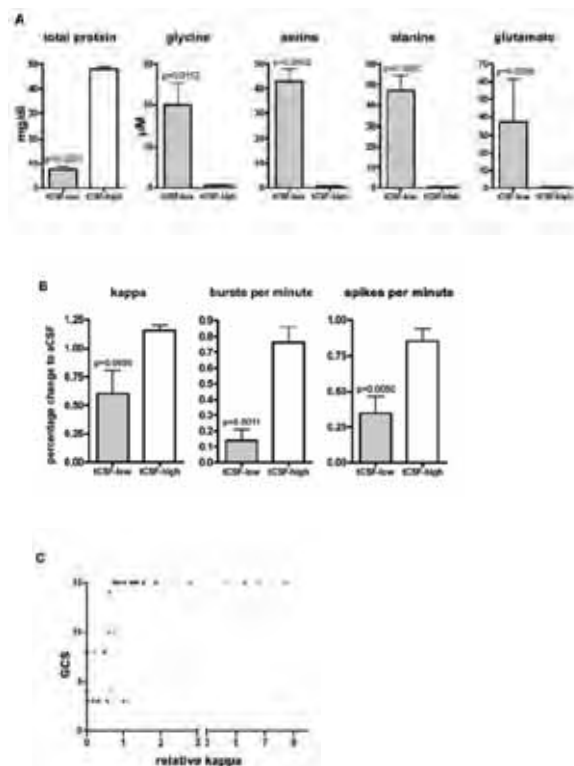


Fig.2 (A) Diagrams show absolute values for total protein content and different amino acids in traumatic cerebrospinal fluid (tCSF)-low or tCSF-high to illustrate efficacy of the dialysis procedure. Values are presented as mean + standard error of the mean (SEM), individual p values are given for tCSF-low versus tCSF-high, the 2-tailed Mann-Whitney U test is used, and n=4. (B) Diagrams show changes in values for kappa, bursts per minute, or spikes per minute in embryonic stem cell (ES)-derived networks after application of tCSF-low or tCSF-high. Values are presented as mean + SEM, individual p values are given for tCSF-low versus tCSF-high, the 2-tailed Mann-Whitney U test is used, and n=4. (C) Relative kappa values (synchrony of network activity) of 5 human CSF (hCSF, blue) and 5 tCSF (pink) specimens on ES cell-derived networks and 12 hCSF (deep blue) and 12 tCSF (brown) specimens on primary cortical networks are plotted against values in Glasgow Coma Scale (GCS) of individual patients. Spearman’s nonparametric correlation test calculated a 2-tailed p value of <0.0001 and a coefficient of correlation of 0.7528. The kappa value of artificial CSF (aCSF) on rat primary cortical or ES cell-derived networks was set to 1 to provide comparability between 2 different neuronal populations. A decrease in synchrony (kappa ratio < 1) was detected in 16 of 17 cases after application of tCSF; hCSF led to increased kappa ratios >1 in 13 out of 17 cases compared with aCSF. Tentatively setting a kappa threshold value of 0.75 to obtain 100% specificity within our limited sample, we found 14 out of 17 tCSF specimens with kappa values <0.75 (sensitivity = 14/17 = 0.82); by definition all 17 hCSF specimens exhibited kappa values >0.75 (from *Ann Neurol* 2009;66:546–555)².

References

- [1] Proescholdt MG, Hutto B, Brady LS, Herkenham M. Studies of cerebrospinal fluid flow and penetration into brain following lateral ventricle and cisterna magna injections of the tracer [¹⁴C]inulin in rat. *Neuroscience*. 2000; 95(2): 577-92.
- [2] Abbott NJ. Evidence for bulk flow of brain interstitial fluid: significance for physiology and pathology. *Neurochem Int*. 2004; 45(4): 545-52.
- [3] Herkenham M. Mismatches between neurotransmitter and receptor localizations in brain: observations and implications. *Neuroscience*. 1987; 23(1): 1-38.

- [4] Schmitt FO. Molecular regulators of brain function: a new view. *Neuroscience*. 1984; 13(4): 991-1001.
- [5] Zoli M, Torri C, Ferrari R, Jansson A, Zini I, Fuxe K, et al. The emergence of the volume transmission concept. *Brain Res Brain Res Rev*. 1998; 26(2-3): 136-47.
- [6] Borges LF, Elliott PJ, Gill R, Iversen SD, Iversen LL. Selective extraction of small and large molecules from the cerebrospinal fluid by Purkinje neurons. *Science*. 1985; 228(4697): 346-8.
- [7] Illes S, Fleischer W, Siebler M, Hartung HP, Dihne M. Development and pharmacological modulation of embryonic stem cell-derived neuronal network activity. *Exp Neurol*. 2007; 207(1): 171-6.
- [8] Illes S, Theiss S, Hartung HP, Siebler M, Dihne M. Niche-dependent development of functional neuronal networks from embryonic stem cell-derived neural populations. *BMC Neurosci*. 2009; 10: 93.
- [9] Otto F, Illes S, Opatz J, Laryea M, Theiss S, Hartung HP, et al. Cerebrospinal fluid of brain trauma patients inhibits in vitro neuronal network function via NMDA receptors. *Ann Neurol*. 2009; 66(4): 546-55.

Application of Micro Electrode Arrays (MEAs) as an Emerging Technology for Developmental Neurotoxicity

Helena T. Hogberg^{1*}, Antonio Novellino², Tomasz Sobanski², Anna K. Bal-Price²

¹ Johns Hopkins Bloomberg School of Public Health, Baltimore, Maryland, USA

² European Commission, Joint Research Centre, Ispra, Italy

* Corresponding author. E-mail address: hhogberg@jhsph.edu

Due to lack of knowledge only a few industrial chemicals have been identified as developmental neurotoxicants. Current developmental neurotoxicity (DNT) guidelines (OECD and EPA) are based entirely on *in vivo* studies that are both time consuming and costly. Consequently, there is a high demand to develop alternative *in vitro* methods for initial screening to prioritize chemicals for further DNT testing. To evaluate if electrical activity could be a suitable endpoint to detect chemicals with DNT effects, primary rat cortical cultures were exposed to domoic acid (DoA), a potential developmental neurotoxicant for up to 4 weeks. The MEA measurements indicate that long-term exposure to DoA increased the spontaneous electrical activity that could lead to possible neuronal malfunctioning. In addition, the response to the GABA_A receptor antagonist bicuculline was lower in the DoA long-term treated cultures compared to the control cultures. The obtained results suggest that the measurement of electrical activity by MEAs could be a useful tool to identify compounds with DNT potential.

1 Introduction

The development of the central nervous system (CNS) in fetuses and children has been shown to be more vulnerable to neurotoxicants as compared to the CNS of adults. This vulnerability is mainly due to the very complex developmental processes involving many different cell types and several different important key events, such as proliferation, migration and differentiation [1, 2].

Due to lack of knowledge only a few industrial chemicals have been identified as developmental neurotoxicants. Current developmental neurotoxicity (DNT) guidelines (OECD TG 426 and EPA712-C-98-239) [3, 4] are based entirely on *in vivo* studies that are both time consuming and costly. Consequently, there is a high demand to develop alternative *in vitro* methods for initial screening to prioritize chemicals for further DNT testing.

Here, to evaluate if electrical activity could be a suitable endpoint to detect chemicals with DNT effects primary rat cortical neurons grown on MEAs were exposed to domoic acid (DoA), a natural occurring toxin produced by diatom algae that accumulate in mussels and shellfish with potential to cause neurological changes in mammals [5].

DoA is structurally related to the excitatory neurotransmitter L-glutamate and activates α -amino-3-hydroxy-5-methyl-4-isoxazolepropionic acid and kainic acid receptors (AMPA/KA-R) which can lead to excitotoxicity [6, 7]. The toxin has mainly been studied in adult animals. However, prenatal exposure to DoA has been associated with neurobehavioral

changes [8, 9], such as an increase in response latency and rate of habituation. Moreover, prenatal exposure to DoA has been associated with e.g. damage to neurons in different brain regions and decreased brain levels of gamma-aminobutyric acid (GABA) and increased glutamate levels [10]. The interference of DoA with excitatory and inhibitory systems could lead to a disturbed overall neuronal activity resulting in serious functional CNS damage.

2 Methods

2.1 Characterization of cortical neuronal cultures by immunocytochemistry

Initially, primary rat cortical neurons grown on MEAs were characterized for different cell markers over time (nestin for neural precursor cells; NF-200 and Map-2 for neurons; GFAP for astrocytes), using immunocytochemistry to evaluate if the model could be suitable for DNT testing.

2.2 Treatment of cortical neuronal cultures

The neuronal cultures were treated with 5 or 50 nM DoA starting at 1 DIV until the cultures were considered mature (28-35 DIV) and the basal spontaneous electrical activity was recorded. Additionally, the response to the neurotransmitter GABA (10 μ M) and the GABA_A receptor antagonist bicuculline (20 μ M) was recorded in control and DoA long-term treated cultures.

2.2 Electrical activity recording

The activity was measured by the MEA120-2-System from Multi Channel Systems, using MEA Amplifier (Gain 1000x) and data were recorded by the MC Rack software at a sampling rate of 10 kHz. A band pass digital filter (60Hz-4000Hz) was applied to the raw signal in order to remove electrical background noise. The data were analyzed using well established methods from custom developed software tools [11, 12]. Various parameters (MBR, MFR, IBI and burst duration) were evaluated to assess the difference in activity between DoA long-term treated and control cultures and compared statistical by one- or two-way repeated measures (RM) ANOVA using the GraphPad Prism 5.0.

3 Results

3.1 Primary cortical neuronal cultures could be a promising *in vitro* model for DNT testing

Our results show that primary cortical neurons could be a promising *in vitro* model for DNT testing since some of the most critical neurodevelopment processes such as progenitor cell commitment, proliferation and differentiation of astrocytes and maturation of neurons are present (Fig. 1).

3.2 Long-term treatment with a low concentration of DoA increased the basal spontaneous activity

Long-term exposure to a low concentration (50 nM) of DoA significantly increased the basal spontaneous electrical activity as measured by spike and burst rates, as compared to the control cultures (Fig. 2).

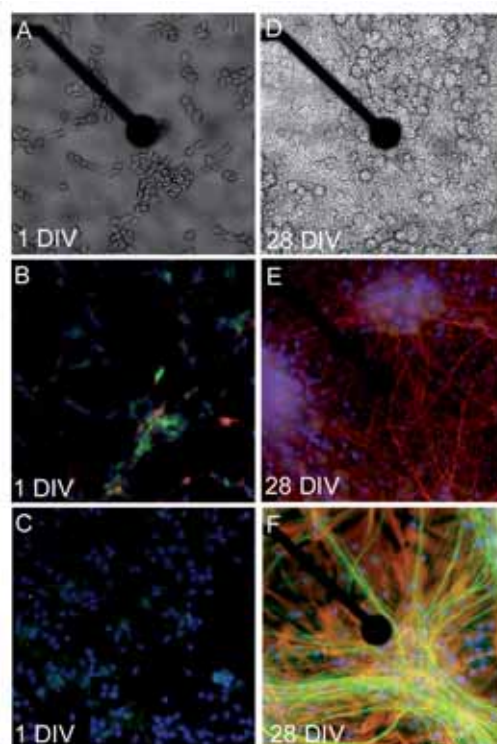


Fig. 1. Primary rat cortical cultures in phase contrast microscopy and characterized by immunocytochemistry over time. Phase contrast microscopy at (A) 1 DIV and (D) 28 DIV shows the cell culture development (note the difference in cell proliferation and differentiation). (B) At 1 DIV most of the cells express nestin (green) while only a few express Map-2 (red). The expression of Map-2 increased with time and nestin decreased (E) at 28. (C) Staining at 1 DIV for NF-200 (green) and GFAP (red) increased (F) at 28 DIV. Magnification: electrode diameter is 30 μ m.

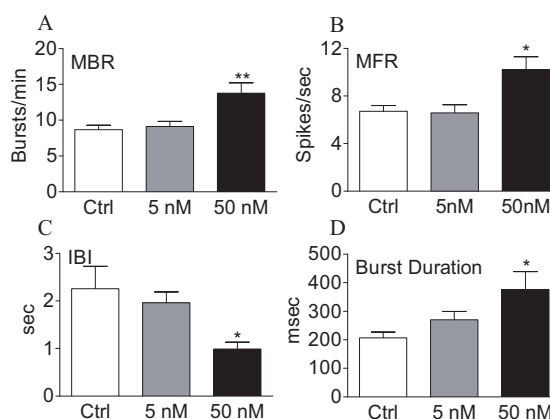


Fig.2. Basal spontaneous electrical activity in control cultures (open bars) and after long-term treatment with DoA 5 nM (grey bars) and 50 nM (black bars). Note the significant increase after long-term treatment with 50 nM DoA for (A) mean burst rate (MBR), (B) mean firing rate (MFR) and (D) burst duration time, while the (E) inter burst interval (IBI) was significantly decreased in the 50 nM DoA treated cultures. Data represent mean \pm S.E.M. of at least five independent experiments. *P<0.05 **P<0.01 comparing the activity between DoA long-term treated and control cultures.

There were no significant differences observed in the effect of the neurotransmitter GABA between DoA long-term treated and control cultures, as both cultures responded with significantly decreased MFR (Fig. 3).

In contrast, treatment with bicuculline induced a significantly different response in DoA long-term treated cultures compared to controls as the amount of total spikes and spikes in bursts did not increase above the basal spontaneous activity (Fig. 3). Even in the case of the cultures long-term treated with the lower concentration of 5 nM DoA, (the basal level of spontaneous activity was not changed) there was no response to bicuculline treatment.

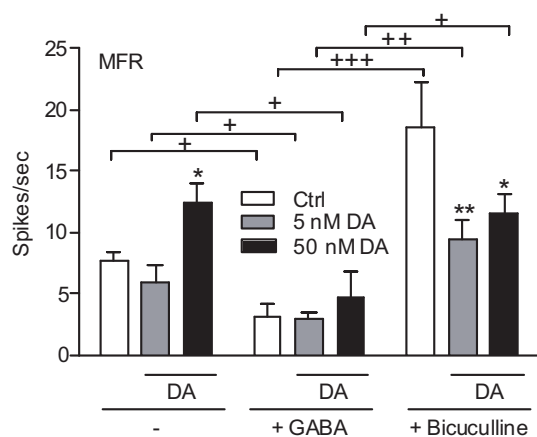


Fig. 3. Changes in electrical activity after treatment with GABA and bicuculline of control rat cortical cultures (open bars) and after long-term exposure to DoA (5 nM, grey bars and 50 nM, black bars) measured by mean firing rate (MFR). Data represent mean \pm S.E.M. of at least five independent experiments. * $P < 0.05$ ** $P < 0.01$ comparing the activity between DoA long-term treated and control cultures. + $P < 0.05$ +++ $P < 0.001$ comparing the activity before and after acute GABA and bicuculline treatment.

Bicuculline is a competitive antagonist of the GABA_A receptor and the treatment would block the effect mediated through this receptor. Our results indicate that the GABA_A receptor is involved in the spontaneous activity since the blocking of this receptor increased the basal level of the activity. The function of the GABA_A receptor seems to be down regulated by the long-term exposure to the DoA when compared with controls, possibly due to lower levels of the neurotransmitter GABA as has been observed in *in vivo* studies [10].

4 Conclusions

The data obtained indicate that electrical activity measurements can be used as a tool to detect chemicals with DNT potential. However, more DNT chemicals as well as non-neurotoxic chemicals (negative controls) should be tested to further confirm that electrical activity measurements could be used as a suitable endpoint for initial DNT screening purposes.

References

- [1] Rice, D. and Barone S Jr (2000). Critical periods of vulnerability for the developing nervous system: evidence from humans and animal models. *Environ Health Perspect* **108 Suppl 3**, 511-533.
- [2] Rodier, P. M. (1994). Vulnerable periods and processes during central nervous system development. *Environ Health Perspect* **102 Suppl 2**, 121-124.
- [3] OECD. (2007). Test Guideline 426. OECD Guideline for Testing of Chemicals. Developmental Neurotoxicity Study. <http://www.oecdbookshop.org/oecd/display.asp?lang=en&sf1=DI&st1=5L4FG25MNKXS>. [accessed 11 May 2010]
- [4] US EPA. (1998). Health Effects Guidelines OPPTS 870.6300 Developmental Neurotoxicity Study. http://www.epa.gov/ocspp/pubs/frs/publications/Test_Guidelines/series870.htm [accessed 11 May 2010]
- [5] Teitelbaum, J. S., Zatorre, R. J., Carpenter, S., Gendron, D., Evans, A. C., Gjedde, A., and Cashman, N. R. (1990). Neurologic sequelae of domoic acid intoxication due to the ingestion of contaminated mussels. *N Engl J Med* **322**, 1781-1787.
- [6] Berman, F. W., LePage, K. T., and Murray, T. F. (2002). Domoic acid neurotoxicity in cultured cerebellar granule neurons is controlled preferentially by the NMDA receptor Ca(2+) influx pathway. *Brain Res* **924**, 20-29.
- [7] Berman, F. W. and Murray, T. F. (1997). Domoic acid neurotoxicity in cultured cerebellar granule neurons is mediated predominantly by NMDA receptors that are activated as a consequence of excitatory amino acid release. *J Neurochem* **69**, 693-703.
- [8] Adams, A. L., Doucette, T. A., James, R., and Ryan, C. L. (2009). Persistent changes in learning and memory in rats following neonatal treatment with domoic acid. *Physiol Behav* **96**, 505-512.
- [9] Levin, E. D., Pizarro, K., Pang, W. G., Harrison, J., and Ramsdell, J. S. (2005). Persisting behavioral consequences of prenatal domoic acid exposure in rats. *Neurotoxicol. Teratol.* **27**, 719-725.
- [10] Dakshinamurti, K., Sharma, S. K., Sundaram, M., and Watanabe, T. (1993). Hippocampal changes in developing postnatal mice following intrauterine exposure to domoic acid. *J Neurosci* **13**, 4486-4495.
- [11] Chiappalone, M., Novellino, A., Vajda, I., Vato, A., and Martinoia, S. (2005). Burst detection algorithms for the analysis of spatio-temporal patterns in cortical networks of neurons. *Neurocomputing* **65-66**, 653-662.
- [12] Novellino, A., Chiappalone, M., Maccione, A., and Morefield, S. (2008). Neural Signal Manager: a collection of classical and innovative tools for multi-channel spike train analysis. *International Journal of Adaptive Control and Signal Processing* doi 10.1002/acs.1076.

Neuronal Networks Coupled To MEAs: A Tool For In Vitro Neurotoxicity Assessment? Results From An Inter-Laboratory Project

Antonio Novellino¹, Anna Price^{1*}, Taina Palosaari¹, Bibiana Scelfo¹, Maurice Whelan¹, Sergio Martinoia^{2,3}, Maria T Tedesco², Paolo D'Angelo², Michela Chiappalone³, Fabio Benfenati^{3,4}, Guenter W Gross⁵, Alexandra Gramowski^{6,7}, Olaf Schroeder⁷, Timothy j Shafer⁸, Andrew FM Johnstone⁸

1 JRC, Institute for Health and Consumer Protection, Ispra, Italy

2 KBTLab – DIBE and ett s.r.l., University of Genoa, Genoa, Italy

3 NeuroTech Lab – NBT, Italian Institute of Technology, Genoa, Italy

4 DIMES, Section of Physiology, University of Genoa, Genoa, Italy

5 Dept. Biol. Sciences and CNNS, University of North Texas, Denton TX, USA

6 Institute of Biological Sciences, University of Rostock, Rostock, Germany

7 NeuroProof GbmH, Rostock, Germany

8 Neurotoxicology Div., U. S. Environmental Protection Agency, RTP, NC, USA

* corresponding author: anna.price@jrc.ec.europa.eu

The functional output of the brain is the electrophysiology and in vitro neuronal networks coupled to micro electrode arrays represent a simplified model for investigating neurons activity in response to external manipulation. The aim of this project is to prove the inter- and intra-laboratory robustness and reproducibility of MEA based measurements for neurotoxicity test. Different laboratories around the world took part to the study and different experimental models, materials and methods have been used, compared and are discussed.

1 Introduction

The gold standard assay for electrophysiological assessment of in vitro electrophysiology is the patch clamp electrophysiology but, although its success is noteworthy, there is a general consensus in the field that progress has been significantly hampered because of the low-throughput nature of the technique.

Novel methods like electrophysiological recordings from in vitro neuronal network coupled to multi electrode array (MEA) chips provide a valuable alternative to conventional techniques.

The MEA is a planar substrate embedded with an array of microelectrodes that are capable of measuring extracellular electrophysiology (i.e. spikes and bursts - packages of spikes) from electro-active tissues.

The MEA are non invasive, label free and provide simpler approach and higher throughput (up to hundreds of recording points) than conventional electrophysiological techniques, and have been started using for monitoring both acute and chronic effects of drugs and toxins.

The aim of this project is to prove the inter- and intra-laboratory robustness and reproducibility of MEA based measurements for neurotoxicity test. Different laboratories around the world took part to the study and different experimental models, materials and methods have been used, compared and are discussed

2 Methods

Six independent laboratories (3 in Italy, 1 in Germany, 2 in USA); 3 test series of cumulative increasing concentration-response curves: Fluoxetine (FLU), Muscimol (MUS), Verapamil (VER); 5 brain models: mouse cortex (E14-15), cryopreserved mouse cortex (E14-15), murine Balb-C (E16) cortex, rat cortex (E16-18), and new born (0-24h) rat cortex; More than 100 independent experiments (about 700 hours of recordings) with different recording systems (Multichannel System, Plexon and custom systems); Common acceptance criteria on morphology and spontaneous electrophysiology; 8 different electrophysiology parameters: mean firing rate, mean bursting rate, burst number, mean burst duration, mean number of spike in burst, mean inter burst interval, spike number, spike in burst vs total.

3 Results

Results show high levels of intra- and inter-laboratories reproducibility and robustness. Network firing rate (i.e. MFR) has been identified as the best parameter for neurotoxicity assessment (Fig.1).

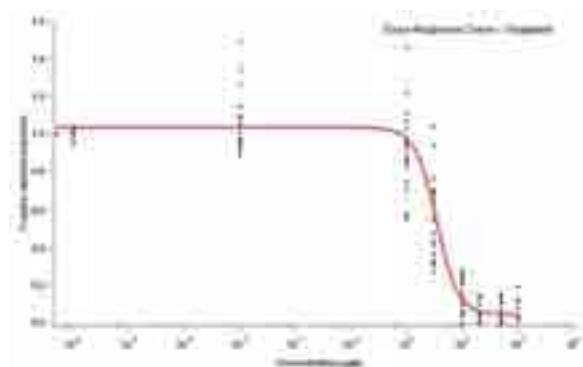


Fig. 1. The dose response curve for the Verapamil

The IC₅₀s have been extracted from normalized mean firing rate (MFR). Tab 1 reports the IC₅₀s for the studied compounds.

Tab.1

	IC ₅₀ [μM]	Stdev [μM]
FLU	2.17	0.21
MUS	0.24	0.03
VER	3.45	0.35

4 Conclusions

Results are very robust and the presence/absence of serum during recording is likely to explain the achieved differences.

Participants used different electrophysiology descriptors to assess the reagents effects but the mean (total) Firing Rate has been identified as the best one: it is sensitive, robust, can be easily extracted and it is less affected by the applied “detection method”.

The quality of the recording depends on the quality of the network that is expressed by the very well defined bursting behaviour, where burst are (relatively) frequent packages of activity separated by periods of silence.

Selection criteria have been discussed and refined, three criteria are left:

1. Quality of bursting activity → the active electrodes have to have well defined burst (with specific frequency (at least 6bursts/min)) where burst is activity in between (relatively long lasting) silent period
2. Spike detection → S/N ratio, minimum requirement 2:1 (around 6times rms)
3. Spiking activity → total number of spike at least 30 spikes/min (not at unit level but at channel level)

In order to be sure that the network expresses the typical bursting activity a minimal culture age of 3 weeks in case of newborn cortex neurons and 4 weeks in case of embryonic cortex neurons is required (i.e. minimal age requirement).

Disclaimer

This abstract does not reflect the policy of the US Environmental Protection Agency).

Bioimpedance spectroscopy of an epithelial cell culture on a MEA chip

H.D. Wanzenboeck¹, C. Peter¹, L. Schneider¹, M. Hufnagl¹, M. Fischeneder¹, A. Hoefler¹, S. Damnjanovic¹, C. Fillafer², M. Wirth², F. Gabor² and E. Bertagnolli¹

¹ Vienna University of Technology, Institute for Solid State Electronics, Floragasse 7/1, A-1040 Vienna, Austria

² University Vienna, Department of Pharmaceutical Technology and Biopharmaceutics

Althanstrasse 14, A-1090 Vienna, Austria

* Corresponding author. Heinz-wanzenboeck@tuwien.ac.at

Bioimpedance measurement of cell cultures during their growth phase has been used to monitor the progressing cell growth of an adherent Caco-2 cell culture. A microelectronic interface with MEAs or IDEs was fabricated on glass substrates by microlithographic methods. A cell culture of Caco-2 cells was grown directly on the sensor surface. The electrode structure was used to measure the impedance of the cell layer in a 2-terminal and 4-terminal measurement configuration. The growth of the adherent cell monolayer could be electrically monitored and showed changes of the impedance by a factor of 8. The electrical impedance showed a good correlation with the biologic growth process of the Caco-2 monolayer.

1 Background / Aims

Pharmacological research increasingly applies cell cultures for drug screening as well as for drug transport studies. The increasing demand for inexpensive and fast scanning of new pharmaceutical substances and testing of their bioavailability have resulted in a rush for cell culturing methods. For orally administered drugs the transport through the epithelial barrier of the intestine is a pharmacologically most relevant process. To test the barrier function of the epithelial monolayer the electrical resistance of the cell layer has been found to be an accurate indicator.

In this study we demonstrate the diagnostic potential of impedance spectroscopy for Caco-2 cell cultures. This adherent epithelial cell line represents an acknowledged pharmaceutical model for the human intestine [1]. The Caco-2 cell culture is seeded on top of the microelectrodes and subsequently grows directly on the microelectrodes. The characteristic electrical properties of human Caco-2 cell cultures are investigated by impedance measurement. The electrochemical analysis of ex-vivo cultures allows continuous, non-destructive analysis of living cells. From the transepithelial electrical resistance (TEER) biological parameters such as cell density or confluence of cell layers have already been successfully derived [3]. The goal of our work was to establish electrochemical impedance sensing as non-invasive, in-situ monitoring method for living Caco-2 cell cultures. This work introduces different microelectronic sensor systems for adherent Caco-2 cell cultures directly grown on the sensor interface.

2 Methods

Using lithographic methods microelectrodes were fabricated on glass substrates. Different configurations including microelectrode arrays (MEAs) of regularly arranged microelectrodes down to $2 \times 2 \mu\text{m}$ size as well as interdigitated electrode sensors (IDES) with 2 electrodes for 2-terminal measurement and with 4 electrodes for 4-terminal measurement were realized (Fig. 1). The electrodes were fabricated from gold by physical sputter deposition. Insulating layers were fabricated by plasma enhanced chemical vapour deposition. The microelectrode substrates were measured by a LCR-meter allowing to measure the impedance in a wide frequency range from 50 Hz up to 1 MHz.

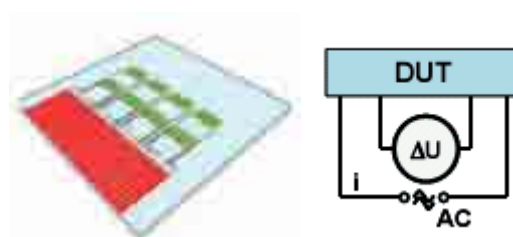


Fig.1. Schematic setup of the impedance chip showing (i) the glass substrate with 8 sensor areas each sensor area has 2 pairs of interdigitated electrodes to facilitate a 4-terminal measurement (ii) schematic illustration of 4-terminal measurement setup.

Caco-2 cell cultures were directly grown on the sensor interface (Fig. 2). The cell suspension was directly seeded on to the sensor areas and cells were allowed to proliferate for up to 14 days in RPMI-medium. Cell culture growth was performed within an incubator to guarantee suitable and constant growth conditions. The microelectrodes were permanently connected to the electrical measurement setup, so that

a continuous measurement became feasible. Data were recorded by a computer.

3 Results

The Caco-2 cells were grown directly on the microstructured surface. A continuous cell layer was observed (Fig. 2) and fluorescence markers specifically bonded on the cell membrane proved a dense package of cells without any gaps.

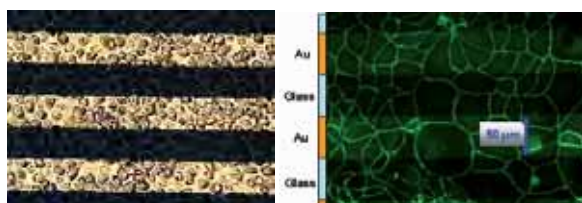


Fig. 2. Microscope images of Caco-2 cells grown on an interdigitated electrode sensor. The metal electrodes are 50 μm wide. (i) Reflected light image of confluent Caco-2 cell layer on the microelectrode sensor. (ii) fluorescent image of Caco-2 cell layer on the microelectrodes with fluorescent dyed cell membranes.

Continuous monitoring of the electrical parameters of cell cultures was performed [2] with impedance measurement systems. An alternate current (AC) signal with voltage amplitudes below 500 mV was introduced to protect cells and nutrient from galvanic reactions. Basolateral and transepithelial electrode configurations with 2-terminal or 4-terminal configuration were evaluated. For evaluation of the different microelectrode setup impedance spectroscopy of inorganic electrolytes including physiological 0,9% NaCl-solution and electrolytes of different pH was performed. A calibration for concentration gradients as well as pH-changes was made. 2-terminal sensors proved sensitive above 5.000 Hz while 4-terminal sensors proved sensitive already above 200 Hz.

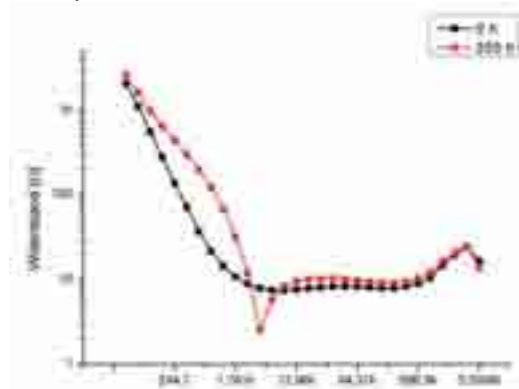


Fig. 3. Frequency dependence of the impedance of (a) a suspension of Caco-2 cells in RPMI-medium at time of seeding ($t=0\text{h}$) and (b) of a Caco-2 cell layer grown on top of the microelectrode sensor area at $t=250\text{h}$ post seeding.

The cell growth was monitored by the frequency-dependence of the systems response and showed

decreasing impedance with increasing frequency (Fig. 3). Especially the range between 200 to 2.000 Hz displayed strong changes of the impedance during growth of the surface adherent Caco-2 monolayer.

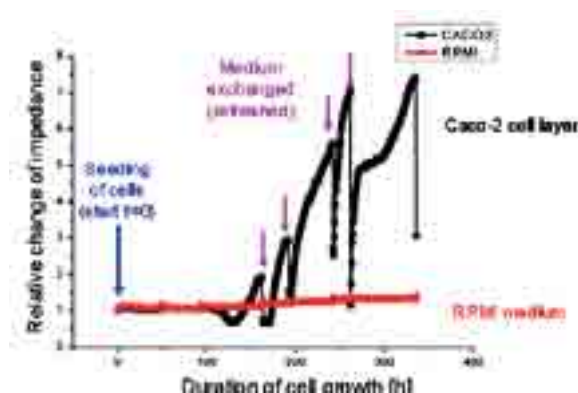


Fig. 4. Time dependent change of the impedance in relation to the start value. The shown time series of the impedance was recorded for a 805 Hz signal. Times when the RPMI medium is refreshed can be identified by a decrease of impedance.

The change of the impedance during Caco-2 cell growth was extracted for the selected frequency of 805 Hz. Changes were illustrated as relative change compared to the initial value. Significant signal changes of the impedance (up to 7-fold) were observed as result of the cell layer growth (Fig. 4).

4 Conclusion

Different microelectronic sensor designs were successfully compared. The 4-terminal sensor proved more sensitive over a wider frequency range than 2-terminal sensors. With 4-terminal probes electrode impedance was strongly reduced so that a lower frequency range became accessible. Ion concentration gradients as well as pH-gradients can be detected by impedance spectroscopy. Electrochemical impedance of living cells could be monitored from seeding to confluence of the cell layer. With the presented approach a continuous, non-destructive monitoring of growth of Caco-2 cells on the sensor was demonstrated by impedance spectroscopy.

Acknowledgement

We thank the Austrian Society for Micro- and Nanoelectronics (GMNE) for support of this study.

References

- [1] Hidalgo, I.J., Raub, T.J., Borchardt, R.T., (1989) Characterization of the human colon carcinoma cell line (Caco-2) as a model system for intestinal epithelial permeability, *Gastroenterology* 96(3), 736-749
- [2] K'Owino, I.O., Sadik, O.A. (2005) Impedance spectroscopy: A powerful tool for rapid biomolecular screening and cell culture monitoring, *Electroanalysis* 17 (23), 2101-2113

Actions Of Pyrethroid Insecticides On Cortical Networks: Comparison Of Relative Potencies Determined Using MEAs To Relative Potencies Determined Using Motor Activity

Andrew F.M. Johnstone¹, Marcello Wolansky², Kevin M. Crofton¹ and Timothy J. Shafer^{1*}

¹ Integrated Systems Toxicology Division, U.S. Environmental Protection Agency, Research Triangle Park, NC, USA

² Departamento de Química Biológica, Universidad de Buenos Aires, Buenos Aires, Argentina

* Corresponding author. E-mail address: shafer.tim@epa.gov

The effects of twelve pyrethroid insecticides on spontaneous electrical activity were investigated in primary cultures of cortical neurons grown on microelectrode arrays. GABAergic transmission was blocked by bicuculline and SCH50911, and concentration-dependent effects of each pyrethroid (1 nM - 50 μ M) were examined. All compounds caused a concentration-dependent reduction in spike frequency (#spikes/min). Cyhalothrin was most potent compound tested, with an IC₅₀ value of 25 nM for spike frequency inhibition. Resmethin was the least potent compounds tested with an an IC₅₀ value of 16.9 μ M for spike frequency inhibition. Relative potency for each compound was determined using deltamethrin (an IC₅₀ value = 175 nM) as an index chemical. These relative potency values were then compared to in vivo relative potency values for eleven of the same chemicals determined using a behavioural activity assay. Despite differences between in vivo and in vitro assays, the relative potencies of the 11 chemicals were qualitatively comparable (how – qualitatively or quantitatively – or both) between the two different assays. These results indicate that MEAs can provide a reliable way to determine the relative potency for pyrethroids.

1 Introduction

Pyrethroid insecticides are utilized in a variety of agricultural, industrial and residential products. The insecticidal and toxicological actions of pyrethroids are mediated via disruption of neuronal voltage-sensitive sodium channel (VSSC) function [1]. VSSCs control the initiation and propagation of action potentials and are critical to control of electrical excitability in neurons. Pyrethroids disrupt the kinetics of VSSC function.

Pyrethroid toxicity is characterized by two different clinical syndromes; Type I syndrome consists of hyperexcitability and tremors, while type II syndrome consists of choreoathetosis and salivation. A small number of compounds exhibit characteristics of both syndromes (mixed) [2]. These different syndromes correlate with the ability of pyrethroids to prolong inactivation of VSSCs as well as with structural moieties. All type I compounds lack a cyano group on the alpha carbon...

We have characterized the actions of 12 different pyrethroid compounds on activity of glutamatergic networks of neurons grown on microelectrode arrays to determine the relative potency of these compounds. The relative potencies of eleven of these compounds have also been determined using their ability to decrease motor activity as a measure of effect [3].

2 Methods

2.1 Solutions

All compounds were provided by their manufacturers and were of known purity and isomer composition [3] with the exception of tetramethrin, which was obtained from ChemService (West Chester, PA). Stock solutions (10 mM) of each compound were prepared daily in 1:1 DMSO:Ethanol, from which serial dilutions were prepared. Total DMSO did not exceed 0.05% (v/v) at any pyrethroid concentration and was without effect on network activity. All recordings were made in culture medium.

2.2 Tissue culture

All animal protocols were approved by the US EPA NHEERL Institutional Animal Use and Care Committee and were designed to minimize animal pain and distress. Cultures of frontal cortex neurons were prepared as described previously for hippocampal neurons [4]. Cortical cells were plated (250,000cells/MEA) on 200/30 TiGR multielectrode arrays (MCS, Reutlingen, Germany).

2.3 Recordings

Extracellular recording of action potentials were made as previously described [4] using hardware and software from Multichannel Systems (Reutlingen, Germany) except that a 128 channel, 4 amplifier system was used. All recordings were made in the presence of 20 μ M bicuculline and 10 μ M SCH50911 to block GABA-A and GABA-B receptors, respectively. Data were saved to a personal computer for later analysis.

3 Results

All twelve pyrethroids inhibited mean network spike rate in a concentration-dependent manner. λ -cyhalothrin was the most potent, while resmethrin was the least potent compound tested. The rank order of potency of the compounds is provided in Table 1. Compounds that are classified as Type II pyrethroids were in general more potent than Type I or mixed type pyrethroids.

4 Summary

The neurotoxicity of pyrethroid insecticides has been widely studied at the whole animal level as well as at the cellular and subcellular level. However, to date, the relative potency of pyrethroids on function of interconnected neurons has not been examined. In fact, relative potency of pyrethroids on mammalian neurons has been lacking for any measure. The data demonstrate that pyrethroids potentially inhibit network activity in cultures of frontal cortex neurons. λ -Cyhalothrin was the most potent compound, while resmethrin was the least potent compound; being 100 fold less potent than deltamethrin. In general, type II compounds were more potent than type I or mixed type compounds. Qualitatively, this observation is consistent with in vivo relative potency estimates for pyrethroids [3]. Collectively, these data demonstrate that MEA approaches can be used to rapidly determine relative potency factors for neuroactive chemicals disrupting network activity such as pyrethroids. Even though toxicokinetic differences are not accounted for by the in vitro MEA measurements, the results are qualitatively consistent with in vivo measures of relative potency.

Acknowledgement

We thank Ms Jadie Baldwin and Sandra Losa, North Carolina State University for technical support.

Disclaimer

The information in this document has been funded by the U.S. Environmental Protection Agency. It has been subjected to review by the National Health and Environmental Effects Research Laboratory and approved for publication. Approval does not signify that the contents reflect the views of the Agency, nor

does mention of trade names or commercial products constitute endorsement or recommendation for use. This is preliminary data and is subject to review and further analysis. Do not cite or quote.

References

- [1] Narahashi, T (1992): Nerve membrane Na^+ channels as targets of insecticides. *Trends Pharmacol Sci.* 13, 236-241
- [2] Soderlund, D.M., Clark, J.M., Sheets, L.P., Mullin, L.S., Piccirillo, V.J., Sargent, D., Stevens, J.T., and Weiner, M.L., 2002. Mechanisms of pyrethroid neurotoxicity: implications for cumulative risk assessment. *Toxicology* 171, 3-59.
- [3] Wolansky MJ, Gennings C, Crofton KM. (2006) Relative potencies for acute effects of pyrethroids on motor function in rats. *Toxicol Sci.* 89, 271-277.
- [4] Meyer D.A, Carter J.M., Johnstone A.F.M, Shafer T.J. (2008) Pyrethroid modulation of spontaneous neuronal excitability and neurotransmission in hippocampal neurons in culture, *Neurotoxicology* 29(2) 213-225.

Table 1 IC_{50} and Relative Potency Values for inhibition of mean spike rate by pyrethroid compounds.

<u>Compound</u>	<u>IC_{50} (nM)</u>	<u>Rel Potency</u>
λ -Cyhalothrin (II)	25	7.000
Deltamethrin (II)	175	1.000
Cypermethrin (II)	181	0.967
β -Cyfluthrin (II)	305	0.574
Bifenthrin (I)	439	0.399
Tefluthrin (I)	499	0.351
Permethrin (I)	719	0.243
Esfenvalerate (I/II)	809	0.216
S-Bioallethrin (I)	1525	0.115
Fenpropathrin (I/II)	1518	0.115
Tetramethrin (I)	3250	0.054
Resmethrin (I)	16850	0.010

Mean spike rate was determined in the absence and presence of increasing concentrations of pyrethroid compounds and the concentration-response data were fitted to a sigmoidal concentration-response using GraphPad Prism to determine IC_{50} values. The relative potency (rel potency) of each compound was then determined using deltamethrin as an index chemical. Deltamethrin was selected as the index chemical due to the large amount of data on this compound and its previous use as an index chemical for in vivo determinations of relative potency [3]. Type I compounds are denoted with (I) following the compound name, type II compounds with (II) and mixed compounds with (I/II).

Profiling of acute neurotoxic effects of insect repellents with MEA-neurochip technology

O. H.-U. Schroeder^{1,*}, D.G. Weiss², K. Jügel¹, A. Gramowski^{1,2}

¹ NeuroProof GmbH, Rostock, Germany

² Institute of Biological Sciences, Cell Biology and Biosystems Technology, University of Rostock, Rostock, Germany

* Corresponding author. E-mail address: olaf.schroeder@neuroproof.com

The microelectrode array (MEA) neurochip technology offers an attractive *in vitro* endpoint for neurotoxicity evaluation of chemicals in the context of regulatory requirements. Currently, neurotoxicity assessment required by the OECD and EC test guidelines is based solely on *in vivo* testing. *In vitro* recordings from cultured neuronal networks on MEAs represent a powerful method to evaluate the dynamics of activity changes in response to chemical exposure. MEA-neurochip technology combined with sophisticated data analysis methods represent a simplified model to study the electrophysiological behavior and are a powerful tool for this objective.

We tested as an example two insect repellents: DEET (diethyltoluamid, N,N-diethyl-3-methylbenzamide) and EBAAP (ethyl 3-[acetyl(butyl)amino]propanoate).

1 Methods/Statistics

With the MEA-neurochip technology, it is possible to generate three different kinds of results. First, with an acute application paradigm it is possible to assess the acute toxicity by determining general EC_{50} values. Second, the comparison of the induced changes of activity patterns with effects of previously tested reference substances can deliver insights into the mechanisms of action. Third, dose repeated treatments can be performed to characterize chronic effects.

We used primary frontal cortex networks on MEA neurochips to study the acute and chronic effects of the substances on the electrical activity regarding inhibition, excitability, synchronicity, oscillation, and burst structure. For all reference and test compounds we calculated 200 activity describing parameters which were used for data analysis.

Through pattern recognition analyses and comparisons with our database of 85 previously established substance profiles we obtain information on the possible physiological roles and modes of action.

2 Results

DEET has a lethal dose of LD_{50} for rats between 2170 and 3664 mg/kg body weight. In acute tests with primary frontal cortex networks on MEA-neurochips we found an EC_{50} value for spike rate activity changes of 413 μ M (Fig. 1)

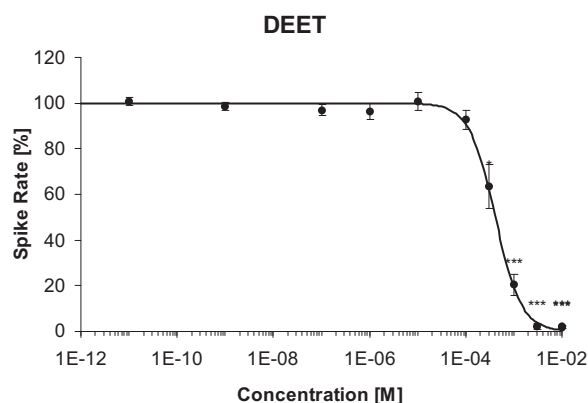


Fig. 1. Dose response curve for DEET.

The LD_{50} of EBAAP is 14.000 mg/kg body weight. In acute tests with MEA-neurochips, the EC_{50} value for spike rate activity changes was 2.48 mM (Fig. 2).

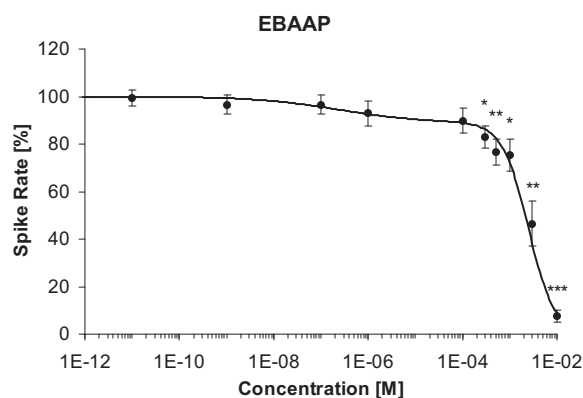


Fig. 2. Dose response curve for EBAAP.

Subsequently, we compared DEET and EBAAP effects with those of 85 electrophysiological activity patterns of substances in our database. For DEET we determined significant similarities (in descending order) to Epibatidine, Apomorphine, Xli093, L-655.708, CTAP, Orexin B, NPY, NMDA, Valproic acid, and Cyclosporine A. For EBAAP, we identified considerable similarities (in descending order) to: Apomorphine, Xli093, Ultiva, AMPA, Zolpidem, lithium chloride, nor-Binaltorphine, Clonazepam, LaCl₃ and SB 205384.

3 Conclusion

We showed that MEA-neurochip technology can deliver predictive quantitative and qualitative information for the assessment of potential neurotoxic effects of compounds. Thus, the MEA neurochip technology provides an attractive *in vitro* endpoint for neurotoxicity evaluation of chemicals in the context of regulatory requirements.

Acknowledgement

Funded by the European Community's 7th Framework Programme, grant 222927, Project: ENAROMaTIC.

New multi-target opioid peptides in drug development: Electrophysiological profiling using MEA neurochip technology

Alexandra Gramowski^{1,2,*}, Olaf Schröder², Konstantin Jügelt², Andrzej Lipkowski³, Aleksandra Misicka-Kesik⁴, Dirk Tourwé⁵, Dieter G. Weiss¹

1 Institute of Biological Sciences, Cell Biology and Biosystems Technology, University of Rostock, Rostock, Germany;

2 NeuroProof GmbH, Rostock, Germany

3 Polish Academy of Science, Medical Research Centre, Warsaw, Poland

4 Faculty of Chemistry Warsaw University, Warsaw, Poland

5 Vrije Universiteit Brussel, Organic Chemistry, Brussel, Belgium

* Corresponding author. E-mail address: alexandra.gramowski@neuroproof.com

Progressive pain associated with advanced stages of cancer is the major factor that destructs the last span of a patient's life. Here more potent analgesics are needed. The focus of the EU project consortium NORMOLIFE is on the development of new, highly effective multi-target analgesics.

1 Methods

We used primary frontal cortex and spinal cord networks on MEA neurochips to study acute affects of peptides on the electrical activity regarding inhibition, excitability, synchronicity, oscillation, and burst structure. For all reference and new compounds we calculated 200 activity describing parameters which were used for data analysis. The complex description of activity changes of neuronal networks co-cultured with glia allows the quantification of the compounds' complex modes of action. Our analyses provide multiparametric information on neuronal activity changes to assess the therapeutic or toxicological potential of neuroactive drugs. Through pattern recognition analyses and comparisons with data of established analgesic drugs we obtain information on the physiological activity and potency of the new synthetic peptides.

2 Results

We investigated the electrophysiological *in vitro* effects of 30 newly synthesised peptides by comparison with a substance database of a variety of well-characterized agonists and antagonists of the three opioid and other pain relevant receptor systems. Further, we developed decision criteria for the prioritization for further development of synthesised peptides as potential new analgesic drug candidates. These decision criteria are: binding affinities, EC values of *in vitro* experiments, multiple modes of action, similarity to the Sufentanil pattern for analgesic properties, and similarity to the Gabapentin pattern for anticonvulsive properties.

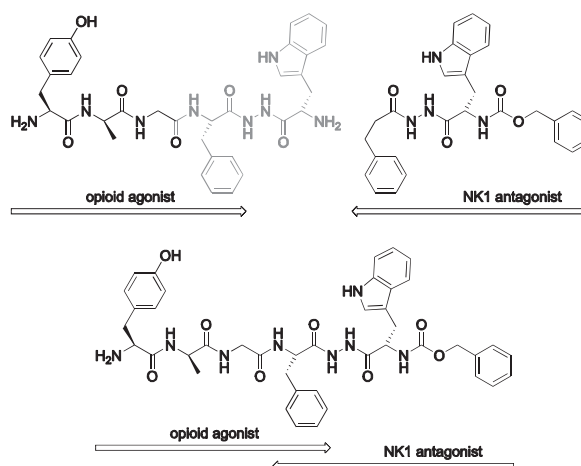


Fig. 1. Multi-target compounds: synthetic chimeric peptides combine molecular parts binding different receptors (opioid and neurokinin-1 receptors).

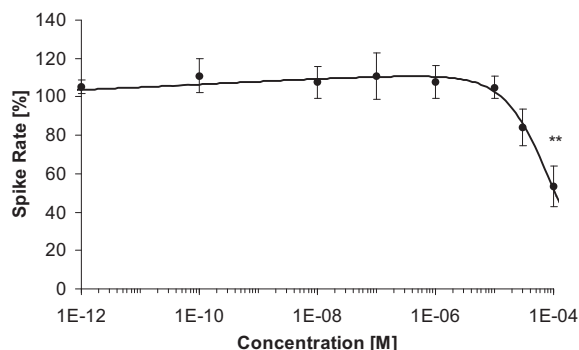


Fig. 2. Dose response curve of a multi-target compound.

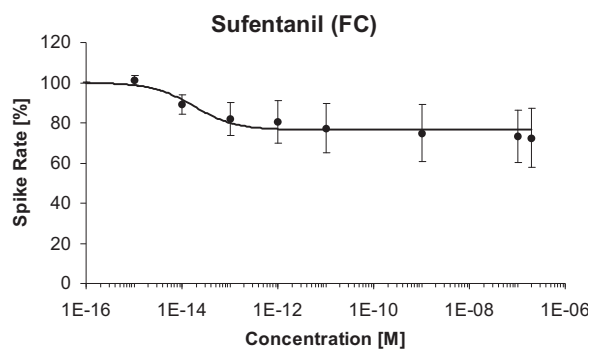


Fig. 2. Dose response curve of sufentanil, the reference compound for analgesic properties.

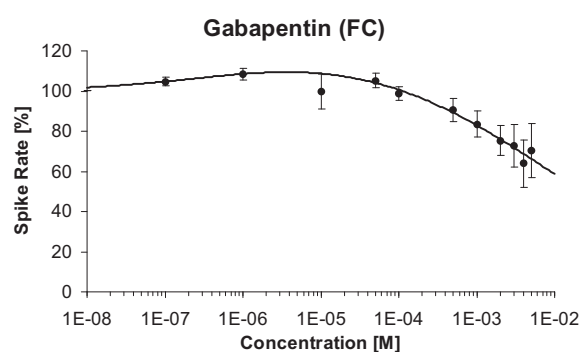


Fig. 2. Dose response curve of gabapentin, the reference compound for anticonvulsant properties.

3 Conclusion

With these results we have for the first time developed a predictive *in vitro* model for the analgesic potency which is not solely based on a single parameter but rather on a description of the global activity changes. We demonstrated that an *in vitro* model is feasible for the prediction of physiological behaviour. This is a promising prospect for the *in vitro* MEA-neurochip technology, as it is a long-standing aim of drug development research.

Acknowledgement

Funded by the European Community's 6th Framework Programme (FP6/2007-2013) grant LSHC-CT-2006-037733.

In vitro toxicity and cytotoxicity of the immunosuppressant cyclosporine A

Konstantin Jügelt¹, Luise Schultz^{1,3}, O. H.-U. Schröder¹, Christophe Landry⁴, Romeo Cecchelli⁴, Dagmar-Christiane Fischer³, Dieter Haffner³, Dieter G. Weiss², Alexandra Gramowski^{1,2,*}

¹ NeuroProof GmbH, Rostock, Germany

² Institute of Biological Sciences, Cell Biology and Biosystems Technology, University of Rostock, Rostock, Germany

³ Department of Pediatrics, University Children's Hospital Rostock, Rostock, Germany

⁴ Université Lille Nord de France, Laboratoire de Physiopathologie de la Barrière Hémato-encéphalique, Lens, France

* Corresponding author. alexandra.gramowski@neuroproof.com

Neurotoxicity of immunosuppressive drugs such as cyclosporine A (CsA) is seen in patients after organ transplantation. The exact mechanisms by which these drugs induce neurotoxicity are unknown, so that we undertook a MEA-based study on the *in vitro* effects of CsA.

1 Methods/Statistics

We investigated neurotoxic vs. cytotoxic effects of acute and chronic treatments with CsA in three *in vitro* models: the MEA neurochip technology, an *in vitro* blood brain barrier (BBB) model, and conventional viability assays based on LDH. This approach can be used as a new tool for the advanced pre-clinical development of CNS pharmaceuticals and for safety pharmacology which lack predictive and reliable *in vitro* models. The MEA technology combines multi-site recordings with optimized multiparametric data analysis to evaluate the dynamics of spontaneous electrophysiological activity in response to chemicals. The *in vitro* BBB model provides important information of the compounds BBB permeability needed to complete *in vitro* neurotoxicity assessment.

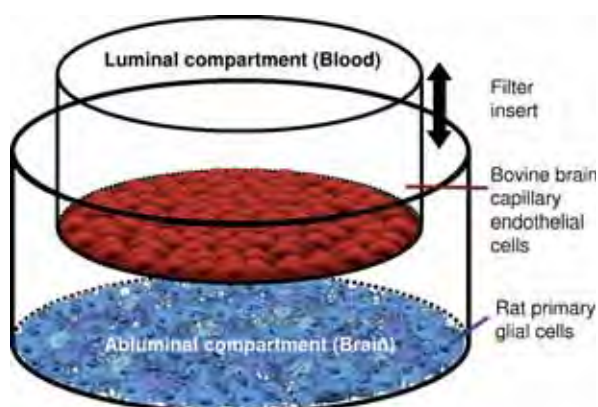


Fig. 1. Illustration of the blood brain barrier model consisting of capillary endothelial cells that separate the glial cells in the "brain" from the "blood" compartment where substances are added.

2 Results

CsA shows toxic effects on the BBB at 100 μ M. Therefore, BBB model experiments have been carried out at 10 μ M. For acute and repeated dose (7days) exposure, BBB permeability coefficients were found to be 0.26×10^{-3} and 0.13×10^{-3} cm/min.

In cortical networks CsA induced an acute biphasic change of the electrical activity: a small decay at very low concentrations and an increase starting at 1 microM, followed by total cessation of the activity at concentrations higher than 100 μ M (Fig. 2).

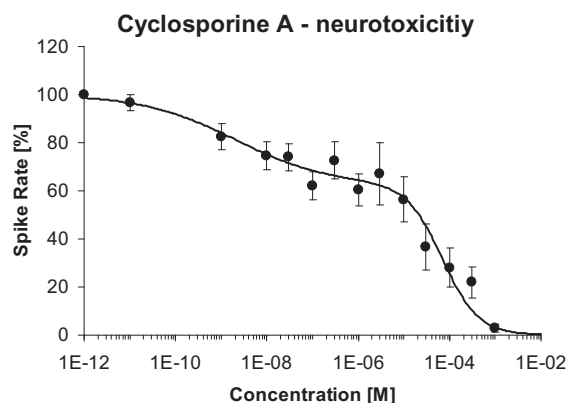


Fig. 2. Dose-response curve of the spontaneous activity of a neuronal network on MEA neurochips in response to accumulating concentrations of cyclosporin A.

Within this concentration range CsA induced only a moderate LDH release of 15% (Fig. 3), indicating a higher sensitivity for functional neurotoxicity over cytotoxicity when overlaying the two functions (Fig. 4)

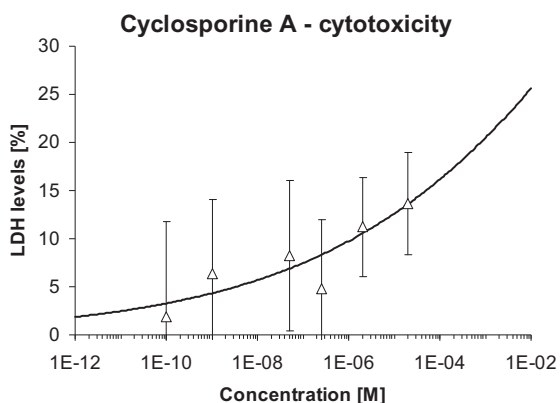


Fig. 3. Acute (1 day) LDH levels in the medium of primary neuronal network cultures indicate a comparatively low cytotoxicity.

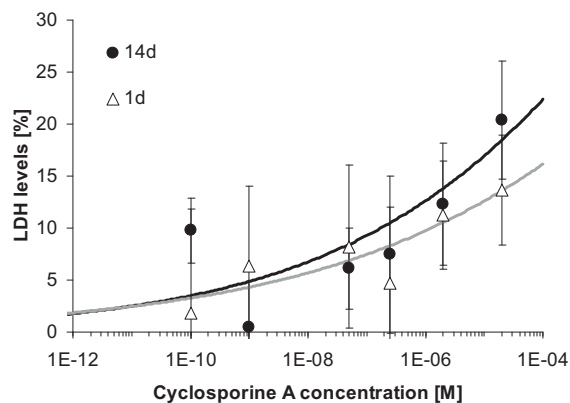


Fig. 5. Acute versus chronic LDH levels after cyclosporin A application on primary neuronal network cultures.

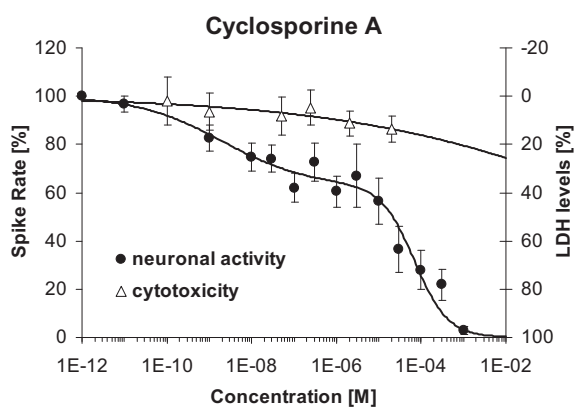


Fig. 4. Comparison of neurotoxicity and acute cytotoxicity. Note that the secondary axis showing the LDH levels as indicators of cytotoxicity has been reversed (as opposed to Fig. 3).

Chronic treatment (7 days) of cortical cultures with CsA revealed an increase in cytotoxicity compared to acute treatment (1 day) (Fig. 5).

3 Conclusion

Taken together the damaging effects of CsA on the BBB and the toxic effects on the neurophysiology at the micromolar range, propose an explanation of its neurological side-effects. Thus, the combination of the MEA neurochip technology with the *in vitro* BBB model enables one to better predict the effects of potential drug candidates on the central nervous system, to define a rough therapeutic range and to indicate possible unwanted neurotoxic side-effects at an early stage in drug development.

Acknowledgement

Funded by the European Community's 7th Framework Programme (FP7/2007-2013), grant 202222, Project PREDICT IV.

Characterization of a mice model of human epilepsy with Multi-Electrode Arrays

Davide Boido^{1,2*}, Enrico Ferrea^{1,2}, Diego Ghezzi¹, Pasqualina Farisello^{1,2}, Pietro Baldelli^{2,1}, Fabio Benfenati^{1,2}.

¹ Department of Neuroscience and Brain Technology, Italian Institute of Technology, Genova, Italy

² Department of Experimental Medicine, Section of Physiology, University of Genova, Genova, Italy

* Corresponding author. E-mail address: davide.boido@iit.it

We applied microelectrode array (MEA) recordings to study the generation and propagation of epileptiform activity in various connected regions of cortico-hippocampal slices obtained from Synapsin I/II/III knockout (TKO) mice and the effects of the synaptic vesicle-targeted antiepileptic drug levetiracetam (LEV). Synapsins (SynI, SynII and SynIII) are synaptic vesicle phosphoproteins playing a role in synaptic transmission and plasticity. TKO mice display an epileptic phenotype and mutation of the *SYN1* gene is associated with epilepsy in man. We found that both interictal (IIC) and ictal (IC) discharges induced by 4AP were more pronounced and widespread in TKO mice, revealing a state of hyperexcitability of TKO networks. To get insight into the frequencies characterizing the IC seizures, we analyzed the average IC power spectral density (PSD) in the 10-50 Hz range in different cortical regions. TKO slices exhibited an increase of power for frequencies above 20Hz with respect to Wild-Type (TWT). To determine whether the hyperexcitability of TKO slices is also reflected by an increased spread of IC discharges and taking advantage of the spatial resolution of the MEA device, we measured the percentage of electrodes recording IC discharges over the total number of cortical electrodes. The spread of excitation was significantly higher in TKO slices than in TWT ones and treatment with LEV decreased the spread of IC discharges in the entorhinal of TKO slices. In order to better characterize the propagation of the IIC events in the hippocampus, we recently coupled MEA recordings with optical imaging using voltage-sensitive dyes by exploiting the possibility of simultaneous recordings with a high spatial and temporal resolution to reveal more detailed patterns of propagation.

1 Introduction

Genetically engineered mouse lines have provided a number of valuable epilepsy models with the potential to link epileptogenesis to changes in both selected genes and neuronal function (Noebels, 2003). The genetic deletion of the Syns in mice is of particular interest in this respect, because it represents the first model of epilepsy based on concomitant alterations of the release of excitatory and inhibitory neurotransmitters and because of the widespread distribution of these SV proteins in the synapses of the central nervous system. TKO provide a unique animal model to investigate cellular and network mechanisms underlying epileptogenesis, because mice are normal at birth but, from the second month of age, they start showing epileptic attacks whose severity increases with age. Moreover a missense mutation of the *SYN1* gene was identified in a four generation family whose male members were affected by partial temporal lobe or frontal lobe epilepsy or by various combinations of epilepsy, learning difficulties, macrocephaly and aggressive behavior (Garcia et al., 2004)

2 Materials and Methods

Acute horizontal cortico-hippocampal slices (250 μm thick) were obtained from 3 weeks-old TWT and TKO mice. Slices were transferred over a planar MEA (500-30 TiN internal reference, Multi Channel System® - MCS, Reutlingen, Germany) coated with poly-ornithine (500 $\mu\text{g}/\text{ml}$), and fixed by the use of a little platinum anchor. Experiments were performed at 34°. Spontaneous and electrically evoked activity was recorded on brain slices treated with 4-aminopyridine (4AP), a potassium channels blocker, that elicited typical epileptiform waveforms consisting of sporadic long-lasting IC seizures and frequent short-lasting IIC events [4]. IC discharges were principally present in the cortex, while IIC events were recorded from both hippocampus and cortex, sometimes propagating among these regions. Evoked epileptic activity was recorded for 3 sec after biphasic stimulation (amplitude: 1mA, duration: 40 μs for each phase) applied on the hilus. PSD analysis has been performed on the frequency range from 10 to 50Hz and the comparison among slices of different genotypes, treated or not with LEV was made with Kolmogorov-Smirnov test on the integral of the PSD distribution. Further experiments were performed on

hippocampal slices by coupling MEA recordings with voltage sensitive dye optical imaging. The voltage sensitive dye RH 795 (Invitrogen) was used to label cell membranes at a concentration of 0.1mg/ml. IIC events, evoked by stimulating in the hilus, were optically monitored with a CCD camera (Red Shirt imaging).

3 Results

Average power spectral density (PSD) histogram and average PSD integral in the 10-50 Hz frequency band were calculated for IC seizures recorded in 3-weeks-old TWT and TKO cortex (Fig. 1A,B). The PSD analysis revealed that IC events in slices from TKO mice were composed of a higher frequency components with respect to TWT (Fig. 1B). Cortical spread of IC events (Fig.1C), calculated as the mean percentage of electrodes recording IC discharges over the total number of the electrodes covering the specific brain area, was used as an estimation of the IC spreading in the entorhinal cortex of TWT, TWT+LEV, TKO and TKO+LEV mice.

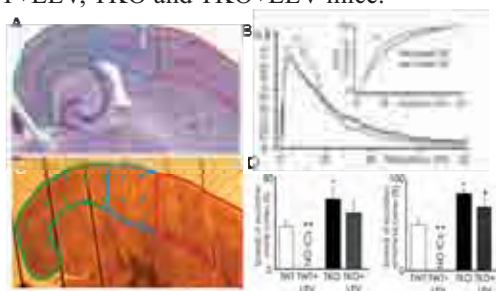


Fig. 1. Anatomical distinction of the regions composing the cortico-hippocampal slices tested in our experiments (A). Analysis of PSD profile (B) and spread of excitation (C, D) of IC seizures

The spread of excitation analysis showed a wider area involved with IC discharges for TKO with respect to TWT in the whole cortex, while LEV succeeded in confining the spread in a area similar to TWT in entorhinal cortex. (Fig. 1D).

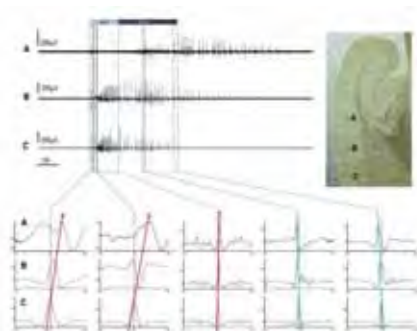


Fig. 2. Propagation of 4-AP induced IC discharges recorded in acute cortico-hippocampal brain slices obtained from 3-weeks-old TKO mice

Fine spatio-temporal monitoring of the propagation of IC events is allowed by MEA recordings. Multi-site recording and cross-correlation algorithms let us measure not only the direction but also the delays of each phase of the IC discharges.

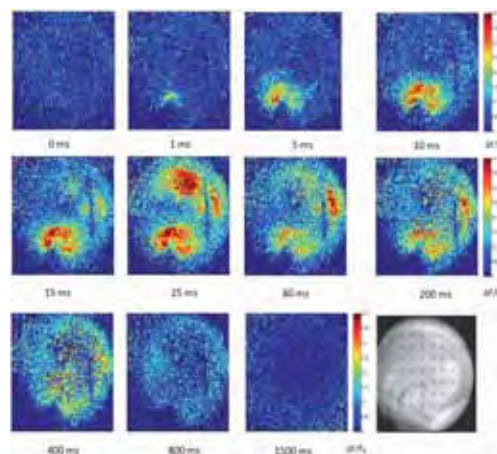


Fig 3. Propagation of evoked epileptic activity in the hippocampus after stimulation in the region of hilus which involves multiple areas. Stimulation on slices treated with 4-AP induces a long lasting depolarization which lasts up to 1 sec.

Moreover, a more precise estimation of the propagation trajectories of IIC events as well as propagation velocities can be evaluated with the voltage sensitive dye optical imaging (Fig.3).

4 Conclusions

MEA recording combined with voltage sensitive dye optical imaging is a very efficient approach to define neurophysiological mechanisms underlying *in vitro* epilepsy in slice preparation. This technique permit to precisely analyse parameters, such as the spread of excitation and cross-correlation among different electrodes, and to address confining and propagation issues on IC discharges.

Acknowledgement

We thank drs. Paul Greengard (The Rockefeller University, New York, NY) and Hung-Teh Kao (Brown University, Providence, RI) for providing us with the mutant mouse strains. This study was supported by research grants from the Compagnia di San Paolo, Torino (to FB, FV and PB), the Italian Ministry of Health Progetto Giovani (to PB), UCB SA Brussels-Belgium and UCB Pharma S.p.A. Milano - Italy. The support of Telethon-Italy (Grant GGP09134 to FB and FV and GGP09066 to PB) is also acknowledged.

References

- [1] Noebels JL, (2003) The biology of epilepsy genes, Annual Review Neuroscience. 26: 599-625.
- [2] C. C. Garcia, et al., (2004): Identification of a mutation in synapsin I, a synaptic vesicle protein, in a family with epilepsy *Journal of Medical Genetics*, 41, 183-186.
- [3] Cavalleri GL et al., (2007) Multicentre search for genetic susceptibility loci in sporadic epilepsy syndrome and seizure types: a case-control study. *Lancet Neurol.* 6:970-980.
- [4] Sudbury JR and Avoli M, (2007) Epileptiform synchronization in the rat insular and perirhinal cortices in vitro, *Eur. J. Neurosci.* Vol. 26, pp. 3571-3582

The A-beta 42/40 Ratio Is a Driver of Acute Synaptotoxicity and LTP Impairment

Iryna Benilova^{1,2,3}, Seon-Ah Chong^{3,7}, Inna Kuperstein^{1,2}, Kerensa Broersen^{4,5}, Joost Schymkowitz^{4,5}, Frederic Rousseau^{4,5}, Carmen Bartic^{3,6}, Geert Callewaert^{7*}, Bart De Strooper^{1,2*}

1 Department for Molecular and Developmental Genetics, Flanders Institute for Biotechnology (VIB), Leuven, Belgium

2 Laboratory for the Research of Neurodegenerative diseases, Center for Human Genetics, KU Leuven, Belgium

3 IMEC, MCP/ART, Heverlee, Belgium

4 SWITCH Lab, VIB, Leuven, Belgium

5 Vrije Universiteit Brussels (VUB), Belgium

6 Department of Physics and Astronomy, KU Leuven, Belgium

7 Research Group Neurodegeneration, KU Leuven, Kortrijk, Belgium

* Corresponding authors. E-mail address: Geert.Callewaert@kuleuven-kortrijk.be and bart.destrooper@cme.vib-kuleuven.be

The amyloid peptides A β 42 and A β 40 contribute differentially to Alzheimer's disease progress. As a rule, A β oligomers but not monomers or fibers are associated with high neurotoxicity, but neither the structure nor conformation of A β toxic species has been determined so far. We show here that small alterations in A β 42/40 ratio significantly affect the synaptotoxic potential of A β peptide assessed in brain slices and primary hippocampal cultures by means of MEA.

1 Methods

1.1 Amyloid-beta preparation

Pre-aggregate free A β 40 and A β 42 solutions were prepared from dry peptides (rPeptide, USA) using HFIP-DMSO based procedure. The final solution was solvent-free, which was confirmed by mass spectrometry. An aggregation of various A β 42/40 ratios in buffer was monitored by means of Thioflavin T-based assay, transmission electron microscopy and FTIR [1].

1.2 Electrophysiology

Hippocampal neurons were isolated from E17-18 mouse embryos and plated on a MEA substrate (Multichannel Systems), Fig. 1. Spontaneous firing in neuronal cultures was recorded at 7th-11th DIV, before and after the treatment with A β , Fig.2. The threshold for spike detection was set to 5 standard deviations of the average noise amplitude.

Hippocampal slices (250 μ m) obtained with a vibratome were kept in ice-cold ACSF solution and they were placed onto MEAs (Fig. 3) for LTP induction and recording. Test stimuli were delivered every 60 s and the amplitude was adjusted to 40% of the maximum field EPSP (fEPSP) response. Slices were perfused with A β dissolved in ACSF solution for 20 min before induction of LTP, and then LTP was induced by 2 trains of HFS (100 Hz) with 20 s interval. During LTP recording, A β solution was replaced with normal ACSF solution.

2 Results

We investigated how the aggregation time and mixture composition determine A β peptide synaptotoxicity in vitro [1]. Spontaneously active neural cultures grown on MEA chips were used for biological evaluation of A β species at sublethal concentrations. The spike firing frequency was taken as a readout of neuron electrical output. By use of MC_Rack software (Multichannel Systems), we computed the rate of firing by integrating all spikes picked up by every active electrode over 60 s [2].

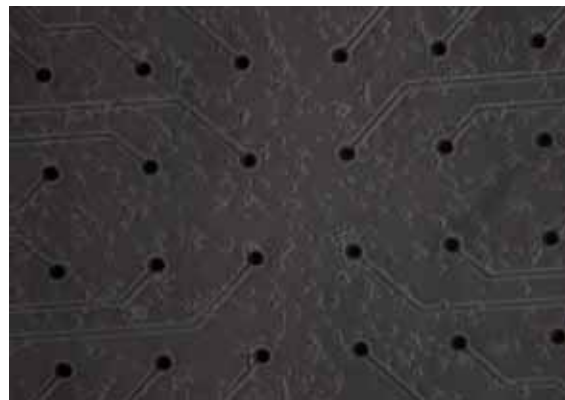


Fig. 1. Hippocampal culture grown on MEA chip for 2 days.

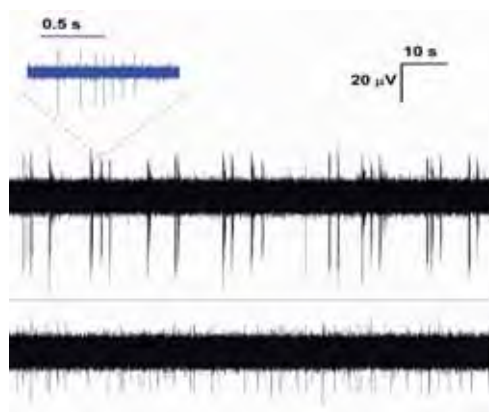


Fig. 2. A β 42 impairs spontaneous synaptic activity. Upper trace: baseline, lower trace: after 30 min of treatment with amyloid.

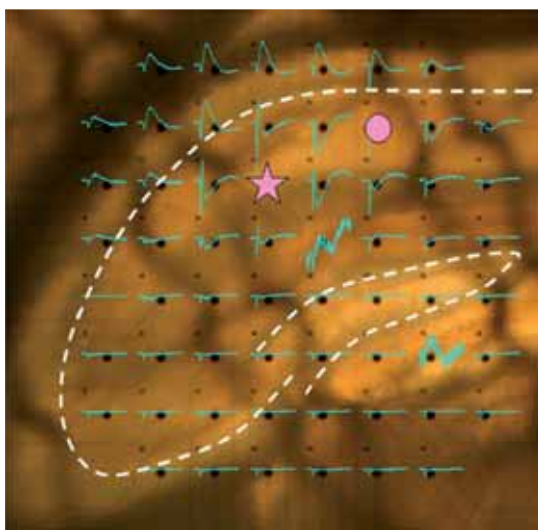


Fig. 3. fEPSP recordings on a hippocampal slice with a 200/30 MEA. The star electrode was used for stimulation and the circle electrode was used for control pathway.

We found that pre-aggregated mixtures containing 90-100% of A β 40 („physiological“ mixtures) had no effect on neuronal electrical activity while pure A β 42 but also some of its mixtures with A β 40 („pathological“ mixtures) could readily suppress the spike firing in less than 30 min [1-2]. These data will be discussed in more detail during presentation. Preperfusion of adult mouse hippocampal slices with „pathological“ A β 42/40 mixtures caused LTP impairment in CA1 region compared to the LTP shown in control slices perfused with ACSF with the buffer instead of A β . On the other hand slices perfused with „physiological“ preparations showed similar level of LTP as that of control slices, corroborating the toxicity pattern obtained on the primary hippocampal cultures.

We next explored the reversibility of acute synaptic dysfunction, and found that pre-treatment of neurons with anti-A β antibodies (6E10 or A11) fully protected the neurons from oligomer-mediated synaptotoxicity. Currently, we try to reveal whether or not immunodepleted A β preparations will fail to induce LTP impairment, too.

Overall, we will show that amyloid oligomer toxicity is a dynamic property which depends upon equilibrium between the two major A β species, A β 40 and A β 42. By means of a MEA-based read-out, we prove that the acute toxic impact of transient A β oligomers is synaptic in nature rather than cytotoxic.

Acknowledgement

This work was supported by the Fund for Scientific Research, Flanders; the Artificial SynApse (IWT ASAP), Federal Office for Scientific Affairs, Belgium IUAP P6/43, a Methusalem grant of the KULeuven and the Flemish Government, and MEMOSAD (F2-2007-200611) of the European Union, an FWO Odysseus grant, and the Alzheimer Research Trust (ART) UK.

References

- [1] Kuperstein I., Broersen K., Benilova I., Rozenski J., Jonckheere W., Debulpaep M., Vandersteen A., Bartic C., D'Hooge R., Martins I., Rousseau F., Schymkowitz J., De Strooper B. (2010), submitted.
- [2] Benilova I., Kuperstein I., Broersen K., Schymkowitz, Rousseau F., Bartic C., De Strooper B. (2009) MEA neurosensor, the tool for synaptic activity detection: acute amyloid- β oligomers synaptotoxicity study. *IFMBE Proceedings 25/VIII*, ed. by O. Dössel and W. Schlegel (Springer), 314-316.

A MEA-based Assay of Adrenal Chromaffin Cells Spontaneous Firing Using Ion Channel Blockers

Andrea Marcantoni¹, Jonathan Rojo-Ruiz¹, Sara Gosso¹, Alberto Pasquarelli², Valentina Carabelli¹, Emilio Carbone^{1*}

¹ Department of Neuroscience; NIS Center, CNISM Research Unit, University of Torino, I-10125 Torino (Italy)

² Institute of Electron Devices and Circuits, Ulm University, 89069 Ulm, Germany

* Corresponding author. E-mail address: emilio.carbone@unito.it

Chromaffin cells express high-densities of Na⁺, Ca²⁺ and K⁺ channels and are able to fire action potentials when depolarized by pA currents. Their electrical activity determines the level of intracellular Ca²⁺ that controls the vesicular release of adrenaline and noradrenaline. Cultured rat chromaffin cells (RCCs) fire spontaneously at low frequencies (0.5-1.5 Hz) in a tonic or burst mode. Two open issues concerning RCCs spontaneous activity are still unanswered: is the firing a true physiological phenomenon or a consequence of cell alteration during intracellular recordings? How many RCC firing-modes do exist and what is their physiological function? We answered these questions using a MEA-based assay and ion channel modulators to understand the ability of these cells to fire spontaneously and to extend our knowledge regarding the involvement of different ion channel conductances in the modulation of the MEA-recorded action potentials shape.

1 Introduction

Rat chromaffin cells (RCCs) of the adrenal medulla have high access resistance at rest and possess sufficient high densities of Na⁺, Ca²⁺ and K⁺ channels to generate all-or-none action potentials (APs) when injecting small amounts of current (3-5 pA) through the cell membrane. In short time culture conditions, RCCs preserve their spherical shape and, unlike neuronal preparations, they do not develop dendrites and form neuronal networks. Unlike the neurons, where the ion channels distribution varies greatly from the soma to the dendrites or the axon, RCCs exhibit a homogeneous distribution of voltage activated channels that sustain spontaneous AP firing, thus decreasing the variability of extracellular waveforms that can be detected with MEA. These properties make the chromaffin cells an interesting model for studying extracellular AP activity.

Considering the different role of Na⁺, Ca²⁺ and K⁺ channels in the generation of action potentials we initiated a detailed study of the spontaneous (autorhythmic) firing of RCCs using a 60 MEA system made of 30 μm electrode diameter separated by 200 μm distance (MCS GmbH, Reutlingen, Germany). The purpose of the study was dual: *1*) to monitor the spontaneous electrical activity of RCCs by means of extracellular recording, thus leaving unaltered and more similar to the physiological conditions the intracellular medium; *2*) to identify the role of ion channels controlling AP firings by analyzing the changes of AP shape and bursting modes induced by selective ion channel blockers.

2 Materials and Methods

Isolated RCCs were plated on a MEA culture chamber and kept in a CO₂ incubator for 2-5 days before recordings. RCCs ready for recordings appeared as round spherical cells inter-dispersed within the 60 MEA. The standard extracellular

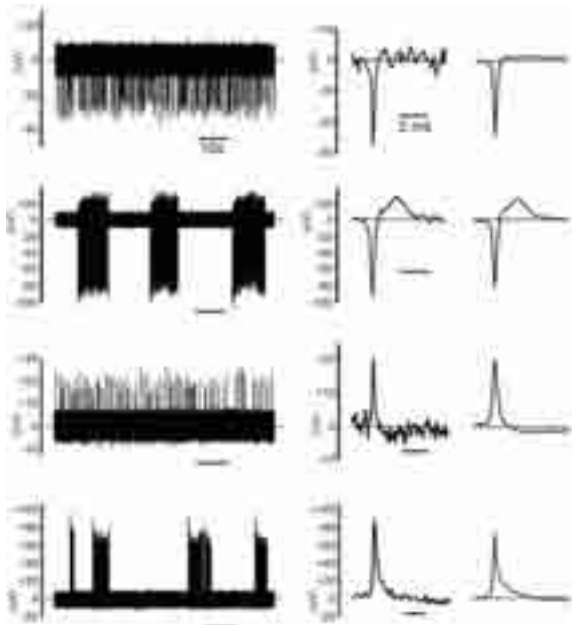


Fig.1: Different action potential waveforms recorded by MEAs. The two top recordings had tonic and burst mode of firing (left) while the APs had anti-capacitative time courses. To the right are shown the fast waveforms of a single and an averaged AP. The two bottom recordings had similar properties but the APs had inverted time course (capacitative response).

solution contained (mM) 135 NaCl, 4 KCl, 2 Ca₂Cl, 2 MgCl₂, 10 Hepes, 10 Glucose (pH 7.4). All the drugs were directly injected in the MEA chamber and the signal were recorded 10 minutes after the administration.

For perforated patch-clamp experiments performed in current clamp mode (not shown) we used the same extracellular solution used for the MEA recordings and the intracellular solution contained (mM): 135 KAsp, 8 NaCl, 20 HEPES, 2 MgCl₂, 5 EGTA.

3 Results and Discussion

RCCs dispersed on MEAs form stable contacts and possess multiple spontaneous activities (Fig. 1) recorded in 25% of the active microelectrodes. RCCs had two distinct firing-modes: tonic (41%) and bursts (59%), which could occur in combination depending on the number of cells contacting the microelectrodes. Spontaneous activity lasted for the entire duration of the experiments and APs had different forms and amplitudes. They were mostly biphasic with either a prominent fast 1st negative peak followed by a smaller

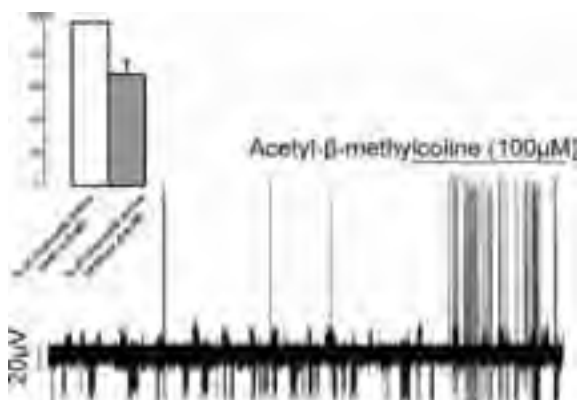


Fig.2: Increased firing frequency induced by the muscarinic agonist methacholine (100 μM) on one RCC generating APs with a strong early positive phase.

and slower 2nd positive peak (anti-capacitative response; proportional to $-\delta V_m/\delta t$) (Fig. 1) or had nearly opposite shape (capacitative response) [1].

We were somehow surprised of the low percentage of microelectrodes that were able to monitor spontaneous firings in normal physiological conditions. This could be due to an intrinsic property of cultured RCCs or to the limited number of cells effectively contacting the MEAs. In order to quantify the amount of cells that were potentially able to fire spontaneously and were in close contact with the electrode, we activated the RCCs with the muscarinic receptor agonist methacholine (100 μM) that is considered to induce spontaneous firing in all RCCs. We then calculated the percentage of cells spontaneously active by comparing them to those that were firing only in the presence of methacholine (Fig. 2). Assuming that the number of active electrodes in the presence of methacholine represents 100% of the

electrodes potentially able to monitor APs, we estimated that 68 ± 8 % of the electrodes were already active before methacholine administration and that in the presence of the agonist the percentage of active electrodes increased only by 32%. This allowed concluding that nearly 70% of cultured RCCs are spontaneously firing in normal physiological conditions.

It has been already demonstrated that RCCs possess high density of Ca²⁺-activated K⁺ channels (BK channels) mainly involved in the fast AP repolarization phase [2]. Recently, we have demonstrated the existence of tight coupling between L-type and BK channels in mouse chromaffin cells [3], thus we wanted to investigate the effect on both the spontaneous firing and AP shape induced by the BK channel blocker paxilline. Our preliminary experiments show that paxilline reduces of the firing frequency and blocks the 2nd positive (or negative) AP peak (Fig. 3). This closely resembled the effects of adding nifedipine and confirms the functional coupling between L-type and BK channels already reported in rat and mouse chromaffin cells [2, 3].

4 Conclusions

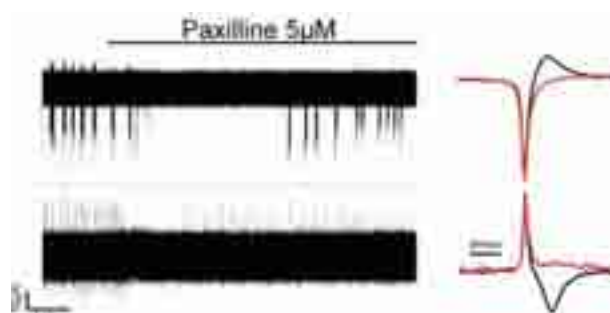


Fig.3: Effect of 5 μM paxilline on AP shape and firing frequency on two distinct MEA electrodes.

Our preliminary experiments demonstrate that the MEA is an effective tool for studying drug action on RCCs excitability, allowing the detection of spontaneous APs from a large number of available cells without altering their intracellular environment as it occurs in patch-clamp experiments.

Acknowledgments

This work was supported by the Marie Curie RTN “CavNET” (contract No. MRTN-CT-2006-035367), and the Foundation Compagnia di San Paolo (contract No 2008.2191 to AM).

References

- [1] Fromherz P. (1999) *Eur Biophys J.* 28: 254-258
- [2] Marcantoni A. et al. (2007) *Cell Calcium* 42: 397-408
- [3] Marcantoni A. et al. (2010) *J Neuroscience* 30: 491-504

Alcohol effects on cortical cultures

Kosmas Deligkaris^{1*}, Jan Stegenga¹, Joost le Feber¹

¹ University of Twente, Enschede, The Netherlands

* Corresponding author. E-mail address: Kraig33@gmail.com

The effects of alcohol on cortical cultures were investigated and analyzed using well-known mathematical and statistical methods. Dissociated cultures were plated on MEAs and ethanol administration took place up to concentrations of 150mM. Analysis included mean firing rates, raster plots, cross-correlation and conditional firing probabilities, complemented by ANOVA tests. Results indicate that although the network's activity is reduced, the strength of individual, persisting connections seems less prone to change by ethanol application.

1 Background

1.1 Effects of alcohol on human behaviour

The 'Alcohol dependence syndrome' has been well described by Edwards [1], presenting several different aspects of alcohol addiction. These effects can be mental or physical, including alcohol tolerance, physical dependence and inability to control intake [2]. It is also established that people stopping chronic alcohol consumption may suffer from epileptic seizures or delirium tremens [3].

1.2 Effects of alcohol on brain mechanisms

The results of alcohol on human behaviour can be attributed to neurological changes in the brains of the individuals. NMDA, AMPA and GABA_A receptors have been implicated in these changes [4-6]. For example, ethanol acts as an NMDA receptor antagonist, while chronic ethanol consumption leads to their upregulation in order to compensate for the acute blockade. Reduced sensitivity to ethanol may lead to tolerance effects, while seizures can be explained by increased NMDA receptor availability after withdrawal [5]. Likewise, decreased GABA_A receptor activation contributes to tolerance [4].

1.3 Effects of alcohol on cortical cultures

In order to understand alcohol mechanisms in the central nervous system (CNS) both cellular and networks studies should take place. Single cell studies provide information about the isolated cellular response. Simple networks may be more appropriate to study brain mechanisms. The aim of this study is to show the effects of ethanol on the network level.

2 Methods

2.1 Preparation and experiments

Cortical cells were extracted from newborn Wistar rats (P1) and plated on a 60 electrode MEA. MEAs were filled with 700ml R12 medium [7] and

stored in an incubator, under standard conditions. A total of 11 experiments were conducted using 4 different cultures, aged between 14 and 19 days in vitro. Ethanol was administered in a sterile environment outside the recording set-up, using a micropipette. We made a stock solution of ethanol in R12, in such concentration that addition of 5ul (<1% of the total volume) to the culture medium yielded a 25mM concentration increase. After the baseline phase, we added 5ul of plain medium to check the procedure's effects (control phase). Then, we increased the ethanol concentration to 50, 100 and 150mM in sequential steps.

2.2 Analysis methods

We analyzed both the activity and connectivity of the network. Activity was analyzed by means of Mean Firing Rates (MFRs) and raster plots, while the connectivity was visualized with cross-correlograms and conditional firing probabilities (CFP) [8]. In a cross-correlogram the peak's absolute value depends on the number of events, making difficult their interpretation and comparison. The CFP algorithm is cross-correlation based and aims at solving this problem. In the CFP algorithm all phases were divided into datablocks of 2¹⁴ spikes each. ANOVA was used to test the significance of the effects.

3. Results

3.1 Activity

Ethanol significantly (ANOVA, P<0.05) reduced the total activity of the network in a dose-dependent way. However, it is evident from the dose-response curve that even at the concentration of 150mM the activity reduction did not saturate (figure 1). Raster plots (figure 2) showed a decrease in both tonic activity and bursts accordingly.

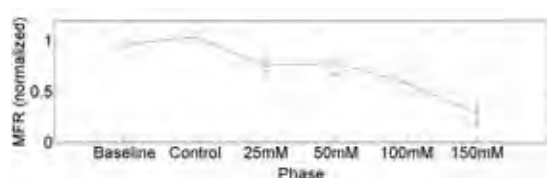


Figure 1. Dose-response curve, presenting the normalized MFRs of all cultures (mean \pm SEM). All curves were normalized to the average of baseline and control phase.

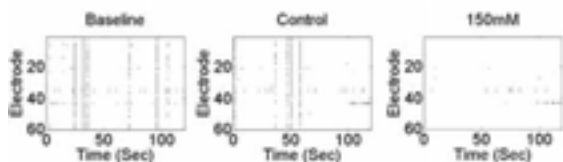


Figure 2. Example of raster-plots. A random two-minute period was chosen in each phase.

3.2 Connectivity

Figures 3-5 show six randomly chosen cross-correlograms among all possible pairs of electrodes. The control phase appears similar to baseline, while ethanol reduced the connection strength. In some cases, the strength of the connection seemed to increase with ethanol administration (figure 5, right). Analysis of individual connections with CFP (figure 6) showed that the strongest connections were, on average, not dependent on ethanol.

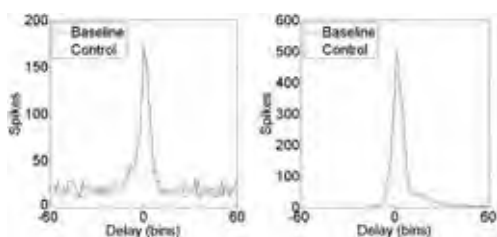


Figure 3. Cross-correlograms of two randomly chosen electrodes

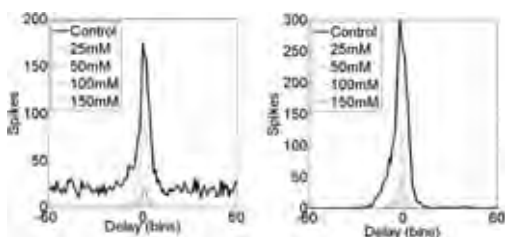


Figure 4. Cross-correlograms of two randomly chosen electrodes illustrating the effect of ethanol.

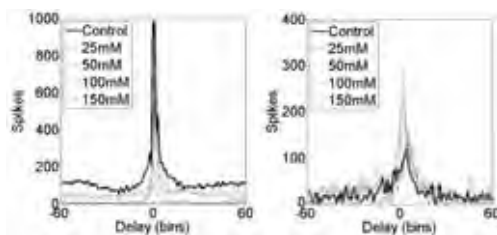


Figure 5. Cross-correlograms of two randomly chosen electrodes illustrating the effect of ethanol.

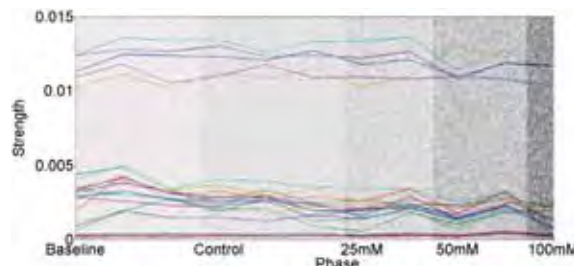


Figure 6. Examples of individual functional connections. Each phase is represented with a different background colour.

4 Discussion

Ethanol administration gradually reduces the network's activity. Our results agree with cellular studies showing a 50% reduction of AMPA and NMDA mediated currents around 150mM [6]. The peaks of cross-correlograms both increased and decreased with ethanol administration. On the contrary, CFP strengths reveal highly stable values. The difference is possibly due to the dependence of the cross-correlogram on the actual number of events. Our finding that the strongest connections remain unaffected, despite the general activity decrease, might indicate that alcohol mainly influences the weaker connections. However, it seems more likely that alcohol enhanced GABAergic responses in the networks. CFP, like all cross-correlation based methods, is more sensitive to excitatory connections. If the decrease in the MFR is mostly due to enhanced GABAergic function this could explain why the connections' strength curves do not follow a decrease similar to that of the MFR.

References

- [1] Edwards G. (1986). *The alcohol dependence syndrome: a concept as stimulus to enquiry*. *Addiction*, **81**(2), 171-183.
- [2] Hoffman P., Tabakoff B. (1996). *Alcohol dependence: a commentary on mechanisms*. *Alcohol and Alcoholism*, **31**(4), 333.
- [3] Hughes J. (2009). *Alcohol withdrawal seizures*. *Epilepsy & Behavior*, **15**(2), 92-97.
- [4] Enoch M. (2008). *The role of GABAA receptors in the development of alcoholism*. *Pharmacology Biochemistry and Behavior*, **90**(1), 95-104.
- [5] Krystal J. et al. (2003). *N-methyl-D-aspartate glutamate receptors and alcoholism: reward, dependence, treatment, and vulnerability*. *Pharmacology and Therapeutics*, **99**(1), 79-94.
- [6] Wirkner K. et al. (2000). *Mechanism of inhibition by ethanol of NMDA and AMPA receptor channel functions in cultured rat cortical neurons*. *Naunyn-Schmiedeberg's Archives of Pharmacology*, **362**(6), 568-576.
- [7] Romijn H. et al. (1984). *Towards an improved serum-free, chemically defined medium for long-term culturing of cerebral cortex tissue*. *Neuroscience and biobehavioral reviews*, **8**(3), 301.
- [8] Le Feber J. et al. (2007). *Conditional firing probabilities in cultured neuronal networks: a stable underlying structure in widely varying spontaneous activity patterns*. *Journal of Neural Engineering*, **4**, 54-67.

Assessment of Neuroprotective Strategies Using MEAs

Geoff Mealing^{1*}, Joseph S Tauskela¹, JP Thivierge^{1,2} Anthony Krantis³

1 National Research Council, Institute for Biological Sciences, Synaptic Therapies & Devices, Building M-54, Montreal Rd Campus, Ottawa, ON, Canada

2 School of Psychology, University of Ottawa, Ottawa, ON, Canada

3 QBM Cell Sciences, Ottawa, ON, Canada

* Corresponding author. E-mail address: geoff.mealing@nrc-cnrc.gc.ca

Our laboratory is identifying neuroprotective strategies against ischemic-like injury in neuronal cultures. Typically, viability/toxicity assays are employed to assess efficacy, but these assays provide no information as to whether neuronal *function* in a network is preserved, either during a drug application alone or during pairing with an injury. Efforts have begun to evaluate if paradigms that induce neural protection (preconditioning-induced tolerance) by live/dead assays preserve neuronal network activity and functional connectivity in cultured cortical neurons.

1 Introduction

Cerebral ischemic stroke is caused by a clot impeding flow of blood, resulting in a core infarct and a surrounding region (penumbra) of at-risk brain tissue. Clinical care entails the use of ‘clot-busting’ drugs within 3 h, a time constraint which results in < 10% of patients receiving treatment. What is urgently required is additional therapy directly targeting causes of neuronal demise (neuroprotection). Conventional viability/toxicity assays provide no information as to whether functional connectivity (i.e., the pattern of neuronal interactions in a network) has been disrupted.

Our laboratory identifies neuroprotective strategies in neuronal cortical cultures against an ischemic-like injury, termed oxygen-glucose deprivation (OGD). Using viability/toxicity assays from 12-well plates, we have identified a neuroprotective platform requiring combination-therapy: first, prior to OGD, pro-survival signal transduction pathways are activated in order to induce a neuroprotective endogenous stress response, a process termed ‘preconditioning’ and; second, since preconditioning only delays – but does not prevent – an excitotoxic build-up of extracellular glutamate during OGD, an anti-excitotoxic receptor antagonist cocktail must be administered at the time of this glutamate surge during OGD.

Multielectrode array interfaces (MEAs) enable non-invasive, chronic recording of spontaneous neuronal activity and provide a means to examine spatiotemporal patterns of network activity. Hence, MEAs may be appropriate in providing high information-content screening of neuroprotective drugs or therapies suitable for eventual translation to the clinic. The immediate goal is to determine if naïve neurons can tolerate drugs used in the neuroprotective

platform, with a longer term goal of determining whether this platform provides functional neuroprotection against OGD.

2 Materials & Methods

Initial efforts are involved in evaluating the suitability of acutely-dissected or cryopreserved (QBM Cell Sciences) primary rat cortical neurons (E18) grown for up to 28 days in vitro (DIV) on MEAs obtained from MultiChannel Systems (MCS). Statistical dependencies across all pairs of electrodes were evaluated by pairwise cross-correlations (CCs) in the occurrence of spikes. CCs provide an estimate of the degree to which different locations on the array interact with each other.

3 Results

Typically, acutely dissected neurons display spontaneous activity characterized by periods of highly synchronized events interspersed by periods of relative quiescence (Fig.1A). Pairwise CCs obtained from 20 min of spontaneous recording show that most pairs of electrodes have a low-to-moderate CC, with a few pairs having relatively high CC (Fig.2A).

Taking the matrix of pairwise CCs as a starting point, we identified “network hubs”, defined as channels that have a high graph betweenness-centrality [1] (Fig.2B). These hubs remained relatively stable over 28 DIV (Fig.2C). Similar results were obtained from cryopreserved neurons (not shown).

Next, we examined the effect of a potent preconditioner, 4-aminopyridine / bicuculline, for which we have shown that a 48 h application to cultured cortical neurons induces a phenotype able to resist otherwise lethal OGD for up to 72 h after 4-AP/bic washout [2]. 4-AP/bic was added to 15 DIV cultures on MEAs for 48 h. One h following

administration of 4-AP/bic, we observed a marked up-regulation of network activity, followed by down-regulation 36 h later (Fig. 1B, C). This reduction in network activity is consistent with down-regulated homeostatic synaptic scaling [3].

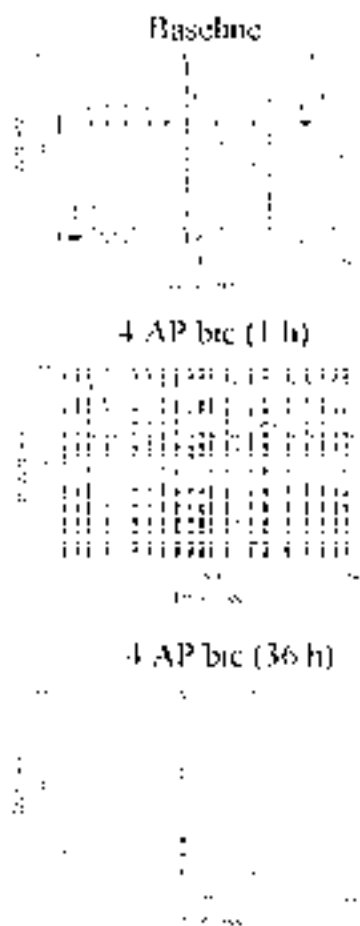
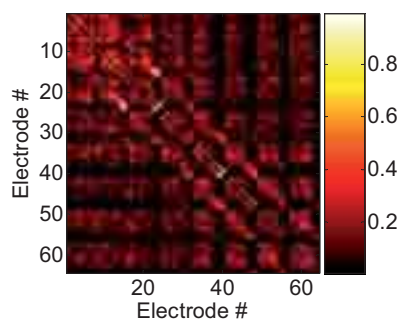
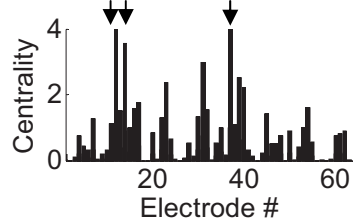


Fig. 1. Raster plots depicting spiking activity before (top panel) and during (middle and bottom panels) exposure to 4-AP/bic.

A.



B.



C.

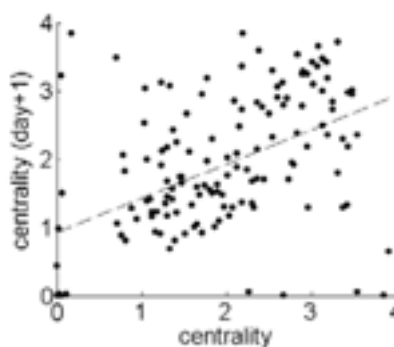


Fig. 2. The graph centrality of different electrodes is stable over days in vitro. A. Example of a 64x64 correlation matrix obtained by computing pairwise cross-correlations across all electrodes of an MEA. B. Betweenness-centrality of all electrodes from graph depicted in A. Arrows identify electrodes with top 5% centrality. C. Betweenness-centrality for each day in vitro (x-axis) compared to the following day (y-axis). Each point is an electrode on the MEA. Dashed line indicates slope of best-fitting linear regression ($r^2=0.25$, $p < .001$).

4 Conclusions

Translation from viability/toxicity assays to MEAs is ongoing, with progress made in understanding how network activity changes during development in cultures, as well as during a neuroprotective regime. 4-AP/bic preconditioning induced a marked down-regulation in network activity, which likely underlies tolerance to OGD. Current efforts are focusing on determining if neuroprotection alters neuronal interactions, and how different preconditioners compare with 4-AP/bic in their effect on activity.

Acknowledgements

We thank Dr. Robert Monette, Ms. Tanya Comas and co-op uOttawa students (O Romanov, S Khair, K Waite, J Lam, and A Farinaccio) for technical help.

References

- [1] Thivierge JP, Cisek P. (2008). Nonperiodic synchronization in heterogeneous networks of spiking neurons. *J Neurosci.*, 28, 7968-7978.
- [2] Tauskela JS, Fang H, Hewitt M, Brunette, Ahuja T, Thivierge JP, Comas T, Mealing G. (2008). Elevated synaptic activity preconditions neurons against an in vitro model of ischemia. *J Biol Chem.*, 283, 34667-34676.
- [3] Turrigiano GG, Nelson SB. (2004). Homeostatic plasticity in the developing nervous system. *Nat Neurosci.*, 5, 97-107.

Importance of multielectrode array recordings in drug discovery

Nicolas Redon¹, Christophe Lanneau¹, Pauline Cervello¹, Bruno Biton^{1*}, Daniel Bertrand³, Florence Oury-Donat² and Patrick Avenet¹

¹ Sanofi-Aventis R&D, Exploratory Unit, Chilly Mazarin, France.

² Sanofi-Aventis R&D, Exploratory Unit, Montpellier, France

³ HiQscreen Sarl, Geneva, Switzerland

* Corresponding author. E-mail address: bruno.biton@sanofi-aventis.com

We have developed in collaboration with MultiChannel Systems a new MEA device aiming at increasing the throughput of antiepileptic drug (AED) screening, using brain slices preparation. Important features of this new device are first, connexion of the entire system through a single USB port, parallel processing of data collected from up to four MEAs on a single computer and possibility to use this system in culture conditions. These developments open new possibilities to epileptogenesis studies on acute slices or on cultures.

1 Introduction

1.1 High value of phenotypic screening for AEDs discovery and its limitation

Considering the most prescribed and efficient anti-epileptic drugs on the market, it is noteworthy that these compounds were identified using a phenotypic screening strategy *in vivo*. Such strategy faces throughput issues, due to ethical and practical considerations. Up to now, *in vitro* phenotypic screening of novel AEDs was also difficult, due to the relatively low throughput of models such as extracellular field recordings in brain slices.

1.2 A new strategy for AED screening

To overcome this bottleneck we developed a new *in vitro* model of epileptiform activity in a 384 well format, using rat cultured hippocampal neurons and low magnesium-induced calcium oscillations. Activity is recorded by a microplate fluorescence reader (Hammamatsu). Using this model we already have screened a 28K proprietary library [1].

The most interesting compounds (about 150) were then directly evaluated *in vivo* in the maximal electroshock model (mouse). A dozen of compounds were found active *in vivo* but for those found inactive, it became mandatory to assess more thoroughly their potential antiepileptic effect *in vitro*, using a more elaborated model *i.e.* hippocampal slices/electrophysiology. Indeed, many parameters such as blood brain barrier penetration or pharmacokinetics parameters were unknown. Given the number of compounds, we needed a higher throughput than those provided by currently available devices,



Fig. 1. Four MEAs and their USB connexion to a single PC.

2 Features of the new MEA device

2.1 Electrode number and connexions

To achieve adequate throughput and realistic recording time we needed to have a MEA system presenting more flexibility than the marketed apparatus. In collaboration with Multichannel Systems we defined the optimal characteristics of such system, including the possibility to record from multiple slices in parallel. For this purpose it was decided to separate the stimulating ($n=12$) from the recording electrodes, whose total number was reduced to thirty-two. In addition, stimulating and recording devices were mounted in a single unit with a USB port connexion. Given the electrical and power characteristics of today's available PC's, up to four units can be connected to a single PC, allowing up to eight slices to be investigated in parallel (2 PC x 4 MEAs). Moreover, each unit was designed in such a way to be compatible with the temperature and humidity of an

incubator in view of long term recording of organotypic cultures.

2.2 Softwares

The MC_Rack program (Multichannel Systems) controls individually each unit. As epileptic activity observed in the zero magnesium conditions is spontaneous, recordings were performed continuously over periods of ten minutes using MC_Rack. While the technical development of a novel stimulation and amplifier system clearly opened new investigation possibilities, it displaced the experimental bottleneck to the analysis.

To overcome such difficulties we conceived a new software (MSlice) that was developed and runs with Matlab. MSlice identifies and classifies spontaneous epileptic bursts, in function of their amplitude and duration. While it would be beyond the scope of this work to describe in more details the MSlice program it suffices to consider that it efficiently reduced the analysis time from about 30 min for a manual inspection of the bursting activity recorded by a single electrode to less than 10 seconds.

3 Experimental protocol and data analysis

3.1 Experimental protocol

Following halothane anaesthesia, the brain of 3 to 8 week old rats were dissected and horizontal slices including the hippocampus and the entorhinal cortex were prepared using a cooled vibroslicer (Leica). Following recovery for at least 1 hour at room temperature in oxygenated artificial cerebrospinal fluid (ACSF), slices were transferred on the MEAs under visual control using a CCD camera connected to the PC (Microvision). The entorhinal cortex was oriented in order to be in contact with the largest number of recording electrodes. ACSF deprived of Mg²⁺ was then superfused and after one hour, the epileptiform activity was recorded during 10 minutes (control). Compounds to be studied were added to the superfusate for 40 minutes and recordings were performed during the last 10 minutes of exposure. All recordings were performed at a controlled temperature of 32 °C (\pm 1°C).

3.2 Data analysis

In view of the synchronous epileptiform activity of electrodes, the activity of a single electrode in the entorhinal cortex was analyzed and well reflected the activity of this structure. Data acquisition of six slices with in average thirty two electrodes and a sample interval of 200 μ s generated about 4.6 Gbs / day of experiment. Using bin of 2 min, MSlice software coupled to a "macro" running with Excel (Microsoft) rapidly provided a picture of the epileptiform pattern

defining the number of epileptiform events and the total time spent in bursting activity, allowing to separate ictal-like from inter-ictal activities (Fig2).

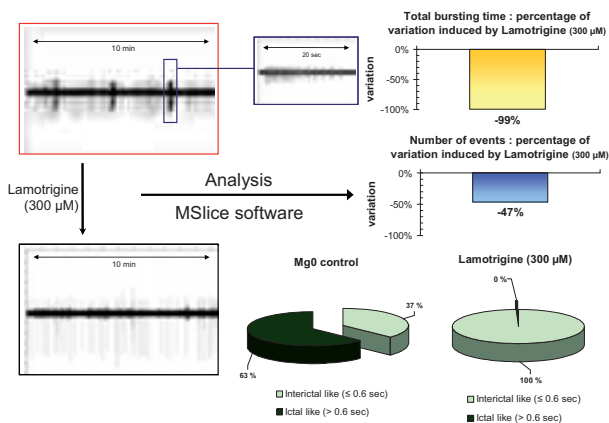


Fig. 2. Typical recording and analysis of epileptiform activity induced by magnesium deprivation.

4 Results and conclusions

We carried out an average of 5.8 successful recorded slices out of 6 running units and we were able to screen about 30 compounds (2 slices per compound) in about 3 weeks (1 FTE), showing the efficiency of the system.

When considering reference compounds, it is of interest to observe that they display significantly different pharmacological profiles. For example retigabine or lamotrigine decreased the overall bursting activity while others such as valproate mainly reduced the total bursting time with no major change in events number. This reveals that while both classes of compounds display efficacious antiepileptic activities their activity profile are clearly distinct. These data well illustrate the advantage of acute slices in analysing the mode of action of compounds. Getting a better understanding of the ictal and interictal activities and their modulation by antiepileptic molecules is expected to open new strategies in the design of active compounds.

Acknowledgement

We thank Multi Channel System for their efficient and constructive collaboration.

References

- [1] Mahmudi N., Boularand S., Roussignol G., Pimoule C., Biton B., Dargazanli G., Avenet P., Oury-Donat F. and Curet C. (2010): Low magnesium-induced synchronized repetitive calcium oscillation recorded in embryonic hippocampal neurons cultured in a 384 well microplate: an vitro model of acute epilepsy suitable for MTS. *FENS abstr.*, vol. 5, 015.36.

Heart

Detailed *Ex Vivo* Electrophysiology Studies in Rabbit Sinoatrial (SA) Node

Geoffrey Lewen^{2*}, Hong Shi¹, Jia L.Zhu¹, Paul Levesque¹

¹ Discovery Toxicology, Bristol-Myers Squibb Company, Princeton, NJ, USA

² Research Informatics, Bristol-Myers Squibb Company, Princeton, NJ, USA

* Corresponding author. E-mail address: geoff.lewen@bms.com

The sinoatrial (SA) node is a complex structure in which pacemaker cells at the node center activate surrounding atrial tissue, leading to spontaneous beating of the heart tissue. Using multielectrode arrays (MEA), we conducted detailed studies of the rabbit sinoatrial node with spatial resolution similar to much more technically demanding methods such as basket electrodes or MEA catheters used *in vivo*. We examined field potential morphology and wavefront conduction in the SA node, comparing the properties of the node center to those of the transition zone to the atrium. We also present an evaluation of the effect of reference ion channel inhibitors under high and low-K conditions which present risk factors for drug-induced arrhythmia: hyperkalemia and hypokalemia.

1 Introduction and Methods

1.1 Introduction

The sinoatrial (SA) node is a complex heart tissue that drives the surrounding atrial muscle from a spontaneously active pacemaking site at the node center. In rabbit, the SA node features a gradual variation in cell type from the center to the peripheral junction with surrounding atrial muscle¹. This diversity of cell type, combined with spontaneous activity, make the SA node an ideal subject for the study of ion channel activity and activation wave propagation *ex vivo*.

1.2 Methods

The SA node-atrial muscle preparation was isolated from rabbit heart and placed over the 60 electrodes of the MEA chip (200/30iR-Ti-gr, MultiChannelSystems, GmBH). The MEA chip was superfused with physiologic buffer with 95% O₂ and 5% CO₂ at 35°C. Spontaneous field potentials were recorded every 5 min during 20-30 min drug treatment following a 30-60 minute equilibration period.

The maximal negative derivative of the field potentials ($-dV/dt$) was taken as the nominal activation time for activation mapping. The conduction velocity was determined by the maximum activation time change within the tissue being sampled by the MEA. Based on real-time activation maps, the tissue sample was repositioned based on the region of interest.

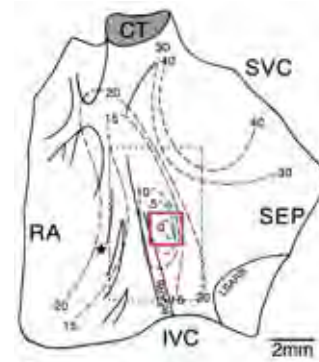


Fig. 1. The location of MEA recordings in rabbit SA node preparation is indicated by the red box, based on the dimensions of the MCS array, 200/30iR-Ti-gr (Adapted from Yamamoto².) SVC: Superior vena cava; CT: Crista terminalis; RA: Right atrium.

2 Discussion and Results

2.1 Results

Localized sampling permits detailed investigation of drug effects

Due to the small array size and high spatial resolution of the MEA, it is possible to isolate a specific region of the sinoatrial node, for instance, the node center (See, for example, Figure 1). Application of the pacemaker current (I_f) blocker BMS-A slightly altered the node center activation pattern, but had a negligible effect on conduction time (Figure 2) and field potential morphology at the SA node center (Figure 3a); however, BMS-A dramatically slowed beat rate (Figure 3b).

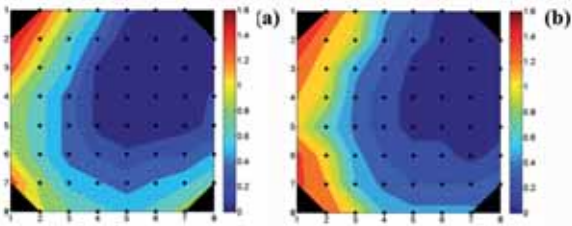


Fig. 2. Compound BMS-A, a pacemaker current blocker, slightly altered the activation pattern at the SA node center but has a negligible effect on conduction time in the node center. (a) control, (b) BMS-A.

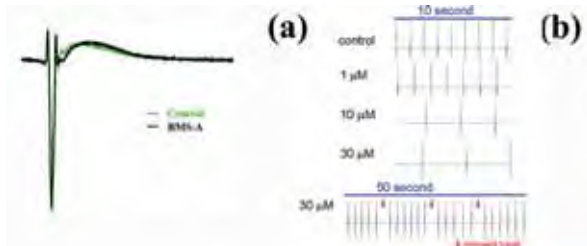


Fig. 3. At a concentration of 30 μ M, BMS-A slightly prolongs SA node center field potentials (a), but has a profound effect on beat rate and rhythm (b).

Ion channel effects vary across the sinoatrial node

Recordings of vehicle or drugs were made at the SA node center, and following a washout of the drug, the sample was repositioned to record from the SA node-atrial boundary region. The Na channel blocker Lidocaine (30 μ M) slowed conduction by a factor of 2 (Figure 4) and eliminated the Na spike in the atrial region of the SA node preparation, but had a minimal effect near the center of the node, where fewer Na channels are expressed (Figure 5).

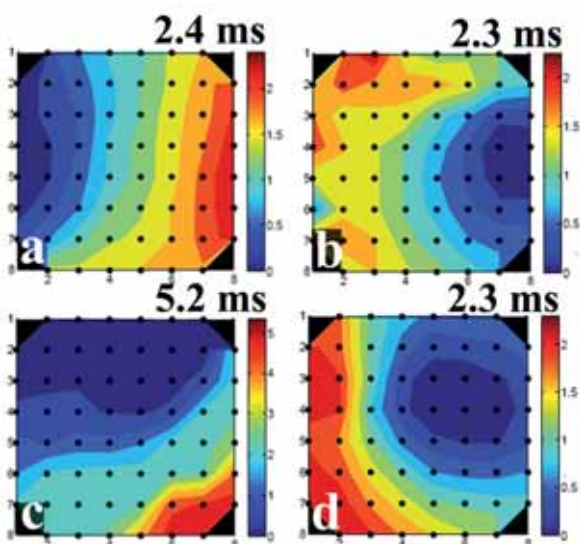


Fig. 4. Application of 10 μ M Lidocaine doubles conduction time in atrial region of SA node (a, c) but has a negligible effect on conduction time in the node center (b, d).

The I_{Kr}/hERG blocker Dofetilide had a minimal effect on conduction velocity in the transition region from SA node-center to atrium but prolonged the field potential duration and slightly lowered the beat rate.

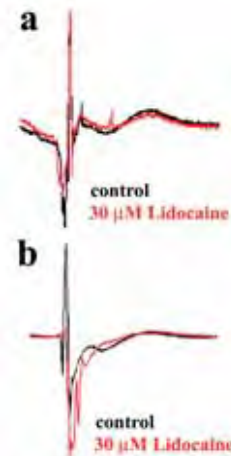


Fig. 5. The effect of the sodium channel blocker Lidocaine on field potentials. (a) In the SA node center, where few sodium channels are expressed, Lidocaine has a minimal effect. (b) Near the SA node-atrial boundary the initial fast sodium peak is eliminated.

MEA sinoatrial node preparations predict toxicity

Reports of profound conduction disturbance and asystole in hyperkalemic (high serum potassium levels) patients treated for arrhythmia with Lidocaine³ prompted us to investigate whether or not the SA node MEA preparation could be used to study the hyperkalemia-lidocaine interaction. A companion study of the interaction of Dofetilide in hypokalemic conditions, a known risk factor for drug-induced arrhythmia, was also conducted.

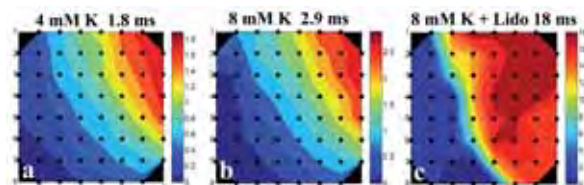


Fig. 6. In hyperkalemic conditions, the proarrhythmic action of Lidocaine is enhanced (a \rightarrow b \rightarrow c). The conduction time enhancement factor above is 7; however, the average for n=5 trials was 3.7.

The conduction times with normal (4 mM) and high potassium levels (8 mM) were compared before and after application of Lidocaine (10 μ M). Hyperkalemic conditions exaggerated the slowing effect of Lidocaine on conduction velocity, decreasing it by an average factor of \sim 4 compared to normal potassium levels (Figure 6).

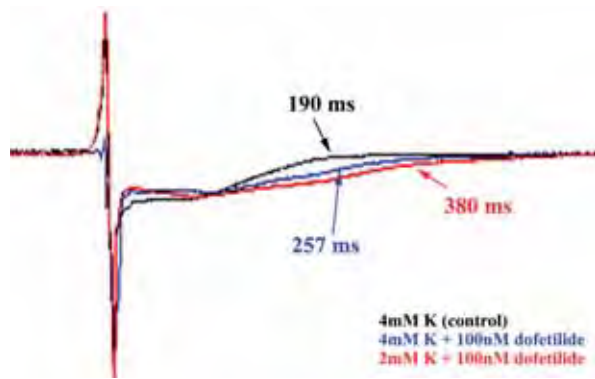


Fig. 7. Dofetilide prolongs the FPD by ~35% in normal potassium levels (4 mM K, black, blue). In hypokalemia (2 mM K, red), the blocking effect of Dofetilide on I_{Kr} currents is enhanced, and the FPD doubles.

Dofetilide had a negligible effect on conduction time when applied under normal (4 mM K) and hypokalemic (2mM K) conditions. However, Dofetilide increased the field potential duration (FPD) by a factor of ~2 in low-K compared to normal-K conditions (Figure 7).

3 Summary and Conclusion

3.1 Conclusion

MEA technology allows detailed, high resolution, spatial analysis of field potential morphology and conduction velocity in sinoatrial node preparations, which present significant challenges due to the variation in cell types over a small area. We demonstrated activity of an I_f -inhibitor in SA node consistent with mechanism and *in vivo* electrophysiology findings; BMS-A slowed spontaneous beat rate of the SA node and induced missed beats in a concentration-dependent manner. We also found that the known risk factor of abnormal extracellular potassium concentration for drug-induced arrhythmia could be reproduced *ex vivo* using the MEA with an isolated sinoatrial node-atrial tissue preparation.

Acknowledgement

We thank Huabin Sun for invaluable discussions and assistance in the development of the mapping software used in these studies.

References

- [1] Boyett, M. R., Honjo, H., Kodama, I. (2000). The sinoatrial node, a heterogeneous pacemaker structure. *Cardiovascular Research*, 47, 658-687.
- [2] Yamamoto, M., Honjo, H., Niwa, R., Kodoma, I. (1998). Low-frequency extracellular potentials recorded from the sinoatrial node. *Cardiovascular Research*, 39, 360-372.
- [3] McLean, S. A., Paul, I. D., Spector, P. S. (2000). Lidocaine-induced conduction disturbance in patients with systemic hyperkalemia. *Annals of Emergency Medicine*, 36(6), 615-618.

MEA-aided investigation of cardiac arrhythmia induced by electrical stimulation

Binbin Xu¹, Sabir Jacquir^{1*}, Stéphane Binczak¹, Gabriel Laurent¹, David Vandroux², Pierre Athias³, Jean-Marie Bilbault¹

¹ Laboratoire Le2i UMR CNRS 5158, Université de Bourgogne, Dijon, France

² NVH Medecinal, Dijon, France

³ Laboratoire LPPCE, CHU de Dijon, France

* Corresponding author. E-mail address: sjacquir@u-bourgogne.fr

To provide insights into the impulse propagation between cardiac myocytes, we performed studies of excitation spread with cellular resolution in confluent monolayers of cultured cardiomyocytes (CM). Multisite field potential have been recorded using microelectrode arrays (MEA) technology in a basal condition and in an arrhythmic condition. This last one has been induced by a high frequency electrical stimulation. In vitro spiral waves observed open a new way to test the anti-arrhythmic drugs or strategies at microscopically level.

1 Introduction

The fibrillation phenomenon is characterized by a high irregular excitation rate responsible for erratic atrial contractions. When it occurs, a wavefront reenters and hence re-excites the same area on the heart repeatedly as opposed to the normal “planar” wavefront emitted by the sinus node that depolarizes the myocardial tissue only once per cardiac cycle. Many studies have been performed and reported that functional reentrant spiral waves (SW) are present in animal cardiac atrial [1-4]. It is commonly accepted that atrial or ventricular fibrillations are both caused by multiple chaotically wandering electrical wavelets leading to chaotic uncoordinated contractions. But the opinions on how these wavelets arise differ. Jalife et al. [5] suggest that wavelets could be the result of a single excitation source. Thanks to the tissue’s heterogeneity, waves with high frequency emitted from this source conduct in all directions and without the same speed on the tissue. In this case, waves collide into wavelets. So the aim of this study is to verify this hypothesis, i.e. to induce an experimental fibrillation phenomenon in order to identify, at a cellular level, the electrophysiological mechanism involved in its initiation and perpetuation. In this paper, some results corresponding to the generation of spiral wave at cellular level are given. For more details, different results can be found in our papers [6-11].

2 Materials and Methods

Neonatal ventricular myocytes were prepared from 1 to 4 days-old Wistar rats by trypsin-based enzymatic. The cell suspension was preplated twice in the culture medium and grown on Microelectrode Array (MEA) which allows non-invasive synchronous

multifocal field potential (FP) recordings. Cardiomyocyte (CM) cultures (> 90%) were seeded at a final density of 10^5 cells per cm^2 in the cultured medium. Cultures were incubated in a humidified incubator and were used after 4-5 days of growth, a step at which confluent and spontaneously beating cell monolayers were obtained. FP corresponding to the extracellular potentials from a 2-5 cells area were recorded to approximate activation maps with one “electrical unit” resolution. The FP parameters (rate, duration ...) derived from these activation maps are confirmed as homogenous throughout the recording area. Then, the CM has been stressed using an external high frequency electrical signal of stimulation. Since this high rate stimulation is able to induce fast and irregular electrical activities which mimic fibrillation patterns, it provides a way to verify the hypothesis proposed by Jalife et al. These fibrillation waves are then analyzed more precisely by reconstructing an electrical activation map.

3 Results

Figure 1. illustrates the FP train for all electrodes without stimulation (4096 samples). The variability of the FP frequency was analyzed. Figure 2 presents the distribution of the first four periods of the FP train corresponding to data presented in Fig. 1. This analysis indicates the slight variability of the FP frequency. This variability may be due to a remodeling phenomenon of gap junctions or the fluctuation of the ionic channels or changes in the propagation path.

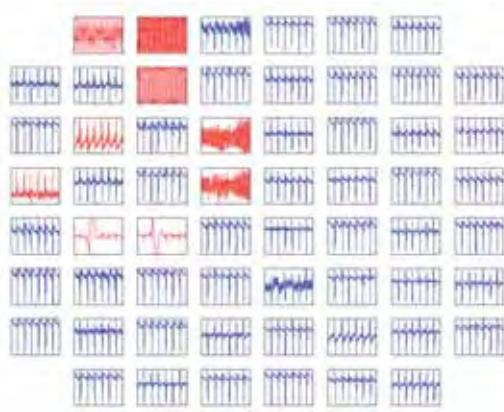


Fig 1. Field potential signals. Each panel corresponds to a single electrode. Correct signals are in blue and artefactual signals are in red.



Fig 3. Field potential signals. Each signal corresponds to one electrode. Conform signal is in blue color and non conform signal is in red color.

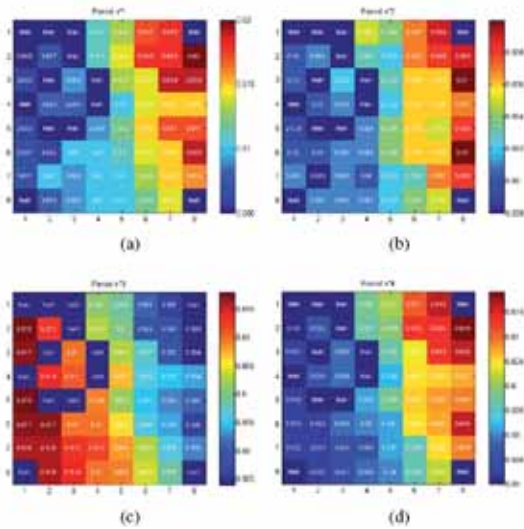


Fig 2. First four periods of the field potential. Panel (a) is the first period and panel (d) is the fourth period.

CM cultures were then stimulated by an external electrical signal, consisting in a stimulation train in one point at the edge of the MEA. After this stimulation protocol, the recorded electrical activities were faster and irregular as illustrated in Fig. 3. The rate was irregular compared to the one in Fig. 1.

Several spiral waves were observed during induced arrhythmias (Fig. 4). The observation of activation map during arrhythmias revealed an average of 3 ± 1 SW within the surface mapped. Rotation waves appeared to be random and could change from one period to another. SW was unstable in location and could move inside or outside the recording area. SW had a mean radius of 400 ± 100 mm and a mean angular velocity of 225 ± 30 rotations per minute. Unstable reentrant and colliding wavefronts were also observed during a total of 180 min per arrhythmic episode.

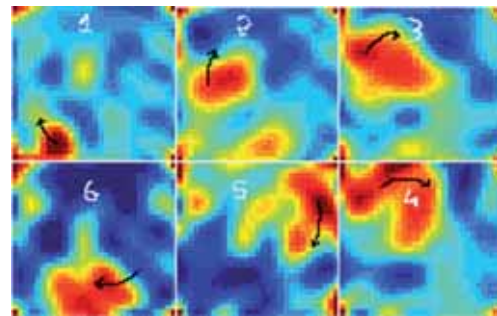


Fig 4. Series of snapshots displaying a relatively stable counter-rotating spiral wave during a sustained induced arrhythmia episode (the arrows indicate the clockwise rotation). Experimental data were smoothed using a cubic spline interpolation. The panel 1 shows the initiation of the SW and the last panel (6) illustrates the termination of the SW. The black color indicates the depolarization of cells and the white color indicates the refractory period.

4 Conclusion

In this work, cardiac impulse propagation has been investigated and sustained fast irregular arrhythmia have been induced in neonatal rat cultured CM. According to the results presented here, unstable spiral waves with randomly changing location and rotation waves can be precisely characterized using a MEA data acquisition system. This novel in vitro

model of sustained induced arrhythmias, mimicking fibrillation patterns, may be helpful in the comprehension of atrial fibrillation in clinical situations and be useful for testing AF interventions. Within the limitations inherent to the preparation used, the cultured CM monolayer is a controlled experimental model that may be useful for further studies on the basic aspects of fibrillation and defibrillation.

References

- [1] Allesie MA, Bonke FIM, Schopman FJG. (1973). Circus movement in rabbit atrial muscle as a mechanism of tachycardia. *Circ. Res.*, 33:54-62.
- [2] Davidenko JM, Kent PF, Chialvo DR, Michaels DC and Jalife J. (1990). Sustained vortex-like waves in normal isolated ventricular muscle. *Proc. Natl. Acad. Sci. U.S.A.*, 87: 8785-8789.
- [3] Davidenko JM, Pertsov AM, Salomonsz R, Baxter W and Jalife J.(1992). Stationary and drifting spiral waves of excitation in isolated cardiac muscle. *Nature*. 335: 349-351.
- [4] Pertsov AM, Davidenko JM, Salomonsz R, Baxter W and Jalife J.(1993). Spiral waves of excitation underlie reentrant activity in isolated cardiac muscle. *Circ. Res.*, 72: 631-650.
- [5] Jalife J.(2000). Ventricular fibrillation: mechanisms of initiation and maintenance. *Annu. Rev. Physiol.*, 62: 2550.
- [6] Athias P., Jacquir S., Tissier C., Vandroux D., Binczak S., Bilbault J-M., Rosse M.(2007). Excitation spread in cardiac myocyte cultures using paired microelectrode and microelectrode array recordings, *Journal of Molecular and Cellular Cardiology, Elsevier*, 42, pp. S3.
- [7] Jacquir S., Binczak S., Rossé M., Vandroux D., Laurent G., Athias P., Bilbault J-M.(2007). Multisite Field Potential Recordings and Analysis of the Impulse Propagation Pattern in Cardiac Cells Culture, *34th International Conference IEEE on Computers in Cardiology, IEEE Proceedings*, 34, pp. 125-128.
- [8] Jacquir S., Tissier C., Vandroux D., Binczak S., Bilbault J-M., Rosse M., Athias P.(2008). Paired microelectrodes and microelectrode array analysis of cardiac impulse propagation in cardiomyocyte cultures, *Fundamental & Clinical Pharmacology*, 22 (1), pp: 51-52.
- [9] Jacquir S., Binczak S., Vandroux D., Laurent G., Athias P., Bilbault J-M.(2008). Cardiac Arrhythmias Induced by an Electrical Stimulation at a Cellular Level, *35th International Conference IEEE on Computers in Cardiology, IEEE Proceedings (ISSN 0276-6574)*, 35, pp. 625-628.
- [10] Jacquir S., Xu B., Bakir T., Bilbault J-M., Binczak S.(2009). Analysis of Cardiac Cells Field Potentials using Wavelet Transform, *36th International Conference IEEE on Computers in Cardiology, IEEE Proceedings (ISSN 0276-6574)*, 36, pp. 401-404.
- [11] Jacquir S., Binczak S., Xu B., Laurent G., Vandroux D., Athias P., and Bilbault J.(2010). Investigation of micro spiral waves at cellular level using a microelectrode arrays technology. *Int. J. Bifurcation Chaos (In press)*.

Organotypic ventricular heart slices of guinea pig and pig to test for drug side effects

Katharina Stürz¹, Elke Guenther¹, Michael Reppel², Jürgen Hescheler³ and Udo Kraushaar^{1*}

¹ Dept. of Electrophysiology, NMI Reutlingen, Germany

² University Medical Center Schleswig-Holstein, Lübeck, Germany

³ Dept. of Physiology, Köln University, Germany

* Corresponding author. E-mail address: udo.kraushaar@nmi.de

The timing of cardiac excitation must be precise in order to maintain a healthy, regular heart beat. The QT interval of an electrocardiogram is a measure for the electrical excitation of the ventricles. A drug-induced prolongation of the QT interval indicates the potential risk of a proarrhythmic drug effect and thus is an important parameter in safety pharmacology. Several systems are available to test for drug side effects on heart function, all with individual disadvantages: Heterologous expression systems yield detailed information on single ion channels without providing ion channel complexity of cardiomyocytes. Isolated cardiomyocytes in turn reflect the heart's ion channel composition but lack multicellular aspects, whereas organ systems like Langendorff heart are costly. In contrast, ventricular heart slices offer a superior alternative, merging the advantages of the above mentioned systems. Here, we developed ventricular heart slice preparations based on the method of Halbach et al. (2006) for guinea pig (GP) and pig, two species widely accepted in safety pharmacology and tested their pharmacological suitability.

1 Methods/Statistics

Hearts were removed and ventricles were cut horizontally or vertically into 300 µm slices in ice cold saline (0 mM Ca²⁺, 30 mM butane-2,3-dione monoxime) using a vibratome (VT-1000, Leica, Germany). After a resting phase of 1 h, a slice subset was recorded directly on 60 channel microelectrode arrays (MEA, Multichannel Systems, Germany) at 37°C in standard extracellular saline or DMEM. Extracellular stimulation was applied by bipolar circular electrodes (Science Products, Germany) mounted on a micromanipulator, and field action potentials (fAP) were elicited. Another subset of slices was cultured for several days prior to recording. Long term signal stability was tested by stimulus application up to one hour. Pharmacological substances were applied by bath perfusion or direct application. Dose-response relations were obtained by cumulative drug application.

2 Results and Conclusion

Freshly prepared heart slices displayed a high viability and could be stimulated repetitively for 1h. fAP duration (221 ± 6 ms GP, 238 ± 21 ms pig; Fig.1A) remained stable (<10 % change after 40 min), a major requirement for substance tests. Inhibitor application of the ether-a-go-go-related gene product, an important potassium channel during repolarization,

prolonged the fAPs substantially (e.g. 300 nM dofetilide: 121 % in GP and 119 % in pig, respectively; Fig 1B), corresponding to a QT-interval prolongation in the intact heart. Signal propagation velocity was prolonged (122.5 % and 121.5 %, respectively).

Slices could be cultured for up to 3 days in GP and 7 days in pig and could be stimulated reliably at 1 Hz during this time. fAP properties were comparable to fresh slices (fAP duration 281 ± 36 ms (GP) and 334 ± 59 ms (pig) indicating a well preserved functional state of the underlying ion channels.

Taken together our data indicate that these organotypic heart slice models combine the convenience of a culture system with the informative value of an organ system. Furthermore signal propagation can be investigated due to the 2D structure of the preparation on the MEA. The capability of long-term culturing of cardiac tissue reduces animal use and allows long term experiments in a controllable in vitro environment.

Acknowledgement

We are grateful to Dr. H.P. Wendel and T.O. Greiner for providing the pig material. This work has been funded by the Bundesministerium für Bildung und Forschung (BMBF; Grant 01GG0710)

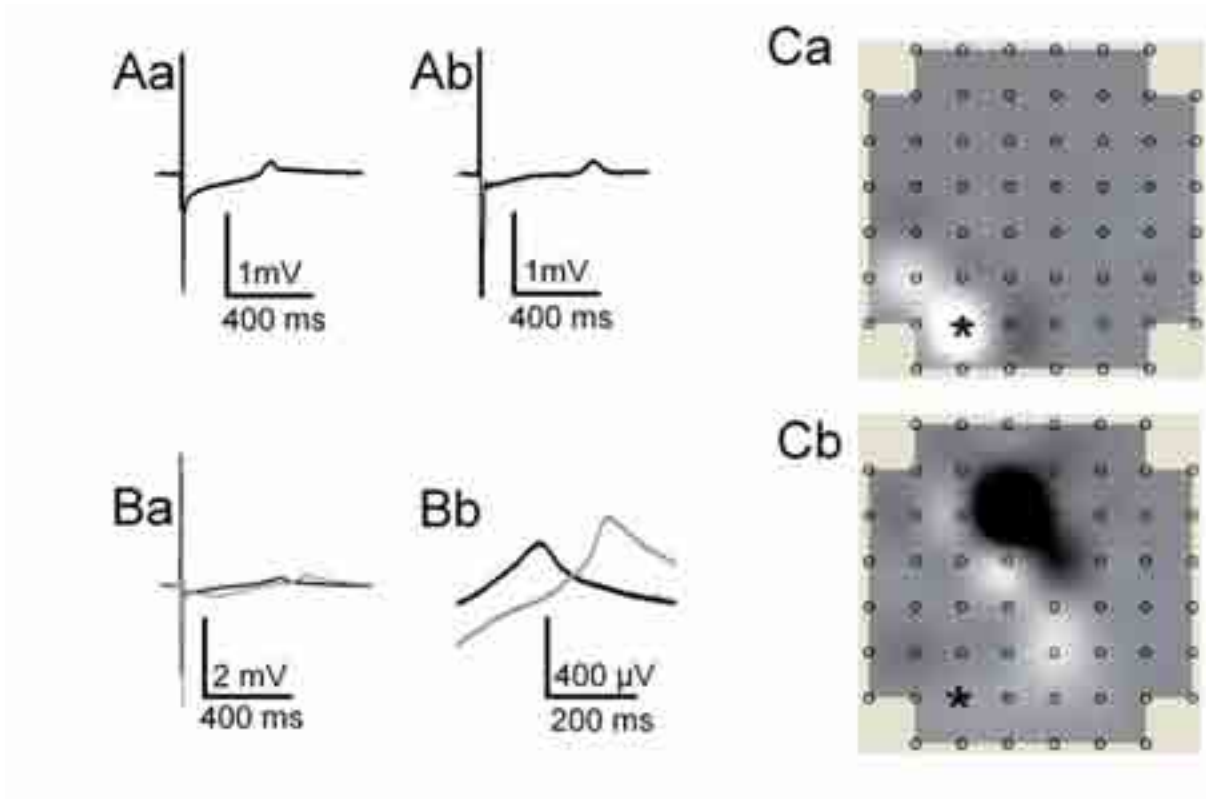


Fig. 1 Field action potential recordings of ventricular pig heart slices. A: fAPs at the day of preparation (Aa) and after 6 days in vitro (Ab). B: Application of dofetilide prolongs the fAP duration. Ba: Superposition of traces during control (black) and in presence of 300 μM dofetilide (grey). Bb: Magnification of the repolarization phase. C: Signal propagation of the fAP. Signal propagation in a ventricular GP slice. Area corresponds to the MEA electrode field, electrodes marked as circles. Voltage deflection is false color coded. White: depolarization, black hyperpolarization. Ca: t=0 ms, Cb: t=14 ms. Star: stimulation point

To Study the Relevance of K_{ATP} Channels in Pharmacological Preconditioning Using MEA

Thomas Pfeiffer¹, Jessica Ka-Yan Law^{2, 3}, John Anthony Rudd², Chi-Kong Yeung², Sven Ingebrandt^{1*}

¹ Department of Informatics and Microsystems Technology, University of Applied Sciences Kaiserslautern, D-66482 Zweibrücken, Germany

² School of Biomedical Sciences, The Chinese University of Hong Kong (CUHK), Shatin, Hong Kong

³ Bioengineering Graduate Program, The Hong Kong University of Science and Technology (HKUST), Clear Water Bay, Hong Kong

* Corresponding author. E-mail address: sven.ingebrandt@fh-kl.de

Adenosine-5'-triphosphate dependent potassium channels (K_{ATP} channels) are believed to be a potential target for pharmacological preconditioning (PPC) [1, 2]. In the present study, the effects of K^+ channel openers (KCOs), pinacidil (PIN), SDZ PCO 400 (SDZ), and diazoxide (DZ) were determined. Furthermore, the effect of PIN was also investigated on metabolically compromised cardiomyocytes induced by a metabolic inhibitor sodium azide (NaN_3). We demonstrated that PIN acts by preconditioning the myocytes by K_{ATP} channel activation thereby providing cardioprotection.

1 Introduction

Preconditioning describes the phenomenon of exposing the heart to one or more short cycles of metabolic conditions to mediate cardioprotective effects. Thus the heart is more resistant in the long-term ischaemia or hypoxia. Even though the preconditioning effect is not fully understood and discussed controversially, it is revised that K_{ATP} channels play a crucial role in both, pharmacological and ischaemic preconditioning. Recently published data considers that the sarcolemmal K_{ATP} (sarc K_{ATP}) opener may have energy saving properties, which may help to overcome metabolically compromised conditions [3].

Investigations into the effects of hypoxia, ischaemia, and the associated PPC have been made possible using the microelectrode array (MEA). This technique has been used by many groups in interdisciplinary cardiovascular research [4, 5, 6]. Contrary to other existing methods, MEA utilises a non-invasive means to study cell functions enabling long-term experiments.

2 Methods

A custom made 64-channel MEA system was used [7]. The (i) beat frequency [beats per minute, bpm], (ii) extracellular action potential (exAP) amplitude [mV], and (iii) propagation velocity through the cultured myocytes layer [cm/s] were measured. Recordings are based on the use of MED64 conductor 3.1 (Alpha MED Sciences Co. Ltd. Japan). Data processing was performed with a custom-made MATLAB[®] implement.

Embryonic cardiomyocytes were isolated from Sprague-Dawley rats (embryonic day 17-19) and cultured for 4 days prior to experiments.

Concentration-response effects of the three KCOs on the electrophysiology of normoxic myocytes were first determined followed by the effect of NaN_3 on normoxic cells. In PPC experiments, the cells were subjected to the presence of 10mM of NaN_3 with or without a 5-min pre-treatment of 50 μ M of PIN (Fig. 1).

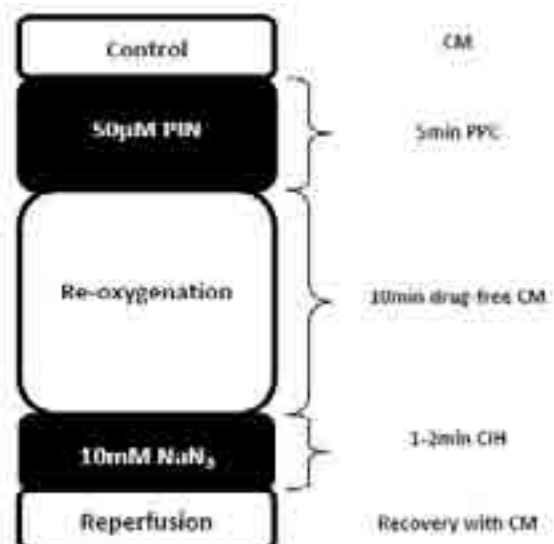


Figure 1: Diagram shows the time chart of the pharmacological preconditioning experiment. PPC was mediated by pinacidil (PIN), while chemical hypoxia was induced (CIH) by NaN_3 . White boxes represent drug-free periods with culture medium (CM) only, whereas black boxes represent medium containing drug.

3 Results

Under normoxic conditions, SDZ, a mitochondrial K_{ATP} (mito K_{ATP}) opener, was more potent than PIN, a sarc K_{ATP} opener, in reducing beat frequency; whereas DZ, another mito K_{ATP} opener, did not have any effect. Similar changes were also observed in terms of exAP amplitude and propagation velocity (Fig. 2).

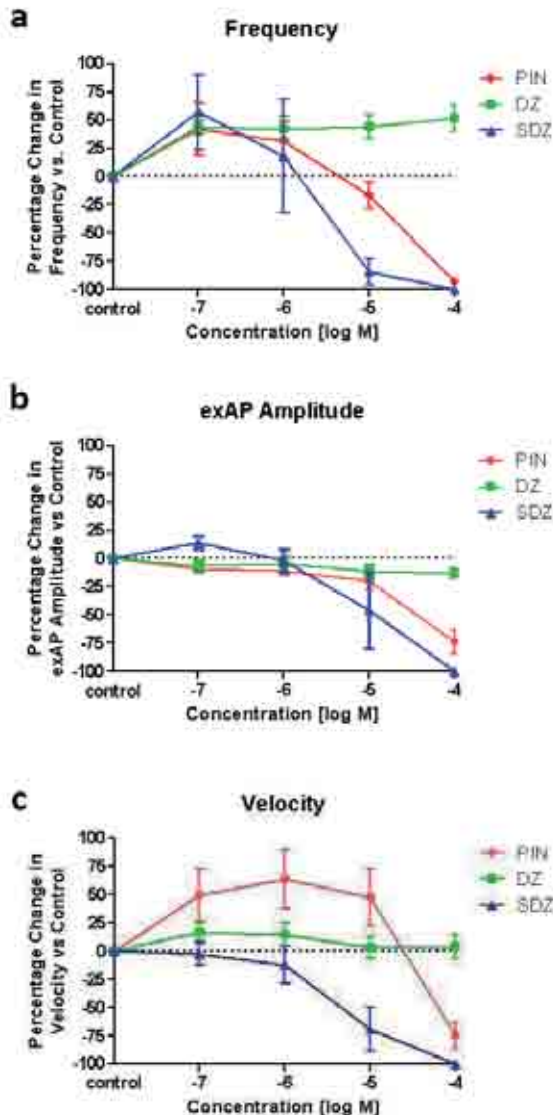


Figure 2: Effects of pinacidil (PIN), diazoxide (DZ), and SDZ PCO400 (SDZ) on beat frequency (a), extracellular action potential amplitude (b), and signal propagation velocity (c) of cardiomyocytes cultured on MEAs (n_{PIN}=18, n_{DZ}=14, n_{SDZ}=5) are shown. The effects of PIN and SDZ were concentration-dependent, with SDZ being more potent. DZ showed a concentration-independent effect on cardiac cells. The data are plotted as the percentage change in respect of the above parameters versus the drug-free control (mean \pm standard error of the mean, SEM) in the presence of different KCO concentrations (log M).

Under hypoxic conditions, myocytes showed a reduction in beat frequency of $83.0\% \pm 4.9\%$ (vs basal values, n = 4). The PIN pre-treated myocytes, however, were affected to a lesser extent with a reduction of only $46.4\% \pm 19.3\%$ (n = 4) (Fig. 3).

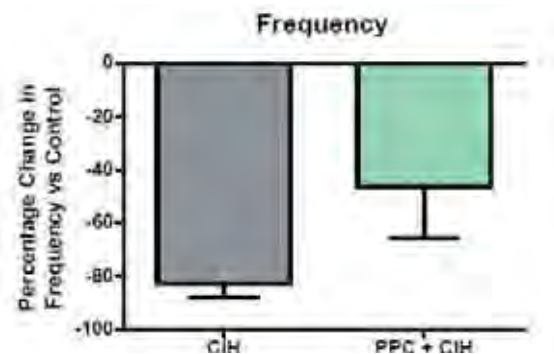


Figure 3: Effects of chemical induced hypoxia (CIH) on beat frequency of embryonic cardiomyocytes cultured on MEAs (n=4) are shown. The cells were exposed to 10 mM of NaN_3 in the absence (left column) or presence (right column) of PIN (50 μ M) pre-treatment. The results are expressed as the percentage change in beat frequency versus the drug-free control (mean \pm standard error of the mean, SEM).

4 Conclusion/Summary

In the present study, PIN activates K_{ATP} channels and provides a cardioprotective effect on hypoxic cardiomyocytes.

The investigation into the effect of KCOs using the MEA may serve as a possible platform for scientists to obtain better insight into cardiac pathology.

However, future work needs to use selective KCO agonists and antagonists in order to characterise whether the beneficial effects of KCOs in preconditioning are due to the activation of sarc K_{ATP} or mito K_{ATP} channels.

Acknowledgement

The authors thank A. Offenhusser, Research Center Juelich, Germany, and his group for development of the MEA devices and amplifier instruments. In addition the authors thank F. Sommerhage, University of Central Florida, USA, for providing an intensive training during project start and the data analysis software.

References

- [1] Cohen MV, et al. (2000): Ischemic Preconditioning: From Adenosine Receptor to K_{ATP} Channel. *Annual Review of Physiology*, 62, 79-109.
- [2] Tamargo J, et al. (2004): Pharmacology of cardiac potassium channels. *Cardiovascular Research*, 62, 9-33.
- [3] Schmid D, et al. (2009): Pinacidil-primed ATP-sensitive potassium channels mediate feedback control of mechanical power output in isolated myocardium of rats and guinea pigs. *European Journal of Pharmacology*, 628, 116-127.
- [4] Reppel M, et al. (2004): Microelectrode arrays: A new tool to measure embryonic heart activity. *Journal of Electrocardiology*, 37104-109.
- [5] Stett A, et al. (2003): Biological application of microelectrode arrays in drug discovery and basic research. *Analytical and Bioanalytical Chemistry*, 486-495.
- [6] Yeung CK, et al. (2009): To establish a pharmacological experimental platform for the study of cardiac hypoxia using the microelectrode array. *Journal of Pharmacological and Toxicological Methods*, 59, 146-152.
- [7] Yeung CK, et al. (2007): Drug profiling using planar microelectrode arrays. *Analytical and Bioanalytical Chemistry*, 387, 2673-2680.

Formation of Cardiac Cell Clusters on Commercial Multi-Electrode Arrays With Well Defined Biochemical Cues

Li Wang¹⁻³, Li Liu¹, Qinghua Yuan¹, N. Magome¹, K. Aglatze¹ and Yong Chen^{1,2*}

1 Institute for Integrated Cell-Material Science, Kyoto University, Kyoto 606-8507, Japan

2 Ecole Normale Supérieure, UMR 8640, 24 rue Lhomond, 75005 Paris, France

3 College of Chemistry and Molecular Science, Wuhan University, 430072, Wuhan, China

Both topographical and chemical patterns play important roles in cell biology and tissue formation studies [1]. In particular, chemical cues for cell culture can be easily obtained by soft lithography or micro contact printing, which have led significant advances in understanding cell growth, migration, proliferation, and survival mechanisms [2]. In the case of cardiac cells, attention has been focused on the single cell patterning and the cell to cell connection at single cell levels [3]. On the other hand, calcium wave propagation in cardiac tissues has been extensively studied but few of them relied on patterned surfaces [4]. It is also known that cardiac cell clusters can be spontaneously formed on a non patterned substrate [5] which results in particular beating properties of the system. It is therefore interesting to investigate the formation of and the coupling between cardiac cell clusters by defining more regular cellular networks with patterned substrates. The purpose of this work is to demonstrate such a controlled network formation with well defined chemical cues on a commercial multi electrode array.

1 Methods

Micro-contact printing [6] has been used to pattern fibronectin on a 60-channel multi electrode arrays (MEA, Multi Channel Systems, Germany). Primary 1 to 2 days old Sprague-Dawley rats were prepared with an enzymatic digestion procedure [7]. Field potentials of cell patterns were then recorded with a MSC preamplifier and a 16-channel analyzer (Powerlab, AD Instruments, USA). By changing the connection pins, the whole MEA mapping area can be covered. During the recording, optical images could also be taken to visualize the contraction and Ca^{2+} wave propagation with fluo 4-AM staining.

2 Results

To check the reliability of the patterning, 100 μm line-and-space strips of fibronectin were printed with alignment on MEA substrates. Optical images of cultured cells confirmed the preferential cell attachment and the formation of cell clusters, as shown in Fig. 1(a) (white arrow indicating the orientation of the strips). Field potential (FP) recordings without stimuli showed spike-like signals, probably due to spontaneous beating of larger cell clusters outside the MEA zone. We noticed that the spike singles appeared randomly in different cell strips (ex. with electrodes 21 to 28) but they clearly showed a correlation on the same cell strip (ex. with electrodes 12 to 82), i.e., the observed spikes appeared successively in a cell strip with a propagation speed of 0.3 m/s, as shown in Fig. 1(b). We also noticed that the appearance of the FP spikes was much more

regular after 5 days culture compared to that of 3 days culture, indicating a maturation of the cell cluster formation.

3 Conclusion

Micro contact printing can be used to pattern cardiac cell clusters. Each cell cluster aligned on a 100 μm width strip forms a stabilized community for electric signal propagation whereas no clear correlation has been observed with different cell cluster strips.

References

- [1] A. Curtis, C. Wilkinson. Trends Biotechnol. 19 (2001) 97.
- [2] M. Thery, et al., Nature Cell Biology 7 (2005) 929.
- [3] T. Kaneko, et al., Analyst, 132 (2007) 892.
- [4] H. Kaji, et al., Biotechnol Bioeng 81(2003) 748.
- [5] T. Harada and A. Isomura, Pro. Theor. Phys. Suppl. 101 (2006) 107.
- [6] R. S. Kane, et al., Biomaterials 20 (1999) 2363. 21
- [7] A. Arutunyan, et al. Am J Physiol Heart, Circ Physiol 280 (2001) H1905.

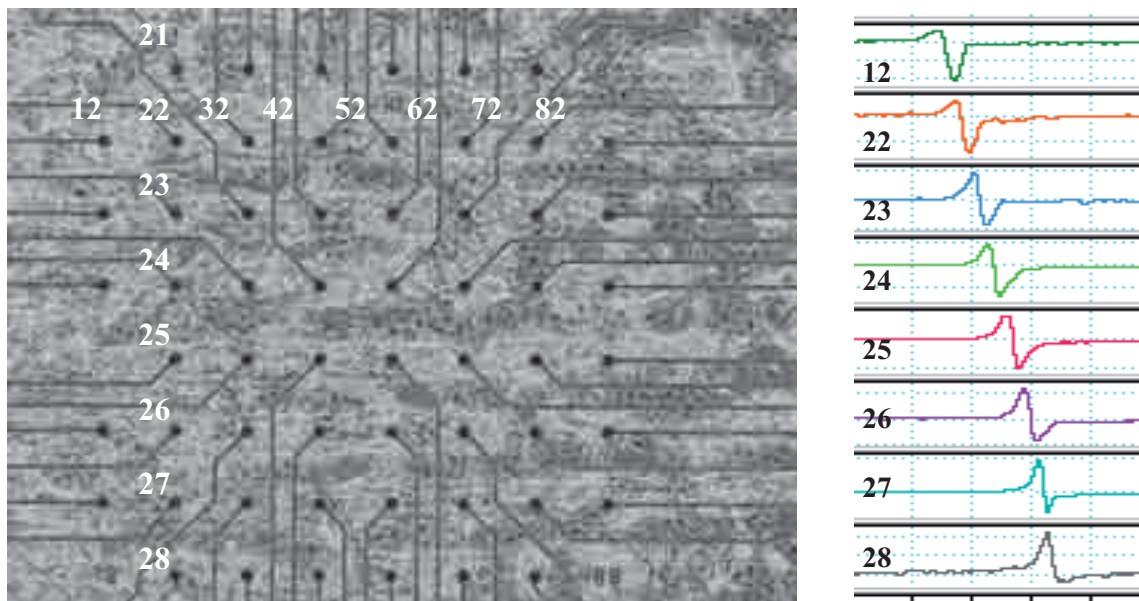


Figure 1. Phase contrast microphotograph (a) and 8-channel field potential recordings of the same cell cluster strip (electrodes #12 to #82) (b) of a MEA sample after 3 days culture.

Electrophysiological Studies of Human Embryonic Stem Cell –Derived Cardiomyocytes with Novel Microelectrode Arrays

Kujala Ville¹, Ryyänen Tomi², Hyttinen Jari³, Leikkala Jukka², Kerkelä Erja¹, Aalto-Setälä Katriina^{1,4*}

1 Regea – Institute for Regenerative Medicine, University of Tampere and Tampere University Hospital, Tampere, Finland

2 Department of Automation Science and Engineering, Tampere University of Technology, Tampere, Finland

3 Department of Biomedical Engineering, Tampere University of Technology, Tampere, Finland

4 Heart Center, Tampere University Hospital, Tampere, Finland

* Corresponding author. E-mail address: katriina.aalto-setala@regea.fi

Microelectrode arrays (MEAs) are a convenient means of studying cardiac electrophysiology long-term in *in vitro* conditions. We have fabricated our own microelectrode arrays to study human pluripotent stem cell –derived cardiomyocytes in order to design models more suitable for our studies. We compared these MEAs to the well established commercial MEAs to see whether they are comparable in terms of detecting cardiac field potentials. Indeed, our own MEAs were able to detect cardiac field potentials generated by the cardiomyocyte clusters, which at best were in the millivolt range. Our aim is to produce custom-made MEAs with modifiable electrode layouts and custom cell culture environments based on this technology.

1 Introduction

Microelectrode arrays (MEAs) are a convenient means of studying cardiac electrophysiology long-term in *in vitro* conditions. Our aim is to manufacture own MEAs with custom electrode systems as well as to study possibilities to integrate other sensors in the custom-build MEAs. To test the capabilities of our fabrication process, we have built our own MEAs with commercially available electrode dimensions and layouts and tested them with human embryonic stem cell –derived cardiomyocytes (hESC-CMs). We compared these MEAs with commercially available standard MEAs (type: 200/30iR-Ti-gr, Multi Channel Systems MCS GmbH, Reutlingen, Germany) to see whether our MEAs are comparable to the well established commercial MEAs to detect cardiac field potentials. Our next step is to produce MEAs with custom electrode layouts and cell culture environments based on this MEA technology.

2 Methods

MEAs were built and designed so that electrodes were wet etched on e-beam evaporated Ti layer on a glass wafer and after that Si₃N₄ was PECVD deposited as insulator layer. Openings for the electrodes and contact pads were made with dry etching. Finally, oxygen plasma treatment was performed to improve the cell adhesion. The resulting layout had 58 square 30 μm x 30 μm electrodes and 200 μm electrode distance resembling their commercial counterpart.

H7 human embryonic stem cells were differentiated to cardiomyocytes by co-culturing them with mouse visceral endoderm –like cells as described before (Mummery et al., 2003). Beating hESC-CMs were mechanically excised from the well-plates and plated onto FBS and 0,1 % gelatine coated commercial and our own MEAs. The MEA signals were recorded with MC_Rack software for three minutes each after a two-minute stabilization period. The hESC-CMs were cultured for two weeks on our own MEAs (n=4).



Fig. 1. Phase contrast picture of a fabricated microelectrode array with adherent cardiomyocyte cluster differentiated from the H7 human embryonic stem cell line.

3 Results

The hESC-CMs adhered well on the MEAs (fig. 1). The contact between the recording electrode surface and the cells improved over the two week time course resulting in larger field potential amplitudes. Our own MEAs were able to detect cardiac field potentials generated by the hESC-CMs. Compared to field potential signals detected with the commercial MEAs, preliminary results show that our MEAs produce comparable signals in terms of detected amplitude and noise levels. At best we could record cardiac field potentials in the millivolt range (fig. 2).

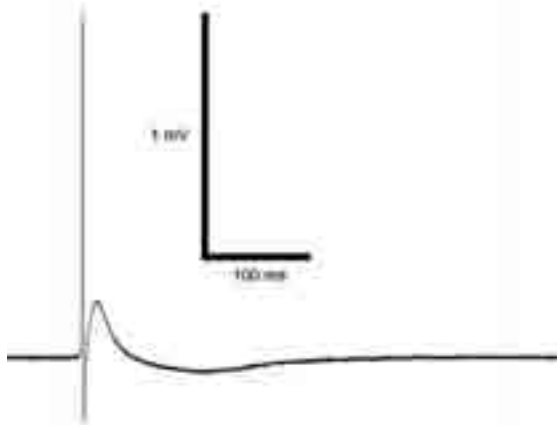


Fig. 2. Cardiac field potential recorded with our own microelectrode array.

4 Conclusions

We set out to investigate whether we could produce our own MEAs to study the electrophysiology of hESC-CMs. We found that these MEAs behave the same way as their commercial counterparts. This test enables us to design custom-made MEA layouts in the future as well as to enhance the platform overall with new features such as integrating sensors for pH, temperature and oxygen.

These MEA prototypes serve as a starting point for subsequent development of the platform. Our aim is to further develop this platform to include application-specific electrode layouts as well as to combine different sensor techniques for online monitoring of, for example, temperature, oxygen and pH levels. We also aim to combine different stimulation features on these MEAs. Our main objective is to combine mechanical and electrical stimulation with the novel sensors and electrode layouts to create an active biomimetic cell culture environment.

References

- [1] Mummery C., Ward-van Oostwaard, D., Doevendans, P., Spijker, R., van den Brink, S., Hassink, R., van der Heyden, M., Opthof, T., Pera, M., de la Riviere, A. B., Passier, R., and Tertoolen, L. (2003). Differentiation of Human Embryonic Stem Cells to Cardiomyocytes: Role of Coculture With Visceral Endoderm-Like Cells. *Circulation* **107**, 2733-2740.

Detection Of Cardiac Activity From Ventricular Heart Slices Using Micro-Electrode Arrays

Chung Yingying¹, Atan Shirhan¹, Zhang Guangqing¹, Wong Philip², Shim Winston¹

¹ Research and Development Unit, National Heart Centre Singapore, Singapore

² Department of Cardiology, National Heart Centre Singapore, Singapore

Heart slice preparation allows the study of cardiac function on the tissue level where the functional integrity of the tissue remains intact. In this study, short axis of the ventricular slices were cut at 300 μ m thickness with the vibrotome. The field potential recordings (FPs) generated by the heart slices were recorded using the Micro-Electrode Array (MEA) system. These ventricular slices were subjected to 1 μ M Isoprenaline (ISO) and 1 μ M Bay K 8644 to examine their response to these drugs. Both ISO and Bay K 8644 increased Ca²⁺ influx. The increased of intracellular Ca²⁺ concentration led to an increase in peak-to-peak amplitude and a decrease in beating frequency. In conclusion, embryonic chick heart slices showed the typical cardiac electrophysiological characteristics.

1 Introduction

Heart slice preparation is a useful approach to study the cardiac function on the tissue level where the functional integrity of the tissue remains intact. In this study, we investigate the electrical activities from ventricular heart slices of embryonic chick using the Micro-Electrode arrays.

2 Methods

The atria of the explanted embryonic chick heart were removed. Following that, the ventricle was mounted in 4% low melting agarose gel. Short axis ventricular slices were cut at 300 μ m thickness via the vibratome in ice-cold Ca²⁺-Free Tyrodes solution. Ventricular heart slices were transferred to ice-cold 0.9mM CaCl₂ Tyrodes solution for 0.5 hour before transporting them into prewarmed DMEM containing 1% Pencillin-Streptomycin and equilibrated with 5% CO₂. The heart slices were kept at 37°C, 5% CO₂ incubator until recording. Approximately 1 hour before recording, the ventricular heart slice was transferred onto the MEA chip and replaced the DMEM with 1.8mM CaCl₂ Tyrodes solution. Field potential recordings were performed using the MEA system. The heart slices were subjected to beta-adrenergic agonist, 1 μ M Isoprenaline (ISO) and specific L-type Ca²⁺ channel agonist, 1 μ M Bay K 8644, to evaluate whether these slices maintain the electrophysiological response of a whole heart.

3 Results

Spontaneous cardiac FPs of the ventricular heart slices were observed across all 60 electrodes when the temperature of the MEA medium was kept at 37°C. These stable and rhythmic spontaneous beatings usually lasted more than 10 minutes in the MEA. The

percentage change in Inter-Spike Interval (ISI) and percentage change in peak-to-peak amplitude of the different drug treated slices with respect to their respective baseline (normal spontaneous beating with no drug treatment) were analysed.

ISO treated slices (n=3) responded with a higher peak-to-peak amplitude with respect to baseline, yielding a Δ percentage of 8.9% as compared to Bay K 8644 treated group (n=3) with a Δ percentage of 1.4%. This implied that the ISO group had a greater increase in Ca²⁺ influx into the sarcoplasm through Ca²⁺ channels in comparison to the Bay K 8644 group.

Both the drug treatment groups showed incremental increase in the ISI that implies a slower beating rates. The ISI Δ percentage of ISO group (114.1%) was approximately 4 times higher than the Bay K 8644 group (27.1%). Thus, beating frequency of ISO group was slower as compared to the Bay K 8644 group despite the larger peak-to-peak amplitude observed in the ISO group. This is likely due to ISO group experienced a much higher sarcoplasmic Ca²⁺ concentration which might have sensitized the Ca²⁺ binding mechanism on the myofilaments. These bounded Ca²⁺ ions may be sequestered momentarily on the troponin C which interfered with efficiency of consecutive cross-bridge cycling. Hence, the decrease in beating frequency of the ISO group when compared to Bay K 8644.

To further confirm the ISO and Bay K 8644 observations, we treated the heart slices with 1 μ M ionomycin (n=3), a carrier ionophore, that is known to translocate Ca²⁺ across cell membrane and mobilising the intracellular Ca²⁺ stores. Hence, the peak-to-peak amplitude of ionomycin group (Δ percentage: 51.2%) was much higher than the baseline. This correlates well with our earlier ISO and Bay K 8644 results

where higher sarcoplasmic Ca^{2+} concentration yielded a higher peak-to-peak amplitude.

Ionomycin greatly reduced the ISI (Δ percentage: -29.9%) which indicated an increased beating frequency with respect to the ISO and Bay K 8644 groups. This may be the result of non-specific leaking of Ca^{2+} out of the sarcoplasm and possibly faster re-uptake of Ca^{2+} back in the sarcoplasmic reticulum, giving rise to higher frequency of contractions.

4 Conclusions

Ventricular heart slices of embryonic chick remained viable in culture for up to 7 days from the slicing and recording procedures. The electrical activities obtained from the ventricular slices manifested the typical cardiac field potential responses. In addition, they showed positive inotropic response to ISO, Bay K 8644 and ionomycin due to the increase uptake of Ca^{2+} intracellularly. However, their chronotropic response to ISO and Bay 8644 may be blunted by Ca^{2+} overloading. Therefore, these ventricular heart slices may serve as a platform to study electrical/contraction coupling and Ca^{2+} overloading in heart failure patients. Furthermore, they can serve as a valuable tool for pharmacological drug screening on cardiac tissue ex vivo.

References

- [1] F. Pillekamp, M. Reppel, V. Dinkelacker, Y. Duan, N. Jazmati, W. Bloch, K. Brockmeier, J. Hescheler, B. Fleischmann & R. Koehling (2005): Establishment and Characterization of a Mouse Embryonic Heart Slice Preparation. *Cell Physiol Biochem.* 16, 127-132
- [2] M. Halbach, F. Pillekamp, K. Brockmeier, J. Hescheler, J. Müller-Ehmsen & M. Reppel. (2006): Ventricular Slices of Adult Mouse Hearts – a new Multicellular In Vitro Model for Electrophysiological Studies. *Cell Physiol Biochem.* 18, 01-08

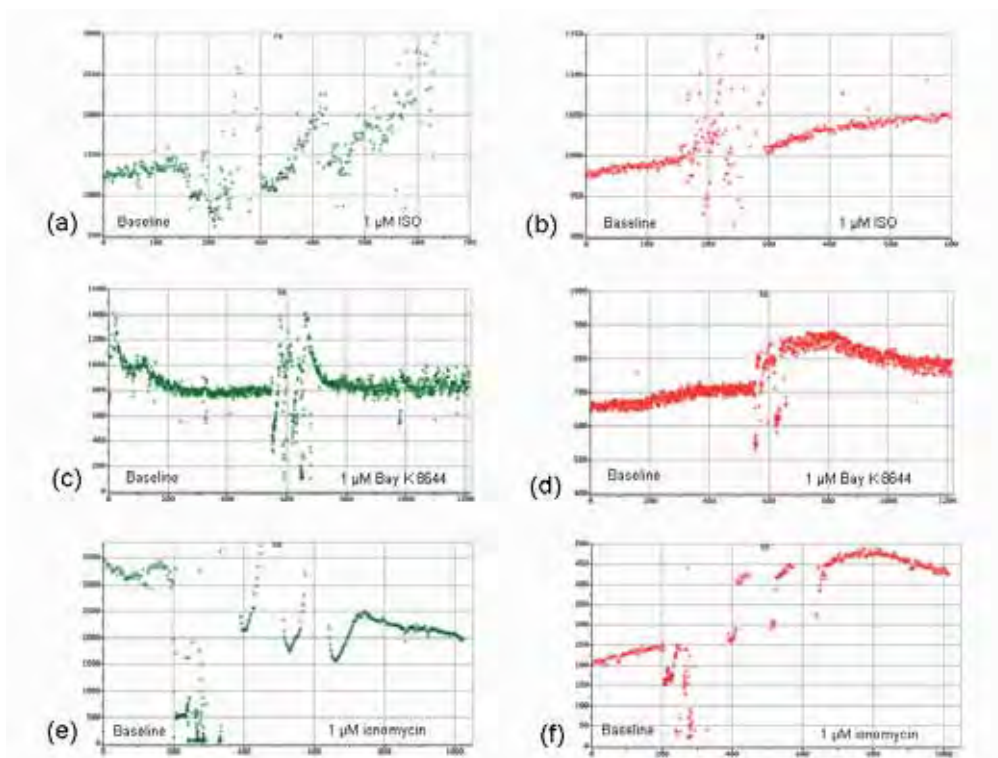


Fig 1. ISI (green) and peak-to-peak amplitude (red) plots of the different drug treatment groups. Both the (a)&(b) ISO group and (c)&(d) Bay K 8644 group showed an increase in ISI and amplitude of the field potentials with their respective baseline. Ionomycin (e)&(f) also showed an increase in peak-to-peak amplitude but a decrease in ISI, hence a higher beating frequency.

QT-time Evaluation for Drug-Screening Using a Rhesus Monkey Embryonic Stem Cell-Derived Cardiomyocyte Based Multi Electrode Array Test System

Martin Lehmann^{1*}, Filomain Nguemo^{1*}, Ulrich Martin², Michael Reppel³, Jürgen Hescheler¹

¹ University of Cologne, Cologne, Germany

² Hannover Medical School, Hannover, Germany

³ Department of Cardiology, Medical University of Lübeck, Lübeck, Germany

* Corresponding author: lehmannm@uni-koeln.de and filo.nguemo@uni-koeln.de

Drug development through the different clinical phases, is a very cost intensive factor for the pharmaceutical industry. In several cases, drugs that were already approved as “safe and effective” by various agencies, had to be retracted after patients suffered from life-threatening proarrhythmic side effects after their use. Being able to exclude compounds with cardio-active properties in pre-clinical trials would be a useful opportunity to improve drug safety and to reduce costs related to this issue. In our approach, we are using rhesus monkey (*macaca mulatta*) stem cell-derived cardiomyocytes (rESCMs) in order to establish a Multi Electrode array (MEA) based drug-screening system to evaluate possible cardio-active drugs effects. After establishing a differentiation protocol to yield sufficient numbers of rESCMs we performed MEA measurements using different drugs with well characterized effects on the QT-interval *in vivo* and on field potential durations (FPD). From these experiments, we then evaluated the inter-spike intervals (ISI) and paired these values with the corresponding FP_{\min} - FP_{\max} time interval (MMI) of single signals. Therefore, it is possible to monitor the relationship between the beating frequency and the repolarisation properties of rESCMs treated with cardio-active drugs.

1 Introduction

1.1 Background

Rhesus monkeys embryonic stem (rES) cells serve as model systems to test drug effects *in vivo* during clinical phases of drug development in the conventional way of this process. It has been proposed that rESCMs are a suitable tool to develop a high-throughput pharmacological drug screening system based on the MEA technique [1, 2]. The extracellular recording signals provided by the MEA system present a huge variability in terms of their morphology, however the recorded FP duration (FPD) linearly correlated to the action potential duration at 90% repolarization (APD_{90}) [3]. With FP_{\min} and FP_{\max} as the most prominent components of the FP signal, we decided to use the time interval between these points (referred to as MMI) as a parameter to evaluate effects of drugs on the repolarisation phase of the FP.

Drug induced arrhythmias occur when the AP repolarisation phase in cardiomyocytes is increased and therefore the relative refractory phase is prolonged. The relative refractory time prolongation increases the chance of the incidence of extra systoles which can lead to arrhythmia. During ECG recordings, QT-interval prolongations and T-wave oscillations are typical indications of imminent arrhythmias of the

heart. Therefore, we analysed single FP signals and took their MMI and ISI values. Using the MMI to represent the FPD and connecting it to the corresponding ISI (or the frequency), should provide a further aspect to conventional analysis using absolute FPD values derived from averaged FP signals.

2 Methods

2.1 Cell culture

In the experiments the rES cell line R366.4 was used. rES cells were cultured and differentiated into cardiomyocytes following modified protocols as have been published by Schwanke *et al.* [1].

2.2 MEA measurements

For the characterization of functional properties of rESCMs, extracellular recording of FPs was performed using a MEA data acquisition system (Multi Channel Systems, Reutlingen, Germany). The standard substrate-integrated MEA culture dish contains 60 titanium nitride-coated gold electrodes (30 μm diameter) arranged in an 8 x 8 electrode grid with an interelectrode distance of 200 μm .

2.3 Data Analysis

For the analysis of single FP signals, recorded data files from the respective MEA measurements were converted into ASCII files using the MC Data Tool (Multi Channel Systems, Reutlingen, Germany). Subsequently data were plotted on a time axis and ISI and the MMI were evaluated. Extracted values were collected in a database for further calculations. The ISI values were used to calculate the frequency. For the MMI values a frequency correction was performed.

3 Results and Discussion

As a first step, we successfully established a differentiation protocol to derive sufficient numbers (15-20% beating embryoid bodies, EBs) of cardiomyocytes from rESCs. These cardiac clusters attached well to the MEA chamber even without specific coating and started to beat spontaneously in parallel with the occurrence of FPs. FP morphology showed similarities to human ES cell-derived cardiac clusters. Preliminary FP recordings showed that in line with clinical observations the FP_{\min} - FP_{\max} interval (MMI) prolonged significantly as a result of the application of known QT-time prolonging drugs (e.g. Sotalol, a K^+ -channel blocker; Fig.1).

It is well known, that the RR-interval and QT-interval in the ECG as well as the AP duration and the repolarisation phase are correlated and are dependent on the beating frequency. Hence, if the FP duration correlates with the APD_{90} [3], FP duration should be also be dependent on the beating frequency. Thus, analysing changes in FP_{dur} , or the MMI as a read-out for FP_{dur} would be useful if they are either plotted against the frequency or when the values are frequency corrected. Thus, correction of FP parameters should be strongly recommended. Furthermore, we noticed that, as compared with averaged FP signals, analysis of single FP signals provides the better way to detect possible variations in the MMI, as is done in the ECG to diagnose imminent arrhythmias based on the occurrence of T-wave oscillations. Using the MMI as a measure for the FP_{dur} allows to detect the interval more easily based on the typical FP signal morphology.

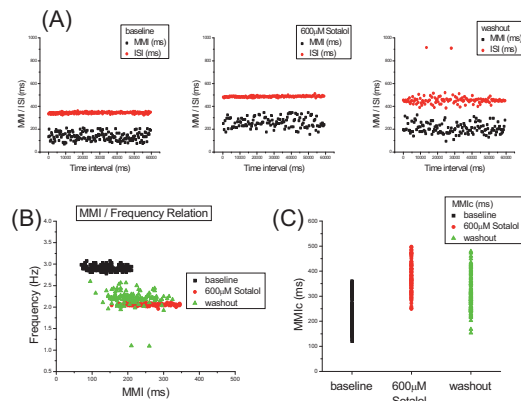


Fig.1: Single signal analysis of FP recording before (baseline), during and after application (washout) of Sotalol ($600\mu\text{M}$); (A) time course of absolute MMI and ISI values (in ms); (B) MMI/ beating frequency plot: distinct populations from paired MMI and beating frequency values; (C) Single MMI values after frequency correction for each measurement.

Acknowledgement

We thank Moritz Hausteiner for skillful technical assistance.

References

- [1] Schwanke, K., et al., Generation and characterization of functional cardiomyocytes from rhesus monkey embryonic stem cells. *Stem Cells*, 2006. 24(6): p. 1423-32.
- [2] Meyer, T., et al., Micro-electrode arrays in cardiac safety pharmacology: a novel tool to study QT interval prolongation. *Drug Saf*, 2004. 27(11): p. 763-72.
- [3] Halbach, M., et al., Estimation of action potential changes from field potential recordings in multicellular mouse cardiac myocyte cultures. *Cell Physiol Biochem*, 2003. 13(5): p. 271-84.

Anti-arrhythmic effects of very low density lipoproteins

Yangzhen Shao, Azra Mijatovic, Sigfus Gizurarson, Truls Råmunddal, Jan Boren, Elmir Omerovic*

Department of Molecular and Clinical Medicine/Cardiology, Wallenberg laboratory, Institute of Medicine at Sahlgrenska Academy, University of Gothenburg

* Corresponding author. E-mail address: elmir@wlab.gu.se

Lysophosphatidylcholine (LPC), a hydrolysis product of (membrane) phospholipid degradation, is one of the most potent pro-arrhythmic substances that accumulate in the human heart in the setting of myocardial ischemia. We need to define new pharmacological targets and therapies for prevention/attenuation of cardiac arrhythmias in the setting of myocardial ischemia. Using the multielectrode array system (MEA) in mouse HL-1 cardiomyocytes (HL-1) exposed to LPC we found that pre-treatment of HL-1 cells with VLDL could ameliorate electrophysiological abnormalities caused by LPC on spontaneous beating rate, spike signal amplitude and duration. Such protection effect from VLDL against LPC were observable even at rather low concentrations. Exogenous VLDL could act as an anti-arrhythmic substance through neutralization of pro-arrhythmic electrophysiological events elicited by LPC.

1 Introduction

LPC, a metabolite originated from the phospholipase A₂ hydrolysis of phospholipids during myocardial ischemia, has been recognized to play an important role in the genesis of ischemic arrhythmias and sudden cardiac death. LPC disrupts normal function of cell membrane, sarcolemma and membrane-associated organelles [1]. VLDL is a lipoprotein produced by the liver with a main function to transport lipids via blood to organs that use lipids as energy substrate. It has been reported that VLDL plays a regulatory role in heart metabolism through VLDL-receptor mediated mechanism and consequently an important role in the maintenance of normal heart functions [2]. We hypothesize that exogenous VLDL (possibly as a donor of exogenous apoB lipoproteins) may have anti-arrhythmic effects to some extent mediated through the neutralization or isolation of pro-arrhythmic substances released from lipid hydrolysis to prevent the electrophysiological events during ischemic states.

2 Method/statistics

Spontaneously beating mouse HL-1 cardiomyocytes of 10^5 - 2.5×10^5 were plated onto micro-electrode array system (MEA) chips and cultured for 3 days. Electrical activities of HL-1 cells were recorded in the form of field potentials (FP). The beating rate (BR), peak-peak amplitude (PP) of FP, FP duration (FPdur), and propagation delay were analyzed after VLDL administration of different doses 5 min before LPC (16 μ M) [3]. Suramin (7mg/ml) - a VLDL receptor blocker - was added 10 min before VLDL. All values are mean \pm SEM. Statistical significance of the recorded data was assessed by

analysis of variance (ANOVA) coupled with post hoc of Turkey test. All values are mean \pm SEM. $P < 0.05$ was considered as significance.

3 Results

We found that application of VLDL could protect BR and PP of FP of HL-1 cardiomyocytes from decreased and prevent the prolongation of FPdur and excitation propagation delay in the presence of LPC. Such protection of VLDL against LPC could be achieved even at a low concentration of 1 μ M and presented in positive dose dependent relationship. However, protection effect of VLDL was not affected by blocking VLDL receptor with suramin. For valuables of BR and PP, the administration of surmain even enforced the protection of VLDL against LPC by $8.2 \pm 0.3\%$ and $10.0 \pm 0.2\%$ respectively at 5 μ M of VLDL (Fig.1 and Fig.2). No significant alterations in electrophysiological properties of HL-1 cardiomyocytes were observed in the only presence of VLDL particles or suramin.

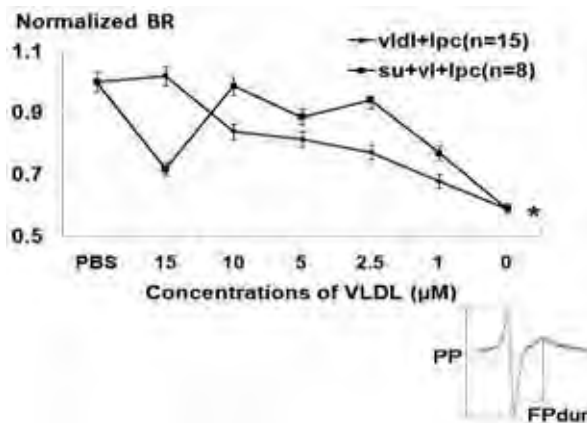


Fig. 1 Protection of VLDL against LPC on beating rate of HE-1 cardiomyocytes vldl+lpc, VLDL and LPC; su+vl+lpc, suramin, VLDL and LPC; PBS, Phosphate Buffered Saline; *, $P < 0.05$, two lines compared.

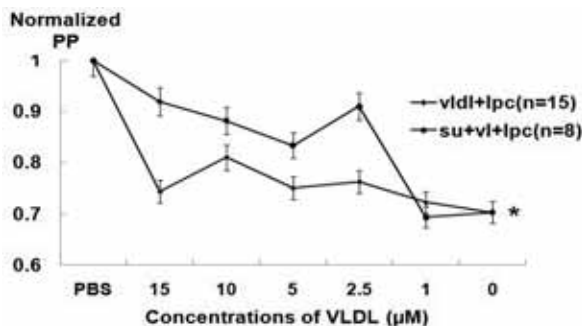


Fig. 2 Protection of VLDL against LPC on peak-peak amplitude of HE-1 cardiomyocytes vldl+lpc, VLDL and LPC; su+vl+lpc, suramin, VLDL and LPC; PBS, Phosphate Buffered Saline; *, $P < 0.05$, two lines compared

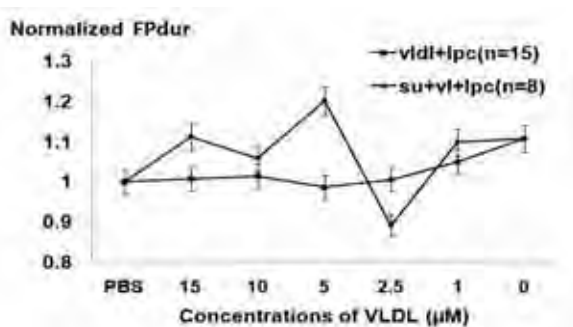


Fig. 3 Protection of VLDL against LPC on FP duration of HE-1 cardiomyocytes vldl+lpc, VLDL and LPC; su+vl+lpc, suramin, VLDL and LPC; PBS, Phosphate Buffered Saline

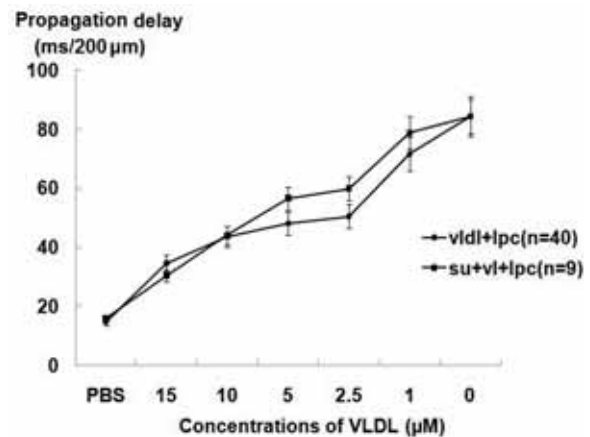


Fig. 4 Protection of VLDL against LPC on propagation time delay of HE-1 cardiomyocytes vldl+lpc, VLDL and LPC; su+vl+lpc, suramin, VLDL and LPC; PBS, Phosphate Buffered Saline.

4 Conclusion

Exogenous VLDL effectively protects cardiomyocytes from pro-arrhythmic effects caused by ischemic metabolite LPC. These effects are independent of receptor-mediated uptake of VLDL which suggests that extracellular sequestering or isolation of LPC within VLDL particles may be the mechanism behind the anti-arrhythmic effects of VLDL. Our study points toward a novel, intriguing and potentially important aspects of lipoprotein biology.

Acknowledgement

The study was supported by grants from Swedish Heart and Lung Foundation, Swedish Scientific Research Council, Gothenburg Medical Society, Medical Faculty at Gothenburg University, Swedish Society for Medical Research, ALF foundation in Västra Götaland.

References

- [1] Arnsdorf MF, Sawicki GJ. (1981): The effects of lysophosphatidylcholine, a toxic metabolite of ischemia, on the components of cardiac excitability in sheep purkinje fibers. *Circ Res*, 49, 16-30.
- [2] Banach K, Halbach MD, Hu P, Hescheler J, Egert U. (2003): Development of electrical activity in cardiac myocyte aggregates derived from mouse embryonic stem cells. *Am J Physiol Heart Circ Physiol*, 284, 2114-2123.
- [3] Niu YG, Hauton D, Evans RD, (2004): Utilization of triacylglycerol-rich lipoproteins by the working rat heart: routes of uptake and metabolic fates. *J Physiol*, 558, 225-237.

An in vitro method for studies of arrhythmogenesis in the heart - Electrophysiological effects of lysophosphatidylcholine on HL-1 cardiomyocytes

Sigfus Gizurarson, Yangzhen Shao, Azra Miljanovic and Elmir Omerovic *

Department of Molecular and Clinical Medicine/Cardiology, Wallenberg laboratory, Institute of Medicine at Sahlgrenska Academy, University of Gothenburg

* Corresponding author. E-mail address: elmir@wlab.gu.se

Sudden death due to malignant ventricular arrhythmias (VA) is the most important cause of death in the setting of myocardial ischemia. Increasing knowledge about arrhythmic mechanism is required for new anti-arrhythmic agents. Using the multielectrode array system (MEA) we demonstrated that lysophosphatidylcholine (LPC), a hydrolysis product of (membrane) phospholipid degradation, could inhibit excitation and exhibit arrhythmogenic properties on HL-1 cardiomyocytes, suggesting LPC to be one of the most potent pro-arrhythmic substances accumulating in the ischemic human heart and partly responsible for VA.

1 Introduction

Lysophosphatidylcholine (LPC), an endogenous amphiphilic compound released from cell membranes with the hydrolysis of phospholipase-A₂, could accumulate in the myocardium after minutes of ischemic events and consequently depolarize membrane potentials and evoke electric disturbance responsible for cardiac arrhythmias. Increasing knowledge about LPC is essential in a search for new pharmacological targets and anti-arrhythmic agents. This requires more complex *in vitro* experiments to assess the electrophysiological properties of LPC in an integrated way besides the effects of LPC on some single certain membrane channels with traditional method of Patch Clamp[1].

2 Method/statistics

Spontaneously beating mouse HL-1 cardiomyocytes of 10^5 - 2.5×10^5 were plated onto micro-electrode array system (MEA) chips and cultured 3 days for electrical activity recording in the form of field potentials (FP). The beating rate (BR), peak-peak amplitude (PP) of FP, and the duration of FP (FPdur) which reflects the Q-T interval, were analyzed with LPC administration of different doses by MC_Rack, and the arrhythmogenic characteristics of LPC was investigated simultaneously [2].

Statistical significance of the recorded data was assessed by one-way analysis of variance (ANOVA) followed with post hoc of Turkey test. Dose-response curves were fitted by Boltzman function to derive potential effect of half maximum effect concentration (EC₅₀). All values are mean \pm SEM. $P < 0.05$ was considered as significance.

3 Results

We found that heart rate (HR) and peak-peak amplitude (PP) of FP significantly decreased at 12 μ M and was inversely proportional to the increased concentrations of LPC. Half-maximal effect concentrations (EC₅₀) were 11.52 ± 0.90 μ M and 12.50 ± 1.60 μ M respectively. The duration of FP (FPdur), which reflects the Q-T interval, was significantly prolonged with LPC of ≥ 12 μ M in a dose-dependent way, with EC₅₀ of 12.25 ± 1.40 μ M. Moreover, LPC induced arrhythmic activity systematically at the concentrations of 16, 20, and 24 μ M. The induced arrhythmia could persist even after LPC washout and disturb the excitation propagation (Fig.5).

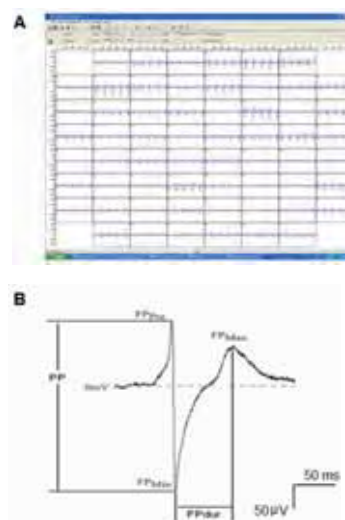


Fig. 1. Field potential recording with MEA system A. Screen shot for electrical signal recorded with MC rack; B. The magnification of one field potential with standardized FP nomenclature.

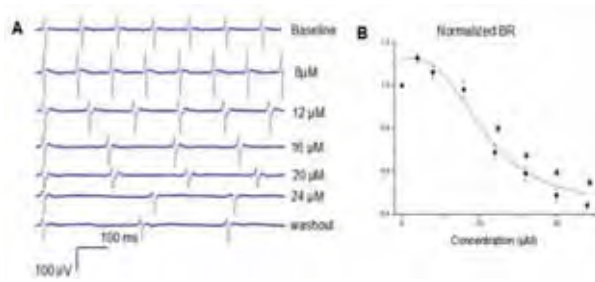


Fig. 2. Effects of LPC on beating rate of HL-1 cardiomyocytes. A. The representative field potential (FP) recorded with MEA at different concentrations of LPC. B. Fitted line of dose response with normalized beating rate, $*P < 0.05$ compared with control, $n = 27$.

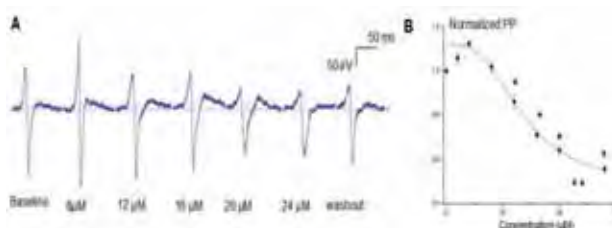


Fig. 3. Effects of LPC on peak-peak amplitude (PP) of HL-1 cardiomyocytes. A. The representative field potential (FP) recorded with MEA at different concentrations of LPC; B. Fitted line of dose response with normalized PP, $*P < 0.05$ compared with control, $n = 27$.

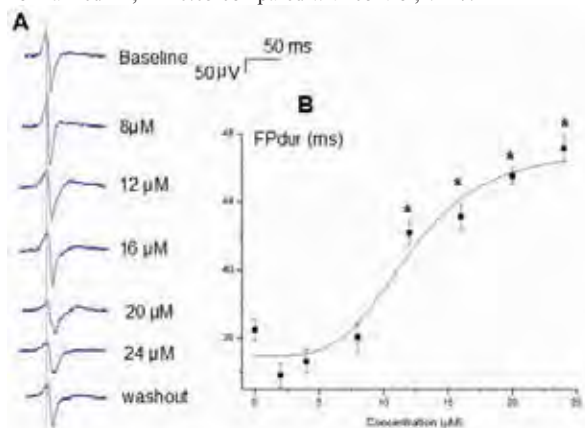


Fig. 4. Effects of LPC on FPdur of HL-1 cardiomyocytes. A. The representative field potential (FP) at different concentrations of LPC; B. Dose response fitted line of FPdur, $*P < 0.05$ compared with control, $n = 27$.

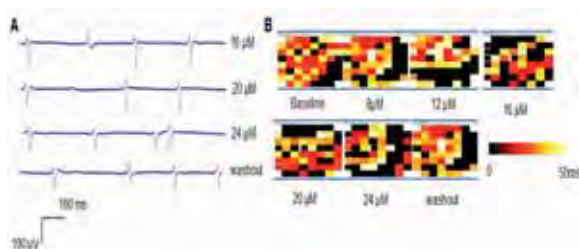


Fig. 5. Induced arrhythmia on HL-1 cardiomyocytes by LPC. A. The representative field potential (FP) recorded with MEA at higher concentrations of LPC. B. Representative excitation maps of higher concentration of LPC.

4 Conclusion

It is the first time for the present study to use MEA to investigate the effects of LPC on the electrical modulation of HL-1 cardiomyocytes in an integrated way by multielectrode extracellular recording, aiming to demonstrate the suitability of such tool in drug studies as well as the potency effect analysis of drugs. We found that LPC could inhibit the electrical activities of HL-1 cardiomyocytes and display the arrhythmogenic properties especially at high concentrations, suggesting that LPC is a potent arrhythmogenic substance with immediate proarrhythmic effects in cardiac tissue, which is partly responsible for ventricular arrhythmia over ischemic state. These methodology with MEA system can be experimentally valuable for basic studies concerning the concentration gradient effects of drugs and proarrhythmic effects of antiarrhythmic drugs for human hearts.

References

- [1] Lundbaek JA, Andersen OS. (1994): Lysophospholipids modulate channel function by altering the mechanical properties of lipid bilayers. *J Gen Physiol*, 104, 645-673.
- [2] Banach K, Halbach MD, Hu P, Hescheler J, Egert U. (2003): Development of electrical activity in cardiac myocyte aggregates derived from mouse embryonic stem cells. *Am J Physiol Heart Circ Physiol*, 284, 2114-2123.

Retinal Signalling

Changing dynamics of spontaneous waves during retinal development: a novel panretinal perspective achieved with the Active Pixel Sensor (APS) 4,096 electrodes array

Evelyne Sernagor^{1*}, Alessandro Maccione², Matthias H. Hennig³, Mauro Gandolfo⁴, Stephen J. Eglén⁵, Luca Berdondini²

¹ Institute of Neuroscience, Newcastle University Medical School, Newcastle upon Tyne, UK

² Department of Neuroscience and Brain Technologies, Italian Institute of Technology, Genova, Italy

³ Institute for Adaptive and Neural Computation, School of Informatics, University of Edinburgh, Edinburgh, UK

⁴ Department of Biophysical and Electronic Engineering, University of Genova, Genova, Italy

⁵ Department of Applied Mathematics and Theoretical Physics, Cambridge University, Cambridge, UK

* Corresponding author. E-mail address: evelyne.sernagor@ncl.ac.uk

Keynote Lecture

The developing retina exhibits spontaneous waves of activity spreading across the ganglion cell layer. These waves are present only during a limited perinatal period, and they are known to play important roles during the wiring of visual connections. Using the APS MEA devices consisting of 4,096 electrodes recording at near cellular resolution, we have been able to achieve panretinal recordings of retinal waves in the neonatal mouse retina. We found that the spatiotemporal patterns of the waves undergo profound developmental changes as retinal synaptic networks mature, switching from slow random events propagating over large retinal areas to faster, spatially more restricted events, following several clear repetitive, non-random propagation patterns. This novel panretinal perspective of wave dynamics provides new clues about the role played by retinal waves during visual map formation.

1 Introduction

During perinatal development, neighboring retinal ganglion cells (RGCs) fire in correlated bursts of action potentials, resulting in waves spreading across the RGC layer (for review see [1,2]). These waves, discovered nearly two decades ago using a multielectrode array (MEA) recording from the RGC layer [3], have been the subject of intense investigation to understand their generation and propagation mechanisms and to decipher their role during the wiring of retinal projections (for review see [2]). Retinal waves have been investigated with MEAs ranging from 60 [2 for review] to 512 electrodes [4] (sampling limited by the distance between electrodes) or with Ca^{2+} imaging [1,2] (sampling limited by the low temporal resolution of Ca^{2+} indicators). With either approach, only a limited window of the retina can be sampled at any given time, and wave dynamics have been extrapolated from these spatially restricted windows. In the mammalian retina, the earliest waves propagate through gap junctions (Stage I) [2,5], followed by propagation through lateral connections between cholinergic starburst amacrine cells (Stage II) [2,6]. Finally, once glutamatergic connections mature and RGCs become driven by light, retinal waves switch from cholinergic to glutamatergic control (Stage III) [2,5,7] before they

disappear completely. Despite these major developmental changes in network connectivity, it is still unclear to what extent wave dynamics change with development. The spatiotemporal wave patterns are hypothesised to provide cues for the establishment of retinal receptive fields and for the binocular organisation and visual map formation in retinal targets. In this study, we have used the APS MEA [8,9] to record retinal waves from the neonatal mouse at P1-P5 (Stage II) and at P9-11 (Stage III). The 64x64 APS MEA records at near cellular resolution (21x21 μm electrodes, 21 μm separation), where all channels can be acquired at high enough temporal resolution (7.8 kHz/channel for full frame acquisition) to detect single spike signals reliably. The channels are integrated over an active area of 2.67x2.67 mm, which is large enough to cover most of the neonatal mouse retina (see Fig. 1A). Hence, with its large size and unprecedented spatiotemporal resolution, the APS MEA provides the ideal experimental tool to investigate developmental changes in retinal waves dynamics.

2 Materials and methods

This study was done using C57b1/6 neonatal mice. Mouse pups were killed by cervical dislocation

and enucleated before retinal isolation. The isolated retina was then transferred to the experimental chamber and placed, RGC layer facing down, onto 64x64 MEAs [8,9]. Better coupling between the tissue and the electrodes was achieved by placing a small piece of polyester membrane filter (5 μm pores) on the retina followed by a custom made slice anchor holder. The retina was kept at 32°C and continuously perfused (2 ml/min) with artificial cerebrospinal fluid containing the following (in mM): 118 NaCl, 25 NaHCO₃, 1 NaH₂PO₄, 3 KCl, 1 MgCl₂, 2 CaCl₂, and 10 glucose, equilibrated with 95% O₂ and 5% CO₂. The retina was usually left for 30-60 min to settle on the MEA before starting the recording, allowing time for coupling to improve and for spontaneous activity to develop.

Electrophysiological signals were acquired from the whole array at 7.8 kHz sampling rate and visualized on screen during recordings. Successively, off-line spike detection was performed by using a recently presented Precise Timing Spike Detection (PTSD) algorithm [10] since it enables a fast and precise identification of the spike events..

Spike trains were used to generate raster plots and activity maps using BrainWave as well as custom designed codes written in Matlab and R.

3 Results

We have investigated the spatiotemporal properties of retinal waves at P1,2,3,4,5 (Stage II) and P9,10,11 (Stage III). For the youngest animals, the entire retina fits on the MEA, and it is even smaller than the active area of the electrodes (2.67x2.67mm). Figure 1A shows a P10 retina on the MEA. The photograph was taken at the end of the recording session, after removal of the anchor and filter paper. In this case, the outer peripheral retina is beyond the limits of the active area. A map of the active electrodes during a 10 minutes recording session is overlaid on the retina. The colours indicate the log of the firing rate on each electrode (see Figure 3 for more details on activity maps). There is no activity at the centre, mostly around the optic disk (red circle), a feature we have observed in most retinas. In this particular retina, there was virtually no activity on the bottom left and left side of the tissue. The lack of activity along the left side was probably due to poor coupling (as verified at the end of the experiment). However, based on visual inspection, the coupling seemed strong in the bottom left part of the MEA, but nevertheless that part of the retina had very little spontaneous activity.

Figure 1B shows an activity raster plot recorded over 15s in the same retina. There were 1180 active channels during that same period. The raster plots (ar-

ranged by electrode rows) show complex propagation patterns across the tissue. However, a 2 dimensional view of the activity is necessary to visualise these patterns. This is shown in time lapse single frames of activity raw data taken at 342, 344, 347, 352 and 354 s. The colour map represents the electrical activity variance calculated over a 0.5s time window. Three clear waves in distinct parts of the array are apparent over the recording period. Figure 1B also illustrates raw data from selected channels scattered across the right side of the array. These channels were active during the network bursts, showing clear activity propagation between them.

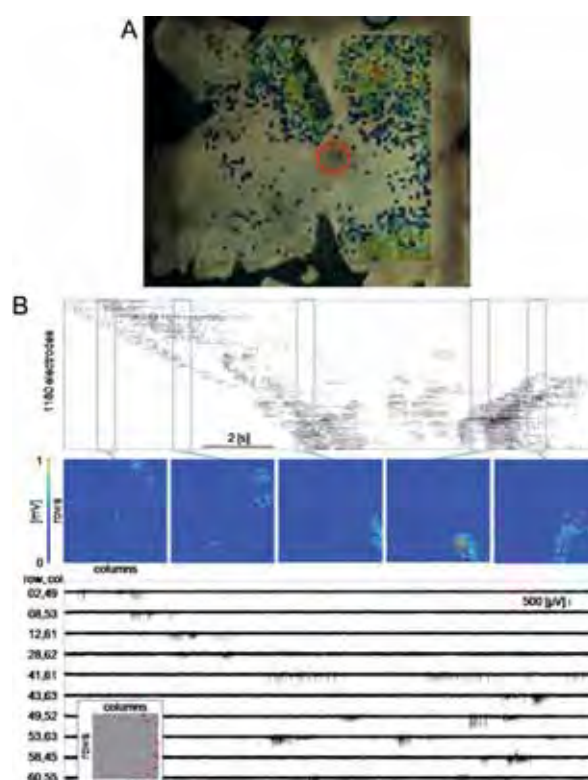


Fig. 1. Spontaneous activity in a P10 retina. **A:** photograph of the retina on the MEA, acquired at the end of the recording session. The overlay represents the map of the activity recorded during a 10 min trial. Dots are colour coded for the log of the firing rate (see fig. 3 for more details). **B:** Activity recorded over 15 s in the same retina. The top panel illustrates the raster plot of the activity, with the channels arranged according to rows on the MEA. The middle panel shows time lapse images of the activity as it propagates across the retina during the same 15 s. See text for more details. The bottom panel shows the raw data for 10 channels selected within the path of the activity on the right side of the array.

Starburst amacrine cholinergic connections initially drive the waves. However, the wave-generation synaptic network undergoes profound changes around P9, when RGCs become driven by light, at the time of the maturation of bipolar glutamatergic connections. Despite these fundamental changes in the network

driving retinal waves, no consistent differences between Stage II and Stage III wave dynamics have been reported in the literature. Experimental limitations due to the relatively small spatial windows in 60 channels MEA recordings, or to the poor temporal resolution in imaging experiments, may indeed prevent achieving a clear overview of perhaps subtle (but nevertheless important from a functional point of view) global wave dynamics changes. With the APS MEA, we have observed fundamental differences in the spatiotemporal properties of Stage II and III waves. Figure 2 illustrates raster plots of spontaneous activity recorded at P4-5 (Stage II) and P9 and P11 (Stage III). In the P4 and P5 retinas, waves are initiated in random locations and they slowly propagate across large retinal areas. At Stage III, however, the waves are often, but not always, spatially more restricted, as clearly revealed in the raster plots. Indeed, most episodes of activity appear to recruit only a limited subset of the RGC population. Another clear difference is that the waves appear to propagate much faster at these later stages.

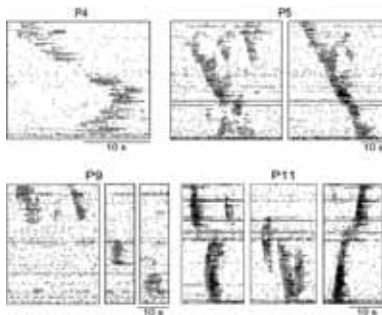


Fig. 2. Raster plots of spontaneous activity at different developmental stages.

Figure 3 provides information on the spatial distribution of the spontaneous activity at these different stages. The figure illustrates activity maps computed over 10 min trials. The dots on the plots represent active electrodes, and the colours of the dots reflect the average firing rate (calculated in log spikes/s) for these channels. At P4, the activity appears completely scattered across the retina, with no distinct patterns of spatial organisation. At P5, the activity is stronger and perhaps slightly more clustered, but still with no clear spatial patterns. At P9, on the other hand, when glutamatergic connections take over from acetylcholine in controlling the waves, the activity becomes clustered in small areas on the array (inspection after the recording session revealed that there was no retina on the right side of the MEA). These clusters appear to tile the retina in a non-overlapping manner. The activity becomes stronger at P10-11, but even so, it appears clustered in the same

specific retinal areas rather than propagating across the entire tissue like at Stage II. Interestingly, Stage II waves are initiated at random locations, both in the center and in the periphery, whereas at Stage III, waves appear to be mostly generated in the periphery and they propagate towards the central retina.

The maturation of GABAergic inhibition is known to play an important role in retinal wave dynamics, causing them to become smaller and more static until they completely disappear [2,5,11]. Hence, GABA may be responsible for the emergence of the activity clusters at Stage III. In the P9 retina illustrated in Figure 3, upon addition of bicuculline (10 μ M), a GABA_A receptor antagonist, the activity became stronger and two new clusters emerged (Figure 3).

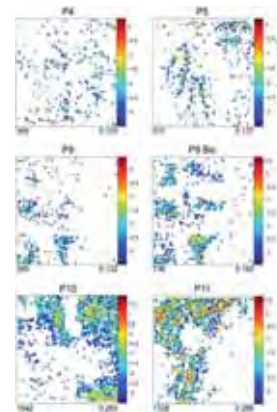


Fig. 3. Spontaneous activity maps computed over the entire MEA during 10 minutes recording sessions at different developmental stages. The activity is colour coded following the log of the firing rate (spikes/s). Left bottom corner number: total number of active channels. Right bottom corner number: average firing rate.

Nevertheless, the activity remained clustered and it did not start to propagate over large retinal areas. GABA_A blockade results in significantly longer bursts and faster wave propagation, as clearly illustrated in the raster plots of Figure 4, suggesting that synaptic inhibition dampens propagation across the network. In addition, in the presence of bicuculline, the activity sometimes seems to “flow” more easily between clusters, such as between the two clusters on the right side of the array at P10 in Figure 3. The top raster plot in Figure 4 represents spontaneous activity in that area of the P10 retina in control condition. The wave front, outlined by the red arrow, clearly shows how activity comes to an almost complete stop in the middle of the episode. In the presence of bicuculline, the activity becomes not only faster, but on occasion, it also succeeds in propagating smoothly from one area to the other (bottom raster plot). However, it is important to point out that in many other episodes, these clusters

remain clearly separated, and often do not occur consecutively.

4 Discussion and concluding remarks

In this study, we have demonstrated that the APS MEA is a powerful tool to investigate the spatiotemporal behaviour of developing retinal networks. Indeed, we have achieved new insights about developmental changes in wave dynamics, during the critical period for wiring of the visual system. Stage II waves are slow and wide spreading in the retina, propagating with a high degree of randomness whereas Stage III are faster and spatially more restricted. Previous studies in chick [12] and turtle [11] (where both acetylcholine and glutamate drive retinal waves in consort) have already demonstrated that acetylcholine is important for the wave spatial extent, whereas glutamate regulates the speed of propagation.

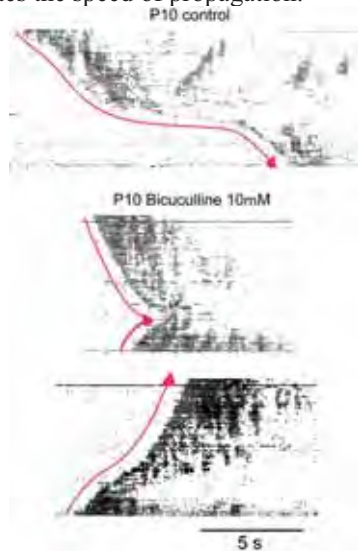


Fig. 4. GABAergic inhibition slows down wave propagation and shortens the duration of the network bursts. Raster plots of spontaneous activity in a P10 retina show that when GABA_A receptors are blocked with bicuculline, waves propagate significantly faster and the bursts are longer.

Here, with the APS MEA, we have shown that indeed, early Stage II cholinergic waves are slow and they propagate over large retinal areas, whereas Stage III glutamatergic waves are faster and spatially more restricted. Stage II waves occur at the time of ocular segregation, when inputs from both eyes compete for a common target, hence requiring synchronization between inputs coming from the same eye. These wide spreading cholinergic waves provide the perfect substrate to achieve this goal. Stage III waves occur at the time of functional map refinement. These faster and spatially more restricted waves provide the perfect substrate for that goal, ensuring coactivation of neigh-

bouring RGCs, hence providing synchronous input to neighbouring cells in their central target. At the same time, however, the clustering and repetitiveness of wave trajectories at Stage III will cause spatially biased neural activity during map refinement, and might therefore interfere with the process of establishing regular ordered retinotopic maps. This novel finding challenges current models of activity-dependent map formation, and calls for a re-investigation of map development at this developmental stage.

Acknowledgement

We thank L. Gasparini at IIT for her help with supplying mouse pups. This work was funded by EPSRC Grant EP/E002331/1 (CARMEN) (ES, SJE), IDEA, FP6-NEST Grant 516432 (LB, AM, MG) and MRC Grant G0900425 (MHH).

References

- [1] Sernagor E., Eglén S.J., Wong R.O.L. (2001). Development of retinal ganglion cell structure and function. *Prog Retin Eye Res*, 20, 139-174.
- [2] Torborg C.L., Feller M.B. (2005). Spontaneous patterned retinal activity and the refinement of retinal projections. *Prog Neurobiol*, 76, 213-235
- [3] Meister M., Wong R.O.L., Baylor D.A., Shatz C.J. (1991). Synchronous bursts of action potentials in ganglion cells of the developing mammalian retina. *Science*, 252, 939-943.
- [4] Stafford B.K., Sher A., Litke A.M., Feldheim D.A. (2009) Spatial-temporal patterns of retinal waves underlying activity-dependent refinement of retinofugal projections. *Neuron*, 64, 200-212.
- [5] Syed M.M., Lee S., Zheng J., Zhou Z.J. (2004). Stage-dependent dynamics and modulation of spontaneous waves in the developing rabbit retina. *J Physiol*, 560, 533-549.
- [6] Zheng J.J., Lee S., Zhou Z.J. (2004). A developmental switch in the excitability and function of the starburst network in the mammalian retina. *Neuron*, 44, 851-864.
- [7] Bansal A., Singer J.H., Hwang B.J., Xu W., Beaudet A., Feller M.B. (2000). Mice lacking specific nicotinic acetylcholine receptor subunits exhibit dramatically altered spontaneous activity patterns and reveal a limited role for retinal waves in forming ON and OFF circuits in the inner retina. *J Neurosci*, 20, 7672-7681.
- [8] Imfeld K., Neukom S., Maccione A., Bornat Y., Martinoia S., Farine P.A., Koudelka-Hep M., Berdondini L. (2008) Large-scale, high-resolution data acquisition system for extracellular recording of electrophysiological activity. *IEEE Trans Biomed Eng*, 55, 2064-2073.
- [9] Berdondini L., Imfeld K., Maccione A., Tedesco M., Neukom S., Koudelka-Hep M., Martinoia S. (2009). Active pixel sensor array for high spatio-temporal resolution electrophysiological recordings from single cell to large scale neuronal networks. *Lab Chip*, 9, 2644-2651.
- [10] Maccione A., Gandolfo M., Massobrio P., Novellino A., Martinoia S., Chiappalone M. (2008). A novel algorithm for precise identification of spikes in extracellularly recorded neuronal signals. *J Neurosci Meth*, 177, 241-249.
- [11] Sernagor E., Young C., Eglén S.J. (2003). Developmental modulation of retinal wave dynamics: shedding light on the GABA saga. *J Neurosci*, 23: 7621-7629.
- [12] Sernagor E., Eglén S.J., O'Donovan M.J. (2000). Differential effects of acetylcholine and glutamate blockade on the spatiotemporal dynamics of retinal waves. *J Neurosci*, 20 (RC56), 1-6.

Network oscillation in *rod degenerated (rd1)* retinas

Günther Zeck^{1,2*} and Jacob Menzler¹

¹ Department of Computational and Systems Neuroscience, Max Planck Institute of Neurobiology, Martinsried, Germany

² NMI, Natural and Medical Sciences Institute at the University of Tübingen, Reutlingen, Germany

* Corresponding author. E-mail address: guenther.zeck@nmi.de

1 Introduction

Pathological neuronal oscillations are associated with diverse CNS disorders including neurodegenerative diseases such as Parkinson or epilepsies. They are characterized by enhanced excitability and oscillatory behaviour of the neurons involved. In rod degenerated mouse (*rd1*) retinas gene defects lead to complete blindness. The disease is accompanied by an increased and rhythmic spontaneous activity in the retinal projection neurons [1-3] – the retinal ganglion cells (RGC). Here we assessed the degree of synchronicity between retinal projection neurons and investigated the mechanism underlying the rhythmic discharge.

2 Methods

We recorded extracellular voltages from *in vitro* mouse retinas using a multi-transistor array with 16384 sensors densely packed in 1mm². The retinas were isolated from adult *rd1* and *wt* mice (P35-P70) respectively. Extracellular signals attributed to retinal ganglion cell (RGC) action potentials were identified using an appropriate filter range (100 Hz – 10 kHz) and taking advantage of the simultaneous recording on many adjacent electrodes. Local field potentials were detected in the low frequency range (1 – 50 Hz) and analyzed adapting concepts from developmental retinal waves.

3 Results

The majority of RGCs (80% per retinal portion) in *rd1* retinas show rhythmic ~10Hz bursting activity. The cross- correlograms between *rd1* spike trains display multiple peaks with the central peak randomly shifted with respect to zero lag. RGC spiking is locked to the minima of Local Field Potentials (LFPs) that occur at the same fundamental frequency. LFPs propagate across *rd1* retinas at average velocities of 5 – 8 mm/sec. Oscillatory spiking and local field potentials were never encountered in *wt* retinas.

Inhibition of RGC spiking using TTX abolished RGC spikes but not the LFPs. Inhibitory glycine and GABA-receptor blockers slowed down RGC rhythmicity and the corresponding LFPs. Local field potentials and the concomitant oscillatory spiking disappeared after application of glutamate receptor blockers or after the application of gap junction blockers.

4 Conclusion

Our results indicate that strong excitation - transmitted through a network of electrically coupled interneurons - leads to aberrant large-scale network oscillations. The spatially confined rhythmic activity may explain forms of photopsias reported by blind patients and may help to develop effective treatment strategies for *retinitis pigmentosa*.

References

- [1] Ye, J.H. & Goo, Y.S.. *Physiol. Measurement* **28**, 1079-1088 (2007)
- [2] Stasheff, SF et al.. *J. Neurophysiol* **99**, 1408 - 1421 (2008)
- [3] Margolis, D.J., et al. *J. Neurosci* **28**, 6526- 6536 (2008).

Spatial and Temporal Patterns and Information Processing in Retinal Neurons

Liang Pei-Ji*, Jing Wei, Liu Wen-Zhong, Gong Hai-Qing, Zhang Pu-Ming

School of Life Sciences and Biotechnology, Shanghai Jiao Tong University, Shanghai, China

* Corresponding author. E-mail address: pjliang@sjtu.edu.cn

The spike activities of bullfrog retinal ganglion cells in response to different visual patterns were recorded using multi-electrode array, and relevant spatio-temporal properties of the retinal ganglion cells activities in response to the visual stimulation were characterized. The adaptation properties were also examined.

1 Background

The first stage for visual information processing in vertebrates occurs in the retina. However, the retinal function is constrained by a number of factors such as the anatomic limitation, the metabolic limitation, and the noise in the neural circuitry. Our research is mainly focused to investigate the reliability and efficiency of information processing of the retinal neurons under such limitations and the related spatial and temporal patterns of the neural activities. In the present study, the spike activities of bullfrog retinal ganglion cells in response to different visual patterns were recorded using multi-electrode array, and relevant spatio-temporal properties of the retinal ganglion cells activities in response to the visual stimulation were characterized. The adaptation properties were also examined.

2 Method

Spikes from bullfrog retinal ganglion cells were recorded by MEA electrodes (8×8, MMEP-4, CNNS UNT, USA) using a commercial multiplexed data acquisition system with a sampling rate of 40 kHz (MEA workstation, Plexon Inc. Texas, USA). Light stimulus was generated from a computer monitor (Iiyama, Vision Master Pro 456, Japan) and was focused to form a 1.1×1.1 mm² image on the isolated retina via a lens system. The stimulation protocols were: (1) Checker-board stimulus consisted of 8×8 sub-squares, with each sub-square covering an area of 132×132 μm² on the retinal piece and was assigned randomly with a value either “1” (white light, 77.7 nW/cm²) or “0” (dark, 0 nW/cm²); (2) Grating (horizontal or vertical) stimuli consisted of light bars (77.7 nW/cm²) and dark bars (0 nW/cm²), with the width of each bar being 177 μm when projected on the retina.

3 Results

In the present study, an analytical tool based on measurement of subsequence distribution discrimination (MSDD) [1,2] analysis was applied to deal with a group of spike train sequences and analyze the spatio-temporal pattern of concerted activities among the neurons. The analytical results show that: (1) In our experimental protocols, each single ganglion cell's firing rate did not change much during its responses elicited by different stimulation pattern; (2) During adaptation to any particular visual pattern, the neuronal firing activities was gradually reduced; (3) By applying MSDD, the spatio-temporal patterns of the neuronal activities in response to different visual patterns were identifiable.

4 Conclusion

The results show that the population adaptation process follows the single neuronal adaptation process in a sense that the neuronal activities were gradually reduced, but the spatio-temporal patterns of population neuronal activities were identifiable, which served for reliable and efficient information processing.

Acknowledgement

This work was supported by the grant from National Basic Research Program of China under Grant No. 2005CB724301.

References

- [1] Fang W.W., Roberts F.S., Ma Z. R. (2001) A measure of discrepancy of multiple sequences. *Information Science*, 137, 75-102.
- [2] Wang G.L., Liu X., Zhang P.M., Liang P. J. (2006) A new method for multiple spike train analysis based on information discrepancy. *LNCS*, 4232, 30-38.

Recording of Neural Activity of Mouse Retinal Ganglion Cells by Means of an Integrated High-Density Microelectrode Array

Michele Fiscella¹, Urs Frey², David Jäckel¹, Jan Müller¹, Ralf Streichan¹, Ian L. Jones¹, Branka Roscic¹, Karl Farrow³, Botond Roska³, Andreas Hierlemann¹.

¹ Bio Engineering Laboratory, ETH Zurich, Basel, Switzerland.

² Bio Engineering Laboratory, ETH Zurich, Basel, Switzerland; now at IBM Research, Zurich, Switzerland.

³ Neural Circuits Laboratory, Friedrich Miescher Institute, Basel, Switzerland.

Retinal ganglion cells form the output layer of the retina and send the encoded visual information to the brain. Using a high-density microelectrode array to scan the ganglion cell layer, we were able to sort the spiking activity of different units and select a defined subset of electrodes to record from a specific group of retinal ganglion cells.

1 Background/Aims

The mammalian retina extracts specific features from the visual input. The final output is computed in the ganglion cell layer and consists of complex spatio-temporal patterns of action potentials [1]. Microelectrode-array (MEA) technology is an ideal tool for recording spike trains of retinal ganglion cell populations.

Here we show the possibility to scan the ganglion cell layer and record the activity of potentially every active retinal ganglion cell on the array.

2 Methods

We used a complementary metal-oxide-semiconductor (CMOS)-based MEA (Fig. 1) providing high spatio-temporal resolution and high signal-to-noise ratio to record neural activity from mouse retinal ganglion cells.

The MEA features 11,011 metal electrodes, placed in an area of $2.0 \times 1.75 \text{ mm}^2$ (126 electrodes at arbitrary positions can be selected for synchronous recording). Each platinum electrode has a diameter of $7 \mu\text{m}$, and the center-to-center distance between the electrodes is $17 \mu\text{m}$. Flexibility in the electrode selection is attained through an analog switch matrix located underneath the electrode array [2].

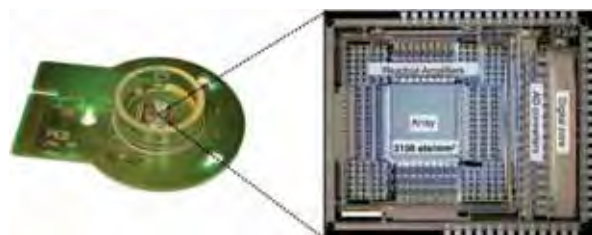


Fig. 1. Packaged high-density MEA device and overall chip micrograph. Scale bar: 1 mm.

The retinae were isolated at ambient light from the C3H/HeNcr1 (*rd1*) mouse strain at P80 in Ringer's medium (in mM: 110 NaCl, 2.5 KCl, 1 CaCl₂, 1.6 MgCl₂, 10 D-glucose, 22 NaHCO₃, bubbled with 5% CO₂/95% O₂). Once a piece of the retina was isolated, it was placed with the ganglion cell side contacting the MEA. The retina was held on the array by a custom-built holder and superfused with Ringer's medium at 36° C.

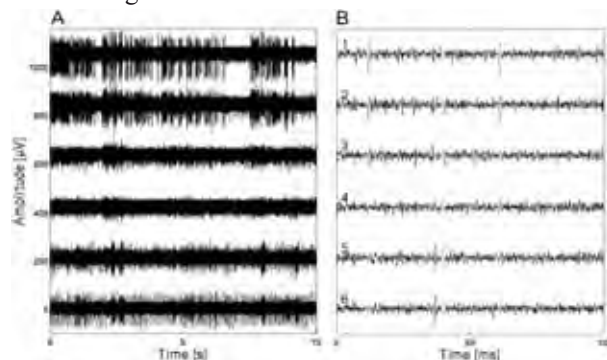


Fig. 2. (A) | Recordings from *rd1* mouse retinal ganglion cells. **(B)** | Zoom into (A) with spikes from 3 units identified after spike sorting and marked in different colors. Note: each unit is detectable on more than one electrode.

3 Results

We used the *rd1* mouse retina to record spontaneous activity [3] from retinal ganglion cells. Action potentials from single ganglion cells were simultaneously recorded on several electrodes (Fig. 2). The highly redundant information provided by our system allows us to use independent-component analysis (ICA) for spike sorting [2]. In most cases we measured somatic signal with amplitudes between 100-300 μV (Fig. 3). In several cases, we were able to measure the propagation of corresponding axonal signals.

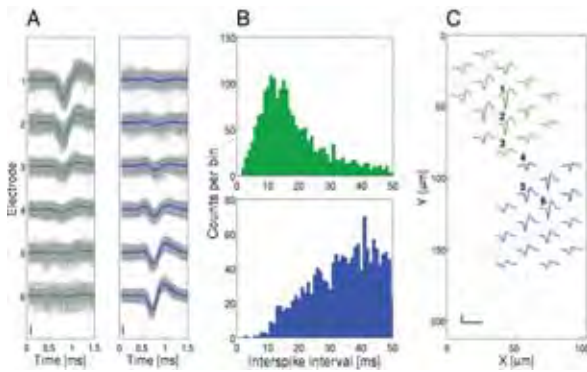


Fig. 3. (A) | Superimposition of events for the green and blue units detected in Fig. 2B during 2 min recording. The averaged signal is marked in color. Scale bar: 50 μ V. (B) | Inter-spike interval histograms; (C) | RGCs footprints. Scale bar: 50 μ V, 1.5 ms

After spike sorting, the spatial position of each ganglion cell can be determined. Consequently, it is possible to select 2-4 electrodes directly underneath any ganglion cell of interest. The electrodes are chosen in a way to most efficiently separate the signal of the cell of interest from those of the surrounding cells (Fig. 4).

The large flexibility in the electrode selection along with the high electrode density is important for two reasons: (1) our system allows to rapidly scan large areas of the ganglion cell layer (2) we can potentially record activity from every ganglion cell on the array (Fig. 5).

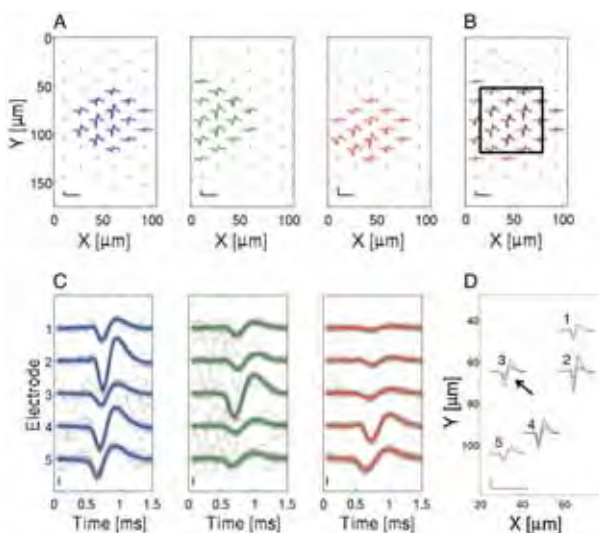
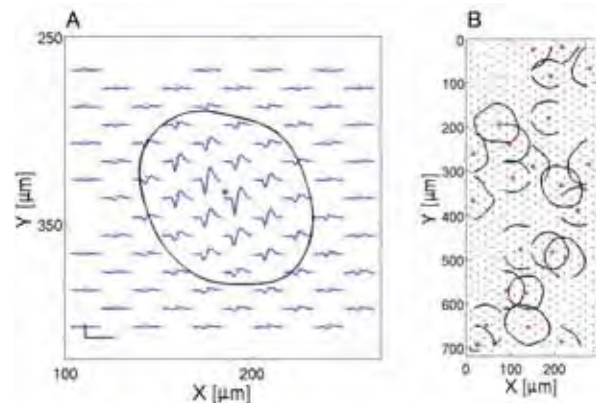


Fig. 4. (A) | Footprints of 3 neighboring cells. Scale bar: 100 μ V, 1.5 ms. (B) | Same cells as in (A) but plotted together. Note the high degree of overlap between the footprints. Scale bar 100 μ V, 1.5 ms. (C) | Superimposition of events from units in (A) on 5 electrodes inside the black rectangle in (B). Scale bar 50 μ V. (D) | The electrode providing best identification of the green cell is indicated by the black arrow. Scale bar 100 μ V, 1.5 ms.

4 Conclusions

The integrated CMOS-based MEA offers the possibility to rapidly scan large retina patches, to identify consistently spiking units, and to record from



selected cells of the ganglion cell layer. This strategy will enable us to record light-evoked activity from functionally identified RGCs in their network context.

Fig. 5. (A) | RGC footprint. The red dot indicates the electrode with the highest spike amplitude. The black contour line represents an equipotential line at half peak amplitude. Scale bar: 100 μ V, 1.5 ms. (B) | RGCs sorted from different overlapping recording blocks, represented in the same way as in (a).

Acknowledgement

This work was supported by the Swiss Initiative in Systems Biology, SystemsX.ch, with an interdisciplinary PhD grant.

References

- [1] Wässle H. Parallel processing in the mammalian retina. *Nat Rev Neurosci.* 2004;5:747-57.
- [2] Frey U, Egert U, Heer F, Hafizovic S, Hierlemann A. Microelectronic system for high-resolution mapping of extracellular electric fields applied to brain slices. *Biosens Bioelectron.* 2009;24:2191-8.
- [3] Stasheff SF. Emergence of sustained spontaneous hyperactivity and temporary preservation of OFF responses in ganglion cells of the retinal degeneration (rd1) mouse. *J Neurophysiol.* 2008;99:1408-21.

Electrical response of rabbit retinal ganglion cells and their intraretinal conduction after optic nerve crush

Christian Leibig^{1*}, Günther Zeck^{2*}

1 Membrane- and Neurophysics, Max Planck Institute for Biochemistry, Martinsried

2 Computational- and Systems Neurobiology, Max Planck Institute of Neurobiology Martinsried, Germany

* Corresponding authors. E-mail addresses: zeck@neuro.mpg.de, leibig@biochem.mpg.de

The optic nerve represents an ideal model to study the degeneration and regeneration of CNS axons after either crush or section.

Here we investigate electrophysiological properties in the rabbit retina following optic nerve crush (ONC). The rabbit retina was selected because we were able to measure intraretinal propagation of individual action potentials at very high spatial (7.8 μm) and temporal (0.1 msec) resolution using a multi-transistor array comprising 16384 extracellular sensor sites. In addition we quantified spontaneous activity and response latencies to flashed spots in populations of retinal ganglion cells from the same retina. Retinas were isolated at three time points following optic nerve crush: after 4, 7 and 14 days respectively.

Intraretinal conduction velocity did not change significantly in retinas isolated four days after ONC compared to control velocities (mean 1.3 m/sec). The average intraretinal velocity dropped to 1.1 m/sec in axons isolated 7 days (n = 14) and 14 days after ONC (n=14).

The median spontaneous firing rate (6 Hz) measured under otherwise identical conditions did not change after optic nerve crush. However, we found in each of the three post-crush conditions cells with firing rates exceeding 30 Hz - a feature not detected in control retinas. The average response latency to flashed spots (mean: 55 ms, n = 40 ON cells per retina) did not change after optic nerve crush.

Our results indicate that two weeks after optic nerve crush intraretinal conduction is reduced but the circuitry presynaptic to the ganglion cells remains functional.

Stem Cell Derived Neuronal Networks

Interactions of P19 cell-derived neuronal networks and mouse cortical networks co-cultured on micro-electrode array

Yuzo Takayama^{*}, Hiroyuki Moriguchi, Atushi Saito, Kiyoshi Kotani, Yasuhiko Jimbo

Graduate School of Frontier Sciences, University of Tokyo, Japan

^{*} Corresponding author. E-mail address: Yuzo_Takayama@ipc.i.u-tokyo.ac.jp

Regeneration of the damaged central nervous system (CNS) is one of the most important themes in neuroscience and neuroengineering. Grafting new neurons derived from stem cells into the damaged brain is essential for restoring appropriate functions. Little is known, however, about network-wide interactions between stem cell-derived neurons and the CNS neurons. In this paper, we tried to establish a co-culture method of stem cell-derived neuronal networks and CNS networks and to observe spontaneous electrical activity in the co-cultured networks by using microfabrication techniques and the MEA-based recording system.

1 Introduction

Due to the morphological and dynamical complexity of neurons in the CNS, local-scale damage of somata or neurites cause the pathogeny of CNS injuries and neurodegenerative diseases, such as Parkinson's disease and spinal cord injury [1]. For CNS regeneration, integrating new neurons derived from pluripotent stem cells with the established host CNS networks and restoring functional network dynamics will be required. However, little is known about network-wide interactions between stem cell-derived neurons and the CNS neurons. In this paper, we attempt to co-culture stem cell-derived neuronal networks and primary CNS neuronal networks and characterize interactions of electrical signals between them. For this purpose, we created a poly(dimethylsiloxane) (PDMS)-based culture device consisted of two compartments and 20 micro conduits and cultured P19-derived neurons and mouse cortical neurons into them. P19 cell is a cell line established from mouse carcinoma, and we chose P19 cells as a model stem cell because neural differentiation pathways in P19 cells resemble those in embryonal development in the mammalian CNS.

2 Methods

To achieve separated co-culture of two types of neuronal networks, we fabricated PDMS-based multicompartiment culture device consisted of two compartments and microconduits, and placed onto MEA substrate coated with 0.1% polyethyleneimine (Fig. 1). In each culture compartment, 32 embedded electrodes were used for recording electrical activity of neurons.

P19EC cells were routinely proliferated on tissue culture dishes in α -MEM containing 10 % fetal bovine serum. To initiate differentiation, cells were plated into bacteria culture dishes, which allow cells to form embryoid bodies, and cultured them in medium with 1×10^{-6} M all-trans retinoic acid. After 4 days, cells were dispersed with 0.25% Trypsin-EDTA and plated on PDMS-combined MEA substrate. Cortical tissues were obtained from 16-day-old ICR mouse embryos and were dissociated by trituration after digestion with 0.25 % Trypsin-EDTA in calcium – and magnesium – free HBSS. The dissociated cells were also plated on PDMS-combined MEA substrate.

3 Results

In two weeks cultures, spontaneous periodic synchronized bursting was observed from both P19 – derived networks and primary cultured cortical networks (Fig. 2A) In particular, although P19 – derived networks showed rarely spontaneous activity at two weeks monocultures, P19 – derived neurons co-cultured with mouse cortical neurons showed extensive synchronized firing. In three weeks cultures, spontaneous activity was rarely recorded from P19 – derived networks despite the presence of highly complicated bursting in primary cultured cortical networks (Fig. 2B). These results suggest that significant interactions were occurred in the integration processes between stem cell – derived networks and CNS neurons.

References

- [1] I.M. Medana and M.M. Esiri. (2003) Axonal damage: a key predictor of outcome in human CNS diseases. *Brain*, 126, 515-530.

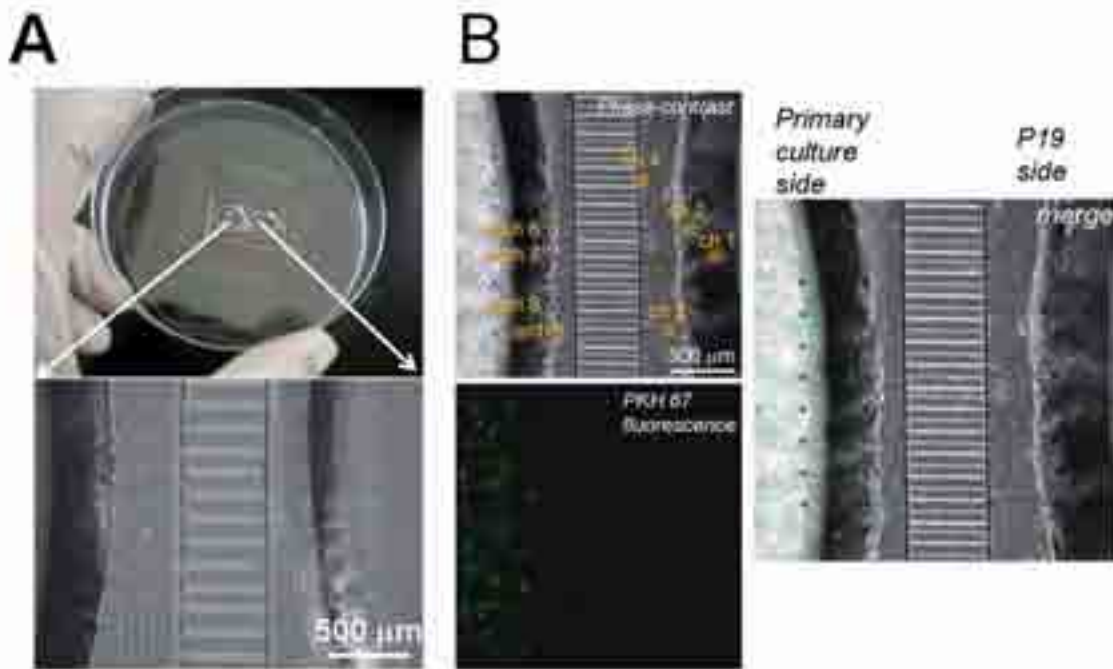


Fig.1 Co-culture of P19 – derived neurons and mouse cortical neurons on MEA. *A*, PDMS – based co-culture chamber was placed onto MEA substrate. *B*, To confirm the distribution of each neuronal type, mouse cortical neurons were labelled with PKH 67 linker and its fluorescent image was obtained.

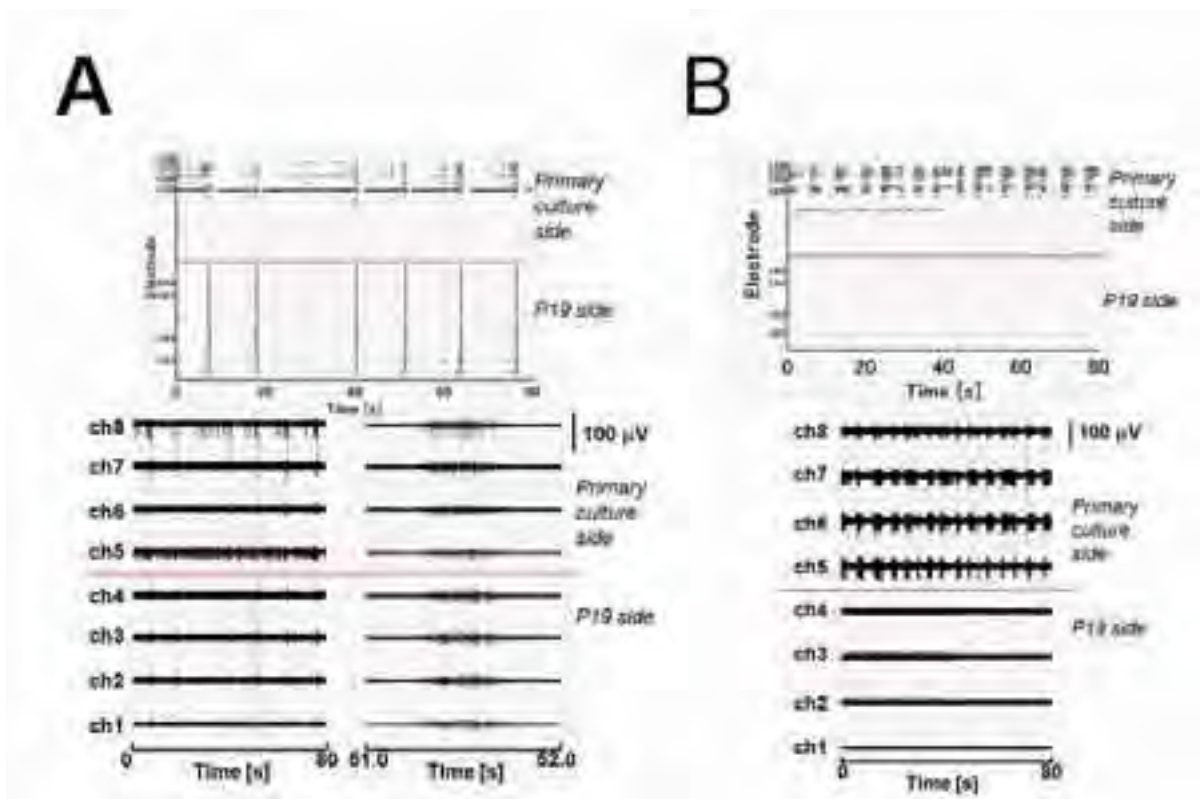


Fig.2 Spontaneous electrical activity in co-cultured networks. Raster plots for all 64 electrodes and 8 waveforms (indicated in Fig. 1B) were showed. *A*, 11 Days in vitro (DIV) *B*, 18 DIV.

Electrophysiological Properties Of Different Embryonic Stem Cell-Derived Neural Populations As Detected By The Microelectrode Array System

Sebastian Illes^{1*}, Stephan Theiss³, Alfons Schnitzler^{1,2}, Marcel Dihn  ^{1,2}

1 Department of Neurology, Heinrich-Heine University, Moorenstr. 5, 40225 D  sseldorf, Germany

2 Institute of Clinical Neuroscience and Medical Psychology, Heinrich-Heine University, Universit  tsstr.1, 40225 D  sseldorf, Germany

3 Result Medical, Friedenstra  e 39, D-40219 D  sseldorf

* Corresponding author. E-mail address: sebastian.illes@gmx.de

1 Introduction

Neural populations cultivated on microelectrode arrays (MEA) can serve as *in vitro* model systems to analyse developmental or pharmacological properties of neuronal network activity. In the last years, it could be shown that embryonic stem (ES) cell-derived neurons can adopt brain area-specific phenotypes, depending on the applied neural differentiation protocols. In addition, it could be demonstrated that ES cell-derived neurons are able to generate functional neuronal networks detected by MEA technology. Therefore, ES cell-derived neuronal networks can be used as a model system to study brain area-specific developmental and pharmacological issues in synaptical interconnected neuronal populations.

To generate ES cell-derived neural populations, two distinct routes of neural pre-differentiation procedures, leading to nearly pure populations of neural cells, are possible (fig.1). Nevertheless, there are major differences. While one neural population consists of pure quantities of homogeneous neural stem (NS) cells (fig.1, i), the other neural population is more heterogeneous and consists of neural stem/progenitor cells as well as mature neural cells (fig. 1, ii-v).

While the molecular phenotypes of both populations have already been described in detail, electrophysiological investigations are scarce. We applied the MEA technology to compare the functional potential of homogeneous and heterogeneous neural cell populations.

2 Results

Immunocytochemical analyses revealed that ES cell-derived homogeneous and heterogeneous neural cell populations differentiate into sufficient quantities of neurons. These neurons expressed either GABA or vesicular-glutamate-transporter-2 (vGlut2) showing that inhibitory and excitatory neurons are present in both neuronal cell populations. However, MEA recordings revealed that only heterogeneous cultures differentiated into synchronously oscillating networks

(fig. 1, vi + vii). In addition, immunocytochemical analyses revealed that neurons derived from homogeneous neural stem cell cultures showed sparsely ramified neurites and a cytoplasmic vGlut2 protein distribution (fig.1, viii-x). In contrast, neurons derived from heterogeneous populations generate a dense neurite network and showed a synaptical vGlut2 protein distribution (fig.1, xi-xiii).

3 Discussion

We demonstrate that homogeneous cultures merely showed uncorrelated spiking activity if differentiated for up to 12 weeks. As a possible reason for the missing network activity in homogeneous cultures, we found evidence for impaired neuronal maturation as indicated by sparsely ramified neurites and a cytoplasmic vGlut2 protein distribution. In contrast, neurons derived from heterogeneous populations appeared to be mature, as indicated by the generation of a dense neurite network and synaptical vGlut2 protein distribution. These findings suggest that the complex environment within heterogeneous neural cell populations is important and supports the generation of mature neurons and functional neuronal networks from ES cell populations.

Acknowledgement

We are grateful to Adrian H  lsewede and Christine Holland for excellent technical support. This work was supported by the "Bundesministerium f  r Bildung und Forschung" (BMBF, 01GN0503).

References

- [1] Illes S, Theiss S, Hartung HP, Siebler M, Dihn   M. (2009) Niche-dependent development of functional neuronal networks from embryonic stem cell-derived neural populations. *BMC Neuroscience*, 10, 93.

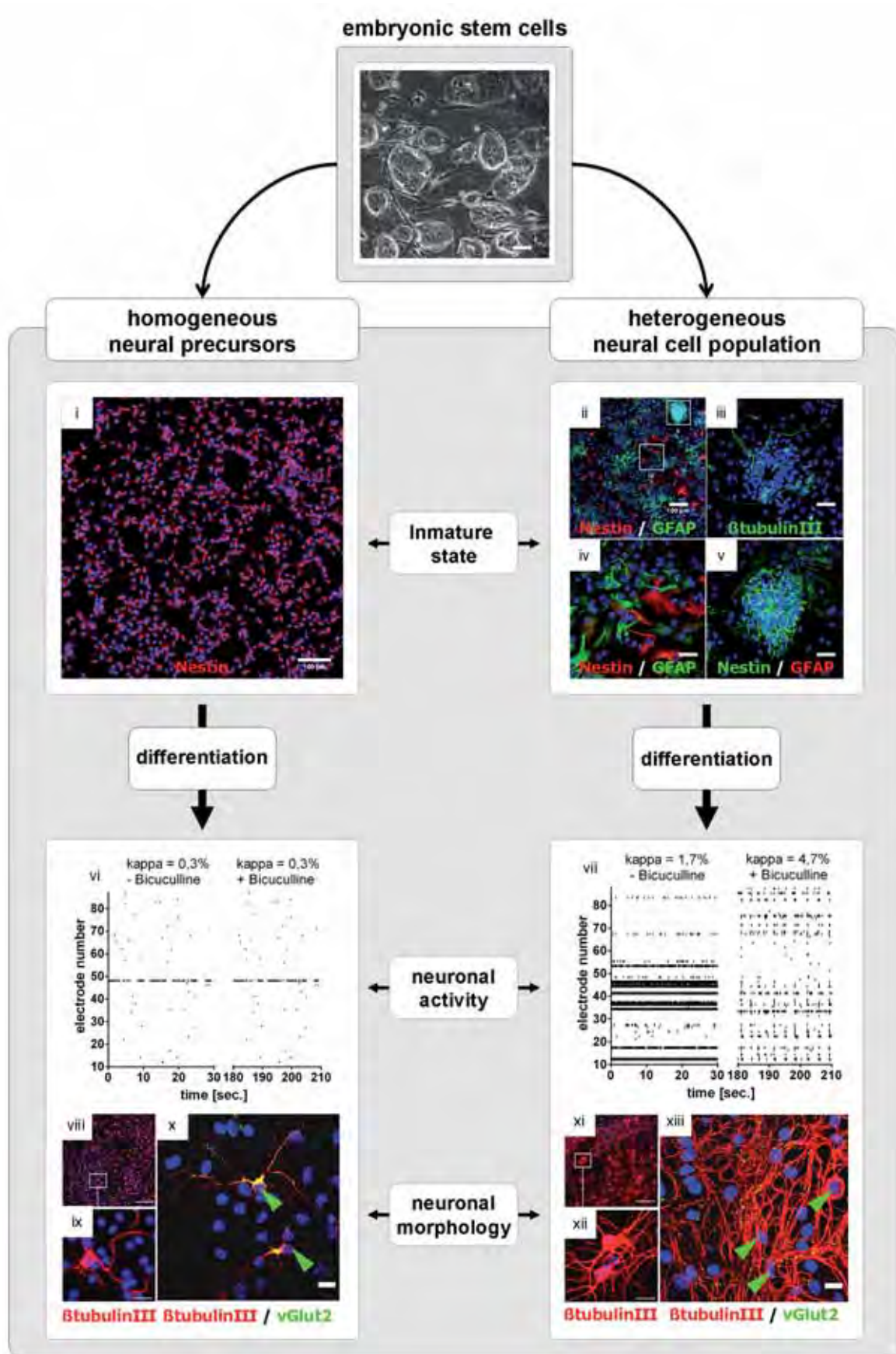


Fig. 1. Electrophysiological and morphological properties of different ES cell-derived neuronal cell populations. For details see main text. Scale bar = 50 μ M (iii-ix) (modified after Illes *et al.* 2009).

The Effects of AC Magnetic Fields on Neuronal Differentiation and Network Activities of P19EC Cells

Atsushi Saito^{*}, Yuzo Takayama, Hiroyuki Moriguchi, Kiyoshi Kotani and Yasuhiko Jimbo

Graduate School of Frontier Sciences, University of Tokyo, Japan

^{*} Corresponding author. asaito@bmpe.k.u-tokyo.ac.jp

Until now, the effects of environmental electromagnetic fields (EMFs) on the neuronal development are not clear. The weak current induced by low frequency alternating current magnetic fields (AC-MFs) are considered the one of the modulation factor of membrane potential, so we exposed the AC-MFs on the mouse P19 embryonal carcinoma (P19EC) cells in neuronal induction and evaluated the effects on the neuronal development and network activity. In our results, the MAP2 that is neuronal marker positive cells and spike frequency recorded by microelectrode array (MEA) were increased by 10 mT AC-MFs (50 Hz, sinusoidal) exposure. And the intensities of induced current were correlated to the percentage of MAP2 positive cells and the size of embryoid bodies (EBs) which formed in the neuronal induction.

1 Introduction

Many reports in the effects of electromagnetic field on the neuronal differentiation include the modulation of neurite outgrowth, synapse formation, gene expression and intracellular calcium oscillation [1]. In these results, low frequency AC-MFs affects the developing and differentiated cell properties, and these modulation cause the matured neuronal network activities were suggested. Therefore, we should evaluate the effects of AC-MFs on the neuronal development during the long-term culture.

In this study, we use P19EC cells as a model of neuronal differentiation, and report the developing spontaneous activities recorded by MEA were dependent on AC-MFs exposure. Here, neuronal differentiation of P19EC cells are controlled precisely by many of intra- and extra-cellular signals. Therefore, we focused on the phase of differentiation that were retinoic acid (RA) induced neuronal gene expression, and performed AC-MFs exposure at this period. On a bases of results, we discussed the AC-MFs exposure as a neuronal modulation factor.

2 Materials and Methods

Undifferentiated P19EC cells were cultured in alpha-MEM containing 10 % fetal bovine serum (FBS) and 1 % penicillin-streptomycin (Pe-St). To induce neuronal and glial cells, P19EC cells were seeded into 85 mm diameter agarose gel coated bacterial grade Petri dishes at a density of 2×10^6 cells/cm² in α -MEM containing 1 μ M RA, and almost all floating cells formed spontaneous aggregates called embryoid bodies (EBs) within 96 hours. To examine the effects of induce current intensity, we made the polydimethylsiloxan (PDMS) based compartment and attached to some dishes. The AC-

MFs exposure (1 or 10 mT) performed chronically at 50 Hz, sinusoidal in Helmholtz coil coupled incubator (HCI). After induction of differentiation, these EBs were dissociated into single cells by trypsin-EDTA and were replated on to polyethylenimine (PEI) coated MEA dishes at a density of 3×10^6 cells/cm² in Neurobasal medium containing 2 % B-27 supplement, 1.25 ml L-glutamine and 1 % Pe-St. One week after induction, spontaneous activities of the exposed and non-exposed P19EC-derived neuronal cells cultured on MEA were detected at three days intervals, and each data were analyzed. In addition, in order to investigate the relationship between the spontaneous activities and the neuronal differentiation, the immunohistochemical images (MAP2/GFAP) and intracellular calcium oscillation were analyzed.

3 Results and Discussion

Development of spontaneous activities of P19EC-derived neuronal networks

Plating on the MEA, neurite outgrowth were started within 2 days (Fig. 1A). *In vitro* neuronal/glial differentiation of P19EC cells are complete at 7 to 14 days after induction [2]. To estimate spontaneous activities during forming of the complex network, the extracellular recording were performed at 5-26 days culture (Fig.1 B,C). The initiation of spikes were detected at 8 days, but there were few number of spikes and detected electrodes. During 11 to 17 days, the number of spikes and detected electrodes were gradually increased, and this tendencies were related with spike frequencies. Over 20 days, however, we observed the predominant cell death and depression of spike. Therefore, the spontaneous activities of P19EC-derived neuronal networks were correlated to the neuronal development and cell death [3].

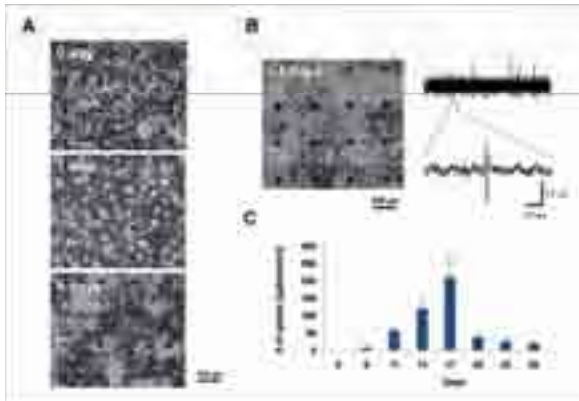


Fig.1 (A) Morphological change of P19EC cells. (B) Typical spikes of P19EC-derived neuronal cells. (C) Time-dependent changes of spontaneous electrical activities. (N=4, \pm SD)

Effects of AC-MFs on spontaneous activities and neuronal/glial differentiation

To determine whether exposure to AC-MFs affects the spontaneous activities of developing neuronal networks, the spike frequency and distribution of exposed and non-exposed cells were evaluated at 14 to 20 days culture (Fig.3A, B). During this period, the spike frequencies and the number of active electrodes of 10 mT exposed cells were increased significantly compared with non-exposed cells. In contrast, the significant differences were not observed in the 1 mT exposed cells at same conditions. Next, in order to confirm the effects on the neuronal and glial differentiation, the region of MAP2 and GFAP positive cells were analyzed. As a result of immunohistochemical analysis, the percentage of MAP2/GFAP in 10 mT exposed cells was higher than the non-exposed and 1 mT exposed cells (Fig.3C). Therefore, these results suggested that the neuronal differentiation and generated network activity of P19EC cells were modulated by 10 mT AC-MF exposure, and the magnetic flux density was one of important parameter.

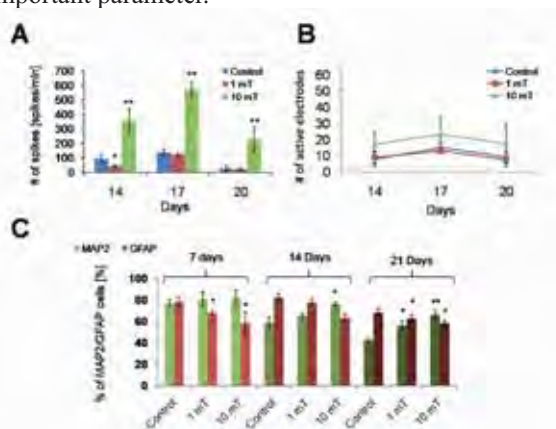


Fig.2 Effects of AC-MFs on the spontaneous electrical activity and differentiation potential. Changes of (A) the spike frequencies and (B) the number of active electrodes. (C) Changes of MAP2/GFAP positive cells. (N=4, \pm SD) * P < 0.05, ** P < 0.01

Effects of induced current intensity on the morphological changes of EBs and intracellular calcium oscillation

The weak electrical current induced by the AC-MFs stimulate cell membrane and regulate gene expression [4]. And the morphological changes during development of EBs were sensitive in the various environmental stimuli [5]. Here, we developed the PDMS based compartment Helmholtz coil attached dish and examined the effects on the development and intracellular calcium oscillation of EBs by AC-MFs exposure. To observe the direct effect of stimulation, we tried 10 mT AC-MF exposure to EBs combined with intracellular calcium imaging (using Fluo-4AM). Using this method, we confirmed the intracellular calcium oscillation of EBs were not correlated with 10 mT magnetic exposure (Fig.3 A). However, the size of EBs were decreased at 10 mT AC-MFs exposed samples (Fig.3 B). Therefore, the induced current did not trigger the direct signal transduction, but the effect through the morphological pathway were suggested.

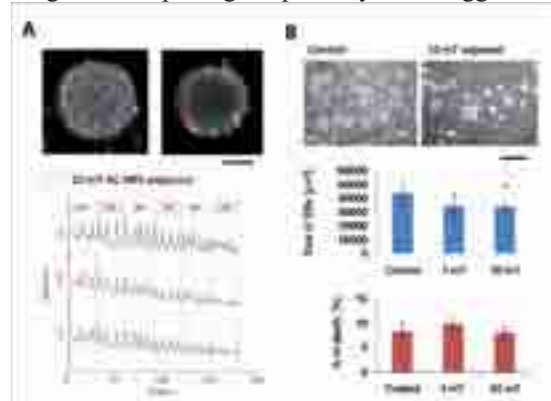


Fig.3 (A) Effects of 10 mT AC-MF exposure on spontaneous calcium oscillation of Ebs. bar=100 μ m (B) Comparison of the size and cell death of EBs induced by 10 mT AC-MF exposure. (N=30, \pm SD) * P < 0.05, bar=400 μ m

Acknowledgement

This work was supported in part by Global COE Program "Medical System Innovation on Multidisciplinary Integration" from MEXT, Japan.

References

- [1] World Health Organization. (2007): Extremely Low Frequency Fields, *Environmental Health Criteria*, No.238.
- [2] Ulrich H., Majumder P. (2006): Neurotransmitter receptor expression and activity during neuronal differentiation of embryonal carcinoma and stem cells: from basic research towards clinical applications, *Cell Prolif*, 39, pp.281-300.
- [3] Yao M., Bain G., Gottlieb D.I. (1995): Neuronal Differentiation of P19 Embryonal Carcinoma Cells in Defined Media, *J. Neurosci Res*, 41, pp.792-804.
- [4] Yamada *et al.* (2007): Electrical Stimulation Modulates Fate Determination of Differentiating Embryonic Stem Cells, *Cell Stem Cells*, 25, pp.562-570.
- [5] Park J. *et al.* (2007): Microfabrication-based modulation of embryonic stem cell differentiation, *Lab Chip*, 7, 1018-1028.

Neural Differentiation of Human Induced Pluripotent Stem Cells: Formation of Functional Neuronal Networks

Riikka Äänismaa^{1*}, Laura Ylä-Outinen¹, Juha Heikkilä¹, Riitta Suuronen^{1,2,3}, Heli Skottman¹, Susanna Narkilahti¹

¹ Regea – Institute for Regenerative Medicine, University of Tampere, Tampere, Finland

² Department of Eye, Ear and Oral Diseases, Tampere University Hospital, Tampere, Finland

³ Department of Biomedical Engineering, Tampere University of Technology, Tampere, Finland

* Corresponding author. E-mail address: riikka.aanismaa@regea.fi

Human pluripotent stem cells are foreseen as a promising source material for *in vitro* modelling and future transplantation therapies. Human embryonic stem (hES) cells can successfully be differentiated toward neuronal cells that hold the capacity of forming spontaneously active neuronal networks. Human induced pluripotent stem (hiPS) cells have also been differentiated toward neuronal cells but the electrical functionality of these cells is currently poorly studied. We differentiated two lines of hiPS cells into neuronal cells with a simple and efficient protocol and studied their network forming capability with microelectrode array (MEA) system. In 14 days after plating the first single spikes were detected in iPSC-derived neuronal networks. During the next 4 weeks the signalling developed into trains and even burst-like activity. The signalling network also responded to pharmacologic stimuli and the cells stained positive for neuronal markers MAP-2 and β -tubulin_{III}. Thus, hiPS cells can be differentiated into young neuronal cells capable of forming electrically active neuronal networks.

1 Background

Isolation and culturing of human embryonic stem (hES) cells were first reported just over a decade ago [1] and since then a lot of research has been conducted to maintain undifferentiated hES cells in defined, controlled culture environment as well as to controllably differentiate the cells into various cell types of the human body. One of the interesting research areas has been the neural differentiation of hES cells and the potential of produced neural cells in treating various neurological diseases and traumas such as Parkinson's disease, spinal cord injury, and ischemic stroke [2]. These diseases have huge negative impact in our society but effective and curative treatments are not discovered yet regardless of the intensive research conducted with various applications. The new significant discovery in stem cell field was the invention of human induced pluripotent stem (hiPS) cells a couple of years ago [3, 4]. These cells are originally differentiated cells, e.g., skin fibroblasts which can be transfected virally with 2-5 genes to form hES cell-like pluripotent cells. These cells open up new possibilities for using patient's own cells for e.g. regenerative purposes. For now, however, the derivation and culture methods of hiPS cells are far from being optimal and far from good manufacturing practice (GMP) level [4]. The use of these cells for *in vitro* modeling of genetic diseases is currently a hot research area. HiPS cells have been reported to differentiate to neural cells [5] similarly as hES cells but the electrical properties and

functionality of these hiPS cell-derived neurons has not been investigated in detail yet. Here, our aim was to differentiate 2 lines of hiPS cells into neuronal cells and study the network forming properties of these cells with microelectrode array (MEA) setup.

2 Results

2.1 Cells on MEA

HiPS cell (lines 5-7 and 6-14, Prof. Timo Otonkoski, Helsinki)-derived neural cells were replated on polyethyleneimine and laminin coated MEA dishes as small aggregates. The neural cells attached properly. Thereafter, the electrical properties of 7 MEA dishes with the hiPS cell-derived neuronal networks and 3 MEA dishes of control cells; hES cell-derived neuronal networks (Regea 08/023), were studied.

2.2 Activity on MEA

HiPS cell-derived neuronal networks exhibited first spontaneous signal spikes after growing on MEA dishes for approximately 14 days. With the first hiPS cell line (6-14), the neuronal networks showed spontaneous activity in 1 out of 3 dishes and with the second line (5-7) the activity was observed in 2 out of 4 dishes. During the next 4 weeks the activity developed into more train- and even burst-like signalling (Figure 1). At the end, pharmacologic

testing showed the networks' response to specific agonists and antagonists.

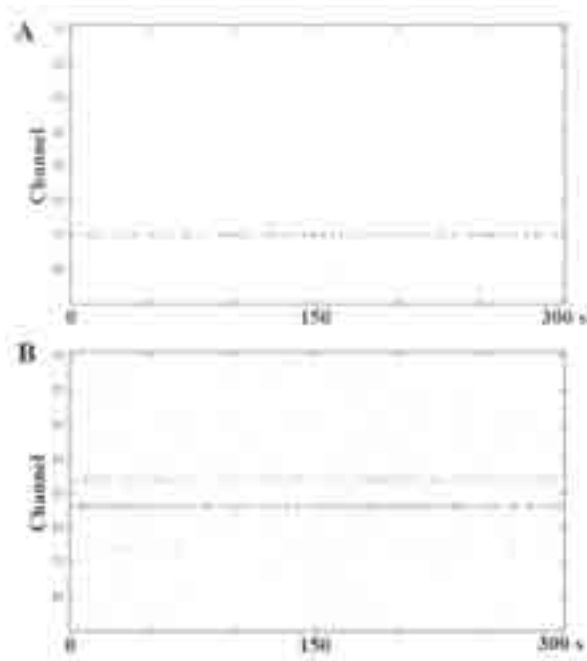


Fig. 1. Raster plot presentation of the electrical activity of hiPS cell line 5-7-derived neuronal network after culturing the cells on MEA for A) 2 weeks and B) 5 weeks. X-axis represents time as seconds (s) and y-axis represents the channels.

3 Conclusions

HiPS cells can be differentiated into neural cells which hold the capacity of forming spontaneously active neuronal networks as previously reported with hES cells [6].

Acknowledgement

Personnel of Regea are acknowledged for support in stem cell research. Professor Timo Otonkoski is acknowledged for providing the hiPS cell lines. The study and MEA equipment was funded by BioneXt Tampere, Academy of Finland, Competitive Funding of Pirkanmaa Hospital District, and ALICE - Alliance for Life Science and Health of University of Tampere, Tampere University of Technology, and University of Jyväskylä.

References

- [1] Thomson, J.A., Itskovitz-Eldor, J., Shapiro, S.S., Waknitz, M.A., Swiergiel, J.J., Marshall, V.S., Jones, J.M. (1998): Embryonic stem cell lines derived from human blastocysts. *Science*, 282, 1145-7.
- [2] Lindvall, O., Kokaia, Z. (2010): Stem cells in human neurological disorders – time for clinical translation? *The Journal of Clinical Investigation*, 120, 29-40.
- [3] Takahashi, K., Tanabe, K., Ohnuki, M., Ichisaka, T., Tomoda, K., Yamanaka, S. (2007): Induction of pluripotent stem cells from adult human fibroblasts by defined factors. *Cell*, 131, 861-872.
- [4] Aalto-Setälä, K., Conklin, B.R., Lo, B. (2009): Obtaining consent for future research with induced pluripotent stem cells: opportunities and challenges. *PLoS Biology*, 7(2), e1000042.
- [5] Karumbayaram, S., Novitsch B.G., Patterson, M., Umbach, J.A., Richter, L., Lindgren, A., Conway, A.E., Clark, A.T., Goldman, S.A., Plath, K., Wiedau-Pazos, M., Kornblum, H.I., Lowry, W.E. (2009): Directed differentiation of human-induced pluripotent stem cells generates active motor neurons. *Stem Cells*, 27, 806-811.
- [6] Heikkilä, T.J., Ylä-Outinen, L., Tanskanen, J.M.A., Lappalainen, R.S., Skottman, H., Suuronen, R., Mikkonen, J.E., Hyttinen, J.A.K., Narkilahti, S. (2009) Human embryonic stem cell-derived neuronal cells form spontaneously active neuronal networks in vitro. *Experimental Neurology*, 218, 109-116.

Plasticity of Human Embryonic Stem Cell –derived Neuronal Networks: Effect of Low-frequency Stimulation

Laura Ylä-Outinen^{1*}, Ismo Korhonen^{1,2}, Jarno E. Mikkonen¹, Jari Hyttinen², Susanna Narkilahti¹

¹ Regea - Institute for Regenerative Medicine, University of Tampere and Tampere University Hospital, Tampere (Finland)

² Department of Biomedical Engineering, Tampere University of Technology, Tampere (Finland)

* Corresponding author. E-mail address: laura.yla-outinen@regea.fi

Human embryonic stem cell (hESC)–derived neuronal cells are potential source for functional studies of developing human brain, disease modeling, drug screening and toxicology, and regenerative medicine. Microelectrode array (MEA) is a useful tool to study the electrical functionality of neuronal cells at network level. In this study, developing electrical activity of the forming neuronal network and the maturation of the network are characterized using MEA system. Our results show that hESC-derived neuronal cells are electrically active and can mature into functional neuronal networks. Moreover, the formed networks responded to low frequency stimulation by increasing the spontaneous activity.

1 Background

Human embryonic stem cell (hESC)–derived neuronal cells are potential source for functional studies of developing human brain, disease modeling, drug screening and toxicology, and regenerative medicine [1,2]. So far, the electrical activity of hESC-derived neuronal networks has not been widely studied. Microelectrode array (MEA) is a useful tool to study the electrical functionality of neuronal cells at network level. In this study, developing electrical activity of the forming neuronal network and the maturation of the network were characterized using MEA system. Further, the plasticity of the hESC derived neuronal network was studied in relation to low frequency stimulation.

2 Materials and Methods

2.1 HESC derived neuronal cells

HESCs are first differentiated into neuronal precursor cells. Shortly, embryonic stem cell colonies were cut into small pieces to suspension culture in neural differentiation medium. Cells were differentiated towards neuronal cells during 8 weeks. Thereafter, the formed neurospheres were cut into smaller pieces ($\varnothing \sim 50 \mu\text{m}$) and plated onto MEA (Multichannel Systems, MCS, Germany) [3].

2.2 Activity measurement and stimulation

Before cell plating onto MEA-plates (30/200, 8×8 layout) plates were coated with PEI and laminin. Cells were let to attach onto MEA plate and form neural network. First measurements were performed after 1

week of plating (7 days in dish, DID). The spontaneous activities of developing networks were measured and the network is let to mature into bursting phase before starting the stimulation experiment. In low frequency stimulation, biphasic pulse is given in frequency of 0.33 Hz, through a pair of electrodes resulting in 30 pair stimulations on the MEA. Stimulation cycles were repeated 11 times. The networks' acute response to stimulation was measured with MCS's equipments and analyzed with Neuroexplorer (NEX Technologies, USA).

3 Results

3.1 Spontaneous activity and maturation

Our results show that hESC-derived neuronal cells are electrically active and can mature into functional neuronal networks.

3.2 Effect of stimulation

Moreover, our data show that hESC-derived neuronal cells response to electrical stimuli. Low frequency stimulus modulates the acute signaling of neuronal network by increasing the bursting activity in particular channels. The representative perievent raster from one stimulation experiments show the increased activity after the stimulus. That is well in accordance to earlier findings with rodent data [4].

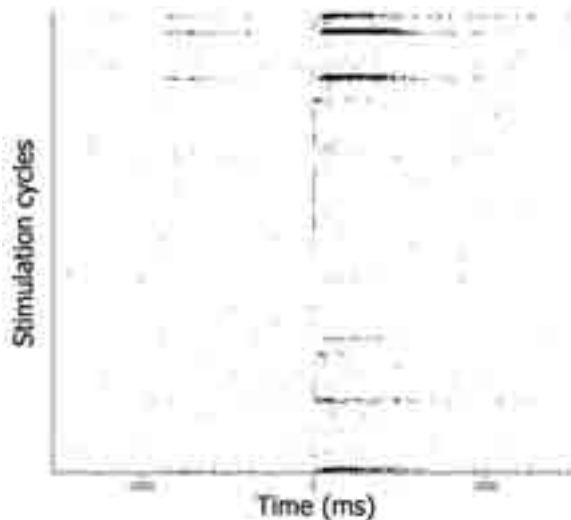


Fig. 1. The effect of stimulation is shown in raster plot. Increased activity of the networks is shown 100-1500 ms after stimulation.

4 Conclusion

To conclude, MEA is an efficient and effective tool to observe the response of hESC-derived neuronal networks to electrical stimuli. This study shows that hESC-derived neuronal networks cultured on MEA can be used as a platform for e.g. developmental studies, and with MEA measurements we can gain new information on the behaviour of human neuronal cells for the future transplantation therapies.

Acknowledgement

The personnel of Regea is acknowledged of stem cell culturing support. This study is funded by Academy of Finland (decision number 123359 and 123233).

References

- [1] Rajala K., Hakala H., Panula S., Aivio S., Pihlajamäki H., Suuronen R., Hovatta O., Skottman H. (2007). Testing of nine different xeno-free culture media for human embryonic stem cell cultures. *Human reproduction (Oxford, England)*. 22(5):1231-8.-99
- [2] Bal-Price AK, Hogberg HT, Buzanska L, Lenas P., van Vliet E., Hartung T. (2009). In vitro developmental neurotoxicity (DNT) testing: Relevant models and endpoints. *Neurotoxicology*. In press.
- [3] Heikkilä T., Ylä-Outinen L., Tanskanen J., Lappalainen R., Skottman H., Suuronen R., Mikkonen J., Hyttinen J., Narkilahti S. (2009). Human embryonic stem cell-derived neuronal cells form spontaneously active neuronal networks in vitro. *Experimental neurology*. 218(1):109-16.
- [4] Jimbo Y., Tateno T., Robinson H. (1999). Simultaneous Induction of Pathway-Specific Potentiation and Depression in Networks of Cortical Neurons. *Biophysical Journal*. 76:670-678

Tracking the Network Development of hESC derived Neurons during Maturation

Fikret Emre Kapucu^{1*}, Jarno M. A. Tanskanen¹, Jarno E. Mikkonen², Laura Ylä-Outinen³, Susanna Narkilahti³, Jari A. K. Hyttinen¹

¹ Department of Biomedical Engineering, Tampere University of Technology, Tampere, Finland

² Department of Signal Processing, Tampere University of Technology, Tampere, Finland

³ Regea – Institute for Regenerative Medicine, University of Tampere and Tampere University Hospital, Tampere, Finland

* Corresponding author. E-mail address: emre.kapucu@tut.fi

In this work, the network activity for maturing human embryonic stem cell (hESC) - derived neuronal cells was tracked by analyzing both temporal and spatial bursting activity of the cultured populations. Bursts are one of the most significant markers for synchronous network activity. We tracked behavioural changes by creating burst density colormaps on microelectrode arrays (MEAs). This provides information on the propagation of network development during maturation.

1 Background and Aims

Human embryonic stem cell (hESC) derived cells are highly promising for the future treatment of neurological disorders and diseases despite the existing challenges in developing neural networks with known functionality and capabilities to integrate in the central nervous system. Hence, it is crucial to understand the maturing process of neural networks. Microelectrode array (MEA) measurements provide the necessary data to analyze the maturing cells. The data consists of spiking trends of the maturing cells obtained from numerous MEA channels. For tracking network relations of neural cell populations, spiking activity analysis is a practical and dependable method. Analysis of the bursting dynamics offers more concrete way to assess the maturity and dynamics of the network. To visualize the spatiotemporal network behaviour, the bursting activity was transferred to MEA spatial colormaps. This sums up the network behaviour when several neurons join the activity seen at a single electrode and at the same time shows the entire MEA activity. Tracking bursting by this method can provide understanding network activity in a more reliable way [1]. Besides, it is able to provide information about plasticity mechanisms.

2 Methods

2.1 Cell Cultures and Electrophysiological Measurements

Human embryonic stem cells were differentiated and neuronal cultures were prepared for MEA dishes to examine the electrophysiological activity of these cultures as described in [2, 3]. In this study, cells were

differentiated as neurospheres 6 to 7 weeks before plating them to MEA dishes. Here, plating on the MEA dish was considered the day zero of the *days in dish (DID)*.

Measurements were recorded from 59-electrode MEAs and each continuous measurement lasted approximately five to ten minutes. In all, the data to be analyzed consisted of measurements performed at 13 time points from 1st to 12th week after DID.

2.2 Data Processing and Analysis

Spike time instants were detected in Matlab by a self-developed algorithm based on *get_spike* function of Wave_Clus toolbox [4]. Threshold was calculated according to standard deviation and mean of the signal. The average threshold was approximately 12.67 μ V. Bursts were detected using the algorithm described by Wagenaar et al. [5] where inter spike intervals was set for 100 ms and minimum number of spikes per burst was set to four. After bursts were detected, average bursts per minute was calculated to obtain normalized and comparable values to track activities on different measurement dates. After bursts per minute were calculated for every channel, the values were placed in a 8x8 matrix. The values were mapped to colors and after interpolation displayed as contours to form a colormap, which allowed spatial aspects of the bursting to be observed efficiently. Temporal evolution was observed by calculating a colormap for each measurement time point. The scale of the colormap was set between 0 to 30, thus burst rates higher than 30 bursts per minute were presented by the same color. This color scale was selected for an optimum display of more rare bursts and frequent bursts in the same colormap.

3 Results

Results were obtained for 13 measurement days from 12 weeks period. Fig. 1 demonstrates 8 time points. Bursts became increasingly frequent during the first 9 weeks and then became gradually more silent afterwards. After the bursts became more significant, it became easier to track how active channels were close to each other spatially (Fig. 1). On the first measurement day of the first week there was no bursting detected whereas the most frequent bursting was seen during the 9th week after DID, when 79,9 bursts per minute was measured on the electrode number 31 (See Fig. 1E). The general spatial distribution of activity was surprisingly constant during the study.

4 Conclusions

Colormaps are basic and effective tools for tracking network activity changes during network maturation or other changes. Their power in visualizing and tracking spatio-temporal changes in the network activity provides for new achievements in the analysis of e.g. stimulated or drug altered networks. Besides, our colormaps are an effective tool for joint analysis and display of burst rates and other image analysis results. Since the colormaps carry spatial information, the results can also be overlaid with, e.g., microscope images.

Here, our exemplary analysis results indicate that, while the cells mature, the bursts become more common and are broadly seen across the channels. This can be a strong sign of maturing cells integrating into a network, whereas such kind of development does not always occur for all maturing cell

populations. Bursting may be observed from a single channel, from a very restricted location or sometimes from many channels where cells are active. Expansion of the bursting activity, and sometimes its fading, is also observable in the results. In conclusion, mature cells can be expected to exhibit clear network behaviour and such kind of behaviour also tends to spread to all active channels. However, there may also be stagnant and even fading activity, which is also worth to analyze in quest of developing hESC derived neuronal cell networks capable of functionally integrating in the recipient neuronal tissue.

Acknowledgement

The work was funded by Academy of Finland (decision numbers: 122947, 122959, and 123233) and Finnish Cultural Foundation 2008 and 2009.

References

- [1] Lisman, J. E. (1997). Bursts as a unit of neural information: making unreliable synapses reliable. *Trends Neurosci*, 20, 38-43
- [2] Nat R., Nilbratt M., Narkilahti S., Winblad B., Hovatto O., Nordberg A. (2007). Neurogenic neuroepithelial and radial glial cells generated from six human embryonic stem cell lines in serum-free suspension and adherent cultures. *Glia*, 55, 385-399.
- [3] Heikkilä T., Tanskanen J., Ylä-Outinen L., Lappalainen R., Suuronen R., Skottman H., Narkilahti S., Hyttinen J. (2008). Culturing and measuring of human embryonic stem cell-derived neuronal cells on MEA. *Proc MEA Meeting 2008*, pp.100. Reutlingen, Germany, July 8-11 2008.
- [4] Quian Quiroga R., Nadasdy Z., Ben-Shaul Y. (2004). Unsupervised spike detection and sorting with wavelets and superparamagnetic clustering. *Neural Comp*, 16, 1661-1687.
- [5] Wagenaar D. A., Pine J., Potter S. M. (2007). Electrophysiological properties of neocortical neurons in vitro. *J Neurophysiol*, 48, 1302-1320.

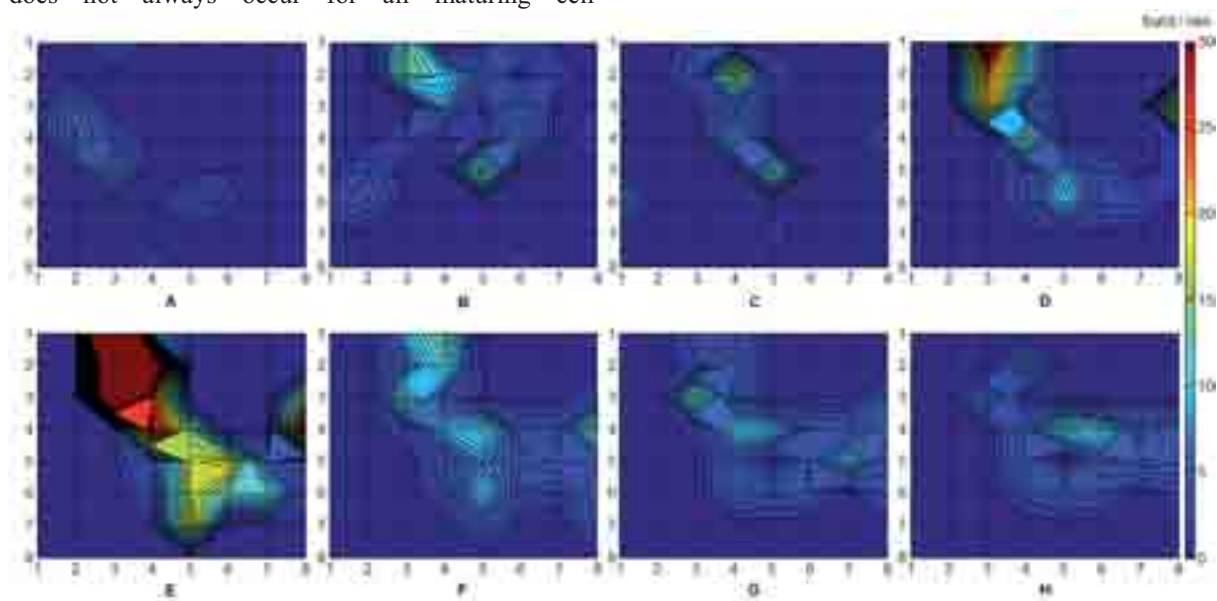


Fig. 1. Change in the bursting activity of maturing hESC derived neuronal cells. The panels A to H demonstrate the bursts per minute for each channel with channels located at the corners of the grids. The channel number can be read by numbers from vertical and horizontal axis (e.g. the point located at the intersection of the 3rd vertical and 4th horizontal grid line represents the channel 34). The panels A to H represents the measurement days recorded on the 1st, 3rd, 5th, 8th, 9th, 11th, 11th and 12th weeks respectively.

Human Pluripotent Stem Cells and Neuronal Networks Derived from Them: In Vitro Modeling, Toxicology Testing, and Patterning Approaches with Microelectrode Array Setup

Laura Ylä-Outinen¹, Juha Heikkilä¹, Heli Skottman¹, Riitta Suuronen^{1,2,3}, Riikka Äänismaa¹, Susanna Narkilahti¹

¹ Regea-Institute for Regenerative Medicine, University of Tampere and Tampere University Hospital, Tampere, Finland

² Department of Eye, Ear, and Oral Diseases, Tampere University Hospital, Tampere Finland

³ Department of Biomedical Engineering, Tampere University of Technology, Tampere Finland

Human pluripotent stem cells and their neuronal and glial derivatives have raised high hopes in the field of regenerative medicine. In addition, these cells would be useful in studies of human development, disease modeling, and drug screening and toxicology. Regardless of the high potential of human pluripotent stem cell-derived cells, some challenges in neural cell production still remain. Especially the accurate and proper electrical functionality of the produced neural cells is so far studied to lesser extend. The function of neural cells *in vivo* is totally dependent on their ability to receive and transmit electric signals, thus the *in vitro* functionality of produced neural cells should be more carefully studied in a controlled and repeatable manner. A good option to measure and monitor the functionality of a neuronal network is microelectrode array (MEA) setup. This MEA setup can be used for e.g. drug screening and *in vitro* modeling. Here, we have studied electrophysiological properties of both human embryonic stem (hES) and human induced pluripotent stem (hiPS) cell-derived neural cells in MEA setup. In addition, we did evaluate the effects of known neurotoxins on network properties.

1 Introduction

Human pluripotent stem cells and their neuronal and glial derivatives have raised high hopes in the field of regenerative medicine. In addition, these cells would be useful in studies of human development, disease modeling, and drug screening and toxicology. These cells could be used as graft material for many devastating neurological diseases and traumas such as multiple sclerosis, spinal cord injury, traumatic brain injury, and ischemic and hemorrhagic strokes [1]. One type of pluripotent stem cells is human embryonic stem (hES) cells which are derived from poor quality surplus embryos donated by couples undergoing *in vitro* fertilization treatments [2]. These cells can differentiate into any cell type of the human body, and successful production of neural progenitor cells and neuronal and glial cells has been accomplished. Other pluripotent stem cell type is newly invented human induced pluripotent stem (hiPS) cells produced by virally transfecting mature differentiated cells, e.g. skin fibroblasts, which in response turn into hESC-like cells. HiPS cells are significant due to the fact that fibroblasts can be taken e.g. from a patient suffering from specific genetic disease and thus patient-specific cells can be produced for *in vitro* modeling or for transplantation therapies in the future [3, 4]. Regardless of the high potential of human pluripotent stem cell-derived cells, some challenges in

neural cell production still remain. Especially the accurate and proper electrical functionality of the produced neural cells is so far studied to lesser extend. The function of neural cells *in vivo* is totally dependent on their ability to receive and transmit electric signals, thus the *in vitro* functionality of produced neural cells should be more carefully studied in a controlled and repeatable manner. A good option to measure and monitor the functionality of a neuronal network is microelectrode array (MEA) setup [5]. This MEA setup can be used for e.g. drug screening and *in vitro* modeling.

2 Methods and Results

We have extensively cultured and measured hES cell-derived neuronal networks in MEA. Also, hiPS cell-derived neuronal networks have been successfully obtained and measured but so far to a lesser extend. All in all, both cell types differentiate towards neural cells which form neuronal networks when replated on MEA dishes. The networks repeatedly show spontaneous activity in approximately 7 days and the signaling further develops into trains and bursts during the following weeks.

Next, we tested known substances, methyl mercury chloride and valproic acid, for their effects on functional neuronal networks. Both of these substances did modify the network properties.

3 Conclusions

In conclusion, functional neuronal networks can be produced from human pluripotent stem cells. These produced functional networks can further be stimulated and used as e.g. toxicology testing platforms. The controllability of the developed platforms is of high importance and requires more effort and new applications. The controllability of the cell seeding, attachment, and network development is one of the key factors in MEA studies and also considered in our study designs.

Acknowledgement

MEA equipment was funded by BioneXt Tampere and researchers were supported by Academy of Finland. Personnel of Regea are acknowledged for their support in stem cell research.

References

- [1] Lindvall, O., Kokaia, Z. (2010): Stem cells in human neurological disorders – time for clinical translation? *The Journal of Clinical Investigation*, 120, 29-40.
- [2] Skottman H, Narkilahti S, Hovatta O. (2007) Challenges and approaches to the culture of pluripotent hESC. *Regen Med. May*;2(3):265-273.
- [3] Takahashi, K., Tanabe, K., Ohnuki, M., Ichisaka, T., Tomoda, K., Yamanaka, S. (2007): Induction of pluripotent stem cells from adult human fibroblasts by defined factors. *Cell*, 131, 861-872.
- [4] Aalto-Setälä, K., Conklin, B.R., Lo, B. (2009): Obtaining consent for future research with induced pluripotent stem cells: opportunities and challenges. *PLoS Biology*, 7(2), e1000042.
- [5] Heikkilä, T.J., Ylä-Outinen, L., Tanskanen, J.M.A., Lappalainen, R.S., Skottman, H., Suuronen, R., Mikkonen, J.E., Hyttinen, J.A.K., Narkilahti, S. (2009) Human embryonic stem cell-derived neuronal cells form spontaneously active neuronal networks in vitro. *Experimental Neurology*, 218, 109-116.

Neuronal Dynamics and Plasticity

Long-term measurement of excitatory and inhibitory synapse densities with electrical activity during development of cultured rat cortical networks

Daisuke Ito^{*}, Takumi Komatsu, Hiroki Tamate, Kazutoshi Gohara

Division of Applied Physics, Faculty of Engineering, Hokkaido University, Sapporo, Japan

^{*} Corresponding author. E-mail address: ditoh@eng.hokudai.ac.jp

Rat cortical neurons were cultured to investigate the long-term development of excitatory and inhibitory synaptic terminals for 35 days in vitro (DIV) and the change of spontaneous electrical activity during this process. Using multi-electrode arrays (MEAs), we show that the network firing rate and synchronized burst rate became saturated toward 35 DIV after an initial increase in these rates in the early stage. Whole synapses, excitatory synapses and inhibitory synapses were detected using antibodies against synapsin 1, vesicular glutamate transporter 1 (VGluT1) and vesicular transporter of γ -amino-butyric acid (VGAT), respectively. Immunocytochemical observation revealed that synapsin 1-labeled synapse density also became saturated at 28 and 35 DIV, whereas it increased toward 21 DIV. Both VGluT1 and VGAT puncta showed a similar tendency during long-term development; however, these distributions were heterogeneous. We show the preliminary results of the developmental distribution of excitatory and inhibitory synapses during long-term culture.

1 Introduction

In the development of the nervous system, neurons autonomously establish rich synaptic connections and transmit their electrical signals via synaptic connections. A recent study has revealed that neuronal network activity correlates with whole synapse density during the developmental stage [1, 2]. However, the network activity is regulated by the balance of excitatory and inhibitory synaptic inputs. It is known that excitatory and inhibitory synaptic terminals are differentially distributed on their postsynaptic target neurons [3]. Therefore, it is necessary to investigate the development and distribution of excitatory and inhibitory synapses with the electrical activity.

Multi-electrode arrays (MEAs) are an effective tool for long-term recording of neuronal network activity [4, 5, 6]. Studies using MEAs have demonstrated that the spontaneous activities of the network become synchronized bursts and that this activity lasts for the lifetime of the culture [7, 8, 9]. In the present study, the spontaneous electrical activity of cultured cortical networks was measured for more than one month. Moreover, we examined separately the excitatory and inhibitory synapses during long-term development of cultured networks using antibodies against vesicular glutamate transporter 1 (VGluT1) and vesicular transporter of γ -aminobutyric acid (VGAT) [10, 11]. Developmental changes of immunocytochemical-labeled synaptic connections were investigated.

2 Materials & Methods

2.1 Cell culture

Cerebral cortices derived from Wister rats on embryonic day 17 were dissociated and plated on a multi-electrode dish (MED) probe (Alpha MED Scientific, Osaka, Japan) or coverslip [12]. The plating density was 2500 cells/mm² for the MED probe and 250 cells/mm² for the coverslip, respectively. The cultures were filled with culture medium and incubated in a humidified atmosphere containing 5% CO₂ and 95% air at 37°C. The culture medium consisted of Dulbecco's modified minimum essential medium (DMEM) supplemented with 5% fetal bovine serum, 5% horse serum, 25 μ g/mL insulin and 1% penicillin-streptomycin. One half of the culture medium was replaced twice a week.

2.2 Spike and synchronized burst detection

The spontaneous electrical activity of each cortical culture was recorded using a MED64 extracellular recording system (Alpha MED Scientific) with a sampling rate of 20 kHz [12, 13, 14]. The activity was recorded twice a week from 7 days in vitro (DIV) to 35 DIV. The spikes were determined when their amplitude exceeded a noise-based threshold in a window of 1 msec. For detection of synchronized bursts, the time window was set to a width of 100 msec. Then the number of spikes (the total for all electrodes) was counted in the window [15]. The number above the threshold of 100 spikes/window was defined as a synchronized burst.

2.3 Immunocytochemistry

The cortical neurons cultured on coverslips were fixed with 4% formaldehyde at 7, 14, 21, 28 and 35 DIV. After permeabilization with 0.5% Triton X-100 in PBS for 10 min, the cultures were incubated with PBS containing 10% goat serum and 0.01% Triton X-100 for 30 min. The cultures were incubated with primary antibodies overnight at 4°C and then incubated with secondary antibodies for 1 h at room temperature. The primary antibodies were anti-microtubule associated protein 2 (MAP2) mouse IgG (a marker of neuronal somata and dendrites; Sigma-Aldrich, St. Louis, MO), anti-synapsin 1 rabbit IgG (a marker of presynapses; Calbiochem, Darmstadt, Germany), anti-VGluT1 rabbit IgG (a marker of excitatory synapses; Frontier Institute Co., Hokkaido, Japan) and anti-VGAT guinea-pig IgG (a marker of inhibitory synapses; Frontier Institute Co.). The secondary antibodies were Alexa Fluor 405-labeled anti-mouse IgG (Molecular Probes, Eugene, OR), 488-labeled anti-rabbit IgG, 488-labeled anti-guinea pig IgG, 546-labeled anti-mouse IgG and 546-labeled anti-rabbit IgG. Fluorescence observation was performed using a confocal laser scanning microscope (FV1000D – IX81; Olympus, Tokyo, Japan).

2.4 Image analysis

Image analysis was performed using Volocity software (Perkin Elmer Inc., Waltham, MA). The number of synapsin 1, VGluT1 and VGAT puncta were counted.

3 Results and discussion

3.1 Recording of electrical activity

Figure 1 shows the developmental changes of the array-wide firing rate and synchronized burst rate of the cortical culture. Spontaneous electrical activity was recorded from 1 week and was found to increase at from 2 to 3 weeks. This activity lasted for up to 5 weeks but varied in intensity from day to day. The synchronized burst rate resembled the firing rate in developmental change. These data indicate that the network activity cultured in vitro become saturated and exhibited synchronized bursts within 1 month.

3.2 Immunocytochemistry and image analysis

Figure 2 shows an example of the immunofluorescence images of MAP2 and synapsin 1 at 3 different culture ages. Synapsin 1 puncta began to form around the neuronal dendrites and somata at 7 DIV and the number of the puncta increased toward 35 DIV. To investigate the development and distribution of excitatory and inhibitory synapse density, double immunostaining of VGluT1 and VGAT was performed (Fig. 3). The

Immunofluorescence micrographs show that both VGluT1 and VGAT puncta also increased around the dendrites and somata over 5 weeks.

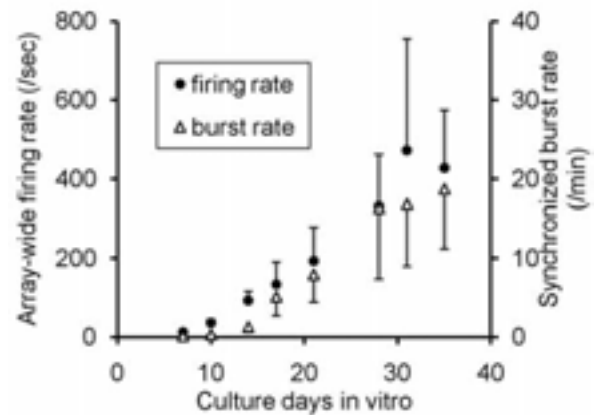


Fig. 1. Developmental change of array-wide firing rate and synchronized burst rate in cortical culture. Firing rate data are shown as the mean+SEM, whereas synchronized burst data are shown as the mean-SEM.

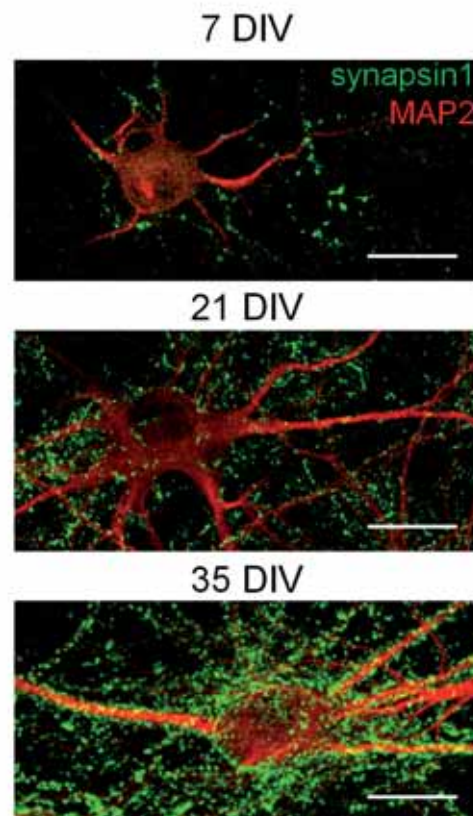


Fig. 2. Immunofluorescence micrographs of cultured cortical networks. Neurons were stained with antibodies to synapsin 1 (green) and to MAP2 (red). Scale bar = 20 μ m.

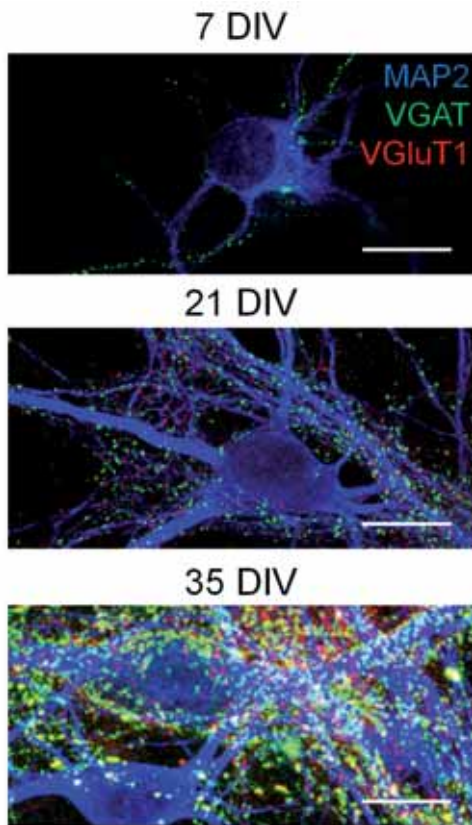


Fig. 3. Immunofluorescence micrographs of cultured cortical networks. Neurons were stained with antibodies to MAP2 (blue), to VGAT (green) and to VGLuT1 (red). Scale bar = 20 μ m.

To clarify the developmental change of synapse density, we counted synapsin 1 puncta using fluorescence images. In this study, we differentially counted the puncta on somata or on dendrites. Figure 4 shows one of the results of quantification, which is a developmental change of the number of synapsin 1-labeled puncta on neuronal somata. The number of the puncta increased gradually along the culture ages from 7 to 21 DIV, whereas the number of the puncta became saturated and did not increase at 28 and 35 DIV. Comparing the synapse density with the electrical activity (i.e., the array-wide firing rate and synchronized burst) shown in Fig. 1, the firing rate and synapse density show similar characteristics. As described previously [1, 2], the firing rate was elevated along with the increase of synapse density during the early development of cortical culture (~21 DIV). At 28 and 35 DIV, both the synaptic density and firing rate did not increase and became saturated.

We also investigated the number of VGLuT1-labeled and VGAT-labeled puncta at different culture ages. The tendency toward developmental change of both puncta numbers resembled the pattern of developmental change of synapsin 1 puncta. However, the distribution of excitatory and inhibitory terminals on

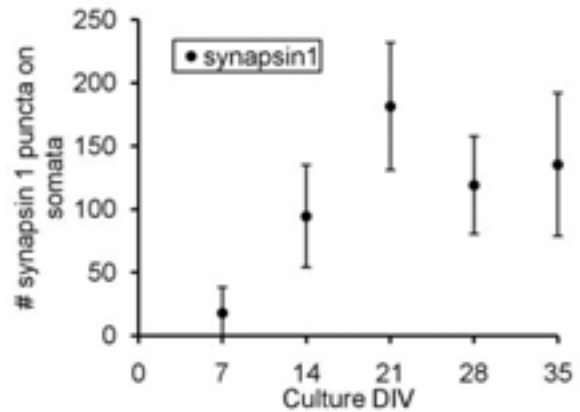


Fig. 4. Developmental change of the number of synapsin 1-labeled puncta on neuron somata. Data are shown as the mean \pm SD.

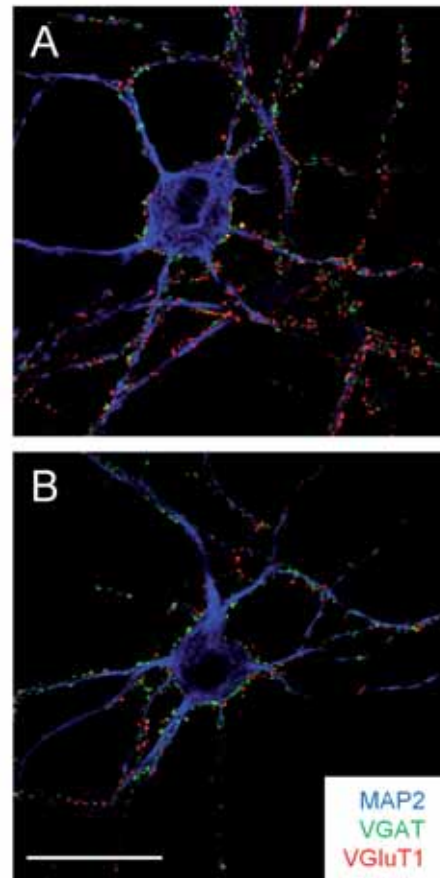


Fig. 5. Examples of immunofluorescence micrographs of cultured cortical neurons for 35 DIV. Neurons were stained with antibodies to MAP2 (blue), to VGAT (green) and to VGLuT1 (red). (A) VGLuT1 and VGAT-labeled puncta were balanced. (B) VGAT-labeled terminals predominated on specific cell somata and dendrites. Scale bar = 20 μ m.

target cell somata and dendrites varied between neurons even in the same cultures. For example, we found that the distribution of VGluT1 and VGAT-labeled puncta were equal in Fig. 5A, whereas the VGAT-labeled terminals predominated and localized on specific cell somata and dendrites in Fig. 5B. In a previous report [3], GABAergic synaptic terminals developed more rapidly and eventually outnumbered non-GABAergic terminals on neuronal somata, whereas non-GABAergic terminals predominated on dendrites in a rat hippocampal culture. Thus, more quantitative analysis of the heterogeneous distribution of excitatory and inhibitory synaptic terminals must be required on the basis of our preliminary results about VGluT1 and VGAT staining. It will be clarify the network dynamics from the point of view of excitatory and inhibitory synapses.

4 Conclusions

We investigated the developmental change of synapse density with spontaneous electrical activity. The network firing rate and synchronized burst rate became saturated, though the intensity varied day to day during 1 month culture. The synapse density (including the density of excitatory and inhibitory synapses) was also saturated throughout the long-term culture. The distribution of the excitatory and inhibitory synaptic terminals on neurons differed from one neuron to another throughout the long-term culture; some neurons had predominant VGAT-labeled synapses and others had equal distribution of VGluT1 and VGAT-labeled synapses. Based on these preliminary results, further detailed analysis of these distributions must be required.

Acknowledgement

This work was partially supported by Grants-in-Aid for Scientific Research from the Japan Society for the Promotion of Science (20240023 and 21650049). We are grateful to Prof. Masahiko Watanabe (Hokkaido University School of Medicine, Japan) for providing the VGluT1 and VGAT antibodies.

References

- [1] Brewer G.J., Boehler M.D., Pearson R.A., DeMaris A.A., Ide A.N., Wheeler B.C. (2009). Neuron network activity scales exponentially with synapse density. *J. Neural Eng.*, 6, 014001.
- [2] Muramoto K., Ichikawa M., Kawahara M., Kobayashi K., Kuroda Y. (1993). Frequency of synchronous oscillations of neuronal activity increases during development and is correlated to the number of synapses in cultured cortical neuron networks. *Neurosci. Lett.*, 163, 163-165.
- [3] Benson D.L. and Cohen P.A. (1996). Activity-independent segregation of excitatory and inhibitory synaptic terminals in cultured hippocampal neurons. *J. Neurosci.*, 16, 6424-6432.
- [4] Gross G.W., Rieske E., Kreutzberg G.W., Meyer A. (1977). A new fixed-array multimicroelectrode system designed for long-term recording. *Neurosci. Lett.*, 6, 101-105.
- [5] Kamioka H., Maeda E., Jimbo Y., Robinson H.P.C., Kawana A. (1996). Spontaneous periodic synchronized bursting during formation of mature patterns of connections in cortical cultures. *Neurosci. Lett.*, 206, 109-112.
- [6] Potter S.M. and DeMarse T.B. (2001). A new approach to neural cell culture for long-term studies. *J. Neurosci. Methods*, 110, 17-24.
- [7] Wagenaar D.A., Pine J., Potter S.M. (2006). An extremely rich repertoire of bursting patterns during the development of cortical culture. *BMC Neurosci.*, 7, 11.
- [8] Chiappalone M., Bove M., Vato A., Tedesco M., Martinoia S. (2006). Dissociated cortical networks show spontaneously correlated activity patterns during in vitro development. *Brain Res.*, 1093, 41-53.
- [9] Van Pelt J., Wolters P.S., Corner M.A., Rutten W.L.C., Ramackers, G.J.A. (2004). Long-term characterization of firing dynamics of spontaneous bursts in cultured neural networks. *IEEE Trans. Biomed. Eng.*, 51, 2051-2062.
- [10] Miyazaki T., Fukaya M., Shimizu H., Masahiko W. (2003). Subtype switching of vesicular glutamate transporters at parallel fibre-purkinje cell synapses in developing mouse cerebellum. *Eur. J. Neurosci.*, 17, 2563-2572.
- [11] Miura E., Fukaya M., Sato M., Sugihara T., Asano M., Yoshioka K., Watanabe M. (2006) Expression and distribution of JNK/SAPK-associated scaffold protein JSAP1 in developing and adult mouse brain. *J. Neurochem.*, 97, 1431-1446.
- [12] Ito D., Tamate H., Nagayama M., Uchida T., Gohara K. (2008). Immunostaining for identification of neuronal-impulse pathway on multielectrode arrays. *Proc. MEA Meeting 2008*, 53-54.
- [13] Kudoh S.N., Hosokawa C., Kiyohara A., Taguchi T., Hayashi I. (2007). Biomodeling system – interaction between living neuronal networks and the other world. *J. Robot. Mech.*, 19, 592-600.
- [14] Honma S., Shirakawa T., Katsuno Y., Namihira M., Honma K. (1998). Circadian periods of single suprachiasmatic neurons in rats. *Neurosci. Lett.*, 250, 157-160.
- [15] Mukai Y., Shiina T., Jimbo Y. (2003) Continuous monitoring of developmental activity changes in cultured cortical networks. *Electr. Eng. Jpn.*, 145, 28-37.

Neuronal dynamics vs. connectivity: a computational model to explain how *in vitro* neuronal networks exhibit well-defined patterns of activity

Paolo Massobrio^{1*}, Matteo Garofalo^{1,2}, Valentina Pasquale², Sergio Martinoia^{1,2}

¹ Neuroengineering and Bio-nano Technology Group (NBT), Department of Biophysical and Electronic Engineering (DIBE), University of Genova, Genova (Italy).

² Department of Neuroscience and Brain Technologies, Italian Institute of Technology (IIT), Genova (Italy).

* Corresponding author. E-mail address: paolo.massobrio@unige.it

In vitro neuronal networks coupled to Micro-Electrode Arrays (MEAs) represent a valid experimental framework to study neuronal dynamics and to understand the principles of brain coding. This preparation is relatively free of predefined constraints and allows neurons to self-organize during development, creating networks that exhibit complex spatio-temporal patterns of activity composed of synchronized bursts, mixed with random spikes. Starting from this experimental evidence, here we address the questions: does a particular network architecture promote such dynamics? Is it possible to predict the activity of a neuronal network on the basis of its connectivity map? In this work we tried to answer such issues by means of a computational approach, considering two different and opposite experimental configurations: randomly connected networks, where each neuron can theoretically link to each other, and patterned-organized networks, where the connections are driven by means of predefined chemical-physical constraints.

1 Introduction

Large random networks of dissociated neurons developing *in vitro* and chronically coupled to Micro-Electrode Arrays (MEAs) represent a valid experimental model for studying the neuronal dynamics and for understanding the principles of brain coding, learning and memory.

This preparation, unlike other experimental models such as acute and cultured cortical slices, is relatively free of predefined constraints and allows neurons to self-organize during their development, creating networks which exhibit complex spatio-temporal patterns of activity and widespread complex dynamics. Mature cultures exhibit a synchronized and distributed bursting activity mixed with a highly variable random spiking activity [1].

In this work, the neuronal dynamics was investigated by trying to correlate such complex electrophysiological patterns to the topological organization of the network, by means of a computational approach. Two different experimental configurations were taken into account. In the first one, we tried to reconstruct and correlate the topology of large-scale randomly-connected networks (Fig. 1a) to the expressed dynamics. From an experimental point of view, the typical network results a sort of hyper-connected neuronal jam which evolves continuously. Under this conditions of high neuronal density (~ 1200 cells/mm², and a few number of

recording sites per MEA (up to 120)), we are not able to reconstruct, the exact topology of the network (structural connectivity). The only possible way is to estimate how neurons are functionally connected [2].

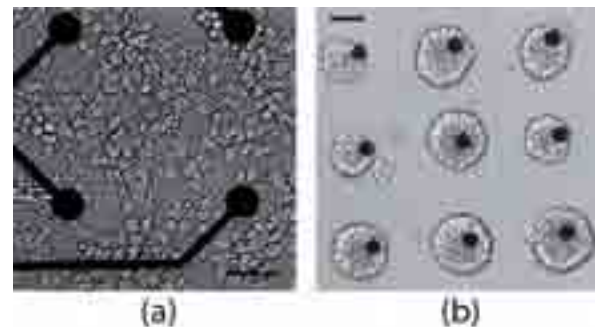


Fig. 1. (a) Randomly connected neuronal networks. (b) Patterned neuronal network. Scale bar is 60 μ m.

Thus, to overcome such limitation, large-scale neuronal networks made up of point spiking neurons described by the Izhikevich equations [3] were developed. Network topologies were designed following the canonical architectures scale-free, random, and small-world [4]. Within this approach, the network is dealt as a graph, where each neuron corresponds to a node, and each synaptically connections to an edge. We simulated the spontaneous activity of such neuronal networks, by sweeping the most common parameters used to characterize these graphs, such as clustering coefficient, mean path length, connection density, etc. [5]. The main finding

which emerges is that although all the network configurations determine a mix of spiking, and bursting activity, the scale-free and partially small-world architectures display a critical behavior, and thus self-organization could be influenced by the network architecture. The second experimental condition consists in more organized and regular patterned neuronal networks (Fig. 1b). However, also in this context some unclear aspects regarding the network connectivity remain. In this context we realized a computational model based on the concept of *meta-neuron*, i.e., a small spatially confined number of actual neurons which perform single macroscopic functions [6]. The two main findings that emerge from the simulations can be summarized as follows: (i) the increasing complexity of the meta-neurons morphology reflects the variations of the network dynamics; (ii) the dynamics displayed by the considered patterned neuronal networks can be explained by hypothesizing the presence of several short- and few long-term distance interactions among small assemblies of neurons (i.e., *meta-neurons*).

2 Materials and Methods

2.1 Modeling randomly-grown networks

The developed model is based on the point Izhikevich neuron model [3]. By means of this neuron model, a neuronal network made up of 1024 spatially distributed and synaptically connected neurons was developed.

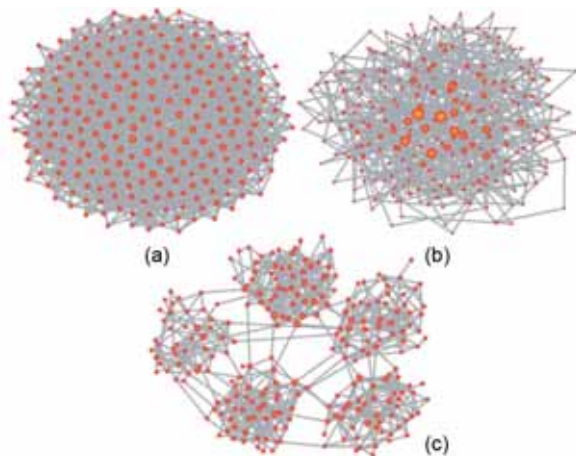


Fig. 2. Schematic representation of (a) random, (b) scale-free, (c) small-world networks.

To model excitatory and inhibitory populations of neurons, two different families of neurons were considered: the family of regular spiking neurons (RS), and the family of fast spiking neurons (FS). Regular spiking neurons fire with a few spikes and short inter-spike-interval (ISI) at the onset of a stimulation. Differently, fast spiking neurons exhibit periodic trains of action potentials at higher frequencies without adaptation. To preserve some characteristics of the composition of *in vitro* cortical

neurons, the ratio between excitatory and inhibitory neurons was set to 4:1 [7]. These two families of neurons were connected in a random (Fig. 2a), scale-free (Fig. 2b), and small-world (Fig. 2c) topology. An important prediction of the random network theory is that, the random placement of links, but most nodes have approximately the same number of links. Indeed, in a random network, the nodes follow a Gaussian distribution. Small-worlds are characterized by the prevalence of short paths linking pairs of nodes within very large networks. Practically, this feature emerges in networks which combine ordered lattice-like connections with a small fraction of random links. Combining elements of order and randomness, such networks were characterized by high degrees of local clustering as well as short path length. Many networks are dominated by a relatively small number of nodes that are connected to many other sites. Networks containing such important nodes, named hubs, tend to be scale-free, in the sense that some hubs have a seemingly unlimited number of links. Differently from the random networks, in the scale-free networks, nodes distribution follows a power law. This law suggests that most nodes have just a few connections and some have a tremendous number of links. In this sense, the system can be considered without a proper scale.

2.2 Modeling patterned-grown networks

To simulate the dynamics exhibited by patterned neuronal networks, we changed the approach to model the neurons: from punctual to compartmentalized neurons. Each neuron (named *meta-neuron*) represents a small spatially confined number of actual neurons which perform single macroscopic functions (Fig. 1b). The morphologies of the neuron models are shown in Figs. 3a-c; all the neuronal structures were made up of a soma, an axon, and a dendritic tree. The electrophysiological properties of the neuronal membrane are based on the Hodgkin-Huxley model [8] for the soma and axon, and on a passive electrical model for the dendrites. Synapses are modeled following a first order kinetic scheme [9]. The network model is made up of 60 meta-neurons arranged according to the MEA layout. Each neuron can establish synaptic connections, preserving the ratio between excitation and inhibition (60-75%). Synapses are placed on the soma and on the dendrites: in this way, axo-dendritic and axo-somatic connections were taken into account as typically happens in actual cortical cultures [7].

In order to investigate the possible mechanisms which drive the connectivity among the clusters of neurons by means of bundles of neurites (Fig.1b), we considered two different connectivity rules, namely One-To-Many (OTM) and One-To-Neighbors (OTN). The OTM rule states that each meta-neuron can establish several random connections (both excitatory

and inhibitory) to the neighbors (maximum value: 30) and few connections (minimum value: 0) as far as the distance increases; the closer are two meta-neurons the more connected they are and thus the synaptic efficacy of the connection is increased. The OTN rule defines a local connectivity and states that each meta-neuron is only connected to the first neighbors (up to 8 meta-neurons). A simplified representation of the OTM and OTN connectivity rules is depicted in Figs. 3d and e, respectively.

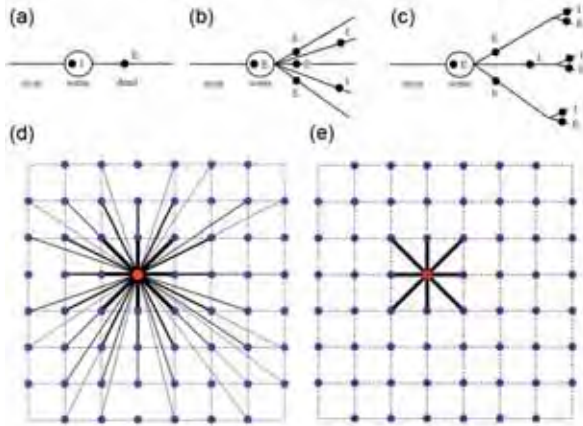


Fig. 3. (a,c) Sketches of the different neuron models with different level of dendritic complexity. (d) A sketch of the network model organized by following the OTM rule. (e) A sketch of the network model organized by following the OTN rule.

3 Results

3.1 Highly connected networks dynamics

We implemented the different network topologies described in the Sec. 2.1 by maintaining uniform for each configuration the number of nodes (1024), and the average degree of connections. Fig. 4 shows the false color map (top), the degree distribution (middle) and the distribution of the cluster coefficient (bottom) for the four aforementioned topologies.

Then, the spontaneous activity of such networks was simulated, as the raster plots of Figs. 5a-c show. A mix of random spiking (mainly due to the inhibitory neurons) and high synchronized bursting activity emerges.

However, a network-organization dependency can be found by investigating the criticality exhibited by the network by looking at the displayed electrophysiological activity. Fig. 5d and e show the avalanche size and lifetime distribution [1]. From the simulation, we can speculate that whether the connectivity is ruled by a scale-free organization, the activity approaches a critical state (red line).

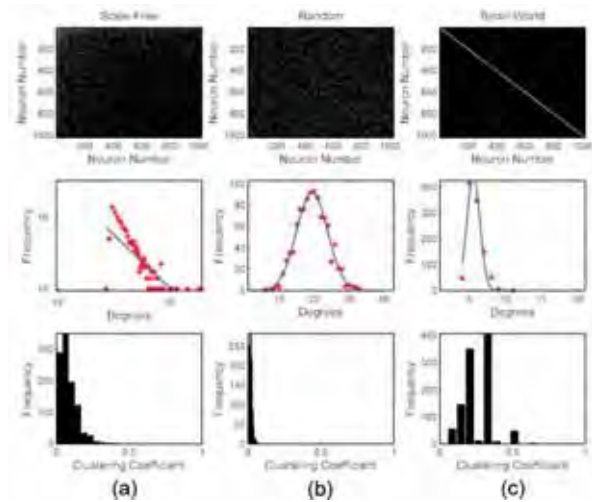


Fig. 4. False color map (top), degree distribution (middle) and cluster coefficient distribution (bottom), relative to scale-free (a), random (b), and small-world(c) topologies.

On the other hand, if the connectivity is ruled by a small-world and random topology, the electrophysiological activity tends to a subcritical, or pseudo-critical (green line), and supercritical regime (blue line) respectively.

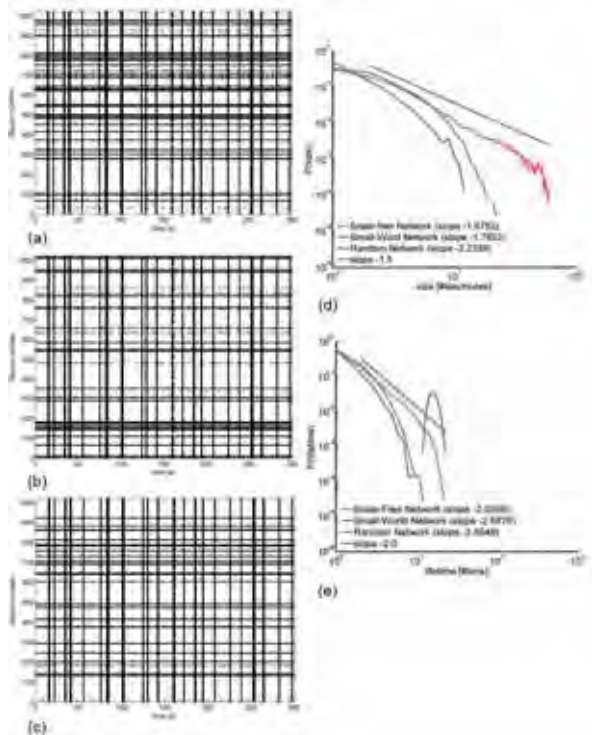


Fig. 5. Electrophysiological activity of 1024 neurons connected following a scale-free (a), random (b), and small-world (c) connectivity rule. (d, e) Avalanche size and lifetime as a function of the network topologies.

3.2 Patterned networks dynamics

Referring to the cluster of microelectrodes in Fig. 6a, voltage stimuli were applied to electrode 67. The response of the network was analyzed by the PSTHs as shown in Fig. 6b. As it might be expected, electrodes 55 and 56 showed site-specific responses

reflecting the functional topographical connectivity of the network: electrode 55, the closest one to the stimulating site, showed a fast response, whereas electrode 56, slightly further apart, exhibited a more delayed response. Moreover, electrodes 37, 46 and 58 produced an attenuate response to the stimulus or, in some cases, no evoked activity (electrodes 38, 45, 47, 48). The network model (made up of 60 meta-neurons) ruled by the OTM connectivity, was used to emulate the experimental condition of focused electrical stimulation. We reproduced the electrical stimulation protocol by means of a current stimuli pulse (width 100 ms; peak-to-peak amplitude 1.0 nA; frequency 0.2 Hz) delivered to one meta-neuron (upper-right corner). As obtained from the experimental conditions, the efficacy of the stimulation involved primarily the adjacent electrodes (Fig. 6c). In fact, the electrodes closest to the stimulation site present a fast and marked response, whereas the others can present a more delayed and attenuate response, or in some case, no evoked activity. Finally, to demonstrate that OTM connectivity is more realistic than OTN connectivity, this stimulation protocol was applied to a network model organized following this kind of topology. The results shown in Fig. 6d highlight that the propagation of the evoked response is confined only to the first next neighbors meta-neurons. A mild response involving all the far meta-neurons is practically absent or negligible.

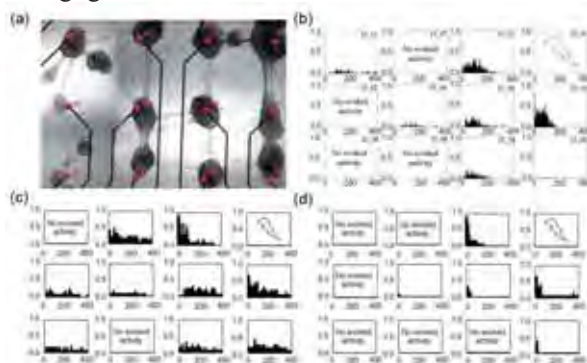


Fig. 6. (a) DIC image of a neuronal network at 27 DIV on an MEA. The scale bar is 100 μm . (b) PSTHs relative to the culture depicted in (a). PSTHs of the simulated neuronal network organized following the (c) OTM, and (d) OTN rule.

4 Discussion and Conclusions

The proposed work pointed out the correlation between network topologies and neuronal dynamics. In particular, we presented the modeling of two typical experimental conditions which can be accomplished by using: randomly grown networks, and patterned networks.

In the first condition, we tried to establish a correlation between network connectivity and critical states of the network. We found that a scale-free, and partially small-world connectivity tend to exhibit critical states. However, preliminary results on MEAs

(data not shown) show a mixed connectivity, i.e., it is practically impossible to get stereotyped rules of connectivity when we deal with dense dissociated cultures whose activity is under-sampled with 60 electrodes.

On the other extreme, to describe the dynamics of patterned neuronal networks, we changed the modeling approach, moving from point to compartmentalized neurons. The proposed model takes into account an important finding regarding the dynamics exhibited by patterned neuronal networks. The obtained experimental results suggest a possible short- and long-term interaction among the clustered neurons that might be mediated by the subsets themselves. The model strengthens the hypothesis that direct connections (by means of neurite bundles) among not-neighboring microelectrodes are also needed, by showing that a simple OTN rule is not suitable to explain both the spontaneous and the stimulus-evoked activity (Figs. 6) of such networks. The obtained simulated results underline the presence of short- and long term distance interactions to support the intrinsic dynamics of such interconnected neuronal populations. The model was developed to be utilized when specific network topologies or patterned neuronal populations are used as experimental models. By using such models and the simulated results, it is possible to obtain useful indications for the design of specific network architectures.

References

- [1] Pasquale V., Massobrio P., Bologna L. L., Chiappalone M. and Martinoia S. (2008). Self-organization and neuronal avalanches in networks of dissociated cortical neurons. *Neuroscience*, 153, 1354-1369.
- [2] Garofalo M., Nieuws T., Massobrio P. and Martinoia S. (2009). Evaluation of the performance of information theory-based methods and cross-correlation to estimate the functional connectivity in cortical networks. *PLoS ONE*, 4,8, e6482.
- [3] Izhikevich E. M. (2003). Simple model of spiking neurons. *IEEE Transactions on Neural Networks*, 6, 1569-1572.
- [4] Albert R. and Barabasi A.-L. (2002). Statistical mechanics of complex networks. *Reviews of Modern Physics*, 74,1, 47-97.
- [5] Bullmore E. and Sporns O. (2009). Complex brain networks: graph theoretical analysis of structural and functional systems. *Nature Reviews*, 10, 186-198.
- [6] Massobrio P. and Martinoia S. (2008). Modelling small-patterned neuronal networks coupled to microelectrode arrays. *Journal of Neural Engineering*, 5,3, 350-359.
- [7] Marom S. and Shahaf G. (2002). Development, learning and memory in large random networks of cortical neurons: lessons beyond anatomy. *Quarterly Reviews of Biophysics*, 35,1, 63-87.
- [8] Hodgkin A. L. and Huxley A. F. (1952). A quantitative description of membrane current and its applications to conduction and excitation in nerve. *Journal of Physiology*, 117, 500-544.
- [9] Destexhe A., Mainen Z. and Sejnowski T. J. (1994). An efficient method for computing synaptic conductances based on a kinetic model of receptor binding. *Neural Computation*, 6, 14-18.

Network Structure And The Origin Of Synchronized Bursts In Vitro

Samora Okujeni^{1,2,3*}, Nila Mönig², Steffen Kandler^{1,2,3}, Oliver Weihberger^{1,2,3}, Ulrich Egert^{1,3}

¹ Bernstein Center Freiburg, University Freiburg, Freiburg, Germany

² Neurobiology & Biophysics, Institute of Biology III, Faculty of Biology, University Freiburg, Germany

³ Biomicrotechnology, Dept. Microsystems Engineering – IMTEK, University Freiburg, Germany

* Corresponding author. E-mail address: okujeni@bcf.uni-freiburg.de

It remains an ongoing matter of research in how far different aspects in the dynamics of neuronal networks depend on particular connectivity statistics. In this study, we focus on structure and dynamics in generic networks of cortical neurons in vitro. We manipulate connectivity in these networks by pharmacological interference with morphological differentiation processes in neurons. Bringing together data from MEA recordings and from histological analyses we discuss how certain connectivity features may determine the propagation of activity and the ability of these isolated networks to self-excite themselves and to maintain recurrent activity states.

1 Introduction

Brain architectures considerably evolve driven by activity-dependent neuronal differentiation processes. The context-dependent and self-organized integration of neurons is partly reflected in the cellular morphology evolving under specific tissue-dependent constraints and input scenarios. Likewise, neurons developing in isolated cultures *ex vivo* integrate themselves into networks based on comparable fundamental principles. The biochemical machinery translating a specific developmental context into the adequate neuronal morphology strongly depends on proteins that regulate the dynamical properties of the cytoskeleton, i.e. structural plasticity. Control of microtubule polymerization via microtubule-associated protein 2 (MAP2) phosphorylation suggests a regulatory loop in which the Protein Kinase C (PKC) takes in a key-position [1]. Various experimental studies demonstrated that manipulation of PKC activity crucially influences neuronal differentiation processes as neurite outgrowth [2], cell migration [3] and pruning [4]. In this study, we investigate dependencies between network structure and dynamics by manipulating the PKC-dependent structural differentiation of neurons.

2 Materials and Methods

Primary cortical cell cultures were prepared as described previously [5]. Cells were derived from cortices of newborn rats by mechanical and enzymatic dissociation and plated onto polyethyleneimine-coated micro-electrode arrays (6x10 with 0.5mm and 32x32 electrodes with 0.3mm spacing; Multichannel Systems). Cultures developed in growth medium (MEM) supplemented with heat-inactivated horse serum (5%), L-glutamine (0.5mM), glucose (20mM) and gentamycin (10µg/ml) under 5% CO₂ and 37°C

incubator conditions. PKC inhibitor Gö6976 1µM was applied starting from DIV1. Staining against MAP2 protein was performed for morphological analysis of dendrites. Recordings were performed under culture conditions (MEA1600-BC and MEA30-1024, Multichannel Systems).

3 Results

We show that cultured cortical neurons developing under chronic inhibition of Protein Kinase C (PKC inh.) form larger dendrites due to enhanced neurite outgrowth and/or impaired pruning and further reduce cluster formation. Stronger and more compact network-wide bursts (NB) are in line with proposed higher network connectivity. Lower overall activity levels based on lower NB frequencies, however, suggest a reduced ability of network self-excitation. We hypothesize that lower activity levels and less complex bursting dynamics result from reduced inhomogeneity i.e. clustering in PKC inh. networks. Conserved isotropic propagation patterns throughout the lifetime of PKC inh. networks further point towards reduced structural reorganization and thereby preservation of the early formed homogeneous connectivity. We assess origins of NB by simultaneous recordings from up to 1000 electrodes spanning almost the entire area of developing networks of 200.000 cultured neurons. By electrical stimulation via micro-electrode arrays at different sites we further probe how activity propagates within the different network structures. We further show that homogeneous networks formed under PKC inhibition are potentially able to operate at much higher activity levels driven by electrical stimulation. We conclude that the formation of neuronal clusters in isolated networks is important for the generation of intrinsic activity by local recurrent amplification of spontaneous excitation.

References

- [1] Quinlan EM, Halpain S (1996) Postsynaptic mechanisms for bidirectional control of MAP2 phosphorylation by glutamate receptors. *Neuron* 16:357-368.
- [2] Metzger F, Kapfhammer JP (2000) Protein kinase C activity modulates dendritic differentiation of rat Purkinje cells in cerebellar slice cultures. *Eur J Neurosci* 12:1993-2005.
- [3] Larsson C (2006) Protein kinase C and the regulation of the actin cytoskeleton. *Cell Signal* 18:276-284.
- [4] Kano M, Hashimoto K, Chen C, Abeliovich A, Aiba A, Kurihara H, Watanabe M, Inoue Y, Tonegawa S (1995) Impaired synapse elimination during cerebellar development in PKC gamma mutant mice. *Cell* 83:1223-1231.
- [5] Shahaf G, Marom S (2001) Learning in networks of cortical neurons. *J Neurosci* 21:8782-8788.

Acknowledgements

We thank Patrick Pauli and Ute Riede for technical assistance. The neuroanatomy Freiburg is gratefully acknowledged for their helpful support.

Funded by the German BMBF (FKZ 01GQ0420 & FKZ 01GQ0830) and by the EC (NEURO, No. 12788).

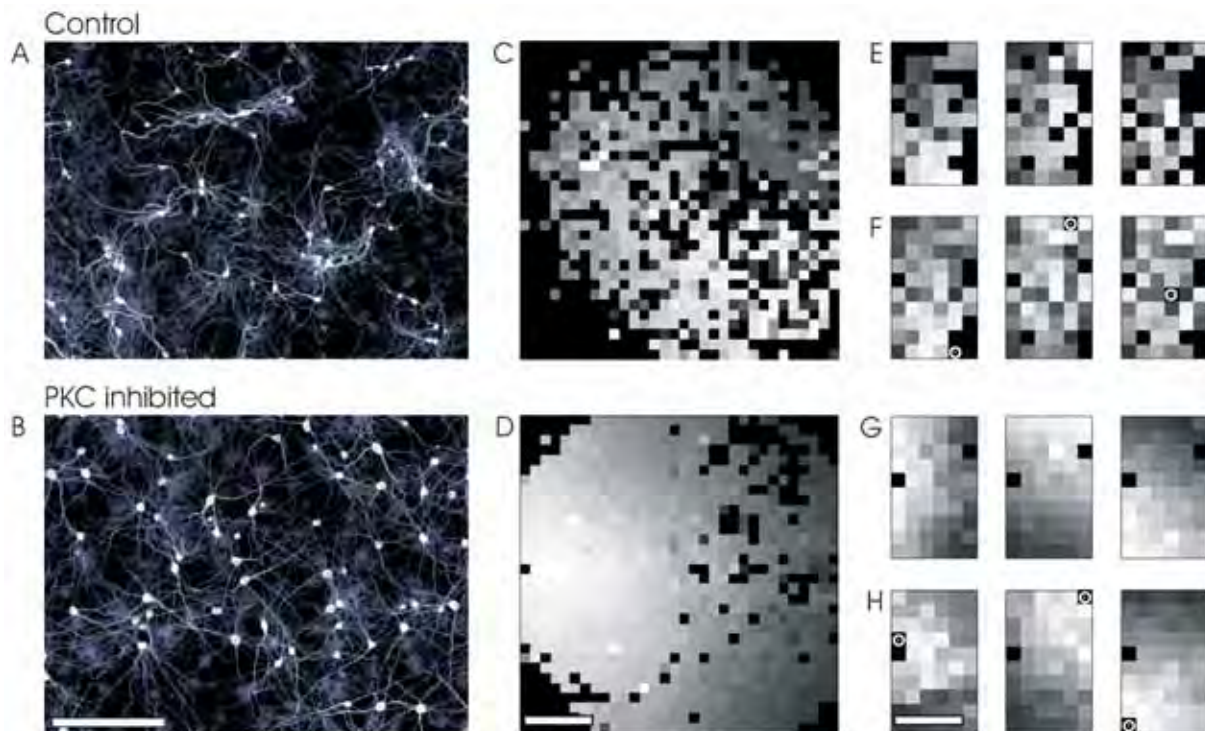


Fig. 1. Structure and dynamics in cortical cell cultures

A, B) MAP2 Staining against dendrites and somata in low density cultures (~ 200 neurons/ mm^2) reveals reduced neuronal clustering and impaired ramification of dendrites within clusters in PKC inh. networks. Scale bars: $200\mu\text{m}$.

C-H) Spatio-temporal propagation of activity (from early in light to late in dark gray; black indicates no activity) during network bursts onset (first spike rank order) in high density cultures (~ 2000 neurons/ mm^2). Arrays with 1000 electrodes span almost the entire culture (C,D; corners lack neurons). PKC inh. networks show preserved isotropic propagation patterns indicating homogeneous connectivity (D). Electrical stimulation via MEAs (white circle) elicits responses with propagation patterns (H) similar to those observed in spontaneous NB (G). Networks developing under normal conditions show much more irregularity in the propagation of spontaneous (C,E) and elicited (F) activity indicating inhomogeneities in the connectivity. Scale bars: 2mm .

Effect of Ghrelin on the Network Development and Activity in Cultured Cortical Neurons of Newborn Rats

Stoyanova Irina*, le Feber Joost, Rutten Wim

Neurotechnology Group, Faculty of Electrical Engineering, Mathematics and Computer Sciences,
University of Twente, Enschede, the Netherlands
Corresponding author. E-mail address: stoyanovai@yahoo.co.uk

Ghrelin is a gastric hormone and a neuropeptide, initially related to the appetite stimulation and growth hormone secretion. Ghrelin has also an important role in the regulation of many other processes, including higher brain functions like memory performance, sleep and wakefulness. Previous studies on the ghrelin activities indicate that the transmitter has an excitatory effect on the neuronal activity of hypothalamic slices *in vitro* by direct synaptic interaction, and controls synaptic plasticity in the hippocampus when applied intravenously. However the effect of ghrelin on developing neuronal networks has not been studied yet. Therefore, we cultured dissociated cortical neurons of newborn rats in a medium containing ghrelin for a period of three weeks and recorded the network activity using multi electrode arrays. In addition, after a cultivation of the cultures for one-, two- and three weeks they were stained immunocytochemically with the ABC method for detection of the synaptic marker Synaptophysin. The control recording experiments included culturing of the neurons in medium without ghrelin. The ghrelin conditioning of the medium led to earlier formation and activation of the networks. The activity pattern we observed at 6 DIV in Ghr cultures normally did not appear before the end of the second week. The immunostaining for synaptophysin revealed that the density of the synapses is much higher in Ghr cultures than in ctrls at all stages of incubation. In conclusion, ghrelin has a strong stimulating effect on functional network formation and earlier collective burst activity. This high level of functional connectivity is a possible consequence of a rapid chemical synaptogenesis, as the immunostaining clearly showed.

1 Introduction

Ghrelin is a gastric hormone and a neuropeptide, initially related to the appetite stimulation and growth hormone (GH) secretion [1]. It is produced mainly in the stomach, but also in the brain by neurons in the hypothalamic arcuate nucleus [2] and paraventricular neurons [3]. Ghrelin is an endogenous ligand of the orphan G-coupled protein receptor – the growth hormone secretagogue receptor (GHS-R), which is greatly expressed in the brain. This distribution suggests that ghrelin has broader functions beyond the control of GH secretion and food intake. Indeed, it has been demonstrated that ghrelin has an important role in the regulation of many other processes, including higher brain functions like memory performance, sleep and wakefulness [4], the cellular basis of which are the synaptic efficacy and plasticity. Previous studies on ghrelin induced activity indicate that the transmitter has an excitatory effect on the neuronal activity of hypothalamic slices *in vitro* by direct synaptic interaction [5], and controls synaptic plasticity in the hippocampus when applied intravenously [6]. However, the importance of ghrelin for developing neuronal networks *in vitro* has not been investigated yet. Therefore, we performed electrophysiological experiments on cultured neuronal

networks coupled to microelectrode arrays (MEAs) combined with immunocytochemistry for synaptic detection.

The pattern of collective electrophysiological activity changes with time during the first three weeks of development widely recognized as a maturation of the network. The natural changes in the activity dynamics comprise two major phases: the first phase is between the first and third week *in vitro*, when the synaptogenesis takes place and the electrophysiological behaviour of the network changes, both in spike and burst activity; and the second phase of maturation (within the fourth and fifth week), characterised by the modulation and shaping of the synaptic connectivity [7,8,9]. The previous work on cultured cortical neurons is mainly connected with the correlation between the age of the culture and the resulting activity pattern, but these are only limited aspects of the complex dynamics in the developing networks *in vivo*, missing the natural input in the developing brain. In this study we focus on the input from the ghrelin system, to see how the network formation and electrophysiological behaviour are influenced.

2 Material and Methods

Dissociated cortical neurons of newborn rats were obtained at post natal day 1 and plated on 60 electrode multi electrode arrays (MEA) (Multi Channel Systems, Reutlingen, Germany) pre-coated with 20mg/ml poly-ethylene-imine (Fluka, Buchs, Switzerland) for enhancement of the cell adhesion. Cells were kept in serum-free R12 medium (*ctrl*) or with additional ghrelin (*Ghr*) 2 μ M, Abcam, Cambridge, UK) under standard conditions of 37°C and 5% CO₂ in air. An initial cell density of approximately 3000 cells/mm² was used in all experiments. The neurons were cultured for a period of at least three weeks, and their activity was recorded for at least one hour on different days. For each culture we plotted the mean firing rate as a function of age. To enable comparison across cultures, the individual curves were normalized to their mean values and then averaged. Finally, all data was grouped in bins of 5 days of age (mean \pm SD) to obtain curves as in Figure 2.

In addition, after one-, two-, and three-week incubation, cultures were fixed in 4% paraformaldehyde in 0.1 M PBS, pH 7.4, and processed immunocytochemically with the ABC (avidin-biotin-horseradish peroxidase) method for detection of the synaptic marker synaptophysin. Briefly, a hydrogen peroxide (0.3% in absolute methanol for 30 min) was used to inactivate endogenous peroxidase. Appropriate washes in PBS followed this and subsequent treatments. Incubation in primary antibody mouse anti-synaptophysin IgG (Abcam, Cambridge, UK dilution 1:1000) lasted for 20 h at room temperature and was followed by 2 h biotinylated donkey anti-mouse IgG (1:500; Jackson ImmunoResearch, West) and 1 h ABC complex (1:500; Vector Labs, Burlingame, CA, USA). Following rinsing, peroxidase activity was visualized using 2.4% SG substrate kit for peroxidase (Vector) in PBS for 5 min, at room temperature. Finally, the cultures were dehydrated in a graded series of alcohols, cleared in xylene, and coverslipped with Entellan (Merck, Darmstadt, Germany). Negative controls included incubation after antigen-antibody preabsorption with the native antigen, at 4 °C for 24 h. After immunostaining, the cultures were photographed with AxioCam MRC digital camera linked to a Zeiss Axioplan 2 research microscope. All digital images were matched for brightness and contrast in Adobe Photoshop 7.0 software.

3 Results

Experimental data presented here were obtained from 8 cultures, coming from different preparations, monitored for at least 3 consecutive weeks. All the cultures exhibited highly variable patterns of spontaneous activity during their temporal maturation.

When the cortical networks were incubated under control conditions, at day 7 *in vitro* (DIV) only random spikes were generated (average 1.1 spikes/sec), and there was no clear evidence of collective bursts (Fig. 1). However, the ghrelin conditioning of the medium led to earlier formation and activation of the networks. At young age, the activity of the Ghr cultures was substantially higher than that of the controls, the Ghr cultures exhibited some activity as early as 3 DIV. The activity pattern we observed at 6 DIV in Ghr cultures normally did not appear before the end of the second week (11-12 DIV) in *ctrl* cultures (Fig. 1). At that age we recorded on average 8.8 spikes/sec, while in the *ctrls* showed no activity before 7 DIV. In Ghr cultures the mean firing rate reached a plateau at day 10-12, which is also considerably earlier than the controls (17-18 DIV) (Fig. 2). The immunostaining for synaptophysin revealed that the density of the synapses is much higher in Ghr cultures than in *ctrls* at all stages of incubation (Fig. 3, 4).

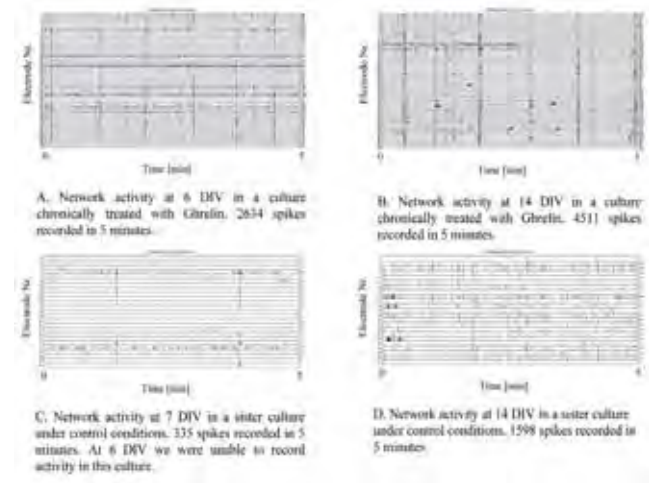


Fig. 1. Raster plots of the neuronal activity recordings in cultures incubated with ghrelin (top panels) and controls (bottom panels).

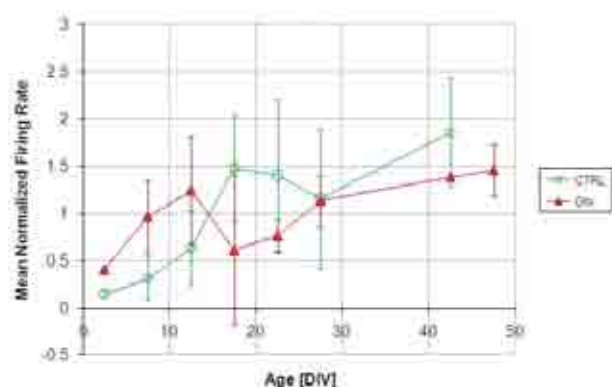


Fig. 2. Development of mean firing rates (normalized) of cultures incubated with ghrelin (Ghr, N=3) and under control conditions (N=5). All data was normalized and pooled into 5 day bins

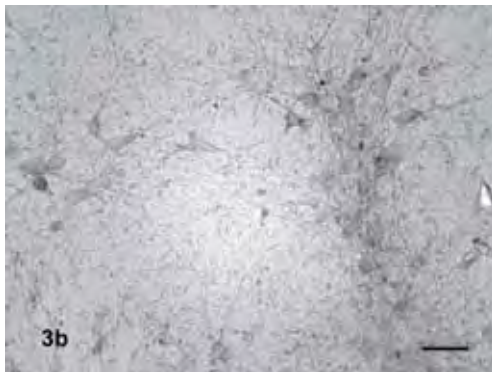


Fig. 3. One-week-old neuronal cultures immunostained for synaptophysin after ghrelin pretreatment (a) and control (b). Synapses appeared as dark-gray dots (arrows). Scale bars 20 μ m.

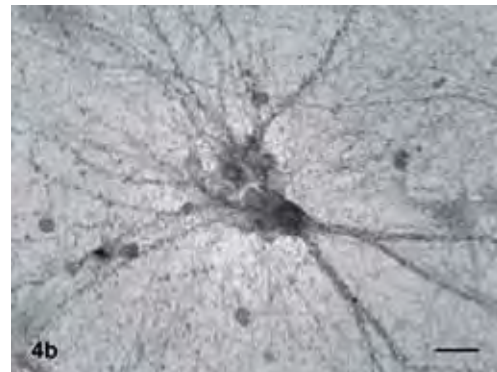
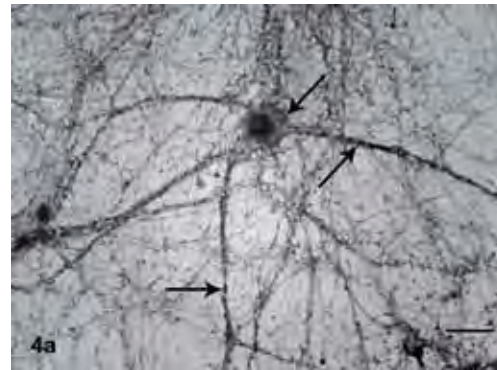


Fig. 4. Immunolabeling for synaptophysin after culturing for three weeks in medium containing ghrelin (a) and a control, incubated in plain medium (b). Arrows point at the synapses on the perikaryon and the neurites. Scale bars 20 μ m.

4 Conclusions

Previous studies on *in vitro* networks of cortical neurons, deprived of external stimuli, report the existence of a correlation between the age of the culture and the resulting activity pattern [10], and characterize the main phases of their development [7]. The results from our study provide clear evidence that chronic application of ghrelin has a strong stimulating effect on functional network formation. Ghrelin increases spike generation, and leads to earlier and better expressed collective burst activity. This high level of functional connectivity is a possible consequence of a rapid chemical synaptogenesis [11]. Indeed, immunostaining clearly showed an increased density of synapses observed in ghr cultures compared with the control experiments. Thus, it supports our electrophysiological findings of higher network activity, and clearly indicates that ghrelin also significantly increases synaptogenesis.

This effect of ghrelin on synaptic formation and function could provide a molecular target in developing novel therapeutics for disorders related to neurodegeneration and impaired synaptic plasticity.

Acknowledgement

We thank Karin Groot Jebbink and Bettie Klomphaar for their assistance in cell culturing. This study is part of the EU research project NEUROVERS-it. It was supported by grant MRTN-CT-2005-019247.

References

- [1] Kojima M, Hosada H, Date Y, Nakazato M, Matsuo H, Kangawa K. Ghrelin is a growth-hormone-releasing acylated peptide from stomach. *Nature* 1999; 402:656-660.
- [2] Lu S, Guan J-L, Wang QP, Uehara K, Yamada S, Goto N, Date Y, Nakazato M, Kojima M, Shioda S. Immunocytochemical observation of ghrelin-containing neurons in the rat arcuate nucleus. *Neurosci. Lett.* 2002; 321:157-160.
- [3] Cowley MA, Smith RG, Diano S, Tschop M, Pronchuk N, Grove KL, Strasburger CJ, Bidlingmaier M, Esterman M, Heiman ML, Garcia-Segura LM, Nillni EA, Mendez P, Low MJ, Sotonyi P, Friedman JM, Liu H, Pinto S, Colmers WF, Cone RD, Horvath TL (2003) The distribution and mechanism of action of ghrelin in the CNS demonstrates a novel hypothalamic circuit regulating energy homeostasis. *Neuron* 37:649-61.
- [4] Tolle V., Bassant, M.H., Zizzari, P., Poindessous-Jazat, F., Tomasetto, C., Epelbaum, J., Bluet-Pajot, M.T., 2002. Ultradian rhythmicity of ghrelin secretion in relation with GH, feeding behavior, and sleep-wake patterns in rats. *Endocrinology* 143, 1353-1361.
- [5] Hori Y, Kageyama H, Guan JL, Kohno D, Yada T, Takenoya F, Nonaka N, Kangawa K, Shioda S, Yoshida T (2008) Synaptic interaction between ghrelin- and ghrelin-containing neurons in the rat hypothalamus. *Regul Pept* 145: 122-127.

- [6] Diano S, Farr SA, Benoit SC, McNay EC, Silva I, Balazs H, Gaskin FS, Nonaka N, Jaeger LB, Banks WA, Morley JE, Pinto S, Sherwin RS, Xu L, Yamada KA, Sleeman MW, Tschop MT, Horvath TL (2006) Ghrelin controls hippocampal spine synapse density and memory performance. *Nat Neurosci* 9 (3): 381-388.
- [7] Chiappalone M, Bove M, Vato A, Tedesco M, Martinoia S (2006) Dissociated cortical networks show spontaneously correlated activity patterns during in vitro development. *Brain Res* 1093:41-53.
- [8] van Pelt J, Vajda I, Wolters PS, Corner MA, Ramakers GJA (2005) Dynamics and plasticity in developing neuronal networks in vitro. *Prog Brain Res* 147: 171-188.
- [9] le Feber J, Rutten WLC, Stegenga J, Wolters PS, Ramakers GJ, et al. (2007) Conditional firing probabilities in cultured neuronal networks: a stable underlying structure in widely varying spontaneous activity patterns. *J Neural Eng* 4: 54-67.
- [10] Kamioka H, Maeda E, Jimbo Y, Robinson HPC, Kawana A (1996) Spontaneous periodic synchronized bursting Turing formation of mature patterns of connections in cortical cultures. *Neurosci Lett* 206: 109-112.
- [11] Lin YC, Huang ZH, Jan IS, Yeh CC, Wu HJ, Chou YC, Chang YC (2002) Development of excitatory synapses in cultured neurons dissociated from the cortices of rat embryos and rat pups at birth. *J Neurosci Res* 67:484-93.

Effects of electrical stimulation to sympathetic neuron-cardiomyocyte coculture

Akimasa Takeuchi^{1*}, Hiromasa Tani¹, Masahide Mori¹, Hiroyuki Moriguchi¹, Keiko Miwa², Jong-Kook Lee², Makoto Noshiro³, Yasuhiko Jimbo¹

¹ Graduate school of Frontier Sciences, University of Tokyo, 5-1-5 Kashiwanoha, Kashiwa, Chiba, 277-8563 Japan

² Research Institute of Environmental Medicine, Nagoya University, Furouchi, Chikusa, Nagoya, Aichi, 464-8601, Japan

³ Graduate School of Medical Sciences, Kitasato University, 1-15-1 Kitasato, Mimami, Sagami-hara, Kanagawa, 252-0373 Japan

* Corresponding author. E-mail address: takeuchi@bmcpe.k.u-tokyo.ac.jp

The autonomic nervous system regulates heart-beating rhythms in response to physiological demand of the body. Recently, the molecular mechanism of signal transmission through these receptors and the effects of neurotrophic factors have been investigated in the culture of the sympathetic neuron and the cardiomyocyte. Little is known, however, the network-level interactions between the sympathetic neurons and the cardiomyocytes. In this study, A co-culture system of superior cervical ganglion (SCG) neurons and ventricular myocytes (VMs) was developed by using a polydimethylsiloxane (PDMS) chamber placed on a microelectrode-array (MEA) substrate. Constant-voltage stimulations (Biphasic square pulses, 1 V in amplitude, 1 ms in duration) were applied to SCG neurons via 16 electrodes which were located in micro compartments. Frequency and pulse number of the stimulation were set to 6 conditions. After applying these kinds of stimulations, beating rate of the VMs increased with an increase in the frequency and pulse number of stimulation. These results suggest that changes in beating rate of VMs after applying electrical stimulations to SCG neurons depend on frequency and pulse number of these stimulations and that the heart-regulating mechanisms as well as that in the body were formed in this co-culture system.

1 Introduction

The autonomic nervous system regulates heart-beating rhythms in response to physiological demand of the body [1,2]. Recently, the molecular mechanism of signal transmission through the adrenergic receptors [3] and the effects of neurotrophic factors [4] have been investigated in the culture of the sympathetic neuron and the cardiomyocyte. Little is known, however, the network-level interactions between the sympathetic neurons and the cardiomyocytes.

In earlier studies, electrophysiological characterization of cultured neurons was evaluated using microfabrication technique, such as a photolithographically-developed structure [5] and microcontact printing [6-8]. Electrical and mechanical dynamics of cardiomyocytes were investigated by photo-thermal etching [9,10] which is one of microfabrication technologies using focused laser beam. However, network-level interactions between sympathetic neurons and cardiac myocytes have not been examined by using microfabrication technology.

In this study, the superior cervical sympathetic ganglion (SCG) neurons and the ventricular myocytes (VMs) were co-cultured in a microfabricated PDMS microchamber placed on a microelectrode-array

(MEA) substrate [11, 12]. And then, to clarify the network-level interactions, functional relationships between them were evaluated by analysing the changes in beating rate of VMs after electrical stimulation to SCG neurons.

2 Materials and Methods

2.1 Culture device

The culture devices for co-culture were photolithographically fabricated. First, a soft-lithography master was produced by using photolithographic approach. Second, 70 mm-thick polydimethylsiloxane (PDMS, Dow Corning Toray) was coated on the soft-lithography master. Finally, a 2 mm-thick PDMS ring was placed on the coated PDMS. The ring acted as a reinforcement when the PDMS microchamber was demolded from the master.

The demolded PDMS microchamber had two compartments, 16 microcompartments and 8 microconduits connecting them (Fig.1). It was put on a microelectrode-array substrate under microscopic observation so that a microcompartment was located to over an electrode on the substrate.

2.2 Cell preparation

The SCG and the VMs were obtained from 2- to 3-day-old Wistar rats and dissociated by trypsin and collagenase.

The culture device was coated by type I collagen (Nitta Gelatin) and filled with the culture medium before dissemination of the SCG neurons and VMs. Dissociated SCG neurons were disseminated into one of the compartment and 16 microcompartments using a glass pipette under phase-contrast microscopic observation. 16-20 hours after dissemination of the SCG neurons, dissociated VMs were disseminated into the other compartment in the same way as the SCG neurons (Fig. 2).

2.3 Stimulation and evaluation

First, spontaneous electrical activities were recorded from the electrodes of the MEA substrate for 3 minutes, and then the constant-voltage stimulations, biphasic square pulses (1 V in amplitude, 1 ms in duration), was applied to the cultured SCG neurons in the microcompartments. The applied current flowed from each electrode under the microcompartment to the reference electrode. The pulse number and the frequency of the stimulation were set to 6 conditions (1 Hz and 60 pulses, 5 Hz and 60 pulses, 10 Hz and 60 pulses, 5 Hz and 300 pulses, 10 Hz and 120 pulses, and 10 Hz and 600 pulses). After the stimulations was discontinued, spontaneous activities were recorded for 1 minute. The same cultures were treated with 1 μ M

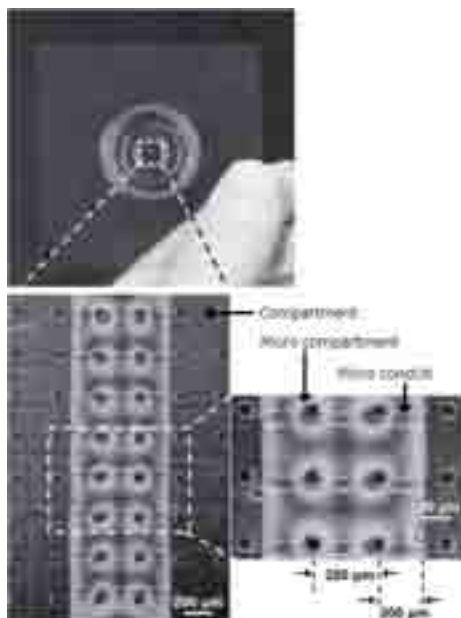


Fig. 1. Culture device on a MEA substrate.

The MEA substrate had 64 electrodes embedded in the center of the culture dish. Each electrode covers an area of $50 \times 50 \mu\text{m}$ square. One electrode is $250 \mu\text{m}$ apart from the other. PDMS microchamber had 16 microcompartments ($60 \mu\text{m}$ in diameter), 2 compartment ($360 \mu\text{m} \times 2.5 \text{mm}$) and microconduits ($50 \mu\text{m}$ in width, $5 \mu\text{m}$ in height) connecting them.

propranolol (Sigma-aldrich), a beta-adrenergic receptor antagonist [13], which blocked the transsynaptic effects between SCG neurons and cardiomyocytes. The treated samples were stimulated by the 600 pulses at a frequency of 10 Hz and the spontaneous activities were observed after stimulation for 1 minute.

The effects of electrical stimulation were evaluated using changes in beating rate of cardiomyocytes. The contraction timings of a cardiomyocytes are estimated by visualizing its spontaneous electrical activities, because a depolarization of the membrane potential is associated with a contraction of muscle fibrils. [14] Beating rate of the VMs was obtained by counting the number of the recorded spontaneous electrical activities. The frequency change ratio was calculated by dividing the beating rate after the stimulation by that before the stimulation.

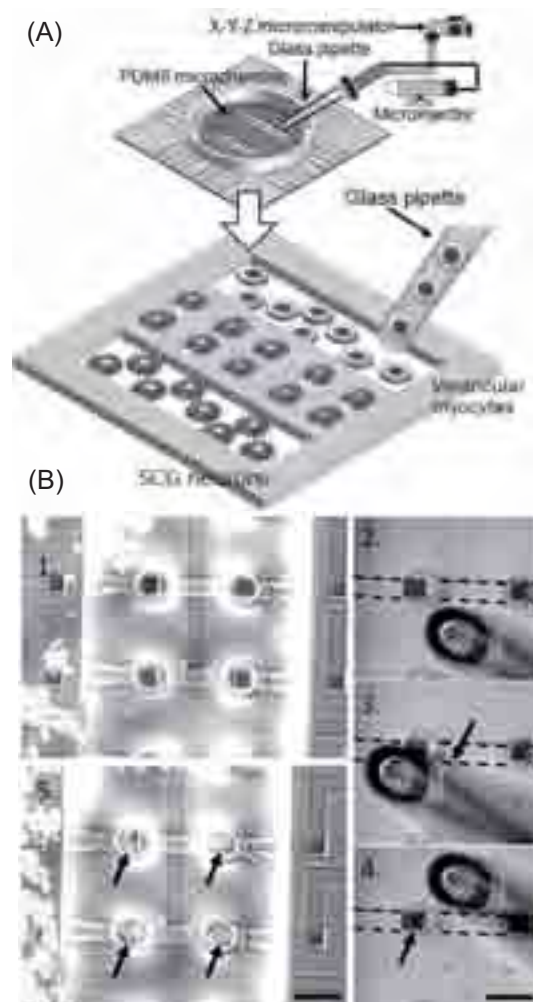


Fig. 2. Process for cell dissemination.

(A) Schematic diagrams of dissemination of the SCG neurons and VMs.

Inner diameter of the tip was set to $70\text{--}80 \mu\text{m}$. (B) Cluster of the SCG neurons (Arrows indicate the clusters of the SCG neurons) was dropped and guided into the microcompartments and one of the compartments by controlling with a microinjector and a micromanipulator. Each scale bar indicates $100 \mu\text{m}$.

3 Results

3.1 Co-culture system

The SCG neurons adhered to one of the compartments and all of the microcompartments, and the VMs to the other compartment. No SCG neuron was mingle with the VMs (Fig. 3). The SCG neurons 3 days after the dissemination of the VMs (3 days *in vitro*, DIV) grew in the left compartment and all of the compartments in the co-culture system. They proliferated more than those 1 hour after the dissemination of the VMs. On the other hand, the VMs proliferated only in the right compartment.

3.2 Effects of the electrical stimulation

Immediately after the electrical stimulation, evoked responses were observed from several electrodes irrespective of the number and frequency of the pulses.

After stimulation to the SCG neurons was stopped, beating rate of the VMs depended on the number and frequency of the pulses.

Figure 4 shows the changes in beating rate of the VMs after 6 different stimulations (5 days *in vitro*). No significant differences were found among beating rate of the VMs with the frequency of the pulses varied and with the number fixed.

Significant differences were found between beating rate 60 and 120 stimulation ($P < 0.01$) and between 60 and 600 stimulation at 10 Hz ($P < 0.01$).

Moreover, Under the presence of propranolol, beating rate after electrical stimulation showed statistically-significant reduction compared with absence of propranolol.

4 Discussion

4.1 Cultured SCG neurons were adrenergic

Beating rate of the VMs increased after the stimulation (600 pulses and frequency of 10 Hz) whereas the increases were not observed in the presence of propranolol. These results strongly suggested that cultured SCG neurons had adrenergic function and formed the synaptic transmission between the neurons and the VMs, and that propranolol prevented beating rate from increasing by inhibiting of the beta- adrenergic receptors on the VMs.

However, earlier studies reported that the SCG neurons cultured together with the cardiomyocytes were switch to cholinergic function [15, 16].

The reason why cultured SCG neurons in our study had adrenergic may be culture period, because of the results of this study were obtained from 5 days in culture. So, temporal changes of synaptic transmission will be closely examined in further study.

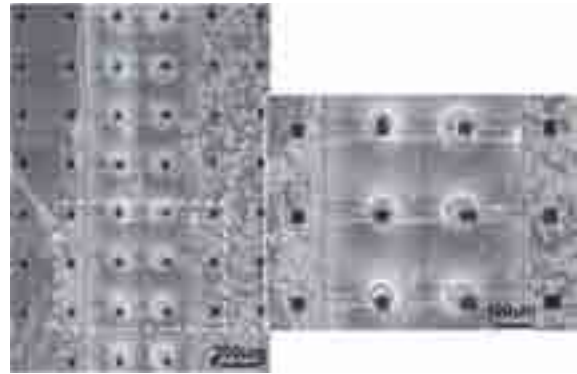


Fig. 3. Co-culture of SCG neurons and VMs.

The SCG neurons are in the left compartment and 16 microcompartments. The VMs are in the right compartment. (3 days *in vitro*; DIV).

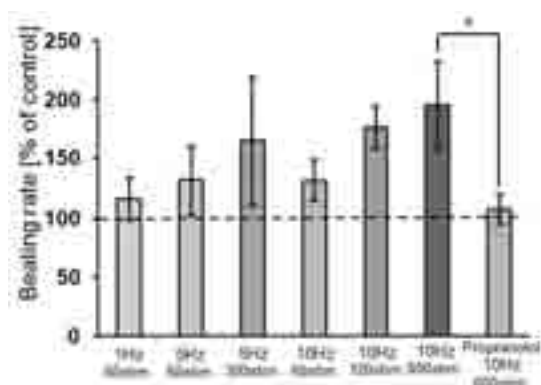


Fig. 4. Effects of electrical stimulation to the SCG neurons co-cultured with the VMs.

Contraction rates of VMs 1 minute after each condition of stimulation ($n=4$, \pm SD). Under the same number of stimulation, no significant change in beating rate after stimulation depended on the frequency of stimulation. However, beating rate significantly increased depend on increasing frequency and number of the stimulation. Asterisk (* $P < 0.05$, according to Student's t-test) indicates statistically significant increases compared with the values of each contraction rate before stimulation.

Moreover, it was still unknown that all of the SCG neurons retain the adrenergic function. So it is necessary to verify the adrenergic neurons in our co-culture system by alternative solutions. Burm and co-workers [17] confirmed the presence of adrenergic neurons directly by immunostaining for dopamine β -hydroxylase (DBH), a catecholamine biosynthesis enzyme.

From their works, immunostaining for the DBH will be performed to verify the presence of the adrenergic synapses between the SCG neurons and VMs in the co-culture system, and the reason why the SCG neurons remained adrenergic function in our experiments in further study.

4.2 Functional property between the cultured SCG neurons and VMs

Beating rate of the VMs increased in response with increasing of pulse number and frequency of the stimulation. From the results, it was suggested that changes in beating rate of the VMs contacting with the SCG neurons depend on the pulse number and frequency of the stimulation to the SCG neurons.

Effects of electrical stimulation to the SCG neuron-cardiomyocyte co-cultures were examined in earlier studies. Wakade and co-workers [18] stimulated electrically rat SCG neurons co-cultured with cardiac cells at the frequency of 0.3, 1 and 10 Hz. As a results, the amounts of released noradrenaline from the SCG neurons has no-significant differences between all stimulating conditions. According to their works, it was still unclear that changes in beating rate of the cardiomyocyte after stimulation to the SCG neurons. On the other hand, the results on this study suggested that changes in beating rate after the electrical stimulation depend on both of the pulse number and the frequency of stimulation in rat co-culture systems. However, the reason why beating rate of the VMs increased with increasing numbers of pulse and frequency of the stimulation was still unclear.

The stimulating conditions such as voltage, duration and pulse number were fixed in Wakade's report. Therefore, the relationship between number and frequency of the pulses and changes in beating rate of the VMs will be closely examined in order to fully investigate the effects of the SCG neurons on the VMs.

Functional properties between the sympathetic nerve and cardiac activities were already examined in animal study. Nakamura and co-workers [19] reported that beating rate of the canine heart increased with an increase in the frequency of the electrical stimulation to the right stellate sympathetic ganglion. According to their work, the increase of beating rate after the stimulation in our study were similar to its previous report. Therefore, it was suggested that functional relationships as well as the heart-regulating mechanisms in the body were formed in this co-culture system.

5 Conclusion

After applying stimulation to SCG neurons co-cultured with VMs, beating rate of the VMs changed with increasing frequency and pulse number of the stimulation.

Overall, these results suggest that the heart-regulating mechanisms as well as that in the body were formed in this co-culture system and that this co-culture system can be applied to study of network-level interactions between the sympathetic neurons and the cardiomyocytes.

References

- [1] Anderson R. H., Yanni J., Boyett M. R., Chandler N. J., Dobrzynski H. (2009). The anatomy of the cardiac conduction system. *Clin Anat.*, **22**, 99-113.
- [2] Langley J. N. (1998), On the Union of Cranial Autonomic (Visceral) Fibres with the Nerve Cells of the Superior Cervical Ganglion. *J. Physiol.*, **23**, 240-270.
- [3] Lockhart S. T., Turrigiano G. G., and Birren S. J. (1997), Nerve growth factor modulates synaptic transmission between sympathetic neurons and cardiac myocytes. *J Neurosci.*, **17**, 9573-9582.
- [4] Miwa K., Lee J.K., Takagushi Y., Kotani K., Horiba M., Hirabayashi M., Jimbo Y., and Kodama I. (2008), GDNF acts as a more potent chemoattractant than NGF for sympathetic innervation in cultured ventricular myocytes. *The 72nd Annual Scientific Meeting of the Japanese Circulation Society*
- [5] Morales R., Riss M., Wang L., Gavin R., Del Río J.A., Alcubilla R., Claverol-Tinturé E. (2008), Integrating multi-unit electrophysiology and plastic culture dishes for network neuroscience. *Lab Chip*, **8**, 1896–1905.
- [6] Mrksich M., Dike L.E., Tien J., Ingber D.E. and Whitesides G.M. (1997). Using microcontact printing to pattern the attachment of mammalian cells to self-assembled monolayers of alkanethiolates on transparent films of gold and silver. *Exp Cell Res*, **235**, 305-313.
- [7] Chang J.C., Brewer G.J. and Wheeler B.C. (2001). Modulation of neural network activity by patterning. *Biosens Bioelectron.*, **16**, 527-533.
- [8] Vogt A.K. G. J., Brewer, T. Decker, S. Böcker-Meffert, V. Jacobsen, M. Kreiter, W. Knolla and A. Offenhäusser, *Neurosci.*, 2005, 134, 783-790.
- [9] Kojima K., Moriguchi H., Hattori A., Kaneko T. and Yasuda K. (2003). Two-dimensional network formation of cardiac myocytes in agar microculture chip with 1480 nm infrared laser photo-thermal etching. *Lab Chip*, **3**, 292–296.
- [10] Suzuki I, Sugio Y, Jimbo Y and Yasuda K. (2005). Stepwise pattern modification of neuronal network in photo-thermally-etched agarose architecture on multi-electrode array chip for individual-cell-based electrophysiological measurement. *Lab Chip*, **5**, 241–247.
- [11] Jimbo Y., Kasai N., Torimitsu K., Tateno T. and Robinson H.P.C., *IEEE Trans Biomed Eng.*, 2003, 50(2), 241-248.
- [12] Stett A., Egert U., Guenther E., Hormann F., Meyer T., Nisch W. and Haemmerle H., *Anal Bioanal Chem.*, 2003, 377(3), 486-495.
- [13] Black J. W., Crowther A. F., Shanks R. G., Smith L. H., Dornhorst A. C. (1964). A New Adrenergic Betareceptor Antagonist. *Lancet*, **1**, 1080-1081.
- [14] Bucher O. M. (1957). A photoelectric recording set for pulsation curves of heart muscle cultures in vitro. *Exp. Cell Res.*, **13**, 109-115.
- [15] Weber M.J. (1981). A diffusible factor responsible for the determination of cholinergic functions in cultured sympathetic neurons. Partial purification and characterization. *J Biol Chem.*, **256**, 3447-3453.
- [16] Weber M. J., Raynaud B., and Delteil C. (1985). Molecular properties of a cholinergic differentiation factor from muscle-conditioned medium. *J Neurochem.*, **45**, 1541-1547.
- [17] Brum P.C., Hurt C.M., Shcherbakova O.G., Kobilka B. and Angelotti T. (2006). Differential targeting and function of alpha2A and alpha2C adrenergic receptor subtypes in cultured sympathetic neurons. *Neuropharmacology*, **51**, 397-413.
- [18] Wakade A. R., Przywara D. A., Bhavé S. V., Mashalkar V. and Wakade T. D. (1995). Cardiac cells control transmitter release and calcium homeostasis in sympathetic neurons cultured from embryonic chick. *J Physiol.*, **488**, 587-600.
- [19] Nakayama Y., Miyano H., Shishido T., Inagaki M., Kawada T., Sugimachi M. and Sunagawa K., (2001). Laterality in direct and indirect inotropic effects of sympathetic stimulation in isolated canine heart. *Jpn J Physiol.*, **51**, 365-370.

Temporal Coordination Of Bursting In Neuronal Cultures

Bikbaev Arthur¹, Frischknecht Renato¹, Heine Martin¹

¹ AG Molecular Physiology, Leibniz Institute for Neurobiology, Magdeburg (Germany)

After maturation, neuronal cultures demonstrate unique spatial distribution of areas that differ by activity and/or temporal involvement into synchronous bursting. However, it remains unclear whether, once developed, the functional relationships between distinct areas in a given culture remain stable or can change over time. To address this question, we analysed network activity in cultures at different time points, and evaluated spatial distribution of and temporal coordination between active areas with respect to age factor.

1 Methods

Rat hippocampal cultures (E18, density 500-750K) were plated on 60-channel multi-electrode arrays and incubated at 37°C. First recordings of network activity were performed in 1 month old cultures (1M group) (MEA-60-INV, MultiChannel Systems, Reutlingen, Germany), which, if survived, were recorded again after 2 or 3 months in vitro (groups 2M and 3M, respectively). Further, we evaluated temporal order of bursting occurred in various channels within events. By events, we considered here a bursting in two or more channels that overlapped in time, i.e. termination of a burst in first channel occurred after commencement of a burst in following channel. Furthermore, active channels in each session were ranked according to certain parameters for following analysis of rank shifts, which was done separately for each culture.

2 Statistics

To evaluate the significance of age factor and the differences between groups, we used non-parametric Kruskal-Wallis ANOVA.

3 Results

We found that cultures surviving for up to 3 months in vitro are characterised by a regular and highly synchronous network activity. Both overall spiking and bursting were significantly higher in 2M and 3M, when compared to 1M cultures (Fig. 1A, 1B). The bursts in old cultures occurred more frequently, were longer and contained more spikes than those recorded in control session in 1M cultures (Fig. 1C-1E). Furthermore, mean firing rate within bursts and total duration of bursting vs. non-bursting modes within recording session were greater in 2M and 3M, than in 1M culture (data not shown). The results of analysis of spatial distribution of “hot spots” demonstrate the presence in all cultures of one or two electrodes/areas that preferentially triggered

synchronous firing (>20% of total event number), but their location in individual cultures varied substantially over time. Additionally, the results of analysis of rank shifts for various parameters revealed prominent changes in spatial location of the most active areas in old cultures in comparison to 1M cultures, and such changes were evident to a similar or larger degree in 3M, when compared to 2M group (Fig. 1F).

4 Conclusions/Summary

These data demonstrate the substantial functional rearrangement that takes place in hippocampal cultures long after their maturation. Further, our findings show that the spatial location of neuronal ensembles, which effectively drive synchronized bursting, can change in cultures over time even without external stimulation. This suggests that the pattern of temporal involvement of different locations into bursting is a subject of dynamic modulation and can undergo plastic changes.

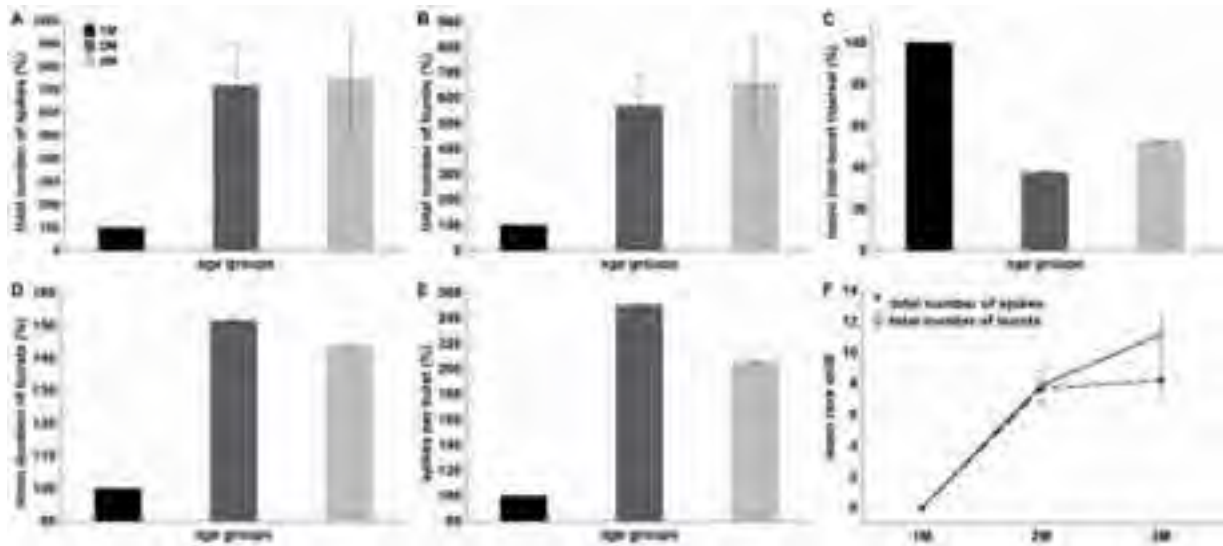


Fig. 1. Extracellular activity in hippocampal cultures that survive for up to 3 months is characterised by enhancement of both spiking and bursting activity and accompanied by functional reconfiguration of the network. For details, see Methods and Results sections. The absolute values for individual channels in 2M and 3M cultures were normalized to respective mean values in 1M group, which were taken as 100%. Results are presented as Mean±S.E.M.

Spontaneous Cortical Column Recurrent Activity and Layer Sensitivity to Electrical Stimulation

Vincent Delattre¹, Michele Giugliano^{1,2} and Henry Markram^{1,*}

¹ Laboratory of Neural Microcircuitry, Ecole Polytechnique Fédérale de Lausanne, Switzerland

² Dept. Biomedical Sciences, Univ. Antwerp, Universiteitsplein 2, B-2610 Wilrijk (Belgium)

* Corresponding author. E-mail address: henry.markram@epfl.ch

The neocortex generates periods of recurrent activity, such as the slow (0.1 - 0.5Hz) oscillations during slow-wave sleep. Such spontaneous oscillations have been observed *in-vitro* in acute ferret brain slices [1], and in rat brain slices [2], with perfusion ionic concentrations mimicking *in-vivo* conditions. We report and describe for the first time spontaneous recurrent activity in rat somato-sensory cortex, as well as a cortical layer specific burst threshold for electrical stimulation.

1 Methods

1.1 Experimental Protocol

The preparation of acute brain slices from p14-p17 juvenile Wistar rats was done accordingly to federal and institutional guidelines. Artificial cerebrospinal fluid (ACSF) contained (in mM) 125 NaCl, 2.5 KCl, 1.25 NaH₂PO₄, 1 MgCl₂, 2 CaCl₂, 25 NaHCO₃, and 25 glucose and was bubbled with 95% O₂-5% CO₂. Slices were mounted with a solution of nitrocellulose (0.14 mg/L in ethanol and 1% methanol) on 3-dimensional Multi Electrode Array (MEA) of 60 pyramidal platinum electrodes; electrode spacing 200 μ m (Ayanda Biosystems SA, Lausanne, Switzerland). Spontaneous oscillations were generated by an *up-state* solution [2,3] with slightly different ionic concentrations from normal ACSF (6.25 KCl, 1.5 CaCl₂, and 0.5 MgCl₂). Electrical stimulation was performed with an STG2008 (Multi Channel System, Reutlingen, Germany). The stimuli (1Hz train of 5 biphasic pulses of 1ms) was simultaneously applied to 4 electrodes.

1.2 Analysis

Recordings were processed off-line by custom C++ software, identifying the time of occurrence of multi-unit activity and its typical extracellular waveforms. Subsequent data analysis was performed in Matlab (The MathWorks, Inc., Natick, MA, USA), involving the manipulation of individual spike times across the MEAs, as well as the computation of the spike times histogram [4].

2 Results

Perfusion of acute rat cortical slices with ionic concentrations mimicking *in-vivo* conditions, generates slow (0.05 - 0.4Hz) spontaneous oscillations (Fig 1). Averaged bursts duration is 100 ms. This recurrent activity persists for 10-30 minutes, and can

be reinitiated by *up-state* perfusion after a washing period of 15 minutes with standard perfusion.

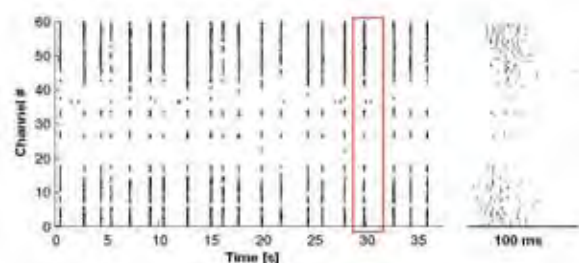


Fig. 1: Highly synchronized recurrent cortical activity is evoked by ionic concentration changes in the environment. A randomly chosen burst (red rectangle) is shown with a larger time scale.

Inter-burst distribution of 90% of detected events is less than one millisecond. Hence, interburst detected activity is almost null (Fig 2).

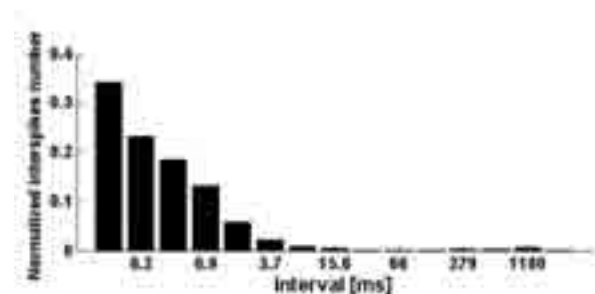


Fig. 2: Interburst distribution of events [0.1 - 5000ms] that occurred during the recording shown on Fig 1.

The average of spike times histogram computed for every channel produces an averaged burst profile, which is then normalized by the total number of events detected during one time bin [4] (Fig 3). We observe that some channels are in advance, and some are late on the averaged activity peak, thus, the average burst profile of each individual channel contains temporal information. Hence, replaying every channels burst profile on the picture of the cortical slice laying on the MEA allows the visualization of the activity spreading in cortical layers (Fig 4). We

report a wave like propagation in the entire column of the recurrent activity which is generated in the cortical layer 5 (N=297 bursts, 4 animals).

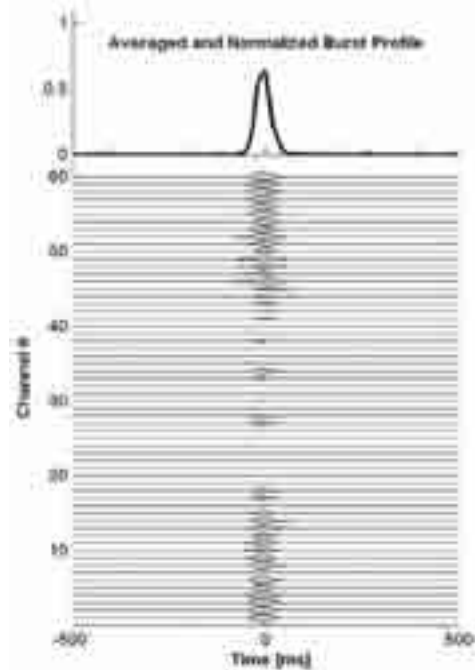


Fig. 3: Averaged and normalized burst profile for the entire MEA (**top**) and averaged burst profile for every individual channel (**bottom**), N=28 bursts over 60s recording.

Once spontaneous oscillations have vanished, we applied electrical stimulations to determine each cortical layer specific burst threshold. For each experiment, layer burst thresholds were normalized by the averaged burst threshold during the experiment. We observed that bursts initiation requires a slightly lower input in layers 2 to 4 than in deeper layers. It might be explained by the morphology of layer 5 pyramidal cells that are believed to initiate the bursting process [5].

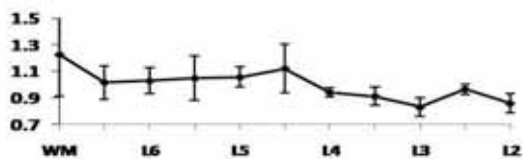


Fig. 5: Normalized cortical layer burst threshold (N=3 to 8).

References

- [1] M.V. Sanchez-Vives and D.A. McCormick, "Cellular and network mechanisms of rhythmic recurrent activity in neocortex", *Nature Neuroscience*, 2000.
- [2] T. Berger et al. "Transient rhythmic network activity in the somatosensory cortex evoked by distributed input in vitro", *Neuroscience*, 2006.
- [3] G. Silberberg et al. "Synaptic dynamics control the timing of neuronal excitation in the activated neocortical microcircuit", *Journal of Physiology*, 2004.
- [4] J. Van Pelt et al. "Longterm stability and developmental changes in spontaneous network burst firing patterns in dissociated rat cerebral cortex cell cultures on multielectrode arrays", *Neuro. Letter*, 2004.

- [5] S. P. Chauvette et al. "Origin of Active States in Local Neocortical Networks during Slow Sleep Oscillations", *Cerebral Cortex*, 2010.

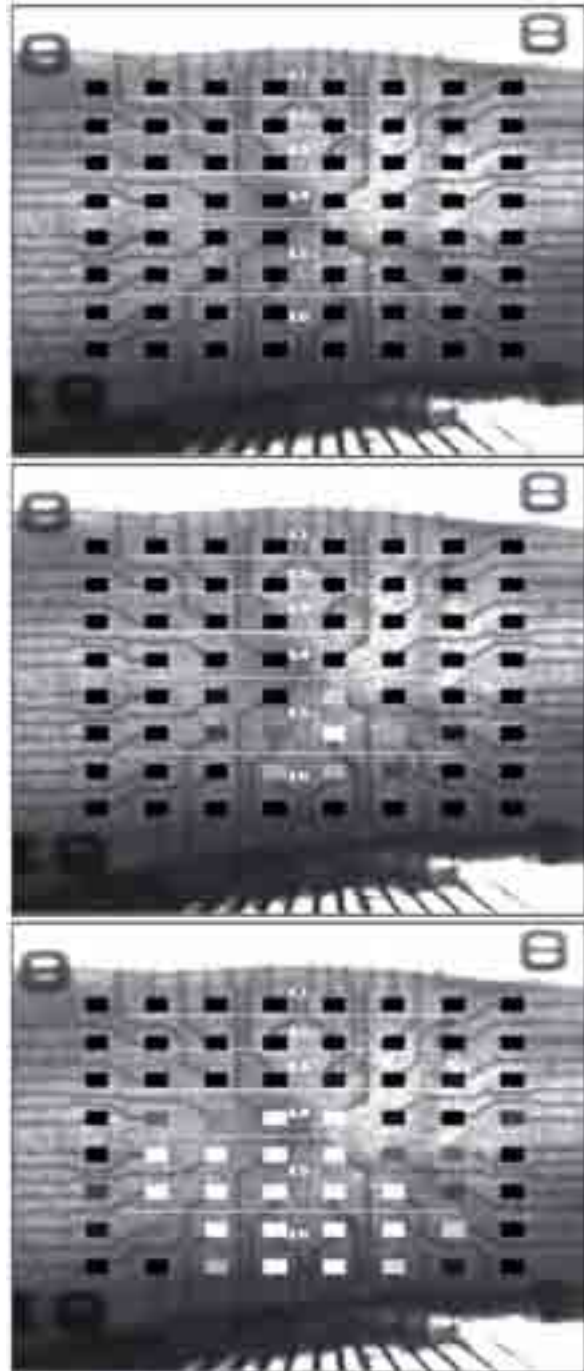


Fig. 4: Bursts are generated in cortical layer 5, and show a wave-like propagation in the entire column. In this example, we recorded 28 bursts over 60s.

Acknowledgement

We thank Luca Gambazzi¹ for providing technical support, the C++ software for MEA data analysis and useful Matlab scripts.

Software providing on-line high-resolution spatial mapping of single neurons

Patrick Dini^{1,2,3*}, Maxime Ambard³, Ulrich Egert^{1,3}

1 IMTEK – Department of Microsystems Engineering; University of Freiburg, Freiburg, Germany

2 Faculty of Biology; University of Freiburg, Freiburg, Germany

3 Bernstein Center for Computational Neuroscience Freiburg

* Corresponding author. E-mail address: patrick.dini@bcf.uni-freiburg.de

New tools such as High-density MEAs provide large amount of information, which help in the understanding of the geometry of single neurons and their embedding in networks activity. However, due to the complexity of such MEAs, a new software interface had to be developed, especially concerning the routing of the channels and the spike-sorting. The latter takes advantage of the capacity of the MEAs to record single neuron external electrical field potentials (EFPs) at different positions. Here we describe our strategy addressing this problem in an on-line fashion.

1 Introduction

Techniques such as patch-clamping, 2-photon microscopy and calcium imaging provide information about the electrical properties of neurons at different locations simultaneously. Nevertheless, they all suffer from trade-offs, which can be limited temporal resolution or short viability of the studied cell. To address these problems, MEAs featuring a high spatial and high temporal resolution [1] can be used. Such devices allow for the recording of the external electric field potentials emitted when a neuron fires, and thus at several locations of the neurons (see Figure 1 for an example of recorded signals). Such MEAs feature 11'016 electrodes, among which 126 are recordable simultaneously. Therefore a re-routing of the channels must be applied in order to target the subset of electrodes recording the activity of the desired neurons. Furthermore, the high spatial resolution was used here to developed an on-line spike-sorter and to compute footprints of individual neurons (see below) in an automatic fashion.

2 Material and Methods

2.1 Cell culture preparation

Neocortical cells from newborn rats were cultured on high-density MEAs and maintained in MEM supplemented with heat-activated horse serum (5%), L-glutamine (0.5mM), and glucose (20mM) at 37 ° C and 5% CO₂. The medium was partially replaced twice a week.

2.2 Material and recordings

High-density MEAs featuring 11'016 electrodes with a pitch of 18 µm were used, which permit the recording of single unit action potentials

from several electrodes simultaneously. A subset of 126 channels are recordable simultaneously, and if necessary, can be re-routed to include other locations on the array.

We developed a flexible interface in C++ and Python. In order to deal with the sheer amount of data during acquisition where only meaningful signals were retained. Moreover, we performed spike-sorting to take advantage of the high spatial resolution. In order to do so, we extended to several channels a method called template-matching [2], which calculates the distance of the recorded signal to a template. Furthermore, it is known that the amplitude of the action potentials varies during a burst. Therefore, an option was implemented in the spike-sorter to rescale the signal before comparison with the template.

2.3 Footprints

Spike triggered averaging over the spiking times at the soma was computed, and footprints of such neurons representing the flux of ions through the membrane near the electrodes location show clear changes in shape and delay from one electrode to another. In order to compute such footprints and to reduce the recording time, an algorithm was developed to automatically route the electrodes in order to track the spatial extent of individual neurons.

2.4 Network bursts

Mature culture networks of neocortical neurons exhibit periods of high synchronous activity called network bursts (NB) [3]. The propagation of activity throughout the network during such NBs follows various reproducible patterns [4], which presumably provide different synaptic inputs to individual neurons. It is of

interest, therefore, to know whether such different patterns of activity have distinguishable effects on the spatial properties of EFPs of individual neurons embedded in the network, especially at the dendritic trees.

Therefore, an on-line classification algorithm based on the recruitment order within a burst was developed and tested.

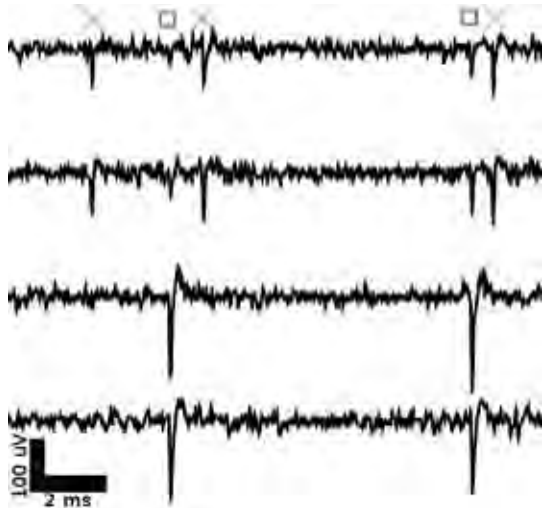


Fig. 1. Example of traces where action potentials were recordable by several electrodes simultaneously. Moreover, spikes from two neurons (red crosses and blue squares) are distinguishable. Applying a simple threshold detection on individual channels would have led to a misinterpretation of the data. For example, if one applies a threshold detection on the second channel from the top, these five spikes would have been attributed to the same neuron.

3 Preliminary results

3.1 Software interface

The software developed allows us to save the data only when activity is detected and reduces considerably the amount of data to be stored. Moreover, spike trains and ISI distribution can be displayed on-line and saved for further analysis.

3.2 Spike-sorting

The discrimination power of the template-matching algorithm applied to several channels improved greatly the quality of the spike-sorting. Qualitative analysis show that this method reduces considerably the number of false positives detected. Moreover, the spike-sorter deals adequately with the change of amplitude of the action potentials during bursts.

3.3 Footprints

The algorithm implemented improves the tracking of the individual neurons, and footprints of such neurons representing the flux of ions through the membrane near the electrodes location, and

show clearly changes in shape and delay from one electrode to another. Under optimal circumstances, electrical fields can be recorded at hundreds of micrometers from the soma. The evaluation of such patterns provides useful insight about the topology of the neuron and of the different transmission delays.

Moreover, several features of individual neurons can be extracted from these footprints: the soma and the dendritic tree can clearly be differentiated due to the inversion of polarity, and smaller external electrical fields, such as the one emitted by single axons, are possibly detectable. In addition to the spatial structure of individual neurons, temporal features representing the flux of ions inside the cell, as well as with the surrounding medium can also be extracted.

3.4 Classification of network bursts

The on-line algorithm succeeded in classifying the network bursts into several reliable patterns. Such feature of the program could be applied in different contexts. It is already possible to compare neuronal footprints of the same neurons embedded in different types of bursts, which is of interest since their synaptic input may vary depending on the network's activity. Moreover, such classification will be useful to apply different feedbacks to the culture while closed-loop experiments will be performed.

Acknowledgement

We thank the group of Prof. Hierlemann for providing the MEAs and for its extensive support, Samora Okujeni and Sebastian Reinartz for the cell culture preparation, and Patrick Pauli for the technical assistance. Funded by the German BMBF (FKZ 01GQ0420 & FKZ 01GQ0830) and by the EC (NEURO, No. 12788).

References

- [1] Frey U, Egert U, Heer F, Hafizovic S, Hierlemann A. (2009): Microelectronic system for high-resolution mapping of extracellular electric fields applied to brain slices. *Biosens Bioelectron.* 2009 Mar 15;24(7):2191-8. Epub 2008 Dec 7.
- [2] Rutishauser U, Schuman EM, Mamelak AN. (2006): Online detection and sorting of extracellularly recorded action potentials in human medial temporal lobe recordings, in vivo. *J Neurosci Methods.* 2006 Jun 30;154(1-2):204-24.
- [3] Wagenaar DA, Pine J, Potter SM. (2006): An extremely rich repertoire of bursting patterns during the development of cortical cultures. *BMC Neurosci.* 2006 Feb 7;7:11.
- [4] Raichman N, Ben-Jacob E. (2008): Identifying repeating motifs in the activation of synchronized bursts in cultured neural networks. *J Neurosci Methods.* 2008 May 15;170(1):96-110. Epub 2008 Jan 11.

Networks in dissociated culture follow native cortical development

Steffen Kandler^{1,2,3*}, Samora Okujeni^{1,2,3}, Sebastian Reinartz³ & Ulrich Egert^{1,3}

1 Bernstein Center Freiburg

2 Neurobiology and Biophysics, Inst. Biology III

3 Biomicrotechnology, Dept. Microsystems Engineering; ALU Freiburg, Germany

* Corresponding author. E-mail address: kandler@bcf.uni-freiburg.de

Synchronization of neuronal activity plays a crucial role for the formation of functional circuits in developing cortical networks. We investigated structural and functional development of cultured networks with combined patch-clamp and microelectrode array (MEA) recordings. We found that maturation processes in culture—e.g. the pairwise correlations of bursting activity—show comparable changes throughout development as observed in neonatal networks *in vivo*. This suggests that identical mechanisms also shape neuronal networks *in vitro*.

1 Introduction

The spontaneous synchronization of network activity during early cortical development supports the formation of basic functional circuits and neuronal assemblies. Recent studies argued that synchronized activity could serve as refinement mechanism of early neuronal maps and that a transition to asynchronous activity states coincides with the integration of sensory inputs, e.g. [1,2]. It suggests that the synchronization of activity has mechanistically a fundamental influence on the emerging computational properties of developing networks.

Here, we investigated the structural and functional embedding of individual neurons into synchronous network bursts (NB) within networks developing in dissociated culture. By monitoring these networks intracellularly and extracellularly with dual patch-clamp electrodes and MEA, we gained insight into the underlying network connectivity and the activity dynamics on a single-neuron and population level.

2 Methods

Neuronal tissue was obtained from frontal cortex of newborn rats following standard procedures [3,4]. Dissociated cells were seeded at densities of 1,500–5,000 neurons per mm^2 on PEI coated MEAs. Cultures were maintained in MEM supplemented with heat-inactivated horse serum (HS; 5%), L-glutamine (0.5 mM), and glucose (20 mM) in a humidified atmosphere at 37°C and 5% CO_2 .

Combined dual patch-clamp and MEA recordings were performed to test for pairwise connectivity at a distance range of max. 400 μm and to record neuronal embedding into NB activity. Recordings were carried out at 35–37°C using a slow perfusion (100 $\mu\text{l}/\text{min}^1$) with carbogenated (95% O_2 , 5% CO_2) culture medium without HS supplement.

3 Results

Networks with seeding densities higher than 2,000 neurons per mm^2 converged to this density within four weeks *in vitro*, indicating that maturation processes limit the final network density (Fig. 1).

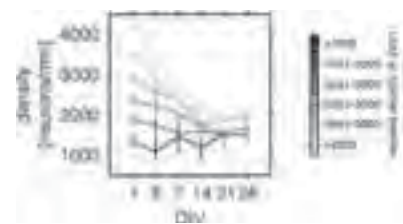


Fig. 1. Developmental decrease of network density depends on seeding density.

We observed that individual neurons were more likely to participate in NBs if those were stronger (*i.e.* higher no. of in-burst spikes or participating units) and if the NB onsets across electrodes were more synchronous (Fig. 2).

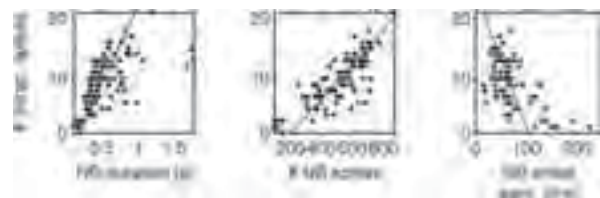


Fig. 2. Individual neuron in-burst activity correlates with NB duration (left), no. of array-wide NB spikes (center), and NB onset synchrony (right), *i.e.* the duration it takes for 25–75% of all neurons to fire their first NB spikes.

The distance dependent pairwise correlations in the firing within spontaneous NBs increased during network maturation, similar as found in native cortex [1] (Fig. 3).



Fig. 3. Age and distance dependent increase of covariance coefficients (CC) from DIV 14–21 and equalization of CCs after DIV 21 for zero-lag CC (left) and max. CC (center). Further, max. CCs have greater delays with increased pairwise distances (right).

The onset of NBs was further restricted to distinct sets of network sites, suggesting that the spatial arrangement and connectivity of neurons in these populations support NB initiation and propagation. Pairwise correlations between intracellular and extracellular NB firing were highly dependent on NB onset latencies, and to little or no degree on the spatial distances to NB onset sites (Fig. 4).

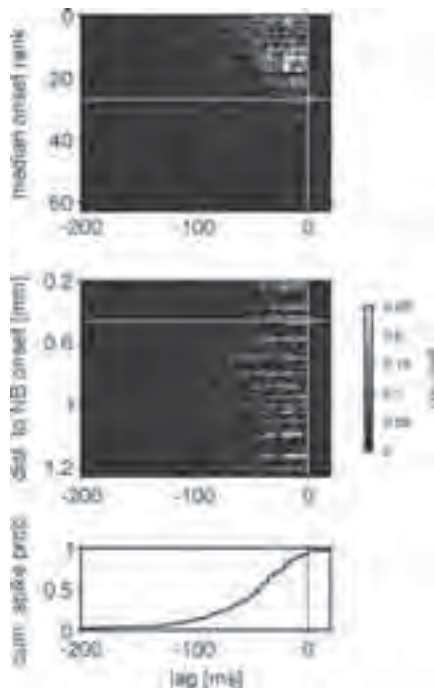


Fig. 4. Sorted pairwise correlations of intra- and extracellular NB spiking are dependent on median NB onset ranks (top) and not distance to NB onset location (center). Cumulative NB spike probability (bottom). Dashed lines indicate zero-lag (vert.) and position of intracellular recording site (horz.).

In 95 pairwise intracellular recordings we found that neurons less than 400 μm apart made connections with a high probability of 49% (Fig. 5) as observed previously [5]. Most connections thereby were unidirectional (23%) or bidirectional (20%) excitatory; only about 6% of all pairs had inhibitory connections. Furthermore, the connection probability was independent of pairwise distance and of the network density at the sampled distances.

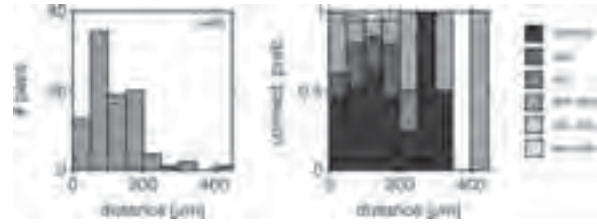


Fig. 5. Distance distribution of intracellularly recorded pairs (left) and their pairwise connection probability (right).

We also observed that EPSP amplitudes were dependent on the pairwise neuron distance and the age of the network. Herein, a separation was found for amplitude distributions of distances shorter resp. larger than 150 μm as well as a systematic shift of higher towards lower amplitudes with increased network age.

4 Discussion

Developmental changes of network synchrony in neuronal cultures show parallels to early cortical development *in vivo*. Especially, the network age dependent changes of pairwise correlations are similar to observations made in native cortex suggesting that cultured networks in principle follow the same mechanisms that refine early network structure and activity in a native context [1]. This is also supported by the developmental decrease of EPSP amplitudes which are subjected to the formation of more and more new synapses and synaptic scaling [6]. We, however, did not observe a transition of NB activity to asynchronous activity as observed *in vivo*. This could be explained by the lack of adequate input and lack of *functional* processing within the cultured networks.

Our results further suggest that a high degree of excitation and interconnectivity supports the spontaneous formation of NBs at distinct locations within the networks. The comparatively low number of inhibitory connections could partly result from maturation processes differentially advanced in excitatory and inhibitory subpopulations at the time of tissue preparation and during culture development [7].

Acknowledgement

Clemens Boucsein is warmly thanked for his support on intracellular recording techniques. Patrick Pauli and Ute Riede are thanked for technical assistance.

This work was supported by the German BMBF (BCCN, FKZ 01GQ0420 & BFNT, FKZ 01GQ0830) and by the EU (NEURO, No. 12788).

References

- [1] Golshani *et al.* (2009) *J Neurosci* 29(35):10890–10899.
- [2] Luczak *et al.* (2007) *PNAS* 104(1):347–352.
- [3] Shahaf & Marom (2001) *J Neurosci* 21(22):8782–8788.
- [4] Potter & DeMarse. (2001) *J Neurosci Meth* 110:17–24.
- [5] Nakanishi & Kukita (1998) *Brain Res* 795:137–146.
- [6] Garner *et al.* (2006) *Cell Tissue Res* 326:249–262.
- [7] De Lima & Voigt (1999) *Eur J Neurosci* 11:3845–3856.

Mapping of Paired-Pulse Activity in Hippocampal Slices with Multi-Transistor-Chip

Christoph Hermann¹, Peter Fromherz^{1*}

¹ Membran and Neurophysics, MPI of Biochemistry, Martinsried/Munich (Germany)

* Corresponding author. E-mail address: fromherz@biochem.mpg.de

We report on the extracellular mapping of field potentials evoked by paired pulse stimulation. For the recording we use a CMOS chip with 16384 transistors on a 1mmx1mm multi-transistor-array (MTA). The pitch between two pixels is 7.8µm and the sample rate is 6kHz. We cultivate organotypic brain slices from rat hippocampus for 2-3 weeks. After stimulation with tungsten electrodes we obtain maps of the extracellular activity in the tissue.

In a first set of experiments, we tested the MTA on functionality by mapping the CA3-CA1 projection at high spatial resolution and imaged the propagation of the fiber volley along the Schaffer Collaterals and the postsynaptic pspike in the CA1 pyramidal neurons. We also induced LTP at the Schaffer Collateral-CA1 pyramidal neuron synapses by presynaptic theta stimulation in stratum pyramidale of CA3.

In a second set of experiments, we mapped the correlated activity evoked by paired-pulse stimulation. We stimulated (i) in CA3 stratum pyramidale/Schaffer Collaterals (orthodromic), (ii) in CA1 stratum oriens/alveus (antidromic) and (iii) orthodromic/antodromic combined at interpulse intervals of 2-40ms. We focused on the response of principal neurons and of interneurons perpendicular to the propagation along cornu ammonis. Therefore we picked a line of sensors along the dendritic axis of the CA1 pyramidal neurons and formed a space-time map by plotting in a 3-dimensional graph field potential versus location versus time to visualize the dendritic location of the CA1 principal cell inputs.

Functional and morphological comparison of patterned and random low density cultures of neurons grown on microelectrode arrays (MEAs)

Marconi Emanuele¹, Messa Mirko¹, Baldelli Pietro¹⁻³, Casagrande Silvia³, Dante Silvia², Maccione Alessandro¹, Berdondini Luca¹, Benfenati Fabio¹

¹ Italian Institute of Technology – NBT Department

² Italian Institute of Technology – Nanophysics Department

³ Università di Genova - DIMES

To date, micro-contact printing (μ CP) proved to be a reliable methodology in creating geometrically ordered neuronal assemblies in *in-vitro* culture. However, the influence of the topology on neuronal networks was recently addressed raising the topic of how network morphology might affect the functionality or connectivity of these models. For this reason it is important to ensure that such cultures, used as models for investigation, maintain the main functional characteristics over all the culturing period and possibly for long term analysis. This is fundamental for morphological and functional characterization as well as the employment of low density cultures that helps in the localization of both single cells and network structures. This should be aimed to providing reliable outcomes as well as to studying functional properties of neuronal cells which appear at later stages of development. In this work, we optimized the microcontact printing (μ CP) technique to create grid-patterned networks on MEAs aligned with the microelectrode array (MEA) by exploring the bio-patterning methodology. Microcontact printing techniques and nano/micro drops deposition were used for engineering the substrate for low density cultures stable for long term analysis (> 21 DIVs). An electrophysiological and morphological comparison was performed on data acquired on random and controlled network assemblies cultured at low cellular density.

1 Methods/Statistics

1.1 Sample preparation

MEAs (8x8 array, 200 μ m pitch) and glass coverslips were prepared using micro contact printing (μ CP) and coated with ECM solution as an adhesion factor. PDMS stamps were used to transfer the adhesion molecules on the target substrates previously coated with an agarose repulsive layer. Low density cultures (< 100 cells/mm²) of E18 rat hippocampal neurons were grown and maintained in vitro for up to 21 DIVs activity.

1.2 Comparison between random and patterned networks

Immunofluorescence staining were performed by means of standard immunolabeling using primary antibodies for structural markers and fluorescently labeled secondary antibodies. Whole patch clamp analysis was performed. Spontaneous activity and evoked currents were recorded from both excitatory and inhibitory neurons. Extracellular currents from micro-printed MEAs were recorded. Electrical stimuli (Probe stimuli and tetanic stimulation) were delivered to selected active electrodes. Bicuculine (30 μ M final concentration) was delivered to the analyzed samples.

2 Results

The μ CP methodology was able to define the network topology and functional activity (i.e. synapse formation, function and plasticity) and maintain the network architecture up to 20-30 DIVs. Currents recorded on patterned MEAs showed higher coupling with electrodes and defined functional connectivity in patterned samples. Signals could be recorded at a very high signal-to-noise ratio even in low density and patterned cultures.

3 Conclusion/Summary

The imposition of a defined topology does not impair the main physiological properties of neurons cultured in geometrically defined conditions. However, benefits are evidenced as demonstrated by the increase in the number of neuronal soma located in close proximity of the electrodes and in the quality of recorded currents. Moreover, neuronal bodies and connection tracking resulted easier, allowing the identification of synaptic connections and enabling the correlation of functional aspects with the morphological structure of the neuronal network. These results were obtained by using low cell densities (70 cells/mm²) in culture, confirming μ CP as a suitable tool for the creation of custom experimental models. These results provide new tools for